Coordination scientifique
Robert JOUMARD

Transports et pollution de l'air
Transport and Air Pollution

12e colloque / *12th Symposium*
Avignon, 16-18 juin / *June* 2003

Actes INRETS n°92 - Vol. 2
Juin 2003

Coordinateur scientifique / *editor*:

Robert JOUMARD est directeur de recherche au Laboratoire Transports et Environnement (LTE)
Robert JOUMARD is a Senior Researcher at the Laboratory Transport and Environment (LTE)

L'unité de recherche :

LTE : Laboratoire Transports et Environnement, INRETS, case 24, 69675 Bron cedex, France
Téléphone : +33 (0)4 72 14 23 00 - Télécopie : +33 (0)4 72 37 68 37
Email : joumard@inrets.fr

Comité scientifique / *Scientific Committee*:

Michel	André	INRETS, F
Richard	Ballaman	OFEFP, CH
Kevin	Bennett	Univ. Cape Town, SA
Mireille	Chiron	INRETS, F
Walter F.	Dabberdt	Vaisala, USA
Asif	Faiz	The World Bank, Nepal
Alan W.	Gertler	Desert Research Inst., USA
Ron	Hamilton	Middlesex Univ., UK
Robert	Joumard	INRETS, F
Sasha	Madronich	NCAR, USA
Tamás	Merétei	KTI, H
Patrice	Mestayer	École Centrale de Nantes, F
Suzana K.	Ribeiro	Federal Univ. Rio de Janeiro, BR
Christian	Sacré	CSTB, F
Zissis	Samaras	Lab. Applied Thermodynamics, GR
Johannes	Staehelin	ETH Zurich, CH
Peter	Sturm	Technical Univ. Graz, A

N°ISBN : 2-85782-588-9N°ISSN : 0769-0266

© Les collections de l'INRETS
PRIX : 15,24 € TTC (TVA 5,5 %)

Les commandes doivent être adressées à l'INRETS - services publications - 2, av. du Général Malleret-Joinville - 94114 ARCUEIL CEDEX, et être accompagnées d'un chèque bancaire ou postal à l'ordre de : l'Agent Comptable de l'INRETS. Déduire la TVA pour l'étranger hors Union Européenne. Pour les pays de l'Union Européenne se reporter à la réglementation intercommunautaire en matière de TVA.

Fiche bibliographique

1 UR (1er auteur) INRETS-LTE		2 Projet n°	3 Actes INRETS n°92 - vol. 2
4 Titre 12e colloque "Transports et pollution de l'air"			
5 Sous-titre			6 Langue F/E
7 Auteur(s) JOUMARD Robert			8 Rattachement ext.
9 Nom adresse financeur, co-éditeur			10 N° contrat, conv.
			11 Date de publication juin 2003
12 Remarques			
13 Résumé Ces actes du 12e colloque organisé par l'INRETS, l'Université de Graz et le National Center for Atmospheric Research à Avignon du 16 au 18 juin 2003 regroupent les communications orales (tome 1) ou sous forme d'affiches (tome 2) sur des sujets aussi variés et complémentaires que les mesures de la qualité de l'air, les effets sur la santé, les modèles de dispersion physico-chimiques, les émissions unitaires, les inventaires d'émissions, les émissions des transports non-routiers, les coûts externes, les nouveaux carburants et technologies véhicule, la gestion des transports urbains, et les politiques de transport.			
14 Mots clés Transports, pollution atmosphérique, impacts, santé, modèles, émissions, technologie, politique de transport		15 Diffusion libre	
16 Nombre de pages 261	17 Prix 15,24 €	18 Confidentiel jusqu'au	19 Bibliographie oui

Publication data form

1 Unit (1st author) INRETS-LTE		2 Project n°	3 INRETS proceedings n°92 - vol. 2
4 Title 12th Symposium "Transport and Air Pollution"			
5 Subtitle			6 Language E / F
7 Author(s) JOUMARD Robert			8 Affiliation INRETS
9 Sponsor, co-editor, name and address			10 Contract, conv. n° 11 Publication date June 2003
12 Notes			
13 Summary These proceedings of the the 12th symposium organised by INRETS, the Technical University of Graz and the National Center for Atmospheric Research in Avignon from 16 to 18 June, 2003, include the oral communications (Vol. 1) and posters (Vol. 2) presented and cover a great variety of items such as air quality measurements, health effects, physico-chemical dispersion models, unit emissions, emission inventories, non-road transport emissions, external costs, new fuels and vehicle technologies, urban traffic management, and transport policies.			
14 Key Words Transport, atmospheric pollution, impacts, health effect, models, emissions, technology, transport policies		15 Distribution statement free	
16 Nb of pages 261	17 Price 15.24 €	18 Declassification date	19 Bibliography yes

Table des matières / *Content*

EFFETS SUR LA SANTE ET LES ECOSYSTEMES / *HEALTH EFFECTS AND ECOSYSTEMS*

Ozone Exposure Assessment for a European City from 1980 to 2020 based on Precursor Emissions in Germany 9
N. Metz - BMW Group (D)

Pollution control of indoor air: an overview 15
A.K. Pandey, K.M. Pandey & J.S. Virk - NIT (India), CPS Coll. (Phil.)

Assessment of vehicular air pollution and its effects on growth and yield of Beta vulgaris L. in periurban area of Allahabad City (U.P.) in India 21
S.B. Agrawal, A. Singh & D. Rathore - Allahabad Agr. Inst. (India)

MODELES DE DISPERSION PHYSICO-CHIMIQUES / *PHYSICO-CHEMICAL DISPERSION MODELS*

Dispersion modelling in a canyon street with application to the Romanian city of Timisoara 27
D. Bisorca, I. Ionel, L. Hanna & K. Cooke - U. Politehnica Timisoara (RO) & Sira Ltd (UK)

Modelling study of urban street canyons 33
N. Dixon & A. Tomlin - Univ. Leeds (UK)

Simulation numérique de la pollution dans la vallée de Chamonix, importance du trafic routier 39
G. Brulfert, C. Chemel & J.-P. Chollet - Univ. Fourrier (F)

Evaluation of highway network contribution to pollution concentration levels in the Bologna area 45
L. Cattozzo & C. Rondinini - Munic. Bologna (I)

Wind driven flow field simulation in narrow urban street canyons 51
F. Murena & F.Vorraro - Univ. Napoli (I)

Model Project Hagen - clean air and action plan in accordance with article 8 of the EC framework Directive 96/62/EG 57
A. Brandt & A. Niederau - LUA NRW, Aviso GmbH (D)

A numerical model for removal of SO2 from atmosphere by rain 63
D. Pal & D. K. Sinha - Santiniketan, Univ. Calcutta (India)

Validation of CALINE4 for CO and NO2 concentrations by an Irish motorway 69
B.M. Broderick, U.G. Budd, B.D. Misstear - Trinity Col. (IRL)

Application of the Lagrangian dispersion model GRAL to assess the air quality in the city of Graz 75
D. Oettl, P. Sturm & R. Almbauer - Graz Univ. Tech. (A)

QUALITE DE L'AIR / *AIR QUALITY*

Transport routier et pollution de l'air : cartographie nationale de la pollution par l'ozone en France 81
E. Fangeat, S. Bouallala, C. Elichegaray, N. Jeannée, M. Ba & J. Colosio - Ademe, Géovariances, Ifen (F)

Pour une méthodologie de la cartographie de la pollution de l'air intégrant l'essentiel des facteurs explicatifs 87
G. Perron, A. Hamadouche & J. Deraisme - ASPA, Géovariances (F)

Étude de la pollution de l'air par les particules fines (PM-10, PM-2,5 et PM -1) et évaluation de l'aérosol acide à Alger en site influencé par les émissions automobiles 93
R. Kerbachi, M. Boughedaoui, F. Boumechhour & N. Oucher - ENP, Univ. Blida (DZ)

Air pollution measurement on the Metropolitan Expressway by vehicle onboard sensor devices 99
Y. Tsubota & H. Kawashima - Keio Univ. (JPN)

Observatoire de la qualité de l'air et méthodologie d'optimisation d'un réseau de mesures à l'aide d'outils statistiques dessinés pour cet effet 105
A. Ionescu, É. de Vanssay, Y. Candau, M. Popounneau & V. Tessauro - Univ. Paris 12, Cap Env. (F)

Remote optical sensing evaluation (ROSE): Pollutant emissions in a street canyon in Germany 111
K. Cooke, B. De Souza, L. Hanna, M. Hilton, M. Welch, P. Kaspersen, L. Brøndo, J. Winkler, P. Neofytou & S. Rafailidis - Sira Ltd, Univ. Reading (UK), NEO (N), TTZ (D), NCSR Demokritos (GR)

Comparison of path-integrated and in situ measurements within a street canyon to produce a validation data set 119
K. Schäfer, S. Emeis, H. Hoffmann, C. Jahn, W. J. Müller, B. Heits, D. Haase, WD. Drunkenmölle, B. Leitl, F. Pascheke, M. Schatzmann & W. Bächlin - IMK-IFU, NLÖ, Hamburg Univ., Lohmeyer (D)

CARACTERISTIQUES DES TRAFICS / TRAFFIC CHARACTERISTICS

A Methodology for Modelling and Measuring Traffic and Emission Performance of Speed Control Traffic Signals 125
M. C. Coelho, T. L. Farias & N. M. Rouphail - IST (P), NCSU (USA)

Air pollutant emissions and dispersion in regional and local transport planning 131
C. Trozzi, R. Vaccaro & S. Crocetti - Techne srl (I)

EMISSIONS UNITAIRES / *UNIT EMISSIONS*

Un modèle de microsimulation pour l'évaluation des émissions polluantes dans les aires urbaines en fonction du régime de marche et pour une typologie véhiculaire 137
S. d'Elia - Univ. Calabria (I)

Impact of Air Conditioning, Ambient Temperature and Humidity on Emissions of Modern Passenger Cars 145
L. Pelkmans, G. Lenaers, P. Debal, M. Van Poppel, T. Hood, G. Hauser & M.R. Delgado - Vito (B), Mira (UK), Cle (D), Idiada (E)

Benzene Emission Factors of the latest Diesel- and Gasoline-fueled Passenger Cars within the Common Artemis Driving Cycle 153
C.J. Saxer, A.M. Forss, M. Weilenmann & N.V. Heeb - Empa (CH)

Correction Factors for Vehicle Emissions Rates Based on the Tauern Tunnel Experimental Data to Improve Vehicle Category Emissions Estimates 159
H. Puxbaum, J. Girard & E. Pucher - Vienna Univ. Technol. (A)

Cold-start emissions performance of late-model EU2 and EU3 passenger cars in low ambient temperature conditions 165
J. Laurikko - VTT (FIN)

Comparison of Different Engine and Fuel Types Regarding their Ozone Forming Potential 171
P. Soltic & C. Bach - EMPA (CH)

Unit PAH emissions at exhausts of recent-technology light vehicles in Europe 177
L. Paturel, E. Combet, O. Devos & P. Tassel - Univ. Savoie, Inrets (F)

Regulated and unregulated exhaust emissions from nine passenger cars 183
B. Mittermaier, D. Klemp & H.-J. Buers - Forschungszentrum Jülich (D)

Comparison of particle size distribution and emissions from heavy-duty diesel engines and gas engines for urban buses 191
J. van Ling, R. van Helden & I. Riemersma - TNO Automotive (NL)

Influence of the driving cycle on average emissions: development of the regression model for a case study 197
M. Rapone, L. Della Ragione, M. V. Prati & G. Meccariello - IM CNR (I)

INVENTAIRES D'EMISSIONS / *EMISSIONS INVENTORIES*

Usage of Non-conventional Power Generation for Controlling Environmental Pollution: A Case Study of Silchar City 203
K.M. Pandey & A.K. Pandey - CPS Coll. (Phil.), REC Silchar (Ind.)

Persistent organic pollutants in transport sector 209
V. Adamec, J. Dufek, J. Jedlicka & R. Cholava - Tranport Res. Centre (CZ)

A non-exhaust particulate emissions inventory for road traffic in Denmark 213
M. Winther - NERI (DK)

MOYENS DE CONTROLE ET REDUCTION / *CONTROL AND REDUCTION*

Competing technologies for reducing catalytic converter cold start emissions 219
P.N. Botsaris & E. Tsioliaridou - Democritus Univ. Thrace (GR)

Comparison of the NO2/NOx Emissions of Heavy-Duty Euro-3 Diesel Engines with and without a CRT™ System 225
P. Soltic & J. Rütter - EMPA (CH)

Cold start emission reduction via partial catalyst bypass 233
A. Karkanis, P. Botsaris & P. Sparis - Democritus Univ. Thrace (GR)

On Board Diagnostic System of Oxygen Sensor Malfunction, Meeting OBD II Requirements 241
E. Golgotiu & R. Drosescu - Tech. Univ. Asachi (RO)

Conversion Capability Estimation Method of an Automotive Catalytic Converter 247
R. Drosescu & E. Golgotiu - Tech. Univ. Asachi (RO)

Ag-Ti-V Impregnated Alumina for Controlling Carbon Monoxide and Hydrocarbons from Auto-exhaust 253
S.K. Rajput, S. Sarkar & D.K. Ghosh - Indian Inst. Tech. (India)

Nickel and Molybdenum Impregnated Catalytic System for Controlling Carbon Monoxide from Auto-exhaust 257
V. K. Pathak, S. Sarkar & D. K. Ghosh - Indian Inst. Tech. (India)

12th International Symposium "Transport and Air Pollution" / 12e Colloque international "Transports et pollution de l'air", Avignon, 16 -18 *June* / juin 2003
proceedings / actes, n°92, tome / Vol. 2, Inrets ed., Arcueil, France, 2003, p. 9-14

Ozone Exposure Assessment For an European City from 1980 to 2020 Based on Precursor Emissions in Germany

Norbert Metz
BMW Group, Department Traffic and Environment, 80788 Munich, Germany, Petuelring 130
Fax: ++ 89 382 4 5760, e-mail: norbert.metz@bmw.de

Abstract
Growing traffic density led in the past to undesirable high concentrations of NMHC and NO_2 in street canyons with limited air exchange. As a consequence O_3-concentrations in the afternoon in the suburbs of cities are exceeding the EU-air quality standards. Emission improvements of vehicles and emission legislation stopped the increasing emission trend since 1985. Despite the growing vehicle fleet air quality for the precursors NMHC and NO_2 in all big cities is improving.
Air quality standards nowadays are exceeded only in extreme adverse meteorological situations (low wind speed, inversion with poor exchange rates of urban air masses). To judge the burden for citizens the trend of annual means for NMHC and NO_2 and 1/2h max. values for O_3 is calculated for the time period 1980 to 2020 and exposure estimations on the basis of active and inactive times outdoors for some populations groups are given.
Keys-words*: exhaust emissions, air quality, health effects*

Introduction

One of the most urgent problems of retrospective epidemiological health effects studies is the examination of the exposure history regarding ambient air quality. Measured air quality data are only available for about 20 years, UBA (2001). For the future calculations are necessary. A suitable solution is to calculate the missing air quality concentrations on the basis of emissions of the main sources, Seika (1996). For kerbside sites exhaust gas emission of road transport are used and for urban background sites emission inventories of the federal states are used, UBA (2001). Forecasts are based on the relevant emission legislation.

Objectives

This paper describes a methodology to estimate the missing air quality data for a German city with a Gaussean dispersion model. Registration numbers of road transport vehicles, stock numbers and mileage from passenger cars, trucks, motor cycles and mopeds together with relevant emission factors during city operation as well as emission estimates from other sources are used as input data. Measured air quality data for NMHC, NO_2 and ozone are used and extrapolated for the forecast. Together with ventilation rates for different population groups the daily intake for different levels of action can be calculated.

Methodology

The exhaust gas emission trend of the precursors NMHC (VOC) and NO_x of all sources are taken from emission inventories for the city, from the federal states and from the German UBA (Environmental Protection Agency), while the road transport emissions are taken from reliable emission calculations, Höpfner (2002), Metz (2002), DIW (2002).

Air quality data are measured until today, UBA (2001), BLU (2003), UMEG (2003), HLUG (2002) and forecasted with a Gauss dispersion model taking into account the development of emission data for all sources and road transport in future years, DIW (2002). It is assumed that in 2010 the EU-air quality standard for ozone will be reached.

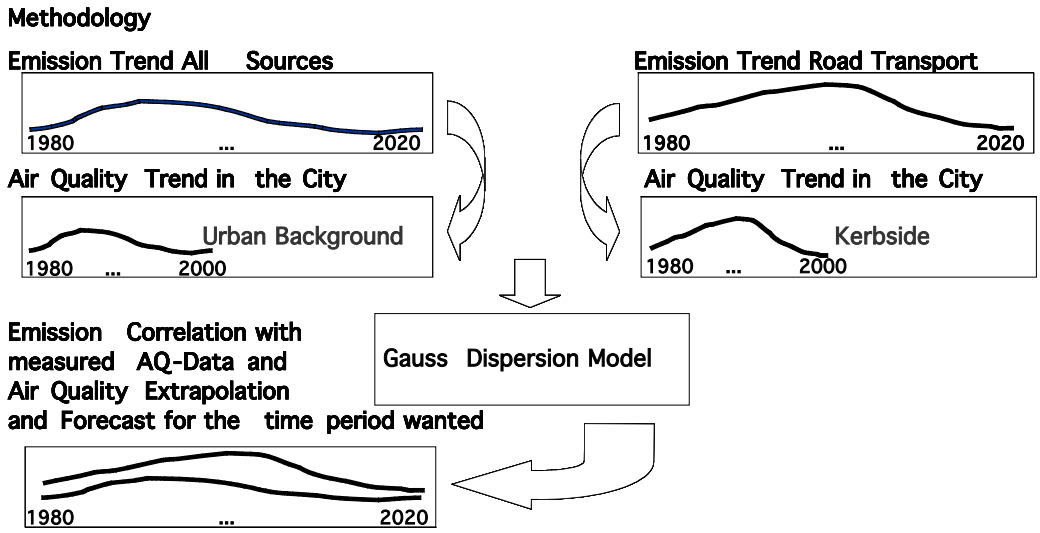

Figure 1: Schematic principle to calculate future air quality on the basis of emission data

Emission Forecast

With the inventories of the German Environmental Agency, UBA (2003) and mileage of road transport vehicles reliable emission forecasts can be calculated for German cities.

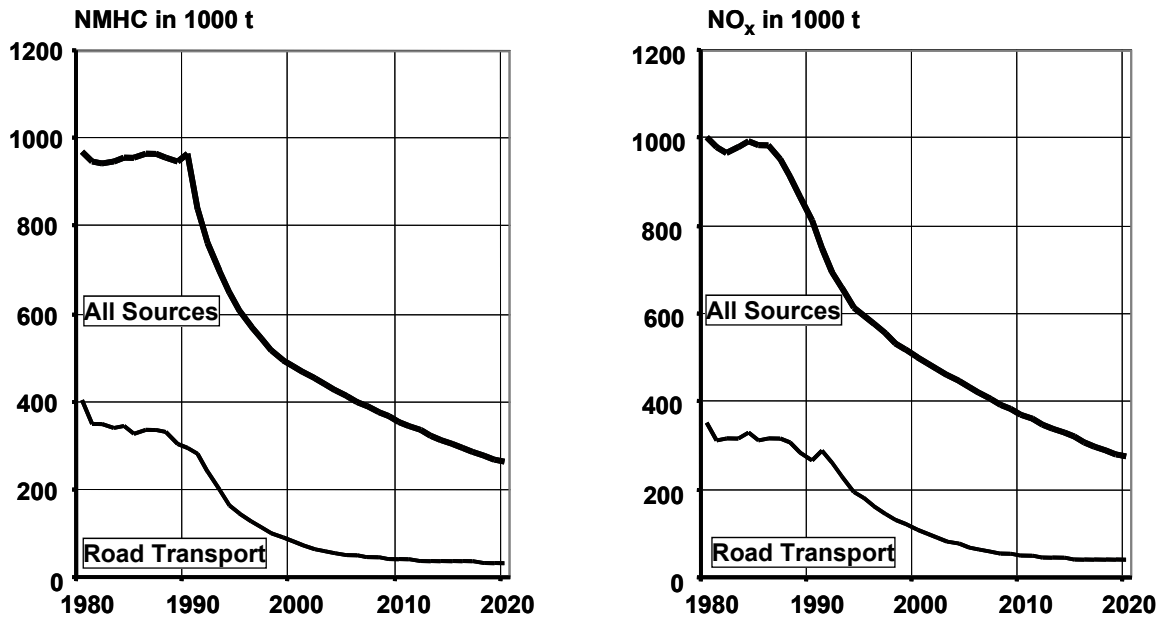

Figure 2: NMHC- and NO_x-emission data of all sources and road transport

Figure 2 shows the development for NMHC (VOC) and NO_x calculated on the basis of the mileage and the emission in cities. The decreasing trend started in 1990 and is still ongoing.

Air Quality

Due to the reduction of emissions the air quality in cities is improving both for kerbside and urban background sites. Together with measured data from 4 federal states Bavaria, Baden-Württem-berg,

Hessen and Rheinland-Pfalz forecasts show an ongoing decreasing trend for NMHC and for NO_2-concentrations, BLU (2003), UMEG (2003), HLUG (2002), LfUG (2002).

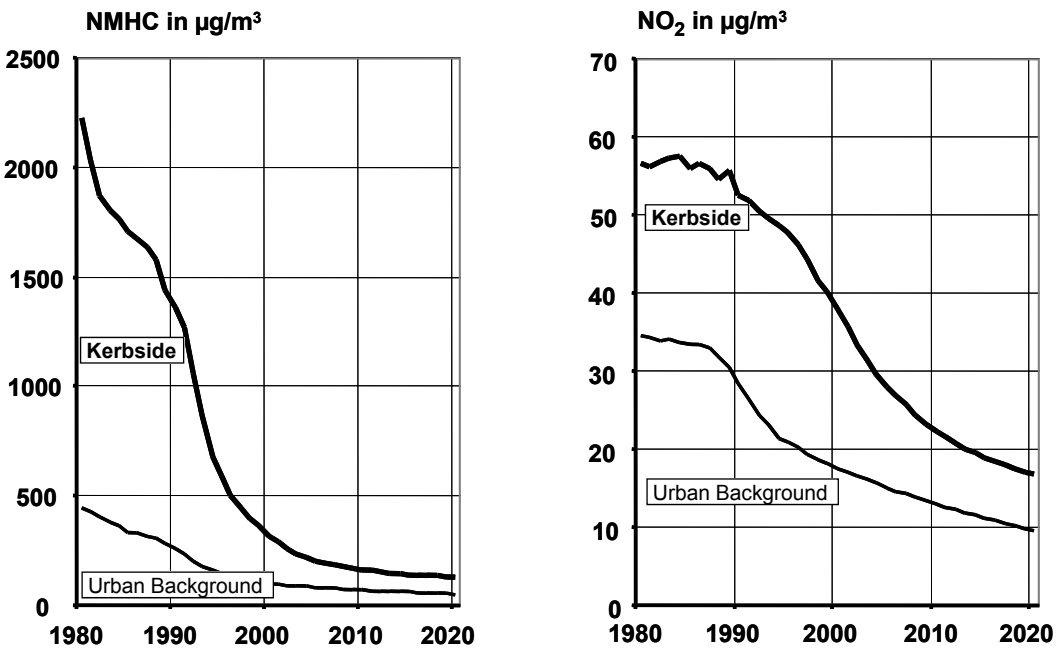

Figure 3: Typical NMHC- and NO_2- concentrations from 1980 until 2020 in German cities

Ozone formation

O_3 formation is a complex phenomena and not only dependent from local emissions. Ozone at ground level is influenced through mixing of NMHC (VOC) and NO_2 and ozone from the lower troposphere and the elevation of the boundary layer in the late morning, BUWAL (1989), Vogel (1996), Memmesheimer (1999).

While yearly average ozone values in cities are slightly increasing at an uncritical value, the max. 1/2h-values are slightly declining, Fricke (2002). In the last 5 years the trend is more or less stable with a small decreasing tendency.

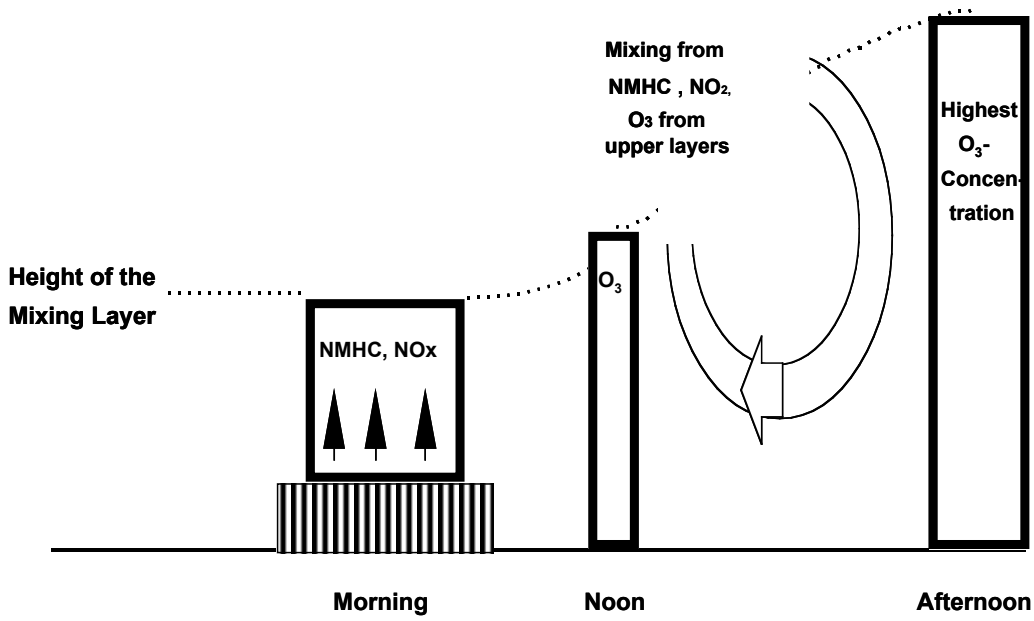

Figure 4: Ozone formation in the course of the day due to the rising height of the mixing layer and the mixing of precursors and ozone from the lower troposhere

To calculate the exposure for different population groups it is important to know the diurnal distribution of ozone during the day, BLU (2003) and the ventilation rates in action and in rest for the different population groups, Geigy (1971). It is apparent regarding ozone that summer and spring season is the most important time.

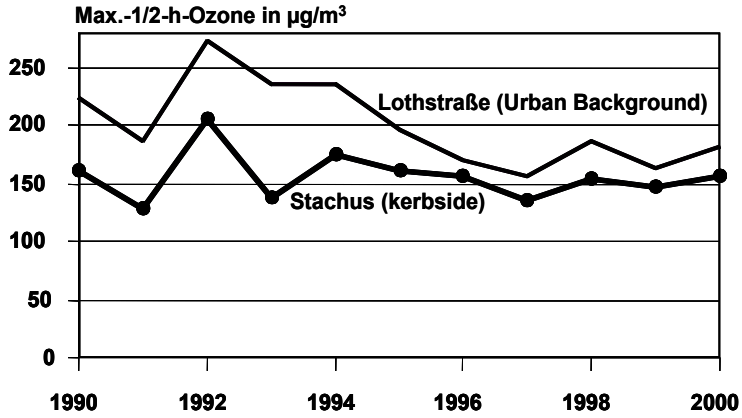

Figure 5: Trend for 1/2h- max. ozone concentrations in Munich for an urban back ground (Lothstr.) and a kerbside (Stachus) site, BLU (2003)

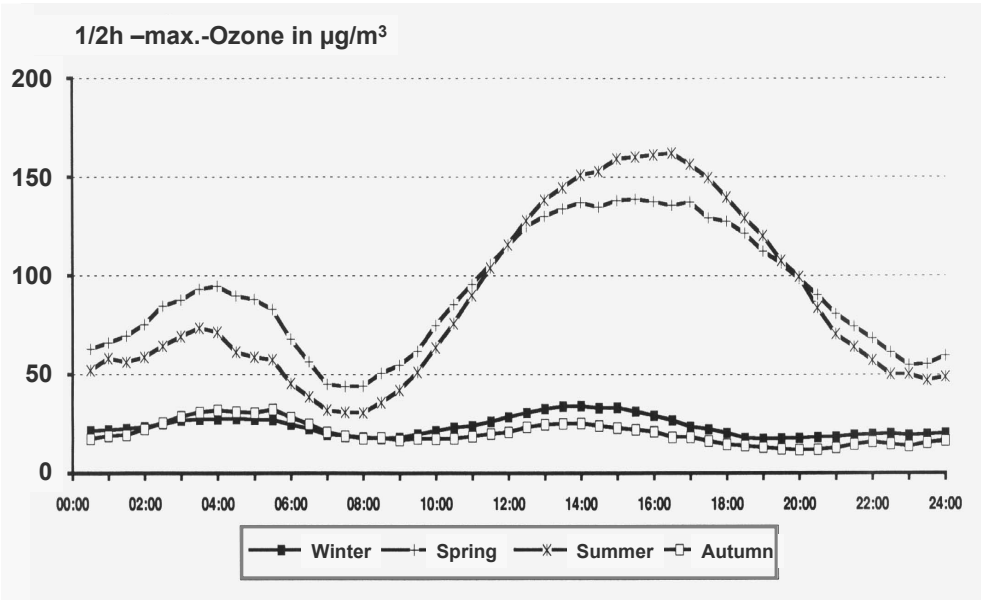

Figure 6: Diurnal distribution of 1/2h-ozone-concentrations for different seasons in 2002 in Munich Stachus

Exposure calculation

To calculate the ozone exposure for different population groups the time is multiplied with the relevant concentration starting at 13:00 for 4 hours assuming that most people are then in an active mode and an 8h outdoor exposure in rest in the time period from 9:00 to 13:00 and from 17:00 to 21:00 with reduced relevant ventilation rates, following the diurnal distribution with the 1/2h max. values for Munich, shown in figure 5.

Results

Due to different ventilation rates of athletics, children and other population groups, Höppe (1995) and of different diurnal ozone concentrations during the day a individual calculation for each population group and activity level must be conducted. As an example some results are given for athletics and children, see table 1.

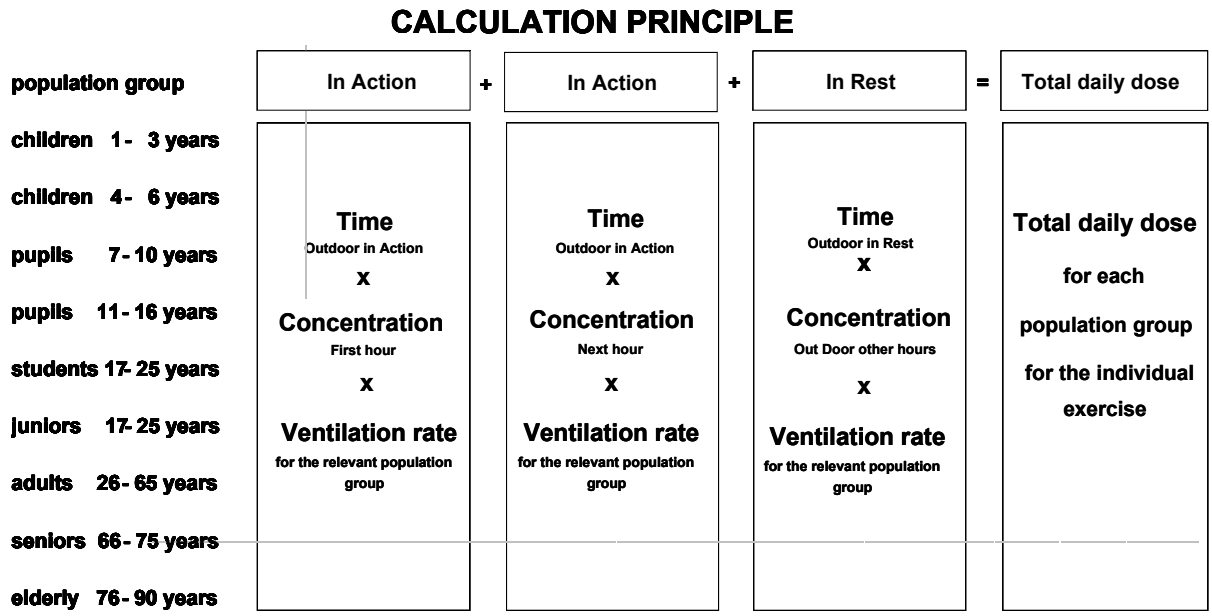

Figure 7: Ozone exposure for different population groups dependent from exercise duration and day time

During exercise athletics inhale almost 400 μg per hour, cumulated for the whole day 1800 μg is reached. Children inhale during exercise up to 130 μg/h, during the whole day up to 700 μg.Dependent from the activity level the inhaled mass of ozone can be different by a factor of 5. Different population groups differ by a factor of 4.For the judgement of health effects it is necessary which quantity per 1h in the respiratory system is metabolized to uncritical substances.

Population Group	Ozone Concentration µg/m^3	Activity mode	Exposure time	Mass of inhaled ozone	Total ozone mass inhaled
Athletics	60	in-rest	1h	30 µg	30 µg
Athletics	75	in-rest	1h	38 µg	68 µg
Athletics	90	in-rest	1h	45 µg	113 µg
Athletics	115	in-rest	1h	58 µg	171 µg
Athletics	130	in-action	1h	312 µg	483 µg
Athletics	150	in-action	1h	360 µg	843 µg
Athletics	160	in-action	1h	385 µg	1128 µg
Athletics	160	in-action	1h	385 µg	1513 µg
Athletics	160	in-rest	1h	80 µg	1593 µg
Athletics	140	in-rest	1h	70 µg	1663 µg
Athletics	125	in-rest	1h	63 µg	1726 µg
Athletics	100	in-rest	1h	50 µg	1776 µg
Children	60	in-rest	1h	15 µg	15 µg
Children	75	in-rest	1h	18 µg	33 µg
Children	90	in-rest	1h	22 µg	55 µg
Children	115	in-rest	1h	28 µg	83 µg
Children	130	in-action	1h	105 µg	188 µg
Children	150	in-action	1h	120 µg	308 µg
Children	160	in-action	1h	130 µg	438 µg
Children	160	in-action	1h	130 µg	568 µg
Children	160	in-rest	1h	40 µg	608 µg
Children	140	in-rest	1h	34 µg	642 µg
Children	125	in-rest	1h	30 µg	672 µg

Children	100	in-rest	1h	24 µg	696 µg

Table 1: Results of selected population groups

Conclusion

On the basis of emission inventories and road traffic emission resulting air quality concentrations can be forecasted also for the future. Air quality measurements for the area of interest must be used to determine the exact exposure history. With the ventilation rates for different population groups and the mode of activity it is possible to calculate the mass of ozone inhaled during 1h and the whole day. Whether these quantities will have negative effects more knowledge is necessary of the ozone mass which is metabolized in the body.

References

BUWAL, Ozon in der Schweiz, Report 101, Bern 1989

BLU, Bayerisches Landesamt für Umweltschutz, Augsburg, Monats- und Jahresbericht sowie pers. Kommunikation, 2003

Cozzarini Ch., Metz N., NO_2 Exposure Assessment for a city in Europe 1950-2050, 2002

DIW, Verkehr in Zahlen, 1970 bis 2002, Deutscher Verkehrsverlag, Hamburg

Fricke W., Pers. Communication, 9/2002

Geigy, Wissenschaftliche Tabellen, 7. Aufl, Basel Juli 1971

HLUG, Hessisches Landesamt für Umwelts und Geologie, 2002

Höpfner U., TREMOD-Calculations TREMOD 2.0, 2002

Höppe P., Environm. Res., Nov.7 , 1995

LfUG, Landesamt für Umweltschutz und Gewerbeaufsicht Rheinland-Pfalz, 2002

Memmesheimer M., Eurad, Uni Köln, 1999

Metz N., UBA-EPA-Wokshop, 11. 10. 2002, Bad Breisig

Seika, M., Evaluation od control strategies for improving urban air quality with London and Berlin as examples, Thesis, Inst. Of publ. A. environm. Health, School of Chem., Faculty of Sci., University of Birmingham Sept. 1996

UBA, Umweltbundesamt, Daten zur Umwelt, E. Schmidt-Verl., Berlin, 2001

UMEG Karlsruhe, und Jahresberichte sowie pers. Kommunikation, 2003

Vogel , Fiedler, Vogel, Ozon-Report, Karlsruhe 1996

12th International Symposium "Transport and Air Pollution" / 12e Colloque international "Transports et pollution de l'air", Avignon, 16 -18 *June* / juin 2003
proceedings / actes, n°92, tome / Vol. 2, Inrets ed., Arcueil, France, 2003, p. 15-20

Pollution control of indoor air : an overview

A.K. Pandey∗, K.M. Pandey and J.S. Virk*****
*Library Assistant, Central Library, N. I.T. Silchar, Assam, India
**Assistant Professor, Department of Mechanical Engineering, N.I.T. Silchar,Assam, India, email: kmpandey2001@yahoo.com
***Director, National Institute of Technology, Silchar, Assam, India

Abstract
People in the world are now facing a variety of risks to their health problems. A growing body of scientific evidence has indicated that the air within homes and other buildings can be more seriously polluted than the outdoor air in even the largest and most industrialized cities. People spend 90 percent of their time indoors. Some health effects can be useful indicators of an indoor air quality problems. Potential sources of indoor air pollution should be identified. It is suggested that there should be source control ventilation improvements and air cleaners should be used. Energy efficient heat recovery ventilators may also be used. A reasonable number of houseplants remove significant quantities of pollutants in homes and offices. It is suggested that the source control is the most effective solution.
Key words: *indoor air pollution, health problems, energy efficient ventilators, air cleaners, source control*

Introduction

All of us face a variety of risks to our health as we go about our day-to-day lives. Driving in cars, flying in planes, engaging in recreational activities, and being exposed to environmental pollutants all pose varying degrees of risk. Some risks are simply unavoidable. Some we choose to accept because to do otherwise would restrict our ability to lead our lives the way we want. And some are risks we might decide to avoid if we had the opportunity to make informed choices. Indoor air pollution is one risk that one can do something about. In the last several years, a growing body of scientific evidence has indicated that the air within homes and other buildings can be more seriously polluted than the outdoor air in even the largest and most industrialized cities. Other research indicates that people spend approximately 90 percent of their time indoors. Thus, for many people, the risks to health may be greater due to exposure to air pollution indoors than outdoors. In addition, people who may be exposed to indoor air pollutants for the longest periods of time are often those most susceptible to the effects of indoor air pollution. Such groups include the young, the elderly, and the chronically ill, especially those suffering from respiratory or cardiovascular disease. While pollutant levels from individual sources may not pose a significant health risk by themselves, most homes have more than one source that contributes to indoor air pollution. There can be a serious risk from the cumulative effects of these sources. Fortunately, there are steps that most people can take both to reduce the risk from existing sources and to prevent new problems from occurring. Indoor pollution sources that release gases or particles into the air are the primary cause of indoor air quality problems in homes. Inadequate ventilation can increase indoor pollutant levels by not bringing in enough outdoor air to dilute emissions from indoor sources and by not carrying indoor air pollutants out of the home. High temperature and humidity levels can also increase concentrations of some pollutants. There are many sources of indoor air pollution in any home. These include combustion sources such as oil, gas, kerosene, coal, wood, and tobacco products;

building materials and furnishings as diverse as deteriorated, asbestos-containing insulation, wet or damp carpet, and cabinetry or furniture made of certain pressed wood products; products for household cleaning and maintenance, personal care, or hobbies; central heating and cooling systems and humidification devices; and outdoor sources such as radon, pesticides, and outdoor air pollution. The relative importance of any single source depends on how much of a given pollutant it emits and how hazardous those emissions are. In some cases, factors such as how old the source is and whether it is properly maintained are significant. For example, an improperly adjusted gas stove can emit significantly more carbon monoxide than one that is properly adjusted.

Some sources, such as building materials, furnishings, and household products like air fresheners, release pollutants more or less continuously. Other sources, related to activities carried out in the home, release pollutants intermittently. These include smoking, the use of unvented or malfunctioning stoves, furnaces, or space heaters, the use of solvents in cleaning and hobby activities, the use of paint strippers in redecorating activities, and the use of cleaning products and pesticides in housekeeping. High pollutant concentrations can remain in the air for long periods after some of these activities. If too little outdoor air enters a home, pollutants can accumulate to levels that can pose health and comfort problems. Unless they are built with special mechanical means of ventilation, homes that are designed and constructed to minimize the amount of outdoor air that can "leak" into and out of the home may have higher pollutant levels than other homes. However, because some weather conditions can drastically reduce the amount of outdoor air that enters a home, pollutants can build up even in homes that are normally considered "leaky." Outdoor air enters and leaves a house by: infiltration, natural ventilation, and mechanical ventilation. In a process known as infiltration, outdoor air flows into the house through openings, joints, and cracks in walls, floors, and ceilings, and around windows and doors. In natural ventilation, air moves through opened windows and doors. Air movement associated with infiltration and natural ventilation is caused by air temperature differences between indoors and outdoors and by wind. Finally, there are a number of mechanical ventilation devices, from outdoor-vented fans that intermittently remove air from a single room, such as bathrooms and kitchen, to air handling systems that use fans and duct work to continuously remove indoor air and distribute filtered and conditioned outdoor air to strategic points throughout the house. The rate at which outdoor air replaces indoor air is described as the air exchange rate. When there is little infiltration, natural ventilation, or mechanical ventilation, the air exchange rate is low and pollutant levels can increase.

Apartments can have the same indoor air problems as single-family homes because many of the pollution sources, such as the interior building materials, furnishings, and household products, are similar. Indoor air problems similar to those in offices are caused by such sources as contaminated ventilation systems, improperly placed outdoor air intakes, or maintenance activities. Solutions to air quality problems in apartments, as in homes and offices, involve such actions as: eliminating or controlling the sources of pollution, increasing ventilation, and installing air cleaning devices. Often a resident can take the appropriate action to improve the indoor air quality by removing a source, altering an activity, unblocking an air supply vent, or opening a window to temporarily increase the ventilation; in other cases, however, only the building owner or manager is in a position to remedy the problem.

1. Improving the air quality in home

Health effects from indoor air pollutants may be experienced soon after exposure or, possibly, years later. Immediate effects may show up after a single exposure or repeated exposures. These include irritation of the eyes, nose, and throat, headaches, dizziness, and fatigue. Such immediate effects are usually short-term and treatable. Sometimes the treatment is simply eliminating the person's exposure to the source of the pollution, if it can be identified. Symptoms of some diseases, including asthma, hypersensitivity pneumonitis, and humidifier fever, may also show up soon after exposure to some indoor air pollutants. The likelihood of immediate reactions to indoor air pollutants depends on several factors. Age and preexisting medical conditions are two important influences. In other

cases, whether a person reacts to a pollutant depends on individual sensitivity, which varies tremendously from person to person. Some people can become sensitized to biological pollutants after repeated exposures, and it appears that some people can become sensitized to chemical pollutants as well.

Certain immediate effects are similar to those from colds or other viral diseases, so it is often difficult to determine if the symptoms are a result of exposure to indoor air pollution. For this reason, it is important to pay attention to the time and place the symptoms occur. If the symptoms fade or go away when a person is away from the home and return when the person returns, an effort should be made to identify indoor air sources that may be possible causes. Some effects may be made worse by an inadequate supply of outdoor air or from the heating, cooling, or humidity conditions prevalent in the home. Other health effects may show up either years after exposure has occurred or only after long or repeated periods of exposure. These effects, which include some respiratory diseases, heart disease, and cancer, can be severely debilitating or fatal. It is prudent to try to improve the indoor air quality in your home even if symptoms are not noticeable. While pollutants commonly found in indoor air are responsible for many harmful effects, there is considerable uncertainty about what concentrations or periods of exposure are necessary to produce specific health problems. People also react very differently to exposure to indoor air pollutants. Further research is needed to better understand which health effects occur after exposure to the average pollutant concentrations found in homes and which occur from the higher concentrations that occur for short periods of time.

2. Air quality problems

Some health effects can be useful indicators of an indoor air quality problem, especially if they appear after a person moves to a new residence, remodels or refurnishes a home, or treats a home with pesticides. If you think that you have symptoms that may be related to your home environment, discuss them with your doctor or your local health department to see if they could be caused by indoor air pollution. You may also want to consult a board-certified allergist or an occupational medicine specialist for answers to your questions. Another way to judge whether your home has or could develop indoor air problems is to identify potential sources of indoor air pollution. Although the presence of such sources does not necessarily mean that you have an indoor air quality problem, being aware of the type and number of potential sources is an important step toward assessing the air quality in your home. A third way to decide whether your home may have poor indoor air quality is to look at your lifestyle and activities. Human activities can be significant sources of indoor air pollution. Finally, look for signs of problems with the ventilation in your home. Signs that can indicate your home may not have enough ventilation include moisture condensation on windows or walls, smelly or stuffy air, dirty central heating and air cooling equipment, and areas where books, shoes, or other items become moldy. To detect odors in your home, step outside for a few minutes, and then upon reentering your home, note whether odors are noticeable. The federal government recommends that you measure the level of radon in your home. Without measurements there is no way to tell whether radon is present because it is a colorless, odorless, radioactive gas. Inexpensive devices are available for measuring radon. EPA provides guidance as to risks associated with different levels of exposure and when the public should consider corrective action. There are specific mitigation techniques that have proven effective in reducing levels of radon in the home. For pollutants other than radon, measurements are most appropriate when there are either health symptoms or signs of poor ventilation and specific sources or pollutants have been identified as possible causes of indoor air quality problems. Testing for many pollutants can be expensive. Before monitoring your home for pollutants besides radon, consult your state or local health department or professionals who have experience in solving indoor air quality problems in nonindustrial buildings. The federal government recommends that homes be weatherized in order to reduce the amount of energy needed for heating and cooling. While weatherization is underway, however, steps should also be taken to minimize pollution from sources inside the home. In addition, residents should be alert to the emergence of signs of inadequate ventilation, such as stuffy air, moisture condensation

on cold surfaces, or mold and mildew growth. Additional weatherization measures should not be undertaken until these problems have been corrected. Weatherization generally does not cause indoor air problems by adding new pollutants to the air. (There are a few exceptions, such as caulking, that can sometimes emit pollutants.) However, measures such as installing storm windows, weather stripping, caulking, and blown-in wall insulation can reduce the amount of outdoor air infiltrating into a home. Consequently, after weatherization, concentrations of indoor air pollutants from sources inside the home can increase.

3. Basic strategies

Source Control

Usually the most effective way to improve indoor air quality is to eliminate individual sources of pollution or to reduce their emissions. Some sources, like those that contain asbestos, can be sealed or enclosed; others, like gas stoves, can be adjusted to decrease the amount of emissions. In many cases, source control is also a more cost-efficient approach to protecting indoor air quality than increasing ventilation because increasing ventilation can increase energy costs. Specific sources of indoor air pollution in your home are listed later in this section.

Ventilation Improvements

Another approach to lowering the concentrations of indoor air pollutants in your home is to increase the amount of outdoor air coming indoors. Most home heating and cooling systems, including forced air heating systems, do not mechanically bring fresh air into the house. Opening windows and doors, operating window or attic fans, when the weather permits, or running a window air conditioner with the vent control open increases the outdoor ventilation rate. Local bathroom or kitchen fans that exhaust outdoors remove contaminants directly from the room where the fan is located and also increase the outdoor air ventilation rate. It is particularly important to take as many of these steps as possible while you are involved in short-term activities that can generate high levels of pollutants--for example, painting, paint stripping, heating with kerosene heaters, cooking, or engaging in maintenance and hobby activities such as welding, soldering, or sanding. You might also choose to do some of these activities outdoors, if you can and if weather permits. Advanced designs of new homes are starting to feature mechanical systems that bring outdoor air into the home. Some of these designs include energy-efficient heat recovery ventilators (also known as air-to-air heat exchangers).

Air Cleaners

There are many types and sizes of air cleaners on the market, ranging from relatively inexpensive table-top models to sophisticated and expensive whole-house systems. Some air cleaners are highly effective at particle removal, while others, including most table-top models, are much less so. Air cleaners are generally not designed to remove gaseous pollutants. The effectiveness of an air cleaner depends on how well it collects pollutants from indoor air (expressed as a percentage efficiency rate) and how much air it draws through the cleaning or filtering element (expressed in cubic feet per minute). A very efficient collector with a low air-circulation rate will not be effective, nor will a cleaner with a high air-circulation rate but a less efficient collector. The long-term performance of any air cleaner depends on maintaining it according to the manufacturer's directions.

Another important factor in determining the effectiveness of an air cleaner is the strength of the pollutant source. Table-top air cleaners, in particular, may not remove satisfactory amounts of pollutants from strong nearby sources. People with a sensitivity to particular sources may find that air cleaners are helpful only in conjunction with concerted efforts to remove the source.

Over the past few years, there has been some publicity suggesting that houseplants have been shown to reduce levels of some chemicals in laboratory experiments. There is currently no evidence, however, that a reasonable number of houseplants remove significant quantities of pollutants in homes and offices. Indoor houseplants should not be over-watered because overly damp soil may promote the growth of microorganisms which can affect allergic individuals. At present, EPA does

not recommend using air cleaners to reduce levels of radon and its decay products. The effectiveness of these devices is uncertain because they only partially remove the radon decay products and do not diminish the amount of radon entering the home. For most indoor air quality problems in the home, source control is the most effective solution. This section takes a source-by-source look at the most common indoor air pollutants, their potential health effects, and ways to reduce levels in the home.

Conclusion

It can be suggested that to control air pollution, source control, and ventilation improvements should be done. Air cleaners can also be used but they are generally not designed to remove gaseous pollutants. For many people the risk to health may be greater due to exposure to indoor air pollution than outdoor air pollution so there should be complete control of indoor air pollution otherwise there is serious risk to life.

References

Our Common Future: Pathways for Environmental Education, The Proceeding of the Australian Association for Environmental Education, International Conference, University of Adelaide, 23-28 September 1990

Mahajan, S.P., Pollution Control in process industries, Tata Mc Graw-Hill Publishing Company Limited, New Delhi, © 1985.

Kormondy, E.J. Concepts of Ecology, Prentice Hall of India Private Limited, New Delhi , 1986.

Rao, C.S, Environmental pollution control engineering, Wiley Eastern limited, © 1991.

Lawrence Folinsbee, "Human Health Effects of Air Pollution," Environmental Health Perspectives, Vol. 100 (1992), pp. 47-48.

World Health Organization and the United Nations Environment Programme, Urban Air Pollution in Megacities of the World (Blackwell Publishers, Oxford, UK, 1992), pp. 10-11.

Health Effects Institute (HEI), Particulate Air Pollution and Daily Mortality: Replication and Validation of Selected Studies (HEI, Cambridge, MA, 1995), p. 4.

12th International Symposium "Transport and Air Pollution" / 12e Colloque international "Transports et pollution de l'air", Avignon, 16 -18 *June* / juin 2003
proceedings / actes, n°92, tome / Vol. 2, Inrets ed., Arcueil, France, 2003, p. 21-26

Assessment of vehicular air pollution and its effects on growth and yield of *Beta vulgaris* L. in periurban areas of Allahabad city (U.P.) in India

S. B. Agrawal, Anoop Singh & Dheeraj Rathore
Department of Botany, Allahabad Agricultural Institute- Deemed University, Allahabad- 211 007, India. email : madhoo@bhu.ac.in, Fax: 91-532-2684394

Abstract
The effect of ambient air pollution on growth and yield of spinach (Beta vulgaris) plants was studied in periurban areas of Allahabad city, India. Increasing pollution load negatively influenced various growth parameters and growth indices. Yield loss of 7.07 to 31.19% was recorded in control plants at different experimental sites depending upon the pollution load. An increase in fertilizer dose showed positive effect by reducing yield losses.
Key words: *Air pollution, vehicles, India, periurban area, growth, Beta vulgaris*

Introduction

The speed with which urban air pollution has grown across the world in the last few decades is alarming. Urbanization has been accompanied by rapid industrial growth and an increase in the vehicle fleets (currently growing at the rate of 10-15 per cent per annum) due to increasing transport demand, giving rise to serious congestion, noise pollution, increase traffic accidents and perhaps most importantly, a grim air pollution problem. The unprecedented spurt in the number of vehicles in developing countries like India, has emerged as the most significant contributor to pollutants in urban air. Crop production is highly dependent upon environmental conditions among which air quality plays a major role. Urban air pollution has direct impact on periurban agriculture due to dispersion of emission in all directions along the wind. Agrawal (2000b) in a long-term study, along a National highway in India showed that air quality along the highway has potential negative impact on plant performance in the area.

Mineral nutrients supply may increase pollutant injury to crops (Pell et al., 1990), however, other studies indicated that plants grown at low fertility levels are more sensitive to air pollutants injury (Ayazloo et al., 1980, Rajput and Agrawal, 1994). Ormrod and Adedipe (1974) have suggested that mineral nutrients modify the responses of plants to air pollutants and responses varies with the specific element and species under consideration. The present investigation was aimed to quantify the growth attributes and yield responses of spinach (*Beta vulgaris* L. var. All green) grown at various sites in Allahabad city at different mineral nutrient concentration in the field.

1. Materials and Methods

The plant species *Beta vulgaris* L. (verna. Palak, family: Chenopodiacae) chosen for present study is a common herb, its leaves and tender twigs are used as vegetable which are a rich source of iron. Field experiment was conducted on seven selected sites viz. Allahabad Agriculture Institute (AAI), Civil lines (CL), Mehdeori (Mh), Jhunsi (Jh), Bahrana (Bh), Arail (Ar) and Rajroop pur (RRP) with four

fertility levels i.e. without fertilizer (F_0), recommended dose(RD) of N, P and K (F_1), one and half times of RD of N, P and K (F_2) and two times of RD of N, P and K (F_3) on spinach (*Beta vulgaris* L. var. All Green). Four plots (1m X 1m) of each treatment having similar edaphic conditions (to eliminate the changes because of soil characteristics, similar soil was used at every site with pH- 7.62, organic carbon- 1.64%, N- 690 mg $100g^{-1}$ soil, P- 16.4 mg $100g^{-1}$ soil and K- 136.2 mg $100g^{-1}$ soil) were prepared at all sites. Air quality monitoring was done with a regular interval of 15 days at all sites for gaseous pollutants.

Samples were collected randomly from each treatment in triplicate to measure various growth parameters. Spinach plants were harvested after 50 days and fresh weights of plants were recorded as yield $plot^{-1}$.

2. Results

The data of ambient air quality are given in Table 1, indicating that RRP was the most polluted site among all sites and Ar was least polluted.

Gaseous pollutants	Experimental Sites						
	CL	Ar	RRP	Mh	Jh	Bh	AAI
Oct., 2001							
SO_2	40.06	15.26	55.7	23.5	30.2	51.23	44.62
NO_2	24.42	8.0	36.6	14.6	20.53	31.87	26.54
O_3	14.33	10.3	27.6	10.0	11.75	22.52	18.64
Nov., 2001							
SO_2	45.72	18.29	65.04	32.55	38.62	60.26	50.45
NO_2	27.52	12.5	42.5	18.66	23.59	37.55	31.62
O_3	20.44	15.3	30.8	15.88	16.89	26.42	24.03

Table 1: Levels of SO_2, NO_2 and O_3 at different sites during experiment ($\mu g\ m^{-3}$).

Plant height, root length, number of leaves, leaf area and total biomass were reduced with increasing pollution levels (Table 2) and recorded maximum in F_2 treatment at all working sites. Maximum plant height (53.37 cm), root length (18.27 cm), leaf number (14.0), leaf area (386.92 cm^2) and total biomass (4.723 g $plant^{-1}$) were observed at Ar in F_2 treatment.

RSR showed positive correlation with pollution levels, while SLW, SLA and NPP negatively correlated (Table 3). Increase in RSR with increasing pollution load showed negative impact of air pollutants, it may be attributed due to more reduction in under ground biomass accumulation in compression to upper ground biomass. Maximum RSR was recorded 0.366 gg^{-1} in F_0 treatment at RRP, which reduced up to 0.327 gg^{-1} due to F_2 treatment. SLW, SLA and NPP were decreased with increasing pollution load and F_2 treatment showed positive impact by increasing them and recorded maximum 0.0097 gg^{-1} cm^{-2}, 118.90 cm^2 g^{-1} and 0.094 g $plant^{-1}$ day^{-1}, respectively at Ar.

Fig. 1 clearly showed negative impact of air pollution on RGR and NAR, as both were decreased with increasing pollution load. F_2 treatment showed positive impact by increasing them at all working sites, and recorded maximum 0.164 g day^{-1} and 92.59 g cm^{-2} day^{-1}, respectively at Ar. Maximum yield was found at Ar (reference site) and reduction in yield was observed with an increase in pollution load (Fig. 2). Maximum yield loss (31.19%) was recorded at RRP in F_0 treatment, which reduced up to 22.04% by F_2 treatment.

Experimental Sites	Treatments			
	F_0	F_1	F_2	F_3
Plant height (cm)				
AAI	42.27±0.14	43.43±0.59	48.93±0.21	42.50±0.75
CL	45.43±0.38	46.80±0.58	51.47±1.08	45.93±0.67
Mh	44.40±0.43	46.53±0.69	50.00±0.90	44.60±0.59
Jh	43.17±0.46	44.53±0.30	49.23±0.90	43.80±0.88
Bh	39.83±0.71	42.73±0.44	47.97±0.13	40.67±0.59
Ar	46.20±1.35	47.53±0.84	53.37±0.83	46.63±1.25
RRP	38.23±0.89	40.77±0.55	46.47±0.27	39.30±0.31
Root length (cm)				
AAI	15.00±0.81	16.80±0.32	20.87±0.36	16.00±0.21
CL	16.83±0.29	18.10±0.29	23.80±0.53	17.77±0.64
Mh	16.27±0.29	17.90±0.82	21.93±0.72	17.86±0.59
Jh	15.67±0.29	17.37±0.40	21.03±0.61	17.27±0.43
Bh	14.10±0.47	15.30±0.57	19.83±0.27	14.83±0.88
Ar	17.20±0.51	18.70±0.84	24.70±0.40	18.27±1.21
RRP	13.90±0.16	15.17±0.15	18.83±0.32	14.67±0.35
Leaf number				
AAI	9.33±0.62	10.33±0.62	12.33±0.62	9.67±0.47
CL	10.33±0.24	11.33±0.24	13.00±0.41	11.00±0.41
Mh	10.00±0.41	11.00±0.41	13.00±0.71	10.33±0.24
Jh	9.67±0.24	10.67±0.24	12.67±0.62	10.00±0.41
Bh	9.00±0.41	10.00±0.82	12.00±0.41	9.33±0.24
Ar	11.00±0.41	12.33±0.62	14.00±0.41	11.67±0.48
RRP	8.00±0.41	9.33±0.62	11.67±0.62	8.67±0.62
Leaf area (cm^2)				
AAI	288.67±15.42	317.42±15.07	343.58±14.66	291.25±19.72
CL	332.25±14.42	346.58±12.79	368.75±10.39	340.58±18.86
Mh	330.00±19.74	335.33±14.83	356.08±12.07	324.50±1.67
Jh	307.50±16.79	331.42±14.30	345.17±14.07	312.92±13.83
Bh	280.33±18.97	311.50±13.79	338.33±14.53	286.25±13.51
Ar	342.25±16.31	366.42±13.29	386.92±12.06	361.42±11.17
RRP	267.33±16.23	292.58±18.03	308.25±15.61	233.17±16.77
Total biomass (g)				
AAI	3.576±0.02	3.871±0.080	4.131±0.015	3.689±0.049
CL	3.973±0.042	4.057±0.041	4.566±0.102	4.017±0.060
Mh	3.880±0.028	3.975±0.080	4.261±0.070	3.923±0.018
Jh	3.748±0.038	3.942±0.037	4.203±0.042	3.847±0.074
Bh	3.326±0.015	3.726±0.039	4.095±0.020	3.537±0.078
Ar	2.953±0.040	4.341±0.039	4.723±0.043	4.056±0.123
RRP	3.328±0.070	3.670±0.065	3.966±0.034	3.517±0.127

Table 2: Effect of different fertility levels on plant height, root length, leaf number, leaf area and total biomass of spinach plants grown at various sites (Mean ±1SE).

Experimental Sites	Treatments			
	F_0	F_1	F_2	F_3
RSR (gg^{-1})				
AAI	0.341±0.001	0.333±0.008	0.311±0.0007	0.340±0.006
CL	0.325±0.004	0.322±0.004	0.317±0.0050	0.323±0.005
Mh	0.318±0.003	0.326±0.009	0.303±0.0050	0.324±0.001
Jh	0.324±0.004	0.328±0.003	0.307±0.0040	0.332±0.009
Bh	0.358±0.008	0.347±0.005	0.315±0.0020	0.355±0.013
Ar	0.333±0.007	0.331±0.006	0.329±0.0040	0.333±0.012
RRP	0.346±0.005	0.348±0.007	0.327±0.0030	0.355±0.028
SLW (gg^{-1} cm-^{2})				
AAI	0.0092±0.0002	0.0092±0.00010	0.0092±0.0008	0.0095±0.0001
CL	0.009±0.00003	0.0089±0.00050	0.0094±0.0006	0.0089±0.0001
Mh	0.0089±0.0002	0.0089±0.00020	0.0092±0.0001	0.0091±0.0002
Jh	0.0092±0.0002	0.0090±0.00002	0.0093±0.0004	0.0092±0.0001
Bh	0.0087±0.0002	0.0089±0.00003	0.0092±0.0001	0.0091±0.0002
Ar	0.0093±0.0004	0.0093±0.00030	0.0097±0.0008	0.0096±0.0005
RRP	0.0086±0.0003	0.0089±0.00030	0.0092±0.0007	0.0084±0.0001
NPP (g $plant^{-1}$ day^{-1})				
AAI	0.072±0.0005	0.077±0.0020	0.083±0.0003	0.074±0.0010
CL	0.079±0.0009	0.081±0.0008	0.091±0.0020	0.080±0.0010
Mh	0.078±0.0008	0.080±0.002	0.085±0.0020	0.078±0.0004
Jh	0.075±0.0008	0.079±0.0008	0.084±0.0009	0.077±0.0010
Bh	0.067±0.0004	0.075±0.0008	0.082±0.0005	0.071±0.0020
Ar	0.079±0.0008	0.087±0.0009	0.094±0.0010	0.081±0.0070
RRP	0.067±0.0020	0.073±0.0010	0.079±0.0007	0.070±0.0030

Table 3: Effect of different fertility levels on root-shoot ratio (RSR), specific leaf weight (SLW) and net primary production (NPP) of spinach plants grown at various sites (Mean ±1SE).

3. Discussion

The number of vehicles has increased in India from 1.86 million in 1971 to 32 million in 1996 (Varshney et al., 1997) and is expected to increase further more than 100 million by year 2020.

The deterioration in air quality has been shown to adversely affect the human health, vegetation and monuments. In the present study, reduction in plant height, root length, leaf number, leaf area and biomass accumulation was noticed with increasing pollution load. It is in conformity with the studies of Agrawal (2000a) on *Vigna radiata* and *Spinacia oleracea* plants exposed in ambient air till harvest. Ayer and Bedi (1991) have also reported that areas receiving higher pollution load showed significant decline in shoot length, leaf area, chlorophyll content, biomass accumulation and yield of wheat compared to control site.

Sites receiving highest SO_2, NO_2 and O_3 concentrations showed minimum values of SLW, NPP, RGR and NAR, while values of RSR were recorded maximum, as compared to the site showing minimum pollution load. Barnes et al. (1990) was also found significant negative correlation between RSR and O_3 concentration. Damage in several crop plants, including chrysanthemums and young endives were reported due to higher levels of SO_2, NO_x and O_3 (Rijsdijk, 1989). Rennenberg et al (1996) suggested that O_3 exposure can diminish the availability of photosyntha1te for growth and development and resulted an increase in shoot to root ratio and an over all reduction in biomass.The ozone concentrations correlated well with ozone injury in tobacco plants in rural Catalonia (Spain) (Ribas and Penuelas, 2003).

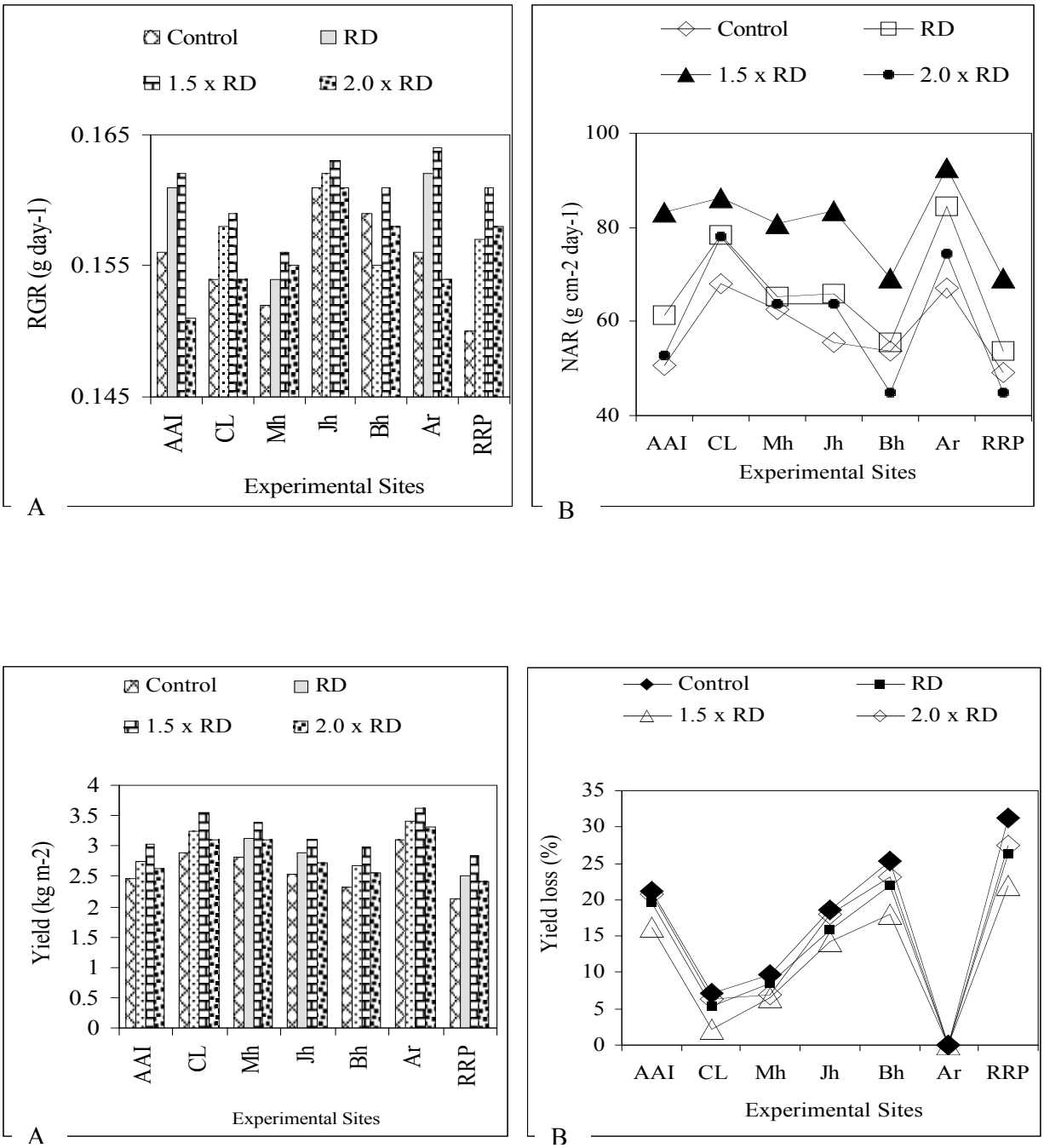

Figure 2: Effect of different fertility levels on spinach production (A) and yield loss (B) at various experimental sites.

Air pollution reduces both yield and nutritional quality of crop plants (Poole et al., 2002). Reduction in yield of various crop plants due to air pollutants was also reported by Agrawal (2000a). Nali et al. (2002) estimated yield losses varied from 8% for corn and alfalfa to 27% for soybean in Florence (Central Italy) and 3% for corn to 17% for soybean in Lucca. Agrawal (2000a) studied on impact of urban air pollution on periurban agriculture and reported that site with highest pollution load showed 79% reduction in yield of *Vigna radiata* and 72.8% reduction in biomass of *Spinacea oleracea*.

Conclusion

The results of present investigation suggest that both air pollution and nutrient deficiency have caused adverse impact on plant height and biomass accumulation. However, different doses of nutrients have ameliorated the adverse effect of air pollution on spinach plants by altering various growth processes. The present investigation also suggests that urban air quality of Allahabad city is affecting the agricultural production unfavorably in periurban areas.

Acknowledgement

Authors are also grateful to C. S. I. R. (New Delhi) for providing financial support in the form of research project.

References

Agrawal, M. (2000a): Effect of air pollution on urban agriculture in and around Varanasi city, Final technical report DIFD Project, Imperial College of Science Tech. and Med. U. K.

Agrawal, S. B. (2000b): Effect of vehicular emission on air quality and plant performance along a highway in India. Proc. 9th int. Symp. "Transport & Air Pollution", Avignon, INERTS, p 71-78.

Ayazloo, M., J. N. B. Bell & S. G. Garsed (1980): Modification of chronic sulphur dioxide injury to *Lolium perenne* L. by different sulphur and nitrogen nutrient treatments. Environ. Pollut., vol. 22. p 295- 307.

Ayer, S. K. & S. J. Bedi (1991): Effect of industrial air pollution on *Triticum aestivum* Proc. Natl. Acad. Sci., India, vol. 61, p 223-229.

Barnes, J. D., D. Velissariou, A. W. Davison & C. D. Holevas (1990): Comparative ozone sensitivity of old and modern Greek cultivars of spring wheat. New Phytol, vol. 116, n° 4. p 707-714.

Nali, C., C. Pucciariello & G. Lorenzini (2002): Ozone distribution in central Italy and its effect on crop productivity. Agriculture, Ecosyst. and Environ., vol. 90. p 277-289.

Ormrod, D. P. & N. O. Adedipe (1974): Protecting horticultural plants from atmospheric pollutants. A review. Hort. Sci. vol. 9. p 108-111.

Pell, E. J., W. E. Winner, C. Vinten-Johansen & H. A. Mooney (1990): Response of radish to multiple stresses. I. Physiological and Growth responses to changes in ozone and nitrogen. New Phytol., vol. 115. p 439-446.

Rajput, M. & M. Agrawal (1994): Responses of soybean plants to sulphur dioxide at varying soil fertility regimes. Biotronics, vol. 23. p 81-92.

Rennenberg, H., C. Herschbach and A. Polle (1996): Consequences of air pollution on shoot-root interactions. J. Pl. Physiol., vol. 148, n° 3-4. p 296-301.

Ribas, A. & J. Penuelas (2003): Biomonitoring of tropospheric ozone phytotoxicity in rural Catalonia. Atmos. Environ., vol. 37. p 63-71.

Rijsdijk, T. (1989): Atmospheric pollution. Damage by air pollution in summer and winter. Groenten en Fruit, vol. 45, n° 22. p 36-37.

Varshney, C. K., M. Agrawal, K. J. Ahmad, P. S. Dubey & S. H. Raja (1997): Effect of air pollution on Indian crop plants. Final report, ODA Project, Imperial College of Sci. Tech. & Med., UK.

12th International Symposium "Transport and Air Pollution" / 12e Colloque international "Transports et pollution de l'air", Avignon, 16 -18 *June* / juin 2003
proceedings / actes, n°92, tome / Vol. 2, Inrets ed., Arcueil, France, 2003, p. 27-32

Dispersion modelling in a canyon street with application to the Romanian city of Timisoara

Daniel Bisorca*, Ioana Ionel*, Lesley Hanna & Kim Cooke****
*"Politehnica" University of Timisoara, Bv. M. Viteazul, 1, 1900 Timisoara, RO
Fax +40 256 403669 - email : ioana_joule@saratoga.ro
** Sira Ltd., South Hill, Chislehurst, Kent, BR7 5EH, UK
Fax +44 20 8467 7097 - email : kim.cooke@sira.co.uk

Abstract
The paper represents the research regarding the air quality inside a street canyon. This research is obtained through the numerical modelling using the FLUENT code, and the TECPLOT code for visualisation. The wind-driven flow patterns and the dispersion of vehicle exhaust pollutant released at street level refer to a real episode from the Blaga Street canyon in Timisoara, and present the results of the dispersion modelling, hoping a later comparison to on line measured air quality values. For the external flow simulations, a hybrid mesh of about 1 million cells is utilised, based on architectural details of the canyon's buildings and surroundings. An exponential profile for the wind velocity as a function of height above the ground is applied. One comes to the conclusion that traffic has a great influence on the three dimensional flow and on the air quality inside the canyon and that modelling might be used for offering suggestion to traffic organisation.
Keys-words: *canyon street, pollution level, air quality, CFD, dispersion modelling.*

Résumé
Cette communication présente les résultats des simulations numériques avec le logicien FLUENT 5.14 et le logicien TECPLOT, concernant les émissions polluantes des véhicules dans un canyon urbain, en conditions réelles, spécifiques pour un épisode d'été à Timisoara. Les conclusions des recherches théorétiques seront complétées par des future mesures on line dans le canyon, pour la validation du logicien. Les résultats sont présentés dans des figures intuitives, en indiquant l'augmentation du nouages polluants, en temps, pour traverser les hautes maisons du canyon.
Mots clés: *pollution, simulation, canyon.*

Introduction

During numerical modelling of the dispersion of car exhaust pollutant in the urban canyon the current state-of-the-art urban roughness as homogeneously distributed on the ground is considered. No attention is given on the details of the physical phenomena occurring in the street canyon. Recent measurements, have shown that the wind flow dynamics, as one approaches the ground, are increasingly influenced by the buildings' architecture and their roofs. As a consequence, results from numerical simulation tools are expected to provide a reliable prediction of the real air pollution levels at street or higher level, places where people might be affected.

1 - Objectives

The dynamic characteristics of air recirculation in street canyon reflects the near-field geometry areas, and, depending on the canyon aspect ratio and the neighbouring roof configuration, different canyon vortex patterns are developed. These influence the re-aeration and result in particular pollution dispersion patterns which characterise each canyon geometry (Rafailidis, 1999).

Focusing on the street level, Oke observes (1988) a different effect from canyon geometry to the long-term pollution levels at pedestrian level. In canyons flanked by *symmetric* buildings, street-level ventilation improves only when the slanted roofs are confined in the surrounding urban canopy, with the effect occurring irrespective of street width. In *asymmetric* canyons, on the other hand, street-level pollution is identical to the reference case at the street sidewalk underneath the slanted roof, whereas it is reduced significantly at the opposite pavement, except in the B/H=1 street geometry and when the slanted roof protrudes above the surrounding buildings; in that case, better ventilation occurs underneath the slanted roof (B is the width, H the height) (Rafailidis, 1999).

As explained by Rafailidis (1997, 1996), when the wind above the roofs rotates or street-level mixing changes due to varying traffic density, one is prevented from using directly the numerical results for pollution level predictions. However, the *relative* changes in the long-term pollution dispersion patterns discussed above, and the identification of the beneficial behaviour of some canyon geometry against others, remain perfectly valid also with wind meandering. Wind-driven air recirculation in urban street canyons results from the combined effect between the wind field above the town, the canyon aspect ratio itself, and the shape and configuration of roofs on the surrounding buildings. The accumulation of pollutant is caused by the lack of advection, generated due to the high walls of the canyon that prevent the polluted air from escaping. Under certain wind conditions also the width may cause a vortex circulation inside the canyon.

2 - Description of the numerical code

Any numerical CDF code for numerical modelling of environmental pollution levels is primary influenced by:

- the local properties of the ground unevenness (denominated scientifically as urban roughness),
- the meteorological conditions, by the type, and
- the intensity of the polluting sources (level of emissions).

Scope of this paper is to demonstrate on a case study that by using FLUENT as CDF modelling tool, one may simulate different pollution aspects in street canyons and come to reasonable conclusions, that might be very useful for planning traffic and street activities in a closed region.

The applied characteristics offered by the code are classified as follows:

1. A coherent geometry and physical modelling is offered for treatment of time dependent transport processes, in a complex three-dimensional domain.

2. The code is based on the finite volume concept, in Cartesian co-ordinate system. Treatment of complex domains is achieved, by allowing a boundary surface, of arbitrary irregularity, to cross a calculation cell. An increase in the terrain complexity does not generally translate in increase of problem complexity.

3. The system is in a thermodynamic equilibrium, i.e., all phases share the same pressure and temperature at each point.

4. The mixture is assumed ideal i.e., the distribution of the pollutant substance over liquid and vapour phase, obeys Raoult's law.

5. The system is in a mechanical non-equilibrium, i.e., the rainfall velocity for the liquid drops is introduced.

6. In order to maintain the computation time and storage at realistic levels, turbulence closure modelling is limited to eddy viscosity/diffusivity concept. Non-isotropic effects are also included.

7. The fluid dynamics and thermodynamics are described by the mixture continuity, momentum and internal energy equations, whereas mass conservation of the pollutant substance is fulfilled, through a separate mass transport equation.

8. The conservation equations include the compressibility effect and the Boussinesq

approximation is not used, although it exists as an option. At ground surface, the conductive and convective fluxes are balanced through the heat budget equation.

10. The model has the ability to simulate stable, neutral and unstable atmospheric conditions, and might be applied to stagnant and non-stagnant atmosphere. It has the capability to account for one and two phase jets.

Thus the survey of the air quality is reasonable and even might be based on hypothetical conditions. The real situations might easily be analysed, in order to come to comparative conclusions.

3 - Real case study on a canyon in Timisoara analysed by the FLUENT 5.14 code

Figure 1 gives the mesh of the analysed canyon and its vicinity.

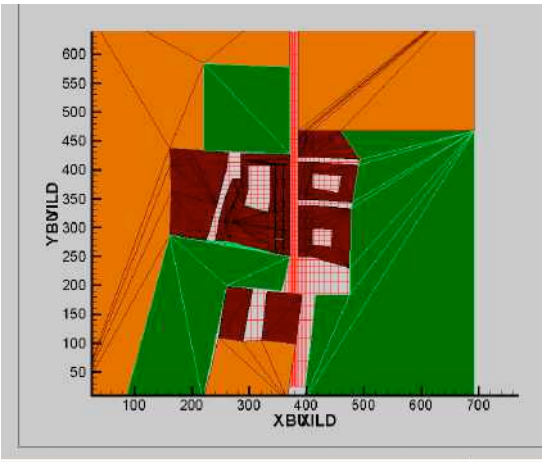

Figure 1: Geometry of the mesh for the street canyon and the neighbourhood.
Figure 1: La géométrie de la discrétisons du rue canyon et le domaine voisin.

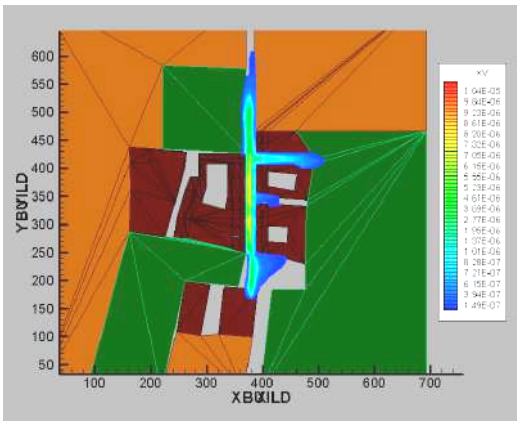

Figure 2: Geometry of the mesh for the street canyon and the position of the cars as pollutant sources.
Figure 2: La géométrie de la discrétisons du rue canyon et la position des automobiles comme sources polluantes.

The dispersion modelling of the exhausted gaseous release through the street canyon is presented in Figure 2 as a 3-dimensional solution, stationary with geometry and cars. FLUENT (***2002) is used as modelling code and TECPLOT (***2002) is used for visualisation.

Road transport represents the dominant source of atmospheric pollution in urban areas. The exhaust pipes of the cars are presented as the jets with a gas release in the opposite direction of the car moving (www/ 2002). The buildings are on flat ground. The ground roughness is 0.12 m. The building roof and walls roughness is 0.001 m (Ionel & Lelea & Bisorca 2003, Bisorca & Ionel

2002). The pollutant flue gas is discharged at ambient temperature and pressure conditions. The pipe diameter is 0.1 m. The gas is released from the nozzle with a speed of 5 m/sec. The mixture kinetics is described, by assuming different velocities between the phases (i.e., the liquid phase may slip with respect to the gas phase). The ambient wind velocity, reasonable far from the building, was measured to be 5 m/sec at 10 m high. The wind is blowing from south-east normal to the street canyon. An exponential profile for the wind velocity as a function of height above the ground is applied as a boundary condition. The atmospheric stability conditions are neutral for the analysed episode. For the external flow simulations, a hybrid mesh of about 1 million cells is utilised, based on engineering drawings of the street canyons buildings. This model spans a geometric region of 800 x 800 x 300 m^3, surrounding the building of interest, containing a typical mesh size of 0.5 m. In the present stage, the fluid under consideration is a binary mixture of ambient gas and pollutant substance in thermodynamic equilibrium, (i.e. substances, sharing the same pressure and temperature). The fluid dynamics is described by the mixture mass, momentum and energy conservation equations. The pollutant substance mass conservation law is fulfilled by its mass transport equation. In order to maintain the computation time and storage in realistic levels, turbulence closure modelling is based on the gradient transport hypothesis and involves application of the eddy viscosity/diffusivity concept.

The vortex in the canyon is determined by the turbulence pattern and is given by Figure 3.

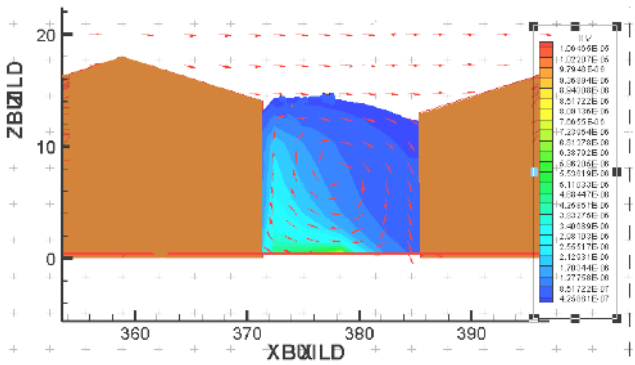

Figure 3: Wind turbulence and velocity in the canyon and the formed vortex.
Figure 3: La vitesse et la turbulence dans le canyon et le vortex formé.

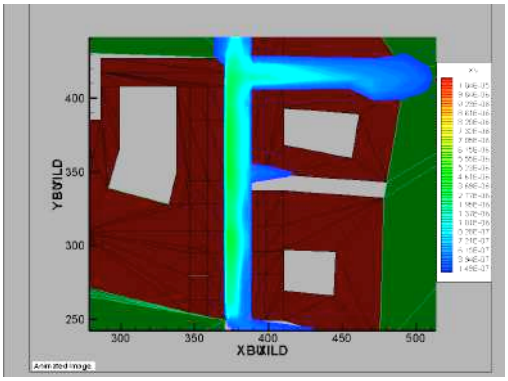

Figure 4: Geometry and position of the CO cloud at 5 m above soil.
Figure 4: La géométrie et la position du nuage polluants á 5 m au-dessus du sol.

In the figures 4, 5, 6, 7, and 8 the CO concentration field at different highs are presented, indicating the modality in which the CO cloud is passing trough the very narrow streets, in the wind direction.

The different pattern indicate that the pollutant cloud is finally escaping the canyon, in the wind direction, trough the narrow streets perpendicular to the canyon or by 'surmounting' the roofs. The soil level is the most polluted and the values might be further used to determine if their are possibilities for some snack bars and restaurants to function 'in open air system', non-harmful in the

area. The location of low roofs gives the pollutant the opportunity of skipping rapidly the canyon. But the next roofs are higher and retain the cloud, only after timing the flux is given the possibility of escaping the canyon.

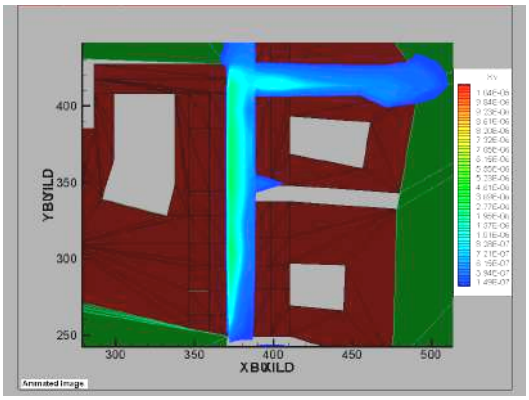

Figure 5: Geometry and position of the CO cloud at 10 m above soil.
Figure 5: La géométrie et la position du nuage polluants á 10 m au-dessus du sol.

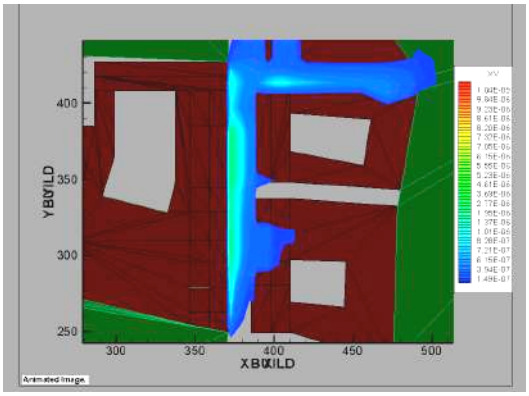

Figure 6: Geometry and position of the CO cloud at 15 m above soil.
Figure 6: La géométrie et la position du nuage polluants á 15 m au-dessus du sol.

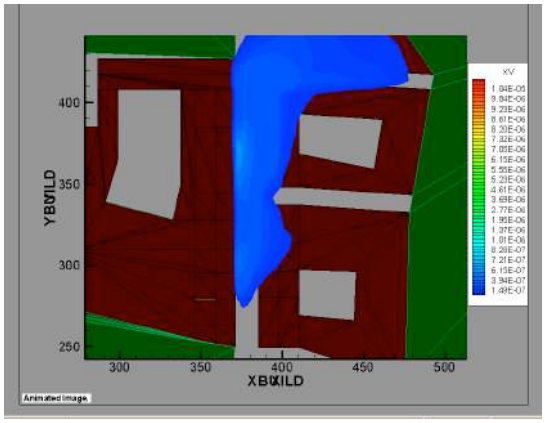

Figure 7: Geometry and position of the CO cloud at 20 m above soil.
Figure 7: La géométrie et la position du nuage polluants á 20 m au-dessus du sol.

4. Conclusions

The following conclusions are summarised:

- The flow field inside the canyon is strongly dependent on the buildings and street geometries.

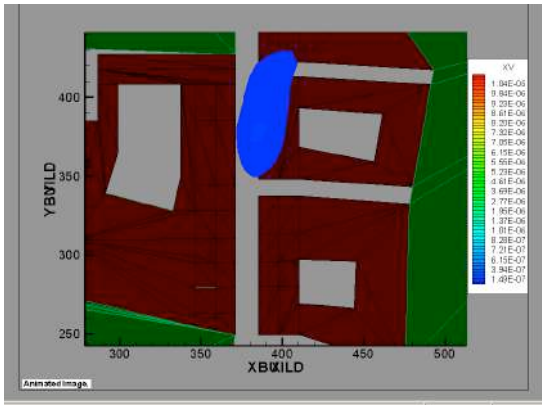

Figure 8: Geometry and position of the CO cloud at 30 m above soil.
Figure 8: La géométrie et la position du nuage polluants á 30 m au-dessus du sol.

- A strong recirculation vortex is established inside the canyon;
- Any changes on the climate conditions induce modification in the pollution level. It is interesting that zones with maximum concentrations are obtained on the opposite side of the canyon, taking the wind direction as reference;
- The traffic composition in the analysed street can be organized in order to minimize the air pollution;

In the present case the climate conditions usual for the Timisoara town have been considered. Thus, comparing the obtained numerical values with real measurements on the particular street programmed for the near future, one can use the data to validate the commercial code applied for moderate continental climate conditions.

Acknowledgement

The authors wish to thank the European Commission's Competitive and Sustainable Growth Programme for founding the research project ROSE (Remote Optical Sensing Evaluation), contract no. GR6D-CT2000-00434. Also the anonymous referees of the paper are warmly acknowledged.

References

Rafailidis S., (1999): Near-Field Geometry Effects on Urban Street Canyon Measurements for Model Validation, International Journal of Environment and Pollution, 8 p.

Rafailidis S. (1997): Influence of Building Arial Density and Roof Shape on the Wind Characteristics above a Town, Boundary-Layer Meteorol. 85, p 255-71.

Oke, T.R. (1988): Street Design and Urban Canopy Layer Climate, Energy and Build., Vol. 11, p 103-113.

Patankar S. (1980): Numerical Heat Transfer and Fluid Flow, Hemisphere, New York.

*** (2002): Guidelines of the FLUENT 5.1 code.

*** (2003): TECPLOT licensed code. Guidelines.

Rafailidis S, Schatzmann, M. (1996): Physical Modelling of Car Exhaust Dispersion in Urban Street Canyons -- The Effect of Slanted Roofs, Air Pollution Modelling and its Application XI, (eds) SE Gryning and F Schiermeier, Plenum Press, p 653-4.

*** (2002): http://www.mi.uni-hamburg.de/data/street02/overview.html

Ionel, I., Lelea, D., Bisorca, D. (2003): Air dispersion modelling of the pollutant gas releases in a street canyon of the Timisoara city, Technical Bulletin, seria EE, al UP Timisoara, in print.

Bisorca, D., Ionel, I. (2002): Numerical application for dispersion modelling of CO in a canyon street in the Romanian city of Timisoara, South-Eastern Europe Fluent Users Group Meeting, Thessaloniki, CD.

12th International Symposium "Transport and Air Pollution" / 12e Colloque international "Transports et pollution de l'air", Avignon, 16 -18 *June* / juin 2003
proceedings / actes, n°92, tome / Vol. 2, Inrets ed., Arcueil, France, 2003, p. 33-38

Modelling study of urban street canyons

Nick Dixon & Alison Tomlin
Energy and Resources Research Institute, Univ. of Leeds, Leeds, LS2 9JT, U.K.
e-mail: fuensd@leeds.ac.uk

Abstract
In this study, a CFD flow model, coupled with a Lagrangian stochastic model of dispersion, is used to determine the ventilation characteristics of some typical street geometries. The flow model used is MISKAM (Eichhorn, 1996), which uses a k-ε turbulence closure scheme to determine the mean wind and turbulence around an arbitrary arrangement of buildings. The wind field and turbulence characteristics are then used as inputs to the Lagrangian model that builds up the distribution of a passive pollutant by emitting thousands of particles into the flow. The combined model shows good agreement with wind tunnel studies of the pollutant concentration in a 2-D street canyon. The model is then used to investigate the ventilation characteristics of symmetric canyons with varying height to width ratios and asymmetric canyons. Results show the ventilation of a step-down canyon is worse than for symmetric or step-up canyons for the specific street width studied here.
Keywords: *Lagrangian stochastic model, street canyon, dispersion, asymmetric.*

Introduction

The fundamental causes of high concentrations of pollutants in urban areas are the large emission rates from traffic sources and the dense arrangement of buildings that inhibit ventilation. In particular, the street canyon is a typical urban street geometry that can lead to the build up of pollutants when the ambient wind is perpendicular to the canyon axis. Numerical models of the dispersion of pollutants within canyons, while greatly simplifying the problem, do give insight into the ventilation characteristics of various street geometries.

The earliest models of traffic pollution in street canyons (e.g. Yamartino and Wiegand 1986) were based on empirical data. More recently, *k*-ε turbulence models have been used to study the flow and dispersion within street canyons (e.g. Johnson and Hunter 1995, Sini et al. 1996). These models employ an Eulerian type of equation to predict the transport of pollutants, in which closure assumptions are made concerning the correlation of fluctuating velocities and concentration. This type of model is known to break down near point sources (Wilson and Sawford 1996).

Here, the alternative Lagrangian approach is used where more assumptions are made about the nature of the turbulence in the flow but these assumptions are independent of the concentration field (Wilson and Sawford 1996). Hence, as long as the flow and turbulence are well described, the Lagrangian approach should lead to a better prediction of the pollutant dispersion. The Lagrangian stochastic model used in this paper is the one derived by Thomson (1987). A similar model has been used to simulate the dispersal of pollutants around a building by Naslund et al. (1994).

The main objective of this paper is to show the use of the Lagrangian stochastic dispersion model coupled with a CFD flow model. The new model results are compared with the wind tunnel data for a symmetric, 2-D canyon. The model is then used to examine the ventilation characteristics of a range of symmetric and asymmetric canyons.

1-Model

The numerical simulation of dispersion in the current model is built up in two stages. First, a steady state flow field over an arbitrary building configuration is calculated using the flow component of the MISKAM urban air quality model (Eichhorn 1996). The flow model uses a k-ε turbulence closure scheme to parameterise the subgrid scale turbulence. Secondly, the derived mean wind and turbulence parameters from MISKAM are used as input to a Lagrangian stochastic model of dispersion using the well-mixed formulation of Thomson (1987).

MISKAM uses a stretched grid in the horizontal and vertical directions, which allows a higher resolution at points where the gradients in wind speed are high. All model runs assume a logarithmic wind profile upstream at the inflow boundary.

The Lagrangian model assumes that for sufficiently small timesteps, the acceleration of particles following the flow is a combination of the 'fading memory' of the particle's velocity at the previous timestep, the drift correction due to inhomogeneities in the flow field and a random diffusion term. The tracer source is specified in the model as a box within which the particles are initially randomly located and given a random velocity assuming a Gaussian velocity distribution.

In each run, at least 50,000 particles are tracked through the model domain. The total amount of time spent by particles in the individual boxes in a specified grid is calculated. These times are converted to a concentration C by

$$C = \frac{Q\sum_i t_{ij}}{NV_j},$$

where Q is the source strength in kg s^{-1}, $\sum_i t_{ij}$ is the total length of time all particles spent in gridbox j and V_j is the volume of that gridbox. Following the example of Meroney et al. (1996) and others, concentrations are converted to non-dimensional K by

$$K = \frac{CU_{ref}HL}{Q},$$

where U_{ref} is the reference level wind speed, H is the height and L is the length of the canyon. In their wind tunnel study, Meroney et al. (1996) showed that the values of K recorded in the canyon were only weakly dependent on the reference wind speed and emission rate.

In all runs, the tracer source is a small line source situated in the middle of the canyon. The exact dimensions of the source were chosen to replicate the line source in the wind tunnel study of Pavageau and Schatzmann (1999). The same source size was used in all other runs to make the comparison easier.

2-Results

Even 2-D canyon with H/W=1

The model was set up to simulate the wind tunnel study of Pavageau and Schatzmann (1999). The domain consisted of a series of canyons separated by buildings of a uniform height and canyon width. The wind flowed perpendicularly to the canyon. In the wind tunnel, the experimental tracer was released at the nineteenth downwind canyon to ensure an urban type roughness upstream of the test canyon. Tests using the model showed that the flow in the canyon did not significantly change after the third canyon. Consequently, the tracer was released from the third canyon in the model.

Figs. 1 and 2 show the distribution of the non-dimensionalised concentration K in the model and the wind tunnel. Overall, the agreement is good, both qualitatively and quantitatively. Notable differences are the relative minimum in the bottom, leeward corner and the maximum on the leeward wall of the model canyon. Neither of these features are observed in the wind tunnel data and both suggest that the turbulence in the model is not as effective as in the wind tunnel.

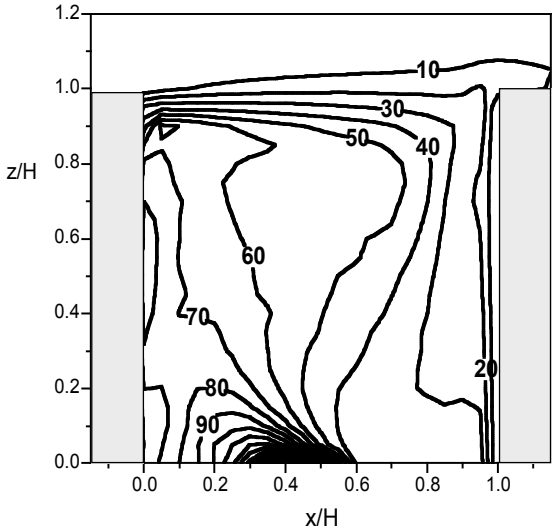

Figure 1: K *in model*

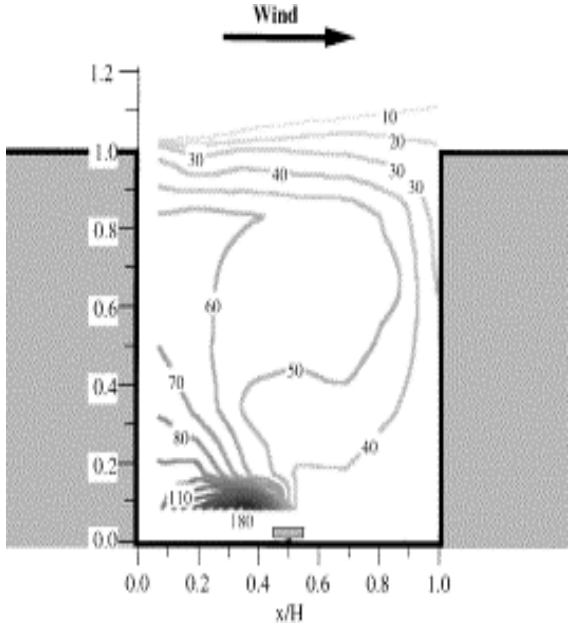

Figure 2: K *from wind tunnel study of Pavageau and Schatzmann (1999*

Effect of varying H/W

The model was set up with a series of canyons again with the same height but the separation between the buildings is now varied. In order to compare the results from the different streets, we need some measure of the ventilation efficiency of the entire canyon. For a steady distribution of concentration to form, the flux of pollutants into the street must be balanced by the turbulent and advective fluxes out of the canyon. Hence, the level of concentration required in the street to match these fluxes is therefore an indication of how well the street is ventilated.

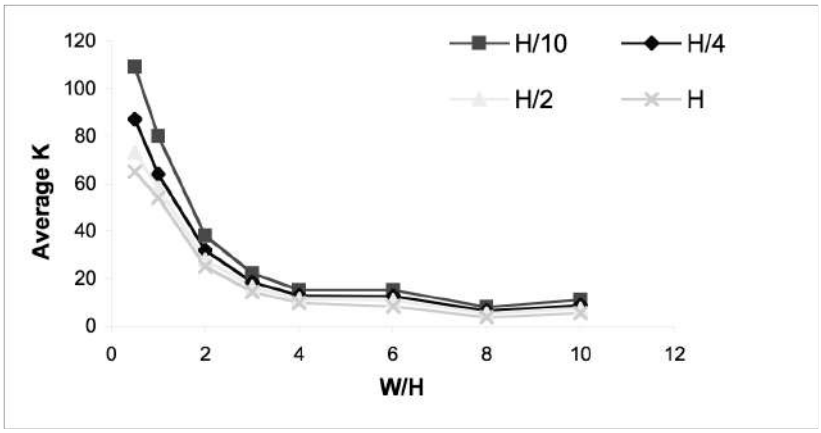

Figure 3: Variation of average K *to various depths with width to height ratio*

Figure 3 shows the average value of *K* from the surface to various depths in the canyon for various width-to-height ratios (W/H). The average concentration is estimated by taking the mean of the concentration in evenly-spaced gridboxes over the required volume. All the results show the marked reduction in average *K* values as the W/H ratio increases from 0.5 to 3. This reflects the problem of high levels of pollution in narrow streets. The fact that the same variation is seen in the averaged *K* values to depths as low as H/10 is useful. It will allow direct comparison with asymmetric canyons where the average over the full depth of the canyon is not always appropriate.

Asymmetric canyons

The domain was set up with five buildings to create four equally-spaced canyons with widths and heights of 20m. The height of the fourth building was varied to produce the combination of a step-up and step-down canyon either side of this building. This section of the domain is shown in Figure 4.

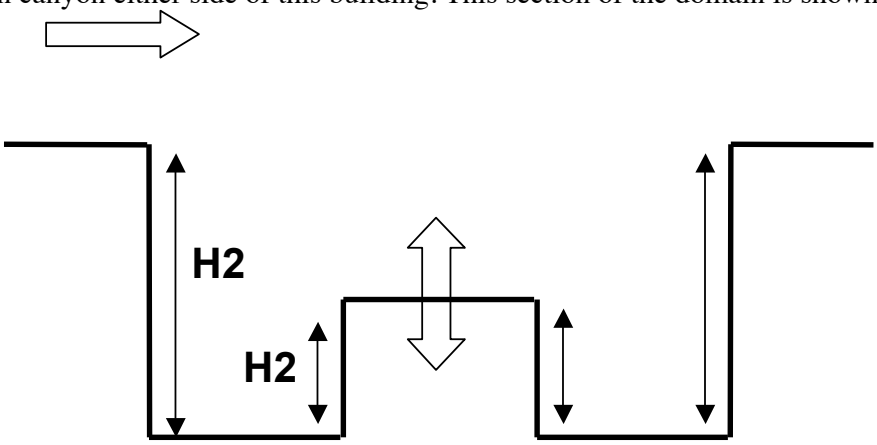

Figure 4: Detail of domain for model runs in asymmetric canyons

Separate runs of the Lagrangian model with a source in the upwind and downwind canyons produced a range of results for different ratios of upstream height H1 over downstream height H2. These results are shown in Figure 5 along with the even canyon result (H1/H2=1). For the step-up situations (H1/H2 < 1), the average concentration of pollutants is reduced compared to the even canyon.

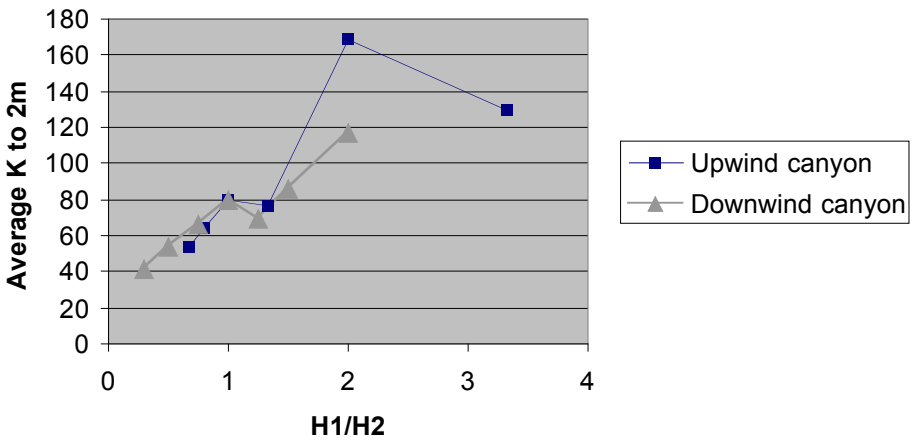

Figure 5: Variation of average K *to a depth of 2m for different asymmetric canyons*

The step-down canyons exhibit a more complex behaviour. For H1/H2 between 1 and 2, the average value of *K* changes only slightly from the even canyon case. For the H1/H2=2 and H1/H2=3.3 runs, the ventilation of the canyon is significantly reduced with the average value of *K* increased by 110% and 60% respectively. This is confirmed by the distribution of *K* in Figure 6.Analysis of the flow fields from these situations shows the single vortex associated with the skimming flow in a narrow even canyon has broken down. Figure 7 shows the flow vectors in the H1/H2=2 step-down canyon. Notice how the reversed flow circulation in the top of the canyon passes over the downstream building. This in turn has induced a secondary circulation in the bottom of the canyon. It is this

double circulation that has inhibited the ventilation of the tracer from the canyon floor.

Conclusion

The coupled *k*-ε flow model of MISKAM and a Lagrangian stochastic dispersion model has been shown to be a useful tool in predicting the dispersion of pollutants in typical street geometries.

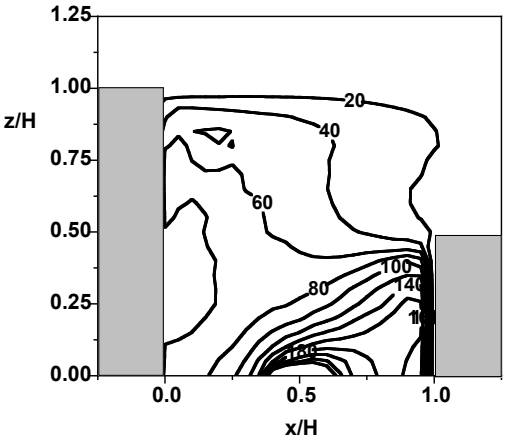

Figure 6: K *in step-down canyon H1/H2=2*

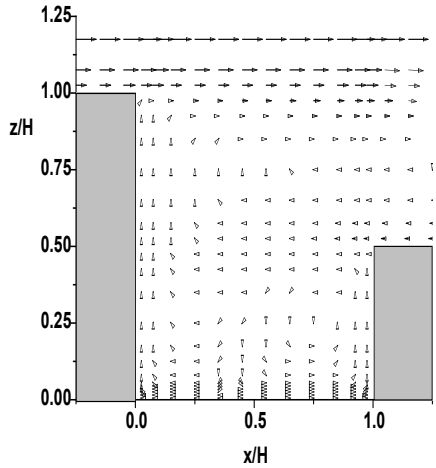

Figure 7: Flow in step-down canyon H1/H2=2

Preliminary results show that the predicted distribution of non-dimensional concentration *K* in an even, W/H = 1 canyon compares well with a wind tunnel simulation. The small differences between the results indicate the turbulence in the model is less effective at dispersing pollutants than in the wind tunnel.

Variation of the average value of *K* in the canyon with the width to height (W/H) ratio showed a steep decline as the W/H ratio increased from 0.5 to 3.

The effect of asymmetry between the heights of the canyon sides was also investigated. There was a general trend for the averaged value of *K* in the canyon to increase as ratio of the upstream wall height H1 to the downstream wall H2 increased.

For extreme cases, where H1/H2 >= 2, the averaged concentration value increased by at least 50%. The flow for these cases showed that the single vortex regime typical of the even canyon had been replaced by two circulations which inhibited the ventilation of the streets.

References

Eichhorn J. (1996): Validation of a microscale pollutant dispersal model. Proceedings of the 21st International Meeting on Air Pollution Modeling and its Application, Baltimore, MD, USA.

Johnson G.T. and L.J. Hunter (1995): A numerical study of dispersion of passive scalars in city canyons. Boundary-Layer Meteorology, vol. 75, p 235-262.

Meroney, R.N., M. Pavageau, S. Rafailidis and M. Schatzmann, (1996): Study of line source characteristics for 2-D physical modelling of pollutant dispersion in street canyons. J. Wind Eng. Ind. Aerodyn., vol. 62, p 37-56.

Naslund, E., H.C. Rodean and J.S. Nasstrom (1994): A comparison between two stochastic models in a complex three-dimensional flow. Boundary-Layer Meteorology, vol. 67, p 369-384.

Pavageau M. & M. Schatzmann (1999): Wind tunnel measurements of concentration fluctuations in an urban street canyon. Atmospheric Environment, vol. 33 p 3961-3971.

Sini J.-F., S. Anquetin and P.G. Mestayer (1996): Pollutant dispersion and thermal effects in urban street canyons. Atmospheric Environment, vol. 30 p 2659-2677.

Thomson, D.J. (1987): Criteria for the selection of stochastic models of particle trajectories in turbulent flows. J. Fluid Mech. vol. 180 p 529-556.

Wilson, J.D. and B.L. Sawford (1996): Review of Lagrangian stochastic models for trajectories in the turbulent atmosphere. Boundary-Layer Meteorology, vol. 78, p 191-210.

Yamartino, R.J. and G. Wiegand (1986): Development and evaluation of simple models for the flow,

turbulence and pollutant concentration fields within an urban street canyon. Atmospheric Environment, vol. 20 p 2137-2156.

12th International Symposium "Transport and Air Pollution" / 12e Colloque international "Transports et pollution de l'air", Avignon, 16 -18 *June* / juin 2003
proceedings / actes, n°92, tome / Vol. 2, Inrets ed., Arcueil, France, 2003, p. 39-44

Simulation numérique de la pollution dans la vallée de Chamonix, importance du trafic routier

Guillaume Brulfert, Charles Chemel & Jean-Pierre Chollet
*Laboratoire des Ecoulements Géophysiques et Industriels, Université Joseph Fourier, INP Grenoble, CNRS, BP53, 38041 Grenoble cedex, France ; brulfert@hmg.inpg.fr

Résumé
Une modélisation numérique est associée aux campagnes POVA (Pollution des Vallées Alpines) de mesure de qualité de l'air dans la vallée de Chamonix avant et après réouverture du tunnel du Mont Blanc. Un modèle de dynamique de l'atmosphère à l'échelle de la vallée est associé à un modèle de photochimie. Les scénarios traités sont des évolutions idéalisées avec les seules circulations convectives ou des champs forcés par une météorologie à échelle régionale. La dispersion des polluants primaires est analysée par suivi de traceurs passifs. L'analyse des concentration de polluants secondaires montre les contributions du trafic des véhicules légers et des poids lourds.
Mots-clés: *simulation numérique, photochimie, scalaires passifs, forçage météorologique, vallée, trafic routier.*

Abstract
Numerical simulation of air quality in Chamonix valley, impact of road traffic.
Road traffic is a serious problem in the Chamonix Valley: traffic flow, noise and above all air pollution worry the inhabitants of the valley. The accident in the Mont-Blanc tunnel made it possible, in the framework of the POVA project (Alpine Valley Pollution), to undertake measurement campaigns with and without heavy-vehicle traffic through the valley, towards Italy (before and after the tunnel re-opening). Modelling in POVA should make it possible to explain the process leading to episodes of atmospheric pollution, both in summer and in winter.
*Atmospheric prediction model ARPS 4.5.2 (Advanced Regional Prediction System), developed at the CAPS (Center for Analysis and Prediction of Storms) of the University of Oklahoma, enables to resolve the dynamics of this terrain where the relief is very complex. A large field of calculation (140 * 140 km) powered by the ALADIN meteorological verticals of the French Meteorological Office France forces the downflow of a small central field (25 * 25 km). This model is coupled to the TAPOM 1.5.2 code of atmospheric chemistry (Transport and Air POllution Model) developed at the air and soil pollution laboratory of the Ecole Polytechnique Fédérale de Lausanne.*
Using 300-metre grid cells to calculate the dynamics and the reactive chemistry thus makes it possible to represent precisely the dynamics in the valley (slope winds) and to process the chemistry on a fine scale.
Dispersion of a passive scalar enables to describe how primary pollutants are either mixed inside the valley or transported beyond the limits of the valley. Species typical of secondary pollutants (HNO_3, PAN) are observed to depend on road traffic especially heavy -vehicles
Keys-words*: numerical simulation, photochemistry, passives scalars, meteorological forcing, valley, road traffic.*

Introduction

Le projet POVA (POllution des Vallées Alpines) permet d'effectuer des campagnes de mesures de la qualité de l'air dans la vallée de Chamonix avant et après la réouverture du tunnel du Mont-Blanc en vue d'évaluer l'impact du trafic routier, en particulier des poids lourds. Ces campagnes montrent

que pour les sites de vallée, la dynamique des mouvements atmosphériques joue un rôle essentiel et conditionne fortement la chimie: canalisation par les reliefs, blocage des inversions dans les zones à basse altitude, vents de pente et vents de vallée.

Pour comprendre les mécanismes dynamique et chimique en jeu, un outil de simulation numérique est mis en place : le modèle de prédiction atmosphérique ARPS 4.5.2 est couplé au code de chimie atmosphérique TAPOM 1.5.2. Les premiers résultats des simulations permettent d'isoler et de comparer les impacts des différentes sources polluantes sur la qualité de l'air.

1 - Dynamique de l'atmosphère et évolution de traceurs scalaires passifs

Un traceur scalaire passif permet une analyse du transfert et du mélange par les mouvements atmosphériques verticaux au sein de la vallée. Ceci permet de distinguer les phénomènes locaux des phénomènes synoptiques.

Présentation du module de suivi de traceurs et paramètres de simulation

Le modèle de prédiction atmosphérique ARPS 4.5.2 (Advanced Regional Prediction System) est un modèle non-hydrostatique de dynamique de l'atmosphère qui permet de traiter des terrains au relief marqué, Xue (2000). L'utilisation de l'imbrication nous permet de forcer les conditions aux limites avec une météorologie réaliste aux échelles locales. Le forçage, issu d'une grille de 140*140 km est appliqué au site de Chamonix. Cette grille force un domaine central de 25*28 km (pas de 300 mètres en discrétisation horizontale). Cette fine résolution permet d'observer les vents de pente et vents de vallée générés par la convection thermique, Anquetin (1998).

L'application d'un nouveau module de suivi de traceurs passifs pour décrire les polluants permet de suivre un ou plusieurs traceurs émis de n'importe quel endroit de la vallée.

Chaque variable instantanée Φ est définie par rapport à son écart $\Delta\Phi$ à un état de référence de l'atmosphère. Cet état de référence est spécifié par l'état hydrostatique pour la pression et la masse volumique et par l'état initial pour les autres variables. Soit S_i le taux d'injection du scalaire, les équations filtrées des champs de vitesse u_i, de température potentielle θ et de fraction massique de traceur Y_i sont les suivantes :

$$\overline{\rho_h}\frac{\partial \overline{u_i}}{\partial t} + \overline{\rho_h}\,\overline{u_k}\frac{\partial \overline{u_i}}{\partial x_k} = -\frac{\partial \overline{\Delta \breve{p}}}{\partial x_i} + \overline{\rho_h}\,\overline{f_i} + \overline{\rho_h B \delta_{i3}} - \frac{\partial \overline{\rho_h \tau_{ij}}}{\partial x_j}$$

$$\overline{\rho_h}\frac{\partial \overline{\Delta\theta}}{\partial t} + \overline{\rho_h}\,\overline{u_k}\frac{\partial \overline{\Delta\theta}}{\partial x_k} = -\overline{\rho_h}\,\overline{w}\frac{\partial \overline{\theta_{init}}}{\partial z} - \frac{\partial \overline{\rho_h \tau_{k\theta}}}{\partial x_k}$$

$$\overline{\rho_h}\frac{\partial \overline{\Delta p}}{\partial t} + \overline{\rho_h}\frac{\partial \overline{u_k \Delta p}}{\partial x_k} = \overline{\rho_h}\,\overline{w}g - \overline{\rho_h}c^2\frac{\partial \overline{u_j}}{\partial x_j}$$

$$\overline{\rho_h}\frac{\partial \overline{Y_i}}{\partial t} + \overline{\rho_h}\,\overline{u_k}\frac{\partial \overline{Y_i}}{\partial x_k} = -\frac{\partial \overline{\rho_h}\tau_k Y_i}{\partial x_k} + \overline{\rho_h}\,\overline{S_i}(\overline{Y_i})$$

Où $\breve{p}$ est le terme de pression modifiée par la trace du tenseur sous-maille, f_i représente les forces volumiques associées à l'accélération de la pesanteur et de Coriolis et B est défini par :

$$B = g\left(\frac{\Delta\theta}{\theta_{init}} - \frac{c_p}{c_v}\frac{\Delta p}{p_h}\right)$$

Nous avons choisi de placer les lieux d'émissions au niveau de l'entrée du tunnel et en deux points du fond de vallée pour analyser les processus de transport et de dispersion des polluants à partir de ces zones caractéristiques d'émission de polluants dues au trafic routier. La simulation présentée est la situation météorologique du 12 août 2001 avec une situation anticyclonique classique pour la vallée à cette période.

Analyse des traceurs scalaires

L'émission de 3 scalaires passifs, à 10h30, dans le fond de la vallée de Chamonix met en évidence la complexité de la dynamique dans cette vallée étroite. La distribution spatiale et temporelle a un caractère fortement local. Le scalaire (2) émis au pied du Mont-Blanc s'accumule dans la vallée alors que les scalaires (1-3) émis aux extrémités de la vallée sont balayés par le vent synoptique (figure 1).

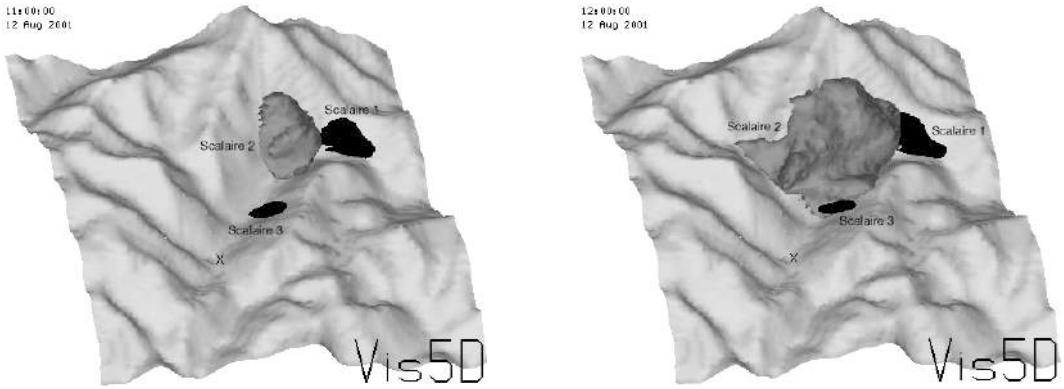

Figure1 : Isosurfaces de concentration, C = 1 g/cm^3, à 11h et 12h. X désigne l'emplacement d'une station de mesure virtuelle

Figure1 : Isosurfaces of concentration, C = 1 g/cm^3, at 11AM et 12AM. X shows the place of the virtual station measurement

Une station de mesure a été virtuellement placée en sortie de vallée, X sur la figure 1. Le relevé des concentrations de scalaires passifs indique une baisse de concentration à 11h20 pour le scalaire (3) émis à proximité de la station de mesure virtuelle figure2). Cet instant correspond à un changement d'orientation du vent en sortie de vallée (figure3).

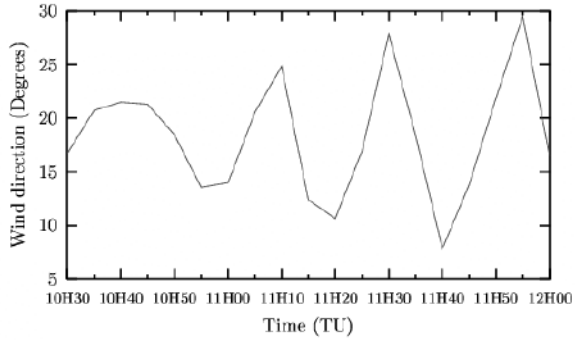

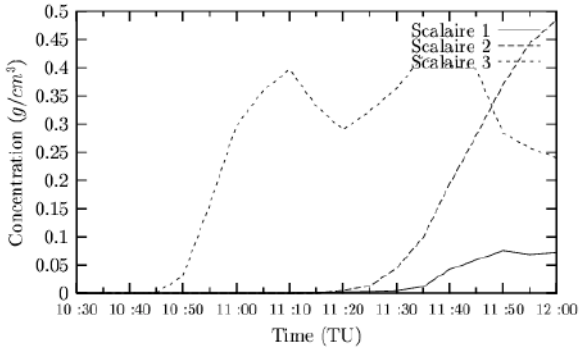

Figure 2 : Relevés des concentrations de traceurs à la station X

Figure 2: Concentrations of scalars at X station.

Figure 2 Relevés des concentrations de traceurs à la station X

Figure 3: Wind direction at X station

L'outil traceur passif peut être utilisé pour estimer le temps de transport des espèces d'un bout à l'autre de la vallée. Le scalaire passif émis en entrée de vallée contamine la station de mesure une heure après son émission (figure2), il a alors parcouru environ 13 km.

2 – Simulation d'épisodes photochimiques dans la vallée de Chamonix

Modèle et simulation

ARPS est couplé avec le modèle de chimie gazeuse TAPOM 1.5.2 (Transport and Air POllution Model) de l'Ecole Polytechnique fédérale de Lausanne (Clappier 1998).

Le code chimique intègre le schéma condensé RACM qui fait intervenir les émissions biogéniques, les réactions photochimiques, à travers 77 espèces et 237 réactions, Stockwell (1997). Des regroupements d'espèces permettent de s'affranchir de la spéciation de l'ensemble des composés

organiques volatils.

L'inventaire des émissions prend en compte les routes et rampes d'accès au tunnel en adaptant les émissions à la pente locale de la route. Le nombre important de poids lourds de fort tonnage (92% de plus de 32 tonnes) circulant oblige à prendre en compte le trafic particulier de la vallée.

Résultats dans le cas de convection pure

Aucun vent synoptique n'intervient dans ces simulations, les seuls vents présents sont générés par forçage thermique. Nous avons réalisé deux simulations avec la même météorologie, seuls les paramètres des émissions étaient différents. Seule la convection et donc les vents de pentes générés par le chauffage solaire sont présents lors de cette journée estivale, le 2 juin. Pour les émissions, deux situations idéalisées ont été choisies : l'une sans aucune source de pollution et l'autre avec le trafic routier d'une journée type dans la vallée de Chamonix. Les différentes catégories prises en compte pour les émissions sont présentées dans le tableau 1. Les espèces de fond sont identiques pour les deux simulations tableau 2.

Commercial boiler	Residential boiler	Gas station
Domestic solvent	Cars	Cars in city
Utilitarian vehicles on motorway	Utilitarian vehicles on road	Heavy vehicles
Aerial traffic	Forest	Grassland

Tableau 1 : Sources d'émissions dans le modèle chimique.
Table 1 : Emissions sources in the chemical model.

Cette situation nous montre qu'en un point donné du fond de la vallée proche de la route, la concentration de NO_2 reste élevée dans les 1000 premiers mètres au dessus du sol lorsque le trafic routier est présent. En effet, on ne retrouve la situation du cas sans aucune source qu'à partir de 2500 mètres (figure 4). Cette altitude est la marque de l'activité convective et correspond à la hauteur de couche limite puisque aucun brassage vertical ne vient mélanger l'atmosphère au dessus de cette altitude.

NO_2	$25\ 10^{-3}$	HNO_3	$9.1\ 10^{-9}$	ACO_3	$2.2\ 10^{-12}$	ETE	$1.5\ 10^{-3}$
NO	$150\ 10^{-3}$	HO_2	$2.2\ 10^{-10}$	ONIT	$5.5\ 10^{-10}$	HNO_4	$1.9\ 10^{-9}$
O_3	$40\ 10^{-3}$	CO	$4.4\ 10^{-1}$	HC5	$8.5\ 10^{-3}$	H_2O_2	$2.5\ 10^{-10}$
HONO	$3.9\ 10^{-9}$	KET	3 10-3	OLI	$0.6\ 10^{-3}$	ISO	$2\ 10^{-14}$
NO_3	$1.9\ 10^{-10}$	DCB	$2.2\ 10^{-9}$	XYL	$1.4\ 10^{-6}$	PAN	$2\ 10^{-4}$
HCHO	$3\ 10^{-3}$	SO_2	$3\ 10^{-3}$	CH_4	1.7	N_2O_5	$3.8\ 10^{-9}$
MO_2	$1.2\ 10^{-9}$	OLT	$1\ 10^{-3}$	CSL	$1.9\ 10^{-10}$		
MGLY	$1.8\ 10^{-9}$	TOL	$1.4\ 10^{-3}$	ALD	$3\ 10^{-3}$		

Tableau 2 : Concentrations (ppm) des espèces de fond de la simulation avec RACM.
Table 2 : Concentrations (ppm) of the background species with RACM.

De plus, cette situation nous montre qu'en l'absence de vent fort la concentration devient élevée, atteignant 120 ppb. Cette concentration maximale semble réaliste au regard des mesures de terrain effectuées au bord de cette route fréquentée en hiver 2003.

Ce calcul est ensuite répété pour le 15 juin: situation convective et espèces de fond correspondant au tableau 2. La topographie de la vallée de Chamonix est présentée figure 5, c'est une vallée très encaissée. Les premiers résultats montrent qu'avec des poids lourds dans la vallée, les concentrations maximales sont plus élevées : 70 au lieu de 62 ppb et situées dans le secteur de l'entrée du tunnel. Les valeurs moyennes sur le domaine sont du même ordre de grandeur. Les conditions aux limites pour les espèces chimiques ne jouent alors que très peu sur les niveaux de pollution observés à Chamonix. En effet, les phénomènes dynamiques observés dans le fond de la vallée sont découplés de la météorologie à plus grande échelle. Ce type de situation est fréquent dans la vallée, tant en hiver qu'en été, puisque des couches d'inversion à très basses altitudes sont observées.

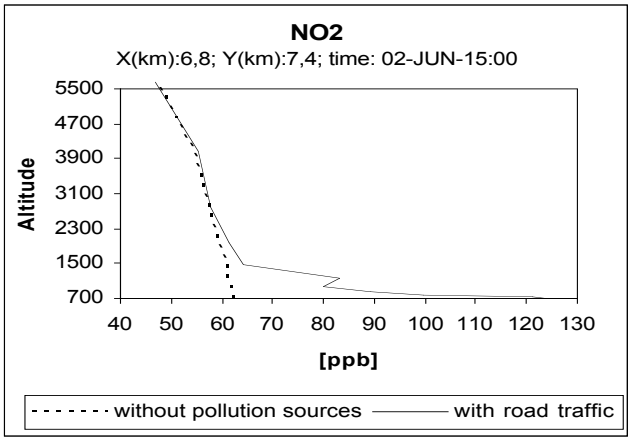

Figure4 : Comparaison de l'évolution du NO2 avec l'altitude avec et sans le trafic routier.

Figure4 : Evolution of NO2 with altitude, with road traffic and without pollution sources.

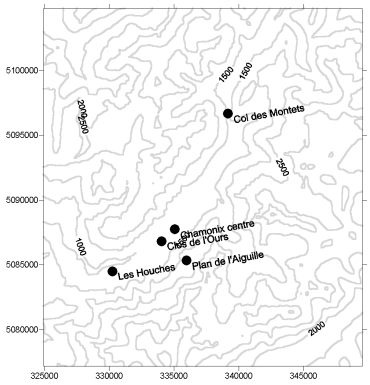

Figure 5 :Topographie de la vallée de Chamonix, principaux sites et coordonnées UTM 32 en mètres.

Figure 5: Topography of Chamonix valley, important places and UTM 32 coordinates in meters.

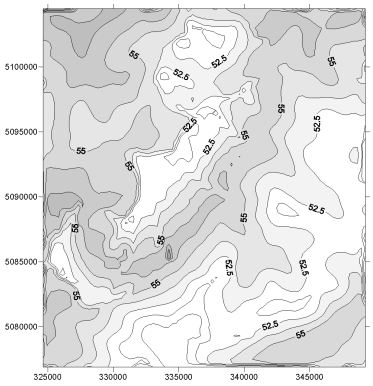

Figure 6 : Concentration de NO_2 dans la vallée de Chamonix, simulation sans les poids lourds mais avec les véhicules légers.

Figure 6: Concentration of NO_2 in Chamonix valley, simulation without heavy-vehicles but with light-vehicles.

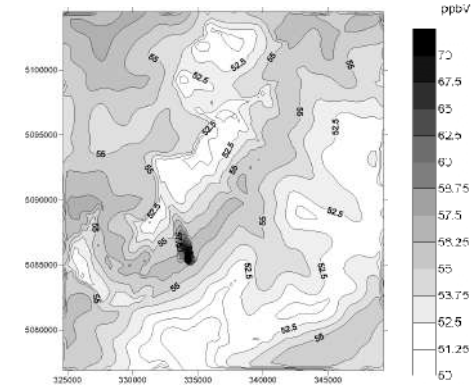

Figure 7 : Concentration de NO_2 dans la vallée de Chamonix, simulation avec les poids lourds mais sans les véhicules légers.

Figure 7: Concentration of NO_2 in Chamonix valley, simulation with heavy-vehicles but without light-vehicles.

Résultats avec forçage dynamique

Des simulations avec forçage dynamique par les champs météorologiques à grande échelle sont également réalisées. La journée du 16 octobre 2002 a été choisie : journée ensoleillée avec un vent venant du sud-ouest balayant la vallée. Deux configurations d'émissions chimiques ont étaient testées avec cette même dynamique, l'une avec l'ensemble du trafic routier (figure 8) et l'autre sans aucune circulation (figure 9). Les espèces constituant le fond sont arbitraires mais réalistes et correspondent à la simulation précédente (tableau 2). On trouve 120 ppb autour du tunnel pour les simulations sans trafic routier et 150 ppb lorsque le trafic est présent. Ces résultats sont du même ordre de grandeur que les résultats des analyses chimiques de la campagne de mesure POVA de l'hiver 2003.

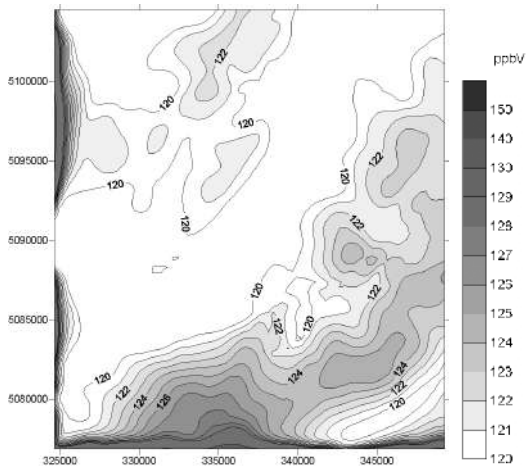

Figure8 : Concentration de NO,au niveau du sol, dans la vallée de Chamonix. Simulation avec l'ensemble du trafic routier.

Figure 8: Concentration of NO2,near the ground, in Chamonix valley. Simulation with all the road traffic.

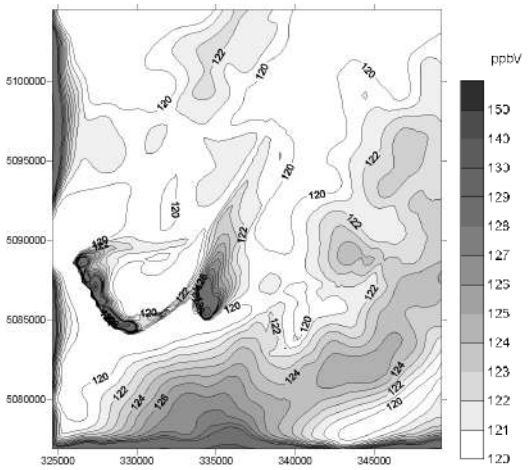

Figure 9 : Concentration de NO, au niveau du sol, dans la vallée de Chamonix. Simulation sans aucun trafic routier.

Figure 9: Concentration of NO2, near the ground, in Chamonix valley. Simulation without any road traffic.

Conclusions

Le suivi de traceur émis à partir de localisations typiques d'émission de polluants montre le découplage entre des écoulements propres à la vallée et des écoulements induits par les vents synoptiques à grande échelle. Les concentrations de traceur subissent de fortes variations au cours du temps sous l'effet des changements de régime de vent : les situations hivernales avec une tendance aux vents descendant la vallée seront donc différentes des situations estivales considérées ici pour lesquelles les vents ont plutôt tendance à remonter la vallée. Cette grande variabilité des champs atmosphériques, en espace et en fonction de l'heure de la journée, affecte les champs de concentration des scalaires passifs qui peuvent être considérés comme représentatifs de certains polluants primaires. L'étape en cours consiste à prendre en compte au mieux la situation réelle des campagnes de mesure, en particulier en ce qui concerne les champ de forçage météorologique. Les résultats présentés pour la modélisation photochimique sont confrontés aux données des campagnes de mesure réalisées en 2000, 2001 et 2003.

Remerciements

Le projet POVA est soutenu par l'ADEME, la région Rhône-Alpes et le réseau de surveillance de la qualité de l'air : Air de l'Ain et des Pays de Savoie. Les calculs sont effectués sur MIRAGE (plate-forme Grenobloise de modélisation numérique de l'environnement et du climat).

Références

Anquetin, S., Guilbaud, C., Chollet, J.P., 1998. The formation and the destruction of inversion layers within a deep valley, Journal of Applied Meteorology 37(12), pp.1547-1560.

Clappier, A., 1998, A correction method for use multidimensionnal time splitting advection algorithms : application to two and three dimensional transport, Mon. Wea. Rev, 126, pp.232-242.

Stockwell, R., Kirchner, F., Kuhn, M., Seefeld, S., November 27, 1997. A new mechanism for atmospheric chemistry modeling, Journal of geophysical research, vol. 102, NO. D22, pp. 25,847-25,879.

Xue, M., Droegemeir, V., Wong, V., 2000. The Advanced Regional Prediction System (ARPS)- A multi-scale nonhydrostatic atmospheric simulation and prediction model. Part I : Model dynamics and verification, Meteorology and atmospheric physics, volume 75, Issue 3 / 4, pp. 161-193.

12th International Symposium "Transport and Air Pollution" / 12e Colloque international "Transports et pollution de l'air", Avignon, 16 -18 *June* / juin 2003
proceedings / actes, n°92, tome / Vol. 2, Inrets ed., Arcueil, France, 2003, p. 45-50

Evaluation of highway network contribution to pollution concentration levels in the Bologna area

Luisa Cattozzo* & Cecilia Rondinini**
*Provincia di Rovigo, 5 Viale della Pace, 45100 Rovigo, (I)
** Comune di Bologna, Environmental Unit, 8 Via Zamboni, 40126 Bologna, Italy
Tel +39.051203174 – Fax +39.051203175 – email: cecilia.rondinini@comune.bologna.it

Abstract
Bologna is a medium-size city (approx. 380.000 inhabitants) located in the northern part of Italy. Two very important motorways - both with high flow of vehicles - pass along its outskirts: the A1 (the Rome-Milan MW) to the west and the A14 (the Bologna-Bari MW) to the north-east. In addition, the city bypass runs parallel to the A14.
Local authorities and air quality managers are interested in understanding if and how much this highway network contributes to the pollution levels that are often very high. A simulation for benzene, nitrogen oxides, and PM10 was performed using the dispersion model ARIA Impact™, produced by Aria Technologies S.A.
We considered 3 selected days, representative of different seasonal and critical situations.
The meteorological data were obtained by means of the diagnostic model CALMET.
Specific attention was paid to traffic flows. Typical available traffic data (output of circulation model and of automatic counters) are too poor for the needs of a pollution simulation, so we tried to improve them with specific measurements in the city centre.
These activities led us to a much more complex set of input data, whose emissions were computed via the TREFIC software. The simulation scheme was a combination of line and area sources, where line sources represent the main roads. The results clearly show that:

- *meteorology – obviously - strongly influences pollution levels and diffusion;*
- *there are problems with emission factors evaluation, especially for benzene (overestimated along the highways) and PM10, where a significant difference measured/simulated is observed;*
- *the highway network contribution to concentration levels in the city centre is not as high as expected: in most cases it is relevant (>25%) only in a strip 1-2 km wide around the path; it is less relevant for benzene than PM10 due to the mix of vehicle types. Anyway, in terms of absolute values, the highway system contributes significantly to pollution on a regional basis.*

Keys-words*: air quality modelling, traffic flow evaluation, emission factors, modelling scheme*

Introduction

Since 1994 the Bologna Municipality produces an annual report on air quality that includes monitoring data, meteorological conditions, traffic situation, and specific studies on air quality. The report is intended to provide a better understanding of the current status and to help defining effective practical solutions for reduction policies.

In the frame of 2001's report we decided to evaluate highway contribution to pollution levels with a dispersion model, in order to estimate the possible effectiveness of urban traffic reduction schemes.

Local authorities and air quality managers are interested in understanding if and how much the highway network around the city contributes to the pollution levels that are often very high. Three pollutants were considered: benzene, nitrogen oxides, and PM10.

This study was made possible by a collaboration between the technical staff of the Bologna Municipality and the companies ARIA Technologies (F) who provided the model and ARIANET (I) who provided technical support and the emission estimate, needed to run the model for PM10 and benzene emissions.

1 – The model

The chosen model was ARIA Impact™, a gaussian model package with user-friendly windows interface, that allows simulation of industrial or traffic emissions over short or long duration. It outputs mean values over a two-dimensional grid or frequency of threshold crossing occurrences. This system is compliant with U.S. EPA recommendations; for moderate and strong winds the algorithm is a linear gaussian model, whilst for weak winds the chosen algorithm is a gaussian puff. The typical spatial scale is between 5 and 30 km.

2 – Building the scenarios

Bologna is a medium-size city (approx. 380.000 inhabitants) located in the northern part of Italy. Two very important motorways - both with high flow of vehicles - pass along its outskirts: the A1 (the Rome-Milan MW) to the west and the A14 (the Bologna-Bari MW) to the north-east. In addition, the city bypass runs parallel to the A14.

The simulation needed accurate hourly traffic data, both in the city centre and along major roads, including cars, light/heavy duty vehicles, and motorcycles. These data are not very common, because traffic departments use models designed to define road sizes according to peak flows, and that are typically unable to represent hourly traffic and different types of vehicles. So we decided to carry out specific traffic measurements in the city centre, with separate counting for cars, bus, light/heavy duty vehicles, and motorcycles over 12 hours a day. Other data were extracted from several environmental impact assessments and official data from public institutions. With this set of data and the traffic model output we were able to reconstruct hourly modulation and traffic composition for each type of road: highway, urban major roads, urban roads, local streets.

The emission estimation was performed via the TREFIC software. This tool integrates the CORINAIR methodology with the IIASA PM10 and individual VOC emission factors. This allows estimation of PM10 and benzene emissions.

The simulation was run for three typical days: a summer sunny day (July 14th), a typical winter day (November 25th) and a worst-case scenario, winter day (January 13th). Meteorological data were provided by the local meteorological service, and are the output of the diagnostic model CALMET run over a larger region including the entire Pianura Padana with a 5 km step.

To have a more realistic distribution of concentrations, we chose a composed scheme of area and line sources (Figure 1). The line sources are the main urban roads and the highway network, while the area sources represent the remaining roads averaged over an urban zone homogeneous in terms of road density and land use.

The output grid step is 500 m; this, and the adopted mixed scheme, means that no local analysis is allowed: in other words, this simulation may only show global pollution effects.

3 – Results

The first general result was a confirmation that meteorological conditions can affect concentrations up to a factor 6. The second main outcome is that modelling may still give poor results when compared with experimental data, depending on pollutant. This may apply both to the value range, and to the spatial distribution.

Benzene (Figures 2 and 3)

Even though the range of the simulated concentration is reasonable, the spatial distribution of the

concentration field is wrong due to an overestimation of benzene emissions from highway network and an underestimation of the city centre contribution. The highway network, in spite of this overestimation, is relevant (>25%) only in a strip 1-2 km wide around the path.

PM10 (Figure 4)

The map shows a significant impact of the highway network, especially due to heavy duty vehicle flows on the A14 Bologna-Milan motorway (more than 9,000 heavy duty vehicles per day).

The absolute values simulated in the critical winter day (~ 50 $\mu g/m^3$) are much lower than the maximum measured values, (~ 150-200 $\mu g/m^3$). This confirms that PM10 has other important sources, secondary formation, and re-immission from the ground.

In general, the results for this day correctly reproduce the pollutant accumulation near the sources; the simulated levels in the very centre of Bologna are similar to the ones near the highway. The measured values show that the pollution peaks in the centre are significantly higher than the values along the highways. This suggests that the medieval structure of the city centre causes "canyon effects".

The simulation shows that the highway system contribution is dominant (>50%) only outside the urban area.

NO_x (Figures 5 and 6)

Bad diffusive conditions during the critical winter day caused very high concentrations (up to 500 $\mu g/m^3$) near the sources; the maximum estimated concentrations are along the highway. This is perhaps the best simulation result, in terms of both value range and spatial distribution. This is surely due to the better knowledge of emissions and diffusion of the pollutant.

The contribution of the highway system is higher for this pollutant, giving contributions greater than 25% even in the city centre.

The summer simulation confirms the strong reduction in pollutant levels due to meteorological conditions that make dispersion easier. Following the favourable meteorological conditions the highway contribution is distributed over a large area with values everywhere less than 75%.

Conclusion

The highway relative contribution to pollutant concentration levels in the city of Bologna is definitely relevant, especially in a 2 km strip along the path, much more extended outward. The city itself is such a large pollutant source that the concentration values measured in the city centre are for the most part due to local traffic and not to the highway system contribution.

Acknowledgements

The authors wish to thank the staff of ARIANET and P. Ferrecchi for their encouragement and technical support.

References

Comune di Bologna (2002): Relazione Annuale della Qualità dell'Aria 2001, p 13-104. www.comune.bologna.it/iperbole/unamb

R.E. Munn et al. (1972): Dispersion and forecasting of air pollution. WMO Technical Note No. 121, p 27-39.

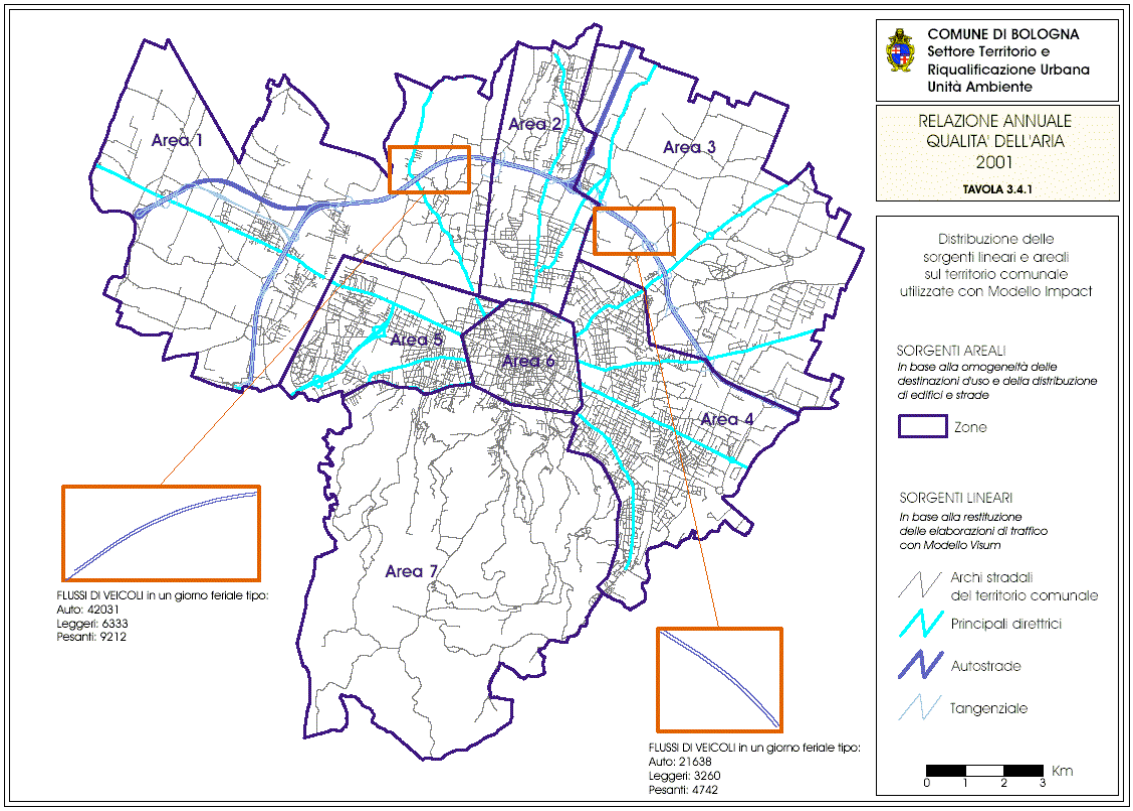

Figure 1: Modelling scheme: area borders are in violet, local and national motorways in blue, main urban roads in cyan

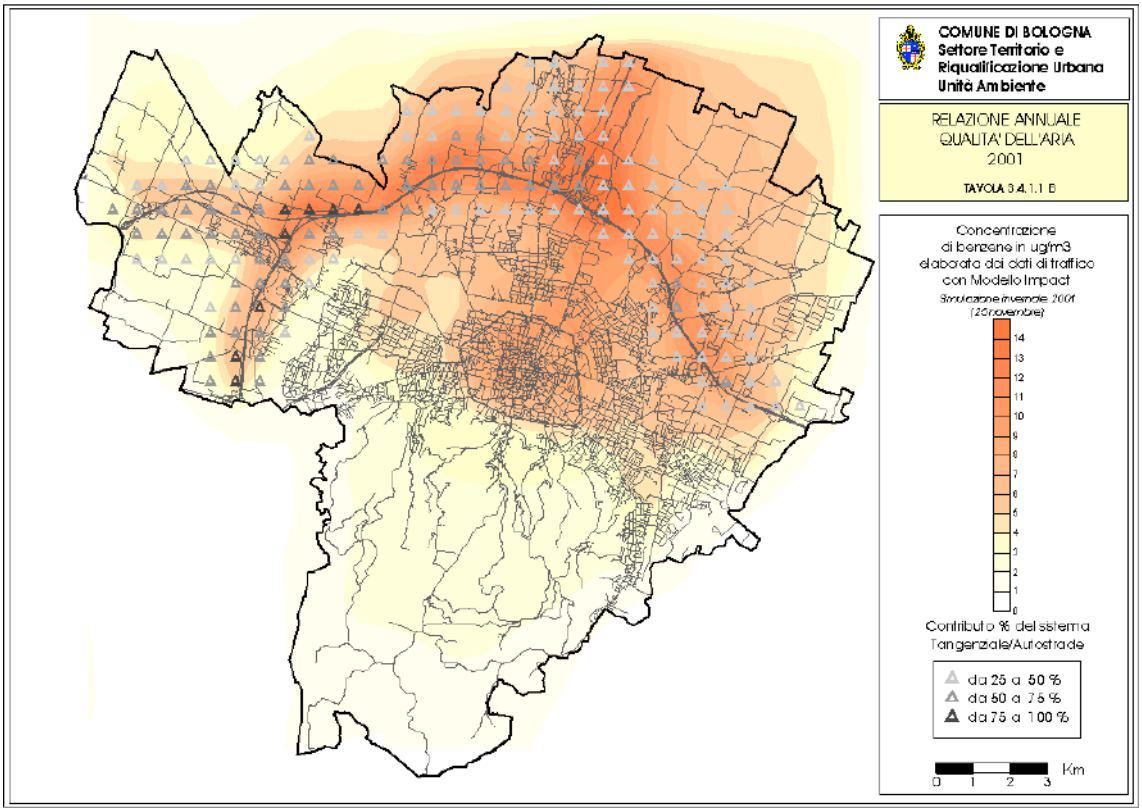

Figure 2: Benzene simulation: concentrations in a typical winter day; a comparison with Figure 3 shows an overestimation along highways and an underestimation in the city centre

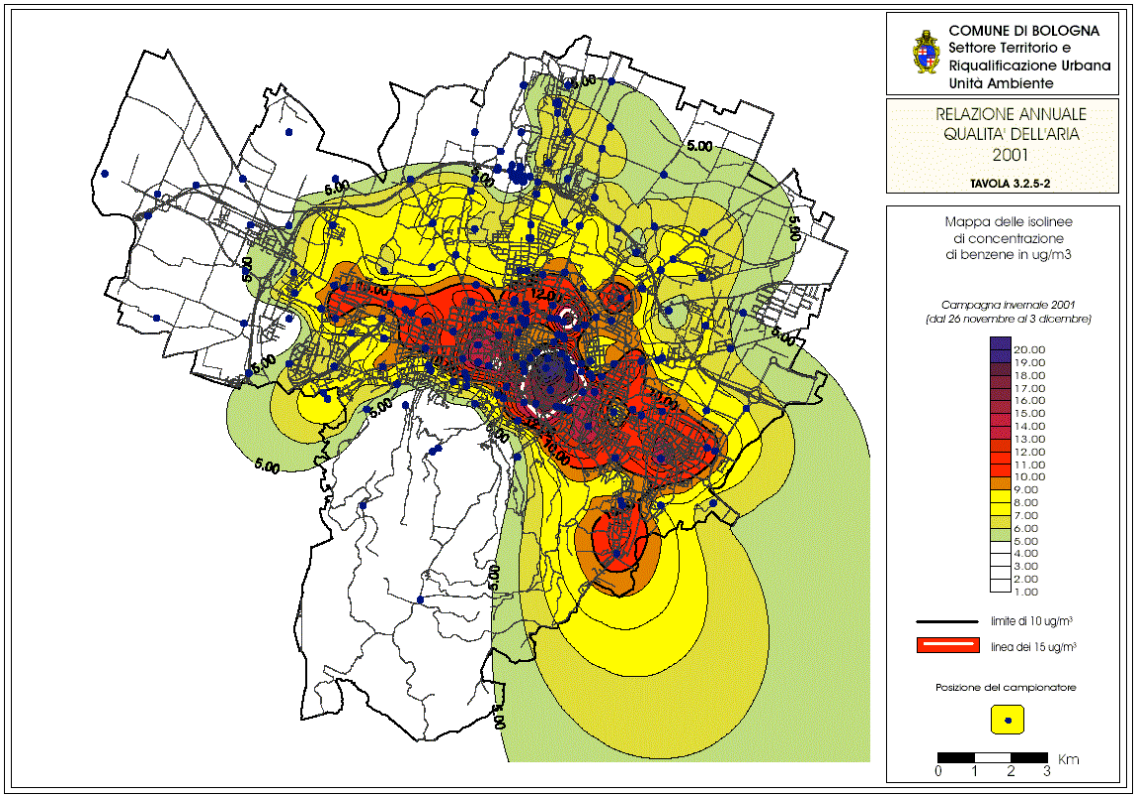

Figure 3 *Benzene measurement: the most critical zone is in the city centre and in the first outskirts*

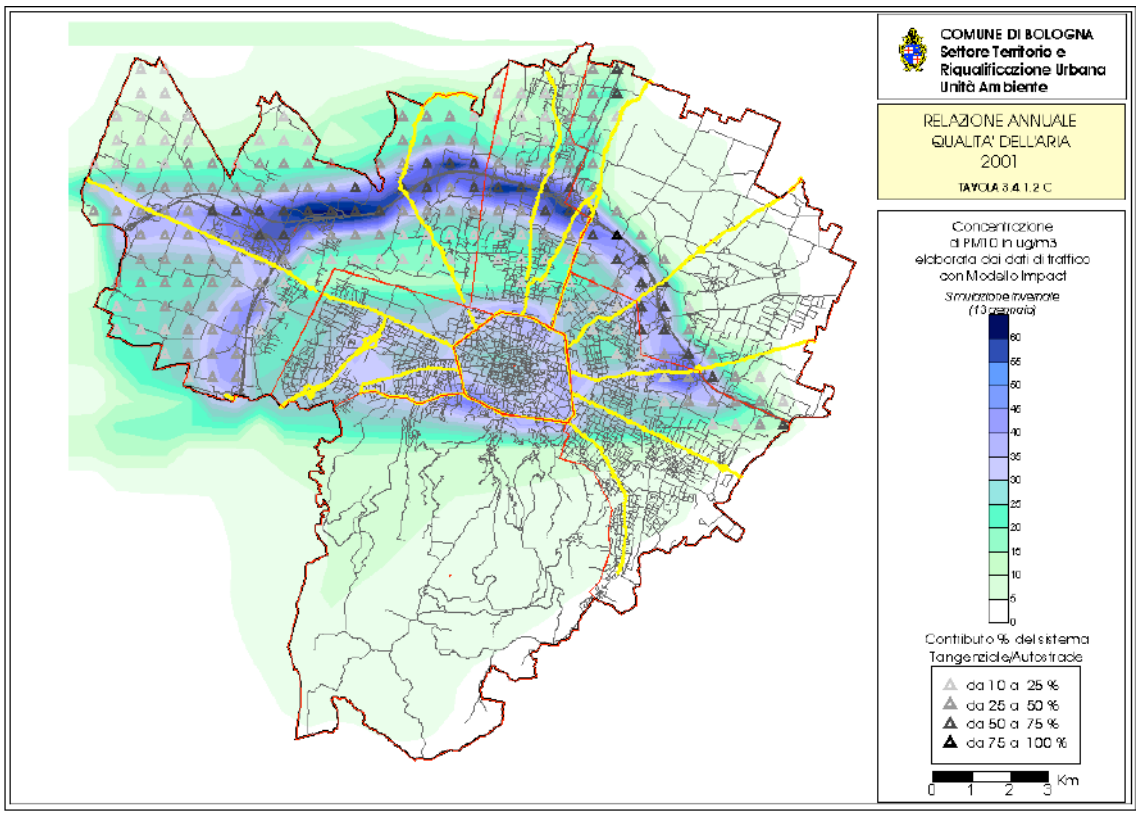

Figure 4: *PM10 simulation: concentrations in a critical winter day tend to remain close to the sources; the city centre is a significant PM10 source*

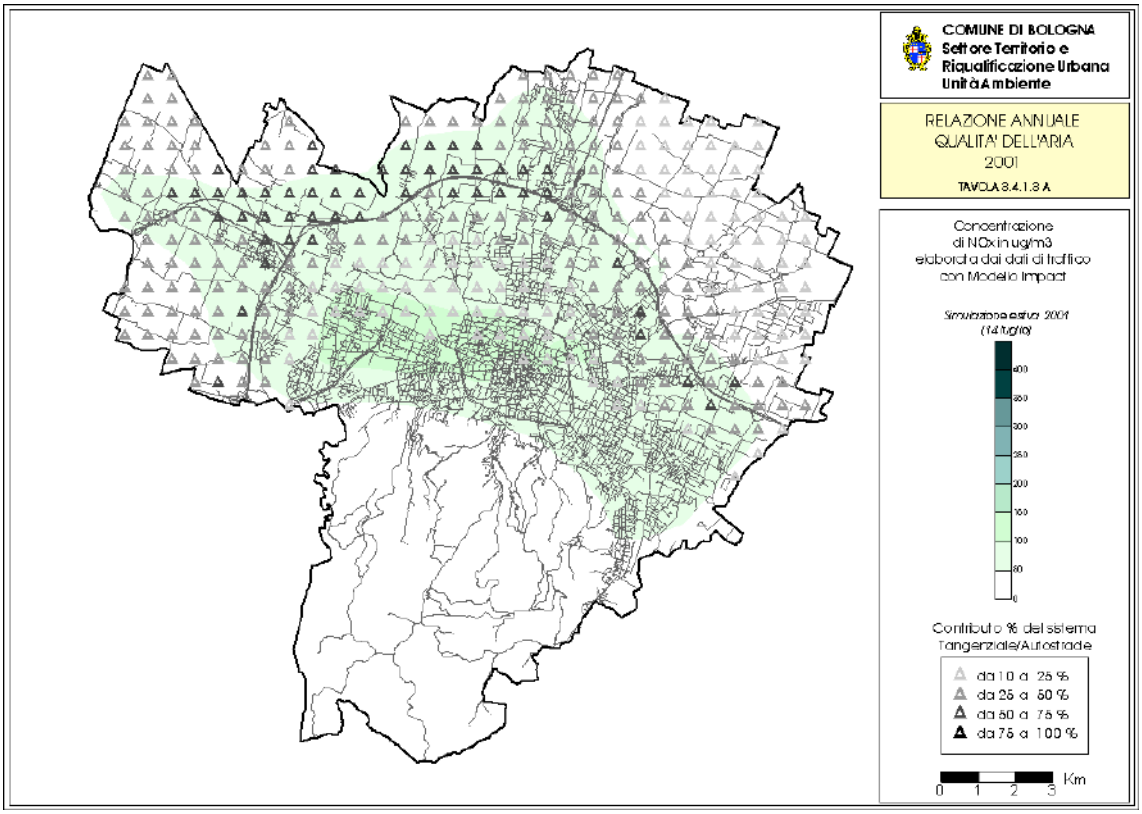

Figure 5: *NO_x simulation: concentrations are low and very well distributed on a typical summer sunny day*

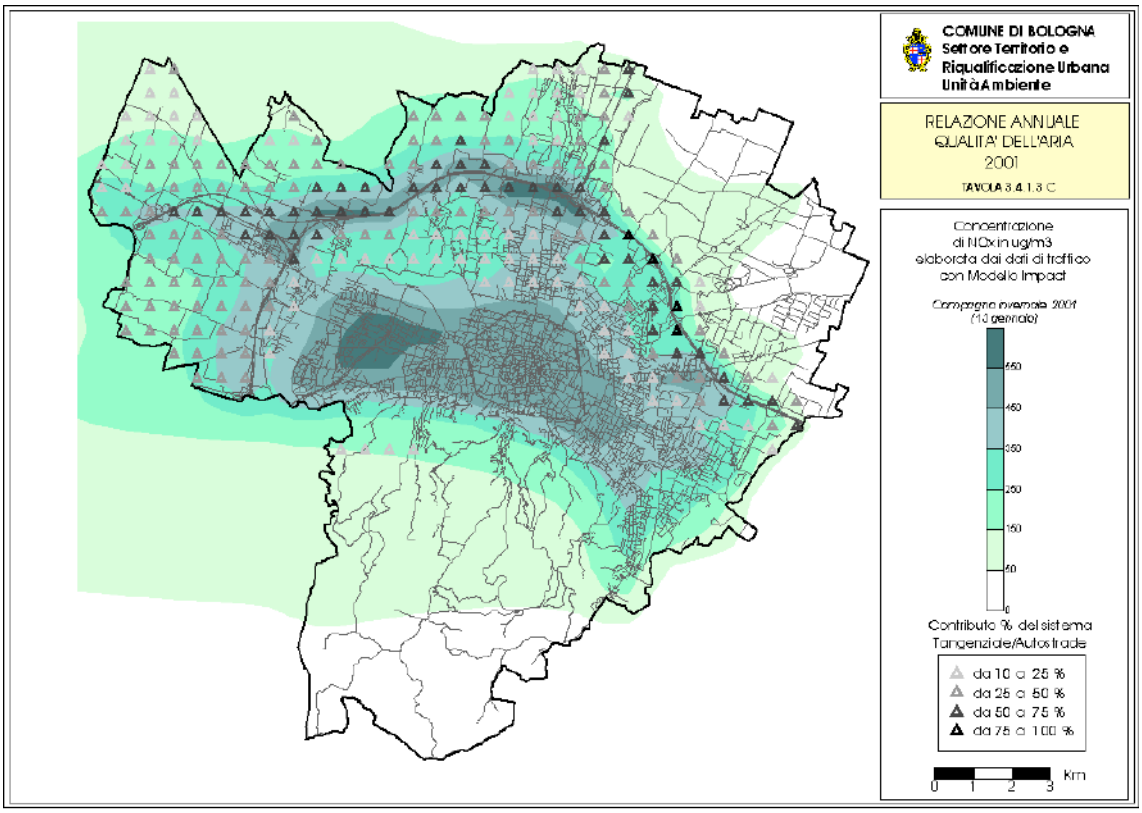

Figure 6: *NO_x simulation: in a critical winter day, concentrations are very high and closer to sources; highway contribution is relevant almost everywhere outside the city centre*

12th International Symposium "Transport and Air Pollution" / 12e Colloque international "Transports et pollution de l'air", Avignon, 16 -18 *June* / juin 2003
proceedings / actes, n°92, tome / Vol. 2, Inrets ed., Arcueil, France, 2003, p. 51-56

Wind driven flow field simulation in narrow urban street canyons

Fabio Murena & Francesco Vorraro
Dip. Ing. Chimica, Univ. Napoli, 80 P.le Tecchio, 80125 Napoli, Italy
Fax +081 2391800 - email : murena@unina.it

Abstract
In the present paper we focus on the numerical investigation of the 2D steady–state isothermal flow patterns that build up in a deep urban street canyon when different wind conditions are superimposed at the roof level. The CFD software FLUENT was used to perform the simulations. The value of the Aspect Ratio of the street canyon was set to AR=H/W=3.3 (W=6 m; H=20 m) because it is in the average of the streets in the old centre of Naples. The typical multiple–vortex flow field was observed. Flow field results were used to evaluate the mass flow rate exchanged between the canyon and the atmosphere and between two consecutive vortices. If vortices are assumed to identify mixed boxes, concentration levels of pollutants can be obtained solving the corresponding mass balance on each mixed volume. An estimation of pollutant concentration as function of wind and emission rate is reported.
Key-words*: street canyon, CFD simulation, pollutant dispersion, turbulence, air quality.*

Résumé
Dans le papier nous concentrons sur la recherche numérique sur les modèles 2D, isothermes stationnaires d'écoulement qui se placent dans un street canyon profonde quand différents états de vent sont superposés au niveau des toits. Le software CFD FLUENT a été employé pour effectuer les simulations. La valeur de l'Aspect Ratio du sreet canyon a été placée à AR=H/W=3.3 (W=6 m; H=20 m) parce qu'il est typique des rues au vieux centre de Naples. On a observé le champ typique d'écoulement à plusieres tourbillonnements.Les résultats du champ d'écoulement ont été employés pour évaluer le taux de la masse échangé entre le street canyon et l'atmosphère et entre deux tourbillonnements consécutifs. Si on assume que les tourbillonnements identifient les volumes mélangés, les niveaux de concentration des polluants peuvent être obtenus résolvant le bilan de matière correspondant sur chaque volume mélangé. Une évaluation de la concentration de polluant comme fonction du vent et de l'émission est rapportée.
Key-words*: street canyon, CFD simulation, pollutant dispersion, turbulence, air quality.*

Introduction

A review on modelling air quality in street canyon is reported by Vardoulakis et al. (2003). Dabberdt et al. (1973) first detected the formation of an helical circulation co - axial with the street giving higher concentrations of the tracer on the leeward side of the street. These features were also reported by DePaul & Sheih (1984, 1986) for wind speed > 1.5 – 2 m s^{-1} and Nakamura & Oke (1988). Oke (1988), on the basis of the wind-tunnel experiments performed by Hussain & Lee (1980), first identified, as AR varies, different flow regimes. The multiple vortices skimming flow regime, typical of deep street canyons, was found to be the less effective in mass exchange between the lower canyon and the upper air. This result was confirmed by Lee & Park (1994), who investigated the influence of flow conditions and structural configurations on pollutants dispersion and found the removal of pollutants to be more difficult in deeper streets, where SF regime establishes. In this case mass exchange is mainly due to turbulent processes, as Baik & Kim (2002) found after studies on a street canyon with AR = 1.

Our aim in this paper is the CFD investigation of the flow fields developed in deep street canyons, with special reference to the historical centre of the city of Naples. All the simulations reported were then performed on a typical deep street canyon of that zone. Average values of width and height of the street were set to $W = 6$ m and $H = 20$ m respectively which correspond to AR=3.3.

1 - Method

In order to gain generality the canyon we focus on would be a modular unit of an even complex cluster of streets. Therefore half building was reported in the integration domain, both on the windward and the leeward side. Its width was assumed to be 20 m on average. The air volume above the roofs has to be deep enough to grant shear-free conditions on the upper limit of the integration domain. Thus we set the value of the air depth to 10 m (nearly 20 times the depth of the turbulent boundary layer rising when air covers 20 m at 10 m s^{-1}). Since a uniform highly refined grid can be chosen without an unbearable CPU time increase (2D flow fields) the entire integration domain was meshed with a uniform 5 cm square grid.

The only boundary conditions to set are concerned with velocities. No-slip condition was imposed on the ground, on the roofs of the buildings and at the windward and leeward walls. Air was allowed to enter and exit the integration domain through velocity inlet boundaries. In order to gain modularity periodic conditions were superimposed at the inlet and outlet boundaries. Finally, velocity of the upper limit of the integration domain was evaluated on the basis of the velocity profiles at the air inlet.

Available closure models (Spalart–Allmaras, κ–ε Standard, κ–ε RNG, κ–ε Realizable, Reynolds Stress Model (RSM)) were used to simulate the 2D steady–state isothermal flow field building up in the street canyon when a plug flow wind of 5 m s^{-1} blows orthogonal to the street axis. It is well known that in this case, due to the low value of AR, multiple vortices are expected to develop within the street canyon, the lowest being the weakest, the highest the strongest (Oke (1988), Sini et ali (1996)). This flow pattern was best described by RSM, followed by κ–ε Realizable with an adequate wall treatment. Thus we decided to undergo the greater computational effort required by the RSM to obtain a reasonable accuracy of the solution in all the simulations reported in the following.

Finally, due to the swirling flow in the street canyon, solution is expected to be quite insensitive to turbulence characteristics of the incoming air. We performed a set of simulations allowing turbulence intensity to vary in the range 0-100% and turbulence length scale in the range (0-10m). Only turbulence intensities higher than 80%, which are unphysical for the problem at hand, affected the solution. Thus we set reference values of turbulence intensity and turbulence length to 10% and 5 m respectively in each simulation reported in the following.

2 - Results

The CFD software FLUENT was used to perform a set of numerical simulation in order to investigate the influence of wind speed, characterized by its mean value and its vertical profile, on the flow field building up in the street canyon and on mass exchange. Vertical velocity profiles generally used (plug-flow, power law in both stable and unstable atmosphere, logarithmic profile) were superimposed at the roof level, with mean speed lying in the range 1÷10 m s^{-1}, typical of poor ventilation conditions and hence of low pollutant dispersion.

Two-vortices flow patterns are observed when the plug-flow vertical wind velocity profile is assumed. In the other cases both two- and three-vortices flow patterns are observed. Stream lines visualisation suggests that the street canyon can be structured in two or three volumes each corresponding to a vortex. Then separation surfaces between consecutive vortices have been identified and assumed as interfaces through which the mass transfer takes place.

To evaluate the turbulent mass exchange between two consecutive vortices a characteristic velocity was evaluated as the standard deviation of the vertical velocity fluctuations

$$v^* = StD\left(v'_y\right) \quad (1)$$

The value of v^* averaged on each interface ($\overline{v^*}$) was assumed as an estimation of the mass flow rate exchanged between two consecutive vortices and between the highest one and the atmosphere. In the latter case $\overline{v^*}$ is roughly proportional to the mean wind speed, especially in the plug-flow case and to a lesser extent when power law profile is assumed. When logarithmic profile is hypothesised, mass flow rate increases less clearly with wind speed.

At the other interfaces it still holds true that the higher mean wind speed the higher $\overline{v^*}$, but proportionality is lost, as one could expect since lower vortices are not directly driven by wind.

Values of $\overline{v^*}$ calculated at the same mean wind speed can differ for different wind profiles. The importance of the right setting of incoming air boundary conditions is thus emphasized. However, it must be recalled that logarithmic law is used to model velocity profile in the turbulent boundary layer, whose depth is a priori unknown when air enters the integration domain; on the other side power law is generally used when wind speed measurements are available at a certain height (typically 10 m) to obtain velocity profile at higher levels on the ground and hence outside the turbulent boundary layer. Therefore, both of them seem to be inadequate for the case at hand. On the contrary, due to the shear effect of the roof, the wind takes the typical boundary layer velocity profile, before flowing over the street cavity, if it enters the integration domain with a plug velocity profile. Therefore we reported in Tab.1 only the results obtained in the plug-flow wind hypothesis.

3 – Air quality model

If vortices are assumed to identify perfectly mixed boxes a simple air quality model can be written for the street canyon. Since in the hypothesis of plug flow wind only two vortices are observed the model is a two-boxes model consisting in two mass balance equations:

for the lower box

$$V_l \frac{dc_l}{dt} = E + Q_{lu}(c_u - c_l) \quad (2)$$

and for the upper box

$$V_u \frac{dc_u}{dt} = Q_{lu}(c_l - c_u) + Q_{ua}(c_a - c_u) \quad (3)$$

Subscripts l and u refer respectively to the lower and the upper box; a to the external air and E is the emission factor due to car exhausts. The mass flow rate among the boxes and the external air (Q_{lu} *and* Q_{ua}) have been evaluated on the basis of the values of $\overline{v^*}$ reported in Tab.1.

Wind speed mean value [m s^{-1}]	H_l [m]	$\overline{v^*}_l$ [m s^{-1}]	$\overline{v^*}_u$ [m s^{-1}]
1	9.16	0.036	0.115
3	7.10 – 8.04	0.088	0.375
5	9.17 – 7.81	0.221	0.552
10	8.76 – 10.29	0.712	1.119

Table1: Results of the CFD simulation (plug flow wind profile)

The values reported in table 1 are H_l = height of the lower box; $\overline{v^*}_l$ = average characteristic velocity between lower and upper box; $\overline{v^*}_l$ = average characteristic velocity between upper box and atmosphere.

Assuming $c_a = 0$ the steady state concentration levels of a generic gaseous passive pollutant have been obtained solving the mass balance equations 2 and 3.

In Fig.1 steady state concentration levels building up in the lower box are reported as function of wind speed, parameterizing the emission factor. Then concentration vs. wind speed data have been modelled assuming an exponential decay law. For a practical use of Fig.1 the emission factor would be evaluated from data of traffic levels in the canyon.

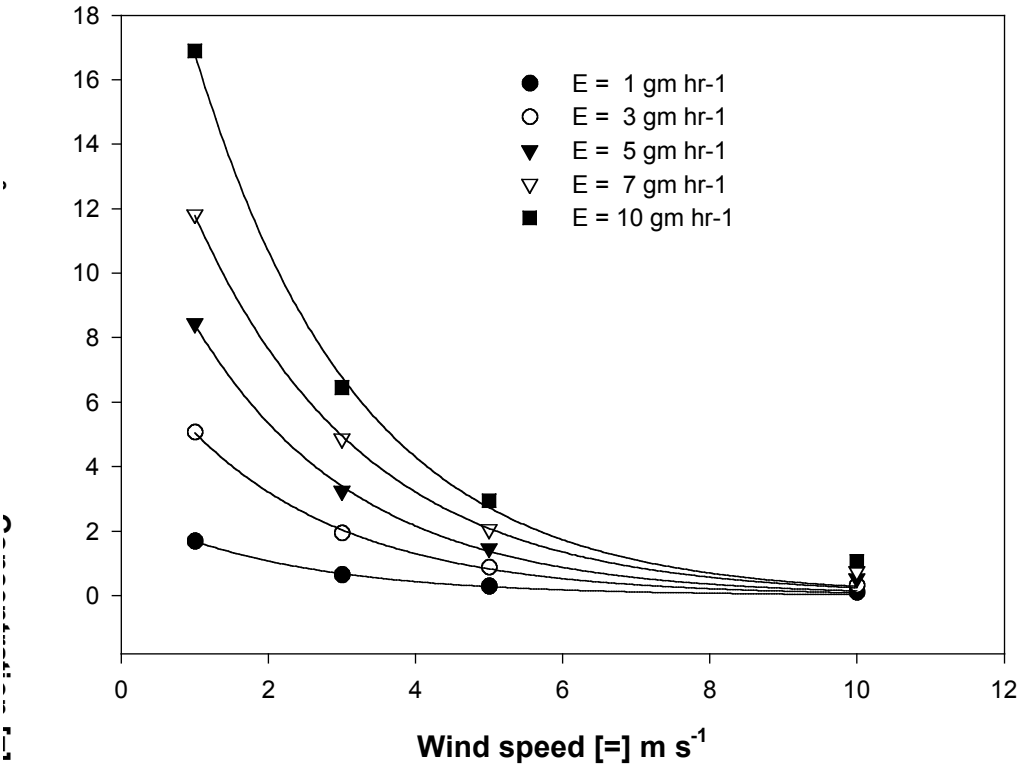

Figure 1: Pollutants concentration vs. wind speed with emission factor as parameter. Results of the air quality model (eq.s 2-3).

Figure 1 : Concentration de polluants contre la vitesse du vent avec le facteur d'émission comme paramètre. Résultats du model de la qualité de l'air (eq.s 2-3).

Conclusions

A simple air quality model in a deep street canyon has been developed for the estimation of passive gaseous pollutants emitted by vehicles circulating in the canyon itself. The model has to be validated by comparison with experimental data produced in monitoring campaigns.

References

Baik J.J. & J.J. Kim (2002): On the escape of pollutants from urban street canyons. Atmospheric Environment, vol. 36, p 527-536.

Dabberdt W.F., F.L. Ludwig & W.B. Johnson (1973): Validation and applications of an urban diffusion model for vehicular pollutants. Atmospheric Environment, vol. 7, p 603-618.

DePaul F.T. & C.M. Sheih (1984): A study of pollutant dispersion in an urban street canyon. Argonne National Laboratory Technical Report, ANL/ER–84-1.

DePaul F.T. & C.M. Sheih (1986): Measurement of wind velocities in a street canyon. Atmospheric Environment, vol. 20, p 455–459.

Hussain M. & B.E. Lee (1980): An investigation of wind forces on three dimensional roughness elements in a simulated atmospheric boundary layer flow - Part II. Flow over large arrays of identical roughness elements and the effect of frontal and side aspect ratio variations. Department of Building Sciences, University of Sheffield. Report, n° BS56.

Lee I.Y. & H.M. Park (1994): Parameterization of the pollutant transport and dispersion in urban street canyons. Atmospheric Environment, vol. 28, p 2343–2349.

Nakamura Y. & T.R. Oke (1988). Wind, temperature and stability conditions in an East – West oriented urban canyon. Atmospheric Environment, vol. 22, p 2691-2700.
Oke T.R. (1998): Street design and urban canopy layer climate. Energy Bldg., vol. 11, p 103–113.
Vardoulakis S., B.E.A. Fisher, K. Pericleous & N. Gonzalez-Flesca (2003): Modelling air quality in street canyons: a review. Atmospheric Environment, vol. 37, p. 155–182.

12th International Symposium "Transport and Air Pollution" / 12e Colloque international "Transports et pollution de l'air", Avignon, 16 -18 *June* / juin 2003
proceedings / actes, n°92, tome / Vol. 2, Inrets ed., Arcueil, France, 2003, p. 57-62

Model Project Hagen - clean air and action plan in accordance with article 8 of the EC framework Directive 96/62/EC

Andreas Brandt* & Arnold Niederau**
* North Rhine-Westphalia State Environment Agency (LUA NRW), P.O.Box 102363, 45023 Essen, Germany - Fax: +49 201 7995 1857 – email: andreas.brandt@lua.nrw.de
** AVISO GmbH; Adalbertsteinweg 34, 52070 Aachen, Germany. Fax: +49 241 9010 969 – email: arnold.niederau@avisogmbh.de

Abstract
To meet the future requirements of the actual EC air quality directives the environmental agency of the Federal State North Rhine-Westphalia (LUA NRW) initiated a model project (clean air plan) for the city of Hagen (~200.000 inhabitants) where the maximum number of daily means of > 50 µg PM10/m^3 are being exceeded. Special focus was put on PM10 modelling from road traffic (exhaust, abrasion of tires, brakes and road surfaces, resuspension). To calculate the contribution of road traffic to the total PM10 concentrations in the survey area, a Lagrange particle model (LASAT, version 2.9) was used for mesoscale dispersion modelling of all PM10 emission sources in and around the survey area with relevance to Hagen. It was found that the contribution of road traffic is dominant nearly over the whole area. So, to reduce the concentrations, first of all road traffic measures must be realised to meet EU air quality standards for Hagen.
***Key words**: clean air plan, PM10, emission, resuspension/abrasion, road traffic, Lagrange particle model, road traffic measures*

Résumé
Pour accomplir les futures exigences des actuelles directives sur la qualité de l´air de la Communauté Européenne l´agence fédéral de l´environnement de la Rhénanie-du-Nord-Westphalie (LUA NRW) a inauguré un modèle projet (plan de la protection de l´air) pour la ville de Hagen (~200.000 habitants) où le nombre maximal de dépassements admis d´une moyenne journalière de >50 µg PM10/m^3 est outrepassé à quelques localités. Beaucoup d´importance a été attachée à la modelage de la PM10 emission due à la circulation routière (l´émissions de moteur, le frottement de pneus, de freins et de surfaces routières). Pour calculer la contribution de la circulation routière aux PM10 concentrations totals dans le domaine d'étude, un modèle de particule de Lagrange (LASAT, la version 2.9) a été utilisé pour le modelage de dispersion mesoscale de tout PM10 sources d´émission dans et vers le domaine d'étude avec la pertinence à Hagen. Il a été trouvé que la contribution de la circulation routière est dominante presque par-dessus le domaine entier. Si, réduire les concentrations, les tout d´abord mesures de circulation routière doivent être réalisées pour accomplir les normes de qualité de l´air de la CE pour Hagen.
***Mots-Clés**: plan de protection de l´air, PM10, émission, resuspension/frottement, circulation routière, modèle de particule de Lagrange, mesures de circulation routière*

Introduction

In the frame of the implementation of the EU air quality framework Directive (Council Directive 96/62/EC of the 27 September 1996 concerning the assessment and control of air quality) and the 1st and 2nd daughter Directives (1999/30/EC relating limit values for sulphur dioxide, nitrogen dioxide and oxides of nitrogen, particulate matter and lead, 2000/69/EC for benzene and carbon monoxide in

ambient air) there is a need on federal state level to assess the air quality for the above mentioned pollutants on the basis of e.g. measurements and model simulations and to set up EC clean air plans for areas that exceed limit values, regarding the allowed tolerance margins.

Table 1 shows the limit values and tolerance margins for nitrogen dioxide and particulate matter (PM10) which are of most importance for the air quality assessment in NRW.

	NO_2	**PM_{10}**	
	Annual mean [µg/m³]	Annual mean [µg/m³]	Number of daily means > 50 µg/m³
EC limit values	40	40	35
In	2010	2005	2005
Tolerance margins 2000	60	48	

Table 1: Limit values and tolerance margins according to Council Directive 1999/30/EG for nitrogen dioxide and particulate matter (PM10)

Tableau 1: Valeurs limites et marges de tolérance de la Directive fille du Conseil 1999/30/EC pour le dioxide d´azote et les particules en suspension (PM10)

In order to test suitable procedures to set up and implement clean air plans, in accordance with the Council Directives, the Environmental Agency (LUA) of the Federal State North Rhine-Westphalia (NRW) was charged with carrying out a model project, which should result in a guideline for setting up EC clean air and action plans for NRW. As model region the greater area of the city of Hagen was selected because of measured high concentrations of nitrogen dioxide and particulate matter and of the high traffic density.

The so called "EC model clean air plan" for Hagen (LUA, 2002) essentially deals with the two pollutants, the focus of the following description lies on PM10.

1 - Description of the model area

The city of Hagen has about 204´266 inhabitants and a surface of 160.37 km^2, so the population density is about 1274 persons/km^2 (state 10/2001). The strong concentration of settlement, commercial and industrial areas leads to high traffic density as well. Three federal motorways (A 1, A 45 and A 46), crossing the area, underline the importance of Hagen. The economy is represented by a lot of mid and small enterprises in the metal industry and the service sector.

The northern part of the area is rather hilly (between 100 and 300 m over sea-level). The deepest point lies 86 m, the highest 438 m over sea-level. Concerning the local climate the situation over the whole area is very different. Especially in the city centre the wind speed is much lower than on the top of the hills. The annual averages of the wind speed differ between 1.3 and 5.9 m/s. The local wind direction distributions also depend on the local situations (down in the valleys or on top of the hills). So the dispersion conditions vary strongly over the whole area. Because of the valley situation nightly inversions occur frequently (KVR, 1997).

2 – Air quality situation

Results of long term measurements of some permanent LUA-locations at Hagen are shown in table 2.

It is true that the annual means of PM10 lowered from 37 μg/m^3 in 1997 to 33 μg/m^3 - the limit values are not exceeded – but there are permanent violations of the allowed number of daily means over 50 μg/m^{3}during the whole analysed time.

Year	PM_{10} annual mean in µg/m³	PM_{10} number of daily means >50µg/m³
2000	33	48
1999	36	49
1998	38	68
1997	37	48

Table 2: Results of long term measurements at Hagen-Emilienplatz location
Tableau 2: Resultats des mesures permanentes à la station Hagen-Emilienplatz

3 – Main sources for PM10 pollution at Hagen

Industrial facilities

In the whole survey area about 144 tons of PM10 were emitted by industrial sources in 1996. The main source of industrial PM10 is the sector of processing stone and ground materials, production of glass, ceramic and building-materials. The share of this sector lies by 87 %.

Transport

The distribution of the annual PM10 emissions from the transport sector is shown in the following table 3. It is obvious that road traffic is the main transport source by far. The results also point out that resuspension and abrasion are nearly 2.6 times higher than the exhaust emissions. This is the special problem when dealing with transport measures for reducing PM10 pollution. The share of the other transport modes is 5.5 % (off-road) and 1.1 % (rail, diesel).

Transport modes	PM_{10} [kg/year]	Year
Road *(exhaust emissions)*	86´205	2000
Road *(resuspension/abrasion)*	308´071	2000
Rail *(diesel, exhaust emissions only)*	4´526	1997
Off-road *(exhaust emissions only)*	23´071	1997-1999
Total	421´873	

Table 3: Distribution of the annual PM10 emissions from the transport sector at Hagen
Tableau 3: Distribution des PM10 emissions dues au secteur de transport à Hagen

Trend calculations for the next years up to 2005 underline that the total PM10 problem from road transport will not decrease. It is true that the exhaust emissions will be nearly 30 % lower than in 2000, but resuspension/abrasion will increase by about 7 %. So the total PM10 emissions from road transport with 392 tons/year will stay nearly the same as in 2000 (calculations by means of the PSM model (Grosch et al., 2000 and AVISO, 2001)).

Total PM10 emissions from the relevant sources

The following figure 1 comprises the total PM10 emissions from all relevant sources at Hagen in a grid resolution of 1 km * 1 km. The map also shows the transport networks and the industrial locations.

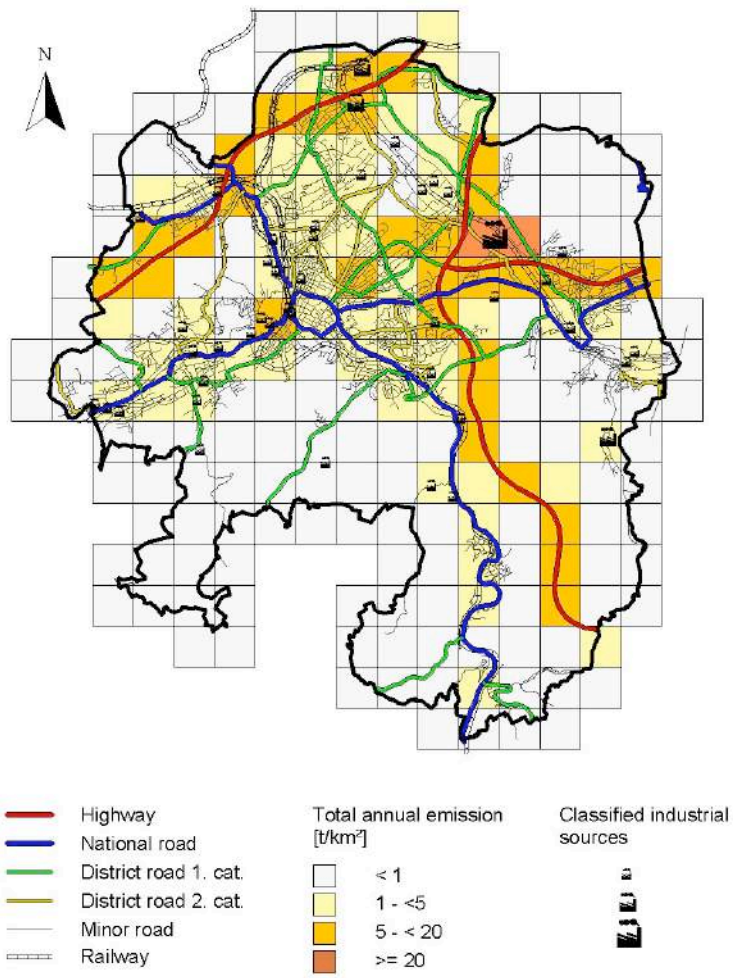

Figure 1: PM10 emissions at Hagen, all relevant sources
Figure 1: PM10 emissions à Hagen, toutes sources pertinentes

4 – Immission simulation

The correlation of the road transport emissions with their calculated spatial contribution to the overall PM10 immission situation 2000 is specified in figure 2. There one can see the share of road transport emissions to the additional grid concentrations, without background. The contribution of road transport mostly lies above 70 %, in the city centre and along the federal motorways between 85 and 100 %. This shows the dominance of road transport with regard to the locally induced PM10 concentrations. The mean background concentration of 23 μg/m³ is substantially determined by long distance transport.

Figure 3 shows the percentage source distribution of the total PM10 concentrations (including background). The background has the highest share (72 % on an average, 64 % at Hagen Emilienplatz, 48 % at Hagen Halden), followed by road transport and industry. The road transport share lies above 30 % in the settlement areas, 24 % on an average over the whole city area. Locally industrial sources can contribute significantly to the total PM10 concentration (16.5 % at the location Hagen Halden).

5 – Measures to reduce PM10 pollution in the Hagen region

Industrial facility-related measures

With the enlargement of two quarries dust measurements have been installed at relevant locations in the neighbourhood, to get some special facts on emission rates, too. Additional measures are not

planned at the moment.

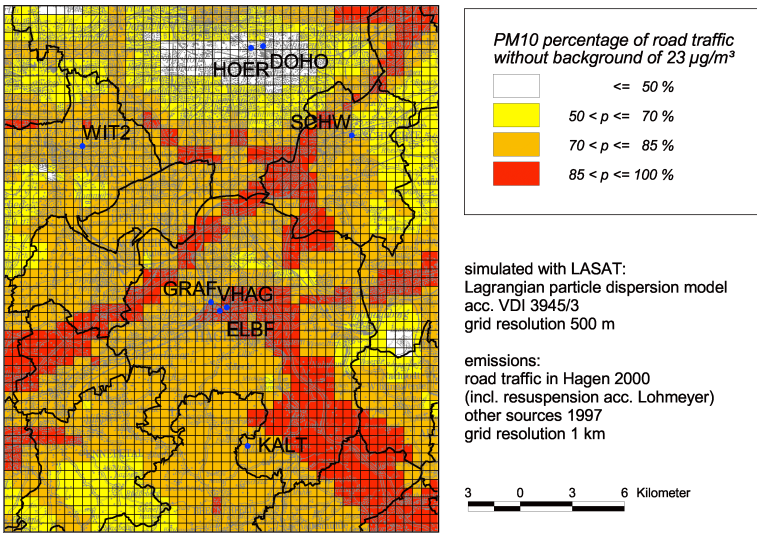

Figure 2: Simulated spatial distribution of the contribution of road transport to the annual means of PM10 concentrations in the model region in 2000 (without background of 23 µg/m³)

Figure 2: Distribution spatiale simulée de la contribution du transport routier aux moyennes annuelles de PM10 concentrations dans le domaine d´étude en 2000 (sans I´arrière-plan de 23 µg/m³)

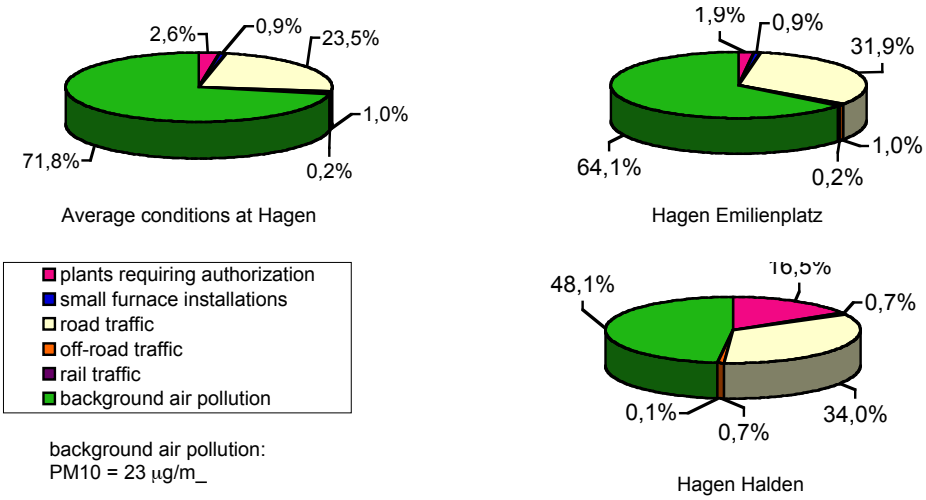

Figure 3: Percentage source distribution of the total PM10 concentrations in 2000 (background of 23 µg/m³ included)

Figure 3: Distribution des sources en pourcentage des PM10 concentrations totals en 2000 (avec l´arrière-plan de 23 µg/m³)

Road transport-related measures

Road transport-related measures should limit traffic volumes with regard to the local emission and immission situation. The measures to be implemented, e.g. at hot spots with violations of 1999/30/EG, must be orientated at the share of the local background concentration, the total traffic volume and the share of the heavy duty vehicles (hdv), as main source of PM10 emissions. And it has to be taken into account that PM10 is not only emitted via tail pipe. Resuspension/abrasion are much more important (Bösinger et al., 2002).

Generally there are two options for measures: 1) the reduction of the total traffic volume focussing

at all vehicle categories; 2) the reduction of heavy duty vehicles up to total local prohibition. For some hot spots in and around the city centre of Hagen simulations were done in accordance to the two general options (Ludes et al., 2001). It was found that to meet the PM10 limit value for the annual mean 2005 the total traffic volumes of 20´ to 40´000 must be reduced between 22 and 61 % (option 1). Realising option 2 up to total prohibition (no thoroughfare) does not reduce the PM10 concentrations under the limit value except one of the 5 hot spots looked on. Effects of alternative route choice with perhaps creating new hot spots, here were not investigated further.

6 – Draft of an action plan "road transport"

The sustainable reduction of high traffic volumes, especially at the localised hot spots, in the future shall be met by the coordinated use of the following three instruments.

Routing concept for hdv

The routing concept for heavy duty vehicles shall assign mainly non-resident drivers to a hdv priority network making a detour round the hot spots. The route guidance will be realised as a permanent static system in a first step.

Concentration-depending dynamic route guidance

To assist the permanent hdv routing concept a dynamic route guidance system shall be installed in a second step. When episodes will be forecasted with violations of limit values and/or tolerance margins the system will be activated in order to reduce peak concentrations by temporarily guiding the drivers through the network, recommending alternative routes up to local traffic prohibition.

City logistics

As most of the high polluted streets lie in and around the city centre it is consistent to influence the delivery traffic, especially with hdvs. The aim of installing and extending city logistics first of all is to reduce hdv traffic. This can be met by replacing heavy with light duty vehicles and optimising trip planning (delivery routes) at the same time.

References

LUA (2002): Modellprojekt zur Erstellung von Luftreinhalteplänen nach Artikel 8 der Richtlinie 96/62/EG des Rates über die Beurteilung und die Kontrolle der Luftqualität. Abschlussbericht, http://www.lua.nrw.de/, Landesumweltamt NRW, Essen, 2002

KVR (1997): Klimaanalyse Hagen. Kommunalverband Ruhrgebiet, Abteilung Karten-, Luftbildwesen, Stadtklimatologie, im Auftrag der Stadt Hagen, Umweltamt, Essen, 1997

Grosch, N.; Heykamps, T.; Niederau, A.; Schneider, C. (2000): Prognose- und Szenarienmodell zur Emissionsmodellierung des Straßenverkehrs in NRW. AVISO GmbH, im Auftrag des Landesumweltamtes NRW, Aachen, 2000

AVISO (2001): Pilotprojekt Hagen, Teilaufgabe im Rahmen der Umsetzung der EU-Luftqualitätsrahmenrichtlinie, Emissionskataster Straßenverkehr, im Auftrag des Landesumweltamtes NRW, Aachen, 2001

Bösinger, R.; Bächlin, W.; Lohmeyer, A. (2002): Erstellung und Validierung eines PM10- Emissionsmodells für den Straßenverkehr in Nordrhein-Westfalen. Ingenieurbüro Dr.-Ing. Achim Lohmeyer, im Auftrag des Landesumweltamtes NRW, Karlsruhe, 2002

Ludes, G.; Schulze-Kegel, D. (2001): Emissionsszenarien für den Hagener Innenstadtring. SimuPLAN-Ingenieurbüro für innerstädtische Simulation, im Auftrag der Stadt Hagen, Mai 2001

12th International Symposium "Transport and Air Pollution" / 12e Colloque international "Transports et pollution de l'air", Avignon, 16 -18 *June* / juin 2003
proceedings / actes, n°92, tome / Vol. 2, Inrets ed., Arcueil, France, 2003, p. 63-68

A numerical model for removal of SO_2 from atmosphere by rain

Dulal Pal[*] & Dilip Kumar Sinha[**]
* Department of Mathematics, Visva-Bharati University, Santiniketan, West Bengal – 731235, *India*. Fax +91 3463 262672 – email : dulalp123@rediffmail.com
** Department of Applied Mathematics, University of Calcutta, 92 A.P.C. Roy Road, Kolkata – 700009, *India*.

Abstract
A time-dependent numerical model for the diffusion of gaseous pollutant in the convective boundary layer is presented in this paper. This model is further extended to include the washout of sulfur dioxide from the atmosphere by rain by incorporating mass transfer of SO_2 into well mixed raindrops. The numerical model presented in this paper describes that the pollutants undergo chemical reaction in gas- and liquid phases. The model is useful for determining the concentration of SO_2 in raindrop under different atmospheric conditions. The effects of various raindrop sizes on concentration of pollutant are also studied in this paper.
Key words: *Atmospheric dispersion, washout, chemical reaction, air pollution, acid rain.*

Introduction

The gaseous pollutant like sulfur dioxide is emitted from industrial stacks in urban areas that are hazardous to the environment. It undergoes several processes before it is being removed from the atmosphere. Some of the important removal mechanisms are dry deposition onto the surface of the Earth, gravitational settling, chemical reaction and wet deposition. These removal processes influence to minimize the ground level concentration that have a great impact on health hazards. The washout of sulfur dioxide from the atmosphere is a phenomenon that contributes to the production of so-called "acid rain" and at the same time helps in the cleansing of the atmosphere. Effective models of the washout process are useful in predicting the composition of rain and the time scale for SO_2 removal. Mathematical models used in the air pollution study vary from simple empirical models to complex numerical models. Although the PBL theory was improved for the convective conditions through field observations (Kaimal et al., 1976) and by its counterpart in laboratory experiments (Willis et al.,1978), the Convective Boundary Layer (CBL), that is the region where mixing occurs due to convective motions associated with upward heat transport from the surface seems to be more appropriate vide Pal and Sinha (1990).

Thus, the main objective of this paper is to develop a time-dependent diffusion model to study the effects of dry deposition and washout of sulfur dioxide from the atmosphere during rainfall on ground level concentration. The pollutant is emitted from a continuous point source for a certain period of time. An in-depth treatment of the problem is greatly facilitated by numerical computations of the atmospheric-diffusion equation with gravitation settling and chemical reaction terms. These bring out the g.l.c. scenario so essential for transport processes of pollutants of different hierarchies.

We have also taken into account of the mass transfer of SO_2 into well mixed-drops. Calculations were made for various drop sizes in the convective boundary layer. We have considered a well-mixed layer of the atmosphere in which concentration of sulfur dioxide is present and rain is formed above this layer before entering the layer. The present model will be useful in estimating the

concentration of sulfur dioxide, composition of rain under different meteorological parameters and also, the time scale for SO_2 removal from the atmosphere.

1. Method of Approach

Let us begin with the description of the model. We have considered a continuous point source at height h_s above the ground emitting chemically reactive pollutant into the atmosphere. Then the atmospheric diffusion equation with first order chemical kinetics and suitable boundary condition as

$$\frac{\partial C_g}{\partial t} = \frac{\partial}{\partial z}\left(K_z \frac{\partial C_g}{\partial z}\right) + W_s \frac{\partial C_g}{\partial z} - R_1 C_g - \lambda C_g + Q\delta(z - h_s) \qquad (1)$$

The boundary conditions that accompany Eq. (1) are:

$$C_g(x, t) = C_o \qquad \text{at } x=0, t=0 \qquad (2a)$$

$$K_z \frac{\partial C_g}{\partial z} + W_s = V_g C_g \qquad \text{at } z=0, \qquad (2b)$$

$$K_z \frac{\partial C_g}{\partial z} + W_s = 0 \qquad \text{at } z=Z_i, \qquad (2c)$$

where, C_g is concentration of the pollutant, K_z is vertical mixing coefficient, V_g is the dry deposition velocity of gaseous species, W_s is the gravitational settling velocity, R_1 is the chemical reaction rate, Q is the source strength, λ is known as washout co-efficient, $\delta(.)$ is Dirac-delta function and h_s is the stack height, C_o is the background concentration of the pollutant species and Z_i is the inversion height.

The rate of accumulation of all compounds of sulfur in each falling rain droplet is taken to be equal to the rate of mass transfer of SO_2 across a fictitious laminar air film surrounding each drop. The total concentration of sulfur dioxide in a raindrop of radius R falling at a constant terminal velocity V_t along

the vertical z-axis can be expressed as (Hill et al., 1977):

$$\frac{dC_w}{dz} = \frac{3k_g}{RV_t}(C_g - H_e C_w) \qquad (3)$$

with boundary condition$C_w = 0$ at $z=Z_i$(4)

where, C_g is the concentration of SO_2, C_w is the liquid phase equilibrium concentration of molecular SO_2, H_e is Henry's law constant, and k_g mass transfer coefficient for interchange of gas between droplet and its surroundings. For purely convective-diffusion transport in the gas-phase k_g can be

obtained from the semi-emperical Frössling equation (Frössling, 1938):

$$S_h = 2 + 0.6\, R_e^{1/2}\, S_c^{1/3} \qquad \text{for } R > 0.06 \text{ cm} \qquad (5a)$$

and $$S_h = 1.56 + 0.616\, R_e^{1/2}\, S_c^{1/3} \qquad \text{for } 0.02 \le R \le 0.06 \text{ cm} \qquad (5b)$$

where, $S_h = 2\, k_g R/ D_g$, $R_e = -2RV_t/ \nu$, $S_c = \nu/ D_g$. Here D_g is the diffusivity of air, V_t is the terminal velocity of raindrop and ν is kinematic viscosity. The terminal velocity of raindrop with respect to height is calculated from a formula by Markowitz (1976) :

$$V_t = 958[\, 1 - \exp\{ - R/ 0.0885\}^{1.147} \}] \,. \qquad (6)$$

Where, R is the radius of raindrop.

The chemical conversion from SO_2 to SO_4 is assumed to be first order. The dry deposition is handled

by means of deposition velocity. The wet deposition flux λ is taken as a function of pH of the precipitation and is calculated from the following expression:

$$\lambda = 0.96\ \beta P^{0.90}\ ,\ \ \log_{10}\beta = -2 + 0.75(pH - 3.9) \tag{7}$$

where, P is rain rate in mm/h.

2. Meteorological Parameters

The variables required for the integration of the equation (1) with its boundary conditions are wind field, eddy diffusivities, chemical transformation rate, deposition velocity, settling velocity, emission rate and mixing height. The wind speed u_z and eddy diffusivity K_z as a function of z for the convective boundary layer are dependent mainly on the stability of the atmosphere. In terms of boundary layer notation, atmospheric stability may be characterized by the parameter L called the Monin-Obukhov length parameter and is defined as

$$L = -\frac{\rho\, c_p T\, u_*^3}{kgH} \tag{8}$$

where u_* is friction velocity, H is the net heat flux to the atmosphere, c_p is the specific heat, T is the temperature of the air, ρ is the air density, k is Karman's constant, and g is the gravitational constant. L has units of length. The friction velocity can be defined in terms of a geostrophic drag coefficient, c_g, and the geostrophic wind velocity u_g as follows:

$u_* = c_g\, u_g$(9) The geostrophic drag, c_g , is a function of the surface Rossby number, $R_o = u_g / z_o f$ and L, where f is the Coriolis parameter of the Earth and z_o is the surface roughness. Direct determination of the L from its definition requires measurement of heat flux and friction velocity. Unfortunately, such measurements are not routinely available. Therefore u_* is derived by using Eq. (9) and the values of net heat flux are obtained from Ragland (1973). For a neutrally stratified atmosphere H = 0, and H = -0.06 ly/min and H = 0.24 ly/min are chosen for stable and unstable flows respectively. The convective scaling velocity w_* which controls turbulence in the convective boundary layer is defined as

$$w_* = u_* \left(-\frac{1}{k}\frac{h}{L}\right)^{1/3}, \tag{10}$$

where u_* is friction velocity, L is the Monin-Obukhov parameter and k is the Von Karman constant (=0.35) suggested by Businger et al (1971).

The wind velocity as a function of z is obtained from the relation

$$u(z) = \frac{u_*}{k}\psi_m(z/L) \tag{11}$$

where, expressions for $\psi_m(z/L)$ are given in Pal and Sinha (1990) for different stability conditions.

The vertical eddy diffusivity as a function of vertical distance are calculated from the expressions given by Jia-Yeong Ku et ali (1987).

3. Methodology

Having described the model we now proceed to develop the methodology in brief. An imlicit finite-difference approach has been used to solve numerically the equation (1-2). We approximate first-order temporal and vertical gradients by forward differencing and second-order spatial derivatives by central differencing. After simplifications, a set of N algebraic equations with N unknowns are represented by a tri-diagonal coefficient and are solved very efficiently by using the Thomas algorithm. An array of 40 boxes vertically and sufficient number of boxes horizontally are chosen for the purpose of the present model. The first ten boxes vertically are 4 m high and remaining 30 boxes are selected to fill the space up to mixing height of 1000 m. A point source is located at 78 m

height. The concentration at the end of the first horizontal rows of boxes is referred to as the ground-level concentration of pollutant. The equation (3) is integrated numerically with appropriate boundary condition (4) after obtaining the concentration of SO_2 from equation (1) at each grid point. The point source, Q, is taken as 10 μg m^{-2} s till the emission is stopped after 1hr. or 4 hrs. depending on the situation. The data set has been taken from the literature (Barrie, 1978) in order to evaluate numerically the concentration of SO_2 in raindrop.

4. Results and Conclusions

Some interesting results have been obtained for the ground level concentration (g.l.c.) of gaseous pollutant from the numerical solution of diffusion equation and the concentration of pollutant in a raindrop for different intensity of rain. It is assumed that raindrop is falling with a constant terminal velocity. The chemical transformation of the pollutants in the atmosphere and the ground deposition of the pollutants are also considered in this present model. The study of g.l.c. is done during rainfall and after the rainfall. In order to have a realistic picture, computations are obtained for, in particular, the emission of the pollutant from a point source which was terminated after 4 hrs and rain stopped after 6 hrs.

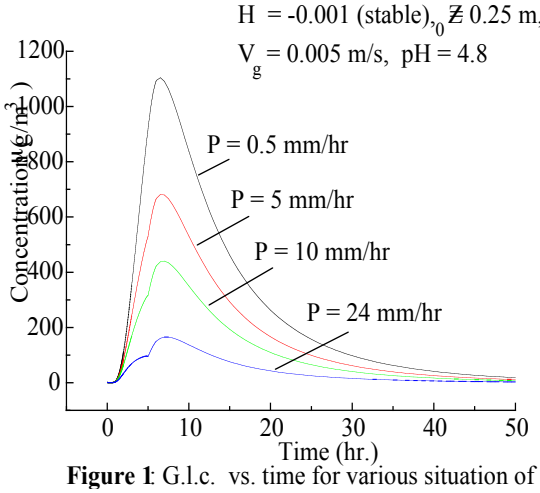

Figure 1: G.l.c. vs. time for various situation of rai

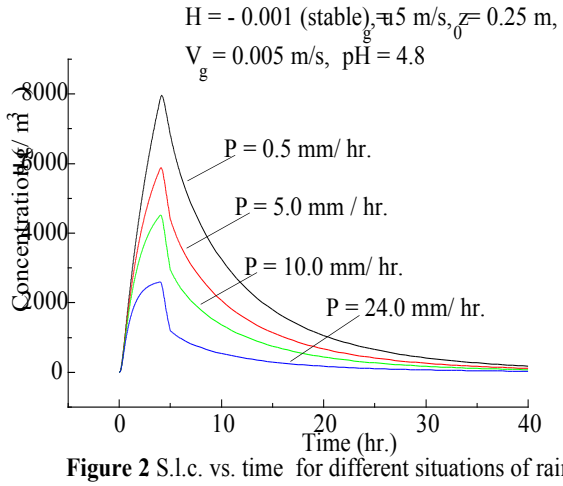

Figure 2 S.l.c. vs. time for different situations of rain r

The simulation is performed for three atmospheric conditions viz. neutral, stable and unstable for calculating g.l.c. under different rain rate and dry deposition velocity. The results are depicted in Figures 1-10. The variation of ground level concentration of SO_2 with rainfall rate for stable atmospheric condition is shown in Fig.1. It is observed from this figure that g.l.c. decreases with increase in the rainfall rate . These show that the g.l.c. increases very rapidly with time till the emission of pollutant is stopped and then decreases very slowly till it attains a very low value of concentration.

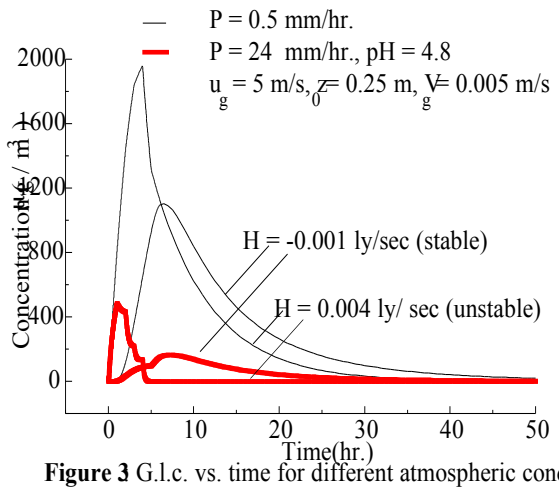

Figure 3 G.l.c. vs. time for different atmospheric conditi

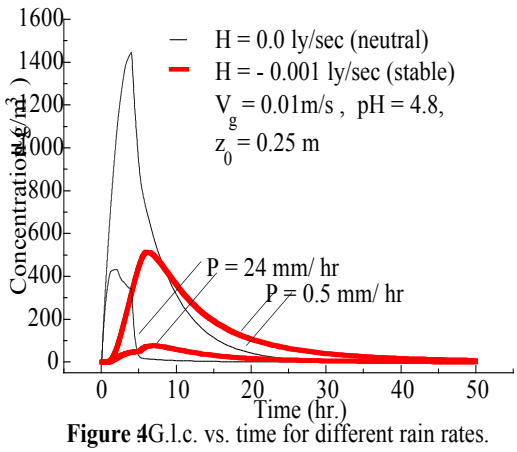

Figure 4 G.l.c. vs. time for different rain rates.

It is interesting to observe that g.l.c. attains its peak after emission of pollutants for four hours. Similar situation is seen in Figure 2 for source level concentration of pollutant. The value of W_s=0.0003 m/s is taken in Figs.1-2 and for others it is assumed to be zero. Figure 3 shows that the variation of g.l.c of gaseous pollutant with time for stable and unstable atmospheric conditions. The concentration increases with time till the emission of pollutant is stopped and thereafter it starts decreasing with time. It is also observed that the values of g.l.c. for unstable atmosphere are higher in comparison with stable atmospheric condition before the emission is stopped and this trend is reversed when the emission is stopped. Similar situation is seen in Figure 4 for neutral and stable atmospheric conditions.

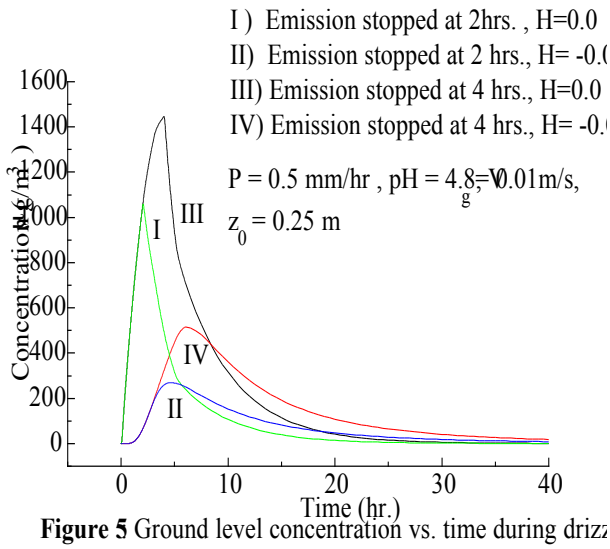

Figure 5 Ground level concentration vs. time during drizz

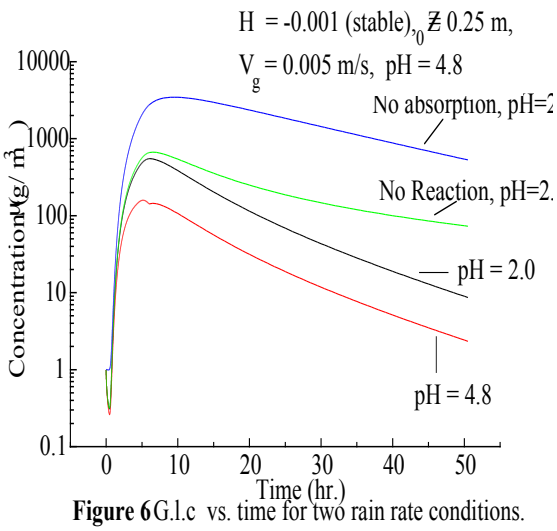

Figure 6 G.l.c vs. time for two rain rate conditions.

Figure 5 shows how the g.l.c. of gaseous pollutant varies with time for different situations of cutoff in source emission during drizzle for different atmospheric conditions. The results which are shown in Figure 6, as expected, points out that the values of g.l.c. are much higher in the absence of any types of ground absorption and chemical reaction. It is interesting to see that the increase in pH value lowers the value of g.l.c. for stable atmospheric stability.

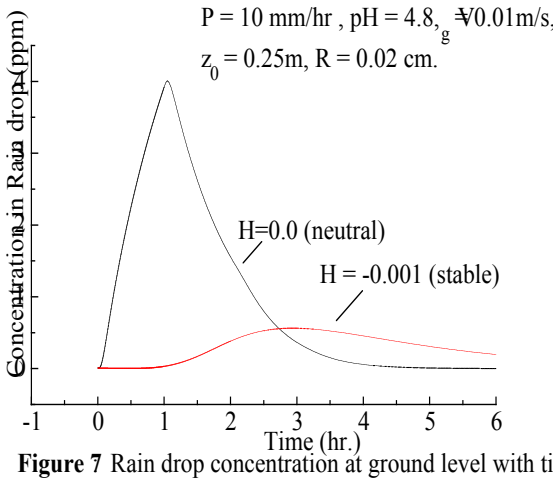

Figure 7 Rain drop concentration at ground level with ti

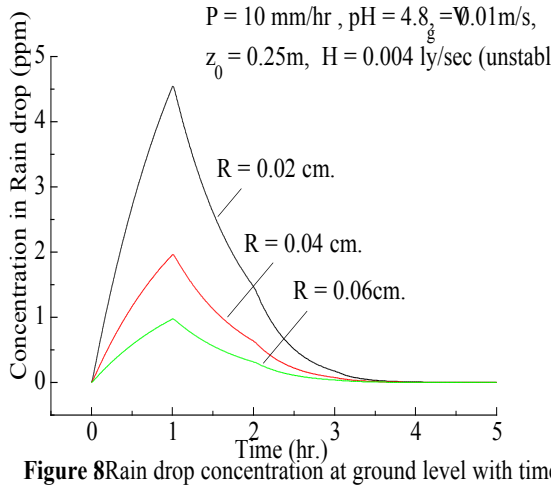

Figure 8 Rain drop concentration at ground level with tim

Some useful results have been obtained for the concentration of pollutant in the raindrop. Figure 7 shows how concentration of SO_2 in raindrop varies with time under different types of atmospheric stability. It is observed that the concentration in raindrop increases with time till the source emission is stopped and decreases after the emission is stopped. It is observed from Figure 8 that the concentration of SO_2 in raindrop of size 0.06cm is much less than the concentration in smaller raindrop of size 0.02 cm. In Figure 9 it is observed that the concentration of pollutant in bigger

raindrop increases gradually even after the emission is stopped at 4 hrs. and starts decreasing after 5.5 hrs. Similar fact is seen in Fig. 10. It is found that the concentration of SO_2 is very small in the raindrop of radius equal to 0.2 cm.

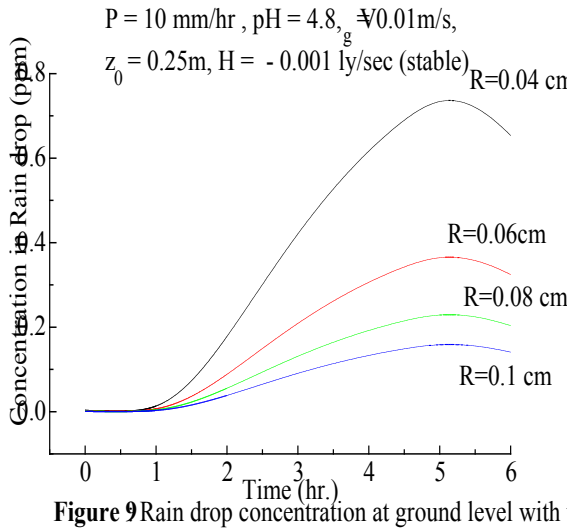

Figure 9 Rain drop concentration at ground level with

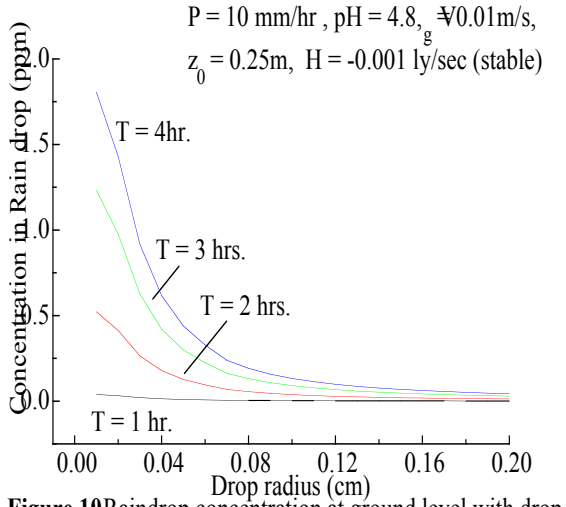

Figure 10 Raindrop concentration at ground level with drop

These concentration profiles lead to some conclusive statements. The values of g.l.c. of the unstable atmospheric condition are less in comparison with stable atmospheric condition when the emission was terminated. The effect of dry deposition velocity is to decrease the g.l.c. for gaseous pollutant. The g.l.c. decreases with increase in the value of rain rate. The concentration of pollutant in raindrop increases with time till the emission is stopped and its concentration is very less in bigger raindrops.

References:

Barrie, L.A. (1978): An improved model of reversible SO_2–washout by rain. Atmos. Environment, vol. 12, p402-412.

Businger J. A., J. C. Wyngaard, Y. Izumi and E. F. Bradley (1971): Flux-profile relationships in the atmospheric surface layer. J. Atmos. Sci., vol. 28, p181-189.

Frössling, N. (1938): The evaporation of falling drops, Gerlands Beitr. Geophys., vol. 53,p170-216.

Hill F. B. & R. F. Adamowicz (1977): A Model for rain composition and the washout of sulfur dioxide. Atmos. Environment, vol. 11, p917-927.

Kaimal J. S., J. C.Wyngaard , D. A.Haugen, O. R.Cote, Y.Izumi, S. J. Caughey & C. J. Readings (1976): Turbulence structure in the convective boundary layer. Atmos. Sci., vol. 33, p2152-2169.

Ku Jia-Yeong, T.S. Rao & K. S. Rao (1987): Numerical simulation of air pollution in urban area: Model development. Atmos. Environment, vol. 21, p201-212.

Markowitz A.H. (1976): Raindrop size distribution expressions, J. Applied Meteorology, vol. 15, p1029-1031.

Pal D. & D.K. Sinha (1990): Numerical Air Pollution Model in the convective Boundary layer, Int. J. Environ.Studies, vol. 35, p215-222.

Ragland K. W. (1973): Multiple box model for dispersion of air pollutants from area sources. Atmos. Environment, vol. 7, p1017-1032.

Rogers R. R. (1976): A short course in cloud physics, Pergamon Press, Oxford, p.225.

Willis G.E. & J. W. Deardorff (1978): A laboratory study of dispersion from an elevated source within a modeled convective planetary boundary layer. Atmos. Environment, vol.12, p1305-1312.

12th International Symposium "Transport and Air Pollution" / 12e Colloque international "Transports et pollution de l'air", Avignon, 16 -18 *June* / juin 2003
proceedings / actes, n°92, tome / Vol. 2, Inrets ed., Arcueil, France, 2003, p. 69-74

Validation of CALINE4 for CO and NO_2 concentrations by an Irish motorway

Brian Broderick, Una Budd & Bruce Misstear
Department of Civil, Structural and Environmental Engineering, Trinity College, Dublin 2, Ireland

Abstract
Atmospheric dispersion model accuracy is dependent not only on the quality of the data used, but also on the methodology of the model and its user. The air pollution dispersion model, CALINE4 is in common usage in Ireland but was developed outside Ireland and has not been validated for use in Irish conditions. The objective of this work was to validate the use of the model for road traffic emissions in Ireland, however the results will also be of wider European interest. The model was assessed using one year of air quality data collected at a free-flowing motorway near Dublin. Model predictions of CO and NO_2 concentrations were not always within ±50% of measured concentrations, and under stable atmospheric conditions, and when wind speeds are low, significant discrepancies may arise. The scarcity of traffic, meteorological and background concentration data was found to be the major difficulty in modelling for the assessment of the environmental impact of Irish road schemes.
Keywords: *air quality monitoring, dispersion modelling, model validation, traffic emissions.*

Introduction

The assessment and management of air quality is required under Council Directive 96/62/EC (CEC, 1996), the Air Quality Framework Directive, and its Daughter Directives which specify the limits for certain pollutants, including carbon monoxide (CO) and nitrogen dioxide (NO_2). Air quality modelling is used to predict the ambient air quality, thus identifying areas which might require monitoring to "avoid prevent and reduce harmful effects on human health and on the environment". The future impact of road improvements cannot be monitored, therefore modelling is used to predict the influence on ambient air quality of any changes in traffic conditions, as part of the Environmental Impact Assessment. The US National Commission on Air Quality found in 1981 that models may typically overpredict or underpredict from actual concentrations by a factor of two. Even twenty years later the UK DETR (2001) concurred that "If the prediction of an annual mean concentration lies within ±50% of the measurement, a user would not consider that the model has behaved badly."

1Method

Site

The monitoring unit was located 20 m to the north of the M4 at Leixlip, 10 miles (16 km) west of Dublin city centre, on the River Liffey. The motorway has two lanes in each direction, which run almost due east-west.

Monitoring

The national weather service, Met Eireann, provided hourly Pasquill stability class, cloud cover, wind speed and direction data from Casement Aerodrome, one km south of the monitoring site. The National Roads Authority measured the hourly traffic flows on the Leixlip section of the M4. CO and NO_2 analysers were sited 20 m north of the M4, where temperature, humidity, wind speed and

direction were also recorded.

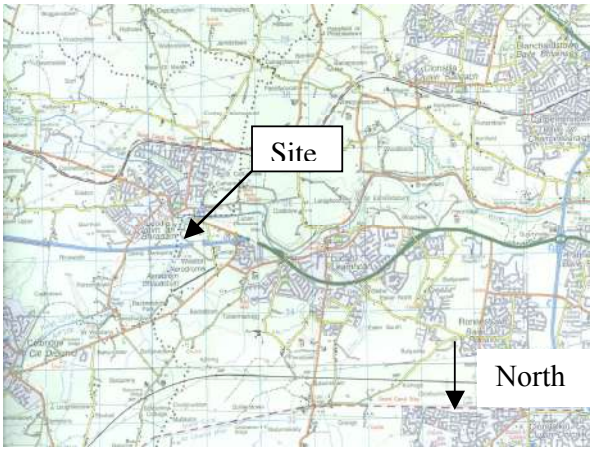

Figure 2.1: Monitoring site location

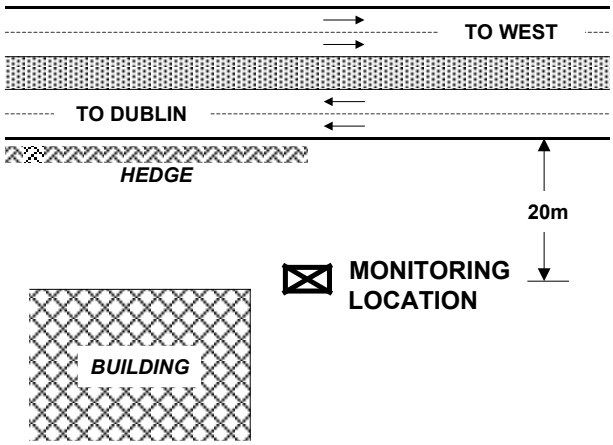

Figure 2.2: Monitoring site layout

Pollutant	Instrument	Method	Sampling interval
CO	API Model 300	Infrared absorption	One hour; 15 minutes
NO_2	API Model 300	Chemiluminescence	One hour; 15 minutes

Table 2.1: Pollutants monitored, method and equipment

Modelling

The model CALINE4 was developed by the US EPA. It requires hourly traffic flows, meteorological parameters and an emission factor which represents the fleet profile of vehicle type, fuel and driving mode. It predicts the hourly concentration at receptors relative to the roadway line source (Benson, 1984). Composite emission factors of 6.62 g/mile CO and 2.24 g/mile NO_2 were calculated for the vehicle fleet of 71% petrol cars, 21% diesel cars and 8% heavy goods vehicles (HGV). Background concentrations of ozone (0.03 ppm), NO (0.01 ppm), NO_2 (0.01 ppm) and a photolysis rate constant of 0.0010 s^{-1} were used for NO_2 modelling.

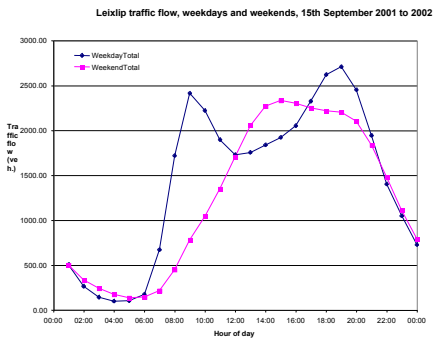

Figure 3.1: Diurnal variation in annual average of hourly traffic flow

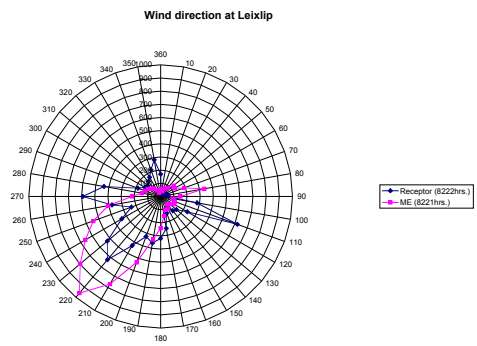

Figure 3.2: Directional variation in annual average of hourly wind direction frequency

2Results

Traffic and meteorology

The annual average peak flow was 2562 vehicles per hour (vph), for the hour ending 19:00 (Figure 3.1: weekday peak 2709 vph at 19:00, weekend peak 2336vph at 15:00). The prevailing winds at the monitoring unit (receptor) were from the south east, south west and west, with a wind shadow cast by a building to the north east (Figure 3.2). Met Eireann, found the prevailing wind to be from

the south west. The highest mean wind speeds of 3.5 m/s were for southerly winds (Figure 3.3). The wind shadow of the building was again clear, with very low wind speeds from the north east. Stable conditions are most frequent with east and north easterly winds (c.60%) and least frequent with westerly winds (<20%) (Figure 3.4). Conditions were never stable (Pasquill Stability Class E, F or G) after 08:00 and before 16:00.

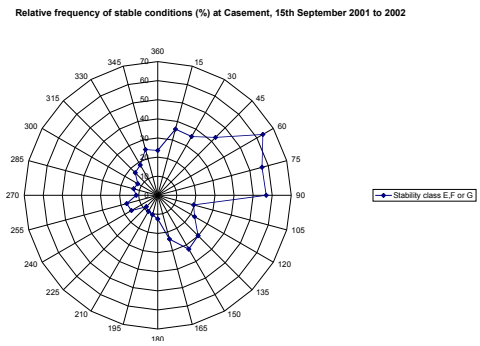

Figure 3.3: Directional variation in annual average of hourly wind speed

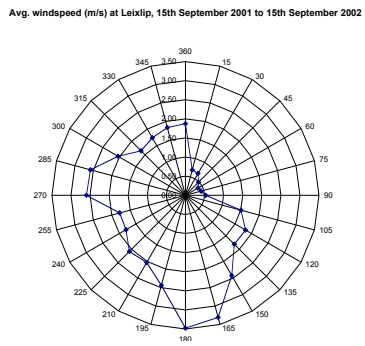

Figure 3.4: Directional variation in annual relative frequency of hourly stability class

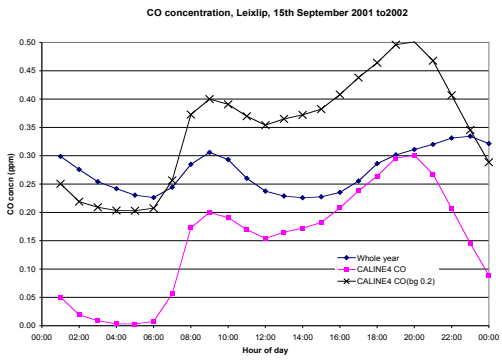

Figure 3.5: Diurnal variation in annual average of hourly CO concentration

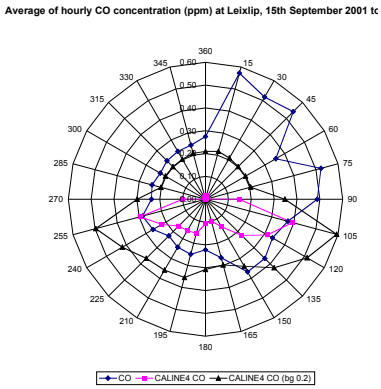

Figure 3.6: Directional variation in annual average of hourly CO concentration

Measured and modelled CO and NO_2

Diurnal and directional annual average hourly concentrations

Figures 3.5 and 3.6 show the measured concentrations of CO compared to the predictions from modelling with background concentrations of 0 and 0.2 ppm CO respectively. The diurnal variation in the modelled CO does not vary when the background concentration is changed, since CO is inert (Figure 3.5). The measured CO is always greater than 0.2 ppm, when averaged diurnally and directionally, hence the background value of 0.2 ppm. The peak annual average hourly CO concentration is 0.33 ppm at 23:00, whereas the modelled peak is 0.30 ppm at 20:00. The highest CO concentrations were measured when the wind was from the north east (0.5 ppm ≤ CO ≥ 0.6 ppm), while the highest predicted CO occurred when winds were near parallel to and from the south of the road (Figure 3.6). With no background concentration of CO, the peak predicted CO (0.39 ppm) was lower than that measured (0.57 ppm), but agreed very well with the measured concentration for the corresponding wind direction (0.37 ppm).

Figures 3.7 and 3.8 show the measured concentrations of NO_2 compared to the predictions from modelling with background concentrations of ozone (0.03 ppm), NO (0.01 ppm) and NO_2 (0.01 ppm). The peak annual average hourly NO_2 concentration is 12 ppb at 21:00, whereas the modelled peak is 22 ppb at 19:00 (Figure 3.7). The highest NO_2 concentrations were measured when the wind was from the north east (12 ppb ≤ NO_2 ≥ 18 ppb), while the highest predicted NO_2 (34.5 ppb)

occurred when winds were near parallel to and from the south of the road (Figure 3.8), as for CO.

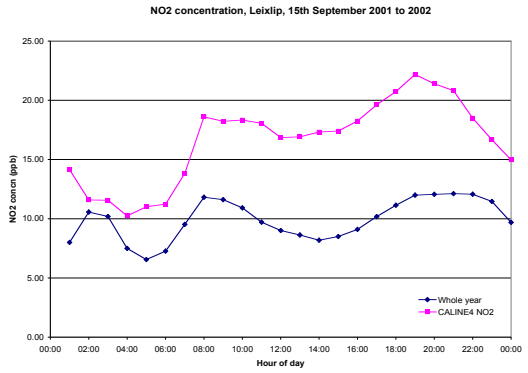

Figure 3.7: Diurnal variation in annual average of hourly NO_2 concentration

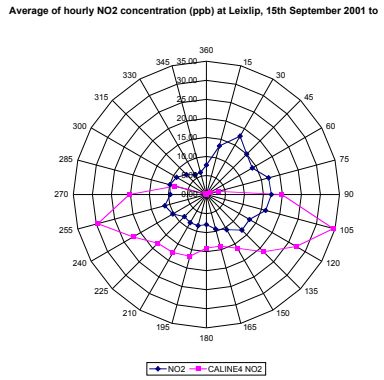

Figure 3.8 Directional variation in annual average of hourly NO_2 concentration

Table 3.1 compares the mean, maximum and 95th%iles of the measured concentrations of CO and of NO_2 with the model predictions. The CO predictions do not include a background concentration. The maximum eight-hour running average for CO, and the 99.8th%ile for NO_2 are compared with the EU limit values set by the Daughter Directives 2000/69/EC and 1999/30/EC (CEC, 1999; CEC, 2000). Also shown are the Upper Assessment Threshold (UAT), below which modelling and (limited) monitoring are required, and the Lower Assessment Threshold (LAT), below which modelling or objective estimation alone suffice.

3Discussion

Directional and diurnal variation

The effect of the road source on concentrations at the monitoring unit is expected to be strongest when the wind is from the south and weakest when the wind is from the north. Winds from the north east are rare, but coincide with the lowest wind speeds and the highest frequency of stable conditions. The model cannot predict these high concentrations since they are not due to the roadway source. Higher concentrations are predicted for near parallel wind directions than for cross winds, due to the larger area of roadway over which the traffic is "upwind" of the receptor and the longer passing time during which pollutants can be emitted.

CO concentration rises as traffic flow increases to the morning peak of 1491 vph at 09:00, then decreases with the lunchtime lull in traffic and with the absence of stable conditions between 09:00 and 16:00. CO rises again after 15:00, though the traffic has increased since 12:00 towards the peak flow of 2562 at 19:00. The CO concentration rises towards its peak of 0.33 ppm at 23:00, due to persistence under stable conditions rather than the corresponding source strength, since the traffic flow decreases sharply after 19:00, reaching its nadir of 112 vph at 05:00.

The variation in CO concentration is more strongly influenced by the weekday traffic pattern with its distinct morning and evening peaks, than by the weekend traffic, which is spread over the afternoon hours. This suggests that CO concentrations decrease during the hours of unstable or neutral conditions (from 09:00 to 16:00) despite relatively high volumes of traffic.

Pollutant		Mean	Maximum	95th%ile	Max. 8hr running average
CO (ppm)	Measured	0.27	2.6	0.6	2.15
	Meas.±50%	0.14-0.40	1.3-3.9		1.08-3.23
	Modelled	0.15	2.3	0.6	1.1
	Limit value	(2000/69/EC	by 2005)		8.6 (10mg/m^3)
	UAT				6.0 (70% of limit)
	LAT				4.3 (50% of limit)
					99.8th%ile
NO_2 (ppb)	Measured	9.9	53.7	25.4	43.2
	Meas.±50%	5.0-14.9	26.9-80.6		21.6-64.8
	Modelled	16.6	60	40	50
	Limit value	20.4 (40µg/m^3)			102 (200µg/m^3)
	UAT				71 (70% of limit)
	LAT				51 (50% of limit)
		1999/30/EC	[≤18 exceedances p.a.]		By 2010

Table 3.1: Measured and modelled CO and NO_2

NO_2 rises with traffic after 05:00. Traffic continues to rise until its morning peak at 09:00 but NO_2 decreases after its morning peak at 08:00, as conditions are no longer stable. From the trough at 14:00, NO_2 concentrations rise to an evening peak, which is maintained from 19:00 to 22:00. The diurnal variation in weekday traffic is reflected in the diurnal variation of NO_2 concentration except that NO_2 concentrations remain high for several hours after the traffic source has decreased.

The predicted peaks coincide with the morning and evening traffic peaks, but the model cannot predict the high CO and NO_2 concentrations after 20:00, which may be due to stable conditions rather than the immediate traffic source, and also due to photochemical effects in the case of NO_2.

Background concentrations of CO

Since CO is inert the background concentration can be added before or after modelling. Modelling CO with a background concentration of 0 ppm gives the diurnal variation in CO due to the traffic source. The predictions are always lower than the measured concentrations, but still fall within 50% of the measured concentrations from 08:00 to 22:00.

From the diurnal and directional averages (Figures 3.5 and 3.6), the measured concentration of CO never falls below 0.2 ppm. Taking this as the background concentration gives predictions that overestimate CO by more than 50% from 13:00 to 20:00, when traffic is flowing strongly.

The difference between the mean measured CO (0.27 ppm) and mean predicted CO (0.15 ppm) is 0.12 ppm. Taking this as the background value ensures that the mean modelled CO concentration agrees with the mean measured CO concentration. However, the resultant predicted diurnal profile also falls within ±50% of that measured. The model overpredicts the afternoon and evening CO concentration, whereas it underpredicts the overnight CO concentration.

Background concentrations for NO_2 modelling

The background values for NO and NO_2 were the lowest permitted by the model. These background concentrations may be conservative since they overestimate the ambient conditions as measured. At least half of both diurnal and directional NO_2 concentrations were measured as less than 0.01 ppm (equivalent to 10 ppb).

Annual statistics

The predicted annual mean, maximum and 95th%ile of hourly CO concentrations and the maximum eight-hour running average CO concentration all lie within ±50% of the measured values. The closest agreement is for the 95th%ile of the annual average of hourly CO concentrations. As predicted by the model, CO concentrations measured at this site are well below even the Lower

Assessment Threshold of 4.3 ppm (eight-hour running average), even with the addition of a conservative background concentration of 0.2 ppm.

The predicted annual mean of hourly NO_2 overestimates that measured. A conservative prediction errs on the side of caution but may result in unnecessary monitoring. The predicted annual maximum and 95th%ile of hourly NO_2 concentrations lie within ±50% of the measured, as does the regulatory 99.8th%ile (equivalent to no more than 18 exceedances per annum: 18/[365*24]=0.2%). As predicted by the model, NO_2 concentrations measured at this site are just below the Lower Assessment Threshold of 51 ppb (99.8th%ile), even with conservative background concentrations of NO and NO_2.

Conclusions

CO background concentration can be calculated after modelling (using a background concentration of 0 ppm CO) from the difference between the means of hourly measurements and predictions. CALINE4 then overpredicts CO concentrations under unstable or neutral conditions, but underpredicts CO concentrations when conditions are stable.

CO concentrations decrease during the hours of unstable or neutral conditions (from 09:00 to 16:00) despite relatively high volumes of traffic.

The predicted peaks coincide with the morning and evening traffic peaks, but the model cannot predict the high CO and NO_2 concentrations observed after 20:00, which may be due to stable conditions rather than the immediate traffic source, and also due to photochemical effects in the case of NO_2.

The model cannot predict the high concentrations observed for north easterly winds since they are not due to the roadway source. North easterly winds rarely occur but frequently coincide with very low wind speeds and stable conditions.

Higher concentrations are predicted for near parallel wind directions than for cross winds, due to the larger area of roadway over which the traffic is "upwind" of the receptor and the longer passing time during which pollutants can be emitted.

The accuracy of predictions is highly dependent on the background concentration assumed.

CALINE4 predictions for comparison with the regulatory limit values (annual maximum eight-hour running mean for CO and 99.8th%ile for NO_2) were within ±50% of the measured values.

Acknowledgements

The Environmental RTDI Programme 2000-2006 of the National Development Plan has funded this project through the Irish Environmental Protection Agency (EPA). Frank McGovern (EPA), Fingal County Council, Derek Brady (NRA), Ben O'Donnell (Met Eireann) and Anne Desmond (TCD).

References

Benson P.E. (1984): CALINE4 – A Dispersion Model For Predicting Air Pollutant Concentrations Near Roadways, Report No. FHWA/CA/TL-84/15, November 1984 (Revised November 1986, June 1989).

CEC (1996): Council Directive 96/62/EC of 27 September 1996 on ambient air quality assessment and management (Air Quality Framework Directive), O.J.E.C. L 296/55 21.11.1996, p 55.

CEC (1999): Council Directive 1999/30/EC of 22 April 1999 relating to limit values for sulphur dioxide, nitrogen dioxide and oxides of nitrogen, particulate matter and lead in ambient air, O.J.E.C. L 163/41 26.6.1999, p 41.

CEC (2000): Council Directive 2000/69/EC of the European Parliament and of the Council of 16 November 2000 relating to limit values for benzene and carbon monoxide in ambient air, O.J.E.C. L 313/12 13.12.2000, p 12.

UK DETR (2001): "Review and Assessment: Selection and Use of Dispersion Models" UK DETR LAQM.TG3(00) Chapter 7 Section 7.22.

12th International Symposium "Transport and Air Pollution" / 12e Colloque international "Transports et pollution de l'air", Avignon, 16 -18 *June* / juin 2003
proceedings / actes, n°92, tome / Vol. 2, Inrets ed., Arcueil, France, 2003, p. 75-79

Application of the Lagrangian dispersion model GRAL to assess the air quality in the city of Graz

Dietmar Oettl, Peter Sturm & Raimund Almbauer
Graz University of Technology, Inffeldgasse 25, 8010 Graz, Austria -
Fax +43 316 873 8081 - email : oettl@vkmb.tu-graz.ac.at

Abstract
In a comprehensive environmental assessment study, the air quality in the city of Graz was investigated using a network of air quality monitoring stations as well as passive samplers, and by applying the Lagrangian dispersion model GRAL. The dispersion model has a special treatment of low wind speed conditions and is therefore well suited for areas with frequent calm wind conditions. Both the observations and simulations reveal that the annual mean concentrations of NO_2 exceed 40 µg/m³ (EU daughter directive 99/30/EC) in large parts of the city. Maximum daily mean concentrations of PM10 were recorded higher than 150 µg/m³. Good agreement was found between observed and modelled NO_2 concentrations, while the model suggests a share of 20-30 % of primary emitted PM10 by vehicles on the total observed PM10 concentrations. Predictions of future NO_2 concentrations levels suggest that 40 µg/m³ will only be exceeded in the vicinity of major streets due to improvements in the vehicle's emissions.
Keys-words*: environmental assessment study, GRAL, air quality, EU daughter directive.*

Introduction

The city of Graz, the second largest city in Austria, situated in a basin south of the Alps, suffers from bad air quality due to frequent low wind speed conditions. For instance, wind speeds below 1.5 m s^{-1} prevail for more than 85 % of the year. Especially in the south of Graz, traffic increases fast due to new companies and shopping centres. In addition, the A2, a major highway, passes this part of the city owing a mean daily traffic of 55,000 vehicles with a 12 % share of heavy duty vehicles. As there exist many residential areas in this part of the city, it was necessary in the frame of an environmental assessment study to investigate the current and future air quality due to traffic emissions.

1 - Method

Based on traffic prognoses for the current state and a future scenario in 2015, the traffic emissions and subsequently the impact on air quality was assessed. Due to the frequent calm wind situations, it was decided to apply the Lagrangian dispersion model (LDM) GRAL, which has a special treatment of low wind speed conditions. In contrast to other LDMs assuming an exponential Lagrangian autocorrelation function in the Langevin equation, autocorrelation functions with a negative lobe are simulated with GRAL for low wind speed conditions. Such peculiar autocorrelation functions were reported by different authors (e.g. Hanna, 1983 or Frenkiel, 1953), but used for the first time in GRAL (Oettl et al., 2001) for dispersion modelling. GRAL uses a time-step probability density function (PDF) with uniform distribution (Wang and Stock, 1992) in the Langevin equations for the horizontal wind components. This means that random time-steps and a negative intercorrelation parameter for the horizontal wind components are used.

$$u'(t+\Delta t_h) = \rho_u \cdot u'(t) + \sigma_u \cdot \sqrt{1-\rho_u^{\,2}} \cdot \chi \qquad (1)$$

$$v'(t+\Delta t_h) = \rho_v \cdot v'(t) + \sigma_v \cdot \sqrt{1-\rho_v^{\,2}} \cdot \chi \tag{2}$$

$$x(t+\Delta t_h) = x(t) + (\bar{u} + u''(t+\Delta t_h)) \cdot \Delta t_h \tag{3}$$

$$y(t+\Delta t_h) = y(t) + (\bar{v} + v''(t+\Delta t_h)) \cdot \Delta t_h \tag{4}$$

Here, u' and v' are the velocity fluctuations for the along and cross-wind component, σ_u and σ_v are the standard deviations of the wind velocity components, χ are random numbers with zero mean and a standard deviation equal to one and a Gaussian probability density function (p.d.f.), ρ_u and ρ_v are the so-called intercorrelation parameters, Δt_h is a random time-step, for which the horizontal velocity fluctuations remain constant, $\bar{u}$ and $\bar{v}$ are the mean Eulerian velocities in *x* and *y* direction, and u'' and v'' are the velocity fluctuations obtained by transformation of the along and cross-wind components (eq.(1) and (2)) in the *x* and *y* direction.

For $\rho_{u,v} \geq 0.9$, eq. (1) and eq. (2) are identical with the classical Langevin equation without drift correction (Wang and Stock, 1992), which satisfies the well-mixed criterion (Thomson, 1987) in one-dimensional, stationary and homogenous turbulence.

For negative intercorrelation parameters the autocorrelation functions of eq. (1)-(2) get a negative lobe (see Fig. 10 in Wang and Stock, 1992). It was shown that a negative lobe in the Lagrangian autocorrelation function results in larger plume spreads compared to the classical approach, where an exponential decrease of the autocorrelation function is assumed (Oettl et al., 2001), and hence lower concentrations result in the vicinity of pollutant sources.

The investigated area covers approximately 45 km². In order to be able to assess the air quality close to the streets a resolution of 20x20 m² was used in the model. The street network comprises all major streets with a total length of 68 km. Roads were segmented into more than 1100 parts to account for changes in traffic flow, street orientation, driving conditions or other features (e.g. noise abatement barriers, dams, etc.).

Meteorological data were recorded with a sonic anemometer mounted on a 10 m high mast and a device observing the differences between solar incoming and terrestrial outgoing irradiation. The latter was used to derive stability classes according to Austrian standards. For convenience, homogenous wind and turbulence conditions were assumed in the horizontal to be able to apply a classification scheme for the wind speed, wind direction, and stability class. This resulted in a time-series of classified meteorological conditions. To account for the daily variability of traffic emissions, an average cycle for the traffic flow was assumed for all streets as a first approximation.

Emissions for passenger cars (PC) were computed according to the Austrian handbook of emission factors (Ministry for environment, youth, and family - Austria, 1997), while emissions for heavy duty vehicles were estimated utilizing new emissions factors derived recently in course of the ARTEMIS project (Hausberger, 2002).

Conversion rates from NO to NO_2 were computed with an empirical relationship between NO_x and NO_2 as given in Romberg et al. (1996).

2 – Results

In Austria there exist air quality standards for the annual mean NO_2-concentrations and the half-hourly maximum NO_2-concentration. Figure 1 depicts a comparison between observed and predicted annual mean NO_2-concentrations. As can be seen in most cases the predictions are within +/- 15 % of the observations. At two passive sampler sites the model overestimates concentrations by 30 %. As expected, the model is not able to predict the maximum half-hourly NO_2-concentration with equal quality (Figure 2). This can be reasoned with large uncertainties regarding the possible influences leading to peak NO_2-concentrations. These are for instance, the conversion rate from NO to NO_2 or peaks in traffic emissions due to e.g. hold ups, etc. Especially, at one site GRAL

overestimates the peak concentration by more than 50 %.

Both observations and simulations reveal, that the threshold value for the annual mean NO_2-concentrations of 40 μg/m³ as proposed in the EU-daughter directive (99/30/EC) is exceeded at certain sites. There is also an exceedence of the national threshold value for peak NO_2-concentrations, which is 200 μg/m³.

The spatial distribution annual mean NO_2-concentrations as modelled with GRAL is shown in Figure 3. The numbers indicate the sampling sites for NO_2. As can be seen 40 μg/m³ are exceeded in most parts of the investigated area. Especially the highway is the major source for air pollution in this region. It was also interesting to note, that east of the highway intersection concentrations are significant lower than west of the intersection. Most probably this is due to the construction of the highway on a 5 m high dam east of the intersection.

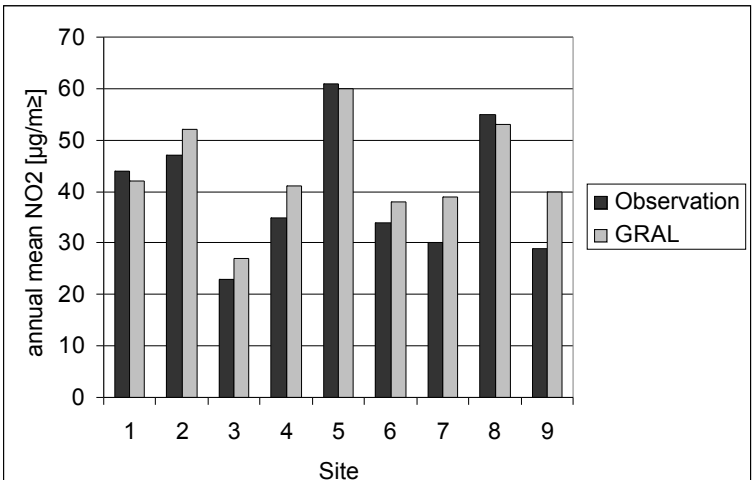

Figure 1: Comparison of observed vs. predicted annual mean NO_2-concentrations.

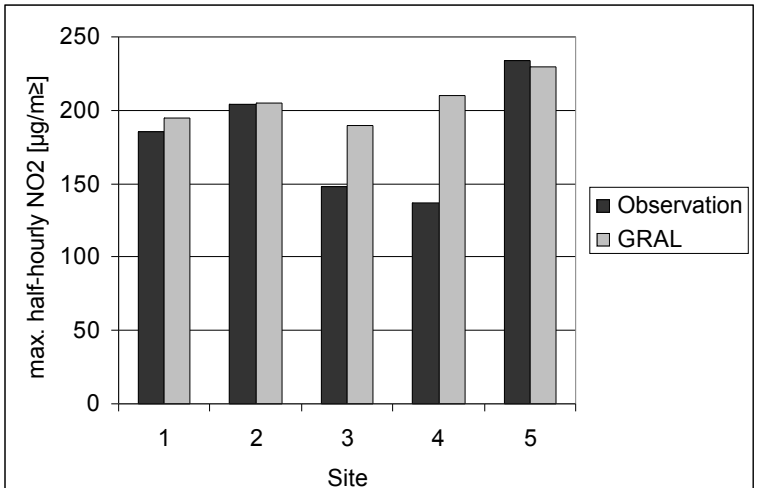

Figure 2: Comparison of observed vs. predicted maximum half-hourly NO_2-concentrations.

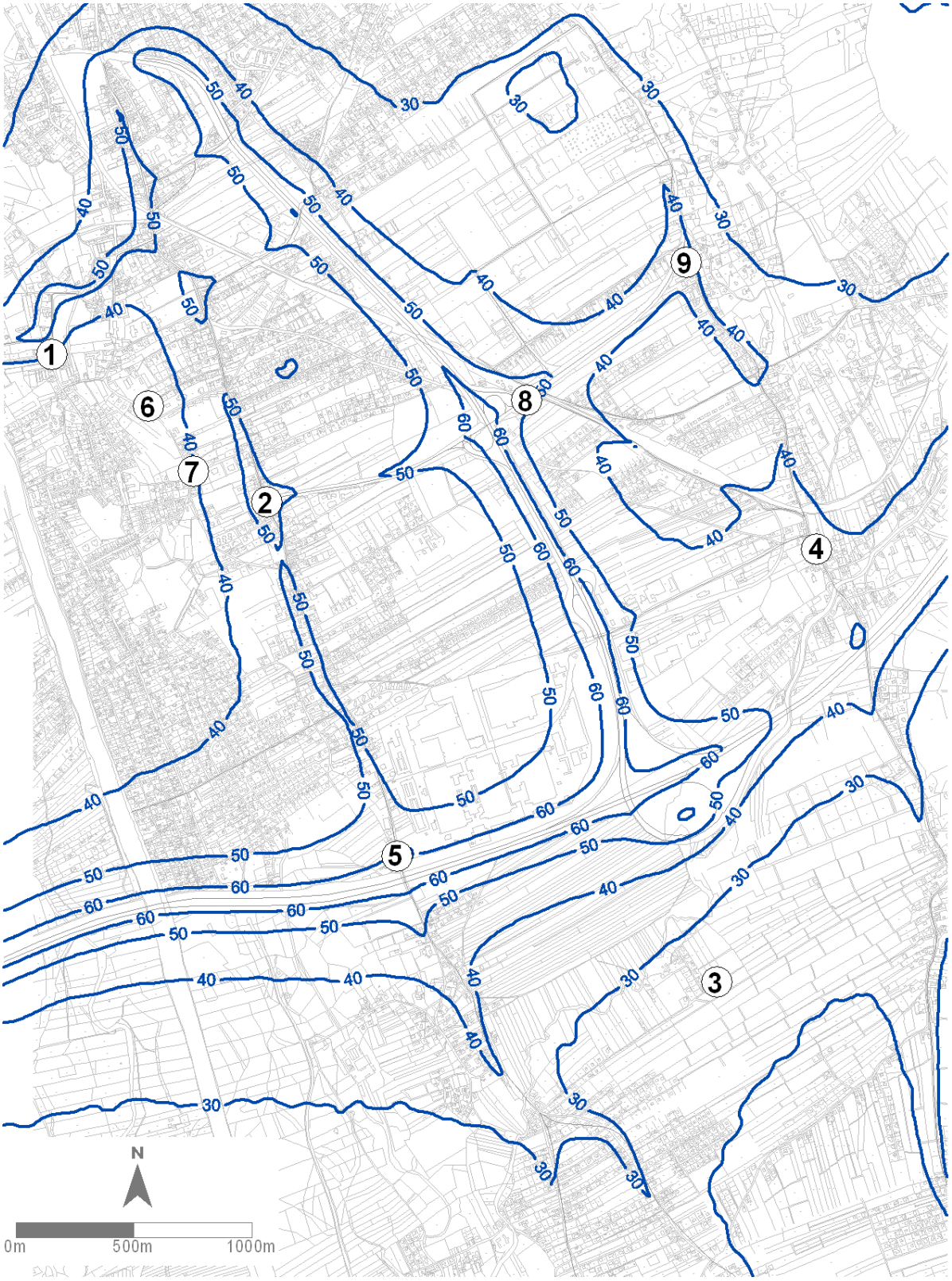

Figure 3: Modelled annual mean NO_2-concentrations for the present state in the south part of the city of Graz (air quality monitoring stations correspond to numbers 1-5, and passive sampler sites correspond to numbers 6-9).

While the model suggests, that the total observed NO_2-concentrations result from local traffic, simulations for PM10 reveal, that the share of primary emitted PM by the local traffic on the total observed PM10-concentrations is only between 20 – 30 %. Currently, there is large uncertainty concerning the possible formation of secondary PM10 due to chemical processes. Thus, no assessment for secondary PM10 was performed in this study.

Simulations for the year 2015 based on possible future traffic scenarios in the region and taking into account new emission standards for vehicles coming up 2005 (EURO 4) and 2008 (EURO 5) suggest, that the annual mean NO_2-concentrations exceed 40 $\mu g/m^3$ only close to the highway. However, the national threshold value for annual mean NO_2-concentrations, set to 30 $\mu g/m^3$ with beginning of 2012, will be exceeded in several residential areas, which certainly needs a careful discussion on possible future economical growth and traffic related strategies in this area.

Conclusions

Traffic related air pollution, especially in cities with considerable economical growth, is an important issue for establishing strategies for street traffic. Most critical seem to be NO_2 and PM10 with respect to a possible exceedence of national or European wide air quality guidelines. It was shown in this study, that sophisticated traffic, emission, and dispersion models are necessary to adequately support the development of traffic plans. Here, the Lagrangian dispersion model GRAL was applied, as the city of Graz faces frequent low wind speed conditions, which need a special treatment. Furthermore, the Lagrangian approach allows for a very detailed resolution of the concentration patterns, which is essential close to streets.

While NO_2-concentrations could be captured reasonably well by the modelling system (traffic, emissions, dispersion, meteorology), there is currently no practical approach available to model e.g. the secondary formation of PM10 from vehicle exhausts. Here, future research is strongly needed to be able to provide reasonable answers for city planners.

References

Frenkiel, F.N. (1953): Turbulent diffusion: mean concentration distribution in a flow field of homogeneous turbulence. Adv. Appl. Mech, vol. 3, p 61-107.

Hanna, S. R. (1983): Lateral turbulence intensity and plume meandering during stable conditions. J. of Appl. Meteor., vol. 22, P 1424-1430.

Hausberger, S. (2002): Simulation of Real Wordl Vehicle Exhaust Emissions. Habilitationsschrift, Graz University of Technology, ISBN , pp 144.

Ministry for environment, youth, and family - Austria (1997): Handbook of emission factors for road traffic - version 1.1A, Vienna.

Oettl D., Almbauer R., Sturm P. J. (2001): A new method to estimate diffusion in low wind, stable conditions. Journal of Applied Meteorology, vol. 40, p 259-268.

Romberg E., Bösinger R., Lohmeyer A., Ruhnke R., Röth E. (1996): NO-NO2-Umwandlung für die Anwendung bei Immissionsprognosen für Kfz-Abgase. Gefahrstoffe-Reinhaltung der Luft, vol. 56, p 215-218.

Thomson, D. J. (1987): Criteria for the selection of stochastic models of particle trajectories in turbulent flows. J. Fluid Mech., vol. 180, p 529-556.

Wang, L.-P., and Stock D.E. (1992): Stochastic Trajectory Models for Turbulent Diffusion: Monte-Carlo Process versus Markov Chains. Atmospheric Environment, vol. 9, p 1599-1607.

12th International Symposium "Transport and Air Pollution" / 12e Colloque international "Transports et pollution de l'air", Avignon, 16 -18 *June* / juin 2003
proceedings / actes, n°92, tome / Vol. 2, Inrets ed., Arcueil, France, 2003, p. 81-86

Transport routier et pollution de l'air : cartographie nationale de la pollution par l'ozone en France

Erwann Fangeat*, Souad Bouallala*, Christian Elichegaray*, Nicolas Jeannée, Mohamedou Ba*** & Joelle Colosio***
* ADEME, 27, rue Louis Vicat, 75015 Paris
** Géovariances, 49bis av. Franklin Roosevelt, BP 91, 77212 Avon Cedex
*** IFEN, 61 bd Alexandre Martin, 45058 ORLEANS

Résumé
L'automobile, par ses rejets de précurseurs (COV et NOx notamment), contribue fortement à la production de l'ozone. La surveillance de ce polluant est assurée en France par un dispositif qui en 2003 comportait 415 sites fixes de mesure gérés par 40 Associations Agréées de Surveillance de la Qualité de l'Air (AASQA). Les données de l'ensemble de ces stations sont collectées au sein d'une base nationale des données de qualité de l'air (BDQA), gérée par l'ADEME et qui permet de faire un bilan de l'ozone en France sur les dix dernières années ainsi qu'une cartographie nationale en utilisant des méthodes géostatistiques.
Mots-clefs : *ozone, pollution photochimique, qualité de l'air, cartographie, géostatistique*

Abstract
Road transport and air pollution: national cartography of pollution by ozone in France
Photochemical pollution designates a complex mixture of pollutants formed chemically in the air, by the effects of ultra-violet solar radiation, from various precursor compounds emitted particularly by natural sources and human activities: nitrogen oxides, volatile organic compounds, carbon monoxide. Motor traffic is thus one of the main causes of emission of ozone precursors in France. Like other European countries, France is regularly subject to episodes of photochemical pollution manifested by high levels of ozone in the troposphere. Ozone constitutes one of the priorities of the CAFE (Clean Air For Europe) programme for the preservation of air quality in Europe, leading in particular to stricter statutory thresholds. Ozone surveillance is carried out in France by a system which in 2003 consisted of 415 fixed measuring sites operated by 40 Approved Associations for Surveillance of Air Quality (AASAQ). The paper will present work in France on ozone from the air-quality data base (AQDB), managed by ADEME, and will be based on an evaluation of exceedance of statutory thresholds, and an evaluation of the last 10 years. An innovative method of ozone-pollution mapping on a national scale, based on annual averages of the ATMO network, assisted by geostatistical methods, will also be presented. Geostatistics is regularly used nowadays to map atmospheric pollution at a local and regional level, particularly within the AASAQ. The value of geostatistics lies in its capacity to refine the pollutant mapping by taking into account auxiliary information (cofactors) linked to the pollutant concentration, thus partially compensating for locally poor coverage of the territory by the fixed measuring stations. In the case of ozone, these different cofactors are: the altitude, the typology of the station or the land use, using Corine Land Cover managed by IFEN.
Keys-words*: surveillance, air quality, photochemical pollution, ozone, ATMO network, geostatistics, cokriging, co-factor, mapping, exposure.*

Introduction

La pollution photochimique désigne un mélange complexe de polluants formés chimiquement dans

l'air, sous l'effet du rayonnement solaire ultra violet, à partir de divers composés précurseurs émis notamment par des sources naturelles et les activités humaines : oxydes d'azote, composés organiques volatils, monoxyde de carbone. Le trafic automobile est ainsi l'un des principaux responsables des émissions des précurseurs de l'ozone en France. L'ozone et les polluants photochimiques présentent des risques pour la santé de l'homme, et peuvent contribuer à l'apparition de dommages sur la végétation et les matériaux. Enfin, l'ozone contribue à l'accroissement de l'effet de serre car ce gaz absorbe en partie la chaleur rayonnée par les sols. Il constitue l'une des priorités du programme CAFE (Clean Air For Europe) en matière de préservation de la qualité de l'air en Europe entraînant notamment une sévérisation des seuils réglementaires. La réglementation actuelle comporte un seuil d'information du public lorsque les niveaux d'ozone dépassent 180 micro grammes par mètre cube d'air en moyenne horaire, et un seuil d'alerte lorsque les niveaux dépassent 360 micro grammes par mètre cube d'air en moyenne horaire.

1 – Bilan de l'ozone en France

La surveillance de l'ozone est assurée en France par un dispositif qui début 2003 comportait 415 sites fixes de mesure gérés par 40 Associations Agréées de Surveillance de la Qualité de l'Air (AASQA). Cette surveillance de terrain est complétée par des outils de modélisation numérique qui permettent de réaliser des prévisions à court terme des épisodes de pollution photochimique. La surveillance de l'ozone permet l'acquisition d'un grand nombre de données, archivées au sein des AASQA et dans une base de données de la qualité de l'air, gérée par l'ADEME, utiles notamment pour l'analyse, sur un historique de 10 ans, des épisodes de pollution mais aussi de la pollution de fond.

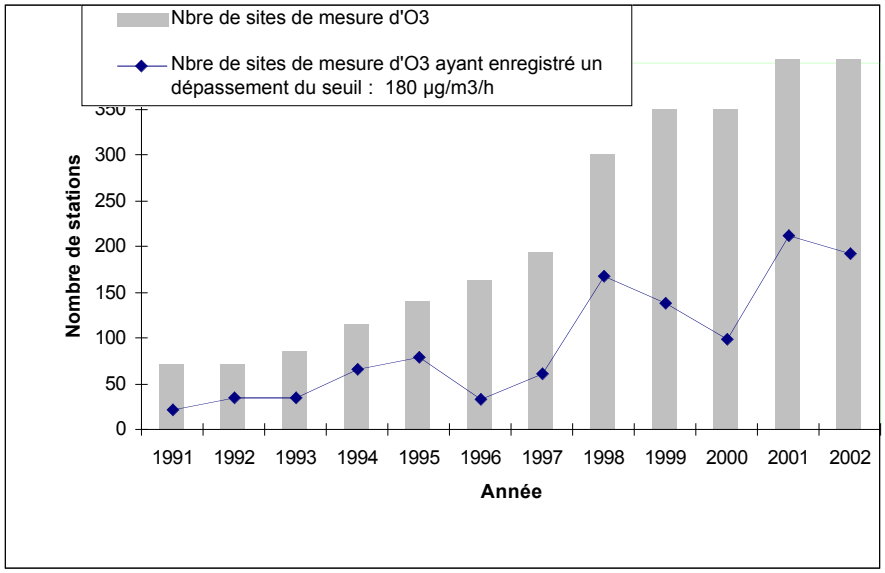

Figure 1 : Nombre de sites mesurant l'ozone et nombre de sites ayant enregistré un dépassement du seuil 180µg/m3

Figure 1 : Number of ozone station with an exceedance of the 180µg/m^3 threshold

Comme d'autres pays, la France est régulièrement soumise à des épisodes de pollution photochimique se traduisant par des niveaux élevés d'ozone dans la troposphère. L'amplitude, la durée, et l'extension spatiale des phénomènes de pollution photochimique dépendent largement des situations météorologiques, et notamment de l'ensoleillement et de la nébulosité. La climatologie de l'ozone est donc très variable d'une année à l'autre, indépendamment des fluctuations qui peuvent être liées par ailleurs aux variations des émissions de polluants par les activités humaines (transport notamment) ou les sources naturelles (les forêts émettent en particulier des composés organiques qui concourent à la production d'ozone).

Une évolution de 1991 à 2002 des épisodes de pollution photochimique est présentée en figure 1.

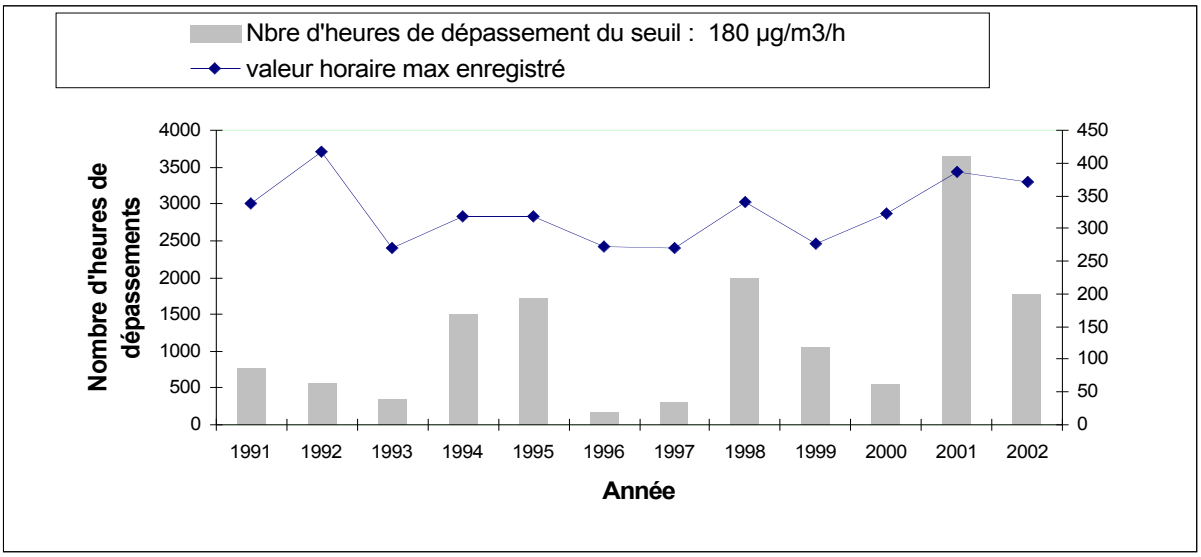

Figure 2 : Nombre d'heure de dépassement du seuil 180µg/m3 et maximum horaire enregistré
Figure 2 : Number of hour concerned by exceedances of the 180µg/m^3 threshold and hourly maximum data

Parmi les 415 sites de mesure, 37 stations ont un historique de plus de 11 ans et montrent une légère tendance à la hausse des médianes des moyennes annuelles, alors que les autres indicateurs statistiques ne présentent pas d'évolution significative sur la période 1991-2002 (figure 3).

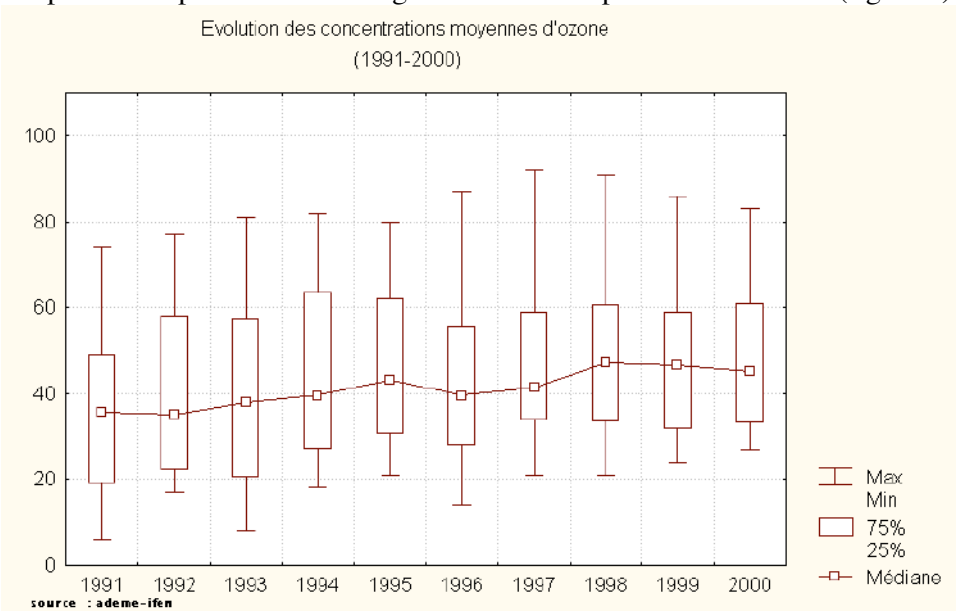

Figure 3 : Distributions de moyennes arithmétiques annuelles d'ozone sur 37 stations du territoire (en microg/m3) ayant 11 ans de mesures continues.
Figure 3: Distribution of ozone arithmetic mean over 37 stations with 11 years of measure

Les concentrations en ozone de fond ont tendance à augmenter alors qu'il y a une grande variabilité sur les valeurs plus élevées, l'ozone étant très dépendant des conditions météorologiques rencontrées d'une année à l'autre.

2 – Cartographie nationale des moyennes annuelles en 2001

La géostatistique est aujourd'hui régulièrement utilisée pour cartographier des pollutions atmosphériques au niveau local et régional, notamment au sein des AASQA. Son intérêt dans le cas présent repose sur la capacité des techniques géostatistiques à :

affiner la cartographie du polluant en prenant en compte des variables auxiliaires liées à la concentration en polluant, palliant ainsi une couverture localement pauvre du territoire par les stations de mesure ;

prendre en compte, lors de la cartographie, les différentes échelles de structuration spatiale de la pollution : localisée, régionale voire nationale

fournir, en plus de l'estimation des concentrations en polluants une carte d'incertitude liée à cette estimation (écart-types de krigeage).

Dans cette étude, seules les stations urbaines, périurbaines et rurales régionales et nationales, constituant 291 stations de fond, ont été utilisées, les autres stations de proximité n'ayant pas à rentrer en compte pour une cartographie de la pollution annuelle de fond en ozone.

Afin de bien cartographier la pollution par l'ozone en utilisant les données issues des stations du réseau ATMO, la recherche de cofacteurs liés à cette pollution est très importante. Les différents cofacteurs utilisés pour affiner la cartographie ont été l'altitude ainsi que 5 postes de la base Corine Land Cover (CLC), gérée par l'IFEN (sur les 44 possibles), en raison de leurs liens potentiels avec la physico-chimie de l'ozone. Ces 5 postes sont les suivants :

111 : tissu urbain continu ; 112 : tissu urbain discontinu ; 121 : zones industrielles et commerciales ; 122 : réseaux routier et ferroviaire et espaces associés ; 312 : forêt de conifères.

Plusieurs combinaisons des cofacteurs ont été envisagées. Nous discutons ici les résultats obtenus à partir d'une régression linéaire multiple, qui vise à expliquer au mieux les concentrations d'ozone observées à partir des cofacteurs.

Cette combinaison linéaire des cofacteurs, explicable physiquement, présente une corrélation non négligeable avec les concentrations en ozone.

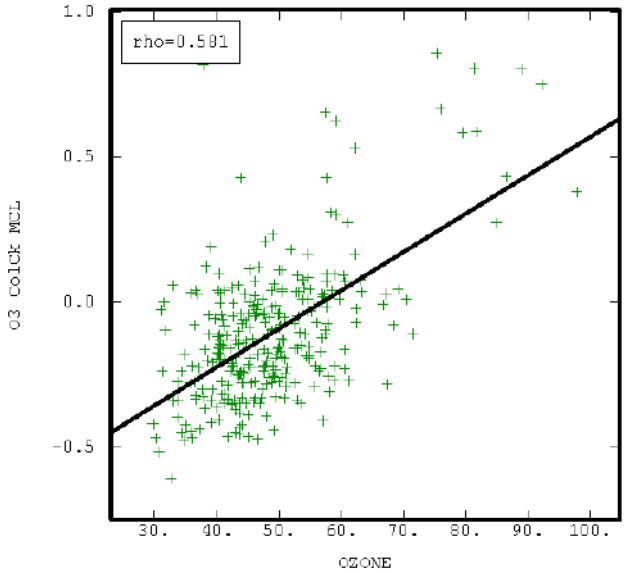

Figure 4 : Nuage de corrélation entre concentration en ozone et la combinaison linéaire des cofacteurs issue de la régression linéaire multiple.

Figure 4: Scatter diagram between ozone concentrations and the linear combination of cofactors obtained through a multilinear regression.

A l'issue de cette réflexion sur les données, plusieurs techniques de cartographie ont été proposées, tout d'abord à partir des concentrations en ozone seules :

une interpolation classique par inverse des distances quadratiques (IDQ), technique rapide servant de référence par rapport aux techniques géostatistiques,

un krigeage ordinaire, obtenu grâce à une modélisation de la structure spatiale des concentrations en ozone ; ce krigeage donne accès aux écart-types de krigeage, qui permettent la reconnaissance qualitative des zones du territoire qui sont sous-échantillonnées, l'estimation des concentrations y étant par conséquent de moins bonne qualité.

L'intégration des cofacteurs a ensuite été envisagée par différents cokrigeages colocalisés avec : l'altitude moyenne, un facteur issu d'une analyse en composantes principales, la combinaison linéaire des cofacteurs conduisant à la meilleure corrélation avec les concentrations en ozone et enfin l'ozone provenant des stations rurales, ajouté au krigeage des résidus urbains.

Ces techniques conduisent à une amélioration de la qualité de l'estimation, les écart-types obtenus étant inférieurs à ceux obtenus lors du krigeage ordinaire. L'importance relative donnée aux différents cofacteurs varie selon la technique.

Finalement, dix jeux de validation ont été choisis aléatoirement afin d'évaluer la qualité des différentes cartographies. Les erreurs quadratiques moyennes entre concentrations vraies (aux points de validation) et estimées, calculées pour chaque jeu de validation et chaque technique d'estimation, montrent des résultats significativement meilleurs pour le cokrigeage colocalisé des concentrations en ozone avec la meilleure combinaison linéaire.

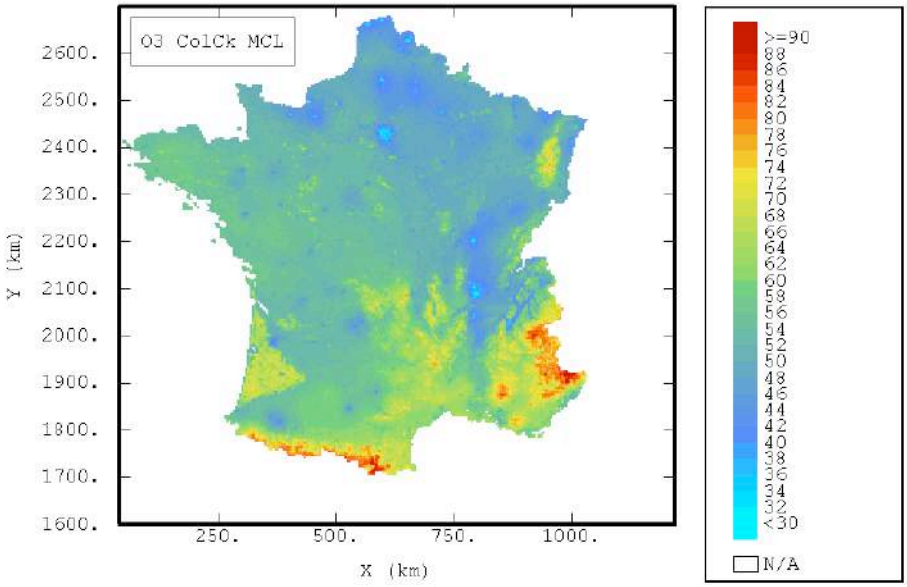

Figure 5 : Estimation de la concentration moyenne annuelle (2001) en ozone par cokrigeage colocalisé avec la meilleure combinaison linéaire de l'altitude moyenne et des postes CLC.

Figure 5: Estimation of the ozone mean concentration over 2001, obtained by colocated cokriging with the best linear combination of the cofactors.

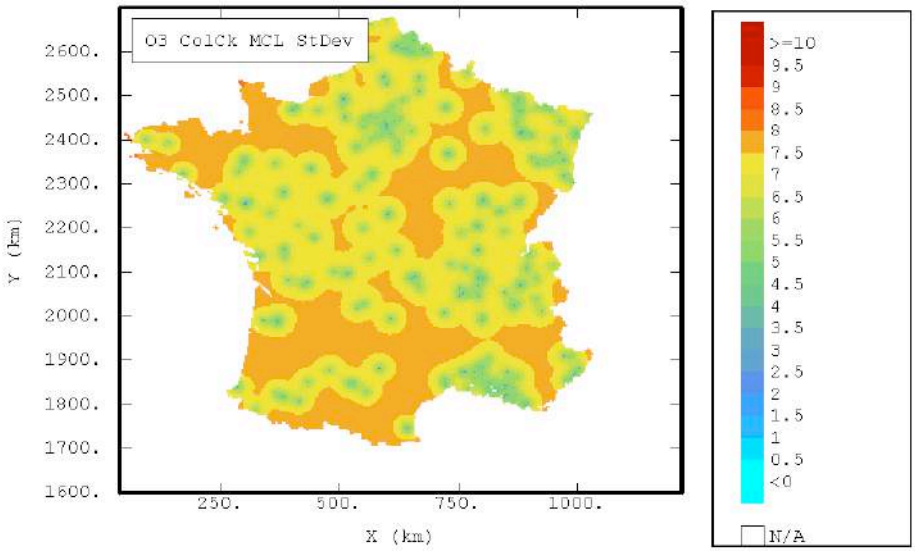

Figure 6 : Ecart-types de l'erreur de cokrigeage colocalisé de la CMA en ozone avec la meilleure combinaison linéaire (postes CLC et altitude moyenne).

Figure 6: Standard deviation of the error of colocated cokriging of mean ozone concentrations with the best linear combination of the cofactors.

Conclusion

Ce bilan sur l'ozone en France souligne toute l'importance que doivent avoir des programmes de préservation de la qualité de l'air comme CAFE afin de diminuer les niveaux rencontrés sur nos régions. Les dépassements du seuil réglementaire de 180 $\mu g/m^3$ en moyenne horaire restent très dépendants des situations météorologiques rencontrées alors que les niveaux de fond semblent avoir tendance à augmenter sur ces dix dernières années, l'ozone contribuant à l'accroissement de l'effet de serre.

Le travail effectué sur la cartographie des concentrations moyennes d'ozone en France permet de conclure au réel intérêt des techniques géostatistiques multivariables, qui permettent de combiner de façon pertinente les différents cofacteurs disponibles. L'utilisation de l'altitude semble incontournable, mais est surpassée dans certains cas par les techniques combinant altitude et postes CLC. La technique la plus satisfaisante semble être la recherche de la meilleure combinaison linéaire et son utilisation par cokrigeage colocalisé. Néanmoins, le choix selon des critères statistiques d'une méthode de cartographie ne doit pas devancer l'avis de l'expert : en effet, la cartographie des concentrations moyennes annuelles en ozone doit avant tout être physiquement plausible et réaliste.

Ce travail de cartographie permet ainsi de dénombrer les populations soumises à des seuils pour une évaluation des risques sanitaires et peut servir également d'outil d'aide à la décision en matière de gestion de la qualité de l'air.

Références

Ozone et propriétés oxydantes de la troposphère. Rapport n° 30 de l'Académie des sciences. Editions Lavoisier Tec&Doc – 1993

Fangeat, Jeannée, Ba : cartographie nationale de la pollution par l'ozone en France, contrat ADEME n° 0262031

Elichegaray, Colosio, Fangeat : la pollution photochimique en France : le climat de l'ozone en 2001 et sur la période 1991-2001 – bilan des dépassements du seuil d'information réglementaire. Pollution Atmosphérique n° 176 octobre-décembre 2002, p515-526.

12th International Symposium "Transport and Air Pollution" / 12e Colloque international "Transports et pollution de l'air", Avignon, 16 -18 *June* / juin 2003
proceedings / actes, n°92, tome / Vol. 2, Inrets ed., Arcueil, France, 2003, p. 87-92

Pour une méthodologie de la cartographie de la pollution de l'air intégrant l'essentiel des facteurs explicatifs.

Gilles Perron[1], Ahmed Hamadouche[1], Jacques Deraisme[2]
[1]Association pour la Surveillance et l'Etude de la Pollution Atmosphérique en Alsace, 5 rue de Madrid 67309 SCHILTIGHEIM
[2]Géovariances, 49bis av. Franklin Roosevelt, BP 91, 77212 AVON Cedex

Résumé
Le krigeage, méthode d'interpolation géostatistique, propose une solution simple et optimale pour fournir une carte des valeurs spatialisées ou champs de pollution à partir de mesures ponctuelles. Les informations à prendre en compte sont nombreuses et concernent les émissions, l'occupation du sol ou des variables d'environnement. Les techniques de krigeage avec dérive externe prennent en compte ces cofacteurs en les considérant comme liés linéairement à la dérive de la pollution. En combinant les techniques statistiques d'analyse multivariable au krigeage avec dérive externe, on aboutit à une méthodologie pertinente et opérationnelle. La démarche se déroule en trois temps. Une analyse en composantes principales de l'ensemble des cofacteurs permet de retenir un nombre limité de facteurs restituant au moins 80% de la variance.
La deuxième étape est une régression linéaire multiple entre un polluant donné et les facteurs précédents. Cette opération combinée à un test itératif de Student conduit à sélectionner les variables auxiliaires les plus significatives d'un point de vue statistique. Les cofacteurs ainsi sélectionnés peuvent varier selon le polluant considéré. La dernière étape consiste en un krigeage avec dérive externe à partir des mesures de pollution.
Mots-clés : *qualité de l'air, tubes à diffusion, krigeage avec dérive externe, analyse en composantes principales, régression linéaire multiple.*

Abstract

For a methodology of air-pollution mapping integrating the essential points of the explicative factors.
A map of pollution values based on selective and dispersed measurements must verify the two criteria of accuracy and precision. The method of geostatistical interpolation, called kriging, offers a simple and optimal solution. The kriging variance then serves as an indicator of the quality of the estimation. However, if further reduction in the kriging variance is desired, more information must be supplied. Before proceeding with a new measurement campaign, it is therefore natural to first consider using the information which indirectly influences the spatial distribution of pollution. This information is relatively plentiful and also concerns emissions, land use or environmental factors such as topography or meteorology.
Kriging techniques with external drift take these co-factors into account by considering them as linearily linked to the pollution trend. However, the number of drift functions needs to be limited, or the usefulness of kriging is reduced until it becomes no more than a classical linear regression. By combining the statistical techniques of multi-variable analysis with kriging with external drift, a pertinent and operational methodology is obtained. The procedure thus takes place in three steps. Firstly, an analysis into principal components of all the co-factors makes it possible to retain a limited number of factors so that at least 80% of the variance is kept.
The second stage (step) consists of a multiple linear regression between a given pollutant and the previous factors. By applying iteratively a Student test the signification of each factor of the

elaborated variable can be determined, then only the co-factors having a significant ratio to the variable are retained. The remaining co-factors change from one element of pollution to another.
The final stage (step) is then kriging with external drift based on pollution measurements. This methodology applied to mapping of NO_2 and C_6H_6 for the Mulhouse urban area gave encouraging results for data obtained from a measurement campaign using passive diffusion tubes.
Key words: *air quality, passive samplers, kriging with external drift, principal components analysis, multiple linear regressions.*

Introduction

En France la loi sur l'air du 30 décembre 1996 et ses textes d'application recommandent de connaître la qualité de l'air en tout point du territoire. Cette connaissance de la qualité de l'air en tout point d'une région donnée, c'est-à-dire en dehors de sites instrumentés, implique le recours à une méthode de spatialisation des données performante et adaptée. Une utilisation rationnelle et objective de l'ensemble des paramètres qui influent sur la diffusion du polluant constitue un enjeu de première importance.

1 - Krigeage ordinaire

Le krigeage ordinaire est un interpolateur linéaire qui prend en compte les corrélations spatiales dans la pondération des données. En ce qui concerne la pollution par le dioxyde d'azote (NO_2), l'analyse des données et particulièrement le variogramme montre que la pollution mesurée en un point a une influence jusqu'à une distance de plusieurs kilomètres.

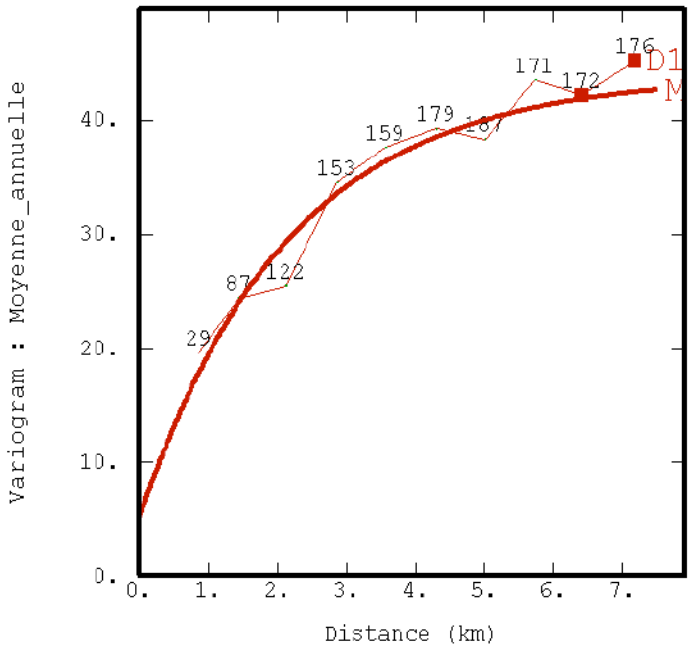

Figure 1 : Experimental variogram of the NO_2 concentration and fitting by a model (model fitting).
Figure 1 : Variogramme expérimental de la concentration en NO_2 et ajustement d'un modèle.

2 - Krigeage avec dérive externe

Le modèle précédent considère que la pollution est un phénomène stationnaire de moyenne constante. Cette représentation du phénomène est légitime dans la mesure où l'interpolation à proximité d'un site sera fortement attirée par la valeur mesurée en ce point. La carte obtenue reflétera les variations des niveaux de pollution dans la zone considérée. Toutefois le krigeage en un point plus éloigné des données se rapprochera de la moyenne générale des données. Ceci est

critiquable et peut être améliorée par l'introduction d'autres informations qui ont un lien direct ou indirect avec la pollution. C'est ce qu'il est possible de réaliser en adoptant un modèle différent, cette fois non stationnaire, qui considère que la pollution peut être représentée par la somme d'une fonction de dérive et d'un résidu stationnaire. La géostatistique fournit une réponse rigoureuse à l'interpolation d'une telle variable, appelée krigeage avec dérive externe. L'application de cette technique requiert toutefois que la dérive de la variable pollution soit une fonction linéaire des variables dérives externes.

Une première tentative consiste à choisir empiriquement les paramètres, ou co-facteurs, les plus significatifs, c'est à dire ceux dont on pense qu'ils influent prioritairement le phénomène de pollution. Cette démarche heuristique n'est validée que par le résultat final sur la qualité des cartes obtenues et nullement par une recherche rigoureuse et objective de ces co-facteurs.

La comparaison des cartes obtenues avec les 2 modèles (stationnaire et non stationnaire avec 2 dérives externes liées à la densité de population et aux émissions de NOx) montre que le second rend mieux compte de l'influence de paramètres externes, en particulier aux abords des principaux axes routiers qui sont à l'origine d'importantes émissions en polluants.

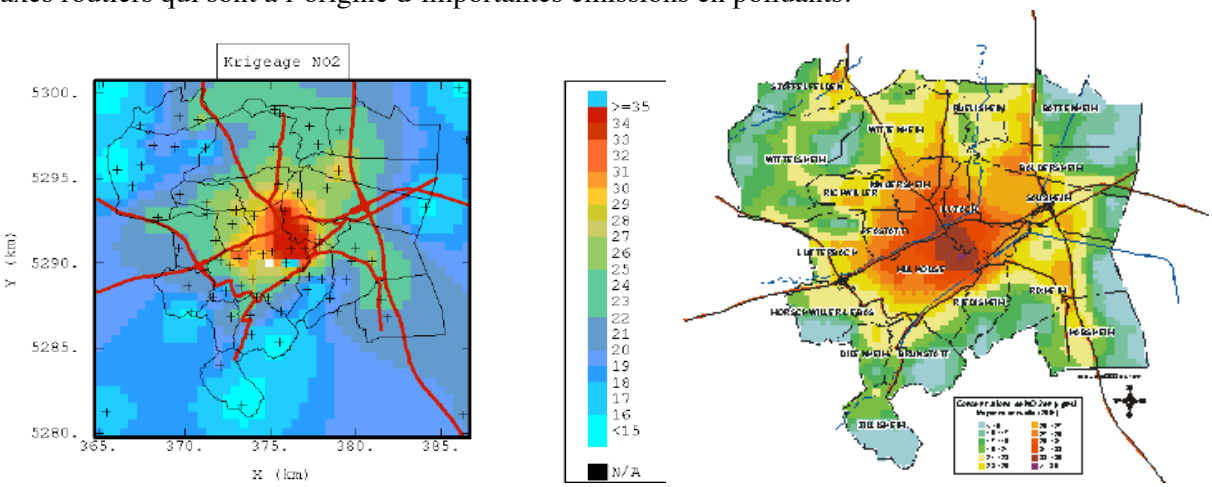

Figure 2: Cartes de NO_2 obtenues par krigeage ordinaire et krigeage avec 2 dérives externes
Figure 2: Maps of NO_2 obtained by ordinary kriging and kriging with 2 external drifts.

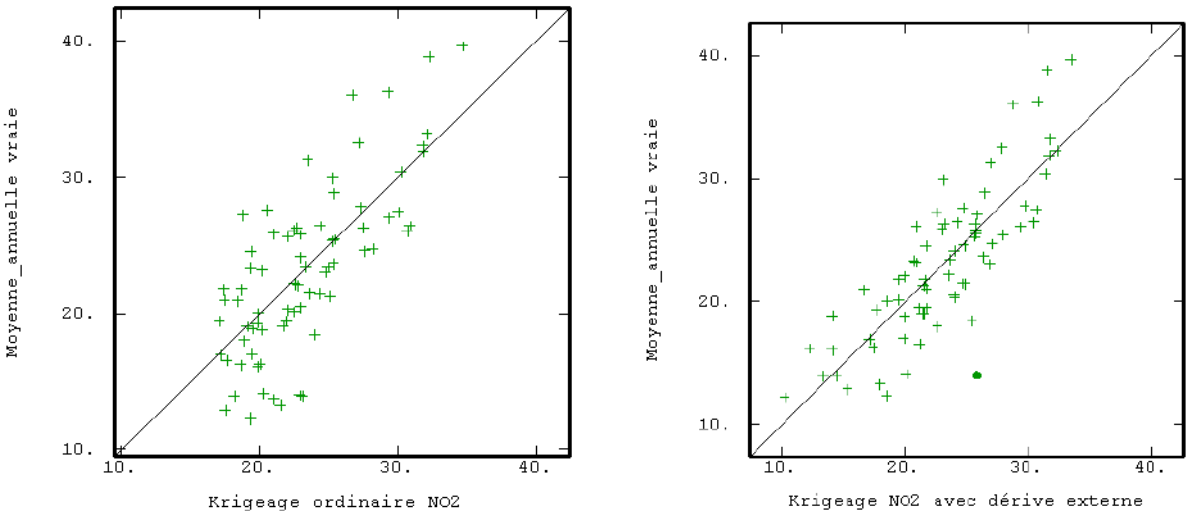

Figure 3 : Nuages de corrélation valeurs vraies/valeurs estimées issues de la validation croisée des données à l'aide du krigeage ordinaire ou du krigeage avec dérive externe.
Figure 3 : Scatter diagrams actual values/estimated values obtained after the cross-validation of the data by ordinary kriging or kriging with external drift.

L'avantage du deuxième modèle est clairement démontré par la validation croisée des données et

encourage donc à approfondir le choix d'un modèle avec dérive le plus approprié. La validation croisée consiste simplement à interpoler à l'aide du modèle choisi chaque point de donnée à l'aide des autres données. Le nuage de corrélation entre les valeurs estimées et les valeurs mesurées montre, dans cet exemple, que les dérives permettent de réduire sensiblement les erreurs d'interpolation.

3 - Recherche systématique des co-facteurs les plus significatifs

Nous avons recensé 17 variables explicatives de la pollution observée dans l'agglomération de Mulhouse et des communes avoisinantes :

- 8 variables caractérisant l'occupation du sol : bâti dense, bâti lâche, industries, types de végétation/cultures.
- 7 variables d'émissions : NOx, Benzène, COV non méthaniques, particules, SO_2, CO, benzo-pyrène.
- la densité de population.
- l'altitude.

Une première étape consiste à rechercher un nombre réduit de facteurs qui permettent de rendre compte approximativement de l'ensemble de l'information initiale. C'est l'objet de l'analyse en composantes principales.

On a ainsi effectué l'analyse en composantes principales sur l'occupation du sol, ce qui a permis de retenir 5 facteurs pour une restitution de 86% de la variance. Ces facteurs peuvent être interprétés par rapport à l'espace bâti, la végétation dominante, les cultures dominantes, les zones d'activités et un type d'essence forestière particulier correspondant aux conifères. L'analyse en composantes principales des émissions a permis de ne retenir que 2 facteurs restituant 80% de la variance. Ces facteurs sont liés au trafic d'une part et à la pollution industrielle d'autre part.

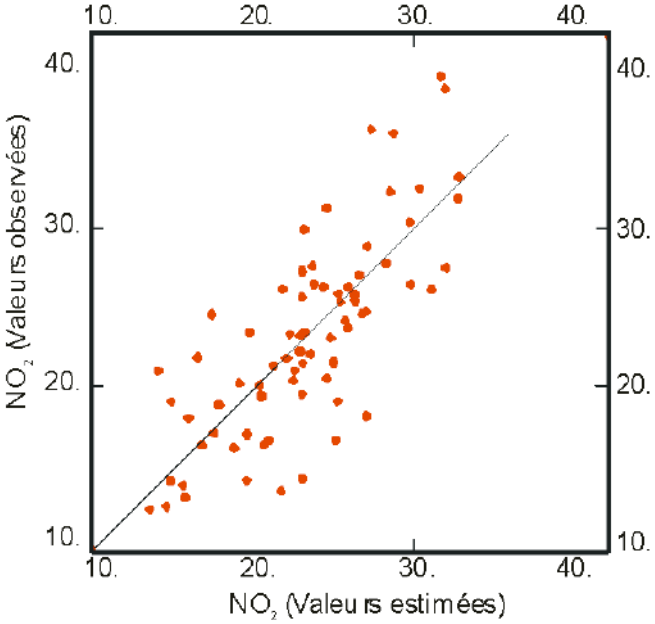

Figure 4 : Nuage de corrélation valeurs vraies/valeurs estimées issues de la validation croisée des données à l'aide du krigeage avec dérives externes résultant de l'analyse statistique multivariable.

Figure 4 : Scatter diagram actual values/estimated values obtained after the cross-validation of the data kriging with the external drifts chosen from the multi-variate statistical analysis.

La deuxième phase de l'étude consiste à examiner pour un polluant donné (ici NO_2)quels sont les facteurs explicatifs les plus significatifs d'un modèle simple de régression linéaire multiple.

$$NO_2 = \beta_0 + \beta_1 X_1 + \beta_2 X_2 + \beta_3 X_3 + \beta_4 X_4 + \beta_5 X_5 + \beta_6 X_6 + \beta_7 X_7 + \beta_8 X_8 + \beta_9 X_9$$

avec X_1 à X_5 facteurs liés à l'occupation du sol, X_6 et X_7 facteurs liés aux émissions X_8 la densité de population et X_9 l'altitude.

L'application d'un test itératif de Student permet de sélectionner 4 coefficients β_α considérés comme significatifs au seuil de 5%. Le modèle finalement retenu pour cartographier NO_2 peut s'écrire de la façon suivante :

$$NO_2 = \beta_0 + \beta_1 X_1 + \beta_6 X_6 + \beta_8 X_8 + \beta_9 X_9 + Résidu$$

Ce modèle peut alors être utilisé pour effectuer le krigeage avec dérive externe. Pour le mettre en œuvre il faut d'abord choisir un modèle de corrélation spatiale non stationnaire que l'on peut également introduire dans une procédure de validation croisée.

Pour réaliser l'interpolation par krigeage avec dérive externe, il est en outre nécessaire de disposer des valeurs numériques des fonctions de dérives aux points de données et aux nœuds de la grille où l'on effectue l'interpolation. Pour ce qui concerne les facteurs résultant de l'analyse en composantes principales, il suffit d'appliquer la matrice de transformation qui permet de passer des variables initiales aux facteurs.

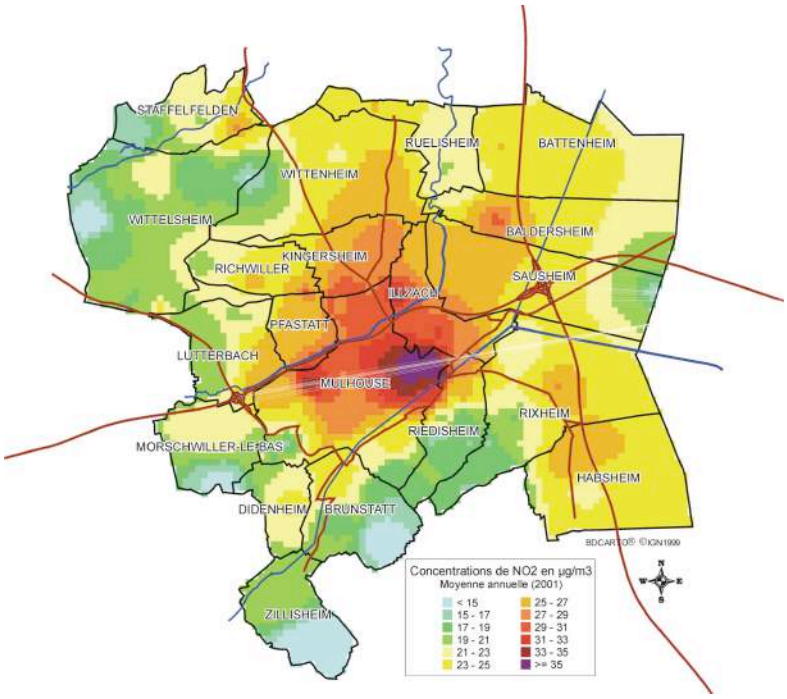

Figure 5: Carte de NO_2 obtenue par krigeage avec 3 dérives externes (type de bâti, population, altitude).

Figure 5: Map of NO_2 obtained by kriging with 3 external drifts (type of construction, population, elevation).

Conclusion

La méthode d'interpolation géostatistique adoptée pour reconstituer les champs de concentration de pollution de fond sur les communes du SIVOM de l'agglomération mulhousienne a permis d'obtenir une cartographie réaliste dont la précision peut être quantifiée. L'analyse statistique multi-variable préliminaire enchaînant une analyse en composantes principale des variables explicatives et une régression linéaire multiple aide à faire un choix objectif et pertinent des variables considérées comme des dérives externes dans le modèle géostatistique. On aboutit ainsi à une utilisation plus objective et rationnelle de l'ensemble des informations. L'implémentation informatique de cette méthodologie au travers de procédures automatisées est actuellement en cours.

Références

Bleinès C. et coll., 2002, Isatis Software Manual, Géovariances.

Chilès J.P et Delfiner P., 1999, Geostatistics Modeling Spatial Uncertainty, Wiley &Sons.

Hamadouche A., 2002, Automatisation du logiciel ISATIS, DESS Mathématiques pour l'industrie, UFR de Mathématiques et d'Informatique.

Perron G. et coll., 2002, Rapport final sur la répartition spatiale de la pollution atmosphérique, Source d'information ASPA 02031901-I-D, ASPA.

Saporta G., 1990, Probabilités, Analyse de Données et Statistique, Editions Technip.

12th International Symposium "Transport and Air Pollution" / 12e Colloque international "Transports et pollution de l'air", Avignon, 16 -18 *June* / juin 2003
proceedings / actes, n°92, tome / Vol. 2, Inrets ed., Arcueil, France, 2003, p. 93-98

Étude de la pollution de l'air par les particules fines (PM-10, PM-2,5 et PM-1) et évaluation de l'aérosol acide à Alger en site influencé par les émissions automobiles

Rabah Kerbachi·, Ménouèr Boughedaoui··, Fatima Boumechhour· & Nassima Oucher·
·École Nationale Polytechnique, Lab. Sciences et Techniques de l'Environnement, Avenue Hacène Badi, 16200 El-Harrach, Algérie. email: Kerbachi@gecos.net
··Université de Blida, BP 270, 09000 Blida, Algérie

Résumé
Les résultats de l'étude effectuée à l'aide d'un HVS-PM-10 équipé d'un cascadeur Andersen à quatre étages dans la banlieue urbaine d'Alger, montrent que la pollution de l'air ambiant par les particules inhalables (PM-10) et les particules respirables (PM-3, PM-2,5 et PM-1) est très élevée. La teneur moyenne en PM-10 s'élève à 81µg/m^3. Avec une teneur de 41µg/m^3, les particules respirables PM-2,5 constituent en masse environ 51 % des PM-10. On relève par ailleurs que plus du 1/3 des PM-10 est constitué par la fraction très fine des PM-1.
L'analyse des sulfates et nitrates montre que la composante acide représente, avec environ 24 % de la masse des PM-3, un taux élevé des particules respirables. Ces particules acides se caractérisent par une faible granulométrie: plus de 80% des sulfates et nitrates sont véhiculés par la fraction respirable. L'exploitation des données recueillies a permis par ailleurs d'établir des corrélations significatives entre divers paramètres mesurés.
Mots-clefs: *Air, Pollution, trafic routier, PM-10, PM-2,5, PM-1, aérosol acide, sulfates, nitrates.*

Abstract
Air pollution by fine particles (PM-10, PM-2,5 and PM-1) and acid aerosol evaluation in Algiers in a site influenced by automobile emissions.
The purpose of the study is the determination of the ambient air pollution levels by inhalable particulates matters (PM-10) and respirable particulates matters (PM-3, PM-2,5 et PM-1) in the suburban area of Algiers. The acid component associated to this particulates matters was also evaluated. Samples were taken near a significant road (trunk road with 2 directions, 4 ways, approximately 25 000 veh./d) using a HVS-PM-10 equipped with a Sierra-Andersen cascadeur with four stages. The results obtained over a period of 10 months of measurements show that pollution by inhalable and respirable particles is very high. The average content of PM-10 rises to 81µg/m^3. A maximum of more than 100 µg/m^3 was often exceeded. The respirable particles (PM-2,5) average content is 41 µg/m^3 which constitute approximately 51 % in mass of the PM-10. The ratio PM-2,5/PM-10 is characteristic of an urban area influenced by the road traffic. Moreover, it is noted that more of the third of the PM-10 is composed of the very fine fraction of PM-1.
The analysis of sulphates and nitrates shows that the acid component constitutes, with approximately 24% of the mass of the PM-3, a high rate of the respirable particles. These acid particles are characterized mainly by a low granulometry: 80% of sulphates and nitrates are associated to the respirable fraction, the PM-2,5. Interesting correlations were made with various measured parameters.
Key–words: *Air pollution, road traffic, PM-10, PM-2,5, PM-1, acid aerosol, sulphates, nitrates*

Introduction

Plusieurs travaux effectués ces dernières années en Europe et surtout aux USA ont montré que, sur

le plan sanitaire, les particules fines représentent en milieu urbain un indicateur majeur de la qualité de l'air (Schroeder et coll., 1987; Jansen et coll., 1997; Chiron et coll., 1997). De nombreuses et cohérentes études leur attribuent une forte responsabilité dans la survenue d'une vaste gamme d'effets biologiques et sanitaires (Dockery et coll., 1993; Pope et coll., 1995). C'est ainsi que plusieurs pays ont récemment révisé les normes existantes ou proposés de nouvelles réglementations. Les sources des particules inhalables et alvéolaires ou respirables, leur nocivité et la contribution des émissions automobiles, particulièrement les émissions diesel, à la fraction très fine sont de nos jours bien connues, mais pour arriver à formuler une stratégie de prévention, il est nécessaire d'avoir des données sur les niveaux et types de pollution, les composés qu'elles véhiculent ainsi que les sources émettrices.

En Algérie où l'urbanisation se développe rapidement, la dégradation de la qualité de l'air et les nuisances sont déjà perçues. Des études récentes ont montré que le Grand Alger (3 millions d'habitants, 600.000 véhicules) est, comme toute grande agglomération urbaine, confronté à une intense pollution atmosphérique (Kerbachi et coll. 1998, 1999). La principale source d'émission est le trafic routier. Aussi et en continuité aux travaux antérieurs effectués sur les particules inhalables (Kerbachi et coll. 2000), nous avons étudié la pollution de l'air par les particules fines par classe granulométrique et évalué les niveaux de pollution par les PM-10, PM-2,5 et PM-1 atteints à Alger en site influencé par le trafic routier. La composante acide (sulfates, nitrates et ammonium) associée à ces particules et sa contribution à la pollution globale a été également étudiée.

1 - Méthodologie

Les prélèvements journaliers ont été effectués à l'Ecole Nationale Polytechnique (ENP) dans la banlieue sud-est à environ 10 Km du centre d'Alger. Le poste de prélèvement est implanté sur la terrasse des salles de cours à 4 m d'altitude et à 10 m du bord de la route nationale N°5. Cet important axe routier est fréquenté par plus de 25000 véhicules/jour dont environ 15% de bus et véhicules lourds diesel. Ce site exposé à la brise de mer subit une bonne ventilation naturelle. Pour les prélèvements par classe granulométrique, un échantillonneur à fort débit, le HVS-PM-10 de la firme Graseby équipé d'un cascadeur Sierra-Andersen Modèle 234 à 4 étages (< 1μm, 1-1,5 μm, 1,5-3 μm, 3-7,2 μm et 7,2-10 μm) a été utilisé. Le débit de prélèvement est de 1m^3/mn. Les particules sont collectées sur des filtres en fibre de verre Whatman. Après extraction à l'eau bidistillée, les sulfates et nitrates véhiculés par les fractions PM-10 et PM-3 sont analysés par chromatographie ionique (Appareil Adionex dx100 détecteur Anion Micromembrane supressor-11).

2- Résultats et discussion

Étude et ampleur de la pollution par les particules fines

L'étude des particules a été effectuée sur une durée globale de 10 mois (de mai 2002 à mars 2003) à raison de 7 à 8 prélèvement par mois. Les mesures ont permis d'accéder au teneurs en PM-10,

PM-7, PM-3, PM-1,5 et PM-1. L'évolution temporelle des teneurs en PM-10, PM-3 et PM-1 ainsi mesurées sont illustrées en figure 1. Le tableau 1 résume les teneurs moyennes et extrêmes. On relève que les teneurs journalières varient dans une large fourchette. Ceci est du, d'une part aux variations dans l'intensité du trafic routier, et d'autre part aux influences météorologiques. Les teneurs moyennes en PM-10, PM-3 et PM-1 s'élèvent respectivement à 80,9 μg/m^3 ; 43,1μg/m^3 et

27,7 μg/m^3 respectivement. A partir du graphe log/probabilité donnant le diamètre des particules en fonction du pourcentage de la masse cumulée inférieur au diamètre (Figure 2), on détermine que le diamètre d_{50} de la masse médiane s'élève à 1,95μm. Ce diamètre est légèrement plus élevé que celui rencontré habituellement dans d'autres villes (Butler, 1979).

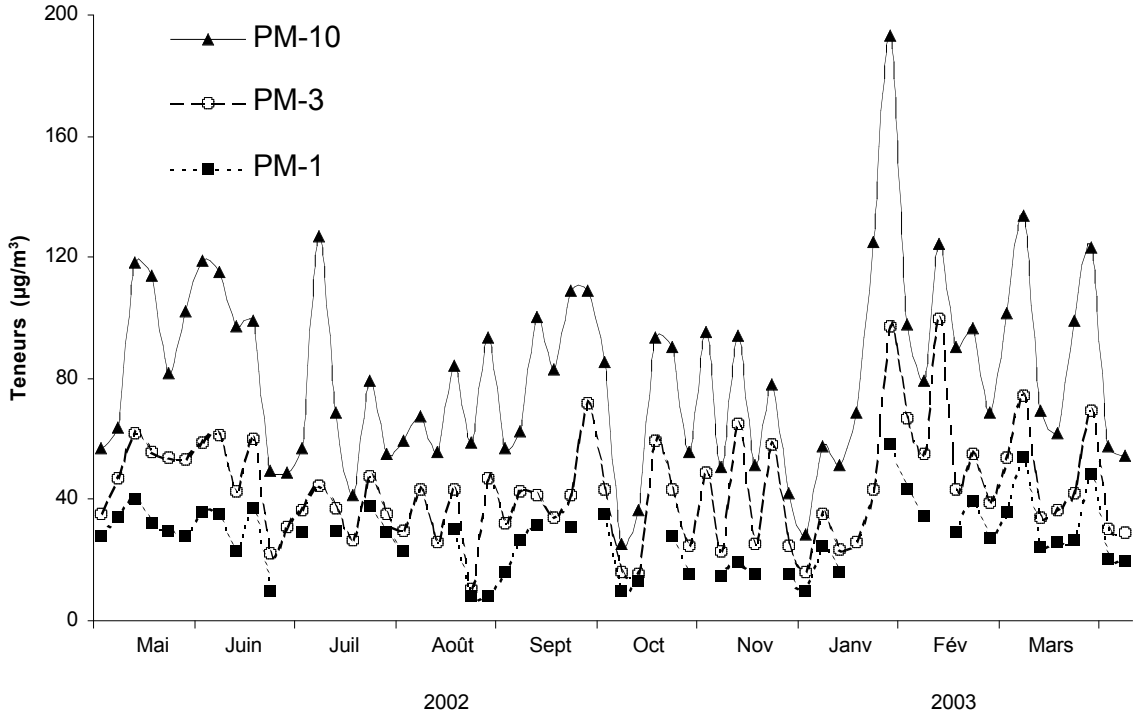

Figure 1: Évolution des PM-10, PM-3 et PM-1 mesurées à Alger
Figure 1: Evolution of the PM-10, PM-3 et PM-1 levels measured in Algiers

Paramètres (µg/m^3)	**PM-1**	**PM-3**	**PM-10**
Min.	7,9	15,5	25,1
Max.	58,2	97,1	193,8
Moy.	27,7	43,1	80,9
Ecart-type	11,2	17,4	30,6

Tableau 1: Teneurs atmosphériques en PM-1, PM-3 et PM-10 mesurées à Alger
Table 1: Atmospherics levels of PM-1, PM-3 and PM-10 measured in Algiers

À partir de ce même graphe, on détermine la teneur moyenne en particules respirables, les PM-2,5, qui s'élève à 41,3 μg/m^3 , soit 96 % du taux des PM-3. La mesure expérimentale des PM-3 par le cascadeur M234 permet ainsi d'accéder avec une bonne approximation aux teneurs en PM-2,5.

La répartition granulométrique des PM-10 illustrée en Figure 3 montre que les particules fines de faible granulométrie sont prédominantes: la fraction alvéolaire (PM-2,5) constitue ainsi 51,1 % des PM-10. La fraction très fines (les PM-1) qui se dépose d'une manière irréversible dans les poches alvéolaires constitue plus du tiers des PM-10 et environ les deux tiers des PM-2,5.

Globalement, on constate qu'en ce site urbain influencé par les émissions du trafic routier, la pollution par les PM-10 et PM-2,5 est très excessive. Les seuils limites en vigueur aux USA et en Union Européenne (US-EPA, 1997; J.O.- CE, 1999) sont largement dépassés.

L'examen de l'évolution des PM-1 en fonction des PM-3, montre qu'il y a une très bonne corrélation entre les deux classes de particules fines qui sont probablement de même origine (figure 4). Une corrélation moins prononcée est obtenue dans le cas de la relation PM-3/PM-10 (figure 5).

Ceci s'explique par le fait que dans les PM-10 interviennent aussi les particules de l'écorce terrestre et celles dues au phénomène de resuspension.

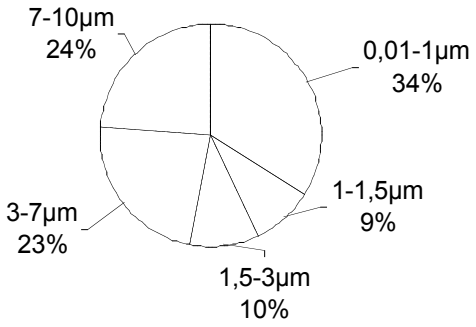

Figure 3: Répartition des PM-10 par classe granulométrique

Figure 3: Percentage of PM-10 in each size range

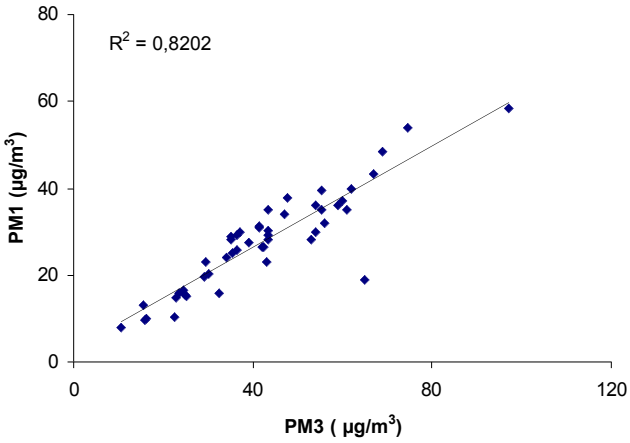

Figure 5: Corrélation PM-1/PM-3

Figure 5: Corrélation PM-1/PM-3

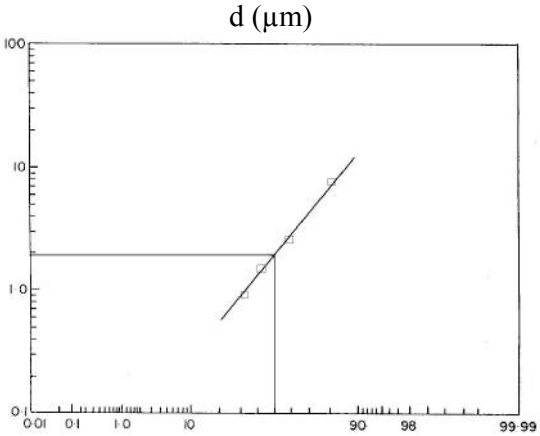

% masse cumulée ≤ diamètre des particules

Figure 4: Distribution des masses cumulées en fonction du diamètre des particules

Figure 4: Distribution of cumulative mass as fonction of particle diameter

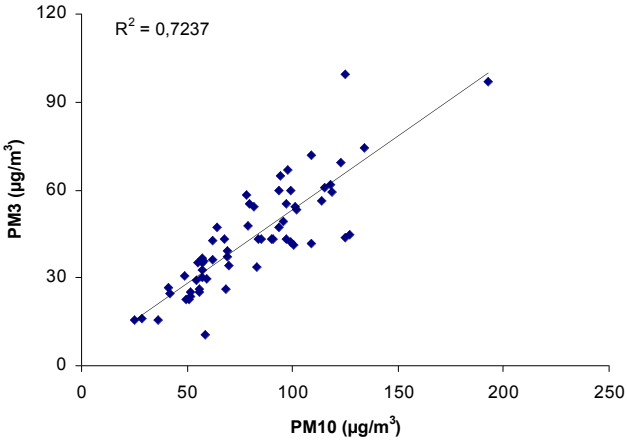

Figure 6: Corrélation PM-3/PM-10

Figure 6: Corrélation PM-3/PM-10

Évaluation de l'aérosol acide

Les teneurs atmosphériques en sulfates et nitrates déterminées dans la fraction soluble des PM-10 et PM-3 sont résumées en tableau 2. Dans les PM-10 et PM-3, les teneurs moyennes en sulfates s'élèvent respectivement à 5,5 et 4,4 $\mu g/m^3$. Les niveaux moyens des nitrates associés aux PM-10 est de 3,5 $\mu g/m^3$. Il est de 3,1$\mu g/m^3$ dans la fraction PM-3. Le rapport sulfates/nitrates varie selon la classe granulométrique de 1,4 à 1,7.

En supposant, comme cela a été formulé par plusieurs auteurs (Chow et coll., 1996, Sweet et coll., 1998), que les sulfates et nitrates se trouvent principalement sous forme de $(NH_4)_2SO_4$ et NH_4NO_3, le calcul stœchiométrique donne pour la teneur atmosphérique en ion ammonium 4,3$\mu g/m^3$ pour la fraction inhalable et 3,0 $\mu g/m^3$ pour la fraction respirable.

Paramètres	PM-3		PM-10	
	SO_4^{--} (µg/m^3)	**NO_3^-** (µg/m^3)	**SO_4^{--}** (µg/m^3)	**NO_3^-** (µg/m^3)
Min.	2,4	0,8	1,9	0,32
Max	10,1	7,6	12,2	8,8
Moy.	4,4	3,1	5,5	3,5
Ecart-type	2,2	1,9	2,1	2,1

Tableau 2: Teneurs atmosphériques en sulfates et nitrates dans les PM-3 et PM-10
Table 2: Atmospheric levels of sulfates and nitrates in the PM-3 and PM-10 size fractions

L'aérosol acide constitue ainsi une fraction massique de 17,9 % dans les PM-10 et 24 % dans les PM-3. La fraction respirable est ainsi plus riche en composants acides. La composition en pourcentage massique de la fraction acide dans les fractions PM-10 et PM-3 est illustrée en figure 7.

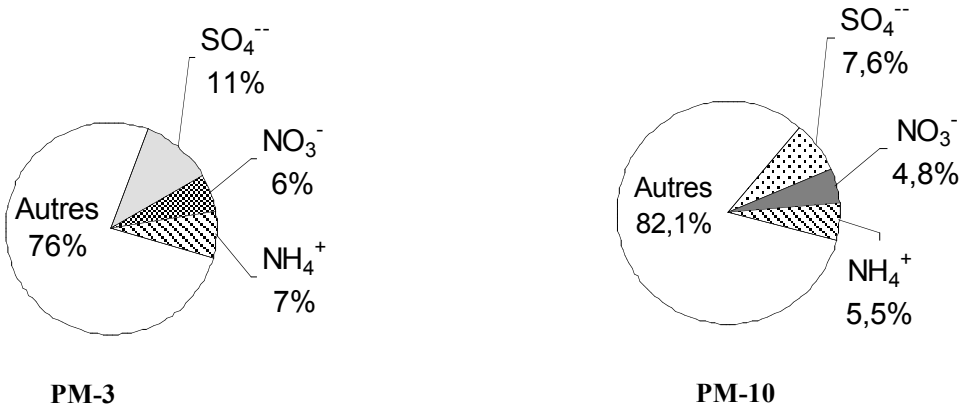

Figure 7: Composition de l'aérosol acide dans les PM-3 et PM-10
Figure7: Composition of the acid aerosol in the PM-3 and PM-10 size fractions

Le rapport $[SO_4^{--}]_{PM-3} / [SO_4^{--}]_{PM-10}$ s'élève à 0,80. Pour les nitrates, ce même rapport s'élève à 0,82. En d'autres termes, plus de 80% des sulfates et nitrates atmosphériques sont véhiculés par les particules fines de moins de 3μm qui pénètrent profondément dans les alvéoles pulmonaires. Des résultats similaires sont obtenues dans diverses études décrites dans la littérature (Cheng et coll., 1998).

Conclusion

L'étude a permis d'évaluer pour la première fois en Algérie les niveaux de pollution atteints par les différentes classes granulométriques des particules fines. Les résultats montrent qu'en site urbain de proximité, les teneurs atmosphériques en PM-10, PM-2,5 et PM-1, qui en moyenne s'élèvent respectivement à 81, 41 et 28 μg/m^3 , sont excessives et dépassent largement les normes en vigueur dans certains pays. Ces particules sont d'autant plus nocives que plus de 50% des PM-10 sont des particules respirables. Ceci se traduit par un diamètre de particule de la masse médiane de 1,95μm . L'exploitation des données montre qu'il existe une corrélation linéaire entre les PM-1 et les PM-3 d'une part, et entre les PM-3 et PM-10 d'autre part.

La composante acide caractérisée par les sulfates, nitrates et ammoniums primaires et secondaires, qui intensifie le pouvoir nocif des particules, constitue une fraction importante des particules inhalables et respirables. Cette fraction s'élève à environ 18% dans les PM-10 et 24% dans les

PM-3. On montre par ailleurs qu'il y a une répartition prédominante des sulfates et nitrates sur la fraction alvéolaire. C'est ainsi que plus de 80% de ces ions sont associés aux particules fines de diamètre inférieur à 3μm.

Il en résulte globalement que dans l'agglomération d'Alger, la pollution par les particules fines est

inquiétante de part son ampleur et de part ses caractéristiques physico-chimiques. L'ampleur de cette pollution résulte sans doute de la mauvaise combustion d'un parc automobile qui n'est pas fortement diéselisé, mais âgé, mal entretenu, dépourvu quasi totalement de pots catalytiques et roulant dans sa presque totalité à l'essence plombée.

Références

Butler J.D. (1979): Air pollution chemistry, Academic Press , London, p 345-352

Cheng L., H.S. Sandhu, R.P. Angle and R. H. Myrick (1998): Characteristics of inhalable particulate matter in Alberta cities, Atm. Env., vol. 32, N° 22, p 3835-3844.

Chiron M., P. Quenel et D. Zmirou (1997) : La pollution atmosphérique d'origine automobile et la santé publique. Poll. Atm., Janvier-mars, p 41-52.

Chow J.C., J.G. Watson, Z. Lu, D.H. Lowenthal, C.A. Frazier, P.A. Solomon, R.H. Thuiller and K. Maglio (1996): Descriptive analysis of PM-2,5 and PM-10 at regionnaly representative locations during Sjvaqs/Auspex, Atm. Env., vol.30, N° 12, p 2079-2112

Dockery D.W., C.A. Pope, X. Xu, J.D. Spengler, M.E. Ware, B.G. Fay, Jr. Ferris and F.E. Speizer (1993) : An association between air pollution and mortality in six US cities. N. Eng. J. Med., 329, p 1753 –1759.

Janssen N. A. H., D. F.M. Van Mansom, K. Van Der Jagd, H. Harsema and G. Hoek (1997) : Mass concentration and elemental composition of airborne particulate matter at street and background locations. Atm. Env., vol. 31, N°8, p 1185-1193.

Journal officiel des Communautés européennes (1999): L 163/41, directive 1999/30/CE du 27 avril 1999, Bruxelles.

Kerbachi R.. M. Boughedaoui, N. Koutai et T. Lakki (1998) : La pollution par les oxydes d'azote et l'ozone dans la ville d'Alger. Poll. Atm., avril-juin, p 89-101.

Kerbachi R., M. Boughedaoui et R. Joumard (1999) : Aromatic hydrocarbons in the ambient air of Algiers. Int. Symp. " Transport and Air Pollution", Graz, Austria, 31. may-2 june 1999.

Kerbachi R., M. Boughedaoui, Y. Kerchich et R. Joumard (2000) : Evaluation de la pollution de l'air par les PM-10 à Alger. Int. Symp. "Transport and Air Pollution", Avignon, France, 31. 5-2 juin 2000.

Pope C.A., M.J. Thun, M. Namboodira, D.W. Dockery, J.S. Evans, F.W. Speizer and Jr. C. W. Heath (1995) : Particulate air pollution as a predictor of mortality in a prospective study of U.S. adults. Am. J. Respir. Crit. Care Med., vol. 151, N°3, p 669-674.

Schroeder W.H. et al. (1987) : Toxic trace elements associated with airborne particulate matter,
A review. JAPCA, 37, 11, , p 1267 – 1285.

Sweet C. W. and D. F. Gatz (1998): short communication, summary and analysis of available PM-2,5 measurements in Illinois, Atm. Env., vol 32, N°6, p 1129-1133

U.S.- Environmental Protection Agency (1997): National ambient air quality standards (NAAQS) for particulate matter, Federal register, vol.62, N° 138.

12th International Symposium "Transport and Air Pollution" / 12e Colloque international "Transports et pollution de l'air", Avignon, 16 -18 *June* / juin 2003
proceedings / actes, n°92, tome / Vol. 2, Inrets ed., Arcueil, France, 2003, p. 99-104

Air pollution measurements on the Metropolitan Expressway by vehicle onboard sensor devices

Yukimasa Tsubota* & Hironao Kawashima**
* 1Earth Science Dept., Keio Senior High School, 4-1-2 Hiyoshi, Kohoku-ku, Yokohama, 223-8524 Japan - Fax +81 45 566 1396 e-mail: tsubota@hc.cc.keio.ac.jp
** Faculty of Science and Technology, Keio University, 3-14-1 Hiyoshi, Kohoku-ku, Yokohama 223-8522, Japan

Abstract
Instantaneous air-pollution levels were measured by vehicle on-board sensor devices on the Metropolitan Expressway. Each vehicle's position was traced via Global Positioning System (GPS) and speed monitored. The nitrogen monoxide (NO), nitrogen dioxide (NO_2) and particulate matter (PM_{10}) showed 100, 2, and 2 times greater than their observed values at static air-quality monitoring stations. Results showed a strong relationship between concentrations of air pollutants and vehicle speeds. The high (low) concentrations of NO, NO_2, and PM_{10} corresponds to the low (high) vehicle speed. Air-pollution measurements using on-board vehicle sensors have also been shown to be a calibration tool for traffic simulation.
***Keys-words**: air pollution, measurement, nitrogen oxide, suspended particulate matter.*

Introduction

The Metropolitan Expressway Public Corporation introduced different tolls on parallel routes (Yokohane Route and Bay Shore Route) to improve their vicinity's residential environments. This 'Environmental Road-Pricing' is used to induce large vehicles on the Yokohane Route to use the Bay Shore Route as shown in Figure 1.

Figure 1. Environmental Road Pricing on the Metropolitan Expressway.

Traffic simulation is normally performed in advance to evaluate this pricing. Traffic emissions are estimated from average vehicle speed, traffic volume and composition. Air pollution levels should

be measured to verify the Environmental Road Pricing's real effects.

Air-pollution levels on the Metropolitan Expressway vary by time and place. The distribution of static air quality-monitoring stations was not dense enough to detect any small-scale variations. Therefore, the existing monitoring stations could not be used to evaluate the effects of the Environmental Road-Pricing.

Vehicle on-board sensor devices were employed to monitor instantaneous air-pollution levels and to establish a verification method for Environmental Road Pricing. The small analysers for nitrogen monoxide (NO), nitrogen dioxide (NO_2), suspended particulate matter (PM_{10}), and CO_2 sensor and a GPS (Global Positioning System) sensor are installed on a small test vehicle.

1 - Methods

Devices

A Mazda GLC four-door sedan (1500cc) was used in our observation. The measurement devices are listed in table 1. Time, latitude, longitude, altitude, and vehicle speed were gleaned from the GPS and logged on a laptop computer in one-second intervals. NO, NO_2, PM_{10}, and CO_2 were recorded on a data logger of NR-200 (Keyence).

GPS	GM-38 Mercury	San Jose Navigation Inc.
	http://www.sanav.com/gm38.htm	
NO	Model 4545	Interscan Co.
NO_2	Model 1152	Interscan Co.
	http://www.gasdetection.com/	
PM_{10}	pDR-1200	Thermo MIE Co.
	http://www.thermo.co.jp/seihin/pDR1200.htm	
CO_2	GMT220	VAISALA
	http://www.vaisala.com/	

Table 1. List of measurement devices.

Outside air was sampled using a suction hose for each NO and NO_2 measurement through the driver's rear window as shown in figure 1. A CO_2 sensor was attached to the rear window frame with these hoses; and the GPS sensor was set upon the roof, with the cable passing through the driver's rear window. The NO and NO_2 Analysers, the laptop computer and data logger were attached to the rear seat by a safety belt as shown in Figure 2.

All of these devices were powered by the vehicle using a 150W electric power-converter plugged into the cigarette lighter.

Date and course

Observations were done during the afternoon and evening rush hours. The observation route and time are shown in Figure 3. The observation route is described in Table 2. These routes were selected to avoid heavy traffic congestion.

Figure 2. Installation of measurement devices.

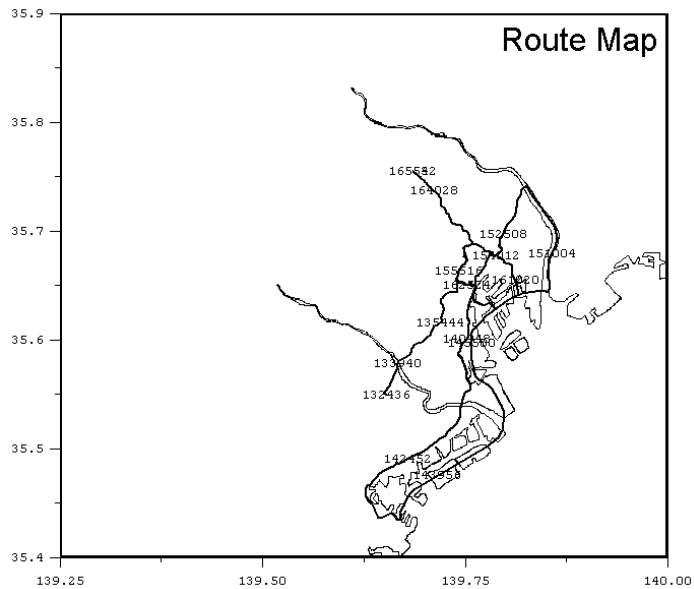

Figure 3. Observation route and time on 2002/4/2.

2002/4/2	13:24:36 - 16:55:42	
Hiyoshi > Meguro Route > Yokohane Route > Wanagan Route > Cuuou Kanjo Route> Toshin Kanjyo Route > Ikebukuro Route		
2002/4/2	17:58:54 - 21:34:26	
Ikebukuro Route > Toshin Kanjyo Route> Daiba Toute > Wangan Route > Fukagawa Route > Toshin Kanjo Route > Shinjyuku Route > Daisan Keihin Route		

Table 2. Detailed information on observation route.

High-pressure (1013 hPa) covered most of Japan's Islands on 2 April 2002 (Figure 4). Winds were weak (less than 3 m/s) in the daytime with south-easterly gusts (5m/s) in the evening. The maximum recorded temperatures was 25 degree Celsius which is above the mean maximum-temperature for this time of the year. This is a typical weather pattern that shows the high concentration levels of air pollutants in the Tokyo Metropolitan area.

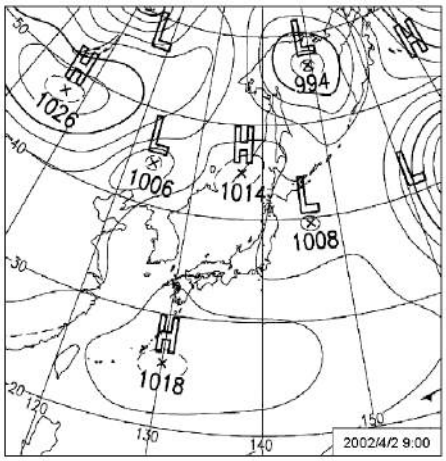

Figure 4: Weather map for 2002/4/2.

2 - Results

The time series data of NO, NO_2 PM_{10} and CO_2 are shown in Figure 5. The NO fluctuations were large so a 60-second running mean was taken. NO and CO_2 indicated similar variations and showed high concentrations on 14:45, 14:55, 15:50, 16:30, 18:40, 19:10, 19:55 and 20:45 JST. The NO, NO_2, PM_{10} and CO_2 concentrations were extremely high during the evening rush hour (around 18:40 Hrs). All the concentration levels became stable after 19:30 hrs, which indicates that evening peak hour had ended by that time.

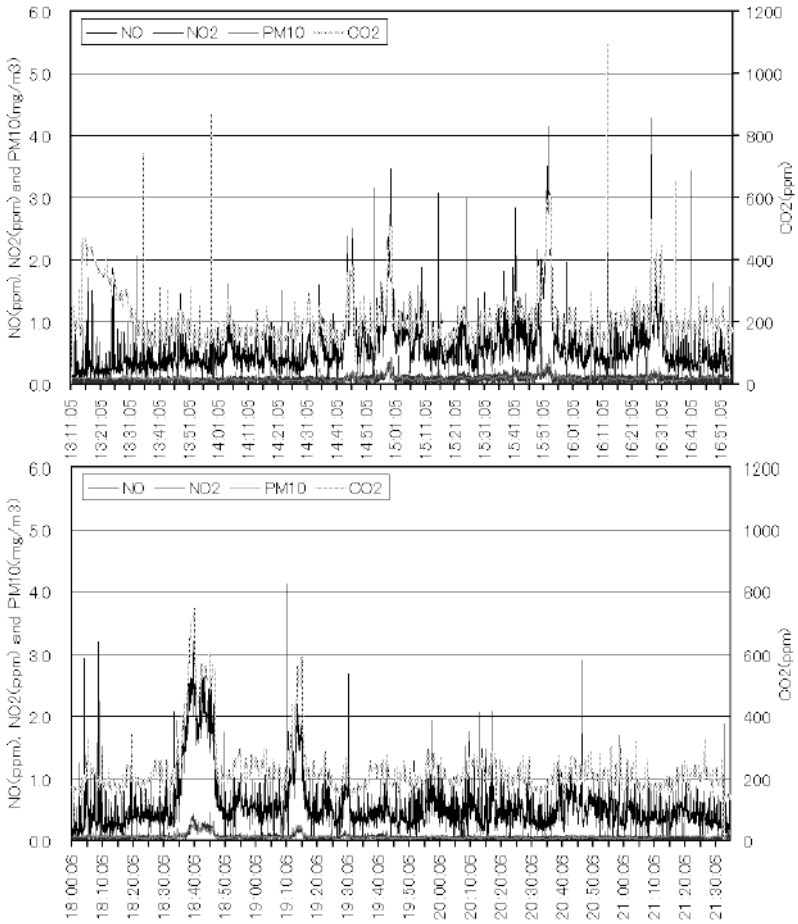

Figure 5: Time series display of NO, NO_2, PM_{10} and CO_2 on 2002/4/2.

The vehicle's speed, NO, NO_2 and PM_{10} distribution are shown in figure 6. Their concentrations are

100x, 2x and 2x greater than their static counterparts. Figure 6 showed that locations of low (high) vehicle speed correspond to the high (low) concentrations.

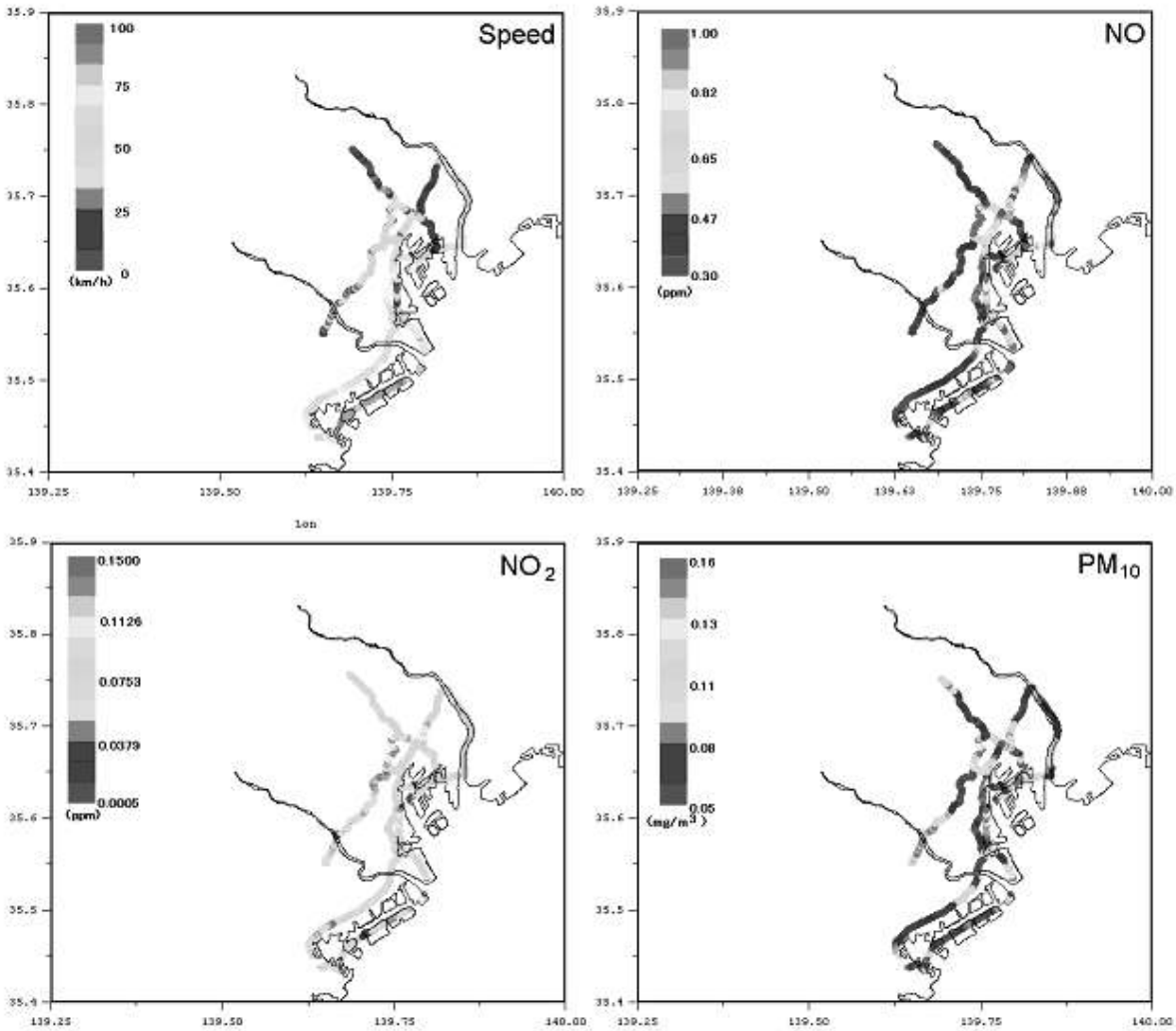

Figure 6: Distributions of Vehicle speed, NO, NO_2 and PM_{10} on 2002/4/2 (13:24:36 - 16:55:42).

3 - Discussion

Before the field measurements, NO and NO_2 analysers were calibrated with the standard NO_x HORIBA AN-3600 analyser. These calibration measurements showed the small analysers for NO and NO_2 can be used above 0.1 ppm concentration.

Field measurements carried out on different dates have assessed the effects of vehicle speed on measured air pollutant concentrations. Results showed that measured air-pollution levels depend slightly on vehicle speed but it can be compensated and/or ignored.

The relationship amongst NO and CO_2, and PM_{10} and CO_2 are shown in Figure 7. Concentrations of NO, NO_2, PM_{10} and CO_2 showed a linear relation but the coefficients depend on the time of day. It must be due to the difference of background air-pollution levels. An inexpensive CO_2 sensor can be used to monitor instantaneous air pollution levels on the road.

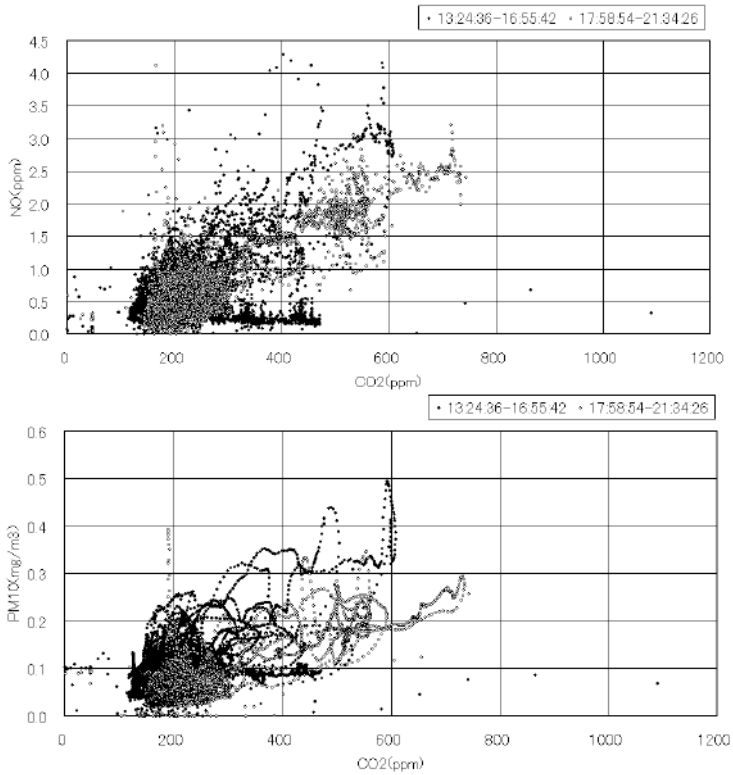

Figure 7 The relationships between NO and CO_2 (top), and PM_{10} and CO_2 (bottom).

Acceleration was computed from vehicle speed gained from GPS. However, any meaningful relationship between acceleration and air-quality level was not found. It must be due to the accuracy of vehicle speed measurements.

Conclusion

We showed that vehicle on-board sensor devices are useful in measuring instantaneous air-pollution levels on the road. The measured air-pollution levels depend slightly on vehicle speed but it can be compensated and/or ignored based on our measurements. The concentrations of NO, NO_2, and PM_{10} are 100 times, two times and two times greater than samples taken from the static air-quality monitoring station, respectively. The concentrations of NO, NO_2, PM_{10} and CO_2 have a linear relationship but their coefficients depend on the time of day. It must be due to the difference of background air-pollution levels. An Inexpensive CO_2 sensor can be used to monitor instantaneous air pollution levels on the road. Results showed the strong relationship between concentrations of air pollutants and vehicle speeds. The high (low) concentrations of NO, NO_2, and PM_{10} corresponds to the low (high) vehicle speed. Air-pollution measurements using vehicle on-board sensors can be used as a calibration tool for traffic simulation.

Acknowledgments

Sincere thanks are extended to Ms. Yasuko Ootsuka for helping with observations and data manipulation and to Mr. Frederick C. Lee for his help in editing the final manuscript. The National Institute commissioned this research for Land and Infrastructure Management.

References

Tsubota Y. & H. Kawashima (2001): Measurements of roadside air pollution and traffic simulations. URBAN TRANSPORT VIII, p 603-611.

12th International Symposium "Transport and Air Pollution" / 12e Colloque international "Transports et pollution de l'air", Avignon, 16 -18 *June* / juin 2003
proceedings / actes, n°92, tome / Vol. 2, Inrets ed., Arcueil, France, 2003, p. 105-110

Observatoire de la qualité de l'air et méthodologie d'optimisation d'un réseau de mesures à l'aide d'outils statistiques dessinés pour cet effet

Anda Ionescu*, Étienne de Vanssay, Yves Candau*, Marie Popounneau** & Vincent Tessauro****
* CERTES, Université Paris XII, Ave. du Général de Gaulle, 94 010 Créteil cedex, France
Fax : + 33 1 45 17 65 51- email : ionescu@univ-paris12.fr
** Cap Environnement, 9bis Passage d'Artois Bidot, 94 106 Saint Maur des Fossés cedex, France

Résumé
Un projet d'aménagement, tel qu'une construction réalisée sur un ouvrage routier, impose des études préliminaires d'impact et d'état initial de la qualité de l'air. C'est dans ce cadre qu'une campagne de mesures a été réalisée à l'aide de tubes passifs répartis sur la zone d'étude afin de caractériser la pollution de fond en NO_2 et benzène. Cet article présentera les outils mathématiques développés pour estimer une cartographie de la pollution à partir des mesures dispersées et la variance de l'erreur de l'estimation associée, ainsi que les résultats obtenus pour ce cas réel. Dans cette étude, l'emplacement des capteurs a été choisi par rapport à la morphologie urbaine et aux autres contraintes annexes. La carte de la variance associée montre que la répartition spatiale des capteurs ainsi choisie n'est pas optimale pour ce type d'interpolation, d'où une réflexion sur une procédure d'optimisation du réseau (basée sur la variance) intégrant la contrainte morphologie urbaine.
Mots-clefs : *état initial de la qualité de l'air, mesures de polluants gazeux, cartographie, interpolation multivariée, fonctions Spline Plaque Mince, Krigeage Intrinsèque, tests "Leave-One-Out", variance de l'erreur de l'estimation, optimisation avec contrainte, aide à la décision.*

Abstract
Air-quality observatory and methodology of optimisation of a measuring network with purpose-designed statistical tools.
A development project such as the construction of ventilation units on a road structure subjects the project manager to an approach which imposes particular research into public health and in particular the effects of atmospheric pollution. An air-quality observatory is to be created over the entire structure, with particular attention to built-up areas. It is within this framework that Cap Environnement was commissioned to draw up an initial air-quality state in an urban-scale research area situated in the Paris region. Cap Environnement undertook a measuring campaign for two pollutants (nitrogen dioxide and benzene) using passive tubes distributed throughout the research area in order to map it. Mapping atmospheric pollution enables to visualise more easily the spatial distribution of pollutants and to analyse it. The estimation of a pollutant concentration field over an area, based on values measured at points spread out over the region, can be carried out using a method of multivariate interpolation. Following a comparative bibliographical study and different tests of interpolation methods applied to air pollution data, it appeared to us that the two most appropriate methods for this purpose are : Thin Plate Spline interpolation and Intrinsic Kriging - equivalent methods in certain conditions. The advantage of interpolation by spline functions is their ease of use, as well as the very short computation time; the advantage of Intrinsic Kriging lies in the fact that it makes it possible to calculate the variance of the estimation-error, which can be used as a basis for the monitoring network optimisation. This paper will firstly present the methodology (based on the two types of interpolation mentioned) used to estimate pollutant spatial distribution and the estimation-error variance map associated to it, followed by the results obtained

in the context of a real study of initial air-quality state at the beginning of a building work on road structures. In this study, monitoring positions have been chosen with respect to urban morphology criteria (e.g. road proximity). The estimation-error variance map shows a non-optimal network for a pollution spatial sampling used as input in this type of mapping. This remark drives in a constrained optimisation (based on the variance error map and constrained by urban morphology criteria).
Keys-words: *initial air-quality state, measurement of gaseous pollutants, mapping, multivariate interpolation, Thin Plate Spline functions, Intrinsic Kriging, Leave-One-Out tests, variance of estimation error, constrained optimisation, decision assistance.*

Introduction

Afin de répondre aux exigences de la Loi sur l'air de décembre 1996, tout projet d'aménagement sur un ouvrage routier devrait soumettre le maître d'ouvrage à une approche qui impose des études particulières sur la santé publique et notamment, les effets de la pollution atmosphérique.

Dans cet esprit, avant la construction d'unités de ventilation sur un ouvrage routier dans la région parisienne, la société Cap Environnement a été mandatée pour réaliser un état initial de la qualité de l'air dans la région. Cap Environnement a réalisé une campagne de mesure en continu de cinq polluants réglementés d'une durée de trois semaines, en un point de la zone d'étude, à l'aide d'un camion laboratoire. Elle a été associée à une campagne de mesures de deux polluants (le dioxyde d'azote et le benzène) à l'aide de tubes passifs répartis sur l'ensemble de la zone d'étude. L'emplacement des tubes passifs a été choisi selon des critères liés à la morphologie urbaine uniquement (à proximité des sources ponctuelles de pollution ou d'axes routiers etc.). Le camion laboratoire a mesuré les cinq polluants à proximité de la future barrière de péage, source potentielle d'émission. Un nombre de quinze tubes passifs pour le dioxyde d'azote et pour le benzène a été jugé suffisant pour couvrir l'ensemble de la zone d'étude, au regard des critères généralement utilisés.

A partir de ces mesures ponctuelles, des distributions spatiales de polluants ont été estimées par interpolation multivariée, et ont servi ensuite comme base d'analyse pour l'état initial de la qualité de l'air. La carte de variance de l'erreur de l'estimation associée peut servir de base à l'optimisation du réseau de mesure. Cette optimisation conduit à la localisation des points de mesure permettant d'obtenir la cartographie (de la pollution) de moindre erreur par la technique d'interpolation choisie. Lorsque certains critères liés à la morphologie urbaine doivent être également pris en compte pour le projet d'un réseau de mesure, alors l'optimisation mentionnée précédemment deviendra une optimisation avec contraintes.

Dans notre cas d'étude, le réseau a été conçu uniquement à partir des critères de morphologie urbaine ou d'autres contraintes annexes. La carte de variance de l'erreur de l'estimation associée à la cartographie réalisée à partir de ces mesures montre que le réseau n'est pas optimal au sens d'obtenir la cartographie de moindre erreur d'estimation, correspondant à une variance de l'erreur de l'estimation minimale. Cette remarque nous a permis de mener une réflexion sur la conception d'un nouveau réseau de mesure : un certain nombre de capteurs doivent être considérés comme des "points-clefs" leur place étant fixe, car la morphologie urbaine l'impose (par exemple, la proximité d'une source), tandis que les autres points de mesure seront placés ensuite, de façon à minimiser la variance de l'erreur de l'estimation.

L'objectif de cet article est de présenter les outils mathématiques développés, de mettre en évidence la pertinence de cette méthodologie et des conclusions qui en ont découlé, ainsi que les bénéfices de cette étude sur la flexibilité de l'outil et sur son utilité pour une politique de communication du maître d'ouvrage.

1 – Méthodologie

Pour l'estimation d'une cartographie de la pollution, le calcul du champ de polluant a été basé sur une méthode d'interpolation multivariée, utilisant les coordonnées des points de mesure et les valeurs mesurées - les fonctions *spline plaque mince*. Cette fonction correspond à la surface qui

passe par les points des coordonnées (*x, y, concentration*) et qui a une énergie de flexion (ou bien une courbure) minimale. L'interprétation physique montre que ce type de fonction est bien adapté aux processus naturels caractérisés par une variation lisse. Ainsi, on retrouve dans l'expression analytique de la fonction une combinaison linéaire des fonctions de type logarithmique (connus pour leur variation assez lente). Pour plus de détails, se reporter à Carasso (1991), Duchon (1976), Ionescu (1998). La sélection de cette méthode, ainsi que sa validation pour le cas de la pollution atmosphérique urbaine ont développées par les auteurs dans des travaux précédents : Ionescu et coll.(1996), Ionescu (1998), Ionescu et coll.(2000).

Afin d'avoir une idée de la qualité des résultats obtenus par interpolation (qui dépend évidemment, à la fois, de la qualité des données d'entrée du modèle, ainsi que du modèle en soi), des tests type *Leave One Out* (*LOO*) ont été appliqués. Ces tests consistent à utiliser (*N-1*) valeurs connues, parmi les *N* mesurées pour estimer la valeur au $N^{ième}$ point (celui qui n'a pas été pris en compte dans le calcul). La valeur mesurée est ensuite comparée à celle estimée.

L'étude des performances d'un réseau comme pouvoir informatif pour une interpolation spatiale peut être réalisée par le biais de la variance de l'erreur de l'estimation. En cartographiant cette variance, on peut identifier les zones où l'information qui devrait être fournie par la mesure est manquante ou bien, redondante – voir Ionescu et Candau (2002). Ensuite, cette carte peut être utilisée comme base pour l'optimisation du réseau, en minimisant la variance de l'erreur de l'estimation.

Les fonctions *spline* sont des fonctions analytiques qui ne permettent pas d'accéder à la variance de l'erreur de l'estimation, c'est pour cela que l'équivalence formelle avec une méthode statistique a été utilisée. En effet, on peut démontrer mathématiquement que les fonctions *spline plaque mince* (combinaisons linéaires des fonctions de base de type logarithmique) sont équivalentes au *Krigeage Intrinsèque* avec des fonctions de covariance généralisée (représentant le modèle de la structure spatiale de notre phénomène de répartition des polluants) de type $c_s r^2 \ln r$. Pour la description du Krigeage Intrinsèque, se reporter à Christakos et Thesing (1993), Cressie (1986), Deutsch et Journel (1992), Journel et Huijbregts (1978) et pour l'équivalence entre les deux méthodes, voir Matheron (1980), (1981), Ionescu (1998).

2 – Résultats et discussion

La distribution spatiale de NO_2 obtenue par interpolation à partir des mesures peut être visualisée grâce aux lignes d'isoconcentration tracées (après géoréférencement) sur le plan de la région, pour faciliter leur analyse. Les niveaux observés (cf. fig. 1) sont ceux couramment enregistrés en région parisienne (niveaux moyens). Les courbes d'isoconcentration sont générées, comme on pouvait s'y attendre, autour du point P13 pour lequel le maximum de concentration a été observé, et situé sur le principal nœud de trafic de la zone étudiée.

Des tests de validation croisée (LOO) concernant l'application de la méthode d'interpolation dans ce cas d'étude précis ont été mis en œuvre. Ces tests ont été appliqués pour tous les points, un par un. Les résultats obtenus (la concentration calculée à partir des 14 mesures au point où la 15ième mesure a été effectuée, sans être prise en compte dans le calcul) sont illustrés sur la (fig. 2).

Les concentrations de NO_2 mesurées par les 15 capteurs conduisent à une valeur moyenne de 50 $\mu g/m^3$ et un écart-type entre les mesures, de 8.6 $\mu g/m^3$. Les quinze valeurs estimées par les tests LOO sont caractérisées par une moyenne de 49 $\mu g/m^3$ et un écart-type de 8.4 $\mu g/m^3$, et les écarts entre les valeurs mesurées et celles estimées par LOO montrent une erreur minimum de –0.3 $\mu g/m^3$ (soit une erreur relative de –0.7%), une erreur maximum de 18.9 $\mu g/m^3$ (soit une erreur relative de 28.5%), l'écart quadratique moyen de ces différentiels étant de 9.1 $\mu g/m^3$, du même ordre de grandeur que l'écart type de mesures (8.6 $\mu g/m^3$). Ces statistiques montrent une certaine robustesse de la méthode d'interpolation pour ce cas d'étude.

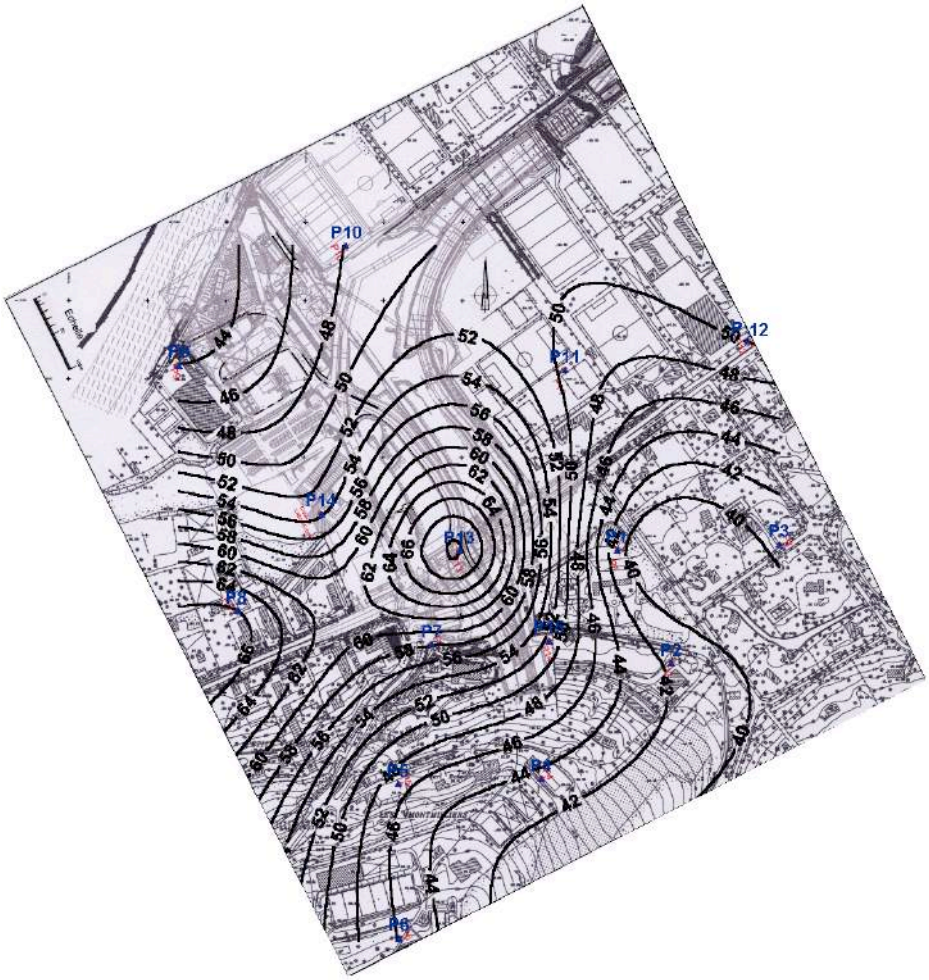

Figure 1: Champ de concentration de NO_2 estimé par interpolation basée sur les fonctions spline plaque mince, à partir des mesures ponctuelles à l'aide des tubes passifs.

Figure 1 : NO_2 concentration field estimated by thin plate spline interpolation applied to measurements given by passive tubes spread over the research area.

Les points pour lesquels l'écart d'estimation a été maximum ont été le point 13 et le point 8 (cf. fig. 2). Pour le point 13, l'explication est évidente, car il constitue la source ponctuelle la plus importante du réseau (le maximum mesuré). Aucune explication théorique ou pratique ne peut être avancée *a priori* pour le point 8. Par contre, la proximité de l'installation de chauffage pourrait expliquer cette valeur inattendue. On peut visualiser sur la (fig. 2) la répartition des points caractérisés par un plus fort différentiel entre la valeur mesurée et celle estimée : il s'agit des points P9, P14, P13, P12 (et P8) alignés sur une courbe. On constate que leur estimation a été moins performante, car à l'intérieur de cette courbe, on manque d'information : il n'y a que deux points de mesure : P10 et P11. D'une manière générale, ces tests montrent que la plupart des capteurs ne sont pas redondants et que le choix de leur emplacement a été fait de façon assez judicieuse et en nombre suffisant.

La carte de variance de l'erreur de l'estimation (cf. fig. 3) permet de visualiser une zone homogène, de faible variance sur la moitié Sud de la région, au centre des points P3, P2, P4, P5, P8, P14, P13, P1, ce qui montre un nombre suffisant et une bonne répartition des capteurs, remarque cohérente avec les meilleurs résultats des tests LOO. Toujours en accord avec les tests précédents, on retrouve des fortes valeurs de variance à l'intérieur (au Nord) de la courbe précédemment définie, ce qui met en évidence, une fois de plus, le manque d'information dans cette région.

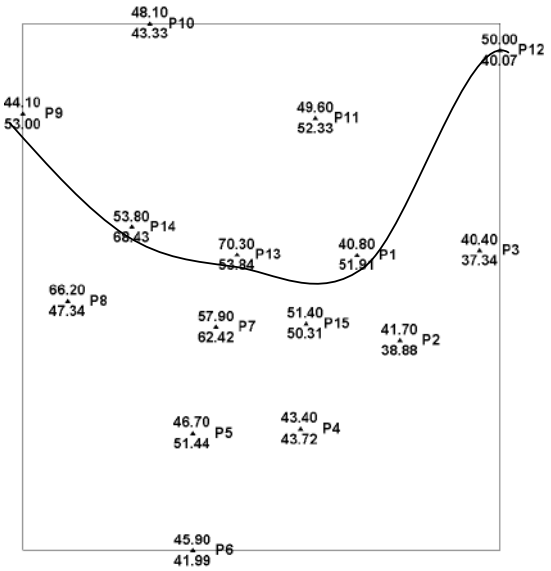

Figure 2: Tests LOO. Les symboles en triangle correspondent aux N points de mesure. La valeur au-dessus du symbole est celle mesurée, tandis que celle en-dessous représente la valeur calculée par interpolation en ce point, à partir des autres N-1 valeurs .

Figure 2 : Leave-One-Out Cross Validation Tests for spline interpolation applied to NO_2. The triangle symbols correspond to the N monitoring locations. The value above the symbol represents the measurement, while the value below the triangle is estimated by interpolation in this point, using all other N-1 measurements .

3 – Conclusion et perspectives

Cette étude a atteint son but, car elle a permis d'évaluer, grâce à une campagne de mesures et une méthodologie validée une fois de plus, sur ce cas précis, l'état initial de la qualité de l'air précédent la construction d'un ouvrage routier. Les niveaux de pollution correspondent à des valeurs moyennes dans la région parisienne.

Les tests de validation croisée ont été en accord avec la carte de variance de l'erreur de l'estimation et représentent ensemble, des outils d'évaluation, d'une part, de la robustesse de l'interpolation, et d'autre part, de la qualité du réseau de mesure. Grâce à la carte de variance, on peut avoir une information sur la fiabilité de l'interpolation pour tout sous-domaine de la zone d'étude. Dans cette étude, la configuration du réseau s'est avérée de bonne qualité et la méthodologie assez robuste.

La carte de variance de l'erreur de l'estimation nous a permis quand même de constater qu'un réseau constitué à partir des critères liés à la morphologie urbaine et aux contraintes annexes n'est pas optimal au sens d'obtenir la cartographie de moindre erreur par la technique d'interpolation choisie. Nous avons alors réfléchi à une procédure à mettre en place lors des projets de réseaux : placer d'abord les points "obligatoires", imposés par des critères liés à la réglementation en vigueur ; ensuite faire différents tests en plaçant les autres capteurs de façon aléatoire et choisir la configuration correspondant à un minimum de variance de l'erreur de l'estimation. Cette procédure peut être un outil d'aide à la décision pour le concepteur d'un réseau de mesure.

References

Carasso C. (1991) : Lissage de données à l'aide de fonctions splines – In "Analyse numérique", Baranger éd., Hermann, Paris, p 357-415.

Christakos G. & Thesing A. (1993) : The Intrinsic Random Field Model in the Study of Sulfate Deposition Processes, Atmospheric Environment vol. 27A, n° 10, p 1521-1540.

Cressie N. (1986) :, Kriging nonstationary data, J. Am. Stat. Ass. n°81, p 625-634.

Deutsch C. V. & Journel A.G. (1992), "Geostatistical Software Library and User's Guide", Oxford University Press.

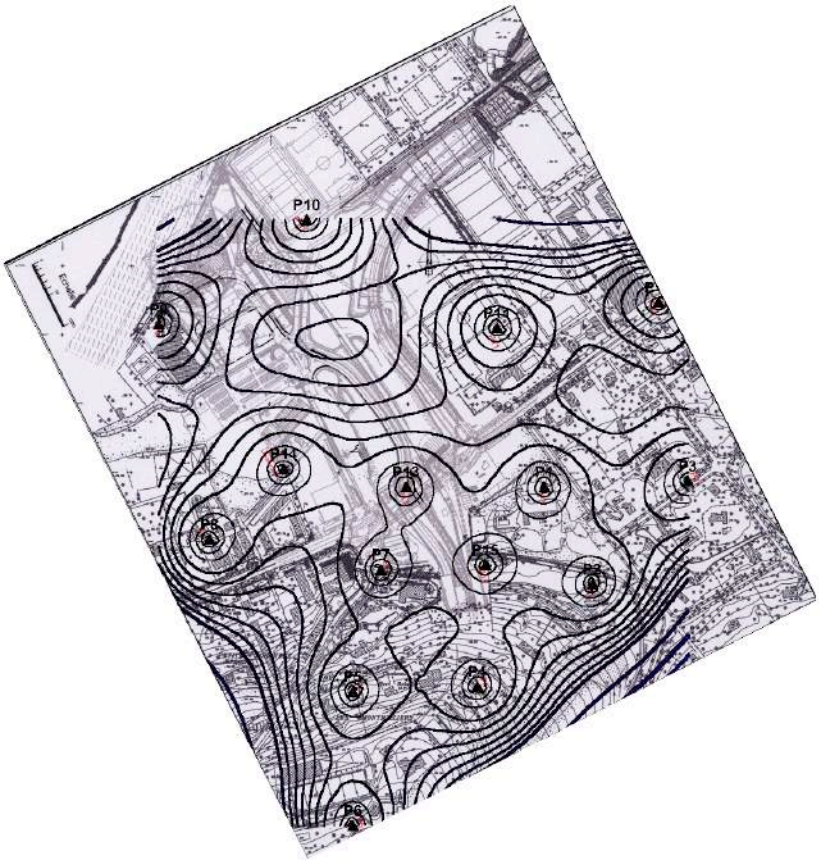

Figure 3: Carte qualitative de la variance de l'erreur de l'estimation par spline plaque mince. L'épaisseur de la ligne d'isovariance est proportionnelle aux valeurs de la variance.

Figure 3 : Qualitative map of variance of the estimation-error using thin plate splines, based on the formal equivalence splines-Kriging . Line width of the isovariance curves is proportional to variance values (thin lines-low variances, thick lines-high ones).

Duchon J. (1976) : Interpolation des fonctions de deux variables suivant le principe de la flexion des plaques minces, R.A.I.R.O. Analyse Numérique, vol.10, n°12, p 5-12.

Ionescu A., Mayer E., Colda I.(1996) : Méthodes mathématiques pour estimer le champ de concentration d'un polluant gazeux à partir des valeurs mesurées aux points dispersés, Pollution atmosphérique, Janvier-Mars, p. 78-89.

Ionescu A.(1998) : Contribution à la compréhension de la dispersion des polluants atmosphériques en zone urbaine, thèse de doctorat de l'Université Paris XII, (1998), Rapport IAURIF(1999) Paris, 224p.

Ionescu A., Mayer E., Candau Y., Colda I. (2000) : Analytical determination and classification of pollutant concentration fields using air pollution monitoring network data. Methodology and application in the case of the Paris area, during episodes with peak nitrogen dioxide levels, Environmental Modelling and Software n° 15, p 565-573.

Ionescu A. & Candau Y.(2002) : Optimization of an Urban Air Monitoring Network, In "Air Pollution Modelling and Simulation", , Sporisse B. éd., Springer, p. 586-588.

Journel A. G. & Huijbregts Ch. (1978) : "Mining Geostatistics", Academic Press, New York.

Matheron G. (1980) : Spline et krigeage : leur équivalence formelle, Doc. Ecole des Mines de Fontainebleau.

Matheron G. (1981) : Remarques sur le krigeage et son dual, Document Ecole des Mines de Fontainebleau.

12th International Symposium "Transport and Air Pollution" / 12e Colloque international "Transports et pollution de l'air", Avignon, 16 -18 *June* / juin 2003
proceedings / actes, n°92, tome / Vol. 2, Inrets ed., Arcueil, France, 2003, p. 111-118

Remote optical sensing evaluation (ROSE): Pollutant emissions in a street canyon in Germany

Kim Cooke*, Barry De Souza*, Lesley Hanna*, Moira Hilton, Mike Welch**, Peter Kaspersen***, Lars Brøndo***, Juergen Winkler****, Panagiotis Neofytou***** & Stylianos Rafailidis*******
*Sira Ltd., South Hill, Chislehurst, Kent, BR7 5EH, UK - Fax +44 20 8467 7097 -
email : kim.cooke@sira.co.uk
** University of Reading, JJ Thompson Physical Laboratory, PO Box 220 Whiteknights, Reading, RG6 6AF, UK
***Norsk Electro Optikk A/S, Solheimveien 62 A, PO Box 384, N-1471 Skarer, Norway
****Technologie Transfer Zentrum Bremerhaven, Umweltinstitut, An der Karlstadt 6, DE-27568 Bremerhaven, Germany
*****Environmental Research Lab., NCSR "Demokritos", Aghia Paraskevi, 15310, Athens, Greece

Abstract
A European consortium has been formed within Framework 5s Competitive and Sustainable Growth programme to carry out a project on Remote Optical Sensing Evaluation (ROSE). The primary objectives of ROSE are the determination of "Best Practise" and performance standards (ROSE, GR6D-CT2000-0434). Within this project an urban field trial has been carried out to measure pollutant emissions in a street canyon in Bremen, Germany, using remote optical measurement techniques. The instruments used included two Fourier Transform Infrared Spectrometers (FTIR) and a Tuneable Diode Laser system (TDLAS), as well as conventional point measurement techniques. The primary species investigated was carbon monoxide. The data obtained and the use of computational fluid dynamic (CFD) modelling to optimise the set up of the instruments at the field site is presented. A clear correlation was observed between the carbon monoxide levels measured and the traffic count, as well as between the carbon monoxide measured by two FTIRs themselves.
***Key Words**: pollutant, emissions, remote optical measurement techniques, street canyon, computational fluid dynamics, urban pollution*

Résumé
L'évaluation du sens optique éloigné (ROSE) : Les émissions polluantes dans un "street canyon" à Bremen en Allemagne
A formé un consortium européen à l'intérieur du "Framework 5s Competitive and Sustainable Growth" programme pour réaliser un projet au sujet de l'évaluation du sens optique éloigné (ROSE). Pour les premiers objectifs de ROSE, il faut déterminer la meilleure practique "Best Practice" et les normes de la performance (ROSE, GR6D-CT200-0434). On a fait un essai dans un "street canyon" à Bremen pour ce projet afin de mesurer des émissions polluantes. On s'est servi des techniques pour les mesures optiques éloignées. On a utilisé les instruments comme 2 "Fourier Transform Infrared Spectrometers" (FTIR) et un "Tuneable Diode Laser system" (TDLAS), aussi bien que des techniques conventionnels pour les mesures exactes. On a examiné les espèces principales comme le carbone monoxide. On vous présente les données obtenues et l'utilisation de modelage de la fluide computationale dynamique (CFD) pour optimiser l'installation des instruments au essai. On a observé une correlation précise entre les niveaux mesurés de carbone monoxide et le compte du trafic, aussi bien que le carbone monoxide mesuré par les 2 FTIRs mêmes.

Introduction

The great advantage of using remote optical measurement techniques (ROMTs) over other more conventional techniques for measuring gaseous pollutants is that they can perform real time, in-situ gas analysis along an open path. Although there have been notable advances in ROMTs in recent years resulting in greater reliability, more portable systems and overall decrease in cost, there is still resistance to using them for routine monitoring of emissions and air quality. The primary reason for this is that there is still no standardisation between systems. This is highlighted particularly well in the World Health Organisation's guidelines for air quality (WHO, 2000), where four out of six of the main "classic" pollutants SO_2, NO_2, CO and O_3 can be measured using remote optical sensors. However, they point out the techniques available do not conform to ISO7996 (ISO1985b), hence stress the need to pay careful attention to instrument calibration and quality assurance to obtain meaningful data.

With ever more air quality legislation and national and international strategies on the horizon, governmental bodies, local authorities and industry alike are under more pressure to deploy monitoring systems in which there is a high degree of confidence in the data produced. A European consortium has been formed within Framework 5's Competitive and Sustainable Growth programme to carry out a project on Remote Optical Sensing Evaluation (ROSE). The primary objectives of ROSE are the determination of "Best Practice" and performance standards, along with a firm theoretical foundation on which to support such statements (ROSE project, GR6D-CT2000-00434). It addresses the problems associated with system and certification approval by inter-comparing five diverse commercially available ROMTs (FTIR, FTUV, DOAS, DIAL and TDLAS, see Table 1) under both field and laboratory conditions. Working alongside this, it also utilizes the advances in Computational Fluid Dynamics (CFD) modelling to reduce the uncertainties in the measurements induced by dispersion and optimise instrument placement in the field. However, while these methods offer the advantage of being able to measure over significantly long paths, often several hundred metres, the uncertainties also associated with point measurements due to dispersion and other interfering mechanisms, become a factor. In the case of open path measurements, this has often placed doubt on the confidence in the collected data.

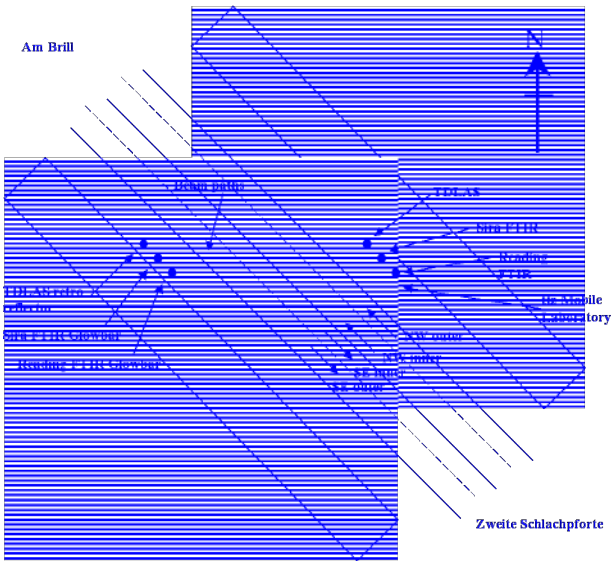

Figure 1: Positioning of instruments and traffic counting (not to scale).

1 – Experimental

A field trial was carried out in Bremen, Germany (Latitude 53° 4' 60N, Longitude 8° 48' 06W, altitude 2m) between 4th-8th November 2002. The objective was primarily to investigate the applicability of remote optical measurement techniques to an urban environment. Martinistrasse was chosen as the street canyon (Figure 1) due to its homogeneity of buildings, having a north west-south east (NW-SE) orientation. The street was made up of 6 to 9 storey buildings, with an average

height of 22 m and a width of 28 m. The building height to street width ratio was 0.79. The local topography is very flat, therefore orographic effects will not influence the city's meteorology. The traffic flow was in both directions consisting of four lanes. Traffic counting was carried out by the traffic authority of Bremen, with the sum of vehicles per hour divided into trucks and cars for the two lanes in each direction during the entire campaign.

Instrument	Species measured	Actual beampath	Height above street level	Sampling Frequency	Limit of Detection
Unicam RS FTIR (Reading) (Bistatic set up with glow bar as external source, resolution 0.25cm^{-1})	CO &CO_2	41.7 m	5.9 m(NE) 4.9 m(SW)	1minute 24 seconds	ppm level
Bomem 100 FTIR (Sira) (Bistatic set up with glow bar as external source, resolution 1cm^{-1})	CO &CO_2	39.5 m	5.8 m(NE) 4.9 m(SW)	2 minutes	ppm level
Norsk Elektro Optikk Near Infrared TDLAS	CO &CO_2	37.7 m	5.9 m (NE) 4.9 m (SW)	1 minute	Not known

Table 1: Remote optical measurement techniques used

Measurement	Instrumentation	Sampling height above street level	Measurable Range	Limit of Detection
CO	Monitor Labs, model 8830, infrared CO analyzer	1.4 m	0 – 50 ppm	0.2 ppm
NOx	API, model 200, chemiluminescent NOx analyzer	1.4 m	0 – 500 ppb	0.5 ppb
SO_2	Monitor Labs, model 8850, fluorescent SO_2 analyzer	1.4 m	0 – 250 ppb	5 ppb
wind-direction and -speed combi-detector temperature humidity-sensor*	Thies Clima Modul System	12.4 m	wind-direction: 0 – 360° wind-speed: 0.4 – 40 m/s temperature: -25 – +50 °C humidity: 10 – 100%	

*Table 2: Point measurements carried out by the Technologiezentrum an der Hochschule Bremerhaven (ttz) mobile laboratory, with a 1 minute sampling frequency (*the humidity sensor was not calibrated, however it gave indicative values)*

Instrumentation

Two Fourier Transform Infrared (FTIR) Spectrometers and a tuneable diode laser (TDLAS) system were used in this trial (Table 1). They were set up at the same heights, with their optical paths as close as possible to allow meaningful inter-comparisons. Carbon monoxide was measured as the main species, although carbon dioxide was also detected. The height and orientation of the optical paths were decided upon using the information supplied by the CFD modelling described in the next

section. A mobile laboratory was placed at the site on the north east side of the street. The point measurements carried out by this laboratory are given in Table 2. Supplementary meteorological data was supplied by the Senator für Umweltschutz (SUS) Bremen air emission monitoring station approximately 1.5 km to the north east of the site and the Deutscher Wetterdienst (DWD)station at Bremen Airport, approximately 3.5 km to the south of the site.

CFD for sighting instruments

The initial scope of the CFD modelling was to specify appropriate locations for instrument placement by numerically simulating the flow and pollution dispersion fields in the vicinity of the site taking into account the wind rose of the area and selecting locations of high pollution concentrations so that non-zero indications of the instruments were assured. This was accomplished by using the CFD code ADREA-HF (Bartzis, 1991), which has been validated (Venetsanos *et al*., 2002; Vlachogiannis *et al.,* 2002) in the past as regards to environmental 3-D flows and pollutant dispersion in complex building terrains.

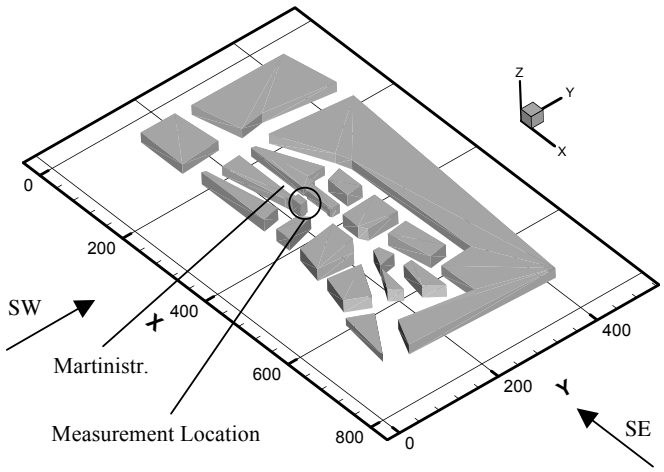

Figure 2: Computational domain of the street-canyon area

The methodology consisted of solving the transient, Reynolds averaged, mass and momentum 3D conservation equations for the mean flow and the mass fraction conservation equation for the pollutant dispersion, until steady state conditions were reached. Turbulence was modelled using an anisotropic one-equation model (Andronopoulos *et al*., 1993). Turbulent diffusivities were obtained using the *Boussinesq* assumption, with the turbulent kinetic energy obtained from its conservation equation, while the anisotropic length scales from algebraic relations, which in the general case depend on the distance from solid surfaces, the atmospheric stability and the asymptotic pressure gradient. The computational domain used for the calculations, shown in Figure 2, encompassed all buildings close to the tested measurement locations in considerable detail.

Calculations were performed for two different incident-wind directions. These were selected according to the wind rose of the area, which indicated that the prevailing winds were south-east (SE) and south-west (SW) with highest free-stream intensity of 9m/s. Seven different beam paths crossing the street were tested as regards to the levels of concentration to be found along the beam. The first three beam-paths were oblique to the street, having the same start and end points as regards to the x,y axes but at different heights (4, 5 and 7 metres above ground). The next three beam-paths had a starting point very near to the starting point of the previous cases but extended normal to the street. The same three different heights mentioned previously were also assumed. In all aforementioned cases the beam extended fully from building wall to opposite wall. The seventh beam path extended from the roof of a building (z=25m) to the first floor balcony (z=4m) exactly opposite as regards to the street. For all cases the same emission rate at street level was assumed. Table 3 provides the integrated Average Concentration*Length values which are what the

instruments would actually measure in relative terms. The values are shown "non-dimensionalised" with the source emission rate kept constant and equally spread across all four road lanes. It can be seen that for the cases of horizontal beams at various heights, height reduces the signal strength to be measured by equal degrees, irrespective of whether the beam is normal or oblique to the street axis. Furthermore, for a normal placement the beam measurement appears to be much more insensitive to wind orientation than in the oblique case. On the other hand, the roof-to-1st-floor opposite placement gives the weakest measurement and in addition to that the rotation of the wind from SW to SE halves the overall signal.

CASE Number		1	2	3	4	5	6	7
Orientation to Street		Oblique	Oblique	Oblique	Normal	Normal	Normal	Normal
Height above Street		4 m	5 m	7 m	4 m	5 m	7 m	4 m to 25 m
Wind Direction	SW	3.55e-7	3.12e-7	2.51e-7	2.92e-7	2.60e-7	2.12e-7	8.42e-8
	SE	2.42e-7	2.03e-7	1.47e-7	2.78e-7	2.38e-7	1.74e-7	4.87e-8

*Table 3: Dimensionless values of Length*Average Concentration of pollutant*

From the discussion of the results it can be drawn that within the cases tested the most advantageous overall placement seems to be the oblique to the street axis as close as possible to the street level (to benefit from higher pollution levels and hence signals).

2 - Results

The results presented are half hourly averages of the data to allow more meaningful inter-comparisons. As can be seen from Figure 3, the meteorological conditions measured within the city and the street canyon differed from the measurements taken at the airport. The wind direction within the street canyon was highly influenced by the street canyon itself, as expected, with overall wind speeds higher within the city. The temperature was also found to be higher within the city due to the urban heat island effect, though all sites exhibited the same diurnal variation.

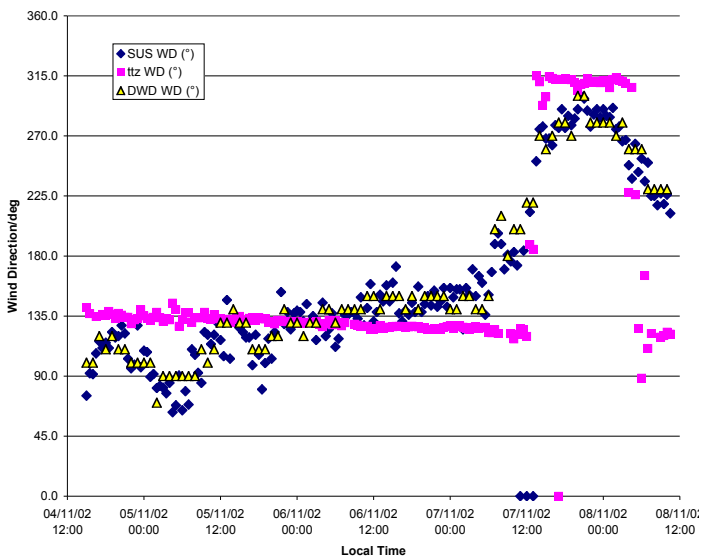

a.

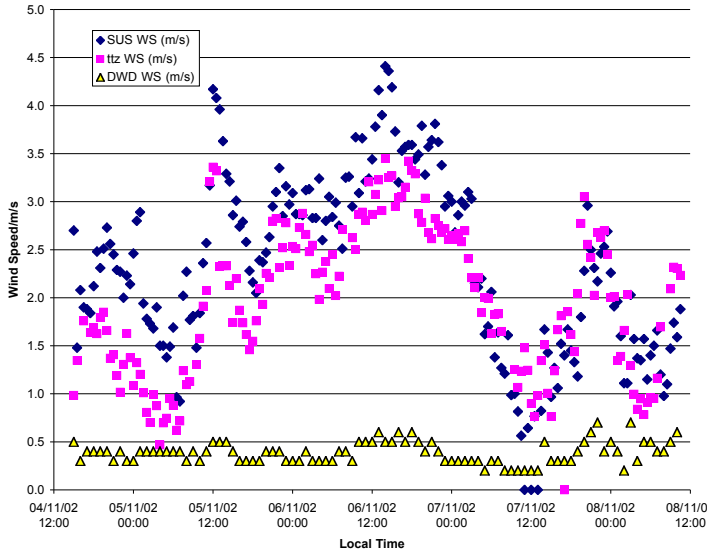

b.

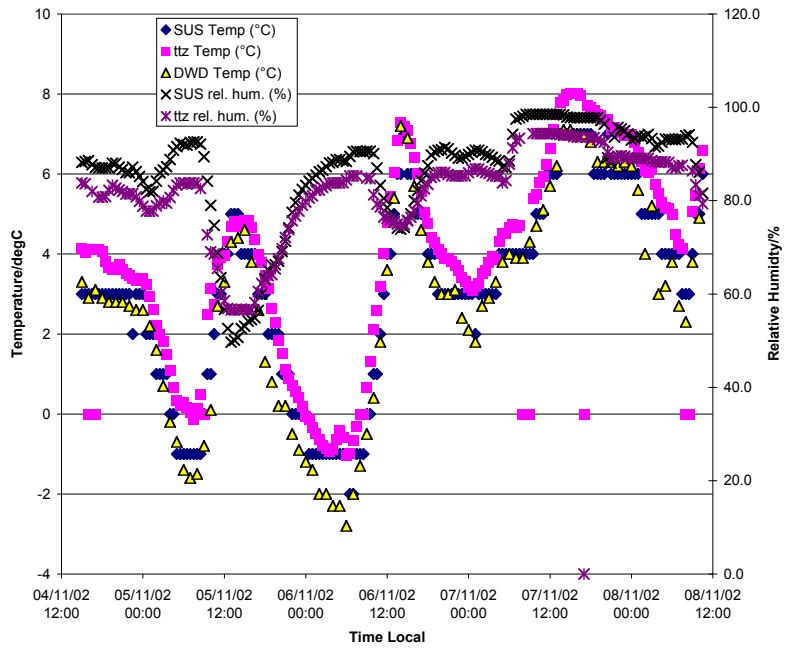

c.

Figure 3: Meteorological Observations for 04.11.02-08.11.02; a. Wind Direction; b. Wind Speed; c. Temperature and Relative Humidity (SUS:Senator für Umweltschutz; DWD:Deutscher Wetterdienst; ttz: Technologiezentrum an der Hochschule Bremerhaven)

Figure 4 gives the results from the car and truck count. There were less trucks than cars, with a majority of the cars travelling in the south east and north west inner lanes. Figure 5 shows the results of the point measurements taken by ttz where a clear diurnal variation of species can be seen. An inter-comparison of the CO data measured using the two FTIRs (Reading and Sira) and a point measurement technique (ttz) are presented in Figure 6. As can be seen the two FTIRs and the point measurement technique exhibit a similar diurnal variation, with peaks appearing in the CO at rush hour. No TDLAS CO measurements are presented as the concentrations were below the detection limit of the system, however the TDLAS did measure CO_2 and the results are presented elsewhere.

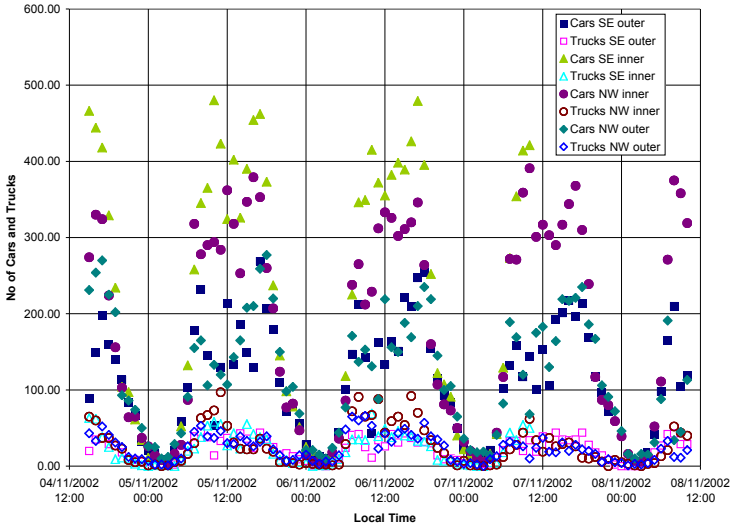

Figure 4: Car and truck count per hour for 04.11.02-08.11.02

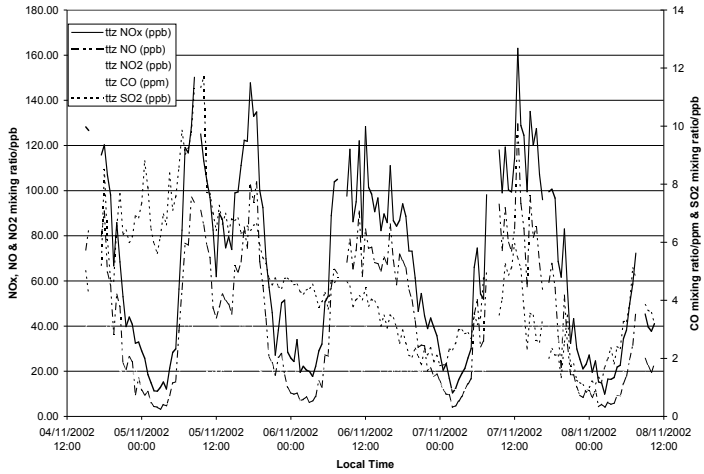

Figure 5: Half-hourly averages of point measurements of NOx, NO, NO_2, CO & SO_2

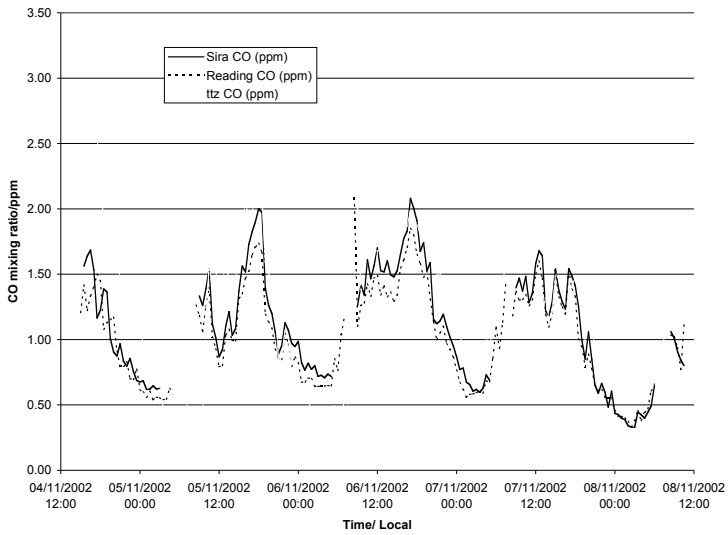

Figure 6: Inter-comparison of the CO measurements made between 04.11.02-08.11.02 (Sira: FTIR; Reading: FTIR; ttz: point measurement)

3 - Discussion

Initial inter-comparisons of the data involved plotting the data against each other looking for linear correlations. A good linear correlation was defined as how close R^2 tended to 1. A clear correlation between the concentration of CO in the street canyon to the amount of traffic was observed where R^2= 0.44, R^2= 0.74 and R^2= 0.75 for the point measurement technique and the two FTIRs respectively, thus inferring, as expected, that traffic is the primary local source of CO. This was further borne out by plotting the CO data against the wind direction and wind speed, giving R^2 values ranging from 0.01-0.07 indicating the CO concentration was not due to wind transport. It must also be noted that a better correlation with traffic was obtained with the remote optical measurement techniques than the point measurement technique.

There was also a good correlation between the FTIRs and point measurements themselves, with the straight line correlation of the ttz point measurements and the Sira open path measurements of R^2=0.53. The plot of the FTIRs gave a straight-line correlation of R^2=0.95, indicative of very good agreement, which is encouraging for the validation of the systems. The close correlation between the point and line ROMT measurements indicates that, due to the channelling effect in the street canyon, a strong canyon vortex does not form but the street pollution is rather advected along with the "street wind" while it disperses laterally. This shows that, for most urban cases in which channelling occurs, ROMT measurements are an equally good, if not a better substitute for point measurements, with the added advantage of monitoring a much larger field and therefore giving a better overview of the urban pollution at the site.

Conclusion

Initial analysis of the results from the field trial in Bremen has been very promising. It has highlighted the potential for remote optical measurement techhniques for the measurement of pollutant in typical urban environments, with the Fourier Transform Infrared Spectrometers performing equally well if not better than traditional point measurements techniques of urban pollution.

Judicious siting of the instruments through the use of computational fluid dynamic modelling beforehand assured that strong signals were measured for almost the entirety of this relatively short field campaign. Further analysis work using computational fluid dynamic modelling is now underway to interpret the results and establish quantitatively their quality assurance within the overall aims of ROSE evaluation.

Acknowledgments

The ROSE (Remote Optical Sensing Evaluation) project, contract no. GR6D-CT2000-00434 is funded by the European Commission's Competitive and Sustainable Growth Programme.

References

Andronopoulos, S., J.G. Bartzis, J. Würtz, & D. Asimakopoulos (1993): Simulation of the Thorney Island dense gas trial No. 8, using the code ADREA-HF, Process Safety Progress, vol 12, p 61-66.

Bartzis, R.J.G., (1991) ADREA-HF: A three-dimensional finite volume code for vapour cloud dispersion in complex terrain, Report EUR 13580 EN.

Venetsanos A.G., J.G. Bartzis, J. Würtz, D.D. Papailiou (2000): Comparative modeling of a passive release from an L-shaped building using one, two and three-dimensional dispersion models. International Journal of Environment and Pollution, vol 14, p 324-333.

Vlachogiannis D., S. Rafailidis, J.G. Bartzis, S. Andronopoulos, A.G. Venetsanos (2002) Modelling of Flow and Pollution Dispersion in Different Urban Canyon Geometries. Water Air and Soil Pollution Focus 2, p 405-417.

12th International Symposium "Transport and Air Pollution" / 12e Colloque international "Transports et pollution de l'air", Avignon, 16 -18 *June* / juin 2003
proceedings / actes, n°92, tome / Vol. 2, Inrets ed., Arcueil, France, 2003, p. 119-124

Comparison of path-integrated and in situ measurements within a street canyon to produce a validation data set

Klaus Schäfer*, Stefan Emeis*, Herbert Hoffmann*, Carsten Jahn*, Wolfgang J. Müller, Bernd Heits**, Dirk Haase**, Wolf-Dieter Drunkenmölle**, Bernd Leitl***, Frauke Pascheke***, Michael Schatzmann*** & Wolfgang Bächlin******
*Institute for Meteorology and Climate Research, Atmospheric Environmental Research (IMK-IFU), Forschungszentrum Karlsruhe GmbH, Kreuzeckbahnstr. 19, 82467 Garmisch-Partenkirchen, Germany - Fax: +49 8821 73573; e-mail: klaus.schaefer@imk.fzk.de
**Lower Saxony State Agency for Ecology (NLOE), Goettinger Str. 14, 30449 Hannover, Germany
***Meteorological Institute of Hamburg University, Bundesstr. 55, 20146 Hamburg, Germany
****Ingenieurbuero Dr. Lohmeyer, An der Rossweid 3, D-76229 Karlsruhe, Germany

Abstract
Measurements inside a street canyon and in the surrounding area of 1 km x 1 km (Goettinger Strasse in Hannover) are performed to produce a validation data set for meso/micro-scale model systems. Air pollutants and meteorological parameters are measured continuously by in situ stations inside the street canyon and in the surroundings. Path-integrating optical measurement techniques as DOAS are used continuously on the ground and roofs of the buildings at the street. A SF_6 tracer line source in the middle of the street is operated during IOPs. At both sidewalks of the street the tracer is measured in situ by air sampling at 12 sites and by path-integrating FTIR spectrometry. The data interpretation is discussed with wind tunnel experiments using a detailed aerodynamic model of this urban area. Data of all methods show the same differences between both side walks during perpendicular wind direction and thus a re-circulating flow pattern inside the street canyon can be concluded.
Key words: *path-integrated measurement techniques, in situ measurement techniques, air pollution, street canyon, DOAS, FTIR, wind tunnel*

Introduction

Tools are needed for the execution of the European Air Quality Framework Directive 96/62/EC and its daughter directives. This set of regulations requires from the EU member states to submit maps that show the spatial distribution of air pollutants for the member state in total, for conurbations with more than 250.000 inhabitants and for micro environments as, e.g., city districts subject to high pollutant concentrations.

In frame of the project VALIUM in the research programme AFO 2000 of the German Federal Ministry of Education and Research these tools are developed and validated (http://www.mi.uni-hamburg.de/technische_meteorologie/valium/index.html).

To produce a validation data set for meso/micro-scale model systems measurements are performed inside a street canyon and in the surrounding area of 1 km x 1 km (Goettinger Strasse in Hannover). The concept of field measurements is designed together with wind tunnel measurements (definition of appropriate weather conditions i.e. wind direction perpendicular to the street canyon, wind speed between 4 and 10 m/s and location of measurement systems). During IOPs an artificial line source for SF_6 is operated in the middle of the street. At both sidewalks of the street the tracer SF_6 is measured. Measurement results of path-integrating techniques and nearby in situ stations will be

compared and discussed together with results from wind tunnel experiments.

1. Measurement set-up and instruments

Since 2001 air pollutants (NO, NO_2, SO_2, O_3, CO, HC, benzene, toluene, p-xylene, dust, PM10, PM2.5, soot) and meteorological parameters (wind speed, wind direction, temperature, global radiation, humidity, pressure, turbulence parameters) are measured by in situ stations at four sites inside the street canyon (HRV1, 2, 3 since beginning of 2001, HRVS long-term station). In the surroundings of the Goettinger Strasse a long-term in situ station (HRSW on the roof of a building in about 42 m above ground) and two in situ measurement stations (HRV4, 5 since July 2001) are operated continuously. Path-integrating optical measurement techniques (up to three DOAS systems, HRT1, 2, 3, 4: NO, NO_2, SO_2, O_3, benzene, toluene, p-xylene) are used continuously on the ground in the street canyon and on the roofs of the buildings at the street. Path-integrated concentrations of CO, CH_4, N_2O, CO_2 and the tracer gas SF_6 of the artificial line source in the middle of the street are measured by FTIR spectrometry at both sidewalks of the street during the four IOPs (HRT5, 6) in 2002 and 2003.

The QA/QC activities are:

- Long-term comparison of different measurement techniques (ISO 13752 Air quality).
- Simultaneous measurements of different techniques in the same air mass 36 hours before / after IOP (e.g. CO concentrations by in situ and FTIR measurements).
- In situ measurement systems of the monitoring network of the Lower Saxony State Agency for Ecology are references.

2. Measurement campaigns and results

DOAS measurements

Inside the street canyon in an altitude of 4 up to 5 m above ground a DOAS system (HRT1) is operated to measure NO_2, benzene, toluene, ozone and SO_2 as described in Bächlin et al. (2003) The 180 m open path is installed from one sidewalk of the street across the lane of the street to the middle of the two-lane street. In this area four container stations for in situ measurements are sited: HRV2 at the emitter of the DOAS, HRVS and HRV1 at the sidewalk nearby the receiver of the DOAS and HRV3 at the other sidewalk opposite to HRV1. The air sampling of the container stations is in 1.5 up to 3 m altitude above ground. These different measurement methods are compared.

Nitrogen dioxide

The altitude variation of the NO_2 concentration was investigated in the last years and it was found that the negative gradient is lower than that of NO and CO. The reason is the continuous oxidation of the emitted NO to NO_2. To study the coincidence of the path-integrated DOAS measurements with in situ measurements at different stations the following half-hourly means were calculated:

- Means of all simultaneous half-hourly means of the stations HRVS, HRV1, HRV2, HRV3,
- Means of all simultaneous half-hourly means of the stations HRV1, HRV2 (located near the receiver and the emitter of the DOAS system).

The following data interpretations were performed:

- Correlation: The correlation of the DOAS measurement with single and averaged in situ measurement results including about 16,000 up to 18,000 values was calculated.
- Classification: The measurement values of each system were classified according to the amount and the absolute and relative standard deviation as discussed in van der Meulen (2003).

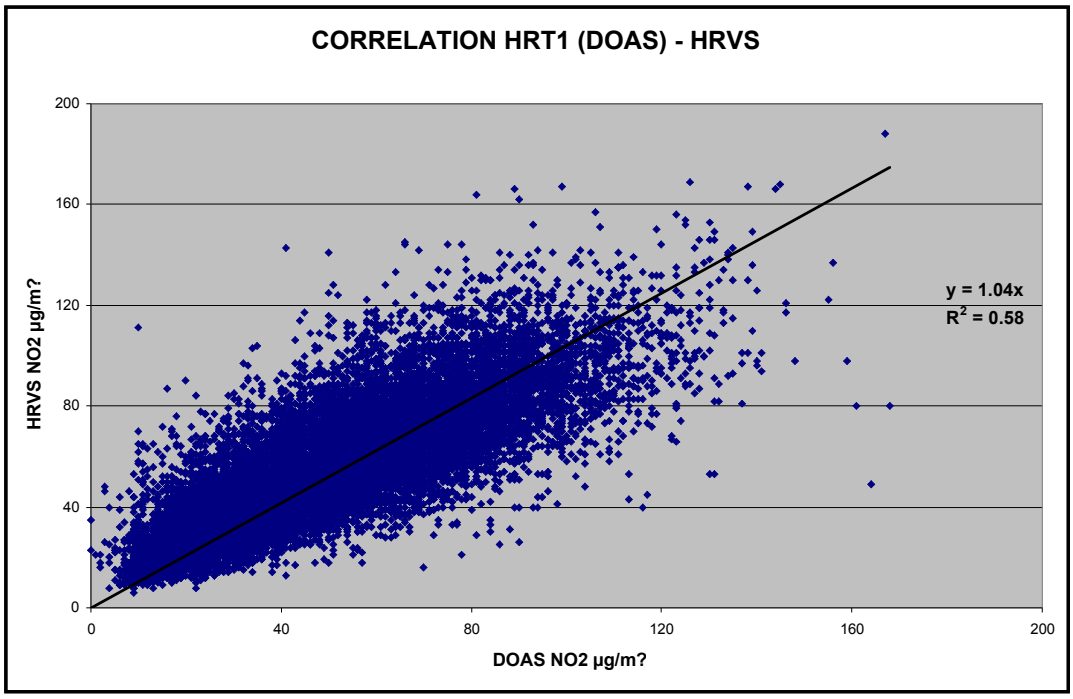

Figure 1: Correlation (gradient, R^2) of DOAS (HRT1) and in situ measurements (HRSV) for NO_2 in the Goettinger Strasse in Hannover in the time frame from February 2001 until May 2002.

The calculated gradients, correlation coefficients (R^2) and standard deviations (S_r) of the stations and the DOAS system given in Table 1 and Figure 1 for NO_2 concentrations show that the gradient of the balance line is near unity. So the measured values of the different measurement methods (DOAS and in situ) are in good coincidence. The best coincidence is found for HRVS and HRV1, which is caused by the installation of both stations very close to a traffic light.

Station	Correlated Station	Correlation		S_r
		Gradient	R^2	%
HRT1	HRVS	1.04	0.58	-
HRT1	HRV1	1.01	0.44	23.6
HRT1	HRV2	0.97	0.32	-
HRT1	HRV1/V2	1.00	0.46	24.1
HRT1	HRVS/V1/V2/V3	0.98	0.55	20.2
HRVS	HRV1	0.94	0.67	18.1

Table 1: Comparison of different NO_2 measurement results of in situ (HRVS, V1, V2, V3) and DOAS (HRT1) systems operated in the Goettinger Strasse in the time period February 2001 - May 2002 in terms of correlation (gradient, R^2) and standard deviation (S_r).

The correlation coefficients are relatively low. The reason could be that most of the measurement values are in the range from 30 up to 70 $\mu g/m^3$ so that the concentration range for the correlation calculation is restricted. It is important that the relative standard deviation between the DOAS system and the in situ stations is similar to the correlation among the in situ stations HRVS and HRV1.

Ozone

A better coincidence is found for ozone with the following correlation results:

- HRV4 and HRV5 with R^2 equal to 0.96,
- HRV4 and HRSW with R^2 equal to 0.95.

The background concentrations of ozone show a limited influence of the street canyon upon the direct surroundings of the living quarter. As the stations in the street canyon are not measuring ozone the DOAS measurement results (HRT1) can be compared with the background station HRSW at a roof of a building at the street in about 42 m altitude only. The correlation of ozone concentration measurements at HRT1 with HRSW is shown in Figure 2. The correlation coefficient is 0.63 and the gradient 1.24 i.e. the ozone concentrations in the street canyon are about 25 % lower than at HRSW, caused by chemical reactions of ozone with the high amount of emitted NO. The long-term mean of ozone is showing the same result: 44 μg/m³ at HRSW and 34 μg/m³ at HRT1. This difference is higher during ozone smog conditions.

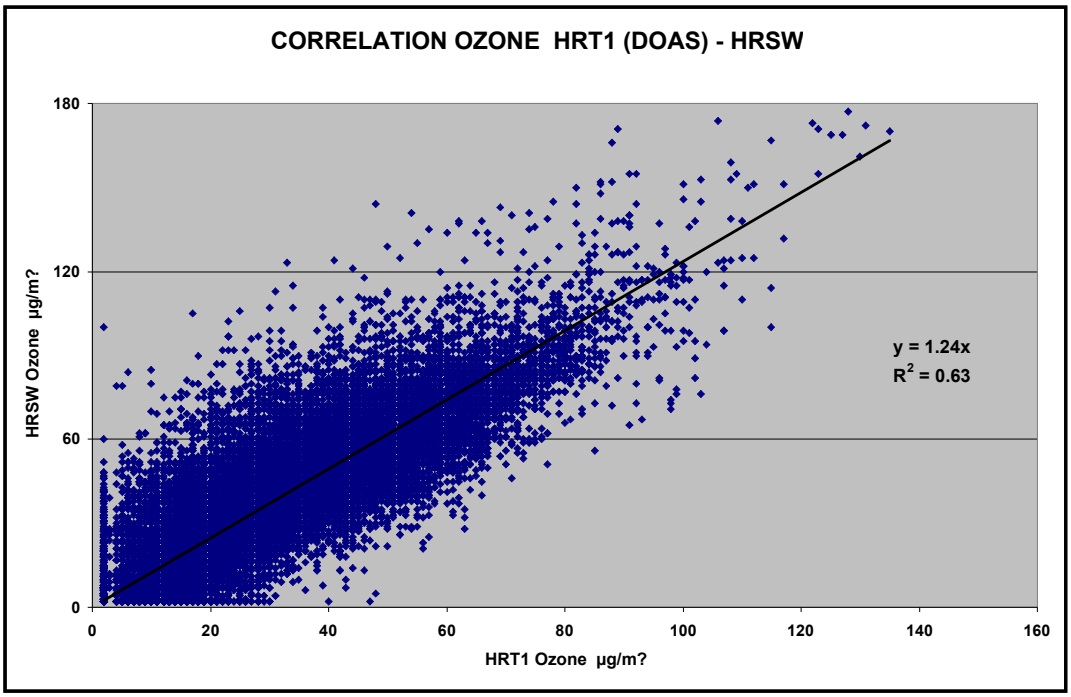

Figure 2: Correlation (gradient, R^2) of DOAS (HRT1) and in situ measurements (HRSV) for ozone in the Goettinger Strasse in Hannover in the time frame from February 2001 until May 2002.

Benzene

The annual mean benzene concentrations in the Goettinger Strasse are about 4 μg/m³. Only during high traffic episodes the values are higher. In general, the concentrations are near the detection limit of the in situ (gas-chromatography) and DOAS instruments. The long-term mean of both systems is similar.

Tracer gas experiment

During the IOPs a SF_6 line source of 96 m length in the middle of the Goettinger Strasse is operated. Measurements by FTIR spectrometry to determine path-integrated concentrations of the tracer gas SF_6 as well as CO, CH_4, N_2O and CO_2 (136 m lengths) are performed at both sidewalks of the street (HRT5, 6) in parallel to the line source. The temporal resolution of these measurements is about 5 minutes. The ambient air is sampled in teflon bags in about 1.5 m altitude at 12 sites on the side walks and at the roofs of the buildings, too. The sampling time of each bag is 30 minutes. The sampled air is analysed in the laboratory by gas-chromatography for SF_6.

Wind tunnel measurements

A detailed aerodynamic model of the urban area around the Goettinger Strasse was built at a scale of 1: 250 including topography. The core of the model covers an area of a 500 m radius and can be extended to an area of about 1 km x 1 km for each wind direction.

Corresponding to the field experiments, high-resolution velocity and concentration measurements were carried out in the large neutrally stratified boundary layer wind tunnel recently inaugurated at the University of Hamburg. The tunnel consists of a 18 m long flow establishment zone followed by a 4 m long test section with a width of 4 m and a height of 3.25 m.

A wind tunnel boundary layer corresponding to the model scale was generated using a combination of vortex generators and roughness elements. The quality of the generated wind tunnel boundary layer was verified and documented by the comparison of all flow and turbulence parameters with default values from nature. Supplementary, all available data from the field site were taken into account.

The experimental program consisted of the following steps: acquisition of time series at the specified sampling locations and additionally at several equidistant positions along the road lines of the street canyon; calculation of mean concentrations and standard deviations for averaging times equivalent to 10, 30 and 60 minutes full scale to quantify the minimum variability of concentration values due to the inhomogeneous turbulent flow field inside the street canyon; variation of the line source length to find the furthermost point of origin of exhaust gases for the specified wind direction; calculation of the operative line source parts related to some specified sampling locations.

3. Results

Along the two road lanes, large variations of the standard deviations were found from wind tunnel investigations. Overall, standard deviations were smaller at the leeward (west) side of the street canyon. Although the standard deviations of the 30 minutes averages were mainly below 20 %, for all locations variations of more than 100 % among consecutive mean concentrations were found. During field conditions, these ratios are likely to enhance due to permanent weather changes. At the other street side, the transport of air close to the ground occurred less frequently, corresponding to bigger standard deviations. It can be concluded that due to a re-circulating flow pattern inside the street canyon, a more or less continuous transport of tracer gas contrary to the mean wind direction occurred close to the ground.

The in situ concentration measurement results along the open paths of FTIR measurements were averaged over the distance between the measurement points giving path-integrated concentrations. Figure 3 shows a comparison between field (FTIR and sampling) and wind tunnel results in terms of path-integrated normalised concentrations c*. The concentration c* is defined as

$$c^* = \frac{c_Z \cdot u_{ref} \cdot h}{Q/L}$$

with $c_Z = (c - c_V)$: concentration of the additional air pollution, Q/L: emission source strengths per length unit, u_{ref}: wind speed in the altitude z_{ref} (in this case HRSW in 42 m altitude), h: normalising parameter (building height). Wind tunnel values given in Figure 3 represent long-term average concentrations whereas the field values correspond to seven 30-minutes averages. c* gives the possibility to compare field and wind tunnel measurements: all methods show the same c* ratio between westerly and easterly side walk. In Figure 3 the scatter bars attached to FTIR results correspond to half-hourly values whereas the scatter of the field sampling and wind tunnel data was calculated as mean relative scatter along the FTIR path.

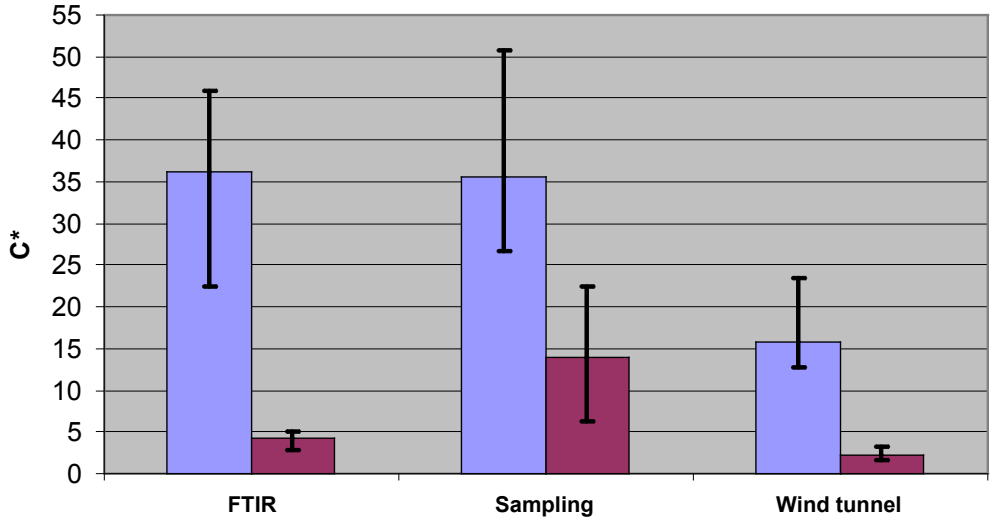

Figure 3: Comparison of c values from field (FTIR, sampling) and wind tunnel measurements with mean wind direction 250°±8° The results cover a time frame from 11:00 until 14:30 LT. Concentrations are calculated from 30 minutes averages. Left column: westerly side walk, right column: easterly side walk. The scatter bars correspond to half-hourly mean values.*

Conclusions and outlook

The measurement results show clear differences in concentration values measured on both side walks. Differences between the field data and the wind tunnel results arise, among other reasons, from the different averaging times inherent in both types of data. Whereas the wind tunnel mean values do represent a statistically safe long-term average of measured concentrations, the field data comprise a total of seven half-hourly mean values only. Consequently, a direct comparison of field results and wind tunnel data requires the scatter of the 30-minutes average values inherent in all field samples to be considered. For the wind tunnel results it must be considered, that the scatter of short-term average values is resulting from turbulent fluctuations only. Thus, the scatter of the short-term average values in the wind tunnel must be smaller than the scatter in the field. Since the scatter bars attached to the field data in Figure 3 have been calculated from 7 half-hourly mean values only, an even bigger scatter must be expected for an increasing number of samples.

Acknowledgements

The authors would like to thank the German Federal Ministry of Education and Research for funding this project with grant 07ATF12.

References

Bächlin W., H. Frantz, A. Lohmeyer, A. Dreiseidler, G. Baumbach, W. Theurer, B. Heits, W.J. Müller & K.-P. Giesen (2003): Feinstaub und Schadgasbelastungen in der Göttinger Strasse, Hannover. Niedersächsisches Landesamt für Ökologie, Nachhaltiges Niedersachsen 23, 28 pp.

Van der Meulen A., D. van Straalen, B.G. van Elzakker, B. Heits, E. Helmholz & H. Rienecker (2003): Field Comparison of Air Monitoring Networks. Niedersächsisches Landesamt für Ökologie, Nachhaltiges Niedersachsen 22, 57 pp.

12th International Symposium "Transport and Air Pollution" / 12e Colloque international "Transports et pollution de l'air", Avignon, 16 -18 *June* / juin 2003
proceedings / actes, n°92, tome / Vol. 2, Inrets ed., Arcueil, France, 2003, p. 125-130

A Methodology for Modelling and Measuring Traffic and Emission Performance of Speed Control Traffic Signals

Margarida Coelho*, Tiago Farias* & Nagui Rouphail**
* Instituto Superior Técnico, Dept. of Mech. Eng., Av. Rovisco Pais, 1049-001 Lisbon, Portugal - Fax +351 21 841 76 40 - email : margarida@navier.ist.utl.pt
** ITRE, NC State University Centennial Campus, Box 6801, Raleigh NC 27695-8601, USA

Abstract
In an attempt to control speeds and reduce crashes, traffic signals are being installed at several locations on highways to serve as speed reduction devices. One concern about these signals is that while they may be effective in reducing high speed crashes, they not only stop traffic that is exceeding the speed limit, but other traffic on the approach that is not. This may result in excessive delays, queuing and speed change cycles for approaching traffic. As a result, vehicle emissions are also likely to increase. An approach, based on experimental measurements, of modelling traffic and emission performance of speed control signals is presented herein to help explain the interaction between the signal control variables (for example minimum signal settings, speed threshold setting and minimum green call scenarios) and performance variables (such as delay, stops and emissions). The experimental data for validation were gathered on Highway N6, connecting Cascais and Lisbon, in Portugal.
Keys-words*: emissions, signals, speed, traffic.*

Résumé
Dans une tentative pour régler des vitesses et réduit des accidents, les signaux de circulation sont installés à plusieurs emplacements sur les routes pour servir d'expédie les appareils de contrôle. Une inquiétude de ces signaux est que pendant qu'ils peuvent être efficace dans réduire les accidents, ils arrêtent non seulement la circulation qui dépasse la vitesse maximum, mais l'autre circulation sur l'approche qui n'est pas. Ceci a pour résultat des retards excessifs, mettre en file d'attente et les cycles de changement de vitesse pour la circulation. Par conséquent, les émissions de véhicule sont aussi probables pour augmenter. Une approche, basée sur les mesures expérimentales, de modelage de circulation et émissions est présentée en ceci pour aider comprend l'interaction entre les variables de contrôle de signal (tel que les montages de signal de minimum, le montage de seuil de vitesse et les scénarios d'appel verts minimum) et les variables d'exécution (tel que le retard, les arrêts et les émissions). Les données expérimentales pour validation on été rassemblées sur la Route N6 qui connecte Cascais et Lisbonne, au Portugal.
Mots-clefs : *émissions, signaux, vitesse, circulation.*

Introduction

In an attempt to control speeds and reduce crashes, traffic signals are being installed at several locations on highways to serve as speed reduction devices. The signal works as follows (see Figure 1). Individual vehicle speeds are detected upstream of the signal and if the detected speed remains below a programmed speed threshold, the signal rests in green. Otherwise, the signal displays a clearance time, followed by a red time and a minimum green time. Depending on the controller settings, any additional “high speed calls” received during the minimum green time could be either ignored (Case A) or could trigger the start of a new cycle as soon as the current (minimum) cycle has elapsed (Case B). A variation of Case A is also considered in this research. In it, any additional

"high speed calls" which occur within a certain amount of time after the previous transgressor had actuated the system result in an extension of the red time by a fixed amount for each high speed call (Case C). As in Case A, any additional "high speed calls" received during the minimum green time are also ignored. One concern about these signals is that while they may be effective in reducing high speed crashes, they not only stop traffic that is exceeding the speed limit, but other traffic on the approach that is not. This may result in excessive delays, queuing and speed change cycles for approaching traffic. As a result, vehicle emissions are also likely to increase.

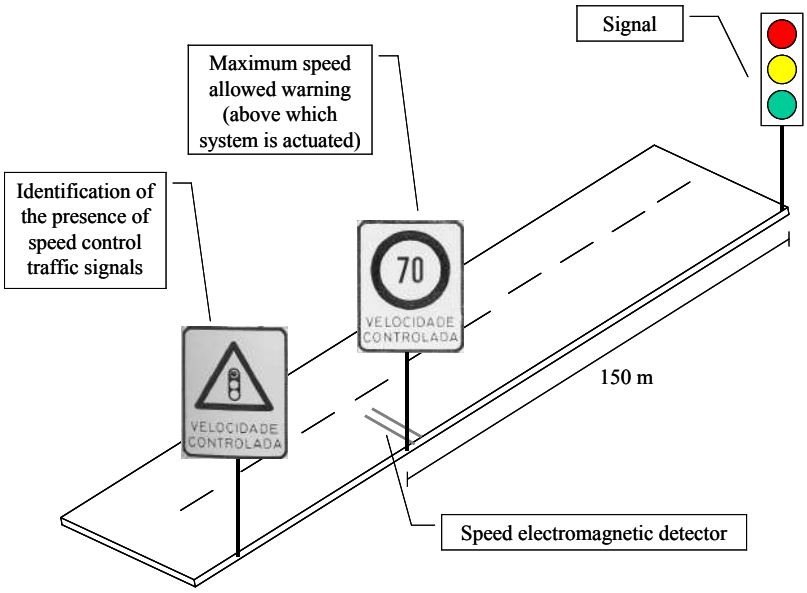

Figure 1: Warning and speed control system with electromagnetic detectors.
Figure 1 : L'avertissement et le système de contrôle de vitesse avec les détecteurs électromagnétique.

The authors are not aware of any current method that can quantify the impact of the speed control signals on traffic and emission performance. An approach, based on experimental measurements, of modelling traffic and emission performance of these signals is presented here in order to explain the interaction between the signal control variables (e.g. minimum signal settings, speed threshold setting and minimum green call scenarios) and performance variables (such as delay, stops and emissions).

1 - Methodology

The main purpose of this research was the development of a numerical predictive model, based on experimental measurements and concepts of traffic flow theory.

The approach presented here is macroscopic and deals mainly with the condition experienced by the average approach vehicle. Thus, all variables represent average conditions and do not include any measure of variability. The numerical method is applied to passenger car traffic only in a single lane, although it can be assumed that lane flows are homogeneous and therefore traffic performance will be similar across all lanes. Acceleration and deceleration models were borrowed from the aaSIDRA computer software, by Akcelik & Associates (2002). These were selected because they were the most detailed and most suitable for emission estimation. The emissions estimation model is founded on the modal emissions approach developed by Frey & Rouphail (2001). This approach categorizes the vehicle operation into four modes: idle, acceleration, deceleration and cruise. Each of the four categories generates a fixed emission rate (in milligrams per second) for the three pollutants considered in this study namely CO, NO and HC.

Several parameters are needed to calculate the performance variables, such as length of the yellow, red and green interval, the approaching traffic flow and vehicles average speed. In order to obtain

the experimental data needed for validation of the proposed methodology, field measurements of signal control and traffic stream variables were performed using video cameras on two different locations (each one with a different type of signal, Cases A and C) of Highway N6, connecting Cascais and Lisbon, in Portugal.

From the experimental measurements obtained, it was concluded that traffic speed on the facility closely follows a normal distribution with a given mean and a standard deviation.

The experimental distribution of time between vehicles exceeding the speed trigger showed that it could not be assumed that transgressors are randomly equally distributed throughout the traffic lane. Results obtained indicate that the distribution of the time between transgressors can be described by a Gamma function (characterised by parameters r and λ), with constant r. In addition, the dependency of parameter λ with traffic flow was assumed as follows: Mean Time = $3{,}600/(Q \cdot P_T) = r/\lambda$, in which P_T is the fraction of all traffic that is travelling above the trigger speed.

A Monte Carlo simulation method was implemented to generate time intervals between transgressors and, thus, relationships between three types of transgressors were found, namely: the fraction of all transgressors that actually actuate the system (F), those that increment the duration of red time (I) - applicable to Case C only - and transgressors that not actuate the system (H). The theoretical average time between speeders is dependent of the hourly traffic volume (Q) approaching the system and can be expressed as $3{,}600/(Q \cdot P_T)$. The proposed expression for the average time between the arrivals of speeders that actuate the system, T_T, is: $T_T = 3{,}600/(Q \cdot P_T \cdot F)$.

2 - Results

Comparison between numerical and experimental results

The authors could not find any real world situation where Case B was implemented. Therefore, only Cases A and C were validated with experimental data. The traffic volumes measured were 992 and 832 vehicles per hour, for Case A and C, respectively. For Case A, there were two approach lanes, while there was only one approach lane for Case C.

The comparison between the numerical and experimental results for both Cases A and C are presented in Tables 1 and 2, respectively.

VARIABLES	*NUMERICAL MODEL*	*EXPERIMENTAL DATA*
Fraction of speed transgressors	0.18	0.21
Average time between speeders (theoretical) [s]	20.64	16.85
Fraction of speed transgressors that actuate the system (F)	**0.46**	0.43
Average time between speeders that actuate the system [s]	44.45	40.12
Average cycle length [s]	44.45	40.12
Average red time [s]	6.42	6.62
Average green time [s]	34.81	30.28
Number of actuations of the system per hour	81	88
Fraction of vehicles stopped	0.30	0.34
Fraction of vehicles unfairly stopped	0.25	0.27
Fraction of vehicles that correctly stop	0.05	0.07
Fraction of vehicles that correctly go	0.58	0.53
Fraction of vehicles that incorrectly go	0.12	0.14

Table 1: Comparison of numerical and experimental results for Case A.
Tableau 1 : Comparaison de résultats numériques et expérimentaux pour Cas A.

VARIABLES	*NUMERICAL MODEL*	*EXPERIMENTAL DATA*
Fraction of speed transgressors	0.39	0.35
Average time between speeders (theoretical) [s]	11.05	**12.55**
Fraction of speed transgressors that actuate the system (F)	0.28	0.25
Fraction of speed transgressors that increment red time (I)	0.33	0.29
Fraction of speed transgressors not actuating the system (H)	0.39	0.46
Average time between speeders that actuate the system [s]	39.78	49.46
Average cycle length [s]	39.78	37.29
Average red time [s]	10.13	7.38
Average green time [s]	25.48	25.75
Number of actuations of the system per hour	91	72
Fraction of vehicles stopped	0.67	0.58
Fraction of vehicles unfairly stopped	0.41	0.38
Fraction of vehicles that correctly stop	0.26	0.20
Fraction of vehicles that correctly go	0.20	0.28
Fraction of vehicles that incorrectly go	0.13	0.15

Table 2: Comparison of numerical and experimental results for Case C.
Tableau 2 : Comparaison de résultats numériques et expérimentaux pour Cas C.

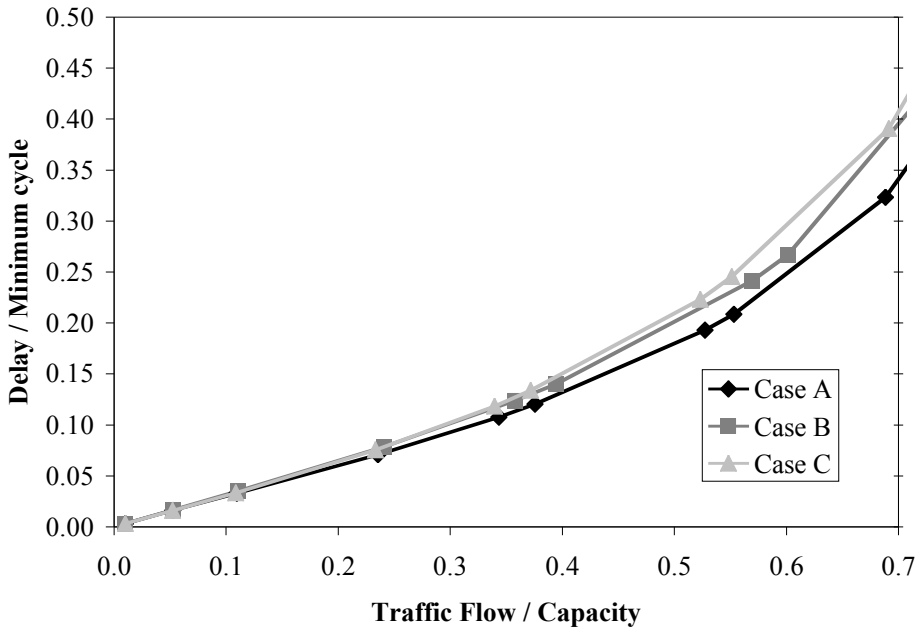

Figure 2: Delay / Minimum Cycle vs. Traffic Flow / Capacity.
Figure 2 : Retard / Minimum Cycle vs. Volume de circulation / Capacité.

Sensitivity analysis

The sensitivity analysis is based on the trade-offs between level of enforcement – how many speed limit abiding drivers should be stopped/penalized for every transgressor that is stopped/penalized – against the cost of added emissions. The inputs for the analysis were the ratios between: traffic flow and capacity; red increment and minimum cycle (applicable to Case C only); minimum green time and sum of yellow and minimum red intervals. These ratios will affect the parameters of traffic control and the emissions. The analysed variables were delay, fraction of vehicles that stop and additional emissions per vehicle caused by the presence of signals (for each pollutant). The most relevant results are represented in Figures 2, 3 and 4.

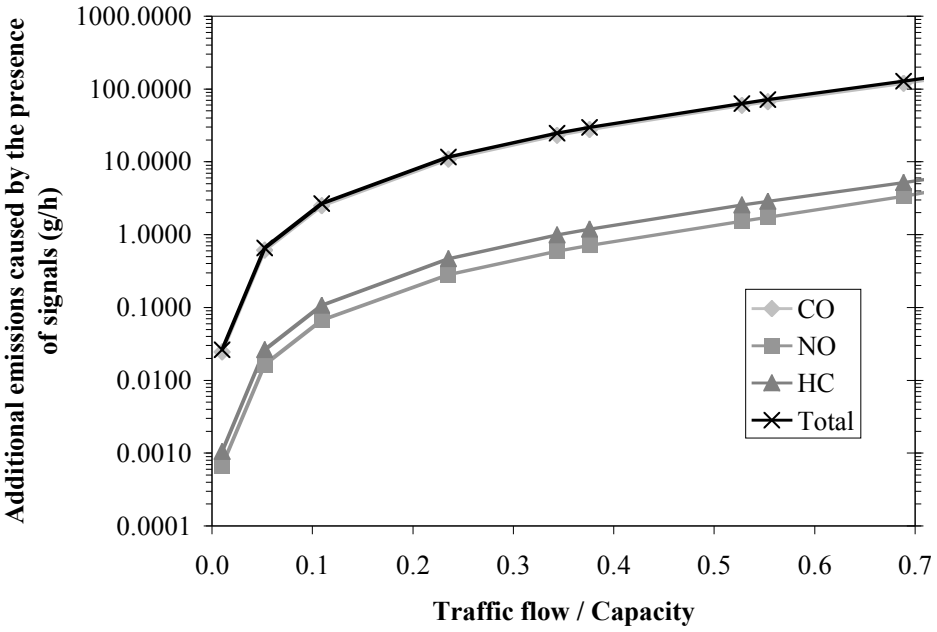

Figure 3: Additional emissions caused by the presence of signals vs. Traffic Flow / Capacity - Case A.

Figure 3 : Émissions supplémentaires causé par la présence de signaux vs. Volume de circulation / Capacité – Cas A.

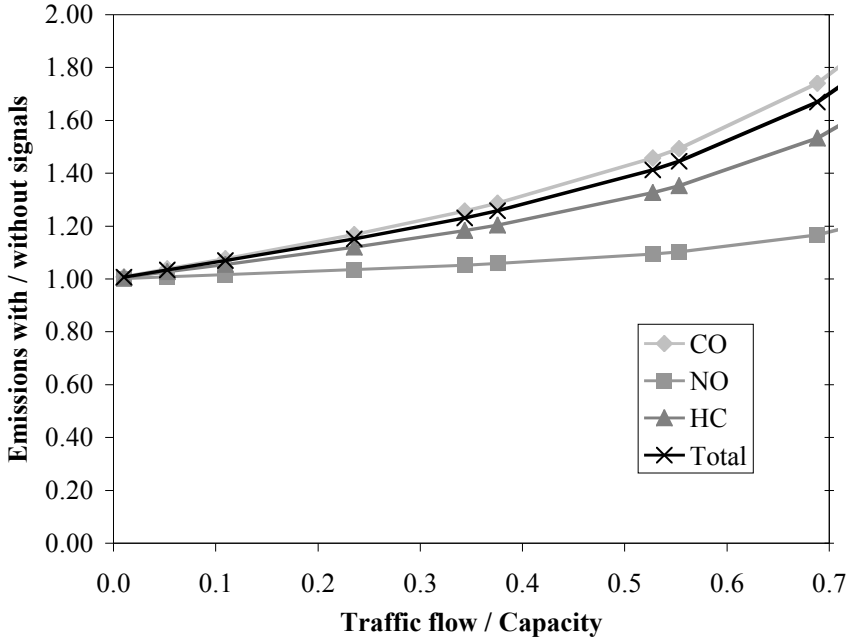

Figure 4: Local increase in emissions caused by the presence of signals vs. Traffic Flow / Capacity - Case A.

Figure 4 : L'augmentation locale dans les émissions causé par la présence de signaux vs. Volume de circulation / Capacité – Cas A.

3 - Discussion

The main interpretations of the results presented in the above tables and figures are summarized below. Looking at Tables 1 and 2, it can be seen that there is not a significant variation between the

numerical and experimental results. However, the existing variations may be due to the fact that the gamma function is not perfectly suited to the experimental data distribution of time between transgressors. To improve these results, a larger amount of experimental data should be gathered.

From the analysis on two specific places of Highway N6, results indicate that the implementation of signals with the system A had the consequence of an additional 119% of CO, 17% NO, 82% HC and 106% in total emissions. The implementation of signals with system C increased emissions by 164% for CO, 41% for NO, 120% for HC and 149% in total emissions. As presented on Figure 2, delay increases with the traffic flow and this increase is worse for Cases B and C. Similarly, the additional emissions caused by the presence of signals increase with traffic flow (see Figure 3). The evolution of the additional emissions for Cases B and C is similar. When the ratio between traffic flow and capacity increases from 0.1 to 0.7, the ratio between total emissions with and without the presence of signals (see Figure 4), considering that the total distance of influence in acceleration and deceleration is about 300 meters, increases by 56%, 82% and 67%, for Cases A, B and C, respectively. It was also concluded (results not shown) that the fraction of vehicles that stop at the signals increases with traffic flow, for all cases, but the variation is more pronounced for Case B.

The trade-off is now clear when experimental data are examined. In Case A, out of the 21% of drivers that were transgressors, about 33% actually stopped, while 67% did not. In the more restrictive Case C, out of the 35% drivers that were transgressors, about 57% stopped while 43% did not. The numerical emission model predicts an increase of 106% for Case A and 149% for Case C. Thus, succeeding in stopping a larger fraction of transgressors will result in higher emissions.

Conclusion

The main motivation of the developed research was the analysis of the compromise between safety and emissions, namely between the trade-offs between level of enforcement – how many vehicles do we want to stop/penalize for every transgressor that is stopped/penalized – against the cost of added emissions. With the proposed methodology some questions could be answered, such as: quantification of the environmental consequences of the installation of speed control traffic signals; identifying which of the control systems (A, B or C) causes more delay (that can result in increased traffic congestion) and more stopped vehicles; and selection of most environmental appropriate stopping time at the signal, in order to minimize the emissions and delay.

The obtained results were very encouraging, confirming the applicability of the proposed numerical methodology to describe the behaviour of traffic in the presence of speed control traffic signals. The described methodology, by estimating and minimizing emissions effects, is very useful because it can help local authorities to decide on the best actions to avoid/reduce those environmental and social problems and educate drivers concerning the environmental impact of a short stop.

Acknowledgments

The research work of Margarida Coelho is supported by a PhD scholarship of the Portuguese Science and Technology Foundation (FCT) and European Social Fund (FSE), within the Third Framework Programme. This research had the support of the Project POCTI/MGS/37601/00, approved by FCT and POCTI, financially supported by the European Community Fund FEDER.

References

Akcelik & Associates (2002): aaSIDRA User Guide. Akcelik and Associates Pty Ltd, Melbourne, Australia, p 46-48 and p 107-120.

Frey, H., N. Rouphail, A. Unal & J. Colyar (2001): Emission Reduction Through Better Traffic Management: An Empirical Evaluation Based Upon On-Road Measurements. North Carolina Department of Transportation, Report No. FHWA/NC/2002-001, United States of America, 333 p.

12th International Symposium "Transport and Air Pollution" / 12e Colloque international "Transports et pollution de l'air", Avignon, 16 -18 *June* / juin 2003
proceedings / actes, n°92, tome / Vol. 2, Inrets ed., Arcueil, France, 2003, p. 131-136

Air pollutant emissions and dispersion in regional and local transport planning

Carlo Trozzi, Rita Vaccaro & Stefano Crocetti
Techne consulting srl, Via G. Ricci Curbastro, 34 - I00153 Roma, Italy
email: carlo.trozzi@techneit.com

Abstract
The paper reports the application of the methodology for air pollutant emissions estimate from road transport developed within the project MEET to regional and local transport planning, in the actual situation and in prevision. The computer program SETS, integrated with the CALINE4 dispersion model, is first introduced. Next, the paper describes the data needs and procedure followed for the emissions estimates in different regional and local situation: regional and urban scale top-down or bottom-up estimates and microscale emissions estimates and dispersion modelling. Finally the use of emissions estimate and dispersion models in microscale level will be discussed.
Keys-words*: air pollutant emissions, regional transport planning, urban roads, highways, Italy.*

Introduction

The paper reports as the methodology for air pollutant emissions estimate from road transport developed within the project MEET (Methodology for Estimate Air Pollutant Emissions from Transport), funded by the European Commission under the transport RTD programme of the 4th framework programme (Hickman J. et al., 1999; Joumard, 1999), has been applied to regional and local transport planning in the actual situation and in prevision.

In air quality management and transport planning there are several needs of air emissions estimate and air quality evaluation. The goals of activities are regional or urban scale top-down and bottom-up estimates, and local or urban scale microscale estimates. Top-down approach estimates emissions on the basis of statistics information at an aggregated geographical scale (region, urban area) and are appropriate for general regional or urban planning while bottom-up approach estimates emissions on the basis of specific information at road by road scale and are appropriate for road network planning. Finally microscale estimates are used for microscale traffic planning.

The different estimates need different approaches but, with some limitation for microscale estimates, can be performed with the same methodology and software. In the following chapter this methodology and software will be introduced and discussed.

The case studies introduced are from regional air quality management plans, regional transport planning, urban air quality measures planning, environmental impact analysis, etc. (Trozzi et al., 1994; 1996; 1997; Trozzi and Colaiezzi, 2000; Trozzi, 2003).

1 – Methodology and software

In order to evaluate the air quality in the road the computer model SETS Diffusion is used (Figure 4). The model integrates an opportune emissions module and a dispersion module.

The emission module (*SETS)* allows the estimate of the air pollutants emissions produced by road traffic (Trozzi et al., 1995). The program has been upgraded to use the methodology developed within the project MEET and recently benzene emissions are introduced utilizing CONCAWE studies (CONCAWE, 1999; 2000). The dispersion module allows the estimate of the air pollutants

concentrations with the CALINE4 dispersion model, developed by California Department of Transportation (State of California, 1989).

In Figure 4 is described the data flow toward the models. From the picture can be deduced the data needs in input to the emissions and dispersion modules. The SETS module produces the emissions information for CALINE dispersion module, while the others geometric, meteorological and chemical data are directed inserted in dispersion module.

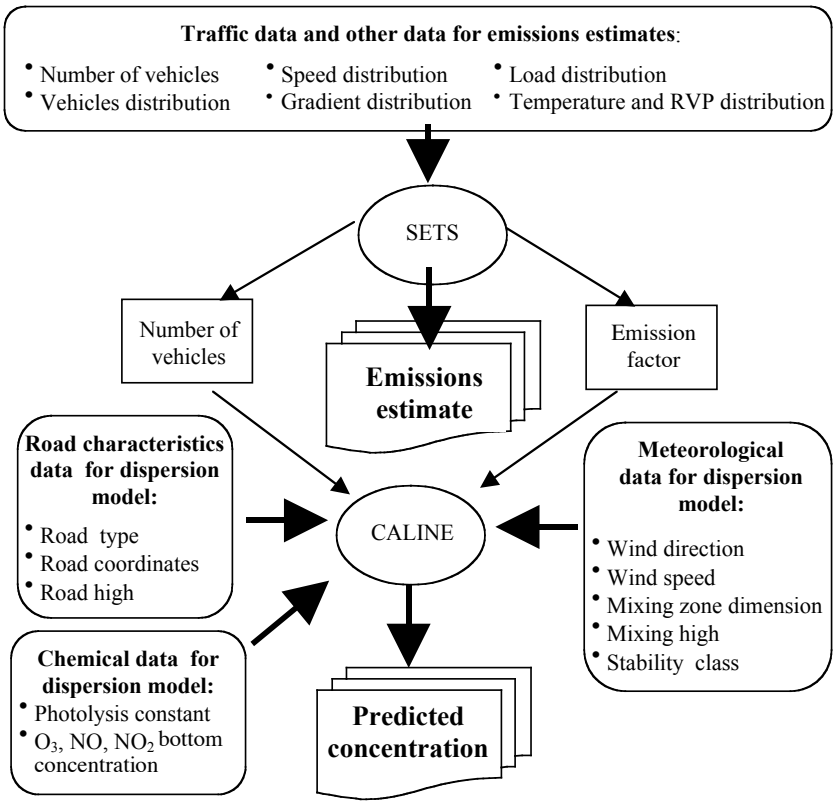

Figure 4: Input/output flow diagram for SETS Diffusion model

In SETS emissions module the user can define a lot of simulations. Each simulation is characterized by number of vehicles circulating subdivided in *categories of vehicles*. A simulation can be referred to a single road or to an area (city, province, region, nation).

The most important data are the number of vehicles circulating. These can be the total number of vehicles registered for a given area or the effective number of vehicles passing a single road section (for example from vehicles counting). The data are introduced with the following general subdivision: cars, two stroke cars, commercial vehicles, urban buses, other buses, motorcycles.

The user can associate to each simulation in the model:

➢a lot of predefined distribution selected between a library of distributions for:

- *vehicles* - as percentage inside each category between fuels, load or engine capacity classes and normative following the MEET classification (usually: *national average*, *regional average*, *regional urban*, *national highway*, etc.);
- *speed* - as percentage inside each category-fuel-load/capacity class between twelve speed classes with an amplitude of 10 km/h, starting from class 10-20 up to class 120-130; usually can be defined regional general or road specific speed frequency distributions (for example *average*, *congested hours*, etc.);
- *load* - as percentage inside each category (actually defined only for commercial vehicles) between loaded and unloaded; usually can be defined regional general or road specific load frequency distributions (for example *average*, *highway*, etc.);
- *gradient* - as percentage inside each category between seven different classes (from [-6%,-

4%] to [4%,6%]); usually can be defined regional general or road specific gradient frequency distributions (for example *average hill*, *average mountains*, *highway*, etc.);

- a lot of predefined monthly profile selected between a library of profiles for:
  - *temperature* - associated with different years or different regions;
  - *RVP (Reid Vapour Pressure as a measure of gasoline volatility) and other fuel characteristics (lead and sulphur contents)* - associated with different years or regions;
  - *mileage* - as monthly percentage inside each category; usually can be defined regional general or road specific monthly mileage distribution (for example *average*, *tourist*, etc.).

For the use of dispersion module are necessary a set of other data on roads geometry, meteorology and pollutant chemistry data.

2 – Regional scale top-down emissions estimates

In the regional scale top-down estimates the model is used:

- to estimate global regional emissions and evaluating the relative contribution of road transport,
- to estimate the monthly, weekly and daily distribution of emissions,
- to evaluate the effect, on regional scale, of modification of vehicles fleet composition, fuel properties, goods transport composition (road-train and road-ships modal shift).

Usually regional scale top-down estimates are used to evaluate urban and extraurban emissions (with the exclusion of highway emissions, mostly evaluated with a bottom-up approach). In this case the following procedure is used:

- retrieval of statistical or regulatory data about:
  - register information (from Public Register of Automobiles) about number of circulating vehicles on a regional basis for vehicle categories (category-fuel-load/capacity),
  - quantity and characteristics of fuels sold in ordinary regional fuels distribution network,
  - average regional temperature data;
- evaluation or estimate of:
  - average mileage for type, class and category of vehicle,
  - average traffic characteristics such as average trip length,
  - average speed, load and (where possible) gradient frequency distribution;
- computation of total fuel consumptions and verification with statistical data about fuels solded.

An iterative process is activated in which the user modify inserted estimate data (trip length, average mileage, etc.) to obtain a fuel consumption estimates compatible with solded fuels.

In conclusion in these cases the emissions:

- are estimated on regional scale;
- are evaluated at municipal level using a lot of proxy variables known at the municipal level; proxy variables allow obtaining information on a certain spatial resolution assuming that it is known for larger spatial resolutions; municipal level in Italy corresponds to level 5 of NUTS (Nomenclature of Territorial Units for Statistics) classification scheme established by Eurostat;
- inside the municipality a square grid mesh (1km x 1km) is built-up to represent emissions on a very detailed scale; to disaggregate emissions to the mesh level, the methodology of proxy variables is used assigning to emissions the same spatial distribution of another variables that it's assumed to have a similar behavior; usually urban areas coverage from land cover maps and extraurban road network from transport maps are used as proxy variables;

An example of regional scale top-down estimate is reported in Figure 5 for Florence Province. In the picture are evident the main urban agglomerates (particularly Florence metropolitan area).

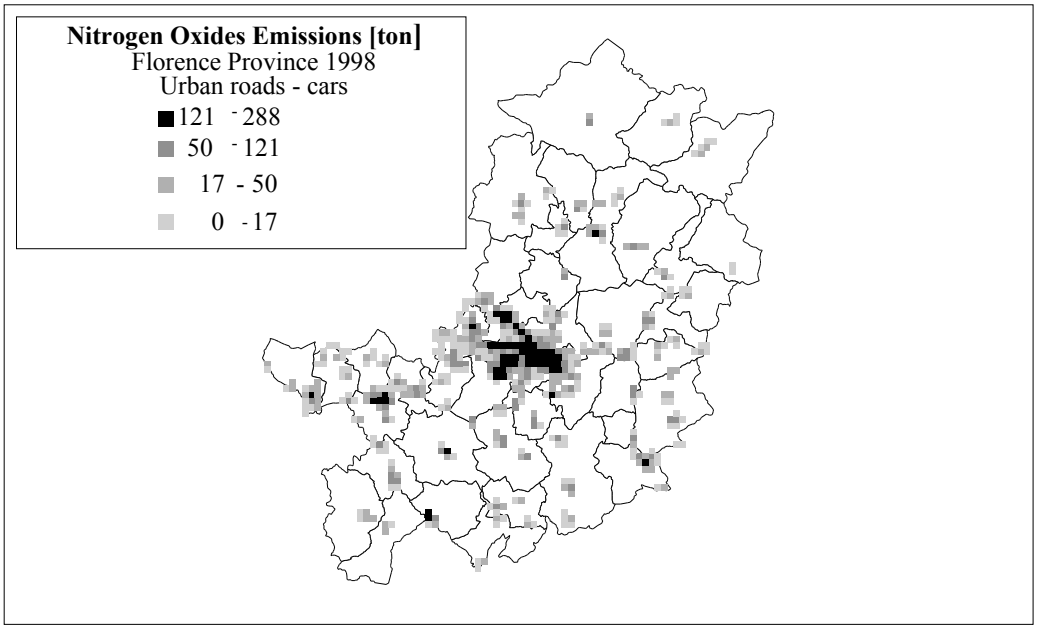

Figure 5: Nitrogen oxide emissions on 1km x 1km grid at regional scale

3 - Regional scale bottom-up emissions estimates

In the regional scale bottom-up estimates the model is used:

- to estimate on road by road basis the emissions on highway and main regional roads;
- to support on road-by-road basis the regional transport policies planning;
- to estimate the monthly, weekly and daily distribution of emissions;
- to evaluate the effect, on single roads, of modification of goods transport composition (road-train and road-ships modal shift).

An example of regional scale bottom-up future emissions estimate is reported in Figure 3 for Bolzano Province, in the frame of regional transport planning. In the picture, relative to an estimate of future Benzene emissions, are clearly represented the main extraurban roads and highways.

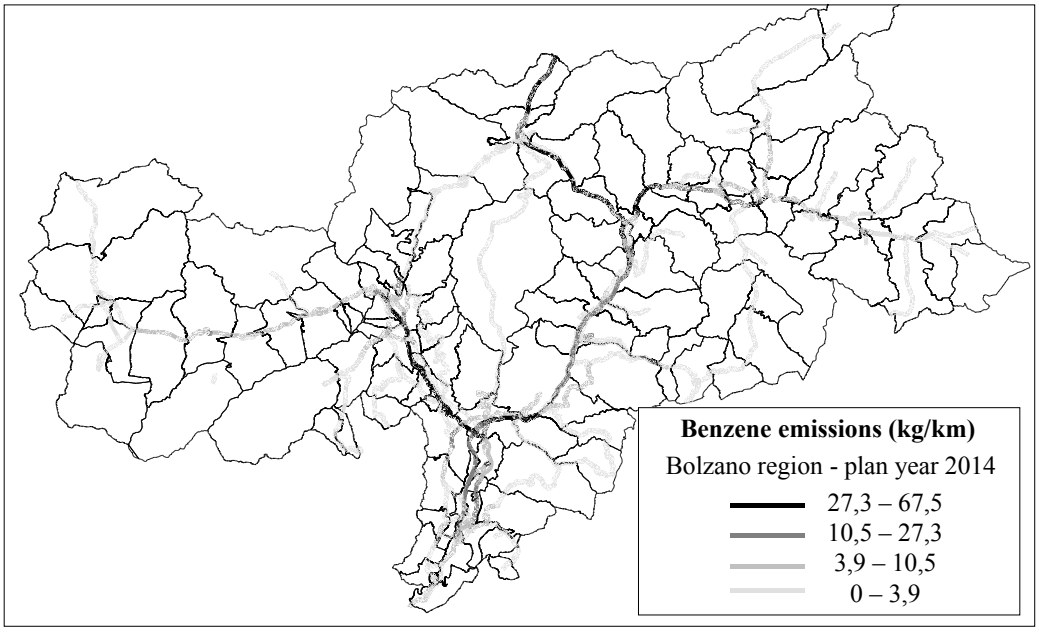

Figure 3 : Benzene 2014 annual emissions in extraurban and highway road segments (kg/km)

Usually regional scale bottom-up estimates are used to evaluate extraurban and highway emissions. In this case the following procedure is used:

- evaluation of specific road sections characteristics such as: length, specific gradient frequency distribution road by road, specific load frequency distribution road by road (or, where not valuable, default one), average temperature data;
- retrieval of counting or traffic models data about: number of vehicles subdivided in *category of vehicles*, average speed, monthly distribution of traffic;
- use of top-down national (for highways) or regional (for other extraurban roads) data about: distribution of circulating vehicles for *categories of vehicle* (category-fuel-load/capacity), characteristics of fuels solded (RVP, sulphur content, lead content);
- evaluation or estimate of specific speed frequency distribution; a lot different speed distributions must be created and associates to the roads based on average speed, measured or defined by the traffic model of assignment of the flows, and of the average inclination of the arc.

Usually cold start emissions are not computed in these cases; however in some extraurban application (very cold climate), a cold start effect can be relevant.

4 - Urban scale top-down emissions estimates

In the urban scale top-down estimates the model is used as in the regional scale and also:
- to evaluate the effect, on urban scale, of limitation of circulation of specific vehicles classes such as "old" passenger cars, heavy duty vehicles, motorcycles, light duty vehicles;
- to evaluate the effect, on urban scale, of modification of fuel properties.

Urban scale top-down emissions estimate is a very difficult task due to a generally lack of information on urban scale. Nevertheless the task is very important, particularly in large metropolitan areas, for urban air quality planning and for use in bottom-up and microscale emissions estimates. In this case the same procedure as in the regional case is used where all the information related at "region" must be evaluated for an area sufficient to include all the "urban area" (usually province area).

In these cases the emissions:
- are estimated on "urban area" scale;
- when emissions are estimate on large metropolitan scale level, can be useful to characterize single main access roads with bottom-up estimates and compute urban emissions as the emissions of remaining traffic;
- inside the "urban area" a square grid mesh (1km x 1km or less) is built-up as in regional case and road network coverage from urban maps can be used as proxy variable.

5 - Local or urban scale bottom-up emissions estimates

In the local or urban scale bottom-up estimates the model is used:
- to support urban traffic models for emissions estimate on urban model network;
- to support local transport policies planning based on traffic models;
- to evaluate emissions on single roads from vehicles counting;
- to estimate the monthly, weekly and daily distribution of emissions;
- to support environmental impact analysis of new road infrastructures through atmospheric diffusion models.

As in the case of regional scale bottom-up emissions estimates that uses as background information regional estimates in these case urban scale top-down emissions estimates are used as as background information for the relevant urban parameters.

6 - Local or urban microscale emissions estimates and dispersion modeling

The local or urban scale microscale emissions estimates can be of different types and in some cases can use the same SETS model; in some other cases specific microscale approach such as instantaneous emission approaches can be useful (Technische Universität Graz, 1999; United States

Environmental Protection Agency, 2001).

Generally, instantaneous emission modeling is not yet validate, some example of application of the SETS model at particular microscale examples are to support the evaluation of microscale measures (such as: new roads, traffic light policies, one way introduction, ring introduction, etc.) and to evaluate emissions for microscale diffusion models. In Italy some application was realized for the study of new infrastructure, the study environmental impact of tunnel, the study of one-way policies in urban road with gradient. From the experience is confirmed as the use of instantaneous emission approaches is recommended only in limited cases where driving behavior and dynamics is of major interest. Average speed models are not appropriate for such tasks.

Conclusion

In the paper is discussed the application of MEET methodology on regional and local scale, with detailed speed, gradient and load frequency distributions. From several Italian experiences is clear the need for more detailed data on traffic speed composition and average trip length. The methodology can be usefully used in some situations also on microscale level.

Acknowledgments

The authors wish to thank the many regional Italy experts in Air quality management that support the work in last years.

References

Joumard R. (ed.) (1999): COST 319 - Estimation of pollutant emissions from transport: Scientific state-of-the-art and network of European scientists. European Commission, DG Transport, n°EUR 18902, ISBN 92-828-6797-8, Luxembourg, 174 p

CONCAWE (1999) : Fuel quality, vehicle technology and their interaction, report no.99/55, Brussels, 66 p

CONCAWE (2000) : An assessment of the reproductive toxicity of gasoline vapour, report no.00/53, 20 p

Hickman J., D. Hassel, R. Joumard, Z. Samaras & S. Sorenson (1999): MEET - Methodology for calculating transport emissions and energy consumption. European Commission, DG VII, ISBN 92-828-6785-4, Luxembourg, 362 p

State of California (1989) : CALINE4 – A dispersion model for predicting air pollution concentrations near roadways, Department of Transportation, Division of New Technology and Research. Final Report, November 1984, Revised June 1989, 205 p

Technische Universität Graz (1999) Instantaneous Emission Data and Their Use in Estimating Passenger Car Emissions Editor: Univ.-Prof. Dr. R. Pischinger Mitteilungen des Institutes für Verbrennungskraftmaschinen und Thermodynamik Heft / Volume 74, 43 p

Trozzi C., R. Vaccaro and S. Crocetti (1994) : Air pollutants emissions estimate from road traffic: application of Corinair baseline methodology in Italy and in Rome metropolitan area. Post. Proc. 3th Int. Symp. "Transport and air pollution", Avignon, France, 6-10 June 1994, pp. 212-217.

Trozzi C., R. Vaccaro, P. Digiovandomenico and S. Crocetti (1995) : SETS: Estimate of air pollutants emission from road traffic. Proc. 4th Intern. Softw. Exhib. Environ. Sc. Engin., Como, Italy, 2-3 march 1995, Pàtron edit., Bologna, pp. 221-226.

Trozzi C., R. Vaccaro and S. Crocetti (1996) : Speed frequency distribution in air pollutants emissions estimate from road traffic. Sc. Tot. Envir. n° 189/190, p 181-185.

Trozzi C., R. Vaccaro, S. Crocetti (1997) : Emission and dispersion in roads with gradients: a case study. Poster Proc. 4th Int. Symp. "Transport and air pollution", Avignon, France, 9-13 June 1997, pp. 231-236.

Trozzi C., M. Colaiezzi (2000) : Actual and future air pollutant emissions and dispersion in urban roads with gradient: Genoa XX Settembre road case study Poster Proc. 9th Int. Symp. "Transport and air pollution", Avignon, France, 5-8 June 2000, pp. 381-388

Trozzi (2003) : Regional air quality management in Italy, in: Regional and Local Aspects of Air Quality Management, D.M. Elsom, J.W.S. Longhurst, (Eds.), WIT Press Southampton, Boston, in press

United States Environmental Protection Agency (2001) : EPA's New Generation Mobile Source Emissions Model: Initial Proposal and Issues, EPA Mobile Source Emissions Modeling Workgroup, EPA420-R-01-007, April 2001, 48 p

12th International Symposium "Transport and Air Pollution" / 12e Colloque international "Transports et pollution de l'air", Avignon, 16 -18 *June* / juin 2003
proceedings / actes, n°92, tome / Vol. 2, Inrets ed., Arcueil, France, 2003, p. 137-143

Un modèle de microsimulation pour l'évaluation des émissions polluantes dans les aires urbaines en fonction du régime de marche et pour une typologie véhiculaire

Sergio d'Elia
Università della Calabria, Dipart. di Pianificazione Territoriale, Ponte Bucci Rende Cosenza -Italia
Fax : 39 0984 496782 - email : sdelia@unical.it

Résumé
Cet article présente un modèle construit pour le calcul des émissions polluantes dans les aires urbaines, et utilise une méthodologie (d'Elia – Danieli) qui permet de mesurer les réelles émissions sur des véhicules équipés, avec des caractéristiques semblables à celles du parc véhiculaire Italien.
Les modèles formulés pour le calcul des émissions polluantes sont nombreux, mais les réelles émissions polluantes en Italie où il existe des conditions de débit très variables même pour la morphologie des infrastructures urbaines existantes (largeur des routes, distances entre les intersections, obstacles, visibilité, etc.) restent peu connues.
Les mesures sont relatives à des cycles de conduite UDC et EUDC de plusieurs véhicules, catalysés et non catalysés, qui ont circulé pendant plusieurs mois, avec des flux variables dans des zones caractérisées par des accélérations et des décélérations continues, ou dans des aires sans trafic.
La base de données obtenue permet la construction et le calibrage d'un modèle de prévision des émissions valide et adhérent à la réalité des villes italiennes.
Le modèle a été ensuite comparé à d'autres modèles pour vérifier les diversités existantes.
Mots-clefs : *modèles de micro-simulation des émissions polluantes.*

Abstract
This paper presents a model for calculating pollutant emissions (CO, NOx, HC) in urban areas, constructed on specially equipped vehicles circulating in Italy, on urban and extra-urban infrastructures.
The measurements relate to UDC and EUDC driving cycles of several vehicles, catalysed and non-catalysed, which were driven during various months, in different conditions, in variable traffic flows in zones characterised by continuous acceleration and deceleration, or in traffic-free areas, but also driven by different drivers in order to obtain data which are independent of the style of driving.
The pollutant emissions were drawn from the relief of the instantaneous parameters of engine movement and operation, along a series of predetermined itineraries, taking into consideration the particular characteristics of the vehicles. The data obtained by the method described above, for each itinerary and vehicle, are representative of the characteristics of the movement (speed and acceleration), of altimetric operation (slope), and of the polluting substances emitted, in function of time and space.
Determination of the polluting substances emitted by a vehicle along an itinerary is achieved through the analysis (by means of software) of the data recorded on instrumented vehicles.
The data consist of signals relating to the engine (number of revolutions), to the wheel (number of revolutions), and to acceleration (throttle opening). The signals are collected instantaneously by a circuit which transforms them so that they can be recorded in a memory (RAM box). At the end of each itinerary the data are downloaded from the RAM to a PC, for subsequent processing.
In this way, it is possible to obtain the characteristics of each trip (speed-time-space diagrams, acceleration-time-space, torque, wheel revolutions/engine revolutions ratio, consumption) and the emissions (g/km and g) of CO (carbon monoxide), NOx (nitrogen oxides), and HC (unburned

hydrocarbons).
On the basis of the above, it was therefore possible to construct a model of regression for selective evaluation of the emissions in function of the phases of movement and the plain/altimetric characteristics of the itinerary.
The emission curves obtained have fairly high regression coefficients and the comparisons carried out lead to the conclusion that the resulting emission values are correct and conform to Italian reality.
Lastly, the resulting curves were compared to other existing models, verifying operation and possible deviations.
***Keys-words**: model microsimulation pollutant emissions.*

Introduction

La méthode se base sur l'utilisation d'un puissant instrument électronique appelé: A.D.C.D. (Advanced Driving Cycle Detector) qui fournit instantanément les valeurs des paramètres nécessaires pour connaître les émissions polluantes à partir du trafic véhiculaire.

Dans cet article est proposé un instrument mathématique mis au point pour la voiture, on possède aussi des données pour d'autres catégories de véhicules. Les émissions polluantes ont été obtenues à travers le relevé de paramètres instantanés du mouvement et du fonctionnement du moteur, après une série de parcours préfixés, considérant les propres caractéristiques des véhicules.

Les données obtenues avec la méthode précédemment décrite, pour chaque parcours et véhicule, sont représentatifs des caractéristiques du mouvement (vitesse et accélération), du parcours altimétrique (pente), et des polluants émis, en fonction du temps et de l'espace. Il est donc possible d'observer des relations existantes entre régime de mouvement et émissions (ex. l'augmentation des émissions de NOx dans les phases d'accélération, ou du CO lors des arrêts). La procédure utilisée a permis en synthèse d'estimer les émissions pour chaque condition possible de vitesse, accélération et pente et pour chaque typologie de véhicule. Les émissions fournies à partir de la base de données sont relatives aux polluants suivants: CO, HC e NOx.

A partir des diagrammes du mouvement obtenu, analysés simultanément avec les émissions instantanées, il est aussi possible de faire des observations à propos de la qualité du débit véhiculaire, parce qu'un régime irrégulier (c'est-à-dire le mouvement variable) est certainement facteur d'augmentation des émissions polluantes. Ceci peut être observé à partir du correspondant diagramme des émissions relâchées le long du parcours (g/km-m); les accélérations correspondent en fait aux pics de NO_x tandis que dans des conditions minimes à celles du CO (moteur diesel). Donc pour un parcours déterminé, on peut connaître l'entité des émissions polluantes relâchées par le véhicule (auto, bus, cyclomoteur), ou à travers le relevé des données nécessaires à l'estimation de ces dernières, ou bien en utilisant des valeurs qui se trouvent dans le tableau relatif à d'autres parcours (dans ce cas, on doit au moins savoir les caractéristiques du mouvement sur le parcours étudié).

Chaque tableau (dont les valeurs sont obtenues comme moyenne de plusieurs relevés) est relative au type d'émission (CO, HC, NOx), véhicule (autos non catalysées, auto catalysées, bus, cyclomoteur) et pente de la nivelette. Après avoir choisi le tableau, les données d'entrées sont la vitesse et l'accélération.

2. L'instrumentation pour le relevé et pour l'élaboration des données.

La détermination des émissions polluantes, relâchées par un véhicule lors d'un trajet dont on connaît les caractéristiques planoaltimétriques, se passe à travers l'élaboration (au moyen de logiciels) des données acquises par l'instrumentation montée sur le véhicule.

Il s'agit de signaux relatifs au moteur (nombre de tours), à la roue (nombre de tours), et à l'accélération (ouverture de la vanne à papillon). Les signaux sont instantanément recueillis par un circuit qui le transforme de façon à pouvoir être enregistrés sur une mémoire (boîte RAM). A la fin

de chaque parcours, les données sont transmises de la RAM à un PC, pour l'élaboration successive. Les données reçues grâce aux relevés doivent être élaborées au moyen de logiciels, après l'introduction du fichier pente, qui contient des données sur l'altimétrie du parcours. On obtient de cette façon les caractéristiques du mouvement propres à la course effectuée (diagramme vitesse-temps-espace, accélération-temps-espace, couple, rapport tours de roues/tours moteur, consommations) et les émissions (g/km et g) du CO (monoxyde de carbone), NOx (oxyde d'azote), et HC (hydrocarbures non brûlés).

Dans le schéma de la fig. 1 la méthodologie adoptée est explicitée aussi bien en phase de relevé qu'en phase successive d'élaboration des données.

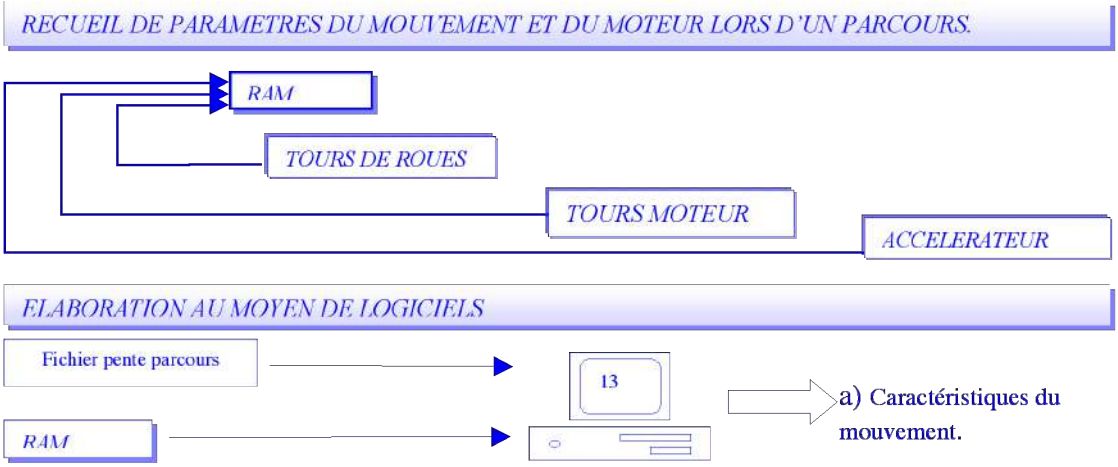

Figure 1: Schéma de la méthodologie dans les deux phases de recueil et d'élaboration des données

En fig. 2, on reporte comme exemple les courbes d'émission du CO exprimées en gr/Km, en fonction de la vitesse instantanée initiale et de l'accélération (positive) sur un parcours ayant une pente en montée moyenne comprise entre 0 et 2%.

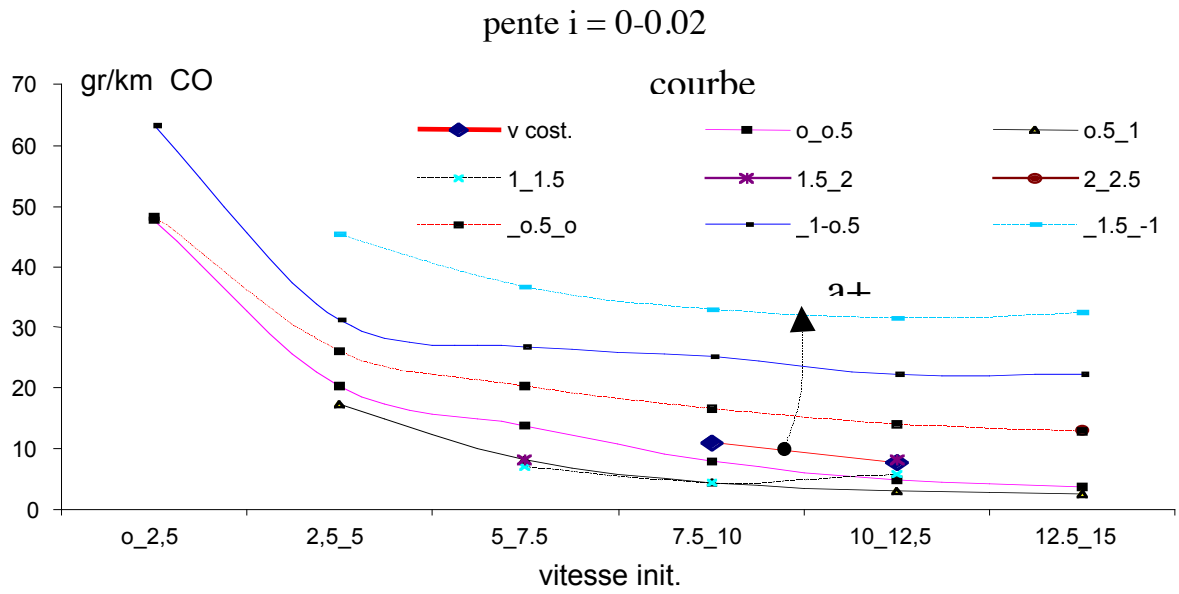

Figure 2: Émissions du CO en fonction de l'accélération et de la vitesse initiale.

La construction du modèle de régression

Selon ce qui a été précédemment dit, il a donc été possible de construire un modèle mathématique pour l'évaluation des émissions ponctuelles qui soit le plus adhérent possible aux différentes situations du mouvement pouvant se présenter sur un parcours déterminé et qui tienne aussi compte de la pente de la section à parcourir.

La base de données s'est donc subdivisée par classes de pente du parcours (Δ = 2 degrés) et on a recherché les équations relatives pour chaque classe de pente, parce que les émissions sont fortement conditionnées par la quote-part de puissance utilisée.

La structure du modèle est polynomiale, de type:

$$Em = \sum_{i=0}^{5} \sum_{j=0}^{5} k_i * \left(\frac{dv}{dt} \right)^j$$

pour $\Delta_i = \cos t_{pref}$. (gradient de pente du parcours: deux degrés de pente)

où: Em = émission du CO, HC, ou de NOx exprimée en gr/Km

K = coefficients du modèle de régression; dv/dt = accélération ou décélération (m/s^2)

La formulation spécifique du modèle qui interpole mieux les données d'émission, dans cette étude assume la forme suivante:

$$Em = a + bx + cx^2 + dx^3 + ex^4 + fx^5$$

où : Em = émission du CO, HC, ou de NOx exprimée en gr/Km

a = point d'interception ; b,c,d,e,f = coefficients; x = accélération (m/s^2)

Pour chaque valeur de la pente de la nivelette sur laquelle le véhicule se déplace, on a deux polynômes distincts, caractérisés par des parcours particuliers, respectivement pour des véhicules en accélération et pour des véhicules en décélération.

La fiabilité des polynômes de régression est déterminée en calculant la valeur du coefficient de détermination R (valeur R au carré). Des valeurs s'avoisinant à un indiquent la bonne correspondance du polynôme aux valeurs expérimentales.

$$R = 1 - \frac{SSE}{SST}$$

où : $SSE = \sum \left(Y - \overline{Y} \right)^2$ et $SST = \sum_n \left(Y^2 \right) - \frac{\sum_n (Y)^2}{n}$

Dans le tableau 1, les valeurs des coefficients a, b, c, d, e, f sont reportées pour un véhicule non catalysé en phase d'accélération; de la même façon dans le tableau 2, on reporte les valeurs des mêmes coefficients pour un véhicule toujours non catalysé, en phase de décélération. De façon analogue, les valeurs des coefficients du polynôme pour une voiture catalysée ont été obtenues aussi bien en accélération qu'en décélération (elles n'ont pas été reportées dans cet article).

Résultats

Le courbes d'émission obtenues ont des coefficients de régression très élevés et les comparaisons effectuées portent à considérer que les valeurs des émissions résultants sont corrects et adhérents à la réalité italienne.

Les courbes sont mises en évidence dans les graphiques reportés dans le paragraphe successif; dans ces dernières, aussi bien les valeurs du modèle en question que celles d'un modèle américain utilisé pour une confrontation et pour vérifier ultérieurement la validité du modèle étudié, sont représentées par un diagramme.

Précédemment, dans un travail présenté au congrès SIDT 1998 à Reggio Calabria, pour vérifier la

qualité de la procédure et des résultats obtenus, on a illustré les différences existantes en comparant les valeurs obtenues à la méthode en question et à ceux dérivant de l'application du modèle Integration.

véhicule en **accélération** - coefficient du polynôme de régression								
émission	pente	**a**	**b**	**c**	**d**	**e**	**f**	R^2
CO	da -6 a -4 %	1,9729	59,7320	-4,2767	-2,3323	0,4605	0,0000	0,9999
	da –2 a 0 %	6,3880	84,1810	-27,0750	7,1936	-1,0011	0,0000	1,0000
	da 0 a 2 %	6,1579	119,3800	-83,0530	38,2540	-6,7538	0,0000	0,9999
	da 2 a 4 %	7,6657	136,9100	-92,4190	44,6280	-8,3206	0,0000	0,9998
HC	da -6 a -4 %	0,2046	1,2120	-0,5682	0,2573	-0,0501	0,0000	0,9997
	da –2 a 0 %	0,6340	1,2517	0,1559	-0,1156	0,0088	0,0000	0,9994
	da 0-2 %	0,6924	2,0485	-0,9966	0,4832	-0,0864	0,0000	0,9992
	da 2-4 %	0,8745	2,1170	-0,6589	0,1937	-0,0316	0,0000	1,0000
NOx	da -6 a -4 %	0,4691	4,1371	-1,8962	0,8827	-0,1730	0,0000	0,9999
	da -2 a 0 %	1,4924	6,3155	-1,2606	0,2047	-0,0061	0,0000	0,9999
	da 0 a 2 %	1,5500	8,9948	-6,2669	3,4912	-0,7237	0,0000	0,9998
	da 2 a 4 %	1,6947	11,7270	-5,1919	2,1480	-0,3770	0,0000	1,0000

Tableau 1: Valeurs des coefficients de régression pour une voiture non catalysé en accélération

véhicule en **décélération** - coefficients du polynôme de régression								
émission	pente	**a**	**b**	**c**	**d**	**e**	**f**	R^2
CO	da -6 a -4 %	1,7840	-35,7150	-37,7510	-16,8610	-2,7076	0,0000	0,9998
	da -2 a 0 %	6,2842	-34,2740	-29,0460	-9,7613	-1,0887	0,0000	0,9965
	da 0 a 2 %	6,0226	-42,9650	-46,9690	-21,6140	-3,5677	0,0000	0,9997
	da 2 a 4 %	7,4098	-45,3230	-77,0970	-61,8720	-23,5360	-3,4137	1,0000
HC	da -6 a -4 %	0,2013	-9,1502	-9,7009	-4,3466	-0,6991	0,0000	0,9998
	da -2 a 0 %	0,6211	-10,9550	-11,5370	-5,2266	-0,8584	0,0000	1,0000
	da 0 a 2 %	0,6796	-13,3820	-23,2710	-19,2950	-7,6020	-1,1396	1,0000
	da 2 a 4 %	0,8720	-12,5190	-19,3130	-14,3910	-5,1845	-0,7228	1,0000
NOx	da -6 a -4 %	0,4621	1,6159	2,2712	1,5371	0,5040	0,0643	1,0000
	da -2 a 0 %	1,4757	5,9722	9,5376	7,3408	2,7218	0,3889	1,0000
	da 0 a 2 %	1,4864	4,2242	4,3008	1,8526	0,2882	0,0000	0,9994
	da 2 a 4 %	1,7000	6,3282	9,1914	6,4431	2,1901	0,2896	1,0000

Tableau 2: Valeurs des coefficients de régression pour une voiture non catalysé en décélération

La comparaison a été concrètement effectuée en appliquant les deux méthodologies sur deux portions distinctes de routes urbaines à Cosenza comprenant deux intersections intermédiaires à des distances différentes entre elles. Les résultats obtenus montraient qu'aussi bien l'HC que le CO estimés en appliquant le présent modèle étaient plus élevés que ceux évalués avec Integration; et ceci était une nouvelle preuve de la qualité des résultats et du fait que le modèle américain se base sur des flux véhiculaires dotés pour leur totalité de pot catalytique et avec combustion quasi parfaite (on ne peut pas en dire autant pour le parc italien).

Dans la comparaison, on a aussi trouvé que les valeurs des émissions des trois polluants en proximité des intersections sont plus importants si on applique le modèle en question, alors qu'ils demeurent quasi indifférents si on applique Integration et cela montre encore une fois la grande adhérence du modèle en question qui utilise des données instantanées de vitesse et accélération sur un parc véhiculaire plus vieux et avec des quote-parts importantes de véhicules non catalysés.

Comparaison avec le modèle K. Ahn, A.A. Trani, H. Rakha et M. Van Aerde

On a aussi voulu vérifier le modèle proposé en le comparant à un modèle analogue de régression, obtenu sur un parc véhiculaire en Virginie de K.Ahn, A.A. Trani, H.Rakha et M.Van Aerde du

Center for Transportation Research, dans le Virginia Polythecnic Institute and State University. Le modèle est de type:

$$F = a + bS + cA^2 + dA^3 + eS + fS^2 + gS^3 + hAS + iAS^2 + jAS^3 + kA^2S + lA^2S^2 + \\ + mA^2S^3 + nA^3S + oA^3S^2 + pA^3S^3$$

dans lequel l'émission (F) du CO, HC, ou de NOx est fonction de l'accélération (A) et de la vitesse (V) selon un polynôme dans lequel a est le point d'interception, b,c,d,e,….., p sont des coefficients. Le modèle ainsi obtenu a été testé et a reporté des coefficients de corrélation égaux à 0,94, 0,85 et 0.90 respectivement pour les émissions du CO, HC et de NOx.

Le modèle est influencé par différentes conditions opératives (départs à froid et des températures du milieu environnant), du parc véhiculaire, de son âge, des restrictions à l'utilisation de véhicules polluants, à l'utilisation du pot catalytique etc. Cette situation provoque des différenciations qui sont clairement mises en évidence à la fig. n. 3, relative au polluant HC reporté comme exemple.

En particulier, une courbe très accentuée des émissions du CO qui s'élève rapidement et devient quasi asymptotique ne semble pas très adhérente quand on accélère déjà d'1 m/sec^2, même si cela reste modeste. En réalité, le fait d'avoir recherché une courbe unique aussi bien en accélération qu'en décélération pourrait être la cause des accroissements élevées d'émissions tant pour les descentes élevées que pour les montées.

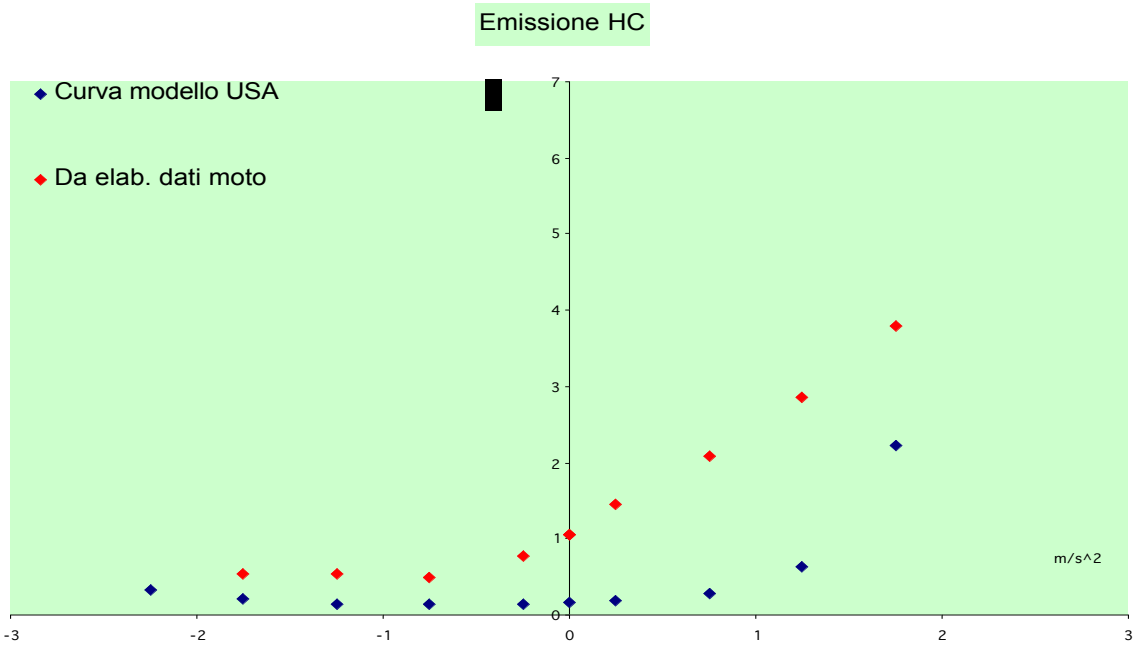

Figure 3: Émission de HC en fonction de l'accélération dans les modèles en examen et de comparaison.

En ce qui concerne l'émission de HC, les deux courbes présentent fondamentalement un parcours similaire. On note en particulier que la courbe obtenue en Italie augmente quand on est en phase d'accélération, plus importante par rapport à celle obtenue aux E.U.; et cela est facilement en raison des restrictions importantes sur les émissions existantes aux Etats-Unis.

Même dans le cas des émissions de Nox, les deux courbes sont analogues avec des valeurs d'émission similaires pour les décélérations et pour les accélérations inférieures à 1 m/sec^2. Pour des accélérations supérieures à cette valeur, on note au contraire une différence notable (zone interne au cercle) parce que dans le modèle américain la courbe augmente asymptotiquement.

Références

H. Rakha, Impact of vehicle stops on energy consumption and emissions, Transportation Research Board '00
Transportation Research Board, 1995 "Expanding Metropolitan Highways Implications for air quality and energy use" special report 255, National Academy Press
National Research Council, (1995) Expanding Metropolitan Highways: Implications for Air quality and Energy Use, National Academy Press, Washington, D.C.
S. d'Elia, G.A. Danieli, "Measuring Real Driving Cycles and Evaluating Relative Emissions for Vehicles in Urban Traffic", Congresso ICE99, Capri, 12-16 September 1999, pp. 393-399
S. d'Elia G.A. Danieli, e S. Ruffolo "Strumentazione per la misura di cicli di effettivo utilizzo su veicoli in traffico urbano", Domanda di Brevetto DP97A005 ricevuta il 14/02/97, concesso 20/12/99, No. 1297898 EEC Directive 91/441.
K.Ahn, A. Trani, H.Rakha e M.Van Aerde: "Microscopic fuel consuption and emission models" , TRB, '99.
S. d'Elia G. A. Danieli: Stima delle emissioni specifiche da autovettura e da veicolo industriale nelle città italiane, Napoli, Congresso S.I.D.T. 1996. pp 666-676 di "I piani urbani del traffico", a cura di M. de Luca e V. Astarita, Società italiana dei docenti di trasporti, Collana Trasporti, Franco Angeli Editore.
S. d'Elia G. A. Danieli: Innovative Methodology for Emission Prediction in Real Traffic on Different Vehicle Typology, Section III, Emission Models and applications, pp. 9-14, 8th International Symposium Transport and air Pollution, including COST 319 Final Conference, Graz, Austria, May 31 - 2 June 1999.
S. d'Elia G. A. Danieli: Environmental Impact Evaluation of the Introduction of a Toll Station in an Italian Motorway, Section III, Emission Models and applications, pp. 57-64, 8th International Symposium Transport and air Pollution, including COST 319 Final Conference, Graz, Austria, May 31/99 – 1999.
S. d'Elia G. A. Danieli: Rilievo dei cicli urbani di effettivo utilizzo su diverse tipologie veicolari e calcolo dell'inquinamento prodotto ATI 99.
d'Elia S. Un modello per la valutazione delle emissioni da inquinante per la presenza di un distributore di carburante, Conferenza Nazionale di informatica e pianificazione urbana e territoriale: INPUT 2001, Isole Tremiti – giugno 2001.

12th International Symposium "Transport and Air Pollution" / 12e Colloque international "Transports et pollution de l'air", Avignon, 16 -18 *June* / juin 2003
proceedings / actes, n°92, tome / Vol. 2, Inrets ed., Arcueil, France, 2003, p. 145-150

Impact of Air Conditioning, Ambient Temperature and Humidity on Emissions of Modern Passenger Cars

Luc Pelkmans*, Guido Lenaers*, Patrick Debal*, Martine Van Poppel*, Tom Hood, Günther Hauser*** & Maria-Rosa Delgado******
* Vito, Boeretang 200, B-2400 Mol, Belgium - Tel. +32 14 33 58 30 – Fax. +32 14 32 11 85 – e-mail : luc.pelkmans@vito.be
** MIRA, Watling Street Nuneaton, Warwickshire CV10 0TU, United Kingdom
*** CLE, Karl-Scharfenberg-Strasse 55-57, D-38229 Salzgitter (Calbrecht), Germany
**** IDIADA, L'Albornar, P.O.Box 20, E-43710 Santa Oliva (Tarragona), Spain

Abstract
Within the EC-funded 'DECADE' project modern passenger cars were tested for various influencing parameters on fuel consumption and emissions. Using a design of experiment (DoE) set-up, specific parameters were brought together in test matrices, to test which parameters have most significant effect on emissions and to determine if there are interactions between these parameters. One of these test matrices focussed on air conditioning, ambient temperature and relative humidity.
Two passenger cars (a Euro 3 diesel car and a Euro 4 petrol car) were tested on chassis dynamometer in a climatic wind tunnel. The tests were carried out in varying ambient circumstances, using a real world traffic based test cycle. The results show that the use of air conditioning may increase fuel consumption and CO_2 emissions by 5 to 25%, depending on the type of traffic. The impact on other emissions may even be bigger, however results depend on the engine and emission control technology. Air temperature and humidity show a modest influence on fuel consumption and CO_2, the impact on other emissions however is substantial.
Key-words*: emissions, fuel consumption, air conditioning, test conditions, test cycle, on-board emission measurement*

Introduction

When quantifying fuel consumption and emissions of modern vehicles, usually the results of the official EU cycle are used. As presented in Pelkmans et al. (2002), these results can be very different from fuel consumption and emissions in real circumstances. The main reason is that the EU cycle is much smoother than real driving and engine manufacturers only have to focus on limited engine operating zones for minimizing the emissions.

Apart from variations in the drive cycle, other parameters will also have impact on emissions. Air conditioning is known to have a substantial influence on fuel consumption, however its impact is not included in the official EU cycle, even if the vehicle is equipped with air conditioning. The influence of air condition is bound to interact with ambient temperature and air humidity. Test results on these influencing parameters will be reported on in this paper.

1 – Design of Experiments (DoE)

Within the European 'DECADE' project, a method has been developed for predicting fuel consumption and regulated vehicle exhaust emissions during dynamic engine behaviour (see Debal et al. (2002)(a)). The calculation methodologies have now been employed in a computer simulation

tool called VeTESS (Vehicle Transient Emissions Simulation Software). The methodology has been tested in detail for three control vehicles (all cars were model year 2000):

- a petrol VW Polo 1.4 16V, with air conditioning (Euro 4 certified, representing small-sized city cars)
- a diesel Skoda Octavia 1.9TDi, with air conditioning (Euro 3 certified, representing medium-sized family passenger cars)
- a diesel PSA Citroen Jumper 2.5D (Euro 2 certified, representing urban delivery vans)

In order to potentially refine the modelling algorithms used within VeTESS, several parameters which were thought to have influence on emissions and fuel consumption, were investigated more in depth. This was achieved using Design of Experiment (DoE) statistical analysis techniques. This way the data set required for the simulation tool was reduced by identifying which vehicle operating parameters or combination of vehicle operating parameters have significant effects on tailpipe emission production. Also the interaction of multiple parameters was to be investigated in order to determine their combined effect on emissions production. Data collection was achieved by running an ordered series of chassis dynamometer experiments.

Three sets of chassis dynamometer emission tests were carried out. Each set of tests would look at the effect on vehicle exhaust emissions of three different parameters. Therefore nine parameters would be investigated in total. Each of the nine parameters would be tested at two conditions or levels. These levels were selected to be at opposite extremes of what a vehicle would face under real world driving conditions. Table 1 shows the sets of DoE tests and the test conditions for each parameter.

DoE SET 1 (chassis dyno, CLE, Germany)

Drive cycle type:ECE15 + EUDC↔US-FTP

Vehicle mass: Empty weight↔+50% of max load

Tyre pressure:-30%↔+30%

DoE SET 2 (chassis dyno, IDIADA, Spain)

Fuel type: Reference fuel↔Commercial fuel

Gear matching: Low rpm gearing↔High rpm gearing

Engine airflow: Nominal airflow↔Restricted air filter

DoE SET 3 (chassis dyno with climatic wind tunnel, MIRA, United Kingdom)

Temperature:-20°C↔+30°C

Humidity:20%RH↔80%RH

Air conditioning: Off↔On

Table 1 : Overall DoE test matrix for influencing parameters (3 cars per set)

All tests were performed with a minimum mileage of 5000km to avoid running in effects of engines and catalysts. The engines were also tested in hot conditions, so the influence of start-up or engine warming-up was not included in the tests.

The emission measurements were performed at chassis dynamometer at three sites: CLE in Germany, IDIADA in Spain and MIRA in the United Kingdom. In all tests a common emission measurement system was used, Vito's VOEMLow mobile emissions measuring equipment. This equipment measures fuel consumption, CO_2, CO, NO_x, HC and PM on a second by second basis (see Debal et al. (2002)(b)).

In every DoE test set there were eight combinations to be tested, with three repeats of every combination for averaging. The number of tests in set 3 (airco, temperature & humidity) was reduced from eight to five. Air conditioning at low temperature was not used, since only engine

heating is needed at that time. At hot temperature the air conditioning is effectively working and using engine power. Humidity was not varied at low temperature, since 80% humidity at -20°C only represents a very low absolute water content in the air (at that temperature level humidity is very hard to control in the climatic wind tunnel). The test matrix was therefore reduced to five tests as shown in the following table.

	Test 1	Test 2	Test 3	Test 4	Test 5
Air temperature (°C)	-20	30	30	30	30
Air humidity (% RH)	80	20	20	80	80
Air conditioning	Off	Off	On	Off	On

Table 2: Adapted test matrix for DoE set 3

The VW Polo and the Skoda Octavia were equipped with air conditioning, so the results of these vehicles will be discussed here.

2 - Test cycle

For the first DoE test experiments, the NEDC cycle was taken as the standard cycle. However it became clear that the EU test cycle cannot be considered representative for real driving (see Pelkmans (2002)). Therefore a real traffic based cycle (called MOL-cycle) was taken for test set-up 3, investigating the influence of air conditioning, ambient air temperature and relative humidity on fuel consumption and emissions. The MOL-cycle is based on previously recorded measurements in and around Mol, Belgium with a 1993 VW Golf 1.9D (42kW). This cycle was proven to have more realistic results than the EU cycle (see Pelkmans et al. (2002)).

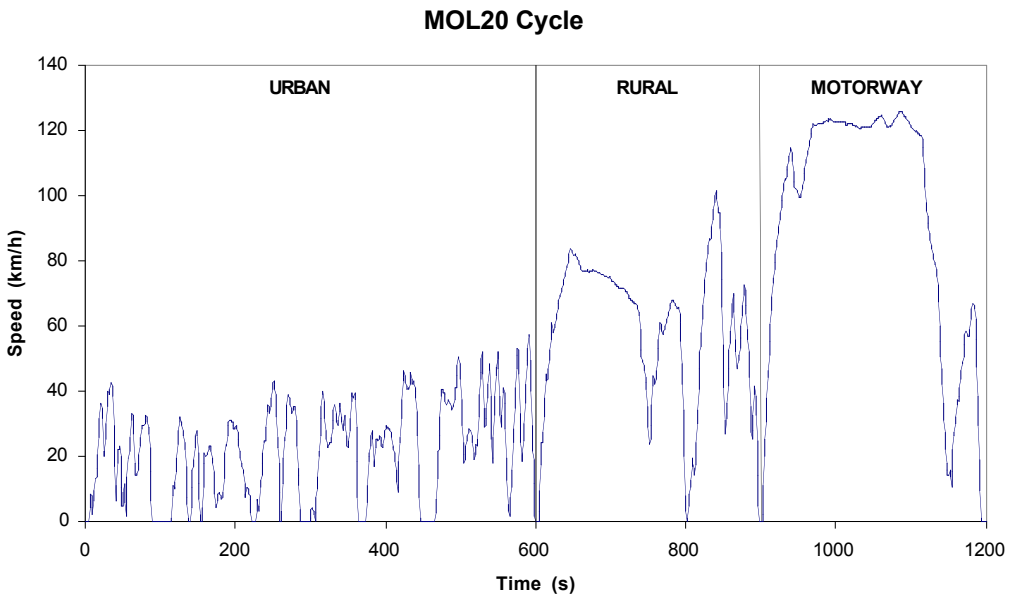

Figure 6: Speed profile of MOL cycle (shortened to 20 minutes)

3 – Test results

The impact of air conditioning, temperature and humidity will be expressed as a relative increase or decrease. Of course the absolute values also matter. For instance a 50% increase of a very low emission value is far less important than a 20% increase of a high emission value. As a basis for comparison Figure 7 gives an idea of the levels of emissions of the two vehicles on the MOL cycle and the EU cycle in standard conditions (25°C, 40%RH, airco off). A distinction is made between the different categories of traffic: city traffic, rural traffic and motorway traffic. Mind that fuel consumption is not mentioned, as it is proportional to CO_2 emissions.

It is clear that the emissions are seriously different between the test cycles. In the real world based cycle, fuel consumption is generally 10 to 20% higher than in the EU cycle. For the diesel vehicle it is striking that NO_x emissions reach almost double the amount measured in the EU cycle. The petrol car has extremely low CO, HC and NO_x emissions in the EU cycle, but in the MOL cycle there is a clear increase of NO_x and CO emissions.

Anyway it can be concluded from the figures that for the diesel vehicle CO and HC emissions are very low, so focus will be on CO_2 (proportional to fuel consumption), NO_x and PM emissions. For the petrol vehicle HC and PM are very low (PM was tested, but below detection limit), so focus will be on CO_2, CO and NO_x emissions.

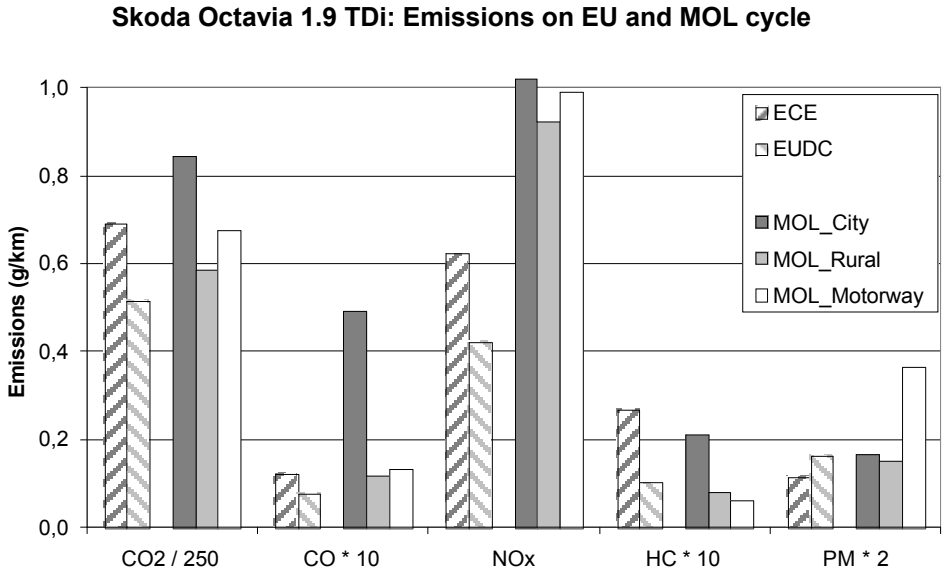

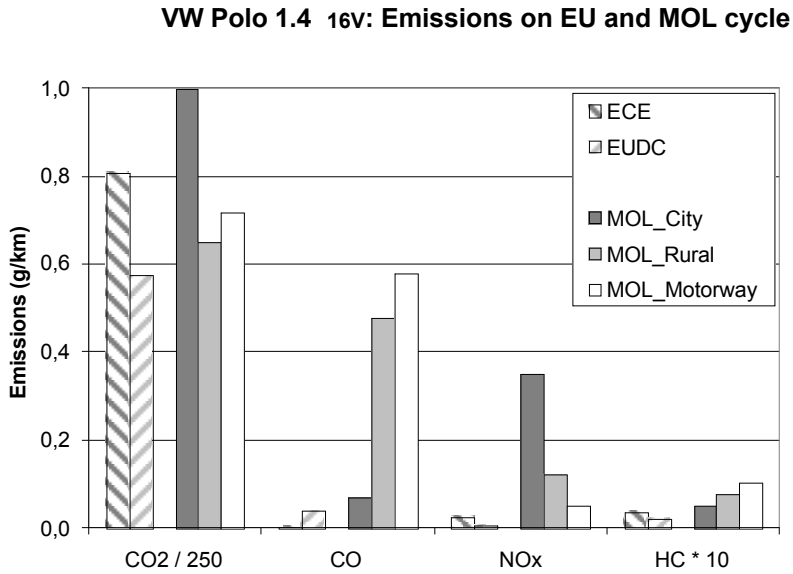

Figure 7: Emissions of Skoda Octavia and VW Polo on EU and MOL cycle

Test results on impact of air conditioning, humidity and air temperature

Figure 8 shows an overview of the impact of air conditioning, humidity and air temperature on the emissions of the Skoda Octavia (medium-sized diesel car).

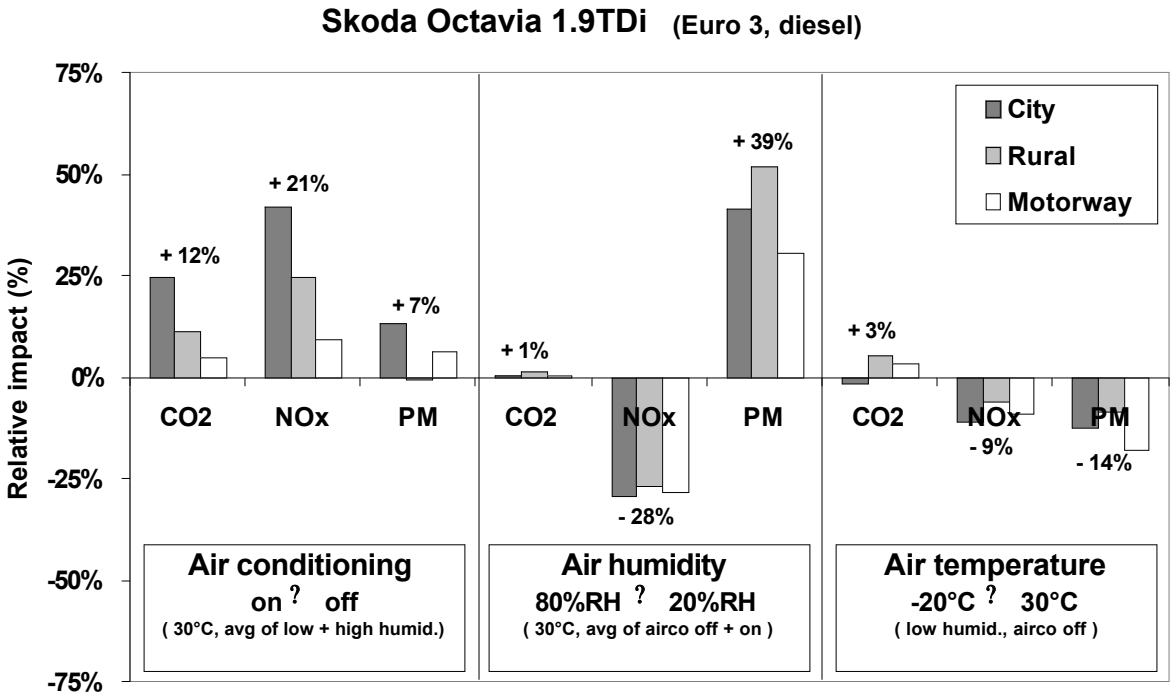

Figure 8 : Skoda Octavia 1.9TDi : impact of air conditioning, relative air humidity and ambient temperature on emissions

The effect of *air conditioning* was tested at an ambient temperature of 30°C, both at high and low relative air humidity. On average air conditioning increases fuel consumption and CO_2 emissions by 12% (at 30°C). However the effect is different when comparing city, rural and motorway traffic. In city traffic, where average engine power is lower, air conditioning has a big impact (fuel consumption increase up to 25%), while in motorway traffic, where average engine power is higher, the effect will only be in the order of a few percent. The impact on other emissions also depends on the kind of traffic. It is remarkable that NO_x emissions of this diesel vehicle are more sensitive to the use of air conditioning than fuel consumption or PM emissions. This has to do with the specific EGR strategy of this engine (see Figure 9). In this strategy, lower EGR is applied at higher loads (to reach higher torque), leading to higher specific NO_x emissions at high torque. The use of air conditioning creates an extra engine load, so the high torque area of engine operation is reached more frequently. The relative trends of the impact of air conditioning were comparable for high and low air humidity.

The effect of ambient air *humidity* was tested at 30°C, both with air conditioning on and off. Air humidity has a very significant effect on NO_x (decrease of 30%) and PM emissions (increase of 40%), while the effect on CO_2 and fuel consumption is quite low. It is known that humidity has a serious influence on NO_x emissions and this is usually compensated in certification tests by a correction factor, depending on temperature, humidity and pressure. The correction factor for 30°C, 20%RH is 0.85, while the correction factor for 30°C, 80%RH is 1.55. So according to the formula used to calculate the correction factor, NO_x emissions are supposed to decrease with 45% when increasing relative humidity from 20% to 80% (at 30°C). The difference measured for the Skoda Octavia was 30%. Mind that the formula for the NO_x correction factor has been derived in the early 1970's and that emission control and fuel management have changed considerably since then (Sierra Research (1998)). The reduced NO_x emissions at high humidity indicate a lower combustion temperature, leading also to an increase in fuel consumption and more PM emissions. The relative trends of the impact of air humidity were comparable for air conditioning switched on or off.

The impact of ambient air *temperature* was tested only for low humidity (cold air can only contain a very low content of water vapour) and with the air conditioning off. It is known that ambient air temperature influences engine operation. From the tests it turned out that CO_2 and fuel consumption

tend to increase a little at low temperature for the diesel engine, while NO_x and PM emissions are decreasing. NO_x emissions decrease because the combustion temperature also drops when the incoming air temperature is lower. The decrease in NO_x is however smaller than expected. It would also be expected that PM would increase at low temperature because of a less complete combustion. However there seems to be a combined effect of lower temperature and the engine management strategy (EGR control), which is also influenced by intake air temperature. In the end this leads to a moderate NO_x decrease and slightly lower PM emissions at lower temperature compared to high temperature.

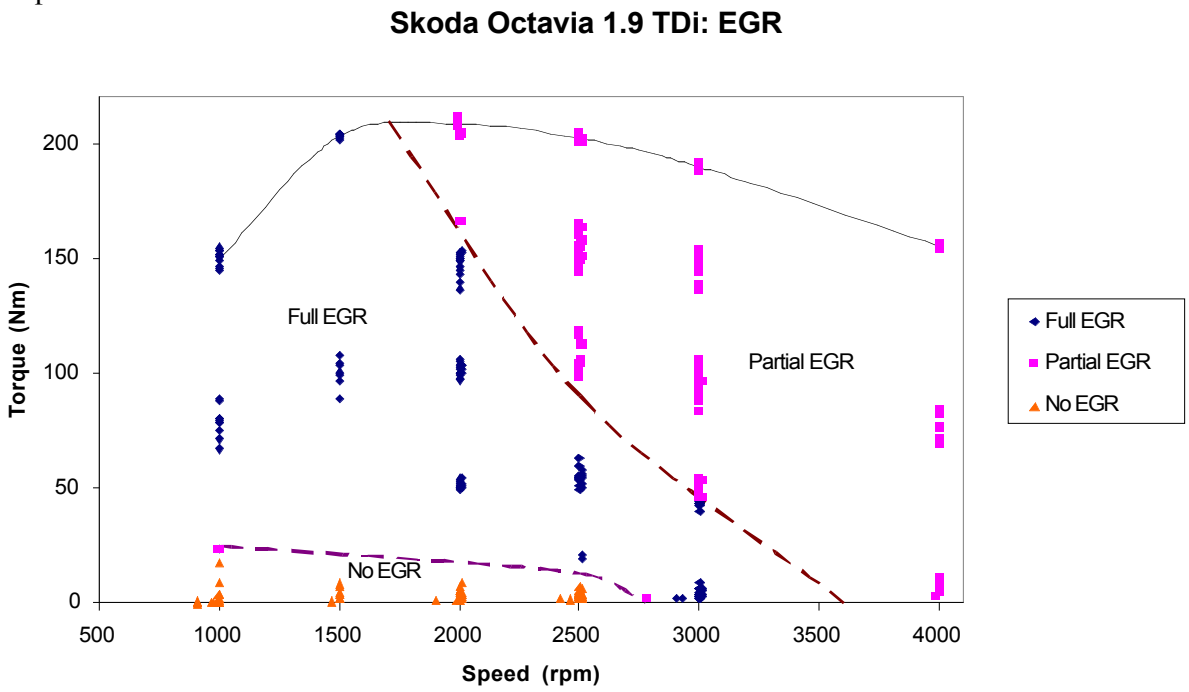

Figure 9 : EGR strategy of Skoda Octavia 1.9TDi engine

Figure 10 shows an overview of the impact of air conditioning, humidity and air temperature on emissions of the VW Polo (= small-sized petrol car). Mind that the scale is much bigger than for the Skoda Octavia (range up to 200% in stead of 75%). The test conditions and boundaries were the same as for the Skoda Octavia.

The effect of *air conditioning* on fuel consumption and CO_2 of the VW Polo is about the same as for the diesel car. There is also the same distinction in traffic conditions, with a higher effect in city traffic and a more moderate effect in motorway traffic. The impact on emissions is much more explicit. CO emissions on average increase more than 80% (with big variations between the traffic conditions); NO_x emissions increase about 60%. These increases are related to a higher average load of the engine, because of which engine operating zones with high CO or high NO_x emissions are used more frequently (see Figure 11).

Air humidity has a similar effect as for the diesel car. NO_x is decreased with about 30%, while CO increases with around 50%. The same remarks as for the Skoda Octavia are valid.

The effect of cold ambient *air temperature* on the other hand is different for the petrol engine. The fuel consumption (and CO_2) increase at low temperatures is more pronounced (+8%) than for the diesel engine. Concerning the other emissions, there are big variations, but in general the emissions increase seriously compared to warm temperature. This seems rather strange for the NO_x emissions. Engine-out NO_x emissions, however, will probably be lower at low ambient temperature (because combustion temperature is lower), while on the other hand the three-way catalyst is also colder and loses some of its NO_x reduction capability.

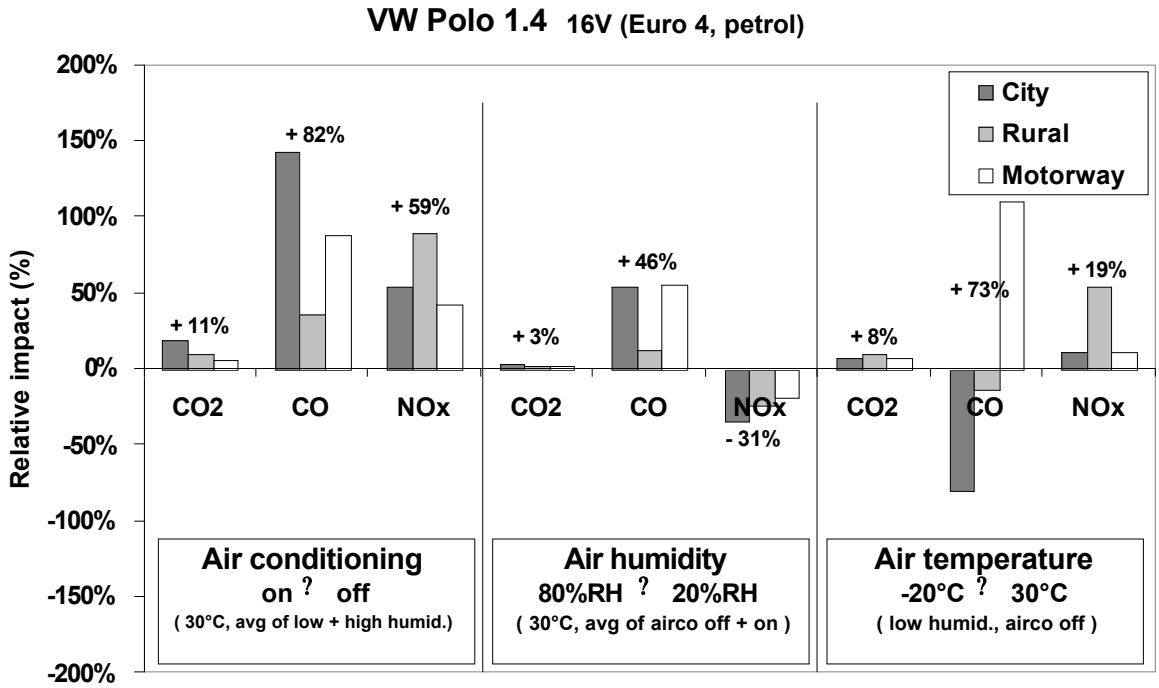

Figure 10 : VW Polo 1.4 : impact of air conditioning, relative air humidity and ambient temperature on emissions

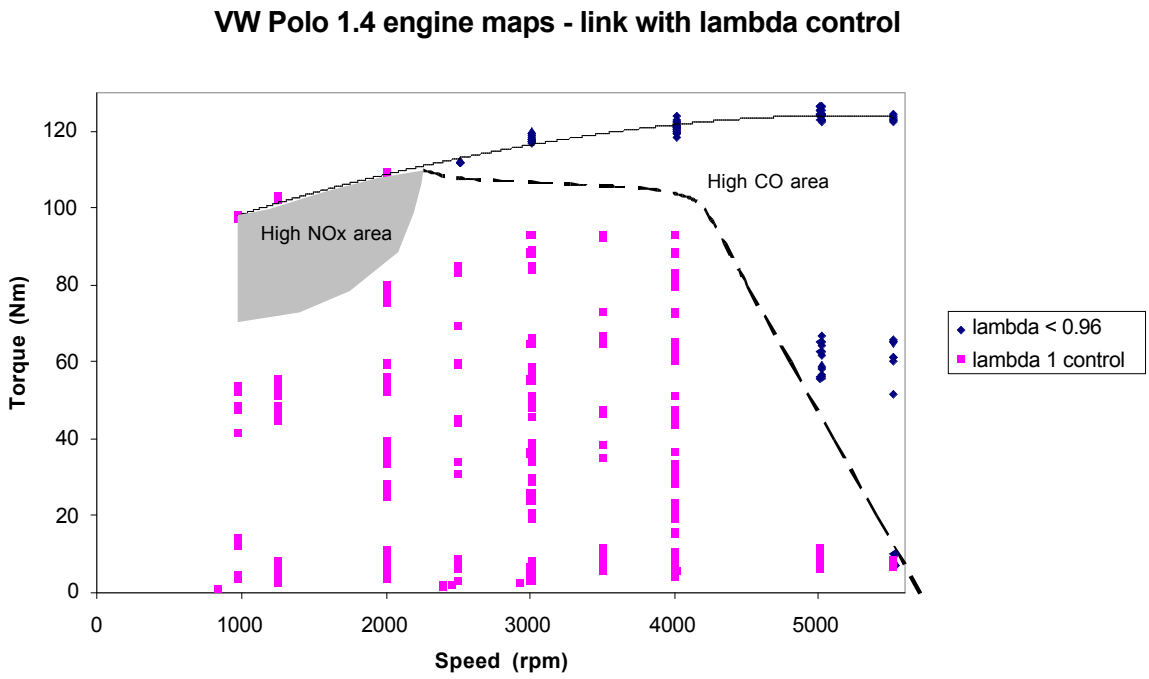

Figure 11 : High NO_x and CO zones in the engine maps of the VW Polo 1.4

Conclusion

In order to quantify the influence of air conditioning, ambient air temperature and humidity, a test matrix was defined and executed for a small sized petrol car, and a medium sized diesel car. The vehicles were tested on chassis dynamometer in a climatic wind tunnel, using a real world based test cycle.

The results show that the use of air conditioning may increase CO_2 emissions (and fuel consumption) by 5 to 25% at warm temperature, depending on the type of traffic. The impact on other emissions may even be bigger, however results depend on the technology with its specific fuel and emission control mechanisms. Humidity of the ambient air has a modest impact on fuel consumption and CO_2, however an increase of humidity leads to a significant decrease of NO_x emissions and increase of CO and PM emissions. Low temperature only has a moderate effect on fuel consumption and emissions of the diesel car (with lower NO_x and PM emissions and slightly higher fuel consumption). On the other hand the petrol car is much more sensitive for low temperatures, both for fuel consumption and emissions. Especially emission reduction in the three-way catalyst is less effective at low temperatures.

Acknowledgments

The authors wish to thank the members of the DECADE consortium for their co-operation in the work program. DECADE is a project of the 5th Framework of the European Union in the programme Energy, Environment and Sustainable Development and is funded as such.

References

Debal P., L. Pelkmans, T. Hood, G. Hauser, M.R. Delgado (2002)(a): Highly accurate emission modelling of vehicles operating in dynamic conditions. Proc. FISITA 2002 World Automotive Congress, Helsinki, Finland, 2-7 June 2002 (available on CD)

Debal P., G. Lenaers, E. Verhaeven (2002)(b): VOEMLow: Emission and Energy Measurement System as Development Tool for Clean Engines, Aftertreatment Systems and Powertrains. Proc. Global Powertrain Congress 2002, Detroit, USA, 24-26 September 2002 (available on CD)

Pelkmans L., G. Lenaers, P. Debal, T. Hood, G. Hauser, M.R. Delgado (2002): Comparison of Fuel Consumption and Emissions of Modern Light Duty Vehicles in the EU-Cycle versus Real World Driving. Proc. Int. Symp. "Transport and air pollution", Graz, Austria, 19-21 June, 2002, vol. 1, p 63-70

Sierra Research (1998): Additional Study of Preconditioning Effects and other IM240 Testing Issues. Sierra Research Report No. SR98-02-01, prepared for US-EPA, February 1998 (reference to p 84 – 98: chapter 8 - Evaluation of NO_x correction factors)

12th International Symposium "Transport and Air Pollution" / 12e Colloque international "Transports et pollution de l'air", Avignon, 16 -18 *June* / juin 2003
proceedings / actes, n°92, tome / Vol. 2, Inrets ed., Arcueil, France, 2003, p.153 158-

Benzene Emission Factors of the latest Diesel- and Gasoline-fueled Passenger Cars within the Common Artemis Driving Cycle

C.J. Saxer [a)], A.-M. Forss [b)], M. Weilenmann [b)], N.V. Heeb [a)]
Laboratory of Organic Chemistry [a)] and Laboratory of I.C. Engines/Furnaces [b)]
Swiss Federal Laboratories for Materials Testing and Research, EMPA, CH-8600 Dübendorf, Switzerland. Tel: +41 1 823 42 62, Fax: +41 1 823 40 41, email: christian.saxer@empa.ch

Abstract
The Common Artemis Driving Cycle (CADC) designed by INRETS is an interesting alternative to the legislative cycles (FTP 75 and EDC). It includes an urban, extra urban and highway phase of similar length with mean velocities of 17, 60 and 120 km h^{-1}, respectively. Within the Artemis project two fleets of the latest diesel- (EURO-2) and gasoline-fueled (EURO-3) passenger cars were investigated for their benzene emissions with chemical ionization mass spectrometry (CI-MS). Herein we report mean benzene (C_6H_6) and the total hydrocarbon (THC) emissions of the two fleets in the CADC at 23, -7 and -20 °C. At 23 °C benzene emission factors of the gasoline-fueled vehicles slightly increased with the velocity from 1.2 (urban) to 2.7 mg/km (highway), whereas those of the diesel-fueled vehicles decreased form 1.8 (urban) to 0.2 mg/km (highway). Reducing the ambient air temperature from 23 to -20 °C resulted in a moderate increase of the benzene and THC emissions for the diesel-vehicles but revealed no significant effect for the gasoline vehicles. Low but stable benzene/THC mass proportions of 1-2% were found for the diesel exhaust gas whereas increased ratios were noticed for the gasoline exhaust gas ranging from 3-5% at urban to 8-10% at highway driving conditions.
Keys-words*: Chemical ionization mass spectrometry (CI-MS), EURO-2 diesel vehicles, EURO-3 gasoline-fueled passenger cars, Common Artemis Driving Cycle (CADC), temperature dependence, Benzene, Total hydrocarbon (THC), time-resolved exhaust gas analysis.*

Introduction

Within the last three decades the driving behavior of the Swiss traffic fleet changed. The proportion of the driving distance on highways increased but both commonly used legislative driving cycles (FTP 75 and EDC) do not adequately weight the highway situation. For that reason the Common Artemis Driving Cycle (CADC), one of the newer cycles developed by INRETS, is a much better choice, since it represents the urban, extra urban and the highway situation with mean velocities of 17, 60 and 120 km/h, respectively. Herein we report a comparison of benzene and THC emission factors of the latest diesel- (EURO-2) and gasoline-fueled (EURO-3) technology obtained from these three driving cycles. In addition, also the influence of the ambient air temperature on the hot engine/catalyst-emissions were studied within the CADC which was immediately performed after the 'INRETS urbain fluide court' cycle (IUFC15). The cold start emissions were also addressed in the Artemis project but are reported separately (Weilenmann et al., 2003).

2- Experimental

Passenger car fleets of 6 EURO-2 diesel- and 6 EURO-3 gasoline-fueled vehicles were driven at the dynamometer test stand at EMPA with a diesel containing 18.8 vol.-% aromatics and a 95 RON gasoline containing 3.0 vol.-% benzene and 37.3 vol.-% aromatics. The diesel-fleet had, on average,

a mileage of 67'300 km, an engine displacement of 2.0 □ with model years between 1997 and 2000 (Table 1). The gasoline-fleet had an average mileage of 28'400 km, an engine displacement of 2.5 □ with model years between 2000 and 2001.

Diluted exhaust gas (constant volume sampling system, HORIBA, Japan) was analyzed with chemical ionization mass spectrometry (CI-MS) for its benzene (C_6H_6) content. A mass spectrometer (Airsense 2000, V&F GmbH, Absam, Austria) was operated in the selected ion monitoring mode at m/z: 78 amu at a frequency of 1-2 Hertz using mercury (Hg^+, 10.4 eV) as ionization gas. The THC content of the exhaust gas was analyzed with a flame ionization detector (FID). Hydrocarbons are oxidized in a hydrogen flame, which is positioned between two electrodes. The measured ion flow difference is proportional to the THC concentration.

3- Results

Benzene concentration in the diluted exhaust gas

Time-resolved benzene emission profiles of a typical diesel- (top) and a gasoline-fueled (bottom) vehicle are given in Fig. 1.

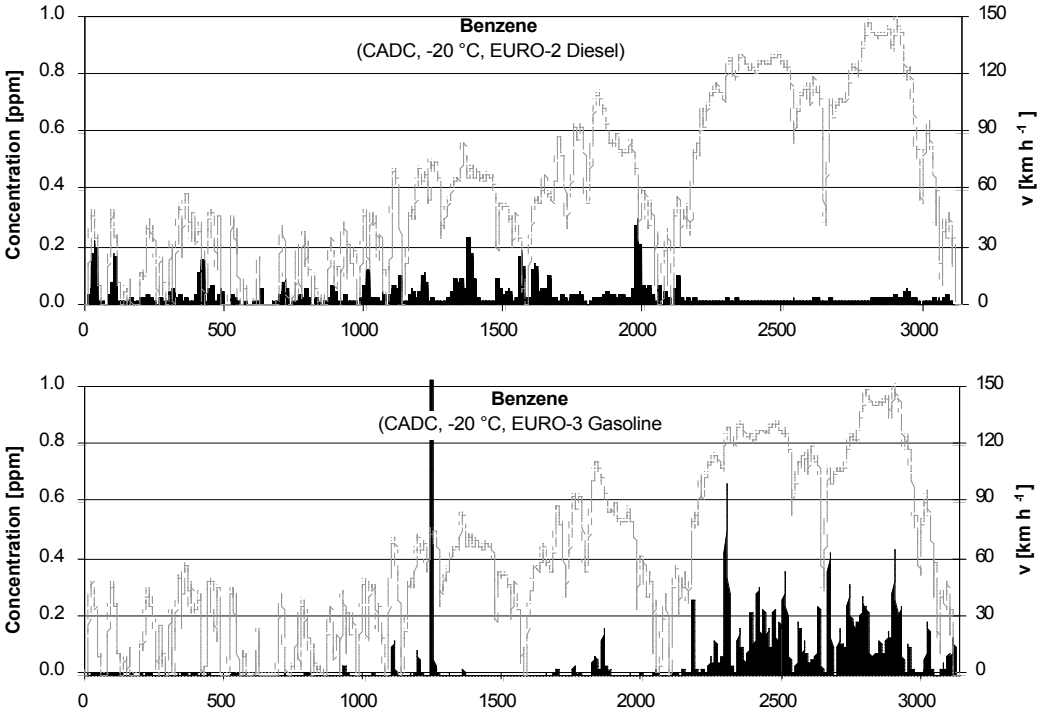

Figure 1: Benzene concentrations (black) in diluted exhaust gas of a VW Passat 1.9 TDI (top) and a Ford Focus 1.6 (bottom). The velocity profile (gray) of the CADC is also given.

In general it was noticed that in the CADC the EURO-2 diesel vehicles emitted more benzene at urban and extra-urban driving (phases I and II) and the EURO-3 gasoline vehicles had increased benzene levels under highway conditions (phase III). It has to be stated that no exhaust gas after-treatment systems are involved for the diesel vehicles but all gasoline cars were equipped with a three-way catalyst. This has to be considered, when comparing the emission characteristic of the investigated vehicle fleets.

Benzene and THC emission factors

Fig. 2 represents the benzene and THC emission factors of the two investigated vehicle fleets. The mean value and as a measure of the observed variation within a fleet also the standard deviation is given for the CADC phases I, II and III, which correspond to urban, extra urban and highway

driving, respectively. Each data set was investigated at ambient air temperatures of 23, -7 and -20 °C.

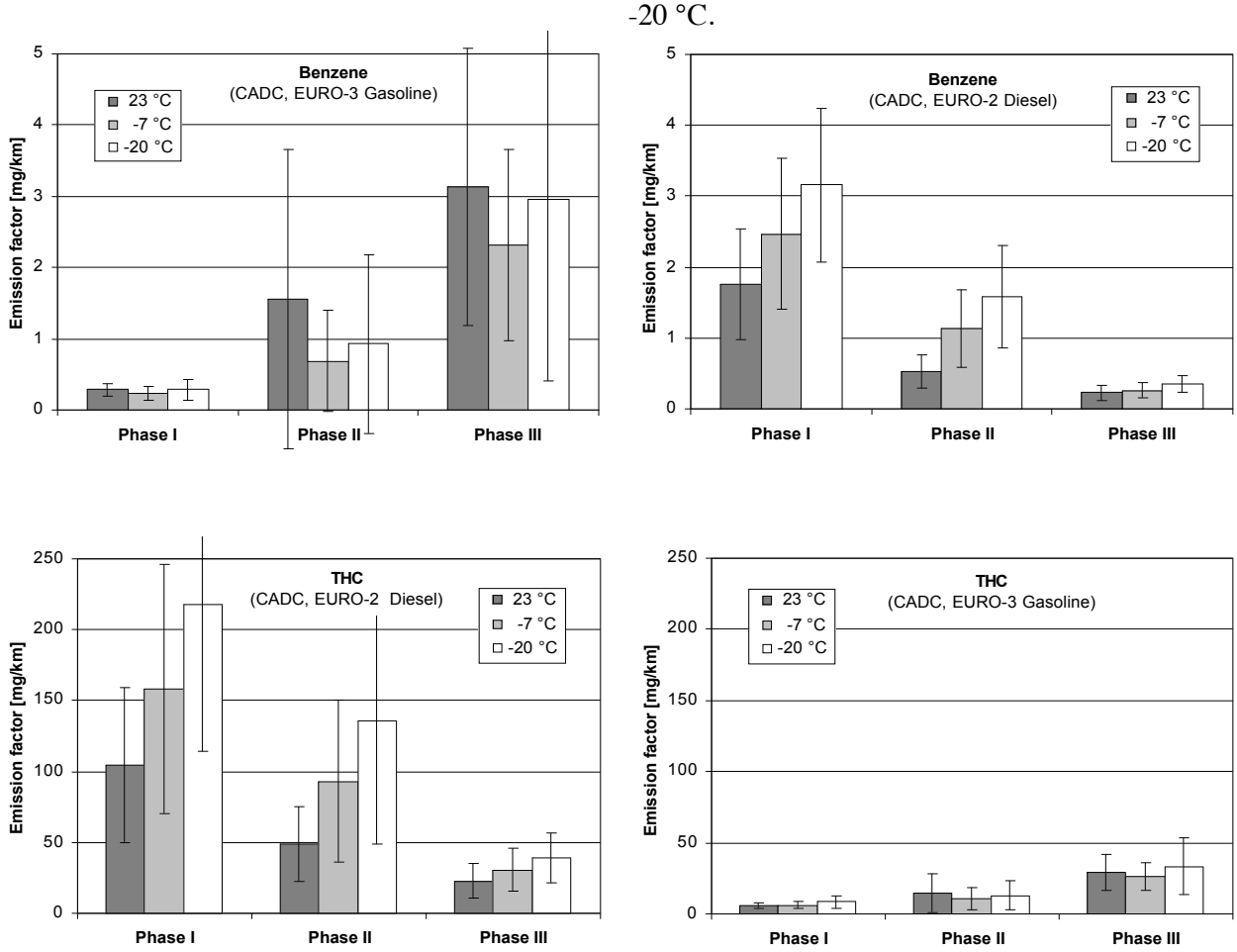

Figure 2: Mean benzene (top) and THC (bottom) emission factors [mg/km] of the EURO-2 diesel- (left) and EURO-3 gasoline-fueled (right) vehicles are given for the three CADC phases at 23, -7 and -20 °C.

As noticed from Fig. 2, the benzene as well as the THC emissions in the CADC similarly respond to velocity and temperature for the diesel vehicles. A different correlation between benzene and THC was observed for the gasoline vehicles. For the diesel-fleet, a reduction of the temperature from 23 to -20 °C induced an increase of the THC as well as the benzene emissions by about a factor of two. No such dependence on the ambient air temperature was noticed for the gasoline vehicles, which as mentioned, are all equipped with a three-way catalyst. This contrasts the strong effect of the temperature on the emissions of these vehicles under cold start conditions, whereas the engine is operated under fuel-rich combustion (choke) and the catalyst has not reached its light-off temperature (Heeb et al., 2003, Saxer, 2001).

Comparable CADC benzene emission factors in the range of 0.2 - 3.1 mg/km were obtained for the gasoline and the diesel fleets (Fig. 2). Under hot engine/catalyst conditions both fleets had significantly lower benzene emissions than previously reported for EURO-1 and EURO-2 fleets with benzene emission factors up to 100 mg/km (Heeb et al., 2001, Heeb et al., 2002). Interestingly, the benzene emissions of the investigated diesel and gasoline vehicles inversely depend on the velocity. Highest emissions (1.8 - 3.2 mg/km) are observed at urban driving for the diesel fleet with minimal levels (0.2 - 0.4 mg/km) at highway conditions, whereas the gasoline vehicles emitted most benzene (2.3 - 3.1 mg/km) at highway driving and lowest levels were found at urban conditions (0.2 - 0.3 mg/km), as reported in Table 1.

Vehicle class (legislation)		**Diesel-fueled passenger cars (EURO-2)**			**Gasoline-fueled passenger cars (EURO-3)**		
Model year		1997 – 2000			2000 – 2001		
Number of vehicles		6			6		
Displacement [ccm]		1'972 ± 199			2'421 ± 1'359		
Mileage [km]		67'300 ± 26'800			28'400 ± 6'200		
	v_{mean}	THC	Benzene	Proportion	THC	Benzene	Proportion
	[km/h]	[mg/km]	[mg/km]	[%]	[mg/km]	[mg/km]	[%]
CADC I (23 °C)	17.5	104 ± 55	1.8 ± 0.8	1.8 ± 0.4	5.8 ± 2.0	0.28 ± 0.08	5.3 ± 1.4
CADC I (-7 °C)	17.5	158 ± 88	2.5 ± 1.1	1.8 ± 0.4	6.3 ± 2.5	0.23 ± 0.10	3.7 ± 1.1
CADC I (-20 °C)	17.5	218 ± 104	3.2 ± 1.1	1.6 ± 0.4	8.4 ± 4.1	0.28 ± 0.15	3.3 ± 0.8
CADC II (23 °C)	60.3	48 ± 26	0.53 ± 0.24	1.2 ± 0.3	15 ± 14	1.6 ± 2.1	7.6 ± 3.8
CADC II (-7 °C)	60.3	93 ± 57	1.1 ± 0.6	1.3 ± 0.4	11 ± 7	0.69 ± 0.71	5.4 ± 2.0
CADC II (-20 °C)	60.3	136 ± 87	1.6 ± 0.7	1.3 ± 0.4	13 ± 10	0.93 ± 1.26	5.4 ± 2.8
CADC III (23 °C)	120.3	23 ± 12	0.23 ± 0.11	1.0 ± 0.2	29 ± 13	3.1 ± 2.0	10 ± 4
CADC III (-7 °C)	120.3	31 ± 15	0.26 ± 0.11	0.9 ± 0.2	26 ± 10	2.3 ± 1.4	8.4 ± 3.9
CADC III (-20 °C)	120.3	39 ± 17	0.35 ± 0.12	1.0 ± 0.3	33 ± 20	3.0 ± 2.6	8.2 ± 3.5
ECE [a)] (23 °C)	17.8	310 ± 80	5.9 ± 1.8	2.0 ± 1.0	325 ± 120	14 ± 4	5.0 ± 1.1
EUDC (23 °C)	62.4	56 ± 24	0.58 ± 0.25	1.1 ± 0.3	8.1 ± 8.1	0.49 ± 0.56	4.3 ± 1.8
BAB (23 °C)	119.0	25 ± 12	0.20 ± 0.08	0.9 ± 0.4	27 ± 14	3.3 ± 1.8	11 ± 5
FTP 75 [a)] I (23 °C)	41.0	100 ± 31	1.9 ± 0.5	2.0 ± 0.6	246 ± 70	11 ± 3	5.2 ± 1.0
FTP 75 II (23 °C)	25.7	99 ± 39	1.7 ± 0.6	1.7 ± 0.3	1.9 ± 0.9	0.11 ± 0.04	6.9 ± 4.0
FTP 75 III (23 °C)	41.0	62 ± 23	0.83 ± 0.24	1.5 ± 0.4	11 ± 7	0.63 ± 0.76	3.7 ± 2.9

a) This cycle phase is effected by cold start emissions

Table 1: Total hydrocarbon (THC) and benzene emission factors [mg/km] as well as the benzene/THC mass proportion [%] of a diesel- (EURO-2) and a gasoline-fueled (EURO-3) passenger car fleet.

Comparison with legislative cycles

Since the CADC is not widely applied yet and data is mainly available for the newer vehicle technology, a comparison was made with emission data of the worldwide used FTP 75 and the European wide known EDC as well as the German highway cycle (BAB).

Mean velocities of 17.5, 60.3 and 120.3 km/h are reported for the three CADC phases which correspond reasonably well with those of the FTP 75 phase II, EUDC and BAB with mean values of 25.7, 62.4 and 119.0 km/h, respectively (Table 1).

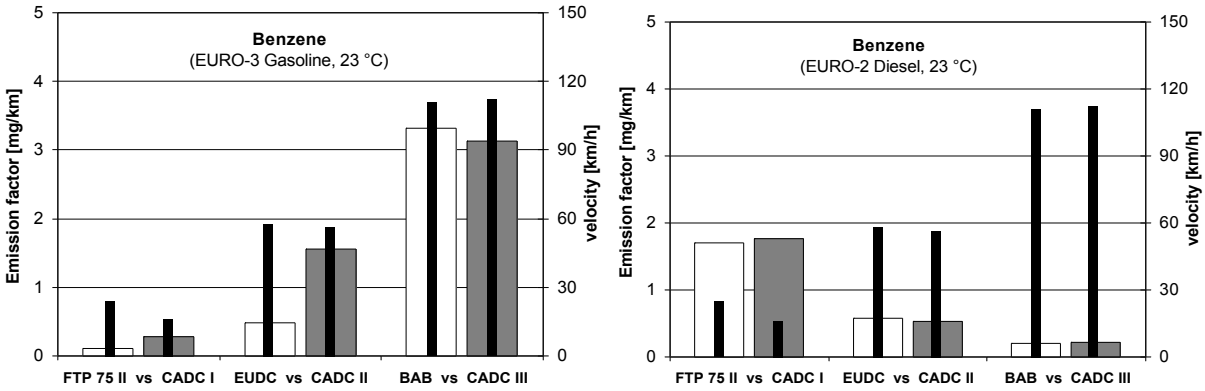

Figure 3: Benzene emission factors (mg/km) of the diesel- (left) and gasoline-fueled (right) fleets for the CADC and comparable phases of legislative driving cycles. The mean velocity (black bar) of a cycle phase is also given.

As shown in Fig. 3, the benzene emission factors of the diesel fleet at urban, extra urban and highway conditions are very similar for the compared driving pattern. Increased CADC benzene emissions factors were observed for the gasoline fleet at urban and extra urban conditions when compared with the FTP 75 phase II and the EUDC data. Related to the legislative cycles differences of +3.3, -8.9 and +12.4% and of +160, +220 and -6% were noticed for the diesel and the gasoline technology, respectively (Fig. 3). It is assumed that increased benzene emissions of the investigated gasoline vehicles at urban and suburban conditions are mainly associated with acceleration situations. Therefore the more dynamic CADC driving pattern is expected to induce more of these short time emission peaks which are not converted efficiently in the catalyst. We previously reported the catalyst-induced benzene formation from gasoline-fueled vehicles of the preceding EURO-1 and EURO-2 technology, (Heeb et al., 2002, Heeb et al., 2000). It is assumed that under highway driving the increased benzene emissions of the investigated EURO-3 vehicles is to some degree also the result of a benzene formation in the three-way catalyst.

Relative benzene/THC mass proportions

Fig. 4 displays the mean benzene/THC mass proportions observed in the exhaust gas of the diesel- and gasoline-fueled vehicles. Independent of the ambient air temperature a moderate decrease of the ratios from about 1.8 to 1.3 and to 1.0% was obtained for the diesel fleet at urban, extra urban and highway driving, respectively (Table 1).

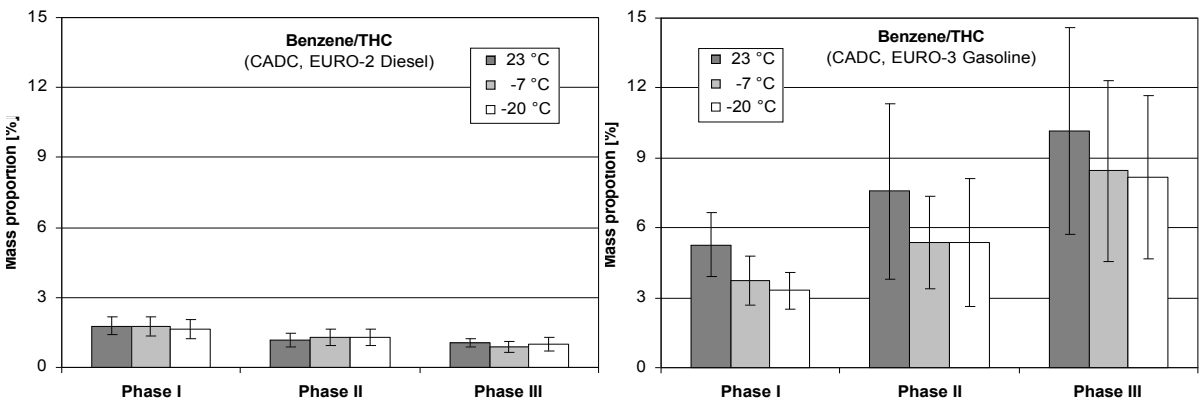

Figure 4: Mean benzene/THC mass proportions [%] of the EURO-2 diesel- (left) and EURO-3 gasoline-fleet (right) are given for the three CADC phases at 23, -7 and -20 °C.

Higher ratios between 3.3 - 10% were noticed for the gasoline vehicles. The benzene proportion increased with the average velocity but slightly decreased when lowering the ambient air

temperature. As mentioned, benzene has to be regarded as a secondary pollutant, which is to some degree formed in a three-way catalyst , (Heeb et al., 2002, Heeb et al., 2000). From the obtained data we conclude that the observed increase of the benzene/THC mass proportions under highway conditions which are associated with the highest catalyst temperatures also indicate a catalyst-induced benzene formation rather than a reduced benzene conversion efficiency. Nevertheless, the benzene emission levels of the observed EURO-3 fleet are significantly reduced when compared with those of the EURO-1 and EURO-2 technology (Heeb et al., 2001, Heeb et al., 2002, Heeb et al., 2000).

Conclusions

Mean benzene and THC emission factors of the latest diesel- and gasoline-fueled passenger cars within the CADC are reported. Comparably low benzene emission factors of 0.2 - 3.2 mg/km were obtained for EURO-3 gasoline- and EURO-2 diesel-fueled vehicles under hot engine/catalyst conditions for a velocity range of 0-150 km/h. Such low benzene emission levels contrast those of the preceding EURO-1 and EURO-2 gasoline vehicles for which emission factors up to 100 mg/km are reported at highway driving (Heeb et al., 2001, Heeb et al., 2002, Heeb et al., 2000). It has to be stated that the investigated EURO-3 vehicle fleet had a rather low mileage and therefore, the overall fleet average might increase when all the foreseen vehicles will be tested.

Nevertheless, the observed emission characteristic was consistent for both vehicle fleets. The benzene emissions of the diesel- and gasoline-fueled vehicles inversely depended on the velocity. The diesel fleet revealed highest emissions at urban driving whereas the gasoline vehicles emitted most benzene under highway conditions. Interestingly, comparable benzene emission factors were observed for both fleets, whereas the THC emissions of the diesel vehicles were increased up to a factor of 20 at urban driving.

A moderate dependence of the benzene and THC emissions on the ambient air temperature was noticed only for the diesel fleet. No significant temperature effects were observed for the gasoline vehicles, which contrasts the findings at cold start conditions (Weilenmann et al., 2003).

Acknowledgments

The authors wish to thank the Swiss Agency for the Environment, Forest and Landscape (BUWAL) and the Swiss Federal Office for Education and Science (BBW) for their financial support in the Artemis project (Assessment and reliability of transport emission models and inventory systems) - a project of the European community within the 5th framework program.

References

Weilenmann, M., Soltic, P., Saxer, C.J., Forss, A.-M., Heeb, N.V., (2003) Regulated and non-regulated diesel and gasoline cold start emissions at different temperatures. Proceedings of 12th International Symposium Transport and Air Pollution, Avignon, France.

Heeb, N.V., Forss, A.-M., Saxer, C.J., Wilhelm, P., (2003) Methane, benzene and alkyl benzene cold start emission data of gasoline-driven passenger cars representing the vehicle technology of the last two decades, Atmospheric Environment 37, accepted.

Saxer, C.J., (2001). Kaltstart-Emissionsmessungen an EURO-0 Fahrzeugen mittels Chemischer Ionisations Massenspektrometrie, Diploma thesis, Dübendorf, Switzerland

Heeb, N.V., Forss, A.-M., Bach, C., Schweizer, T., (2001). Velocity-dependent benzene emission factors of three-way catalyst passenger cars and light duty vehicles form time-resolved exhaust gas analysis. International Journal of Vehicle Design 27, 296-305.

Heeb, N.V., Forss, A.-M., Weilenmann, M., (2002) Pre- and post-catalyst-, fuel-, velocity- and acceleration-dependent benzene emission data of gasoline-driven EURO-2 passenger cars and light duty vehicles. Atmospheric Environment 36, 4745-4756.

Heeb, N.V., Forss, A.-M., Bach, C., Mattrel, P., (2000) Velocity-dependent emission factors of benzene, toluene and C_2-benzenes of a passenger car equipped with and without a regulated 3-way catalyst. Atmospheric Environment 34, 1123-1137.

12th International Symposium "Transport and Air Pollution" / 12e Colloque international "Transports et pollution de l'air", Avignon, 16 -18 *June* / juin 2003
proceedings / actes, n°92, tome / Vol. 2, Inrets ed., Arcueil, France, 2003, p. 159-164

Correction Factors for Vehicle Emissions Rates Based on the Tauern Tunnel Experimental Data to Improve Vehicle Category Emissions Estimates

Hans Puxbaum* James Girard* & Ernst Pucher**
*Institute of Chemical Technologies and Analytics
**Institute for Internal combustion Engines and Automotive Engineering
Vienna University of Technology, A-1060 Vienna, Getreidemarkt 9
Email: james.girard@cleaner-drive.info

Abstract
Previous data has been acquired from tunnel experiments where concentrations of more than 100 exhaust gas constituents were measured and the vehicle categories were recorded. The vehicle fleet is broken up into categories of: passenger car with/without trailer, light duty trucks, heavy duty trucks with/without trailer, semi trailer trucks, buses and motorcycles. Three models, based on linear regression were used to characterize the sources. They used the number of vehicles, the CO_2-emissions per vehicle category (LDV and HDV) and the CO_2-emissions per fuel type (gasoline and diesel) as input values. The determination method was based on the measurement of the concentrations of the components and the air-flow of the tunnel full cross ventilation. Therefore it is possible to use the difference of input air concentrations to output air concentrations to calculate the mass of exhaust emissions. Modelling work has also been done to estimate the levels of emissions given the composition of the vehicle fleet. Based on data sets of the "Handbook Emission Factors" CO and HC emissions were overestimated. Nitrogen oxide emissions were underestimated. The differences in CO and HC seem to be due to older altitude correction factors. The lower level of the calculated NO_x-emissions can be explained by higher real life emissions from heavy duty vehicles. This paper uses the experimental data from the tunnel experiments to calculate correction factors for emissions of various vehicle categories. The experimental data is ideal for this work because the measurements take place in a controlled environment where the operating conditions of the vehicle fleet are fairly simple – for example the vehicles have a relatively steady speed. This means good correlation to the heavy duty vehicle certification test procedure, etc. For this paper correction factors are found for NO_x, CO and hydrocarbons, as well as new emissions rates for some non-regulated exhaust constituents.
Keywords: *Emissions, Real-life, Correction Factors, Automobile, CO, HC, NO_x*

Introduction

The ability to properly estimate emissions levels based on traffic volumes and vehicle categories is essential for many aspects of planning for cities, highways, etc. Emissions levels are typically estimated based on emissions factors, including those in the Handbook of Emission Factors (UBA, BUWAL 1995). The importance placed on these emissions factors makes it essential that the level of confidence in these factors be sufficient. The Vienna University of Technology has taken a series of exhaust emissions measurements from real traffic in the controlled environment of an alpine tunnel. Because these experiments were taken in a tunnel, the emissions levels can be calculated quite accurately. Additionally the types of vehicles passing through the tunnel in the measurement periods were recorded, so that the emissions levels can be related to the vehicle categories. This allows an independent check of previously published emission factors.

Experimental Setup

The Tauern Tunnel is located on federal highway A-10 in Austria from kilometre 80 to kilometre 87 (northern portal to southern portal). The tunnel elevation is 1244 m at the northern portal and 1340 m at the southern portal, leading to a slope of approximately 1.5%.

The tunnel has a full cross-flow ventilation. The tunnel has four ventilation sections of approximately equal length. The cross-flow, caused by the ventilation system and the traffic, leads to a fairly homogeneous gas concentration across any given section. Thus it is possible to obtain the mass of exhaust emissions by taking the difference between the concentration of the incoming and outgoing air flows from the ventilation system. Measurements for this research were taken between the middle two ventilation sections. The ventilation can be seen in Figure 1, below, which gives a schematic of the tunnel.

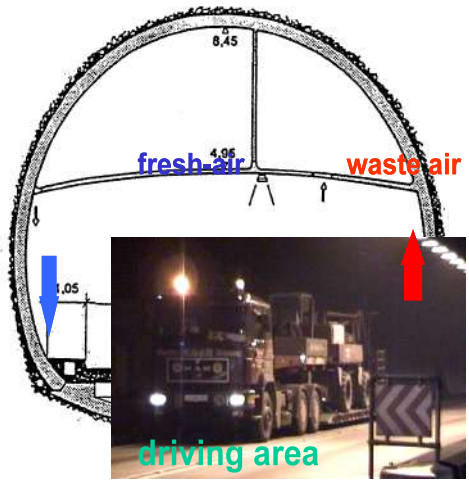

Figure 1: Schematic of Tunnel Showing Ventilation

Automatic and manual counting methods, as well as a video recording for the duration of the measurements, provided data on the traffic volume, distribution of various vehicle categories, individual vehicle speeds, ages and countries of origin. The exhaust emissions were measured continuously using commercial ambient air analysers (see Schmidt et al., 2001 for details).

Traffic Composition and Driving Conditions

The speed was measured for each vehicle and broken down to vehicle categories. Countries of origin of the vehicles were also recorded, and statistical data for the vehicle fleet composition were obtained from statistical offices of the various countries of origin. Additionally the age distribution, engine displacement class and average mileage were recorded.

The traffic flow parameters measured included the total traffic volume, the share of each vehicle categories, street profile influence (length-wise slope and altitude), number of driving lanes and speed limit. Experiments were carried out on two separate days, so that some information as to the daily variations in vehicle fleet composition could be obtained. The total traffic volume on the two days was similar, at around 470 vehicles per half hour at cruising speed. The speed was measured with radar, and the average speed was between 65 and 75 km/h. The standard deviation of the speed varied from 5 to 10 km/h.

For the weekday test, the truck share of the total traffic volume was 16.5%, vs. around 1.5% for the Sunday measurement. This is due to a ban on weekend truck traffic in Austria…only vehicles carrying perishables are allowed on Sundays. The share of cars (passenger car plus passenger car

with trailer) was 72.5% on the weekday vs. 90% on Sunday. Motorcycles had an average share of 0.62%, but the motorcycle share fluctuated from 0 to 3.13% when broken down to half-hour measurement periods. On Sunday the north-bound traffic flow was 1.5 times higher than the south-bound flow, primarily due to weekend return traffic. The traffic volume by vehicle categories is shown in Figure 2 for the various measurement periods.

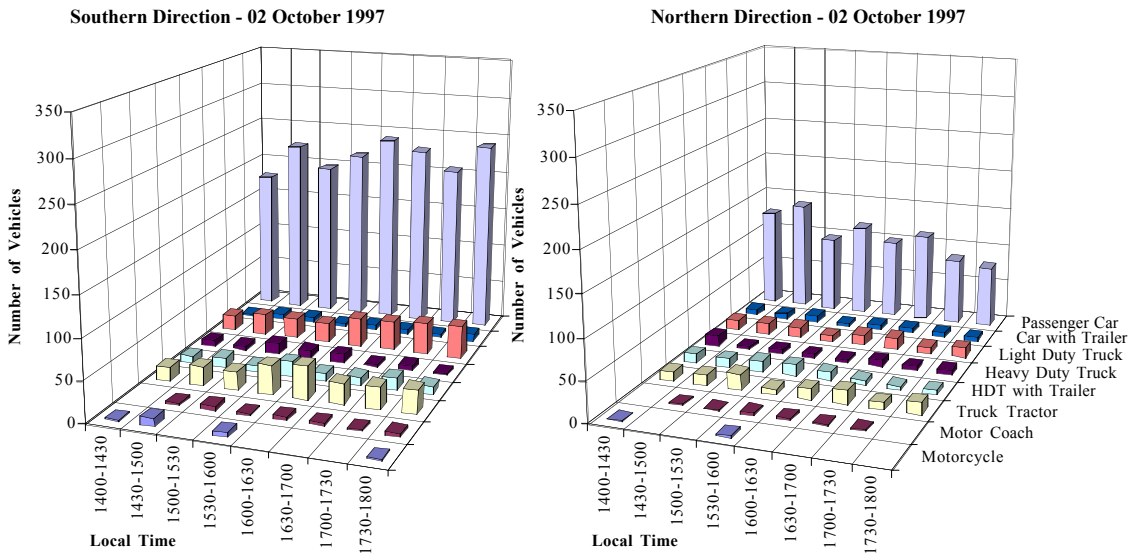

Figure 2: Distribution of Vehicle Categories for the North-Bound and South-Bound Traffic

Calculation of Emissions Factors

Based on the traffic data presented in the previous section, emissions factors were calculated based on the published values in the German "Handbuch des Strassenverkehrs" (UBA, BUWAL 1995). Most of the vehicles in the Tauern Tunnel testing were from Germany, making this the most appropriate set of published values. The published emissions factors were corrected for the upward and downward slope and the altitude of the Tauern Tunnel. The correction factors for altitude and slope are applied to the base emission factor as shown in equation 1:

$$M_{K1,2} = f_K * k_{LN1,2} * k_{Alt} * N_{Veh1,2} \quad (1)$$

Where $M_{K1,2}$ is the emitted mass of an exhaust component in a time interval in g/km, f_K is the emission factor of an exhaust component for a given street section in g/km, k_{LN} is the slope correction factor, k_{Alt} is the altitude (height above sea level) correction factor, N_{Veh} is the number of vehicles during the measured time interval, and the indexes 1 and 2 correspond to upward and downward slope, respectively.

From equation 1 it can be seen that the altitude and slope factors can play a large role for a given set of data. For example, for CO of passenger cars at the Tauern Tunnel the upward slope factor is around 2.3 and the altitude correction is about 2.2, making the corrected value about five times higher than the baseline value. Thus having proper correction factors is essential for any type of accuracy when applying the published emission factors to a road section such as the Tauern Tunnel.

Performance of Published Emission Factors vs. Experiment

Performing calculations using forms of equation 1 for each vehicle category and given the measured traffic information the exhaust concentration has been calculated for CO_2, CO, HC, NO_x, Benzene and Particulate Matter, among other exhaust components. These calculations are then compared with the experimentally measured concentrations from the Tauern Tunnel experiments. The results for CO_2 are given in Figure 3, below. These results show that the fuel consumption calculations are correct for the model.

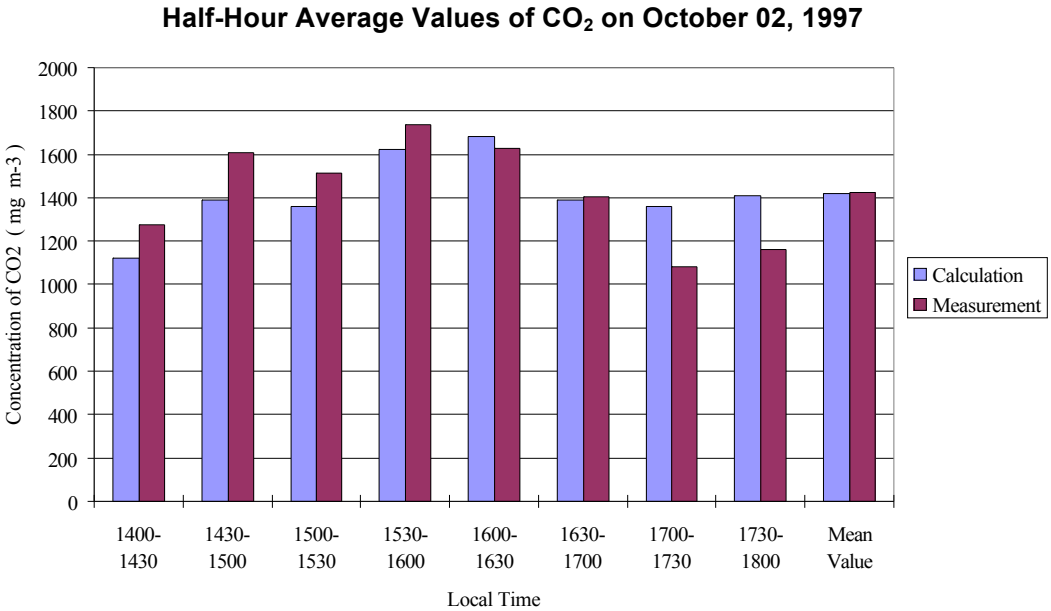

Figure 3: Comparison of CO_2 concentrations, measured and calculated from emission factors

Figures 4-5 Give the comparisons of the measured emissions values with the calculated values showing the effects of the altitude and slope corrections on the calculated emissions levels. The CO comparison is given in Figure 4. It can be seen that the published emission factors with altitude and slope correction factors overestimated the CO emissions vs. the experiment.

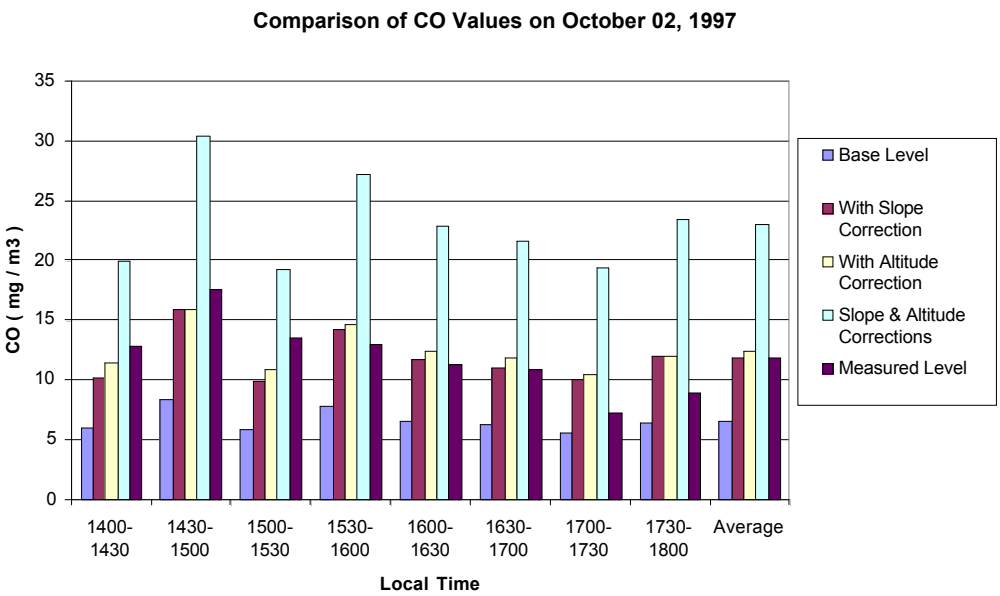

Figure 4: Effects of Altitude and Slope Correction Factors on Calculated CO Emission Levels in Comparison with Measured Values

Figure 5 gives similar comparisons for other emissions components. Since the daily averages were representative of the half-hour average values, only the daily averages are given in these figures for simplicity. It can be seen that the HC emissions are overestimated, while NO_x emissions are underestimated using the published values.

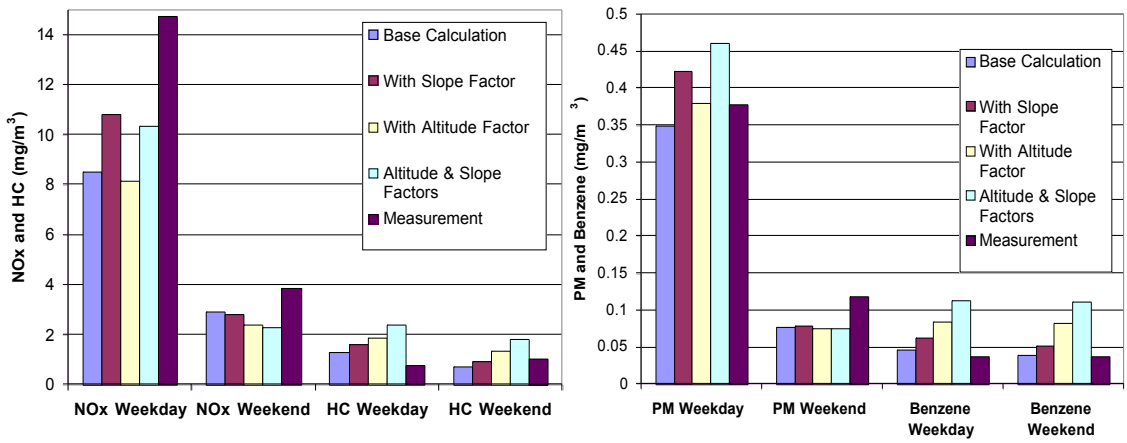

Figure 5: Effects of Altitude and Slope Correction Factors on Calculated Emission Levels for Various Components in Comparison with Measured Values

For the CO and HC emissions the trend is consistent in that the published values and published correction factors lead to over-predictions vs. experiment. These over-predictions were found through our analysis to be caused mainly by inaccuracies in the altitude correction factors for passenger cars and light duty trucks. As can be seen from Figure 4 the altitude correction factors alter the emission factors substantially for the conditions of the Tauern Tunnel.

For NO_x, the calculated concentrations were higher than the measured values. This trend was more pronounced for the weekday measurement than for the weekend. As noted, the heavy duty vehicle traffic was 16.5% of the total traffic volume on the weekday vs. only 1.5% for the Sunday. It was found that the difference in the NO_x concentrations was caused by underestimated base emissions factors for the heavy-duty vehicles and light trucks. Additionally, the negative altitude adjustment factors for the passenger cars and light trucks were found to be too large for NO_x. For the weekend, approximately 50% of the NO_x was due to passenger cars and light duty trucks due to the small numbers of heavy duty vehicles, so that the altitude factors for these vehicle classes were important in obtaining correct calculations.

Based on these findings the corrections to the published emission factors are given in Table 1. The altitude correction factors for passenger cars and light trucks are significantly lower. Also, the base NOx emission factors have to be increased by 42% for heavy duty vehicles and by 20% for light trucks to meet the measured values. Figure 6 shows the new calculated emission rates.

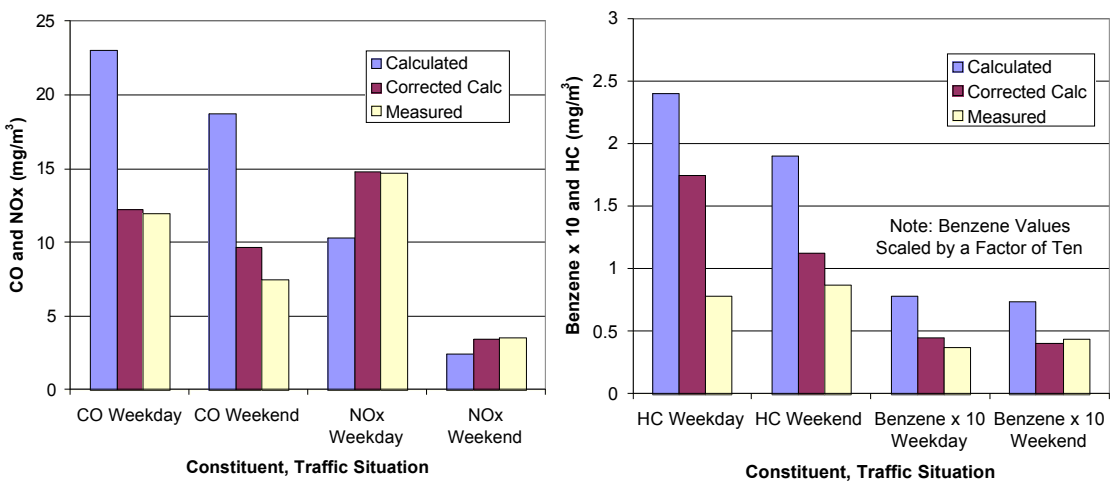

Figure 6: Predictions with Corrected Factors

	Base Value	Base Value New	Altitude Factor Old	Altitude Factor New	Slope Factor Uphill Old	Slope Factor Uphill New	Slope Factor Downhill Old	Slope Factor Downhill New
	(g/km per vehicle)							
CO Passenger Cars	1.15	1.15	2.20	1.35	2.32	1.45	1.16	1.16
CO Light Trucks	1.52	1.52	1.47	1.20	1.91	1.45	1.11	1.11
CO Heavy Trucks	varies by class	same as base	1.35	1.35	1.50	1.50	0.837	0.837
HC Passenger Cars	0.129	0.129	2.09	1.10	1.42	1.42	1.31	1.31
HC Light Trucks	0.192	0.192	1.67	1.10	1.46	1.46	1.31	1.31
HC Heavy Trucks	varies by class	same as base	1.09	1.09	1.21	1.21	1.07	1.07
NO_x Passenger Cars	0.442	0.442	0.737	1.0	1.39	1.39	0.759	0.759
NO_x Light Trucks	0.971	+ 20% = 1.164	0.821	1.0	1.367	1.367	0.759	0.759
NO_x Heavy Trucks	varies by class	base + 42%	1.01	1.01	1.62	1.62	0.734	0.734
Benzene Passenger Cars	0.00413	0.00413	2.20	1.35	1.45	1.45	1.33	1.10
Benzene Light Trucks	0.00432	0.00432	1.47	1.20	1.40	1.40	1.31	1.10
Benzene Heavy Trucks	varies by class	same as base	1.35	1.09	1.21	1.21	1.08	1.00

Table 1: Base Emissions Values and Altitude/Slope Adjustments, with Corrected Values Based on Experiment.

Summary

The high level of detail in the tunnel measurements allowed for the determination of correction factors to improve the published exhaust emission factors. It was found that the published HC and CO emission levels had altitude correction factors that were too large for the experimental conditions of the Tauern Tunnel. The NO_x emissions had base levels for heavy vehicles and light trucks that were too low in comparison to the measured values. Additionally, the negative NO_x altitude adjustment factors for the passenger cars and light trucks were too large. Particulate matter and CO_2 values were predicted correctly based on the published values. Benzene emissions were over-predicted using the published data, and it was found that both the altitude correction and the base emission level for passenger cars resulted in the over-predictions.

References

BUWAL (1995), Luftschadstoffemissionen des Strassenverkehrs 1950-2010, Schriftenreihe Umwelt Nr. 255 Bundesamt für Umwelt, Wald und Landschaft, Luft, Bern.

Schmid, H., Pucher, E., Biebl, P., Puxbaum, H. (2001), *Atmos. Environ.,* **35**, 3585-3593.

UBA, BUWAL (1995) Handbuch für Emissionsfaktoren des Strassenverkehrs, Version 1.1, UBA (Umweltbundesamt), Berlin.

12th International Symposium "Transport and Air Pollution" / 12e Colloque international "Transports et pollution de l'air", Avignon, 16 -18 *June* / juin 2003
proceedings / actes, n°92, tome / Vol. 2, Inrets ed., Arcueil, France, 2003, p. 165-170

Cold-start emissions performance of late-model EU2 and EU3 passenger cars in low ambient temperature conditions

Juhani Laurikko
VTT Technical Research Centre of Finland, VTT Processes, Engines and Vehicles, P.O.Box 1601, FIN-02044 VTT, Finland. Email: Juhani.Laurikko@vtt.fi

Abstract
Latest development of engines and emission control devices in passenger cars to bring them in compliance with the amended European directives for exhaust emissions (EU2 and EU3) has apparently improved also their performance in regard of cold-start related emissions, even if the targeted test procedure to specificly measure and control these emissions was included in the type approval requirements as late as year 2002. However, as the test results presented in this paper demonstrate, cold-start performance has been gradually improved, and emission rates measured at low ambient temperatures (-7 ºC) have declined. According the results, elevated emission levels at cold-start are also mostly associated with petrol-fuelled cars, as much lower levels were recorded for those with diesel engines.
Key-words*: cold-start emissions, passenger cars, petrol, diesel.*

Background

European Union introduced more stringent exhaust emission control for passenger cars in 1998, when the directive 98/69/EC, amending the directive 70/220/EEC, was adopted. This amendment directive by the EU Commission (1998) included features that were targeted to make manufacturers to enhance the performance of the emission control especially in the cold-start phase. One such feature was the modification of the test procedure to omit the 40 seconds idle that has been in the beginning of the test, and start collecting the exhaust sample immediately after the engine has fired-up. Therefore, the exhausts from the most-critical cold-start phase were not anymore by-passed, but included in the sample. This modification was expected to make the manufacturers more careful in their programming of the cold-start enrichment, and force them to bring the catalytic converter closer to the engine for faster warm-up and subsequent light-off Maus (1999), Holy (2000). According to Memorandum form the EU Commission (2000) both of these features were expected to greatly improve the performance of the system right after the start-up. And they really succeeded, which could be demonstrated e.g. by testing these Euro 3 compliant vehicles using the old test procedure.

Furthermore, the revamped directive included a separate test at low operating temperatures, namely at –7 °C. This test consists of just the UDC phase of the revised European dynamometer driving schedule. As it is slightly over 4 km in length, it can be regarded as a fair representative of a short urban cold-start trip. Naturally, this test has its own set of standards. Limit values are given for CO (≤ 15 g/km) and total hydrocarbons (≤ 1.8 g/km), as NOx is not expected to increase markedly. Although part of the package, this additional requirement was not, however, introduced at the same time as Euro 3 standards (1.1.2000 for new type approvals), but two years after. And even then, it was only for new types. Therefore, the implementation has been rather slow, as not so many new types have been introduced during the past year. Even so, testing has shown that the modifications of the emission control system required due to this revised test procedure in the normal temperature have greatly improved the performance at low ambient temperature, as well.

1- Objective

VTT has evaluated the cold-start performance of new cars for a decade. Each year a batch of some 10 to 20 cars representing that particular model year has been tested. The objective of this work has been to make an assessment, how the cold-start performance has been developing, and to provide first-hand results for the motoring press of those cars for their annual evaluation tests.

2 - Methodology

The selection of each annual fleet has been rather random, but favoured cars of high sales volumes in Finland. The eventual choice of cars was made by the motor magazines that initiated the testing. Most of the cars were fairly new, with odometer readings below 5,000 km.

Tests were run at –7 ºC, and using ECE15 urban driving cycle. Thus, they conform with the specifications of the Directive 98/69/EU, and the results can be compared to the official limit values. Even those cars that were originally type approved according to Euro 2 (EU2) specification, i.e. using the NEDC test cycle, were tested with the new procedure to give comparative assessment of their performance. Furthermore, all cars were tested also over the same driving cycle, but now after a thorough warm-up (EUDC cycle). This cycle was initiated with a hot engine restart after a 1 minute pause. Such a test gave the opportunity of assessing the difference between the results, and after deducting the hot restart value from the cold-start results, gave an estimate of the cold-start/warm-up excess emissions.

The objective of this work was, however, neither to make an official check of the emissions output, nor to assess the conformity of production. Therefore, all tests were run using commercial fuel (RON 95) of good quality.

Vehicle preparation and preconditioning was also carried out according to the definitions in the Directive. Accordingly, cars were soaked in the test cell for at least 12 hours, but not more than 24 hours, although the certification procedure allows cold-soak up to 36 hours. Dynamometer settings were based on reference mass and the corresponding factors taken from the look-up table in the Directive.

A normal PDP-CVS system was used for all exhaust dilution and sampling, and an AMA2000 exhaust emission analysis system from Pierburg AG (FRG) was used for the regulated emissions.

3 - Results and discussion

Petrol fuelled Euro 2 and Euro 3 cars

A good comparison between the performances of Euro 2 and Euro 3 cars can be made on the basis of one 16 car fleet of model year (MY) 1999. This consisted solely of Euro 2 cars, and two 19 car fleets, one of which is MY2001, with the majority of Euro 2 cars, but a few Euro 3 cars. However, the MY 2003 fleet consisted exclusively of Euro 3 compliant types. Figure 1 illustrates the test results for CO and HC emissions. Both constituents are presented as a cold-start result, comparable to the cold-start test described in Directive 96/69/EU, as well as a hot-restart value, all derived from identical ECE15 driving cycles at –7 °C ambient. As the lowering of temperature does not usually increase the emission of NOx, the results are not presented, even if NOx was measured.

As the figure clearly shows, CO performance has been constantly improved over this period. This is the case, even if none cars tested, do not necessarily have type approved to comply with the cold-ambient test of Directive 96/69/EU that went into force for new types of cars after 1 January, 2002.

Mostly the improvement has probably resulted from the various improvements that the manufacturers have made to the engines and the associated emissions control systems, when they have seeked compliance with Euro 3 level of standards. Because Euro 3 requires testing with the revised European Test, without the 40 second idle, the emphasis is clearly now much more fast warm-up performance of the catalyst, and using sensible cold-start enrichment strategies. Therefore, also low-

ambient temperature performance is enhanced.

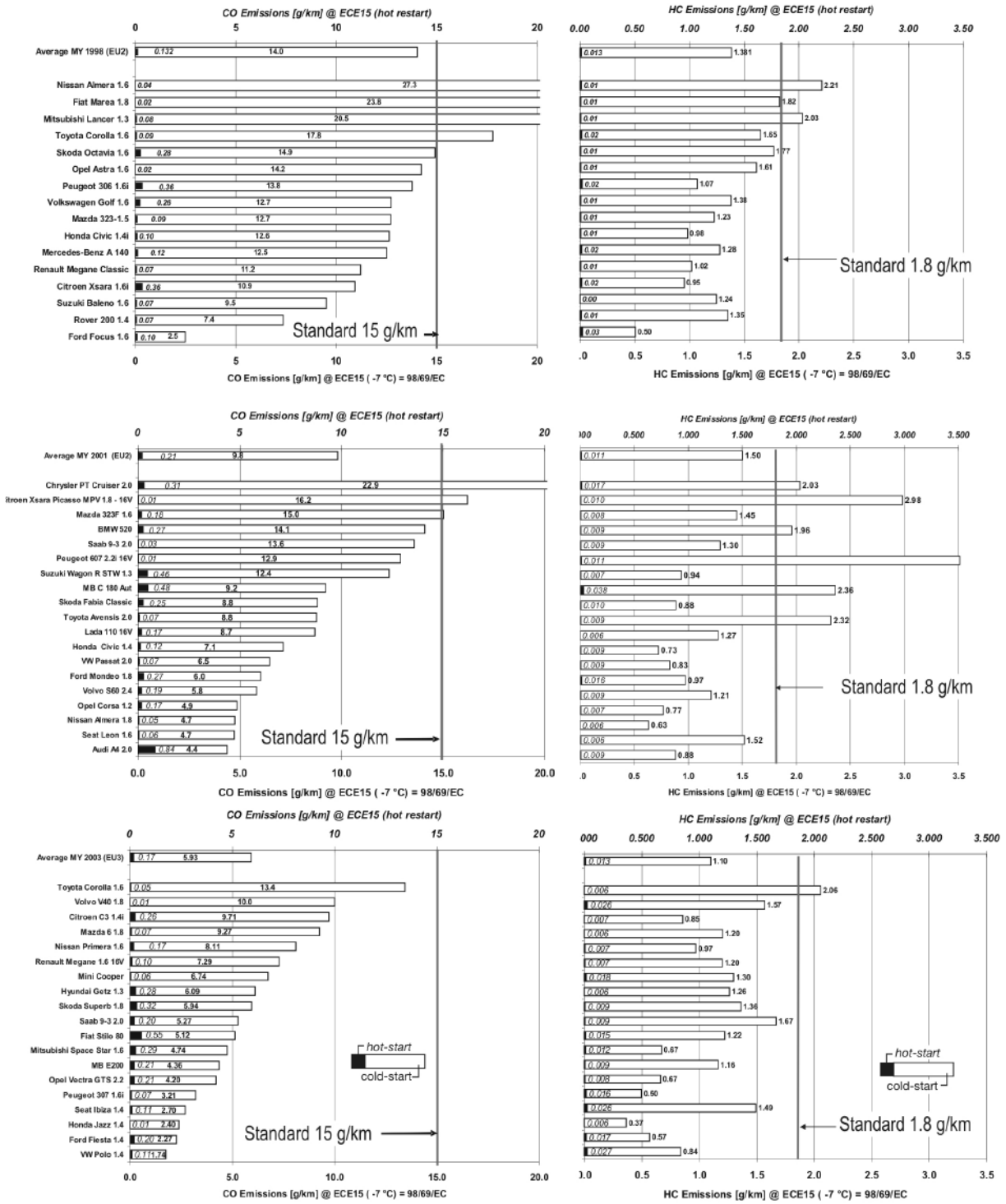

Figure 1: CO Results for three tested fleets, MY'99 (EU2), MY'01 (EU2,EU3) and MY'03 (EU3)

However, the case seems to be somewhat different for total hydrocarbons (HC). The recorded results do not much vary between the fleets, and the highest values seem to be associated with the MY2001 fleet. There is not, however, any straightforward explanation to this kind of trend. Our experience suggest though, that low HC and low CO do not necessarily come together, as in many cases the cars with extremely low cold-start CO can show higher values of HC, than those with slightly higher CO output. This may be a result of a too lean air-fuel ratio setting during cold-start phase resulting in rough running and non-firing working cycles releasing unburned hydrocarbons in the exhaust.

With a sensible enrichment, CO may be slightly higher, but with more stable combustion and less non-firing cycles, the HC output remains lower.

This can also be seen from the illustrations in Fig. 1, where the plotted data has been sorted so that in each subgroup the CO values are highest at the top, and lowering when going down. Consequently, the HC values are plotted with the cars in the same order. Thus the phenomenon just described, gives the HC graph a slight U-shape, with the lowest values usually falling somewhere in the mid-to-low section, and not at the bottom. However, with these three graphs at hand, this is not a very clear case. Most clearly this can be seen in MY1999 graph, less in the MY2001 and MY2003 graphs.

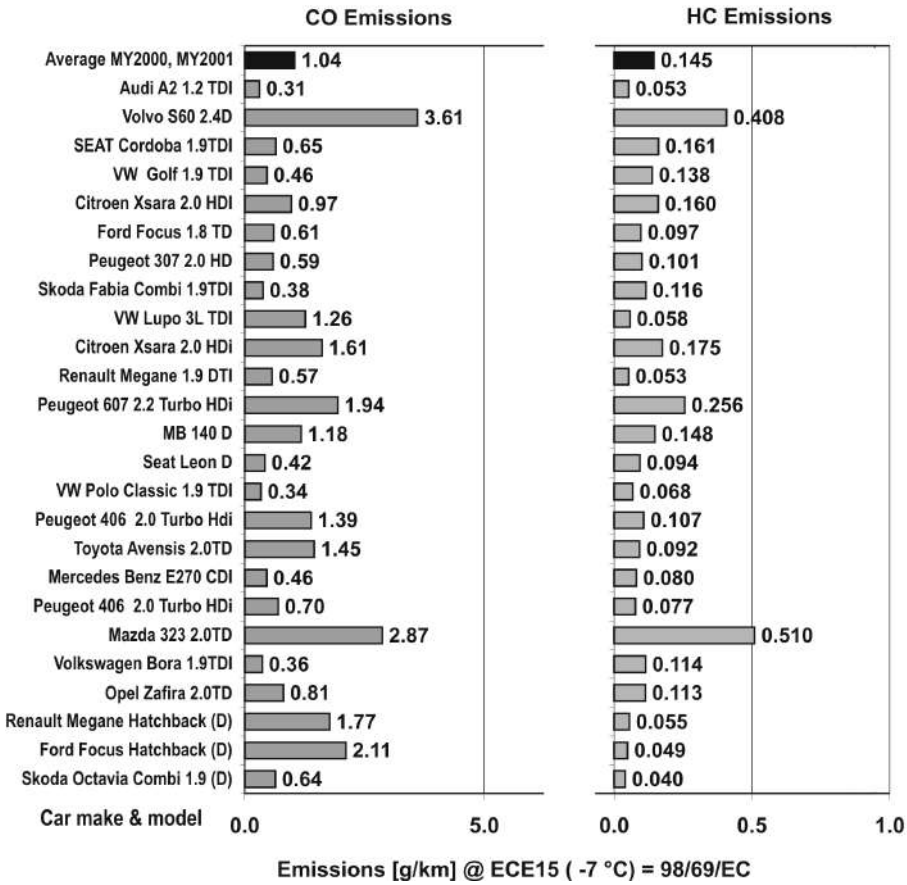

Figure 2: Cold-start CO for diesel-fuelled cars of MY2000 and MY2001

Diesel-fuelled cars

Although cold-start excess emissions are primarily associated with petrol-fuelled cars, we have also tested some diesel passenger cars, because emission inventories do need cold-start data also for diesel cars. Figure 2 graphs these results.

As we can see, when the scales in Fig. 3, diesel-fuelled cars do emit much less CO and HC when started at a cold ambient temperature. Overall, the difference is almost of an order of magnitude. However, the figures also show that the worst performing diesel cars are close to the best-performing petrol cars, i.e. between 2.5 to 3 for CO and 0,5 g/km for HC.

Overall comparison and a perspective view

Comparative data over a longer period of time is also available, since this same kind of test methodology has been employed since 1998. Figures 3 and 4 show a summary of these results.

When looking at the average cold-start CO results for various test fleets between MY1998 and MY2003, illustrated in Figure 3, one can see that there has been almost a steady downward trend. Exceptions to this pattern do exist, but that may be the effect of choice of cars in that particular fleet,

as it has been quite random, and the fleet reasonable small. Therefore, a different choice of makes and models could have produced a slightly different average for that particular year. The number of cars emitting CO more than the legislative limit value (15 g/km) has also decreased, even if the mandatory cold-start type approval was implemented as late as January 1, 2002.

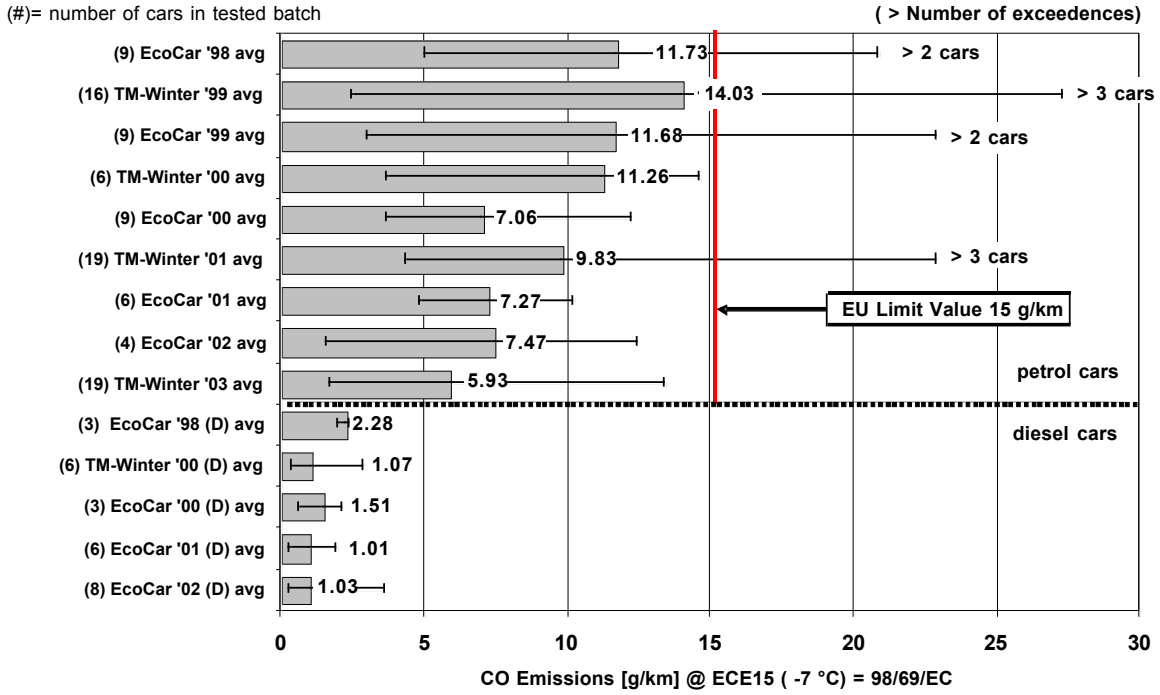

Figure 3: Comparison of different fleet average cold-start CO emissions from petrol and diesel cars.

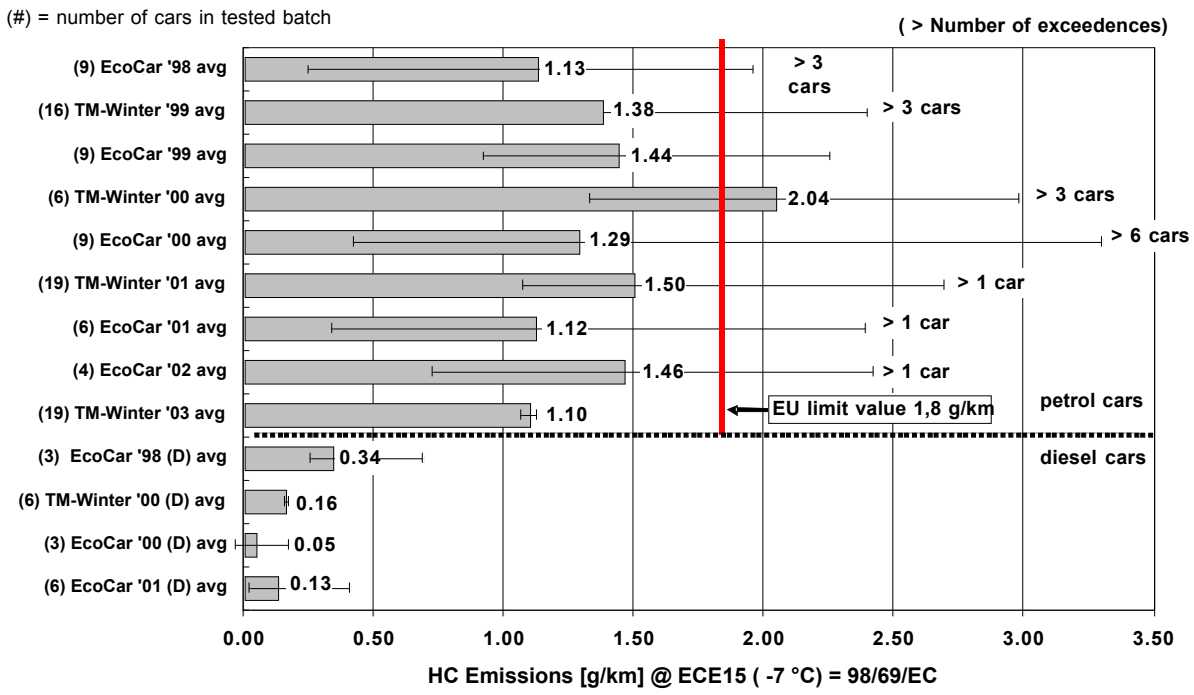

Figure 4: Comparison of different fleet average cold-start HC emissions from petrol and diesel cars

The total hydrocarbon (HC) emissions have had somewhat different evolution based on the values presented in Figure 4. They have been the highest in late 1999 early 2000 cars and exceedences to

the legislative limit values, although not imposed on these cars yet, have been great in number, and counted for every fleet but the last consisting of MY2003 Euro 3 compliant cars.

The difference between diesel and petrol-fuelled cars, as already described, can clearly be seen also here, when comparing the group of lowest bars that represent average values for the diesel car fleets, to the ones on the top half of the graphs. For instance, the average CO levels in late-model diesel cars are about 1 to 1.5 g/km, which is only some 15 to 20 % of the level of fleet averages from comparable petrol-fuelled cars fleets, which is from 6 to 7,5 g/km. In case of HC, the difference is even more enhanced, as the average levels for diesel-fuelled cars tested in 2000 and 2001 were in the region of 0.1 g/km, which is only some 10% of the levels emitted by the petrol-fuelled cars of the same model years, as hydrocarbons at levels from 1.1 to 1.5 g/km were recorded for these fleets. However, as already stated, the worst diesel cars are equal to the best petrol-fuelled ones.

Conclusions

The annual testing of new motor cars for cold-temperature emissions performed at VTT shows, that even if the Directive 96/69/EU has imposed a cold-start emissions test at –7 °C with separate limit values for new type approvals as late as after January 1, 2002, cold-start emissions performance of petrol-fuelled cars has greatly improved over a period of last five years. The average cold-start CO emission result has fallen by nearly 50 %. However, HC emissions have not improved with the same magnitude, but remained on average almost on the same level. Extremely high values have been cut down, though, especially with the introduction of the latest Euro 3 cars.

The collected test results maintain the status that cold-start excess emissions are primarily associated with petrol-fuelled cars, and the difference is almost of an order of magnitude. However, the worst performing diesel cars are close or on par with the best-performing petrol cars.

References

EU Commission, Directive 98/69/EC of The European Parliament and of The Council of 13 October 1998 relating to measures to be taken against air pollution by emissions from motor vehicles and amending Council Directive 70/220/EEC. Official Journal of the European Communities (OJ), L 350/1, 28.12.1998. 56 p.

EU Commission, Explanatory Memorandum (as part of) a Proposal for a Directive of the European Parliament and of the Council amending Council Directive 70/220/EEC concerning measures to be taken against air pollution by emissions from motor vehicles /* COM/2000/0487 final - COD 2000/0211 */ Official Journal (OJ) C 365 E, 19/12/2000. pp. 0268 – 0269.

Holy, G., Brück R., Hirth P., Improved Catalyst Systems for SULEV Legislation: First Practical Experience. SAE Paper 2000-01-0500, Society of Automotive Engineers, Inc., 2000. 7 p.

Maus, W., Brück, R., Holy, G., Technologies for Spark-Ignition Engines - The Next Generation of Super Ultra Low Emission Vehicles. Proceedings of the International Congress in Graz, September 2 & 3, 1999. 13 p.

12th International Symposium "Transport and Air Pollution" / 12e Colloque international "Transports et pollution de l'air", Avignon, 16 -18 *June* / juin 2003
proceedings / actes, n°92, tome / Vol. 2, Inrets ed., Arcueil, France, 2003, p. 171-176

Comparison of Different Engine Types and Fuels Regarding their Ozone Forming Potential

Patrik Soltic & Christian Bach
EMPA, Überlandstrasse 129, 8600 Dübendorf, Switzerland -
Fax +41 (0)1 823 40 12 - email : patrik.soltic@empa.ch

Abstract
The most pollutant emissions have been reduced during the last decades; this applies also for the ozone-precursors NO_x and VOC. However, this clear lowering of the precursors did not affect the measured ozone concentration as one would expect. It is well known that the VOC/NO_x ratio plays a major roll in the ozone forming photochemical VOC/NO_x cycle as well as the composition of the VOC is important. The most frequent VOC-to-NO_x ratio during summer moved in the agglomeration of Zürich from around 3-7 in the early 1990s to around 2-6 in the mid and late 1990s. It is likely that the lower VOC-to-NO_x ratios increased the relevancy of VOC emissions for the ozone forming and that they could lead thereby to higher ozone forming, even at lower precursor concentrations.
Nowadays, European traffic is dominated by gasoline-driven spark-ignition engines and diesel-fuel-driven compression-ignition engines. It is likely that other fuels will gain importance in the near future, mainly because of possible advantages in the CO_2 balance. The most discussed approaches are CNG (Compressed Natural Gas which consists mainly of methane), LPG (Liquefied Petroleum Gas which consists mainly of propane and butane) and gaseous and liquid bio fuels. Blend of diesel, gasoline or natural gas with bio fuels are also promoted. The fuel has an impact on the engine thermodynamics but also on the level and composition of the exhaust gas emissions. To estimate the effects on the ozone levels, this work compares the composition of the hydrocarbon emissions, the ozone forming potential and the NO_x emissions of passenger cars for several engine/fuel combinations.
Keys-words*: CNG, LPG, gasoline, diesel, ethanol, methane, propane, VOC, NO_x, ozone.*

Introduction

Ozone is built in a "clean" troposphere and by the presence of intense sunlight by the photolysis of NO_2 and its reaction with O_2 ($NO_2 + O_2$ □ $NO + O_3$). NO_2 can therefore be regarded as the fuel for the ozone production (forward reaction) whereas NO lowers the ozone concentration (backward reaction). This leads to the situation that increased NO emissions can locally result in lower ozone levels. It is also obvious that NO_2 emissions are much more harmful than NO emissions because they directly increase the ozone level. The reaction scheme is massively more complicated in a "dirty" troposphere where volatile organic compounds (VOCs) build-up NO_2 from NO without "consuming" ozone. NO_2 acts as a catalyst in such a situation. The build-up of NO_2 is done with help of the photolysis of VOCs were the hydroxyl radical (HO) plays a major role. The net result is the well-known relation that, depending on the VOC-to-NO_x ratio (NO_x summarises NO and NO_2), either the NO or the VOC level determines the ozone production rate.

The term "VOC" includes all organics (hydrocarbons, aldehydes, alcohols) which react in the troposphere and contribute to the ozone formation. The magnitude of the contribution is different for each VOC and depends on the local stoichiometry (level of NO_x, VOC and ozone). Since individual and commercial traffic accounts for roughly 50 % of the VOC and 75 % of the NO_x emissions in Swiss cities during summertime, the composition of these emissions is important to estimate their

influence on the ozone levels. Although both levels, VOC and NO_x, were roughly halved since the maximum emission period in the mid-eighties, the ozone levels did not show a clear decrease, see section 1 of this paper. That the ozone decline is weaker that one would expect or even that the ozone levels increase is the result of the underlying nonlinear mechanisms. It is very likely that the actual mix of VOCs and NO_x as well as the partitioning of the NO_x emissions has changed in such a way that ozone is built up more efficiently. This is why this paper gives a brief overview of the immission situation over the last decade and it compares the composition of the emissions for different engine types, for different engine generations and for different fuels (gasoline, diesel and their blends with ethanol, natural gas and liquefied petroleum gas).

1- Immission situation

EMPA operates the Swiss national air pollution monitoring network (NABEL) under the supervision of the Swiss Agency for the Environment, Forests and Landscape (SAEFL). The main task of the NABEL is to measure the ambient air quality in Switzerland and to provide high quality long-term measurement series of air pollutants. The monitoring network consists of 16 monitoring stations that are located all over Switzerland. Some of the rural monitoring sites are integrated into the European Monitoring and Evaluation Program (EMEP), and the high-alpine site at Jungfraujoch is a part of the Global Atmosphere Watch program (GAW). Figure 1 shows the measurements for NO_2 (yearly average) and ozone (98 % value of the half-hour values of the worst months). The Swiss limit values are also drawn.

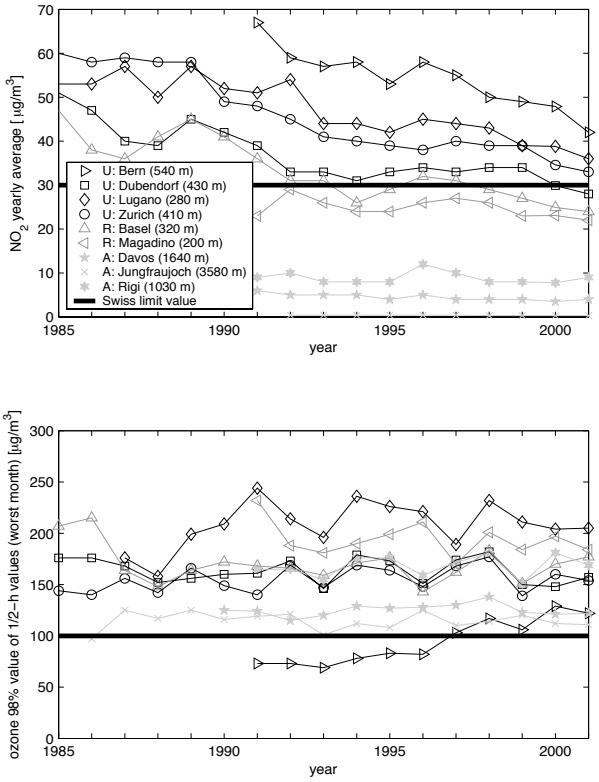

Figure 1: NABEL measurement values for NO_2 and ozone of nine different sites (U = urban, R = rural, A = alpine or pre-alpine, the altitude above sea level is indicated in the brackets)

The trend of lower immission levels for NO_2 can clearly be seen for all urban and rural sites over the last 1.5 decades. This clear trend does not exist for the ozone immissions. Very interesting is to see that the site with the highest NO_2 imissions (Bern) shows the lowest ozone immissions. Whereas the NO_2 imissions were lowered during the in the last decade in Bern, the ozone imissions increased. The VOCs are not measured in all NABEL sites but only in Zürich and Dübendorf. Figure 2 shows the frequency distribution of the VOC-to-NOx ratio in Zürich (left diagram) and Dübendorf (right

diagram) for summer days.

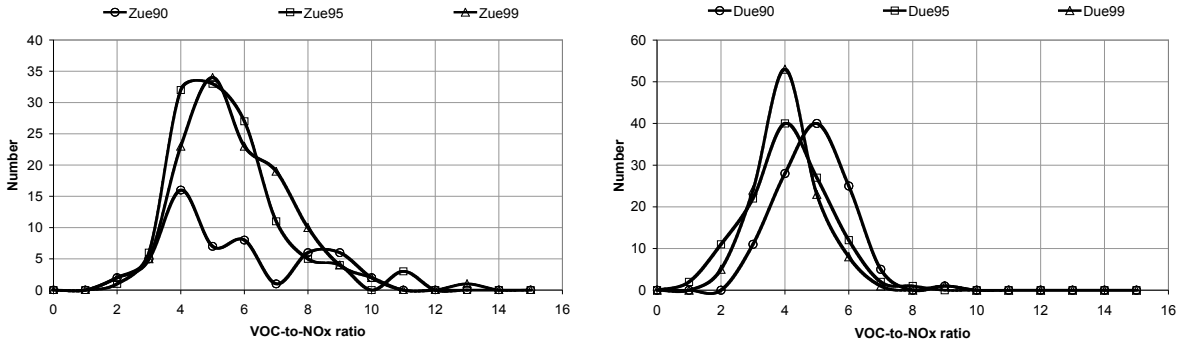

Figure 2: Frequency distribution of the VOC-to-NO_x ratio in Zürich and Dübendorf for summer days (May-August)

The frequency distributions show for Zürich that the most VOC-to-NO_x ratios during summertime lie between 3 to 9 and no clear trend to lower the higher ratios can be observed during this decade. Especially the values for 1995 and 1999 are similar. The most VOC-to-NO_x ratios for Dübendorf (agglomeration near Zurich) lie between 2 and 7 during the same period and a trend to lower VOC-to-NO_x ratios can be observed.

2- Ozone reactivity

The computation of incremental reactivities (IR) is a meaningful method to quantify the contribution of an individual VOC to ozone. The IR denotes the increase of molecules of ozone per C atom of the VOC added for a given initial condition. IRs are usually computed numerically for a specific VOC as a function of the VOC-to-NO_x ratio using complex reaction schemes. Figure 3 shows the incremental reactivities for several VOCs. Interesting is the observation that toluene and benzene are capable to lower the ozone level (negative IR values) for large VOC-to-NO_x ratios and benzaldehyde always lowers the ozone level. Almost all VOCs show a maximum incremental reactivity (MIR) at VOC-to-NO_x ratios of around six.

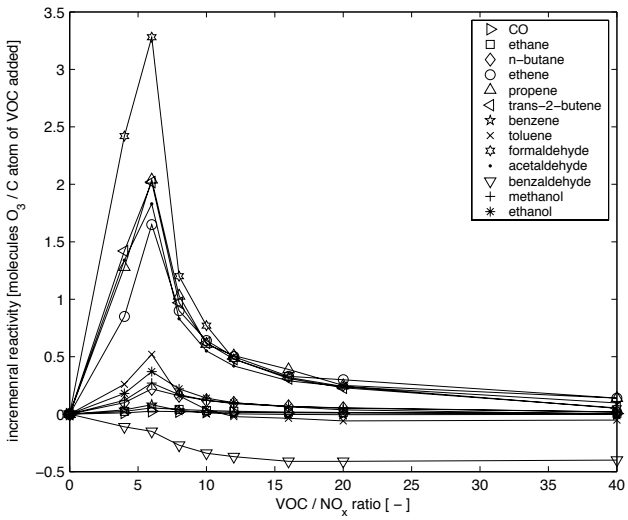

Figure 3: Incremental reactivities versus the VOC-to-NO_x ratio from Carter & Atkinson (1989).

The immission data shows that the VOC-to-NO_x ratios of Zurich and Dübendorf are in the regions with the Maximum Incremental Reactivities (MIR) of the VOCs. This means that during several sunny summer days the whole ozone forming potential of the VOCs is exploited for ozone production. One would expect that the observed slight shift to lower VOC-to-NO_x ratios in Dübendorf would result in lower ozone levels because the incremental reactivities show a clear

declination for VOC-to-NO_x ratios smaller than six. This ozone trend cannot be seen in the immission data in Figure 1 because only the worst 98 % value of the half-hour values is plotted. However, the observation that very high ozone levels are nowadays less frequent than in the early nineties can be attributed to the lower frequency of VOC-to-NO_x ratios around six.

3 - Emission situation

Different engine concepts and different fuels used result in different VOC compositions regarding the hydrocarbon (HC) emissions. Not only the VOC composition differs but also the portion of the tailpipe NO_2 emissions out of the usually measured NO_x emissions can differ significantly for different engines and/or aftertreatment systems see Soltic & Weilenmann (2002) and Soltic & Rütter (2003). Therefore, different vehicle concepts can contribute more or less to the ozone problem depending on their individual composition of the VOC and NO_x emissions. Unfortunately, no comprehensive survey of different vehicles, different certifications levels and different fuels regarding their NO_x partitioning and total hydrocarbon (T.HC) speciation could be found in the literature. Table 1 shows eleven measured vehicle/fuel combinations where the T.HC speciation was done at EMPA.

Case	Vehicle / Engine displacement [l]	Combustion system	Fuel	Certification level
1	A / 1.4	spark ignition	100 % gasoline	Euro-2
2	A / 1.4	spark ignition	CNG (methane)	Euro-2
3	A / 1.4	spark ignition	72 % propane , 28 % butane	Euro-2
4	A / 1.4	compression ignition	100 % diesel	Euro-2
5	B / 1.2	spark ignition	100 % gasoline	Euro-3
6	B / 1.2	spark ignition	85 % propane, 15 % butane	Euro-3
7	B / 1.2	spark ignition	30 % propane, 70 % butane	Euro-3
8	C / 1.6	spark ignition	100 % gasoline	Euro-4
9	C / 1.6	spark ignition	95 % gasoline, 5 % ethanol	Euro-4
10	D / 1.9	compression ignition	100 % diesel	Euro-3
11	D / 1.9	compression ignition	90 % diesel, 10 % ethanol	Euro-3

Table 1: Vehicles measured in the New European Driving Cycle (NEDC).

Case	NO_x [g/km]	T.HC [g/km]	NMHC [g/km]	OBP [g/km]
1	0.155	0.400	0.383	1.560
2	0.055	0.580	0.084	0.020
3	0.245	0.428	0.342	0.656
4	0.500	0.130	0.121	0.541
5	0.038	0.212	0.198	1.136
6	0.050	0.321	0.288	0.559
7	0.040	0.208	0.175	0.573
8	0.124	0.112	not determined	0.593
9	0.114	0.109	not determined	0.714
10	0.490	0.061	0.052	0.338
11	0.537	0.075	0.064	0.446

Table 2: NOx and HC emissions, ozone building potentials and specific reactivities in the urban part of the NEDC (ECE).

In the cases 1 to 4, the same vehicle A was measured in the gasoline, compressed natural gas (CNG), liquid petroleum gas (LPG) and diesel versions. In the cases 5 to 7, the same vehicle B was measured in the gasoline and two different LPG versions. In the case 8 to 11, the two vehicles C and

D were measured in the gasoline or diesel version. Once with the pure fuel and once with the ethanol blended fuel.

The T.HC emissions were speciated and the ozone building potential (OBP) was evaluated according to the California Non-Methane Organic Gas Test Procedures. The results are listed in Table 2 for the eleven cases described in Table 1.

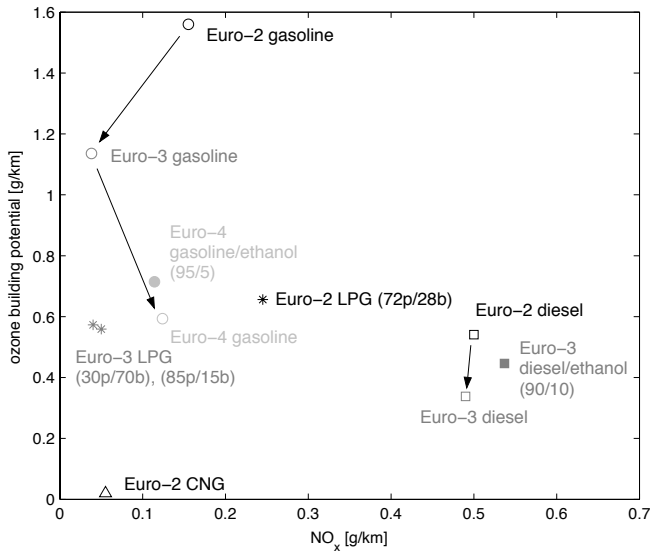

Figure 4: Ozone building potentials versus NO_x emissions (p=propane, b=butane) in the ECE.

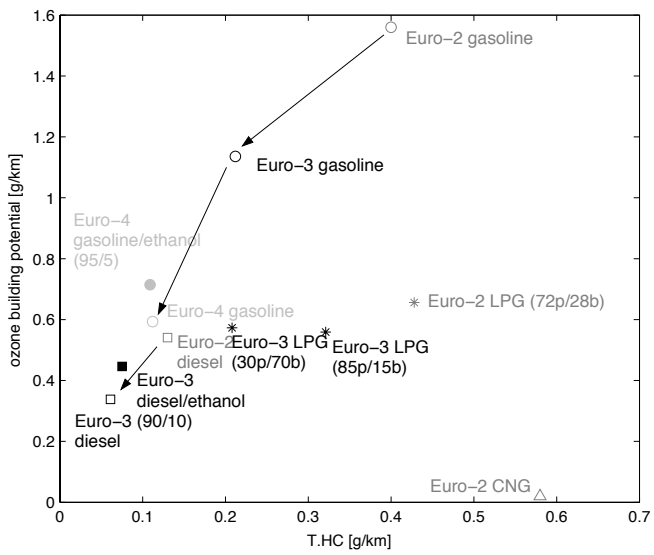

Figure 5: Ozone building potentials versus T.HC emissions (p=propane, b =butane,) in the ECE.

The ozone building potential of the eleven cases is plotted against the NO_x or T.HC emissions in the figures 4 and 5. It can clearly be seen that the ozone building potential for gasoline as well as for diesel engines decreases with higher certification level for the ECE cycle where the cold start has a significant influence on the emissions. This is most likely because the T.HC level is reduced and the reactivity of the T.HC emissions does not change very much. The LPG vehicles show a decrease in the T.HC emissions but not a clear decrease in the ozone building potential. Therefore, the reactivity of the T.HC emissions seems to increase for newer LPG vehicles. However, the CNG vehicle shows clearly the lowest ozone building potential because the T.HC emissions consist mainly from rather inert methane.

Conclusions

Even though the VOC as well as the NO_x emissions show a clear decrease over the last decades in Switzerland, the ozone problem is far away for being solved. The immission VOC-to-NO_x ratio shows a slight shift form higher VOC-to-NO_x ratios in the early nineties to lower VOC-to-NO_x ratios in the late nineties. As studies of the incremental reactivities show, this changed tropospheric stoichiometry can cause a more efficient ozone build-up with the photolytic VOC/NO_x cycle. The emissions have been massively lowered with better emission aftertreatment technology so that the resulting ozone building potentials for the newest generation of vehicles is very similar for gasoline, diesel and LPG. The blending of gasoline or ethanol shows a small increase of the ozone building potentials. However, CNG vehicles are the best option with an ozone building potential close to zero.

Acknowledgments

The authors wish to thank the Organic Chemistry Laboratory at EMPA for the HC speciations and the Air Pollution/Environmental Technology Laboratory at EMPA for the VOC and NOx immission datas.

References

Carter W. P. L. & Atkinson R. (1989): Computer modeling study of incremental hydrocarbon reactivitiy. Environ. Sci. Technol., vol. 23, p 864

Soltic P. & Weilenmann M. (2002): Partitioning of NOx emissions for gasoline passenger cars and light duty trucks, Int. Symp. "Transport and air pollution", Graz, Austria, 19-21 June, 2002, proceedings vol. II, p 49-56.

Soltic P. & Rütter J. (2003): Comparison of the NO2/NOx emissions of heavy-duty Euro-3 diesel engines with and without a CRT™ system, Int. Symp. "Transport and air pollution", Avignon, France, 6-10 June, 2003.

California Air Resources Board: California Non-Methane Organic Gas Test Procedures, August 1999

12th International Symposium "Transport and Air Pollution" / 12e Colloque international "Transports et pollution de l'air", Avignon, 16 -18 *June* / juin 2003
proceedings / actes, n°92, tome / Vol. 2, Inrets ed., Arcueil, France, 2003, p. 177-182

Unit PAH emissions at exhausts of recent-technology passenger cars in Europe

L. Paturel[*], E. Combet[*], O. Devos[*], P. Tassel[**]
[*] Université de Savoie, Ecole Supérieure d'Ingénieurs de Chambéry, LCME, 73376, Le Bourget du Lac Cedex, France. Fax 33 04 79 75 86 74 - e-mail : laurent.paturel@univ-savoie.fr
[**] Institut National de Recherche sur les Transports et leur Sécurité, LTE, case 24, 69675 Bron Cedex, France.

Abstract
The purpose of the study is to extend knowledge of the emission of non-regulated pollutants at the exhausts of private cars for recent technologies.
It deals with measurement of Polycyclic Aromatic Hydrocarbon (PAH) emissions of passenger cars according to 3 driving cycles(2 urban and 1 motorway). The effect of cold or hot start is carried out with the short urban INRETS cycle. The PAH distribution in particle and gaseous phases is studied for all of the vehicles for the four types of driving.
The quantification of 16 PAHs referenced by the U.S. Environmental Protection Agency (USEPA) was carried out by HPLC with fluorometric detection from a sample of 13 gasoline vehicles and 17 diesel vehicles registered from 1990 to 2002.
The effects of technology, type of engine start (hot or cold) and vehicle reglementation are analysed from the set of quantitative results obtained.
Key words : *PAH, HPLC, unit emission, passenger cars, gasoline, diesel, pollutant.*

Résumé
Mesure par HPLC des émissions unitaires d'HAP à l'échappement de véhicules légers de technologies récentes en Europe.
L'étude vise à étendre la connaissance de l'émission des polluants non réglementés à l'échappement des voitures particulières pour des technologies récentes.
Elle concerne la mesure des émissions des Hydrocarbures Aromatiques Polycycliques (HAP) des véhicules légers selon 3 cycles de conduite (2 urbains et 1 autoroutier). L'influence du démarrage du moteur à froid ou à chaud est étudiée sur le cycle INRETS urbain court. La répartition des HAP sous forme particulaire et gazeuse est étudiée pour l'ensemble des véhicules pour les quatre types de conduite.
La quantification de 16 HAP référencés par l' U.S. Environmental Protection Agency (USEPA) a été réalisée par HPLC avec détection fluorimétrique à partir d'un échantillon de 13 véhicules essence et 17 diesels mis en circulation de 1990 à 2002.
Les influences de la technologie, du type de démarrage (chaud ou froid) et de la réglementation du vehicule sont analysées à partir de l'ensemble des résultats quantitatifs obtenus.
Mots-clefs : *HAP, HPLC, émission unitaire, véhicule léger, essence, diesel, polluant.*

Introduction

Transport activities contribute significantly to air pollution in Europe. Reliable and credible emission estimates are a central prerequisite. Some of the priority research topics in atmospheric transport emissions [Joumard (1999a)] are the estimation of non regulated pollutants (NRP), the impact of cold engine start [Joumard (1996)] and the database updating of unitary emission for recent vehicles.

Previous studies have been achieved on this topic [Combet (1993), Paturel (1996), Miguel (1998), Shauer (2002) and the different PAH results obtained need to be completed.

Thirty vehicles (gasoline and diesel) have been tested with a chassis dynamometer on three driving cycles representative of real-world driving conditions [Joumard (1999b)]. The quantitative analysis of 16 PAHs (selected by the US Environmental Protection Agency as priority pollutants) is carried out using High Performance Liquid Chromatography with fluorometric detection.

These results have been obtained as part of ARTEMIS (Commission of the European Communities) and PRIMEQUAL-PREDIT (ADEME) projects. These projects will first result in the determination of the transport emission factors for regulated and non regulated pollutants.

1 - Methods

Driving cycles

The cycles were carried out on a controlled bracking chassis dynanometer. Each vehicle was tested over two types of driving cycles [André (2002)]:

- two cycles which are representative of the actual driving conditions in Europe, called Artemis urban and Artemis motorway, under hot engine start conditions.
- one short cycle called Inrets short urban free-flow, repeated 15 times with the first cycle being carried out under cold or hot engine start condition.

The main characteristics of these cycles are given in Table 1.

Cycle name	NRP sampling part	Short name	Duration (s)	Distance (km)	Average speed on the sampling part ($km.h^{-1}$)	Engine start
Artemis (start + urban)	urban	arturb	2834	15.3	19.4	hot
Artemis (pre + motorway + post)	motorway	artmwy	727	23.8	117.8	hot
Inrets short urban free-flow repeated 15 times	urban	repf	940	4.8	18.4	cold
		rephot				hot

Table 1: Name and description of the cycles used during PAH sampling.
Tableau 1: Nom et description des cycles utilisés pour le prélèvement des HAP.

Vehicle characteristics

Thirty passenger cars (17 diesel and 13 gasoline) registered from 1990 to 2002 and representative of european fleet have been tested. Table 2 shows the number of vehicles for each reglementation.

Reglementation	Gasoline	Diesel	
Euro 1	2	4	6
Euro 2	6	12	18
Euro 3	5	1	6
	13	17	

Table 2: Vehicle repartition.
Tableau 2 : Répartition des véhicules.

Sample collecting and processing

A classical Constant Volume Sampling (CVS) system was used. In parallel to the emissions of regulated pollutants, PAHs are collected at the end of the dilution tunnel at ambient temperature by means of a filter and an adsorber as described previously [Paturel (1996)]. The system consists of two stainless steel cartridges separated by a stainless steel grid and filled with 15g of Teflon wool and 20g of XAD2 Amberlite polymer which are well suitable respectively for particulate and gaseous PAH sampling.

These supports were prepared and purified in the laboratory.

All PAHs were extracted by cyclohexane ultrasonic method performed over 30min at 37°C. After evaporation near to dryness, extracts were dissolved in n-octane. To eliminate polar compounds a clean-up was performed on silica cartridges with an elution by n-hexane. After evaporation, residues were dissolved in acetonitrile.

All solvents used were of spectrometric grade.

HPLC analysis

The analysis of PAHs was carried out using High Performance Liquid Chromatography (HPLC, Merck) with fluorescence and absorption UV detection. The HPLC analysis was performed at 20°C using a LiChroCART 250-4 LiChrospher PAH column with an ACN/H_2O gradient at a flow rate of 1mL.min^{-1}. The 16 PAH calibration was realized with a custom mixture supplied by Supelco.

Average recovery factors for the whole procedure are calculated for each PAH using spiked Teflon wool and XAD2 Amberlite resin.

PAH	PAH abbreviation	Fluorescence conditions (nm) λex/ λem	Range of calibration (ng.mL^{-1})	Limit of detection (ng.mL^{-1})	Recovery factor (%)
Naphtalene	N	**220/320**	0,93 / 46,62	0,23	5
Acenaphthene	Ace	220/320	0,23 / 11,66	0,12	15
Fluorene	Flu	220/320	0,65 / 32,64	0,65	40
Phenanthrene	Phe	250/362	0,19 / 9,33	0,05	50
Anthracene	An	244/400	0,04 / 1,86	0,02	65
Fluoranthene	Fla	286/460	0,33 / 16,32	0,16	100
Pyrene	Pyr	333/382	0,28 / 14,00	0,07	100
Benzo[a]anthracene	BaA	265/380	0,19 / 9,33	0,09	100
Chrysene	Chr	265/380	0,09 / 4,67	0,05	100
Benzo[b]fluoranthene	BbF	296/425	0,23 / 11,66	0,08	100
Benzo[k]fluoranthene	BkF	296/425	0,04 / 1,86	0,02	100
Benzo[a]pyrene	BaP	296/425	0,11 / 5,60	0,04	100
Dibenzo[ah]anthracene	DBahA	296/425	0,19 / 9,33	0,06	100
Benzo[ghi]perylene	BghiP	296/425	0,51 / 25,64	0,13	100
Indeno[1,2,3-cd]pyrene	IP	302/500	2,05 /102,57	0,68	100

Table 3: HPLC analytical conditions.
Tableau 3: Conditions analytiques pour la CLHP.

Table 3 shows the main HPLC conditions and the recovery factors for the 15 PAHs detected by fluorescence. Acenaphthylene (Acy) was detected with UV absorption at 254 nm . This PAH was rarely quantified in emissions due to high limit of detection and poor selectivity. Consequently, the results for Acy are not presented.

Unit emissions (μg.km^{-1}) are corrected for analytical blanks, air dilution and recovery factors.

2 - Results and discussion

PAH distribution profile

An example of total PAH distributions for gasoline and diesel vehicles are presented in Figure 1.

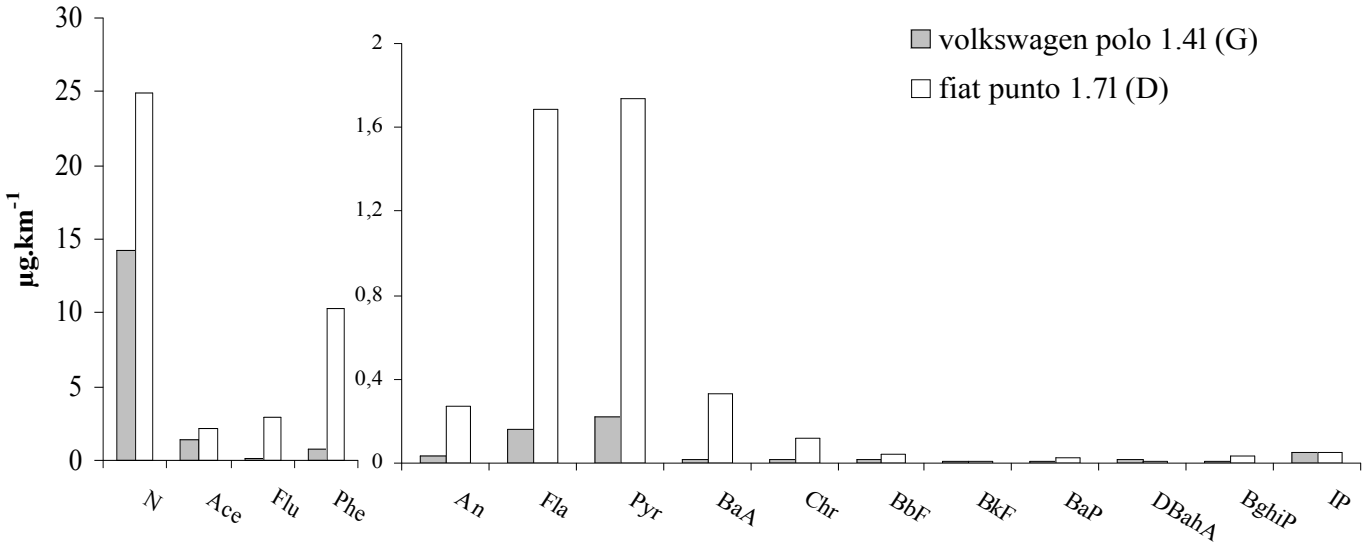

Figure 1: PAH distribution for gasoline (G) and diesel (D) vehicles and for Artemis urban cycle.
Figure 1 : Distribution des HAP pour les véhicules essence et diesel pour le cycle Artemis urbain.

Very similar PAH distributions are observed for these two gasoline and diesel vehicles. A relation between the values of unit emissions and the volatility of the PAHs appears : N with 2 rings is predominant (~60/80% of the sums expressed in mass) and then a decrease is pointed out for the 3 rings (Ace, Flu, An, Phe), the 4 rings (Fla, Pyr, BaA, Chr) and the 5 and 6 rings (BbF, BkF, BaP, BghiP, IP, DbahA) with respectively 25, 5 and 1% of the total. This distribution is similar to the one obtained by Mi et al. (1998).

All patterns of results are quite similar for all driving cycles and all cars.

Very low recovery factors (5 to 40%) and important errors are observed for N, Ace, Flu due to their volatility (Boiling point < 300 °C, Henry constant : about 1.10^{-4} $atm.m^3.mol^{-1}$) responsible of important losses during extraction processes. So, results will be expressed per individual PAH, as sums of the 12 less volatile PAHs, and some of the 6 most carcinogenic PAHs (BaA, BbF, BkF, BaP, DBahA, IP) [IARC (1983), IARC (1987)].

Reglementation influence

Mean emissions of the 12 PAH sums for gasoline (13) and diesel (17) are presented for the 4 driving cycles in Figure 2. Gasoline Euro1 and diesel Euro3 reglementation concern respectively 2 and 1 vehicles ; consequently, the evolution observed needs a confirmation. Furthermore, emission values for Inrets urban fluid cycle with cold engine start and Artemis european motorway cycle are not available for gasoline Euro1. The histogram (Figure 2) highlights from Euro1 to Euro3 that reglementation has a large influence on the diesel emissions (decrease of 5 to 20 times according to cycle) and that the gasoline classes show a weak decrease in the emissions except for Inrets short urban free-flow cycle with cold engine start.

For the both technologies in the case of hot cycles the two urban (Inrets and Artemis) lead to similar mean values.

In the case of cold engine start, the PAH emission increase is especially enhanced for gasoline vehicles: the ratios of emissions between cold and hot engine starts are respectively 4 and 1.25 for

gasoline and diesel vehicles.

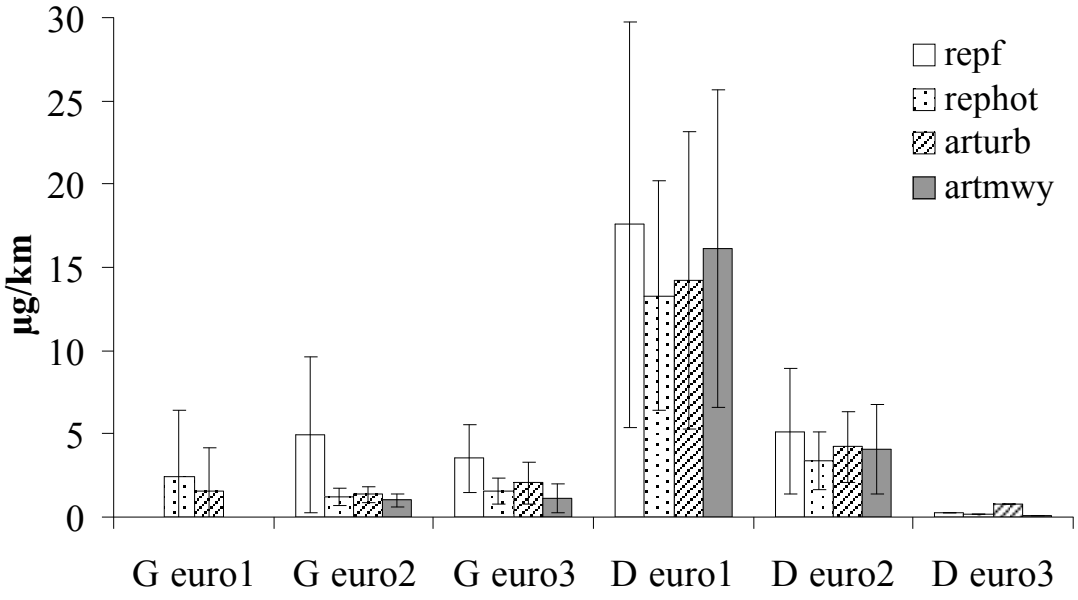

Figure 2: Mean emissions of the 12 PAH sum according to the reglementation for the 4 driving cycles. Confidence interval deviation is calculated as 2 times the standard deviation.

Figure 2 : Emissions moyennes de la somme des 12 HAP selon la réglementation pour les 4 cycles de conduite. L'intervalle de confiance est égal à deux fois l'écart type.

Gaseous and particulate distribution

For the two technologies, Table 4 shows the gaseous and particulate distribution for the more volatile, the less volatile and the 6 carcinogenic PAHs. The majority of volatile PAHs are principally in the gaseous phase (60/65 %) while the less volatile or the carcinogenic PAHs are more adsorbed on particulates (70/76%). The distribution of PAHs on particulates is sligthly more important for diesel vehicles.

PAH sums	Gasoline	Diesel
3 PAHs (volatile : N, Ace, Flu)	65/ 35	61.5 / 38.5
12 PAHs (less volatile)	29.5 / 70.5	23.5 / 76.5
6 PAHs (carcinogenic)	32 / 68	25.5 / 74.5

Table 4: Average gaseous and particulate distribution (%) for hot cycles.

Tableau 4 : Distribution moyenne entre phases gazeuse et particulaire pour les cycles chauds.

Conclusion

This work shows that the unit emissions of the 12 less volatile PAHs are very similar according to hot driving cycles. For gasoline cars an important over emission is observed for the INRETS urban free-flow cycle with cold engine start.

Sampling of PAHs both in particulate and gaseous phases is indispensable to have a good quantification of these non regulated pollutants (NRP) in the vehicular emissions particularly for volatile PAHs (two to four rings).

Finally, for all hot cycles, a large decrease is observed for the emissions of PAHs according to the evolution of reglementation for the diesels. In the case of gasoline vehicles, decrease is especially important for the cold engine start cycle.

As less volatile PAH emissions from modern technology vehicles continue to decrease to near detectable limits, more advanced technologies for sampling these pollutants such as Solid Phase

Micro Extraction (SPME) for gaseous phases and longer driving cycles should be investigated for a good determination of polycyclic aromatic hydrocarbons.

Acknowledgements

We would like to thank the French Environmental Protection Agency ADEME and the European Commission (ARTEMIS) for their financial support.

References

Andre M. (2002) : The ARTEMIS European driving cycles for measurements of the passenger cars pollutant emissions. Seventh Highway and urban Pollution Symposium. Barcelona, 20-23 May.

Combet E., Jarosz J., Martin Bouyer M., Paturel L. & Saber A.I. (1993): Mesure par spectrofluorimétrie Shpol'skii des émissions unitaires en HAP de 30 véhicules légers à essence et diesels selon huit cycles représentatifs. Sci. Total Envir., vol. 134, n° 1-3, p 147-160.

IARC (1983): Polynuclear Aromatic Compounds Part 1 Chemical, Environmental and Experimental data. IARC monographs, vol. 32.

[En ligne]. AdresseURL : http://193.51.164.11/htdocs/Indexes/Vol32Index.html

IARC (1987): Overall Evaluations of Carcinogenicity: An updating of IARC Monographs, vol.1-42, supplement n°7.

[En ligne]. AdresseURL : http://193.51.164.11/htdocs/Indexes/Suppl7Index.html

Joumard R. (1999a): Methods of estimation of atmospheric emissions from transport: European scientist network and scientific state-of-the art. DG VII, n°EUR 18902, ISBN 92-828-6797-8, Luxembourg, 175 p.

Joumard R., André M., Vidon R., Tassel P. & Pruvost C. (1999b): Influence du cycle de conduite sur les émissions unitaires de polluants des voitures particulières. INRETS report, n° LTE 9902, Bron, France, 60 p.

Joumard R., Vidon R., Paturel L. & de Soete G. (1996): Changes in pollutant emissions from passenger cars under cold start conditions, SAE technical paper series, 961133, p 23-34.

Mi H.H., Lee W.J., Chen S.J., Lin T.C., Wu T.L., Hu J.C. (1998): Effect of the gasoline additives on PAH emission. Chemosphere, vol. 36, n° 9, 2031-2041.

Miguel A.H., Kirchstetter T.W., Harley R.A. & Hering S.V. (1998): On-road emissions of particulate Polycyclic Aromatic Hydrocarbons and black carbon from gasoline and diesel vehicles. Environ. Sci. and Technol., 10, p 450-455.

Paturel L., Saber A.I., Combet E. & Joumard R. (1996): Analysis of PAH emissions from passenger cars by high resolution Shpol'skii spectrofluorometry. Polycyclic Aromatic Compounds, vol. 9, p 331-339.

Shauer J.J., Kleeman M.S., Cass G.R. & Simoneit B.R.T. (2002): Measurement of emissions from air pollution sources C1-C31 organic compounds from gasoline-powered motor vehicles. Environ. Sci. and Technol., 36, p 1169-1180.

12th International Symposium "Transport and Air Pollution" / 12e Colloque international "Transports et pollution de l'air", Avignon, 16 -18 *June* / juin 2003
proceedings / actes, n°92, tome / Vol. 2, Inrets ed., Arcueil, France, 2003, p. 183-190

Regulated and unregulated exhaust emissions from nine passenger cars

Bernhard Mittermaier, Dieter Klemp & Hermann-Josef Buers
FZ Jülich, Institut für Chemie und Dynamik der Geosphäre, ICG II: Troposphäre, D-52425 Jülich
Fax +49 24 61 61 32 40 - email: b.mittermaier@fz-juelich.de

Abstract
Nine different cars with latest exhaust gas treatment systems were tested on a chassis dynamometer in the certification cycles MVEG and FTP-75 as well as in two more demanding driving cycles. The cars had different engine concepts, i.e. conventional gasoline engine, gasoline engine with direct fuel injection and diesel engine. While all cars fulfilled the exhaust limits in the certification cycle, some severe exceedances were found in other cycles, especially for carbon monoxide in the case of gasoline engines. High emissions of NO_x - and here especially nitrogen dioxide - from diesel engines and gasoline engines with direct fuel injection are especially interesting from the perspective of air quality due to their relevance for ozone chemistry.
Keys-words*: exhaust, emissions, gasoline, diesel, ozone.*

Résumé
Émissions de gaz d'échappement régulées et non-régulées de neuf voitures
Neuf voitures différentes avec les systèmes les plus modernes de traitement de gaz d'échappement ont été testées sur un banc d'essai à dynamomètre sous les conditions des cycles de certification MVEG et FTP-75 et dans deux cycles de conduite encore plus exigeants. Les véhicules avaient des concepts de propulsion différents, à savoir des moteurs Otto conventionnels, des moteurs Otto à injection directe ainsi que des moteurs Diesel. Dans le cycle de certification, les véhicules étaient conformes aux normes pour les gaz d'échappement, mais dans d'autres cycles de test des dépassements considérables ont été constatés, notamment en ce qui concerne les monoxydes de carbone dans le cas des moteurs Otto. Les émissions élevées en NO_x – et ici notamment en NO_2 – des véhicules Diesel et des moteurs à injection directe ont une importance particulière du point de vue de la qualité de l'air dû à leur importance pour la chimie de l'ozone.
Mots clefs: *gaz d'èchappement, émissions, essence, diesel, ozone.*

Introduction

Emissions of passenger cars were first regulated at European level in the early 1970s by the directives 70/220/EEC (gasoline engines) and 72/306/EEC (diesel engines). Thereafter, several directives have sharpened the limits considerably. Today, the EURO3-limits are effective, and most new gasoline cars already fulfill the EURO4-limits, which is not mandatory before the year 2005. Nevertheless, the type approval figures do not necessarily reflect the real world emissions of vehicles because the approval testing cycle MVEG is quite undemanding (Hassel 1994), even though cold start emissions were included for EURO3- and EURO4-cars. Therefore it seems to be important to quantify the emissions of modern cars under rather realistic conditions.

Furthermore it has to be noted that from the perspectives of air quality and climate not only the regulated compounds CO, NO_x, HC and PM play major roles. For example, NO and NO_2 are recorded as sum NO_x although they play contrary roles in ozone chemistry. Therefore, several in-depth investigations beyond the regulated compounds seem to be necessary (Harrison 1996).

In this work, nine different cars were tested on a chassis dynamometer. The cars had different engine

concepts, i.e. conventional gasoline engine, gasoline engine with direct fuel injection and diesel engine. Besides the well-known European and American driving cycles MVEG and FTP-75 which are used in type approvals, all cars were tested also in the "Autobahn-cycle", which represents the driving on German highways, and in the "MOBINET-cycle" which represents driving in the city of Munich. O_2, CO, CO_2, N_2O, NO, NO_2, HC, fuel consumption and air mass were recorded on a second-by-second basis. A brief overview of the literature was recently given by the authors (Mittermaier 2003).

1 - Experimental

Vehicles and driving conditions

The measuring program included eight different cars of the model years 2000 and later which were compliant with EURO3, EURO4, D3 or D4-exhaust regulation standard. For reasons of comparison to older cars, one EURO2 car (model year 1996) was tested either. Three cars had conventional gasoline engines (spark ignition, SI), three cars had SI-engines with direct fuel injection (SI-DI) and three cars had diesel engines (compression ignition, CI) with direct injection. All SI-engines had three-way-catalysts; the diesel engines were equipped with oxidative catalytic converters. For details see Table 1.

n°	Name	Engine type	Capacity [cm³]	Power [kW]	Model Year	Mileage [km]	Exhaust limit	Source
1	Ford Mondeo	SI	1796	85	2000	6.100	D4	FZ Jülich
2	VW Golf IV	SI	1984	85	2000	83.600	D4	FZ Jülich
3	Ford KA	SI	1299	44	2001	53.400	D4	car rental
4	VW Polo FSI	SI-DI	1390	63	2002	5.900	EURO4	Volkswagen AG
5	Mitsubishi GDI Space Star	SI-DI	1834	90	2001	38.200	D3	car rental
6	VW Golf FSI	SI-DI	1598	81	2002	13.300	EURO4	car rental
7	VW Golf III TDI	CI	1896	66	1996	146.800	EURO2	private
8	VW Golf IV TDI	CI	1896	85	2002	16.300	EURO3	car rental
9	Mercedes-Benz C220 CDI	CI	2148	105	2002	19.600	EURO3	car rental

Table 1: Overview of the test vehicles. SI=spark ignition, SI-DI = spark ignition with direct fuel injection, CI=combustion ignition. D3 and D4 are special German exhaust limits. With regard to taxation such cars are treated like EURO3 and EURO4, respectively.

Tableau 1 : Aperçu des véhicules testés. SI=moteur Otto, SI-DI=moteur Otto à injection directe, CI=moteur Diesel. D3 et D4 sont des normes de gas d'échappement allemandes spéciales, qui fiscalement correspondent à EURO3 et EURO4.

All cars were driven with commercial fuel according to the manufacturer's guidelines without further specification. The emission measurements were performed on the chassis dynamometer of RWTÜV Fahrzeug GmbH in Essen, Germany. They were carried out under the conditions of four different driving cycles (Figure 1 and 2):

MVEG: Certification cycle for all new cars in the EU. The cycle begins with a cold start. Therefore, the cars are pre-conditioned at 20 °C - 30 °C for at least 12 hours. The cold start is followed by 40 seconds with idle engine for EURO1/2 and D3/D4 cars. Sampling begins after these 40 seconds. For EURO3 and EURO4 cars the 40 seconds are omitted; sampling starts right from the beginning. The cycle is divided into two phases. Phase 1 consists of 4 repetitive parts that shall reflect urban driving. The average speed is 19 km/h. The second phase reflects extra-urban driving with a speed

up to 120 km/h at an average of 63 km/h. The MVEG cycle is quite undemanding due to low engine loads and moderate accelerations. For example, the beginning of the extra-urban part is an acceleration from 0 km/h to 70 km/h in 41 seconds.

FTP-75: Certification cycle for new cars in the US and several other countries. The FTP test is divided into three phases. The test begins with a cold start. In the first test phase an average speed of 41 km/h is driven. In the second test phase the average speed is only 26 km/h. After the second test phase the engine is shut off for 10 minutes and then the test continues with a warm start. The driving pattern of this third phase is identical with the first phase. By comparing the emissions obtained in the first and in the third test phase, the effects caused by the cold start procedure can be derived from the data. This cycle reflects the driving behavior in the US satisfactorily; engine load and maximum speed are comparable to the conditions in the US.

Autobahn-cycle: This cycle was developed by by Hassel (1994), TÜV Rheinland, Germany. It represents driving behavior on the German expressways "Autobahn". Again this cycle consists of three phases. After a running start at 95 km/h, the average velocity is increasing. In the third phase of the test cycle the cars have to accelerate from 127 km/h to the maximum speed of 162 km/h in 40 seconds. This means high engine loads which are neither covered in the FTP-75 cycle nor in the MVEG cycle.

MOBINET-cycle: This cycle was developed within the BMBF-funded project MOBINET by Klemp (2002). It is representative for the driving in the city of Munich because its distributions of velocity (v), acceleration (a) and engine load (v*a) are the same as the observed ones in Munich during 20 trips with a total of 70.000 second-by-second-values. The cycle consists of parts which were actually driven on a road, whereas MVEG and Autobahn are artificial. The MOBINET-cycle begins with a warm start, followed by normal urban driving controlled by traffic lights. This phase ends with one part recorded on a 4-lane-street with a speed maximum of 80 km/h. The second phase reflects stop-and-go with an average velocity of only 5 km/h, whereas the third phase shows the driving on a city-highway with a speed limit of 120 km/h. At the dynamometer, this phase is driven in duplicate in order to reach the detection limits for the sampling bags (cf. the next section).

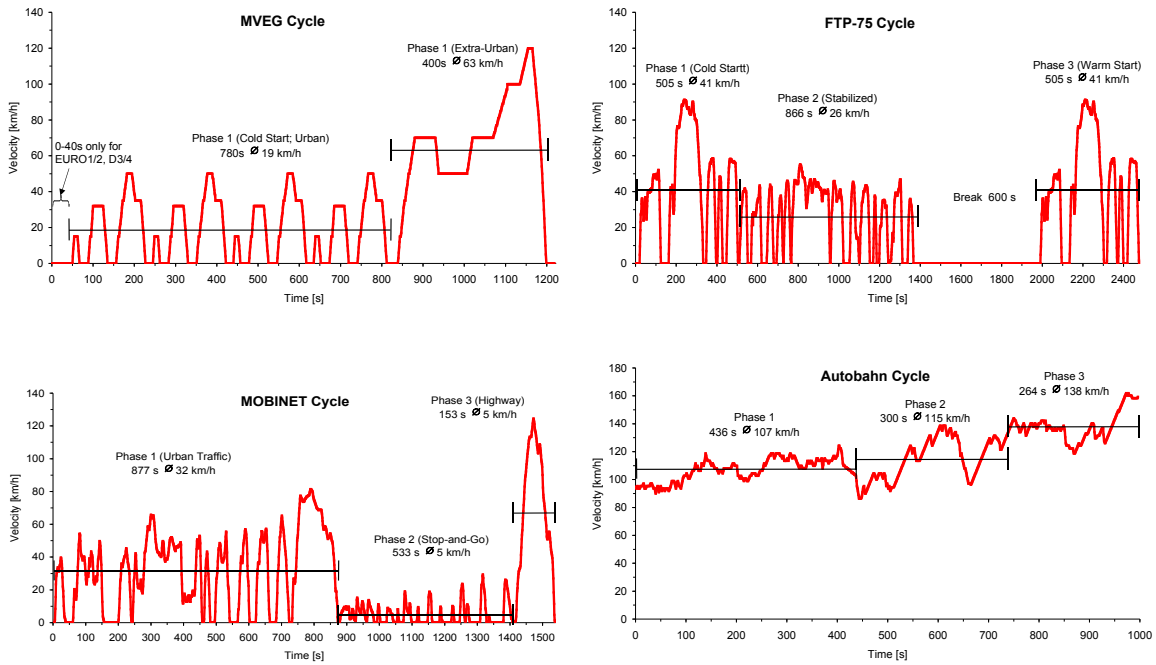

Figure 1: Driving cycles of the measuring program.
Figure 1: Cycles de conduite dans le programme de mesure

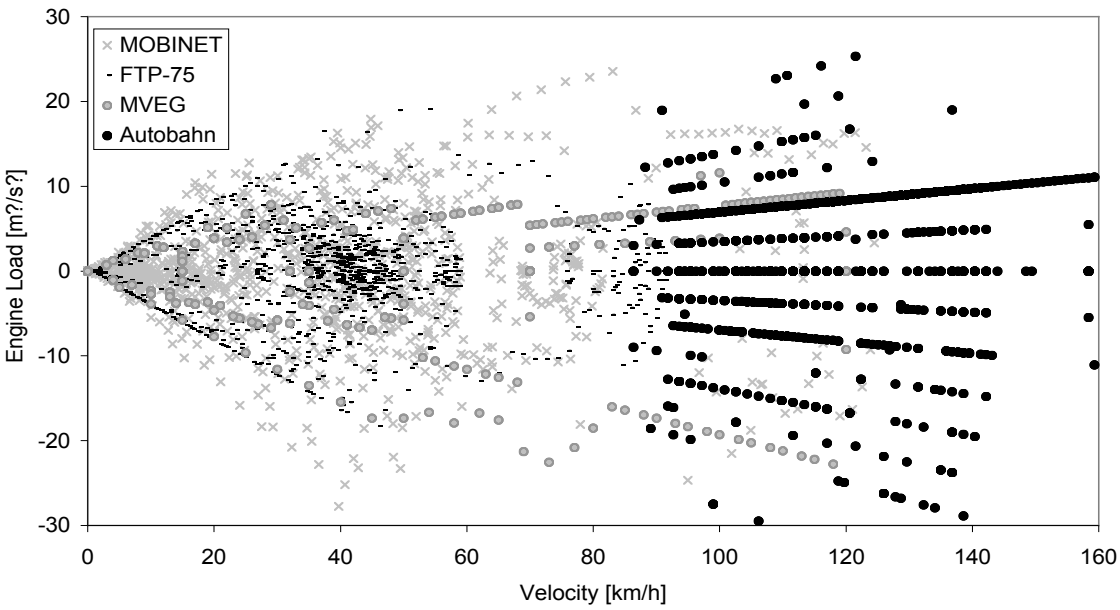

Figure 2: Distribution of engine load (velocity times acceleration) vs. velocity.
Figure 2: Répartition de la charge spécifique (produit de vitesse et d'accélération) vs. vitesse

Analysis

Fuel consumption (PLU 401-108, Pierburg Corp.), lambda value and the signal from the air mass sensor were recorded every second by our data acquisition system. As pointed out by Lenaers (1996), the current total exhaust gas mass flow can be calculated from the signals from the air mass sensor, the respective lambda value and the momentary fuel consumption. From the exhaust stream a flow of around 5 L/min is sucked in and analyzed by our gas analytics. NO, N_2O, CO and CO_2 mixing ratios in the exhaust gas are measured by means of commercially available gas analyzers (URAS, ABB Corp.) using non-dispersive infrared (NDIR) detection principle. The NO and NO_2 content of the exhaust gas is analyzed by UV-absorption (LIMAS, ABB Corp.). The total HC content is measured by a FID system (ABB Corp.). Low mixing ratios of CO were also measured by a modified trace gas analyzer (TE 48 C, Thermo Instruments). Emission values of CO, CO_2, NO, NO_2 and HC in g/s and g/km were calculated from the measured mixing ratios using the respective total exhaust gas mass flows, taking into account the individual time shifts between engine exhaust output and analyzing time for the different gas analyzers. Data of the vehicle velocities were provided by RWTÜV, together with measurements of the emissions with three independent devices. The four measurements (one by FZ Jülich, three by RWTÜV) generally agreed better than 10% (Klemp 2002). A detailed comparison will be published elsewhere. In this work, only the measurements of FZ Jülich are used.

2 - Results

Demand of the different driving cycles

A comparison of the three vehicles with conventional gasoline engines (No. 1-3 in Table 1), all compliant with the D4-exhaust regulation level, shows the bandwidth of emissions that exist in the broad range of velocities and engine loads which are present in the four different driving cycles. Table 2 shows the emissions of the regulated compounds of these cars in the respective driving cycle, together with the D4-exhaust limit. Except for a small excess in NO_x-emissions of the Ford Mondeo, all cars were compliant with the D4-limit in the MVEG-cycle. In the other driving cycles, considerable differences can be found:

- Only the Golf IV exceeded the D4-limits in neither driving cycle. Both the MOBINET-cycle with quite demanding urban driving and the Autobahn-cycle with its high velocities yield

emissions comparable to the MVEG. Relatively large differences can be found only between MVEG and FTP-75. This might be due to the fact that the FTP-75 includes a whole cold start, whereas in the MVEG the first 40 seconds after the cold start are omitted. MOBINET and Autobahn do not include cold starts.

- In the Autobahn-cycle with velocities up to 160 km/h, both the Ford Mondeo and the Ford KA exceed the D4-limit for NO_x substantially. The emissions relative to distance exceed the ones from the MVEG by a factor of 2-3.

	Limit D4	MVEG	FTP-75	MOBINET	Autobahn
Ford Mondeo					
CO [g/km]	0.70	0.43	0.89	3.37	2.89
NO_x [g/km]	0.07	0.09	0.19	0.09	0.18
HC [g/km]	0.08	0.08	0.08	0.05	0.08
VW Golf IV					
CO [g/km]	0.70	0.20	0.74	0.50	0.47
NO_x [g/km]	0.07	0.04	0.06	0.06	0.04
HC [g/km]	0.08	0.02	0.04	0.01	0.01
Ford KA					
CO [g/km]	0.70	0.59	0.82	3.10	13.07
NO_x [g/km]	0.07	0.07	0.06	0.08	0.13
HC [g/km]	0.08	0.05	0.09	0.08	0.09

Table 2: Emissions of the cars with conventional gasoline engine in the different driving cycles (g/km).

Tableau 2 : Emissions des véhicules avec moteur Otto conventionnel dans les différents cycles de conduite (g/km).

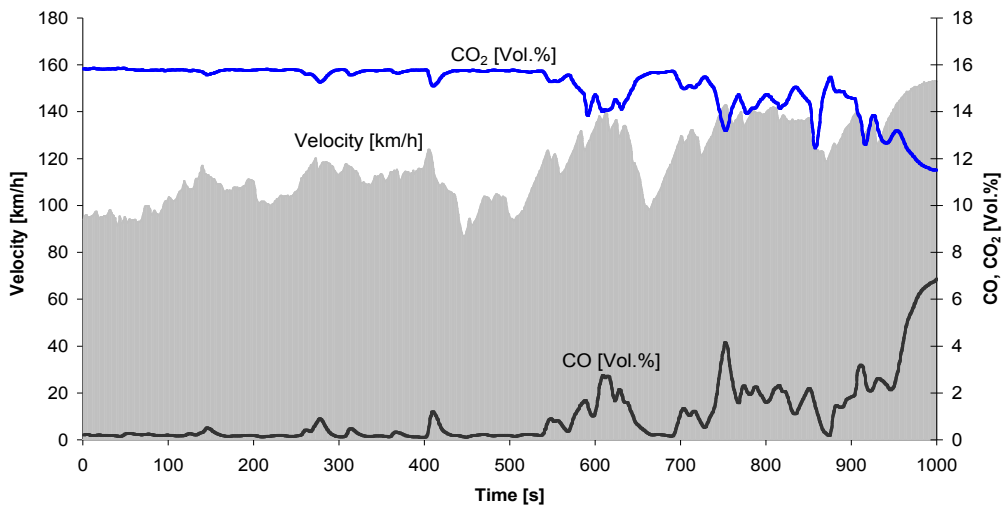

Figure 3: Emissions of carbon monoxide (CO) and carbon dioxide (CO_2) by the Ford KA in the Autobahn-cycle.

Figure 3: Emissions de monoxyde de carbone (CO) et de dioxyde de carbone (CO_2) de la Ford KA dans le cycle Autobahn.

- The most significant exceedances of the D4-limits happened for CO with the Ford Mondeo and Ford KA in the two demanding cycles MOBINET and Autobahn. The Ford Mondeo exceeded the D4-limits by a Factor of 5 in the MOBINET-cycle and by a factor of 4 in the Autobahn-cycle. For the Ford KA, who had the lowest-powered engine in the measuring program, CO-emissions

in MOBINET-cycle and Autobahn-cycle grew dramatically by a factor of 5 and 20, as compared to MVEG. In the last part of the Autobahn-cycle, CO-emissions reached 7 Vol. % (see Figure 3) probably due to full power enrichment. Such emission levels are expected to be reached by non-catalyst-cars.

Comparison of different model years / aged cars

The measuring program included one older car, a 6-years-old VW Golf III TDI with a mileage of almost 150.000 km. This car was compared to a VW Golf IV TDI from 2002 with little more than a tenth of the mileage. Both cars have engines with the same concept and the same capacity, but the Golf IV has more power (86 kW instead of 66 kW) and fulfills EURO3 instead of only EURO2.

	Limit	MVEG	FTP-75	MOBINET	Autobahn
VW Golf III TDI EURO2					
CO [g/km]	1.00	0.62	N/A	0.30	0.17
NO_x [g/km]	-	0.37	N/A	0.58	0.86
HC [g/km]	-	0.13	N/A	0.04	0.06
NO_x + HC [g/km]	0.90	0.50	N/A	0.62	0.92
VW Golf IV TDI EURO3					
CO [g/km]	0.64	0.13	0.10	0.11	0.09
NO_x [g/km]	0.50	0.39	0.39	0.46	0.69
HC [g/km]	-	0.01	0.01	0.00	0.00
NO_x + HC [g/km]	0.56	0.40	0.40	0.46	0.69

Table 3: Emissions of the diesel-engine driven cars Golf III TDI and Golf IV TDI in the different driving cycles. Due to a handling error, no valid results were obtained for the Golf III TDI in the FTP-75 cycle.

Tableau 3 : Emissions des voitures Diesel Golf III TDI et Golf IV TDI dans les différents cycles de conduite. A cause d'une erreur de manipulation, aucun résultat valable n'a pu être obtenu pour la Golf III TDI.

Both cars fulfilled the requirements of their respective emission limits in the MVEG (Table 3). The trends in the emissions in the perspective of technical progress seem to be interesting:

- CO emissions have been reduced considerably by 50-80%, depending on the driving cycle. The smallest reduction refer to the Autobahn-cycle which has the highest velocities.
- HC-emissions have been reduced by one order of magnitude to a very low level. The Golf IV TDI emits HCs almost exclusively during the cold start, which is part of MVEG and FTP-75. When the engine is warm (MOBINET and Autobahn), less than 10 mg HC are emitted per kilometer.
- NOx emissions practically remain on the same level. While there is even a slight increase in emissions during the MVEG (though not directly comparable due to the 40s-idle-period in the test for the Golf III, see Figure 1), emissions in the other cycles have been reduced by only 20%.

These findings lead to the conclusion that from the perspective of air chemistry and air quality a shift in the relevance of the exhaust compounds can be expected: While CO- and HC-levels will decrease in the future, NO_x-emissions will rather increase. This will take place especially because of the rising share of diesel cars in the fleet of passenger cars. Diesel cars emit approximately five times more NO_x than gasoline cars. The findings from these two cars have to be assured statistically.

Importance of speciated nitrogen oxide analysis

The nitrogen oxides NO (nitric oxide) and NO_2 (nitrogen dioxide) are usually recorded as sum value NO_x. Both species can be transformed into each other through the reaction with ozone:

$$NO + O_3 \Leftrightarrow NO_2 + O_2$$

For many conditions the Leighton relationship holds (Leighton 1961), according to which these species are in balance [J(NO_2) is the photolysis rate of NO_2]:

$$\frac{[O_3][NO]}{[NO_2]} = const. \cdot J(NO_2)$$

This means that in dependence of the kind of nitrogen oxide emitted, ozone is either produced (from NO_2-emissions) or destroyed (from NO-emissions). While conventional gasoline engines almost exclusively emit NO (> 99%), the share of NO_2 from NO_x in DI-SI engines and in CI-engines is between 10% and 60%, see Figure 4 and Figure 5. Increasing shares of NO_2 lead to several effects:

- Less ozone coming from rural background air into the cities will be destroyed due to a smaller amount of NO. This is equivalent to rising ozone levels in the cities, which is consistent with the observation of increasing ozone levels in the last years, according to Umweltbundesamt (2002).

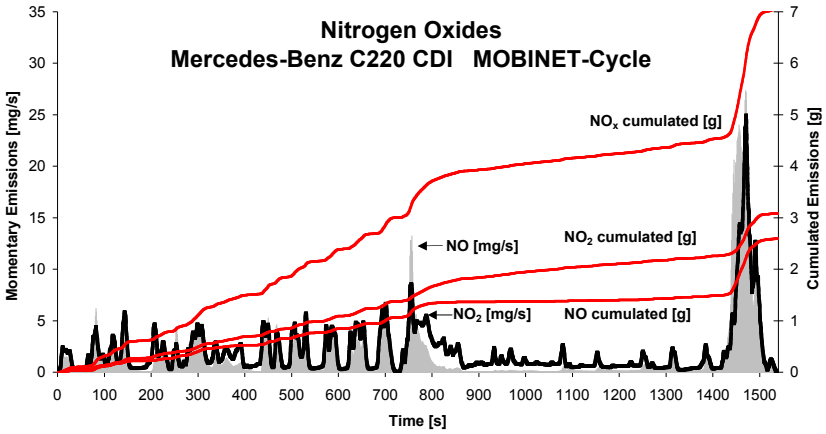

Figure 4: Emissions of nitrogen oxides by Mercedes-Benz C220 CDI in the MOBINET-cycle
Figure 4: Emissions d'oxydes d'azote de la Mercedes-Benz C220 CDI dans le cycle MOBINET

- Nitrous acid, HONO, is mainly formed heterogeneously on surfaces in the presence of water and NO_2 and is also directly emitted from diesel engines, as found by Kurtenbach (2001). HONO is a source of the most important daytime radical, the hydroxyl radical OH, which acts as initiator of multiple photochemical cycles.

$$2\ NO_2 + H_2O \rightarrow HNO_3 + HONO$$
$$HONO + h\nu \rightarrow OH + NO$$

- Increasing ozone levels and increasing HONO levels both result in higher OH concentrations and therefore in an acceleration of many photochemical reactions.

Worth mentioning is furthermore the emission of NO by the Polo FSI *after* the driving cycle (Figure 5). This car is equipped with a NO_X-storage catalyst, described by Glück (2000), which bases on the reversible reaction of NO with barium oxide:

$$BaO + 2\ NO + 1.5\ O_2 \Leftrightarrow Ba(NO_3)_2$$

It seems that after the cycle the back reaction took place, leading to the emission of NO. Other pollutants have not been emitted during that time.

Conclusion

In the last years, emissions of new cars have been reduced substantially. Nevertheless, a close look at the different pollutants is still necessary. While modern catalyst effectively convert hydrocarbons, NO_x and especially nitrogen dioxide stay a problem, aggregative due to the rising share of diesel engines and gasoline engines with direct fuel injection. They result in higher ozone levels and faster photochemistry. Furthermore, some cars emit high amounts of carbon monoxide during high engine loads and velocities. Therefore, not only the certification cycle MVEG but also more demanding

driving cycles which rather realistic driving patterns must be taken into account.

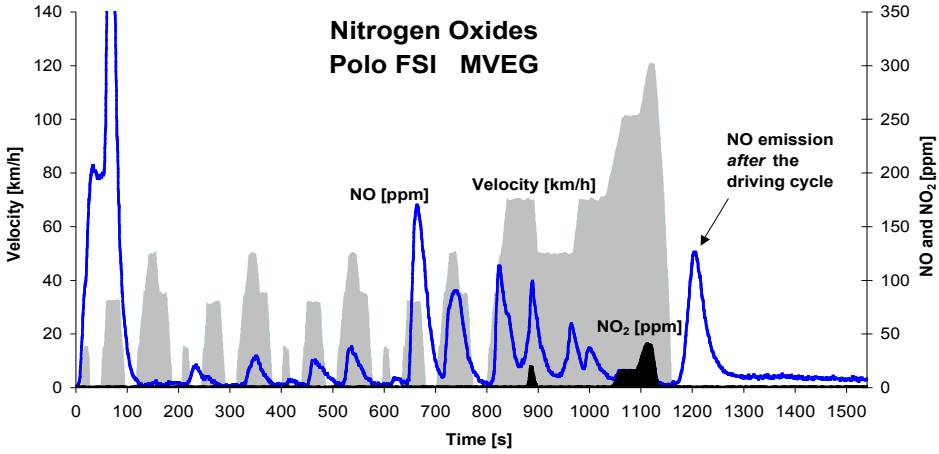

Figure 5: Emissions of nitrogen oxides by the Polo FSI in the MVEG

Figure 5: Emissions d'oxydes d'azote de la Polo FSI dans le MVEG

Acknowledgments

The authors wish to thank Volkswagen AG for providing the Polo FSI. This work was supported by BMBF in the project "MOBINET".

References

Glück K.H., Göbel U., Hahn H., Höhne J., Krebs R., Kreuzer T. & Pott E. (2000): Die Abgasreinigung der FSI-Motoren von Volkswagen. MTZ, vol. 61, n° 6, p 402-412

Harrison R.M. & Shi J.P (1996): Sources of nitrogen dioxide in winter smog episodes. Sci. Tot. Environ. vol. 189-190, p 391-399

Hassel D., Jost P., Weber F.J., Dursbeck K., Sonnborn S. & Plettau D. (1994) Abgas-Emissionsfaktoren von Pkw in der Bundesrepublik Deutschland. Umweltbundesamt (Ed) Erich Schmidt Verlag Berlin, p 6.2-6.5

Klemp D., Mittermaier B., Buers H.J. & Schmitz Th. (2002): Determination of temporaly highly resolved passenger car emissions of important exhaust components by means of on-board measurements under real traffic conditions. Proc. Int. Symp. "Transport and air pollution", Graz, Austria, vol 2, p 41-48.

Kurtenbach, R. Becker K.H., Gomes J.A.G., Kleffmann J., Lörzer J.C., Spittler M., Wiesen P., Ackermann R., Geyer A. & Platt U. (2001): Investigations of emissions and heterogeneous formation of HONO in a road traffic tunnel, Atmos. Environ. vol. 35, n° 20, p 3385-3394

Leighton, P.A. (1961) Photochemistry of air pollution, Academic Press, New York and London, p 152-157

Lenaers, G. (1996): On board real life emission measurements on a 3 way catalyst gasoline car in motor way-, rural- and city traffic and on two Euro-1 diesel city buses. Sci. Tot. Environ., 189/190, p. 39-147

Mittermaier B., Schmitz Th., Hassel D., Weber F.J. & Klemp D. (2003): VOC-Split of Gasoline and Diesel Passenger Cars. In : Friedrich R. & Reis S. : Emissions of air pollutants – measurements, calculation, uncertainties : Results from the EUROTRAC subproject GENEMIS, Springer Berlin, in publication

Platt U., Perner D., Harris G.W., Winer A.M. & Pitts J.N. (1980): Observations of nitrous acid in an urban atmosphere by differential optical absorption, Nature, vol. 285, p 312-314

Umweltbundesamt (2002): Umweltdaten Deutschland 2002. www.umweltbundesamt.de/udd/udd2002.pdf, p 36

12th International Symposium "Transport and Air Pollution" / 12e Colloque international "Transports et pollution de l'air", Avignon, 16 -18 *June* / juin 2003
proceedings / actes, n°92, tome / Vol. 2, Inrets ed., Arcueil, France, 2003, p. 191-196

Comparison of particle size distribution and emissions from heavy-duty diesel engines and gas engines for urban buses

Joep van Ling, Rinie van Helden, Iddo Riemersma
TNO Automotive, Powertrains, P.O.B 6033, 2600 JA Delft, The Netherlands
fax: +31 15 269 68 74; email: vanling@wt.tno.nl

Abstract
Ordered by Novem, the Netherlands Agency for Energy and the Environment, emission tests were carried out with several bus engines on a transient engine dynamometer according to the European transient test (ETC) and the Dutch urban bus transient cycle (DBTC). Additional tests were carried out in order to determine particle size distributions of the engines in the steady-state 13-mode test (ESC).
The stoichiometric gas engines met the emission targets for EEVs and the expected Euro 5 standards for 2008. The diesel engine with diesel particulate filter (DPF) had very low particulate emissions which were comparable with those of the gas engines, however, the NO_2 emission was increased with a factor 5 compared with the conventional diesel engine.
Particle size distribution measurements showed very low particle numbers with all gas engines and with the diesel engine with DPF.
The test results can be used by public transport companies during the decision process of purchasing Enhanced Environmentally friendly Vehicles (EEVs).
Key-words: Urban busses, EEV, Euro 3 ETC, particle distribution, LPG, CNG, diesel.

Introduction

Since the introduction of the European Euro 3 emission standards in October 2000 for new types of heavy-duty vehicles and engines, conventional diesel engines including those fitted with electronic fuel injection equipment, exhaust gas recirculation (EGR), and/or oxidation catalyst are tested according to the European Steady-state 13-mode Cycle (ESC). Diesel engines fitted with advanced exhaust aftertreatment systems including the NO_x catalysts and/or diesel particulate filters (DPF), shall additionally be tested on the new European Transient Cycle (ETC). For gas engines the emissions shall be determined only on the ETC test.

Ordered by Novem, the Dutch Agency for Energy and the Environment, a test programme was carried out by which the following aspects with regard to emissions of bus engines could be evaluated.

- The emission behaviour of gas engines, both lean burn and stoichiometric (λ= 1), during the transient ETC test and comparison of the emissions with real-world emissions during Dutch city driving (Dutch Bus Transient Cycle, DBTC test (van de Weijer, 1997).
- Comparison of the emissions of gas engines with Euro 3 diesel emissions determined in the ETC test and in the DBTC test.
- Comparison of the particulate matter (PM) emissions of a diesel engine equipped with diesel particulate filter with the PM emissions of gas engines with oxidation catalyst or three-way catalyst.
- Effect of the diesel particulate filter on the NO_2 emission.

- Additional tests were carried out with the same engines and an extra natural gas engine in order to determine particle size distribution during the steady-state ESC test.

The following engine types have been selected for the test programme. The power range was within 160 to 240 kW.

- LPG gas engine; stoichiometric with three-way catalyst.
- Natural gas engine; lean burn with oxidation catalyst.
- Natural gas engine; stoichiometric with three-way catalyst.
- Diesel engine; Euro 3 without aftertreatment system
- Diesel engine; Euro 3 with a continuously regenerating diesel particulate filter.

The particle size distribution in the diluted exhaust gas was determined with a Scanning Mobility Particle Sizer (SMPS) including an Electrostatic Classifier and a Condensation Particle Counter (CPC).

The fuels used were commercial LPG with a minimum motor octane number (MON) of 92.5, Dutch L (low calorific) compressed natural gas (CNG), commercial diesel fuel (290 mg/kg sulfur) and ultra-low sulfur diesel fuel (13 mg/kg).

2. Results of the gaseous emissions and particulate mass emission tests

All engines were tested according to the European Transient Cycle (ETC) and the Dutch Bus Transient Cycle (DBTC). The results are given in Table 1 together with the ETC and EEV emission limits.

The EU Member States may make provision for tax incentives applied to all new vehicles which comply with the EEV limits. The purpose is to stimulate the introduction of Enhanced Environmentally friendly Vehicles (EEVs).

The two λ=1 engines (LPG and CNG) have been optimised by the manufacturers to reach the EEV limits. The lean burn CNG engine was optimised to reach the Euro 3 ETC standard of 2000. The prototype diesel engine, optimised for the European Steady-state Cycle (ESC, Euro 3), run the ETC test without modification with and without diesel particulate filter (DPF).

The kind of hydrocarbon emissions determined in the ETC test differ from the HC emissions in the ESC test. Instead of total hydrocarbons (THC) nonmethane HC (NMHC) is measured in the ETC test because methane does not contribute to the reactivity of HCs with regard to summer smog (ozone) formation. Methane is considered as a greenhouse gas, which is the reason that a limit is introduced, in spite of the fact that methane is not a pollutant. Adding the global warming potential of methane to the CO_2 emission would be more realistic.

NMHC and CH_4 emissions

The engines with aftertreatment system (LPG, CNG and Diesel with DPF) have all low or extremely low NMHC emissions in both test cycles. The LPG and diesel engines do not emit much CH_4 engine-out; that is why the methane limit does not apply for these engines. Due to the fact that methane is a stable molecule, the three-way catalyst or oxidation catalyst of a CNG engine has to be optimised with regard to methane conversion efficiency. The three-way catalysts and the oxidation catalyst have very good methane conversion efficiencies.

CO emissions

The CO emissions of all engines are below the EEV limit. Today carbon monoxide is not a point of concern any more.

NO_x and NO_2 emissions

The NO_x emissions show clearly the difference in emission performance of λ=1 gas engines with three-way catalyst and engines running with air excess (CNG lean burn and the Diesel engine). With the λ=1 gas engines it is possible to meet the EEV limit of 2.0 g/kWh NO_x. The emission of the lean

burn gas engine and the diesel engine (with and without DPF) are between 4 g/kWh and 6.5 g/kWh. All NO_x emissions are somewhat higher in the DBTC test.

Engine type	Test cycle	NMHC	CH_4	CO	NO_x	NO_2	PM
		g/kWh	g/kWh	g/kWh	g/kWh	g/kWh	g/kWh
LPG λ= 1	ETC	0.0	0.0	1.8	0.1	0.0	0.009
	DBTC	0.0	0.0	0.1	0.6	0.0	0.007
CNG λ= 1	ETC	0.0	0.2	0.4	1.6	0.4	0.014
	DBTC	0.0	0.1	0.1	2.0	0.0	0.015
CNG lean burn	ETC	0.0	0.2	0.0	3.9	0.6	0.012
	DBTC	0.1	0.6	0.0	4.9	0.5	0.012
Diesel	ETC	0.3	0.0	2.5	5.6	0.5	0.109
	DBTC	0.3	0.0	2.2	6.4	0.4	0.114
Diesel + DPF	ETC	0.0	0.0	0.0	5.6	2.6	0.005
	DBTC	0.0	0.0	0.0	6.5	2.9	0.007
Limits			NG only				diesel
Euro 3 2000	ETC	0.78	1.60	5.45	5.0	-	0.160
Euro 4 2005	ETC	0.55	1.10	4.00	3.5	-	0.030
Euro 5 2008	ETC	0.55	1.10	4.00	2.0	-	0.030
EEV 2000	ETC	0.40	0.65	3.00	2.0	-	0.020*)

*Table 1: Comparison of NonMethaneHC, CH_4 , CO, NO_x NO_2 and PM emissions in the European Transient Cycle (ETC) and the Dutch Bus Transient Cycle (DBTC). *) also for gas engines*

The emissions of NO_2 of the gas engines and the diesel engine without DPF are relatively low. The diesel engine with Pt loaded DPF has a 5 times higher NO_2 emission than the conventional diesel engine. In order to remove carbon particles in the filter NO is oxidised to NO_2 by a high loading of platinum on an oxidation catalyst upstream of the filter. NO_2 reacts with the carbon particles to form CO_2 , N_2 and oxygen. Normally more NO_2 is formed than necessary to convert the carbon and NO_2 is leaving the exhaust unmodified. NO_2 is a direct toxic compound which causes breathing problems and lung damage. The EU standards have no limit for NO_2, despite the fact that the maximum exposure limit of NO_2 is 5 to 25 times lower than that of NO (nitric oxide).

Particulate matter (PM) emissions

It appears that the ETC particulate emission results of all engines are representative for the situation during urban driving according to the DBTC test.

The particulate emissions of the gas engines are very low (EEV level). The PM emission with the diesel particulate filter is even lower than measured with the gas engines, however, the PM level of all these engines is around the detection limit.

Only the diesel engine without DPF gives much higher PM emissions.

3. Particle size distribution measurements

During the nineties of the last century concern was growing on the health hazards of very small, so-called, nanometer size particles (size 10 nm to 1000 nm). It was already known that the mass of particles in the ambient air smaller than 10 µm must be monitored (PM_{10}) because there is a clear association with adverse health effects. Many medical experts consider that nanometer size particles, that may be insignificant to the total mass of particulates, may be more significant in terms of health effects.

Nanometer size particles are divided into very fine particles (< 1000 nm), ultrafine particles (< 100 nm) and nano-particles (< 50 nm).

The smallest particles in the nanometer size range < 40 to 50 nm are often referred to as the nucleation mode particles and are mainly condensed volatile materials. The larger particles > 50 nm

consist mainly of carbonaceous material and are often referred to as accumulation mode particles.

The existing method to determine particles is based on a gravimetric method by which total particulate matter is measured on a mass basis. With new technologies, such as the diesel particulate filter, alternative fuels and advanced combustion systems, the effective measurement limit of this system will be approached.

The above mentioned aspects, health effects of nanometer size particles and accuracy of the existing method, are the reason why the Working Group on Pollution and Energy (GRPE) of the UNECE started the sub-group Particle Measurement Programme (PMP) (ref. UNECE Website). The aim is to monitor emerging evidence on the health effects of particles and, related to that evidence, to develop new systems for the measurement of particles emitted from the exhaust of motor vehicles/engines. The programme started in March 2001 and will end in 2003. The output will be a draft text for use as a proposal that may replace or supplement the current systems set out in UNECE emission Regulation 83 (light-duty vehicles) and Regulation 49 (heavy-duty vehicles/engines).

Results of particle size distribution tests at steady-state conditions

All measurements, using an SMPS particle sizer in the range from 12 nm to 600 nm , were carried out during selected points of the steady-state 13 mode test. The results were weighted in order to reach a representative particle size distribution of each engine type.

Figure 1 shows the normalised particle size distribution of the Euro 3 diesel engine without diesel particulate filter (DPF) with 290 mg/kg sulfur in the fuel and the engine with DPF with 13 mg/kg sulfur fuel. For comparison the data of the same Euro 3 engine without DPF tested with 13 mg/kg sulfur are also plotted in the graph.

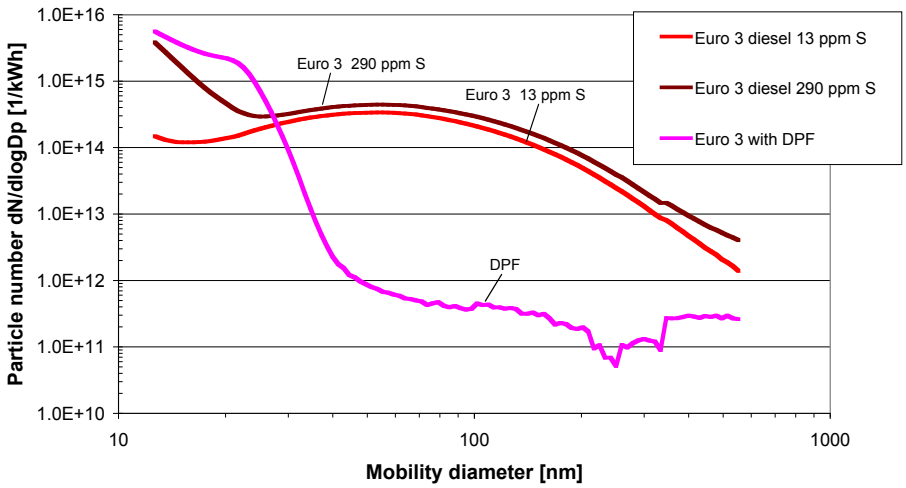

Figure 1: Particle size distribution. Diesel engine with and without particulate filter.

It appears that the sulfur content has an influence on the number of nano-particles smaller than 25 nm in the nucleation mode. These particles are formed by homogeneous condensation of sulfate and hydrocarbons when they cool down in the dilution tunnel. Further investigation is necessary to find out if this is a typical laboratory problem caused by the dilution factors between 10 to 20, which are relatively low compared with ambient dilution factors (>1000). Recent information, however, shows that nucleation mode particles also may occur in real world (Kittelson, 2000 and Keuken, 1997), especially when ambient temperature goes down. The measurement with the DPF shows very low particle numbers in the accumulation mode (>50 nm). In the nucleation mode there is a sharp increase below 40 nm, even exceeding the engine out numbers. This can be explained by the fact that more sulfate is formed in the oxidation catalyst of the DPF, even with the ultra-low sulfur fuel. With the absence of accumulation mode particles, mainly comprising of adsorptive carbonaceous material (Andersson and Wedekind, 2001), this volatile material is not adsorbed allowing nucleation mode particles to be formed.

It can be concluded that only fuel with zero sulfur and with light hydrocarbon fractions yields low numbers of these very small nano-particles.

Figure 2 shows the normalised particle size distributions measured with four gas fuelled engines.

Three stoichiometric gas engines were measured (one LPG and two CNG engines) and one lean burn CNG engine. The lean burn and λ= 1 CNG engines (of the same make) show very low particle numbers over the complete nanometer size range, which means that the nucleation mode particle numbers are extremely low. The λ= 1 LPG engine has also low nucleation mode numbers; the accumulation mode has higher numbers than the two mentioned CNG engines but still two magnitudes lower than the diesel engine without DPF.

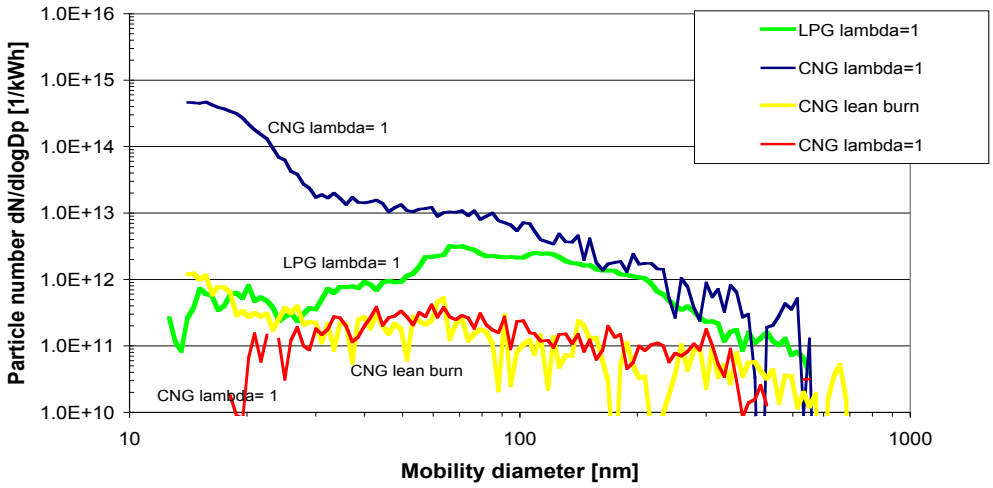

Figure 2: Particle size distribution. Gas engines, 13-mode test

The second λ= 1 CNG engine shows accumulation mode particles comparable with the LPG engine, however, nano-particles are increasing below 30 nm. This effect is the contribution of only one measuring point (25 % load at 1300/min) and cannot be explained. The other measuring points did not show any increase below 30 nm.

The difference between particle numbers of the gas engines may be explained by different oil consumption behaviour in combination with a different catalyst behaviour regarding the oxidation of oil particles.

ESC 13-mode Particle number [Pno/kWh]	Diesel Euro 3 290 mg/kg S $*10^{14}$	Diesel Euro 3 13 mg/kg S $*10^{14}$	Diesel + DPF Euro 3 13 mg/kg S $*10^{14}$	LPG λ= 1 $*10^{14}$	CNG1 λ= 1 $*10^{14}$	CNG Lean Burn $*10^{14}$	CNG2 λ= 1 $*10^{14}$
< 50 nm	4.8	1.3	9	0.003	0.800	0.002	0.001
> 50 nm	1.8	1.3	0.003	0.013	0.040	0.001	0.001
Total	6.6	2.6	9	0.016	0.840	0.003	0.002
Particulate mass ETC [g/kWh]	0.109	0.100	0.005	0.009	0.014	0.012	0.012

Table 2: Particle numbers with diesel and gas engines < 50 nm, > 50 nm and total between 12 and 600 nm.

After measurement of the background particle numbers in the dilution air, the following can be concluded. It appears that the particle numbers determined in the diluted exhaust gas of two of the CNG engines and the diesel engine with DPF are of the same order of magnitude as the number of particles measured in the dilution air especially in the accumulation mode range.

Total particle numbers

In Table 2 the total particle numbers per kWh in the ranges lower and higher than 50 nm are given for all measured engines. The order of magnitude is the same as the normalised numbers in the Figures 1 and 2 so that the table can be considered as a summary of the size distribution in actual numbers. The conclusions do not differ much from those discussed before.

Conclusion

The following conclusions can be drawn from the results of the test programme.

- The stoichiometric gas engines (λ= 1 with three-way catalyst) on LPG and natural gas have very low gaseous emissions both at steady-state and during transient conditions in the ETC (European Transient Cycle) and the Dutch urban Bus Transient Cycle (DBTC).
  Both gas engines meet the emission targets for EEVs (Enhanced Environmentally friendly Vehicles) and expected Euro 5 standards for 2008.
- The lean burn natural gas engine has a higher NO_x emission than the stoichiometric engines. However, all other emissions, especially particulate matter (PM), are very low.
- The diesel engine without diesel particulate filter (DPF) has much higher NO_x and PM emissions than the stoichiometric gas engines.
- The diesel engine with platinum loaded DPF aftertreatment system has very low PM emissions comparable with those of all gas engines, however, the NO_2 emission as part of the NO_x (NO + NO_2) emission increases from 10 % (with conventional diesel engines) to 50 %.
  With the introduction of the diesel particulate filter with catalytic supported regeneration the proportion NO_2 /NO_x has changed depending on the combination of diesel engine and DPF. In the US, platinum-based DPFs are banned from use in coal mines (DieselNet Website, 2002).
- For all engines the NO_x emissions in the DBTC test are 10 to 20 % higher than measured in the ETC test.
- Particle size distribution measurements show very low numbers with all gas engines and with the diesel engine with DPF. They are several orders of magnitude lower than the numbers determined with the conventional diesel engine without filter of which the total particle number is between 10^{14} and 10^{15} particles per kWh.
- Some of the gas engines show particle numbers which are equal to the numbers determined in the dilution air of the constant volume sampling system with disconnected exhaust.
- Despite the ultra-low sulfur content (13 mg/kg) of the diesel fuel used for the engine with DPF, the nano-particle numbers (< 50 nm) are very high due to sulfate formation in the DPF.

Acknowledgements

The authors like to thank the truck manufacturers MAN, IVECO and DAF for making available several engines for the tests.

References

Andersson Jon and Wedekind Barbara (May 2001): DETR/SMMT/CONCAWE, Particulate Research Programme 1998-2001. Ricardo Consulting Engineers, DP01/0515.

DieselNet UPDATE (July 2002): Pt-based particulate filters banned from coal mines. www.dieselnet.com.

Keuken M.P (1997): Emission from light-duty and heavy-duty traffic in the Drecht tunnel (in Dutch), TNO-MEP – Report no. 97/378.

Kittelson (2000): Oral speech. Nano-particle measurement. Zürich.

UNECE: PMP sub-group. ww.unece.org/trans/main/wp29/wp29wgs/wp29grpe/grpeage.html.

van de Weijer C.J.T. (1997): Heavy-Duty Emission Factors. Development of representative driving cycles and prediction of emissions in real-life. Dissertation. TU Graz, Austria.

12th International Symposium "Transport and Air Pollution" / 12e Colloque international "Transports et pollution de l'air", Avignon, 16 -18 *June* / juin 2003
proceedings / actes, n°92, tome / Vol. 2, Inrets ed., Arcueil, France, 2003, p. 197-202

Influence of the driving cycle on average emissions: development of the regression model for a case study

Mario Rapone, Livia Della Ragione, Maria Vittoria Prati & Giovanni Meccariello
Istituto Motori CNR, via Marconi 8 80125 Naples Italy - Fax +39 081 2396097
email : m.rapone@im.cnr.it; l.della ragione@im.cnr.it; m.v.prati@im.cnr.it; g.meccariello@im.cnr.it

Abstract
The case study relative to emission measurements performed by IM within the task 3141 Driving Cycles of ARTEMIS project is analysed in this paper. Measurements have been performed using 34 driving cycles representative of different driving and traffic characteristics. A statistical approach based on Partial Least Square regression method has been utilized. By this way the most important quantities (defined to assess the different characteristics of each driving cycles) to explain data variation have been determined. Moreover, the relationship among emissions and driving cycles characteristics has been quantitatively determined by building the regression model. The analysis of results show a good coherence of the model with phenomena explaining emission production by the engine
Keys-words*: average emission factors, kinematic parameters, regression model .*

Introduction

The objective of the study in progress is the development of a statistical modelling approach capable to evaluate real use average emissions as a function of variables characterizing the dynamic behaviour of a vehicle in the traffic. The basic observation here considered is a driving cycle, defined as the time series of vehicle velocity where homogenous kinematic characteristics can be detected.

Within the task 3141 of ARTEMIS project, a 1.2 l catalyst car (LANCIA Y) has been tested performing driving conditions precisely defined in (Andrè 2002). Following the experimental program the driving cycles have been divided into parts (or sub-cycles), emissions have been collected in one bag for each part. In the following the driving pattern relative to each bag is mentioned, to simplify, as a driving cycle (DC), by this way 34 driving cycles have been determined. These driving cycles represent a wide and complete scenario of operating conditions detectable in different traffic and road situations.

In the paper emission data are analysed to outline the mechanisms by which driving cycles determine exhaust emissions. The effects of basic kinematic parameters on emissions are investigated to envisage a potential structure of a model capable to assess emission factors. Results are based on a single vehicle tests, thus their validity cannot be extended to other vehicle types before testing themselves: digital logic of current engine electronic control does not allow one to extrapolate results to different vehicles or, for the same vehicle, to operating conditions different from tested ones (Barth 2002). Results have to be considered as preliminary, aiming at describing the capability of a model structure to be tested in the application to a wider emission data base relative to different vehicles.

The Partial Least Square method has been used to make the statistical analysis and build the regression model (Tenenhaus 1998). This method builds the regression model among two sets of variables, the response variables **Y** (emissions) and explicative variables **X** (quantities used to

characterize each DC), by the decomposition of **X** variables into principal components **t** and regression of **Y** over **t**. By the development of the model it is possible to estimate the relationship among response and groups of explicative variables, each group characterizing DC's under a specific aspect, quantitatively summarized by a principal component t_h. In particular CO2 resulted negatively related to parameters higher for fast and fluent DC (percentage of driving time, max speed) and positively related to speed and gear attributes (V20 and cambio1) representative of slow and congested DC, strictly coherent with basic phenomenon of CO2 production by the engine, which presents a bathtub trend of CO2 with the lowest values in the zone of engine highest efficiency. HC and CO variations are firstly explained by transient phenomena considered in the model structure by time spent in different classes of positive and negative acceleration. The transient conditions are critical for engine injection system open loop control, especially in presence of strong accelerations at high load.

1 - Model Building

Experimental data relative to DC average emissions measured in the testing of a LANCIA Y EURO 3 (towards EURO 4) have been considered to build the emission model. A detailed analysis of DC characteristics is reported in (Andrè 2002). The list of variables used to quantify the different aspects characterizing each DC is reported in table 1.

Variable	Description	**Variable**	Description
v_mean	average speed	**cambio4**	%time gear = 4
v_max_t_c	ratio vmax/driving time	**cambio5**	%time gear = 5
V20	%time speed <20	**paccel1**	class of acceleration (m/s^2) [-∞;-1.4]
V30	%time 20<speed<30	**paccel2**	class of acceleration (m/s^2) [-1.4;-0.6]
V40	%time 30<speed<40	**paccel3**	class of acceleration (m/s^2) [-0.6;-0.2]
V100	%time speed>40	**paccel4**	class of acceleration (m/s^2) [-0.2;0.2]
tseq	time duration	**paccel5**	class of acceleration (m/s^2) [0.2;0.6]
dist	distance covered	**paccel6**	class of acceleration (m/s^2) [0.6;1.4]
pdr_time	%driving time	**paccel7**	class of acceleration (m/s^2) [1.4;+∞]
seq	number of sequences	**nerv**	number of peaks
acc1t	time with acc>0.15 m/s^2	**Tral**	idling time
cambio0	%time gear = 0	**v_a**	sum of (acceleration per v) when acc>0
cambio1	%time gear = 1	**vmax**	max speed
cambio2	%time gear = 2	**tdr_sum**	total driving time
cambio3	%time gear = 3		

Table 1: Variables characterizing driving cycles.

As a first step all variables listed in table 1 have been considered in the development of the regression model by PLS method to better differentiate the variants of DC kinematic patterns.

The existence of outliers in the set of experimental data has been analysed by means of the normal probability plot of residuals in the model. Data relative to ArtLoMWY 3 driving cycles exceeds 4 standard deviation interval assumed as threshold and thus it has been considered as an outlier. It has been excluded from data set and a second regression model was then fitted to data (model 2).

In order to better outline DC kinematic parameters statistically significant in the model, variables more relevant to explain emission variation for the specific dataset have been determined using the statistical index VIP (Variable Importance in the Projection), function of explained variance in the prediction. 12 variables have been retained, having a VIP larger than 1, which is the critical threshold widely used in the literature to select more important variables. Thus a third model (model 3) was built based on these 12 variables.

An analysis of kinematic characteristics of 33 driving cycles tested can be made in figure 1, where points relative to DC's are plotted in the space of the two principal components t(1) and t(3) of X variables. The structure of t(1) and t(3) as a function of X variables as well as their correlation with Y variables can be recognized in the figure 2, where coefficients (Y-loadings c and X-weights w)

relating emission data (response variables) and DC variables (explicative variables) with principal components **t**'s (as it follows from PLS regression equations **t**=**wX** ; **Y=ct**) are reported.

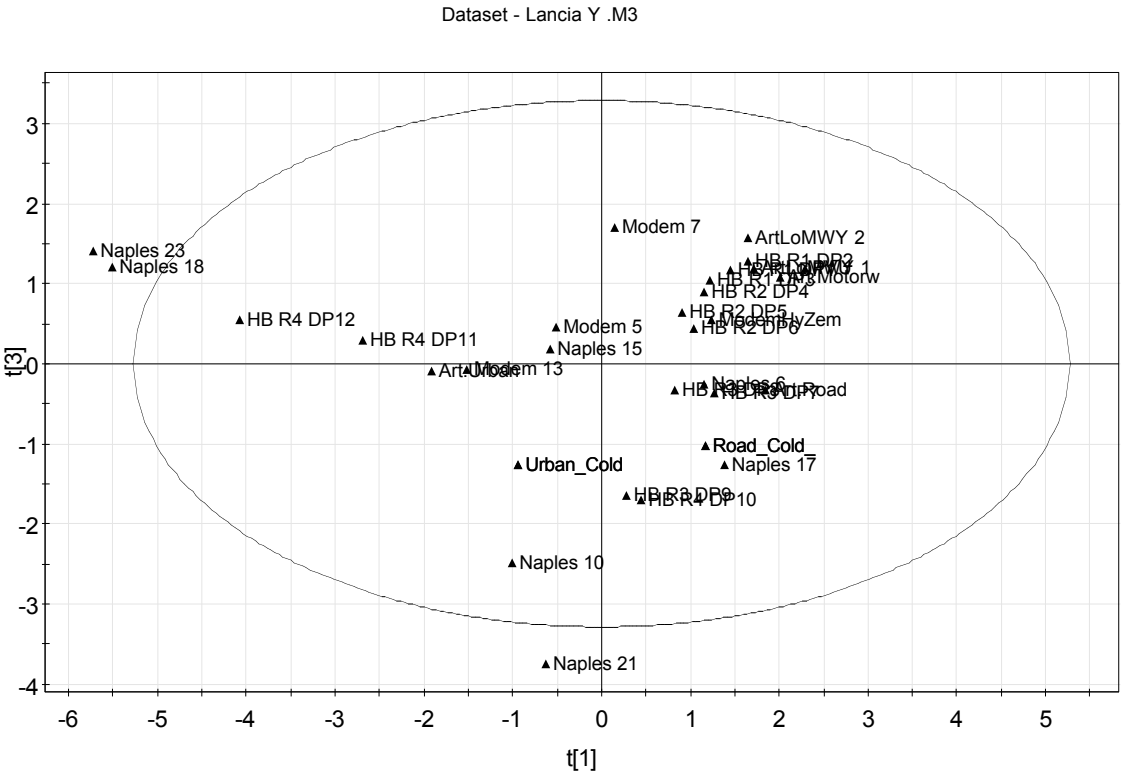

Figure 1: Driving cycles in the space of principal components T1 and T3.

The first axis t(1) explains variation of driving cycles respect to speed attributes separating faster driving cycles representing fluent conditions from slower ones, representing more congested traffic situations. The axis t(3) explains mostly variations respect to acceleration.

From the figure 2 correlation among emissions and kinematic parameters can be argued. CO2 is independent from the others and results negatively related to parameters higher for fast and fluent DC (percentage of driving time, max speed) and positively correlated to speed and gear attributes (V20 and cambio1) representative of slow and congested traffic situations. HC and CO are highly correlated, they are positively proportional to the percentage of time spent in the maximum deceleration (Paccel1), to the percentage of time spent in the maximum positive acceleration (Paccel7) and to max speed (vmax), while are negatively related to higher speed and gear (v30 and cambio3). NOX is independent from the others and has a low weight in the principal components, it has very low values and variations.

Thus, the plan of figure 1 can be divided into different characteristics zones: the upper zone refers to higher emissions of CO and HC and strong transient driving cycles, while the left zone refers to higher emissions of CO2 and slow stop and go DC's. In the residual zones lower pollutants driving cycles are situated. A further model (M4) has been fitted to observations with CO values less than 1.5 g/km to deepen the analysis of parameters for lower pollutant DC's, trends and parameters similar to M3 result for CO2, while results for CO and HC are different (from the model M3): data variation is explained by the same first component (and related variables) relevant for CO2.

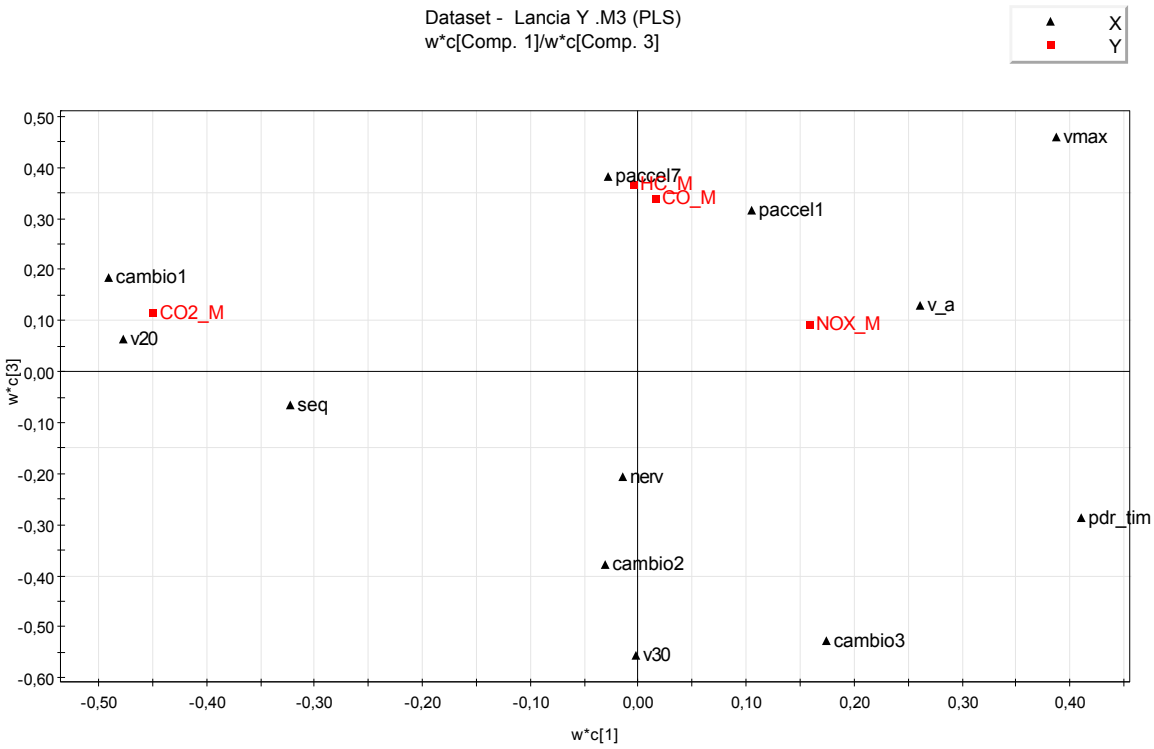

Figure 2: Variables correlation with (T1,T3).

Var ID (Primary)	**CO_M**	**HC_M**	**NOX_M**	**CO2_M**
Constant	1,17289	0,971893	1,90976	1,55727
vmax	0,323526	0,291032	0,0740697	-0,123474
nerv	0,0809275	-0,0783903	-0,222778	0,0413683
v20	0,0338531	0,00776709	-0,145937	0,229609
v30	-0,140901	-0,168631	-0,16704	-0,104693
cambio1	0,0528744	0,0299916	-0,0819516	0,275292
cambio2	0,004863	-0,0288359	-0,230964	-0,103521
cambio3	-0,410598	-0,34156	0,437339	-0,0190011
paccel1	0,31377	0,390753	0,236934	-0,0581837
paccel7	0,428107	0,462765	0,039432	-0,027134
seq	-0,0698899	-0,0256466	0,202072	0,197379
v_a	0,163958	0,105778	0,212342	-0,00831133
pdr_time	-0,162997	-0,168625	-0,0918432	-0,262112

Table 2: Regression coefficients .

The weight of each variable in the model for different emissions can be detected in the table 2 relative to standardized and centred coefficients.

The fit of model to data is reported in the figures 3,4 for CO and CO2 emissions, where measured (triangles) and predicted (squares) values are shown versus the most significant principal component (pooling the effect of different variables) for CO and versus mean speed for CO2.

In the table 3 goodness of fit indexes for each principal component and cumulative values are reported. R2X (and R2Y) are "Sum of squares" of all the X's (and Y's) explained by the extracted components, while Q2 is an index to assess the contribute of each principal component to the reduction of residual in the prediction (significant for Q2 >.05).

A	R2X	R2XCUM	R2Y	R2YCUM	Q2
1	0,366	0,366	0,239	0,239	0,195
2	0,237	0.603	0,203	0,442	0,0544
3	0,148	0,751	0,111	0,553	0,0655
4	0,070	0,821	0,113	0,665	0,187
5	0,11	0,931	0,012	0,677	-0,125

Table 3: R2 and Q2 indexes .

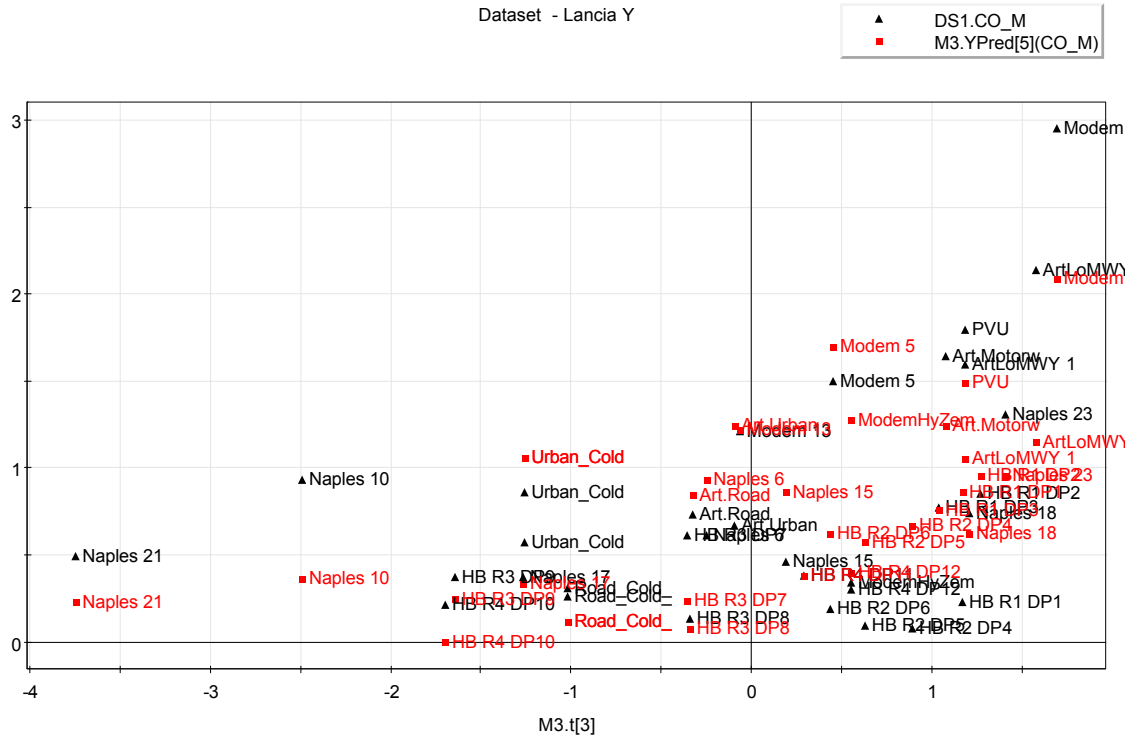

Figure 3: Measured and predicted values of CO versus t(3).

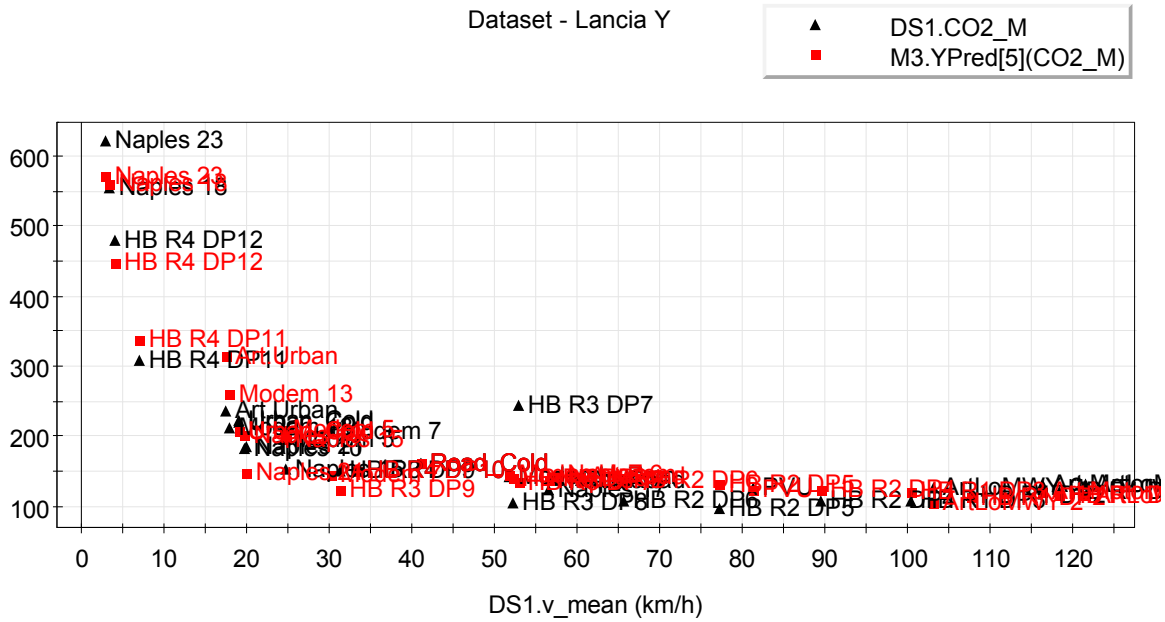

Figure 4: Measured and predicted values of CO2 versus v_mean.

Conclusion

Emission measurements performed with a car and a wide spectrum of driving cycles showed that understanding of real use emission pattern is a complex task, because the emission resulting from a specific driving cycle is the sum of many contrasting effect due to the peculiar combination of many parameters for each specific driving cycle. This fact is still more emphasized by the digital nature of current cars causing an individual unpredictable behaviour of engine/catalyst system in the performance plan of car.

The regression model obtained by the PLS method based on principal components, together with estimated statistical coefficients, represents a useful tool to analyse the relations among different emissions and kinematic aspects of driving cycles and quantify the effect of each parameter. Considering a consistent number of explicative variables in the model allows one to differentiate in a sensible way peculiar kinematic characteristics of different driving cycles and to individuate why a driving cycle produces higher (or lower) emissions respect to similar DC's.

Acknowledgments

The research was carried out and funded within the V European Framework Project ARTEMIS.

References

Andre M. (2002) WP3141 Influence of the driving cycle NRETS report, , Bron, France, 29 p.

Tenenhaus M (1998): La regression PLS Theorie et Pratique. Editions Technip Paris 1998

Matthew Barth and others (2002) Mobile Source Emissions New Generation Model: Using a Hybrid Database Prediction Technique, report prepared for U.S. EPA, University of California, Riverside, CA (2002)

12th International Symposium "Transport and Air Pollution" / 12e Colloque international "Transports et pollution de l'air", Avignon, 16 -18 *June* / juin 2003
proceedings / actes, n°92, tome / Vol. 2, Inrets ed., Arcueil, France, 2003, p. 203-208

Usage of Non-conventional Power Generation for Controlling Environmental Pollution: A Case Study of Silchar City

K .M. Pandey* & A. K. Pandey**
* Assistant Professor, Department of Mechanical Engineering, National Institute of Technology, Silchar-788010, Assam, India. email: kmpandey2001@yahoo.com, Fax:91-3842-233797
** Library Assistant, Central Library, N.I.T. Silchar, Assam, India.

Abstract
In the present work graphs are plotted, which compares the level of pollution on the roads of Silchar city. After a radius of 2 km, it can be said that the effects of suspended particulate matter concentration falls suddenly due to wind speed and directional effects so the area of Silchar medical college and REC Silchar can be declared as pollution free zone, but inside the municipal area, heavy dust is there as well as roads are narrow and the concentration of pollution is very high in municipal area of the city so pollution control techniques must be used for a healthy life. The situation of air pollution is alarming due to lack of an inefficient implementation of a preventive environmental management strategy. Most of the metropolitan cities in India are facing high levels of particulate matter and gaseous pollution in the environment. If non-conventional energy systems are used, the level of air pollution will decrease. It is suggested that for Silchar city small micro hydel power plants and solar systems will be more effective.
Key words: *non-conventional energy, air pollution, emission level, gaseous*

Introduction

A plenty of energy is needed to sustain the industrial growth and agricultural production. The existing sources of energy such as coal, oil, uranium etc. may not be adequate to meet the ever increasing energy demands. These conventional sources of energy are also depleting and may be exhausted at the end of the century or beginning of the next century. Consequently sincere and untiring efforts shall have to be made by the scientist and engineers in exploring the possibility of harnessing energy from several non-conventional energy sources. The various non-conventional energy sources are as follows: solar energy, wind energy, energy from biomass and bio gas, ocean thermal energy conversion, tidal energy, geo thermal energy, hydrogen energy, fuel cells, magneto-hydrodynamics generator, thermionic converter, thermoelectric power. Hydro-electric and solar power generation plants have no polluting effect on the environment the hydro-electric project does not pollute the atmosphere at all, but it can be argued that the solar power station in the long run may upset the balance in nature. To extend the argument to the logical end, imagine a very vast area of land is covered by solar collections of different forms.

Then the minimum required suns rays may not reach the earth's surface. This will certainly kill the vegetation on the earth and also the bacteria that are destroyed by sun's rays may survive giving rise to new types of health problems. Further, the evaporation of water and consequent rains may change their cycles. Added to these, the average temperatures of the earth and ocean may change. This may result in new balances among the living creatures, which cannot be easily predicted. Since we don't envisage such a large-scale coverage of earth's surface in the near future, we can safely state that the solar energy power plants do not pollute the atmosphere. According to energy experts the non-conventional energy sources can be used with advantage for power generation as well as other applications in a large number of locations and situations in our country.

Adopting the following can also control the green house effect:

- Increase of use of natural gas,
- Use of more hydro power,
- Use of alternative energy systems,
- Use of nuclear power,
- Use of efficient equipments,
- Removing CFCS from refrigeration industry,
- International reforestation and stopping of deforestation,
- Carbon charges,
- Increase in sink capacity

1 Methodology

All the vehicles like two wheeler, three wheeler, cars, buses, trucks and LCV etc were counted moving on roads at different intervals of time, road lengths were measured and calculations were made based on emission factors for different type of vehicles (Source – Indian Institute of Petroleum, Dehradun, India, 1985). Thus the amounts of pollutants generated were calculated on roads.

Vehicle Type	CO	HC	NO_x	SO_2	Pb	TSP
Two-wheelers	8.30	5.18	-	0.013	0.0028	-
Three wheelers	12.25	7.65	-	0.029	0.0063	-
Cars	24.03	3.57	1.57	0.053	0.0116	
Buses						
Sub Urban	5.87	2.27	11.10	1.930	-	0.37
Urban	4.51	1.75	8.52	1.480	-	0.28
Trucks	3.52	1.36	6.66	1.160	-	0.22
LCV	1.30	0.50	2.50	0.400		0.10

Table 1: Emission factors for different vehicles, g/km

Sl . No.	Length of Road	NAME OF ROAD
1	$L_a = 0.29$	Premtola Road
2	$L_b = 0.22$	Central Road
3	$L_c = 0.17$	Central Road
4	$L_d = 0.21$	Janiganj Road
5	Le = 0.12	Thana Road
6	Lf = 0.17	Fathak Bazar Road
7	$L_g = 0.13$	Panpatty Road
8	$L_h = 0.28$	U.D. Sarani Road
9	$L_i = 0.26$	Jail Road
10	$L_{ao} = 0.41$	Shillong Pattty Road
11	$L_{aa} = 0.16$	Vowel Road
12	$L_{ab} = 0.89$	Central Road
13	$L_{ac} = 0.27$	Park Road
14	$L_{ad} = 0.25$	Park Road
15	$L_{ae} = 0.28$	Central Road
16	$L_{af} = 0.68$	Central Road
17	$L_{ag} = 0.21$	Stadium Road
18	$L_{ah} = 0.13$	Central Road
19	$L_{ai} = 0.14$	Sadarghat Road
20	$L_{bo} = 0.14$	Central Road/Club Road

21	$L_{ba} = 0.92$	Cachar College Road
22	$L_{bb} = 0.17$	Malugram Road
23	$L_{bc} = 0.28$	Cachar College Road
24	$L_{bd} = 0.08$	Sadharghat Road
25	$L_{be} = 0.29$	Udharbond Road
26	$L_{bf} = 0.3$	Janigaj Road
27	$L_{bg} = 0.89$	Court Road
28	$L_{bh} = 0.32$	Janiganj Road
29	$L_{bi} = 0.85$	Janiganj Road
30	$L_{co} = 0.68$	Thana Road
31	$L_{ca} = 0.22$	Kalibari Road
32	$L_{cb} = 0.14$	Bhuiyar Gaddhi Road
33	$L_{cc} = 0.06$	Janiganj Road
34	$L_{cd} = 0.17$	Maidhan Road
35	$L_{ce} = 0.19$	P.W.D. Road
36	$L_{cf} = 0.27$	Tarapur Road
37	$L_{cg} = 0.32$	Tarapur Road
38	$L_{ch} = 089$	Station Road

Table 2: Nomenclature of roads

2 Results and discussion

The combustion of fuels and their products is responsible for a sizeable amount of anthropogenic air pollution, and this problem is particularly acute areas. Motor vehicles in urban areas produce hydrocarbons, CO, NO_x, and lead particles. The problem is further aggravated by the formation of secondary pollutants in the atmosphere due to complex chemical reactions. Photochemical smog, the product of such reactions, gives rise to the familiar haze (particularly in summer) and to vegetation damage, eye irritation, and respiratory distress.In urban areas, the most noticeable effect of air pollution is the reduction in visibility. This results from the scattering of light by airborne liquid and solid particles, particularly in the sub micron range from 0.1 to 1 μm, leading to safety hazards. Air pollution also affects urban climate with respect to increased fog formation and reduced solar radiation. It is estimated that urban areas receive 15 to 20 percent less total solar radiation than the rural areas due to pollution. The weather is also affected because a city forms a heat island, i.e., the temperature within an urban area may be many degrees higher than that of surrounding rural area. In addition, pollutants such as SO_2 in sulphurous smog and ozone in photochemical smog may intensify the greenhouse effect over urban regions, leading to even higher ambient temperatures.This can be seen from the graphs that in Silchar city maximum pollution occurs due to cars and two wheelers. TSP is present in the atmosphere due to buses, LCV and trucks. The emission of lead is there due to 2 wheelers, 3 wheelers and cars. Here, the peak traffic occurs between 0900h to 1100h in the morning and between 1700h to 1900h in the evening everywhere. Two wheelers contribute much for CO and HC emission in the atmosphere. The development of emission factors for vehicles under Indian conditions should be given priority in order to assess the emission from vehicles more comprehensively. This can be concluded that if non-conventional energy systems are used in day to day life like hydroelectric power plants, solar photovoltaic, it will control environmental pollution to a larger extent. The roads of Silchar city are highly congested and there is lot of dust also so much care is required. There are frequent traffic jams also which increase the pollution. People of Silchar city require awareness also about prevention of air pollution.The present investigation for the vehicular emission gases carried out for the Silchar city for

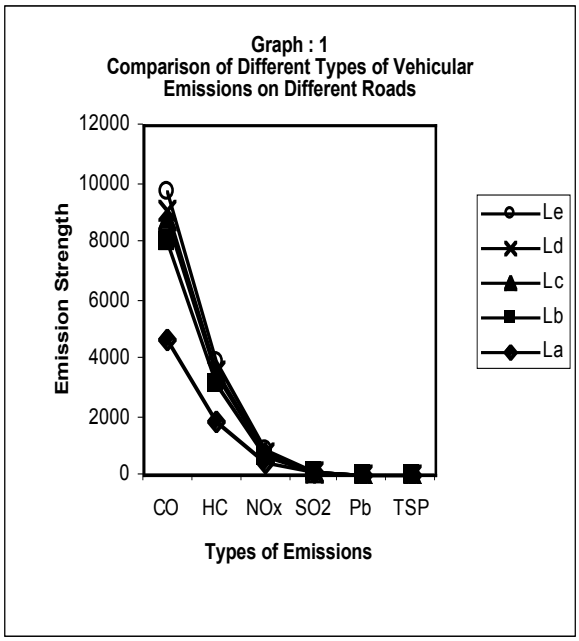
Graph : 1
Comparison of Different Types of Vehicular Emissions on Different Roads
Emission Strength
12000
10000
8000
6000
4000
2000
0
CO
HC
NOx
SO2
Pb
TSP
Types of Emissions
Le
Ld
Lc
Lb
La

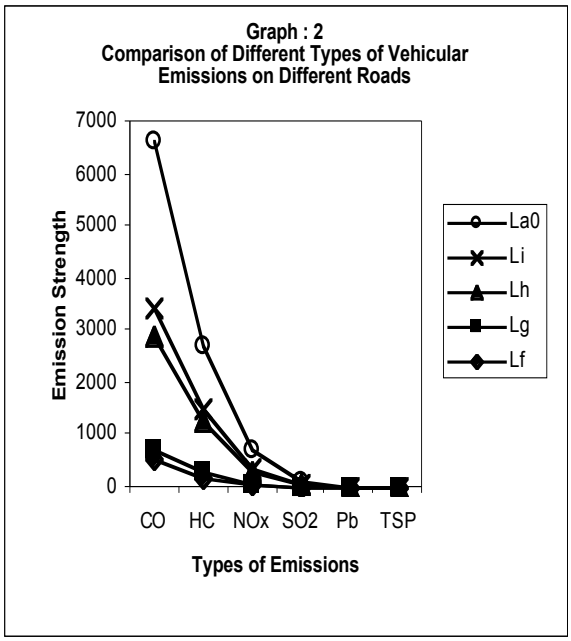
Graph : 2
Comparison of Different Types of Vehicular Emissions on Different Roads
Emission Strength
7000
6000
5000
4000
3000
2000
1000
0
CO
HC
NOx
SO2
Pb
TSP
Types of Emissions
La0
Li
Lh
Lg
Lf

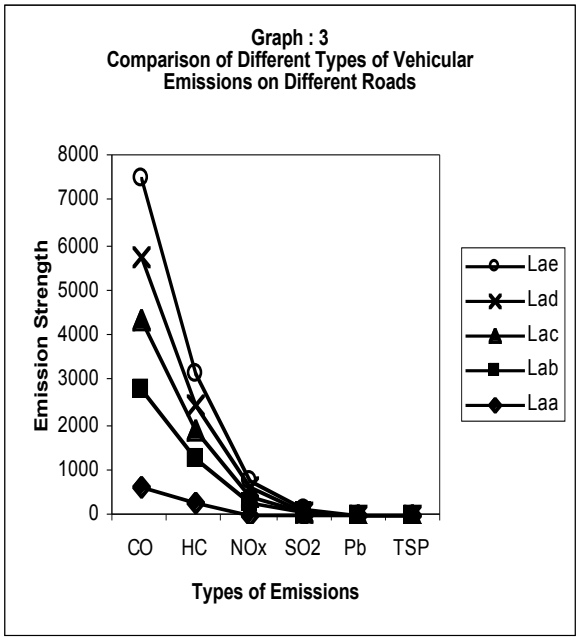
Graph : 3
Comparison of Different Types of Vehicular Emissions on Different Roads
Emission Strength
8000
7000
6000
5000
4000
3000
2000
1000
0
CO
HC
NOx
SO2
Pb
TSP
Types of Emissions
Lae
Lad
Lac
Lab
Laa

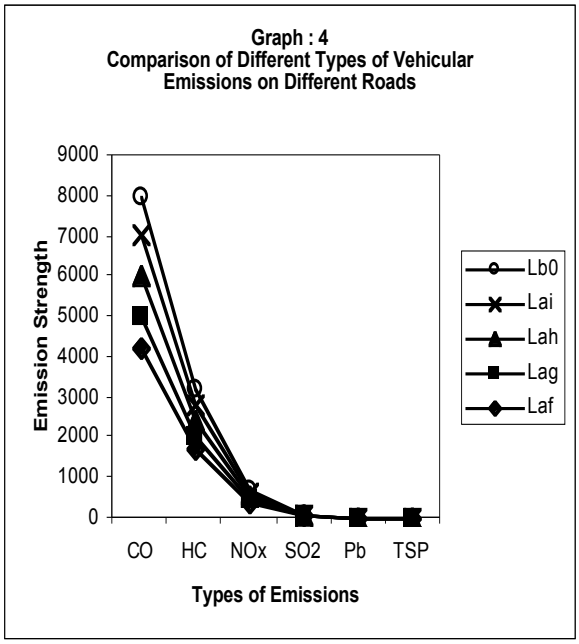
Graph : 4
Comparison of Different Types of Vehicular Emissions on Different Roads
Emission Strength
9000
8000
7000
6000
5000
4000
3000
2000
1000
0
CO
HC
NOx
SO2
Pb
TSP
Types of Emissions
Lb0
Lai
Lah
Lag
Laf

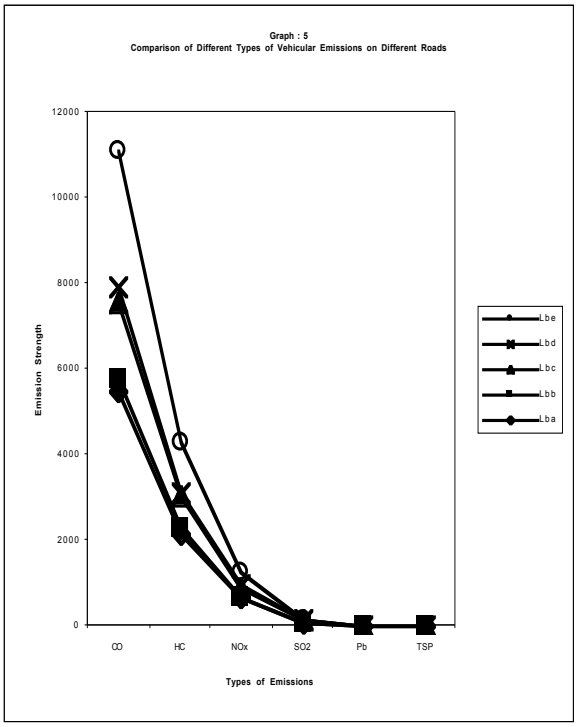
Graph : 5
Comparison of Different Types of Vehicular Emissions on Different Roads
Emission Strength
Types of Emissions
CO
HC
NOx
SO2
Pb
TSP
Lbe
Lbd
Lbc
Lbb
Lba

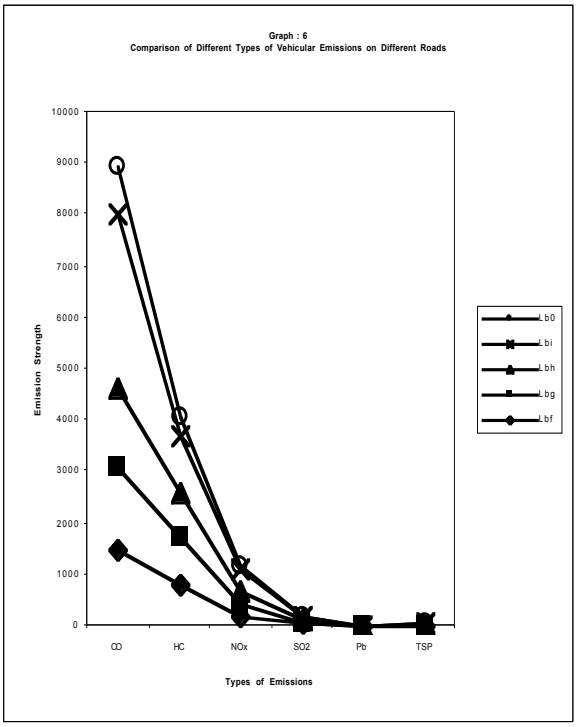
Graph : 6
Comparison of Different Types of Vehicular Emissions on Different Roads
Emission Strength
Types of Emissions
CO
HC
NOx
SO2
Pb
TSP
Lb0
Lbi
Lbh
Lbg
Lbf

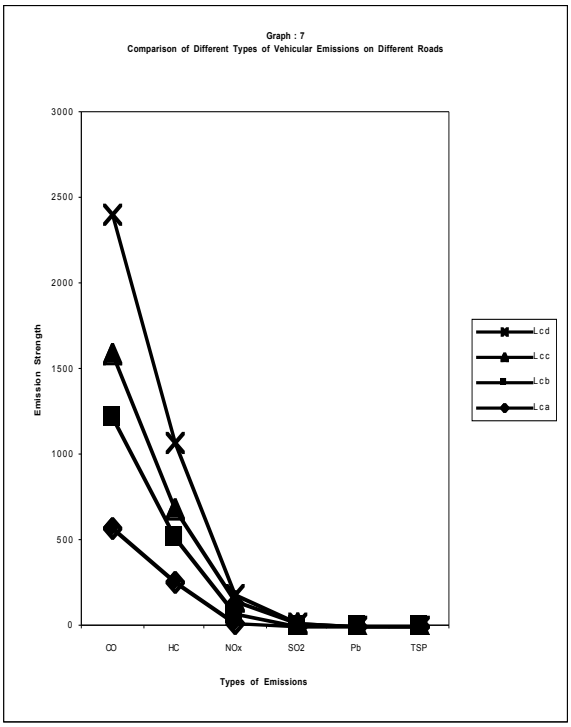
Graph : 7
Comparison of Different Types of Vehicular Emissions on Different Roads
Emission Strength
Types of Emissions
CO
HC
NOx
SO2
Pb
TSP
Lcd
Lcc
Lcb
Lca

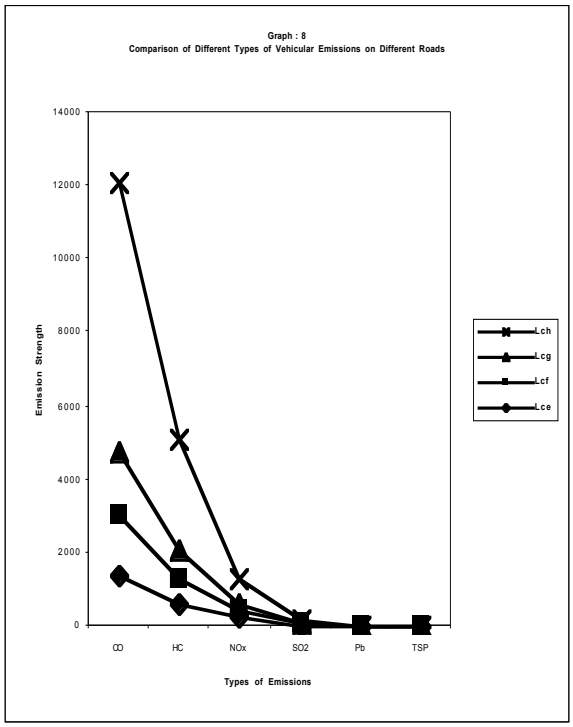
Graph : 8
Comparison of Different Types of Vehicular Emissions on Different Roads
Emission Strength
Types of Emissions
CO
HC
NOx
SO2
Pb
TSP
Lch
Lcg
Lcf
Lce

vehicles like 3 wheeler, 2 wheeler, cars, trucks buses and low commercial vehicles and emission gases like NO_x, SO_2, HC, CO, Pb, TSP are measured by the empirical formula given by Indian Institute of Petroleum as given in Table i.e. between 0900h to 1100h and 1700h to 1900h is taken for the present investigation. The emission for different roads for different type of vehicles are measured for the different pollutants example CO, HC, SO_2, NO_x etc. To study the vehicles emissions of Silchar City the number of vehicle running in the different roads were counted and by measuring the length of the different roads. The emission factor was used for estimate the pollution of the Silchar City. The tables of Roads show the road and pollutant specific emission in gm for two hour study from 0900h to 1100h and 1700h to 1900h. However to find the daily pollution load (Kg/day) the study for 24 hr. should be taken, but by two hour study, we can find the one hour emission of the different types of vehicle i.e. 2 & 3 wheelers, Cars, Bus, & Trucks and the pollutants i.e. Co, HC, NO_x, So_2, Pb, TSP. This gives the total emission for the whole city.

Conclusion

It is concluded that if non – conventional energy sources like solar photovoltaic, hydel and wind energy systems are used, the emissions of carbon dioxide and carbon monoxide will be less and as these damage respiratory systems and they also cause toxicity, blood poisoning and CO_2 is toxic in large quantities and CO_2 also leads to hyphoxia so in Silchar city as dust is also more so non – conventional energy sources must be promoted. Dust increases respiratory diseases, toxicity from metallic dusts, Silicosis and Asbestosis from specific dusts. Asbestos dust cause pulmonary fibrosis, pleural calcification and lung cancer also. Barak valley is very prone to cancer. From the graphs it is obvious that the level of pollution is very high at Silchar city so much care is needed now. In fact, micro hydel power plants and solar systems are effective solution to this problem.

References

Mahajan, S.P., Pollution Control in process industries, Tata Mc Graw-Hill Publishing Company Limited, New Delhi, © 1985.

Kormondy, E.J. Concepts of Ecology, Prentice Hall of India Private Limited, New Delhi , 1986.

Rao, C.S, Environmental pollution control engineering, Wiley Eastern limited, © 1991.

Lawrence Folinsbee, "Human Health Effects of Air Pollution," Environmental Health Perspectives, Vol. 100 (1992), pp. 47-48.

World Health Organization and the United Nations Environment Programme, Urban Air Pollution in Megacities of the World (Blackwell Publishers, Oxford, UK, 1992), pp. 10-11.

Health Effects Institute (HEI), Particulate Air Pollution and Daily Mortality: Replication and Validation of Selected Studies (HEI, Cambridge, MA, 1995), p. 4.

R. Bertollini et al., Environment and Health 1: Overview and Main European Issues, WHO Regional Publications, European Series, No. 68 (World Health Organization, Copenhagen, 1996), pp. 34-38.

A. Peters et al., "Acute Effects of Exposure to High Levels of Air Pollution in Eastern Europe," American Journal of Epidemiology, Vol. 144, No. 6 (1996), pp. 570, 578-80.

12th International Symposium "Transport and Air Pollution" / 12e Colloque international "Transports et pollution de l'air", Avignon, 16 -18 *June* / juin 2003
proceedings / actes, n°92, tome / Vol. 2, Inrets ed., Arcueil, France, 2003, p. 209-212

Persistent organic pollutants in transport sector

Vladimir Adamec, Jiri Duffek, Jiri Jedlicka & Rudolf Cholava
Transport Research Centre, Lisenska 33a, 636 00 Brno, Czech Republic
Fax: +420 541 633 742, email: adamec@cdv.cz

Abstract
This paper introduces the present situation of POPs transport emissions in the Czech Republic including the prediction to 2010 year, determination of emission factors, possibilities of its reduction and legislative framework. From achieved results it is evident that the emissions from the road and railway transport exceed 17 tons in 2001 year. The naphtalene creates more than 90% at emissions of vehicles fulfilling EURO I-III limits. The phenanthrene (about 50% of PAHs) predominates in emissions of older gasoline vehicles that do not fulfil EURO limits, naphtalene content is about 10%. at such vehicles. Total emissions of PCDDs and PCDFs are very low – in milligrams. Mostly older vehicles, before EURO produce them. Its total decrease is given by gradual changes of vehicle fleet in the Czech Republic.
Keywords: *polyaromatic hydrocarbons, polychlorinated bifenyls, polychlorinated dibenzo-dioxines, polychlorinated dibenzo-furanes, emissions, emission factors, air pollution, transport.*

Introduction

In the past decades transport has become the important factor which affects the environment both in the positive and the negative way. The most serious problem is air contamination by emissions, especially due to their effect on human health, particularly in big towns with the large volume of motor vehicle traffic. Exhaust gases from motor vehicles contain hundreds of chemical substances in different concentrations and with different effects on living organisms. Besides „classical“ monitored pollutants such as e.g. nitrogen oxides (NO_X), carbon monoxide (CO), carbon dioxide (CO_2) or sulphur dioxide (SO_2), lately the attention is also paid to persistent organic pollutants (POPs) such as e.g. polycyclic aromatic hydrocarbons (PAHs), polychlorinated biphenyls (PCBs), polychlorinated dibenzo-p-dioxins (PCDDs) and polychlorinated dibenzofurans (PCDFs).

Method

Regarding the fact that POPs do not belong among limited components, the measurement of emission factors of these pollutants is very limited. The situation is also complicated by the fact that values so far obtained have relatively large dispersion. The calculation and the audit of the amount of POPs emissions from transport start from the following woks: Adamec (2003), Ntziachristos and Samaras (2000) and Krobl (2001).

Emission factor (Ef) of a pollutant is always presented in the mass per the unit of energy ($g.MJ^{-1}$), the length of transport ($g.km^{-1}$), the mass of consumed fuel ($g.kgfuel^{-1}$) or power of the engine ($g.kWh^{-1}$). Ef of limited pollutants such as e.g. CO, NO_x, hydrocarbons (C_xH_y), particular matters (PM) are compulsorily measured (periodical technical inspections) but the measurement of POPs emissions from transport is not so far controlled by any legislative directive. That is why POPs emissions from vehicles are not usually measured and these measurements are especially connected with the experimental field. For this purpose, the authors made the database of Ef of selected POPs produced by transport (Dufek et al., 2002a). Results from national and foreign measurements, which

are the sources, are continuously completed (updated) and evaluated statistically. The following Table 1 presents used emissions factors of selected POPs produced by transport which were used for the elaboration of the emission inventory. Calculations of total emissions used average values for each category of means of transport.

VEHICLE CATEGORY	PAH total	PCDD	PCDF
	$\mu g.km^{-1}$	$pg.km^{-1}$	$pg.km^{-1}$
motorcycles	131,64	10,3	21,2
gasoline conventional cars	260,29	10,3	21,2
gasoline cars fulfilling EURO standards	143,84	-	-
diesel passenger cars	1277,44	0,5	1,0
LPG passenger cars	49,46	-	-
gasoline light duty vehicles	378,11	10,3	21,2
diesel light duty vehicles	1601,16	0,5	1,0
diesel heavy duty vehicles	241,86	3	7,9

Table 1: Emission factors of selected POPs produced by transport

Results and discussion

For determination of POPs emissions there were applied Methodology of the calculation of air polluting emissions from transport (Dufek et al., 2002b) which uses data about the amount of sold fuels. After the substraction of non-transport sources i.e. consumption in farming, forestry, civil engineering and army (especially concerning diesel), the amount of sold fuel is split by means of transport performances into particular modes of transport:

- individual road passenger transport (ID)
- public road passenger transport (SOD)
- road freight transport (SND)
- public urban transport - buses (MHD)
- railway transport – motor traction (ZD)
- waterway transport (VD)
- air transport (LD).

The mentioned modes of transport are split into 23 categories according to used fuel and equipment with catalytic converters. From this split consumption, emissions are calculated by means of average emission factors. For each of the given category there is used the average emission factor ($g.kgfuel^{-1}$) which is based on the measured and statistically processed values. For selected categories of road transport with very different yearly mileages in kilometers, fuel consumption of this category is calculated from these mileages concurrently with calculations of fuel consumption by means of transport performances. Yearly mileages correspond to results from the national traffic census on motorway and road network which is worked out once in five years.

For elaboration of emission inventory there were used consumptions of particular fuels determined by the mentioned methodology and emission factors presented in Table 1, evaluated statistically in the database of emission factors and recalculated from $g.km^{-1}$ to $g.kgfuel^{-1}$. The emission inventory includes PAHs, PCDDs, PCDFs and PCBs emissions.

Emissions from air transport are not included in the mentioned emission audit because there is not known the share of PAHs in emissions of hydrocarbons produced by combustion of airplane fuels.

Mode of transport	Year											
	1990	1991	1992	1993	1994	1995	1996	1997	1998	1999	2000	2001
ID	5265	4592	5620	6127	6642	7105	8249	8541	8591	9223	9206	9625
SOD	379	282	256	209	167	194	197	176	271	266	307	347
SND	2389	2039	2388	2220	3003	4003	5206	5810	5160	5572	5837	7316
MHD	169	132	138	125	109	138	170	172	190	221	250	296
ZD	449	320	296	195	163	233	249	206	214	190	165	186
VD	43	35	33	27	23	30	40	20	23	24	21	18
Total	8694	7400	8731	8903	10106	11703	14111	14926	14448	15496	15786	17788

Table 2: Total PAHs emissions in the Czech Republic (kg)

According to the mentioned calculations, the yearly amount of PAHs emissions in the Czech Republic from transport exceeds 17,8 tons in 2001. The naphtalene creates more than 90% of PAHs emissions from petrol vehicles which meet EURO emission limits and from diesel vehicles. The phenanthrene (about 50% of PAHs) predominates in emissions from older petrol vehicles which do not meet EURO emission limits, naphtalene content is less than 10% in the case of these vehicles. We find by comparison of PAHs emission factors from various sources that there are not strong differences between new and older vehicles as in the case of VOC because PAHs are not limited by any standard. So this results in the considerable increase in the amount of these emissions which corresponds to the increase in consumption of petrol and diesel and transport performances in the field of the individual road passenger transport and road freight transport.

Mode of transport	Year											
	1990	1991	1992	1993	1994	1995	1996	1997	1998	1999	2000	2001
ID	168,5	147,2	179,9	195,1	214,9	209,6	219,9	211,2	178,1	163,6	123,2	97,3
SOD	5,1	3,8	3,5	2,9	2,4	2,8	2,8	2,5	3,7	3,5	4,0	4,5
SND	13,7	13,4	17,5	17,9	29,0	32,9	38,1	45,8	37,0	43,1	46,1	48,1
MHD	2,1	1,6	1,7	1,5	1,3	1,7	2,0	2,0	2,1	2,0	2,2	2,4
ZD	5,6	4,0	3,7	2,4	2,0	2,9	3,1	2,5	2,6	2,3	2,0	2,3
VD	0,5	0,4	0,4	0,3	0,3	0,4	0,5	0,2	0,3	0,3	0,3	0,2
Total	195,5	170,5	206,7	220,2	250,0	250,2	266,4	264,2	223,8	214,8	177,8	154,8

Table 3: Total PCDDs emissions in the Czech Republic (mg)

Mode of transport	Year											
	1990	1991	1992	1993	1994	1995	1996	1997	1998	1999	2000	2001
ID	348,4	304,4	372,0	403,2	444,4	433,3	454,6	436,6	368,2	338,0	254,6	201,1
SOD	5,7	4,3	4,0	3,4	2,9	3,4	3,3	2,9	4,2	4,1	4,6	5,1
SND	23,2	23,5	31,4	32,8	54,7	61,3	69,9	84,5	67,6	80,0	84,8	88,8
MHD	2,1	1,6	1,7	1,5	1,3	1,7	2,0	2,0	2,1	2,0	2,2	2,4
ZD	5,6	4,0	3,7	2,4	2,0	2,9	3,1	2,5	2,6	2,3	2,0	2,3
VD	0,5	0,4	0,4	0,3	0,3	0,4	0,5	0,2	0,3	0,3	0,3	0,2
Total	385,5	338,2	413,2	443,7	505,6	502,9	533,4	528,9	445,0	426,7	348,5	299,8

Table 4: Total PCDFs emissions in the Czech Republic (mg)

PCDDs and PCDFs emissions from transport reach totally milligrams. They are mostly produced by older vehicles which do not meet EURO 1 – 3 emission limits. The downward trend in the production of these emissions from transport is caused by renewal of the vehicle fleet especially in the individual road passenger transport. From the COPERT database of emission factors there is not however possible to find if these emissions from older vehicles are fixed on the so-called halogenated scavengers or if they originate from trace amounts of chlorine in petrol. Emission factors of PCDDs and PCDFs are very low, in $pg.km^{-1}$, hence there is the probable origin of this minimum amount also by burning fuels which do not contain halogenated scavengers. This assumption is also supported by the fact that the database includes emission factors of diesel vehicles as well, where halogenated ingredients were not applied.

Mode of transport	Year											
	1990	1991	1992	1993	1994	1995	1996	1997	1998	1999	2000	2001
ID	143,2	125,3	154,3	169,0	190,1	192,4	212,0	218,8	204,7	224,4	216,1	222,4
SOD	0,4	0,3	0,4	0,3	0,4	0,4	0,4	0,3	0,4	0,4	0,4	0,4
SND	6,1	6,6	9,3	10,0	17,5	19,1	21,2	26,0	20,3	24,7	26,1	26,9
MHD	-	-	-	-	-	-	-	-	-	-	-	-
ZD	-	-	-	-	-	-	-	-	-	-	-	-
VD	-	-	-	-	-	-	-	-	-	-	-	-
Total	149,8	132,3	163,9	179,3	208,0	211,9	233,6	245,1	225,5	249,6	242,6	249,8

Table 5: Total PCBs emissions in the Czech Republic (mg) – petrol vehicles

Note: PCBs emissions were calculated only for petrol vehicles because no measurements of emission factors of PCBs of diesel vehicles were found.

Conclusion

The PAHs and POPs emissions are a part of total hydrocarbon emissions, that are limited by UN ECE standards. But the PAHs themselves are not limited and these emissions are not regularly measured. That is why their significant increase in the Czech Republic is found out from the 1990 until now. This fact can mean the threat of air quality and the increase of negative impacts of traffic on human health.

There seems that the elaboration of the inventory of emissions from combustion of fuels is the least problematic. Emission factors, categories of vehicles and fuel consumption are mostly known. POPs emissions from mobile sources are negatively affected by the high old age of the vehicle fleet in the Czech Republic. Only its renewal by modern vehicles, equipped with suitable technologies for the reduction of POPs, will contribute to the decrease of their total production.

Acknowledgements

The study was supported by the Czech Ministry of Transport as research project VaV 801/210/109.

References

Adamec V. (2003): Research of Environmental Burden from Transport. TRC, Brno, Czech Republic, 200 p. (In Czech).

Dufek J. & V. Adamec (2002a): Database of Measured Emission Factors from Transport Sector. TRC, Brno, Czech Republic (In Czech).

Dufek J. & V. Adamec (2002b): Methodology of the Calculation of Air Polluting Emissions for All Transport Modes. TRC, Brno, Czech Republic, 24 p. (In Czech).

Ntziachristos L. & Z. Samaras (2000): COPERT III - Computer Programme to Calculate Emissions from Road Transport. Methodology and Emission Factors (Version 2.1). EEA, Copenhagen, Denmark, 84 p.

Krobl L. (2001): Survey of Emission Factors of Road Motor Vehicles. ÚVMV, Prague, Czech Republic, 35 p. (In Czech).

12th International Symposium "Transport and Air Pollution" / 12e Colloque international "Transports et pollution de l'air", Avignon, 16 -18 *June* / juin 2003
proceedings / actes, n°92, tome / Vol. 2, Inrets ed., Arcueil, France, 2003, p. 213-218

A non-exhaust particulate emissions inventory for road traffic in Denmark

Morten Winther
National Environmental Research Institute, Frederiksborgvej 399, 4000 Roskilde, Denmark
Fax: +45 4630 1212 - e-mail: mwi@dmu.dk

Abstract
The Danish emissions of TSP, PM_{10} and $PM_{2.5}$ from brake and tyre wear and road abrasion are calculated using vehicle fleet and mileage data behind the national COPERT III exhaust emission estimates and CEPMEIP emission factors modified in some parts on the basis of a literature survey. Brake and tyre wear emission factors are determined with the most accuracy for passenger cars. The emission factors for road abrasion are still very unprecise. The level of non-exhaust particulate emissions from road transport is still uncertain but has increased with traffic growth in the later years. In 2001 the non-exhaust emission shares of TSP, PM_{10} and $PM_{2.5}$ are around 80, 25 and 10%. The relative importance of non-exhaust emissions will become even bigger in the future due to the step-wise strenghtening of emission standards for road transportation vehicles.
Keys-words*: TSP, PM_{10}, $PM_{2.5}$, tyre wear, brake wear, road abrasion.*

Introduction

An increased attention has been given to the adverse health effects on humans that particulates can cause depending on their numbers, sizes and chemical compositions and now particulates are subject to large research activities in many countries. The increased research efforts have lead the attention to the non-exhaust sources such as tyre and brake wear, road abrasion and the resuspension of road dust recognising them as well to be important contributors to the overall emission total.

In Denmark a four-year research programme has been launched in 2001 to shed light on particulate emissions and their related impact on environment. Focus is on describing particle size distributions, chemical compositions and the emission contribution from different sources. Other elements of the programme are to identify critical exposure events and population groups at special risk, to carry out welfare-economic analyses, to make health effect assessments and to investigate emission reduction options for transport.

An integrated part of the research programme is to determine exhaust as well as non-exhaust emission factors for road transportation vehicles as an input to dispersion and exposure models. The establishment of proper emission factors also has an overlap with the national obligations in terms of emission inventories and emissions reporting to different international bodies.

This paper serves as a documentation of the Danish inventory for the road transport non-exhaust emissions of TSP, PM_{10} and $PM_{2.5}$ according to the new UNECE convention guidelines (CORINAIR, 2002). The particulate emission sources included are tyre and brake wear and road abrasion. Another purpose of the present work is to identify the weak parts of the inventory where better data should become available in order to improve the accuracy of the emissions estimates.

1 - Method

The emissions from brake and tyre wear and road abrasion are calculated by multiplying the total annual mileage per vehicle category with the correspondent average emission factors for each source

type. The calculation procedure is consistent with the European COPERT III model approach, see Ntziachristos et al. (2000), used in Denmark to estimate the national emissions coming from exhaust.

Activity data

From the Danish Road Directorate information of the vehicle stock and annual mileage is obtained. This covers data for the number of vehicles in relevant sub-categories, annual mileage and mileage split between urban, rural and highway driving. The annual mileages are not the original figures from the Danish Road Directorate: The figures shown are modified to obtain an equilibrium between the simulated fuel use in COPERT III and the statistical fuel sale totals from the Danish Energy Agency (DEA).

Vehicle class	Population [No.]	Mileage [km]	Mileage distribution Urban [%]	Rural [%]	Highway [%]
Passenger cars	1,932,929	19,157	35	46	19
Light duty vehicles	282,846	29,116	35	50	15
Heavy duty trucks	48,809	55,443	21	45	34
Buses	9,820	84,154	42	44	14
Mopeds	165,000	1,175	81	19	0
Motorcycles	77,427	5,563	47	39	14

Table 1: Vehicle fleet and mileage data for Danish road transport in 2001.

Non exhaust emission factors

Different factors affect tyre wear such as tyre construction, composition and size, accumulated mileage, driving behaviour, vehicle type, vehicle settings and maintenance, road surface characteristics and weather. Brake wear only occurs during forced decelerations, and therefore most of the emissions should be observed near busy junctions, traffic lights, pedestrian crossings, and corners.

The emission factors used in the Danish inventory mainly come from TNO (2001) which has conducted a literature study (CEPMEIP) targeted at proposing particulate emission factors of TSP, PM_{10} and $PM_{2.5}$ relevant for national inventories in the context of the UNECE convention. The non-exhaust particulate data in CEPMEIP originate from Dutch road-side measurements, as the only source of information (Brink 1996).

The tyre and brake wear factors have been established from mass balance experiments for passenger cars, while for other vehicle types the tyre wear factors have been estimated using information from people employed in the tyre business and industry. Brake wear factors for the same vehicle types have been estimated using the same ratio between brake and tyre wear as for passenger cars.

The road abrasion factors are taken from an emission inventory by RIZA (Institute for Inland Water Management and Waste Water Treatment) in the Netherlands in 1994. Here a total road abrasion mass was found to be 60% higher than the figure for total tyre abrasion mass. This factor (1.6) was then used to derive the road abrasion factors from the tyre wear factors. In the CEPMEIP database the factor is somewhat changed to be around 2.1.

Extensive literature surveys are made by Luhana et al (2002) and Gustafsson (2001) in order to summarise the current knowledge about particulate emissions arising from tyre, brake and asphalt road pavement wear. The work by Luhana et al (2002) is made as a part of the 5th framework project Particulates. Both surveys consider aspects of particulate chemical characteristics, emissions and health and environmental effects. The two surveys refer data for particulate size distribution and emission rates which deviates largely.

Luhana et al. (2002) and Gustafsson (2001) refer to some studies which suggest that tyre, brake and road wear particles appear in all size ranges, see e. g. Fauser (1999). This conflicts with the particle data from CEPMEIP; here all brake wear particulates are reported as $PM_{2.5}$ whereas for the same

size-range zero particulates are reported from tyre and road asphalt wear. The disagreement of particulate size fractions justifies some changes in the factors to be used in Denmark.

	Brake wear			Tyre wear			Road abrasion		
Vehicle category	TSP	PM_{10}	$PM_{2.5}$	TSP	PM_{10}	$PM_{2.5}$	TSP	PM_{10}	$PM_{2.5}$
Passenger cars	6	5.9	2.4	69	3.5	2.5	145	7.3	0
Light duty veh.	7.5	7.4	3.0	90	4.5	3.2	190	9.5	0
Heavy duty veh.	32.25	31.6	12.9	371.25	18.6	13.0	783	39.2	0
Buses	32.25	31.6	12.9	371.25	18.6	13.0	783	39.2	0
Mopeds	1.5	1.5	0.6	17.25	0.9	0.6	36.5	1.85	0
Motorcycles	3	2.9	1.2	34.5	1.7	1.2	73	3.7	0

Table 2: Emission factors (mg/km) per vehicle category in the Danish inventory.

For tyre wear the Danish TSP emission factor (CEPMEIP) remains unchanged. A variety of emission factors has been reported in the literature so far. The CEPMEIP factor of 69 mg/km is within this interval and is moreover supported by the findings of 97 mg/km in the experimental part of Particulates (Luhana et al., 2002). On the basis of their literature review the latter source further suggest that between 1 and 10% of all emitted particles from tyres can be classed as PM_{10}. This is in accordance with the PM_{10} fraction of 5% used in CEPMEIP. However, USEPA (1995) and TNO (1997) suggest that 70% of PM_{10} is emitted as $PM_{2.5}$, a size fraction which is adapted to calculate new Danish $PM_{2.5}$ factors for tyre wear.

Also the Danish TSP factor for brake wear is maintained for the same reasons as for tyre wear. New PM_{10} and $PM_{2.5}$ emission factors are calculated using the findings from USEPA (1995) and TNO (1997). In these two studies PM_{10} and $PM_{2.5}$ shares of total TSP are reported to be 98 and 40% respectively.

At present being it is not possible to determine road abrasion emission factors with some degree of certainty from the available literature. Road abrasion is typically included in the emission factor for total non-exhaust particulate matter; the sum of tyre and brake wear, road abrasion and resuspended material from the road surface. Due to missing data no changes will be made to the factors used in the Danish inventory (see also section Results).

Generally the non-exhaust emission factors must be considered as preliminary and may be subject to revisions when new information becomes available.

	Brake wear (tons)			Tyre wear (tons)			Road abrasion (tons)			Total (tons)		
Vehicle category	TSP	PM_{10}	$PM_{2.5}$	TSP	PM_{10}	$PM_{2.5}$	TSP	PM_{10}	$PM_{2.5}$	TSP	PM_{10}	$PM_{2.5}$
Passenger cars	222	218	89	2,555	130	91	5,369	270	0	8,146	618	180
Light duty veh.	62	61	25	741	37	26	1,565	78	0	2,368	176	51
Heavy duty veh.	87	86	35	1,005	50	35	2,119	106	0	3,211	242	70
Buses	27	26	11	307	15	11	647	32	0	981	74	21
Mopeds	0	0	0	3	0	0	7	0	0	11	1	0
Motorcycles	1	1	1	15	1	1	31	2	0	48	4	1
Grand total	399	391	160	4,626	233	163	9,738	489	0	14,764	1,114	323

Table 3: Non exhaust emissions per vehicle category in the Danish 2001 inventory.

2 - Results

The emissions from brake and tyre wear and road abrasion are calculated by multiplying the total annual mileage per vehicle category with the correspondent average emission factors for each source type.

In terms of total emissions Gustafsson (2001) gives estimates for the Swedish TSP for tyre and brake wear. The estimates are around twice as high as the Danish 2001 estimates. Taking into account the larger Swedish fleet and route network the Swedish and the present study's results are comparable. For road abrasion Gustafsson (2001) suggest total emissions which are an order of

magnitude higher than the Danish result. The large difference is due to the extensive use of studded tyres in Sweden.

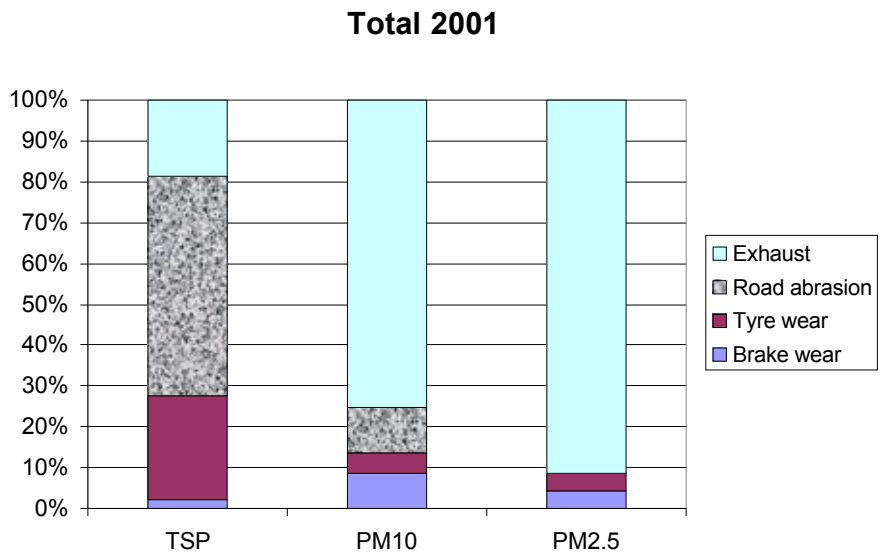

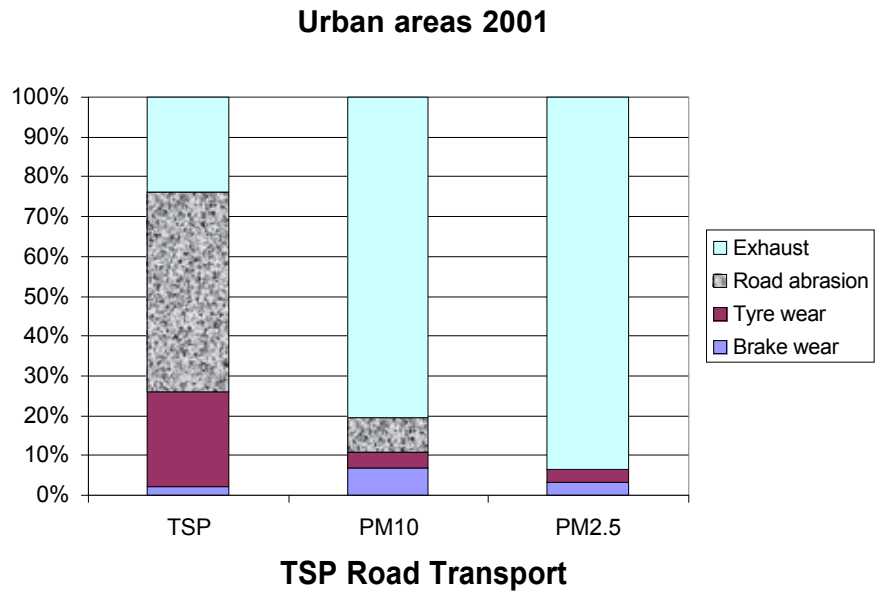

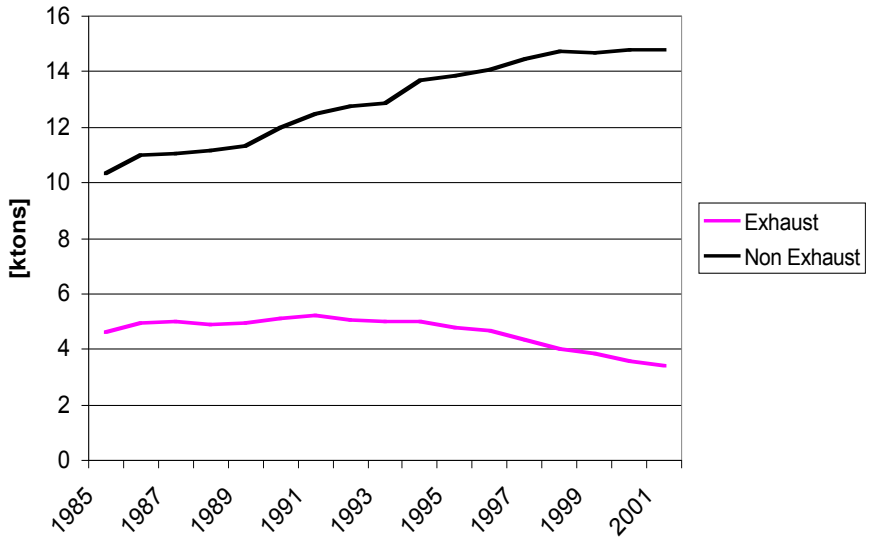

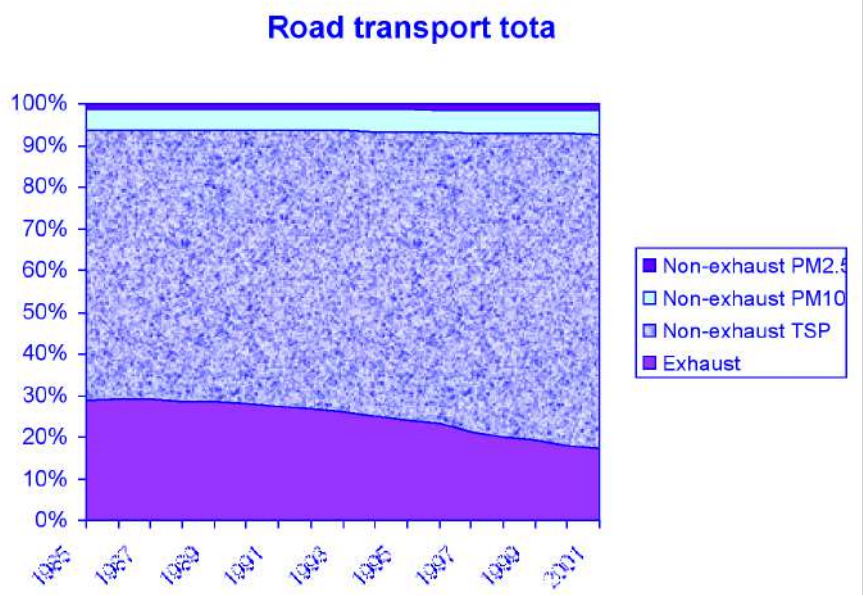

Figure 1: Danish exhaust and non-exhaust particulate emission results in 2001 and as trends.

For brake emissions Salway et al. (1997) report an estimate of 3,900 tons in the UK for PM_{10}, which is comparable to the Danish total assuming that differences in population and hence traffic amount give proportional emission changes. No consistence in tyre wear totals can be derived from the results for Germany (Rauterberg-Wulff, 1999), the UK (Salway et al., 1997) and Denmark.

The Danish emission inventories comprise estimates for all sectors including tailpipe emissions from road transportation vehicles (DMU, 2003). In 2001 around 80, 25 and 10% of the total road traffic TSP, PM_{10} and $PM_{2.5}$ emissions come from non-exhaust sources. In urban areas the emissions in many cases are more harmful. Here the exhaust emission share is a little larger.

In the years up to 2001 the non-exhaust emissions have increased proportionally with the traffic growth. During the same time period a significant decrease in the exhaust emissions is observed in step with the gradual strenghtening of exhaust emission standards for all road transportation vehicles. In the future the non-exhaust share of total particulate emissions will increase even further.

The Danish PM_{10} emissions for urban areas are markedly lower than 50% as suggested by Düring et al. (2002). In a total emissions perspective two main reasons explain why no changes are made to the CEPMEIP road abrasion factors in the Danish inventory.

Primarily, annual emission calculations must be regarded as average results made to provide environmental information in emission trends. Consequently the national vehicle fleet and mileage data behind the estimations are not able to reflect real world fleet composition and traffic behaviour in single streets. Secondly, local conditions such as weather conditions, road material and road surface maintenance level also have a strong effect on the resulting road abrasion rates. As an end result correspondent air quality measurements and traffic counts are essential on a local street scale if more qualified reverse calculations of the road abrasion factors should be made. The feasibility of making such reverse calculation estimates must be investigated in the remaining part of the Danish research project.

Conclusion

For non-exhaust particulate sources the emission factors for brake and tyre wear are determined with the most accuracy. Still there is a lack of data derived from experiments on vehicle types other than passenger cars. The emission factors for road abrasion are still very unprecise. Hardly no data exist in this area and there is a destinct need for further research. Road abrasion rates are difficult to determine since they are highly dependent on factors such as weather conditions, road material and maintenance level.

Modifications of the CEPMEIP emission factors behind the Danish inventory is made for brake wear using PM_{10} and $PM_{2.5}$ fractions of 98 and 40% of total TSP derived from the findings in other studies. In the same way a new $PM_{2.5}$ emission factors is estimated for tyre wear as 70% of the existing factor for PM_{10}. It is decided to maintain the factors for road abrasion and instead let the outcome of parallel research at NERI and other non-exhaust emission research activities be the basis for future emission factor improvements.

The level of non-exhaust particulate emissions from road transport is still uncertain but emissions have increased with traffic growth in the later years. This increase will continue in the future and in relative terms the importance of non-exhaust emissions will become even bigger due to the step-wise strenghtening of emission standards for road transportation vehicles.

References

v.d. Brink R. M. M. (1996): Particulate emissions from road traffic: emission factors, size distribution and chemical composition. RIVM Report, 773002008, 57 p. (in dutch).

EMEP/CORINAIR Emission Inventory Guidebook - 3rd edition October 2002 UPDATE Technical report No 30. European Environment Agency, Copenhagen (http://reports.eea.eu.int/EMEPCORINAIR3/en).

DMU (2003): Inventories for the Convention on Long-range Transboundary Air Pollution (www.dmu.dk/1_Viden/2_Miljoe-tilstand/3_luft/4_adaei/default_en.asp).

Düring I., Jacob J., Lohmeyer A., Lutz M., Reichenbächer W. (2002): Estimation of the "Non-Exhaust Pipe" PM_{10} Emissions of Streets for Practical Traffic Air Pollution Modelling. In: Sturm, P. J. (ed): 11th International Symposium Transport and Air Pollution. Report of the Institute for Internal Combustion Engines and Thermodynamics. Volume 81-1, p 309-316.

Fauser P (1999): Particulate air pollution with emphasis on traffic generated aerosols. Risø National Laboratory, Denmark, Risø-R-1053(EN), 149 p.

Gustafsson (2001): Icke-avgasrelaterede partiklar i vägmiljön. Litteraturöversikt, Väg- och transportforskningsinstitutet, Sweden, VTI meddelande 910, 52 p. (in Swedish).

Luhana, L., Sokhi, R., Warner, L., Mao, H., Boulter, P., McCrae, I., Wright, J., Reeves, N., Osborn, D. (2002): Characterisation of Exhaust Particulate Emissions from Road Vehicles (PARTICULATES). Deliverable no. 8. Non-exhaust particulate measurements: results, Version 1.0 – July 2002, 93 p.

Ntziachristos, L., Samaras, Z. (2000): COPERT III Computer Programme to Calculate Emissions from Road Transport - Methodology and Emission Factors (Version 2.1). Tehnical report No 49, 86 p, European Environment Agency, Copenhagen, Denmark.

Particulates (2002): A 5FP Project of the European Commission in the Competitive and Sustainable Growth (GROWTH) Programme, sponsored by DG TREN Contract No: 2000-RD.10429 (www. vergina.eng.auth.gr/mech/lat/particulates).

Rauterberg-Wulff A. (1999): Determination of Emission Factors for Tyre Wear Particles up to 10µm by Tunnel Measurements. In: Sturm, P. J. (ed): 8th International Symposium Transport and Air Pollution. Report of the Institute for Internal Combustion Engines and Thermodynamics. Volume 76-1, p 265-272.

Salway A.G., Goodwin J.W.L., Eggleston H.S., Murrells T.P. (1997): UK Emissions of Air Pollutants 1970-1995, National Environmental Technology Centre, AEA Technology, Culham, Report AEAT-1746, Issue 1.

TNO (1997): Particulate Matter Emissions (PM_{10}, $PM_{2.5}$, $PM_{0.1}$) in Europe in 1990 and 1993. TNO Institute of Environmental Sciences, Energy Research and Process Innovation, Apeldoorn, TNO-MEP Report R96/472.

TNO (2001): TNO CEPMEIP database (www.air.sk/tno/cepmeip).

USEPA (1995): Compilation of Air Pollutant Emission Factors. USEPA Report AP-42, Volume I, 5th Edition, 63 p.

12th International Symposium "Transport and Air Pollution" / 12e Colloque international "Transports et pollution de l'air", Avignon, 16 -18 *June* / juin 2003
proceedings / actes, n°92, tome / Vol. 2, Inrets ed., Arcueil, France, 2003, p. 219-224

Competing technologies for reducing catalytic converter cold start emissions

P. N. Botsaris & E. Tsioliaridou
Democritus Univ. of Thrace, Dep. of Electrical & Computer Eng., Faculty of Energy Systems, Laboratory of Mechanical Eng., 1 Vas.Sofias, 67100 Xanthi, Greece,
tel: +3 (0)541 28941, fax:+3 (0)541 64324, email: leeboss@mailcity.com

Abstract
The development of new efficient and reliable technologies is a fact in nowadays for the reduction of cold start emissions apart the behavior of the powerplant itself, in order to meet the stringent regulations in Europe, United States of America or Japan. Carrying out a comprehensive study in this field, the present research group aimed to present the current and future possible solutions to this challenge. Lately, beside the tried technologies like electrically heated catalytic converter, secondary converter or catalyst placement near to the exhaust manifold, new promising technologies are presented. Afterburner chamber, secondary air into exhaust, converter with phase-change materials,, chemically heated converter, non-thermal plasma heated converter, HC-traps, or emission tanks are some of the new technologies.
This study seeks to provide a cleaner view of positives and negatives involved in these technologies and to offer an insight into development activities pursued by the world automotive makers in this area.
*Keywords**:** cold start emissions, fast light off, emissions.*

Introduction

Three-way catalysts control the vehicle emissions in hydrocarbons (HC), carbon monoxide (CO) and nitrogen oxides (NO_x). To achieve, though, ULEV, many control functions of the gasoline vehicles have to be improved. This paper presents current developments and test result of the techniques used to attain low emission levels. In order to compare and estimate the above-mentioned techniques, common factors and parameters have to be considered and discussed. Comparison of parameters such as conversion efficiency of HC, CO and NO_x, excess power or fuel consumption and complexity of each catalytic system, will help reach some conclusions as far as fast light-off techniques are concerned.

1. Catalyst Fast Light-Off Techniques

Electrically Heated Catalyst

A. Electrically Heated (pre) Catalyst (EHC)

The EHC is a well-known effective technology for the reduction of cold- start emissions. An electrically heated catalyst, when used as an addition to the main catalytic converter causes the latter to reach light- off temperature much faster. The main advantage of this system is that the EHC approaches light- off temperature (400 ^{o}C) in 15- 20 sec. Using electrical energy to quickly heat a catalyst is a proven means of reducing hydrocarbon (HC) and carbon oxides (CO) emissions, by more than 50 and 40%, respectively, whereas the reduction of NO_x is up to 30% Kirchner, Eigenberger (1996). However, EHC is a battery- powered system and requires more than 2 KW from a 12V battery for a minimum period of 20 sec Shimasaki et. al. (1997).

B. Alternator- Powered Electrically Heated Catalyst (APEHC)

Either an additional battery or the alternator can alternatively supply EHC. The idea of using an Alternator- Powered EHC is to minimize the impact on the existing vehicle battery, by extracting sufficient power directly from the alternator. During the first 20 sec, 2,4 KW of power are required by the EHC. Furthermore, tests have shown a great reduction in exhaust gas emissions. HC, CO and NO_x emission levels are respectively 70, 90 and 30% below ULEV standards Laing, Paul (1994), Roychoudhury et al. (1994).

C. Electrically Initiated Chemically Heated Catalyst (EICHC)

When heating a catalytic converter electrically, the vehicle may not have sufficient time for recharging the battery that supplies power to the EHC. Apart from that, the catalyst does not reach light- off temperature in less than 15- 20 sec. EICHC is another method for an almost instantaneous heating of catalyst. This is achieved by means of electrical heating followed by chemical heating. EICHC reduces the electrical energy provided by the battery (2,1 KW for 4.8 sec) and hence, minimizes the dependence on it. Catalyst light- off temperature (300 ° C) is reached in 7- 12 sec Murphy et. al. (1999).

Phase Change Material (PCM)

The system described in this paragraph consists of a metal catalytic converter, embedded in a phase-change-material. PCM is composed of an eutectic mixture with additives, has a melting point at 353 ° C and operates best in combination with a variable-conductance-insulation (VCI). According to this method once the catalyst reaches light-off temperature, some of the thermal energy of the exhaust gases is stored in the PCM as the material melts. Since phase-change transition temperature is closed to the light-off temperature (310 ° C, in 1-2 min.) of the catalyst, PCM is used to absorb, store and then release heat, when needed. After the engine is turned off (during parking), PCM is being partially solidified, keeping the catalyst temperature above the highest light-off temperature for 4 hours. Results of tests demonstrate that the conversion efficiency is more than 65% for HC, 73% for CO and 85% for NO_x. PCM system is however effective only for a specific length of time after the engine is turned off Korin et al. (1998).

Pre-Catalyst

The main ceramic converter remains in its initial position, whereas the monolith pre-catalyst is situated either close to the main converter (close coupled) or close to the exhaust manifold (stand-alone). Pre-catalyst operation is based on its high heat and mass transfer coefficient as well as on its geometric surface area. Pollutant emission levels can be met with or without secondary air. However, when secondary air is supplied to the pre-catalyst, time to reach light off temperature (300 ° C) drops from 30sec to 5 sec. HC and CO levels are 50 and 80% respectively, below ULEV, whereas NO_x emission levels are reduced to 20% below ULEV Roychoudhury et al. (1997), Truex, Timothy (1988).

Close Coupled Catalyst

Placing the main converter closer to the exhaust manifold is an efficient technique to achieve a minimum operating temperature light off of 250- 350 ° C and a minimum pollutant emission level. Close to the engine, the catalyst receives more heat from the exhaust gases and warms up quickly. With the aid of secondary air light off temperature of 250 ° C can be met in 20 sec. Close coupled converter though, is also exposed to high operating temperatures and severe vibrations. Therefore the catalyst should be coated and insulated with a material of high temperature resistance. This will reduce heat transfer to the engine components and maximize the engine performance. Close-coupled catalyst not only meets the ULEV standards, but is also approximately 40% below the HC, 80% below the CO and 70% below the NO_x standards Truex et. al. (1988).

Chemically Heated Catalyst (CHC)

In contrast to electrically heated catalyst, CHC uses a chemical means of producing the energy

necessary to preheat the main converter. In this system, no power from the engine- battery is needed, since the energy used to heat the catalyst is produced by chemical reactions between hydrogen and oxygen. These exothermic reactions take place on the catalyst surface and simply improve the efficiency of the existing catalyst system. After reaching light off temperature (300 ° C in a few seconds), the engine is switched from hydrogen to gasoline, resulting in the elimination of HC, CO and NO_x emissions (below the SULEV). Another advantage of this system is the absence of any moving or wearing components on the car, since the solid-state electrolyzer is steadily mounted on the vehicle.

Burner Heated Catalyst (BHC)

In this case gasoline is burned to obtain a hot exhaust gas steam, which heats the main catalyst faster. The burner is located in front of the converter to ensure heat transfer and it is turned on until the main catalyst reaches light-off temperature. The catalyst temperature rises up to 800 ° C in 20-sec. Total conversion of HC is limited to 70% during the first 7-sec, whereas total combustion of HC and CO can be reached after 15 and 8 sec respectively. Burners used in this method are up to 15 KW, meaning that gasoline consumption is much higher for a vehicle. Consequently, it should be mentioned that BHCs are high complexity, microprocessor controlled systems, making this method rather expensive and complicated Kirchner, Eigenberger (1997), Koltsakis, Stamatelos (1997).

Exhaust Gas Ignition (EGI)

In order to avoid added cost and complexities, associated with BHC, Exhaust Gas Ignition (EGI) has been utilized. During cold-start emission, engine operation is modified for a few seconds to supply a richer fuel-air mixture. With the aid of an electric pump, additional air is provided into the combustion chamber. By burning excess HC, exhaust gas mixture reaches the catalyst inlet and is ignited, in order to heat up the main converter. The technique described in this paragraph requires a combustion chamber, a glow plug and a temperature sensor placed between two catalyst monoliths. The rates of HC and CO are remarkably low, compared to ULEV, since conversion efficiencies are very high Koltsakis, Stamatelos (1997).

Plasma Catalyst System

One of the primary pollutants produced by engines, diesel or gasoline, are oxides of nitrogen (NO_x). Researchers and engineers, in order to solve this problem, have developed a device, which generates non- thermal plasma in the exhaust stream of a vehicle. The system uses plasma to convert NO_x to acids that react with ammonia. Ammonia is then added to the gas stream to produce ammonium nitrate (NH_4NO_3), which is removed through the use of scrubbers. Plasma catalyst removes 50% of the initial NO_x, as well as 50% of HC and 80% of CO, emitted by a vehicle. Even though, power consumption is not regarded as a disadvantage in this method (plasma uses only 0,025KW for a few seconds), harmful by-products, which may be formed in the process, are to be taken under serious consideration Herling et. al. (2000).

Hydrocarbon Absorber systems

Hydrocarbon Absorber Systems incorporate special materials, such as zeolites, into or ahead of the catalyst. At low temperatures, zeolite absorbs HC from the exhaust gas, and as the catalyst approaches its operating temperature, HC are the absorbed (at about 200 ° C). By that time the main catalyst is ready to receive and destroy hydrocarbons, reducing their emissions levels up to 45-75%. When the catalyst is still cold, exhaust gas passes through the absorber substrate and is being trapped in it until the converter is heated up. Although HC emissions decrease significantly with this method, no such results can be seen as far as CO and NO_x conversion is concerned Koltsakis, Stamatelos (1998).

Comparing diagrams

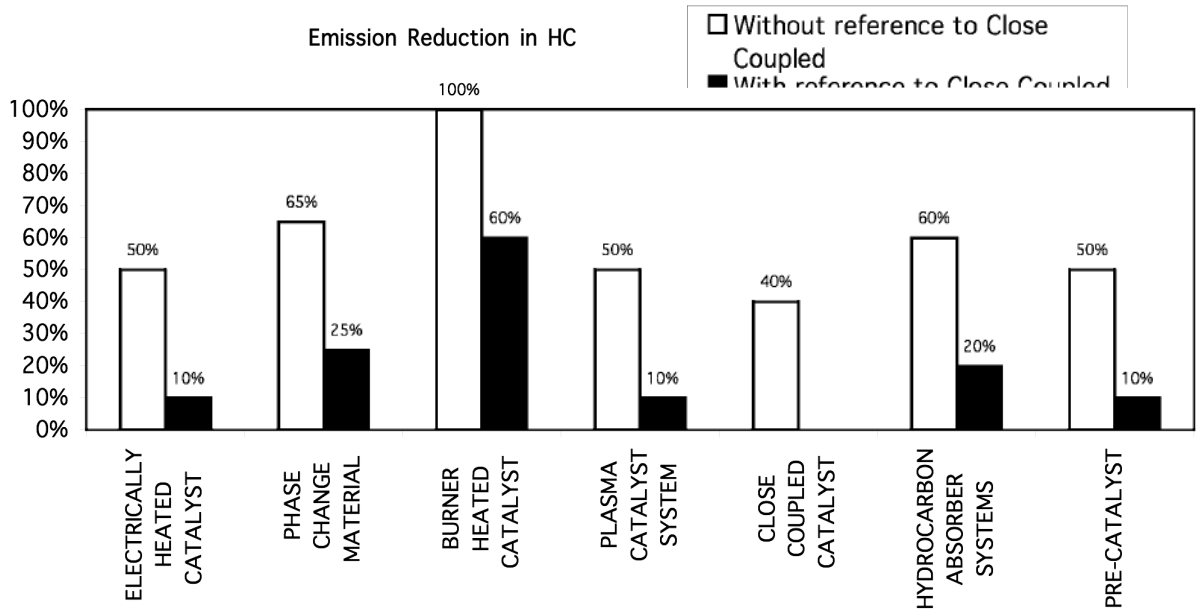

Figure 1: Emission Reduction in HC

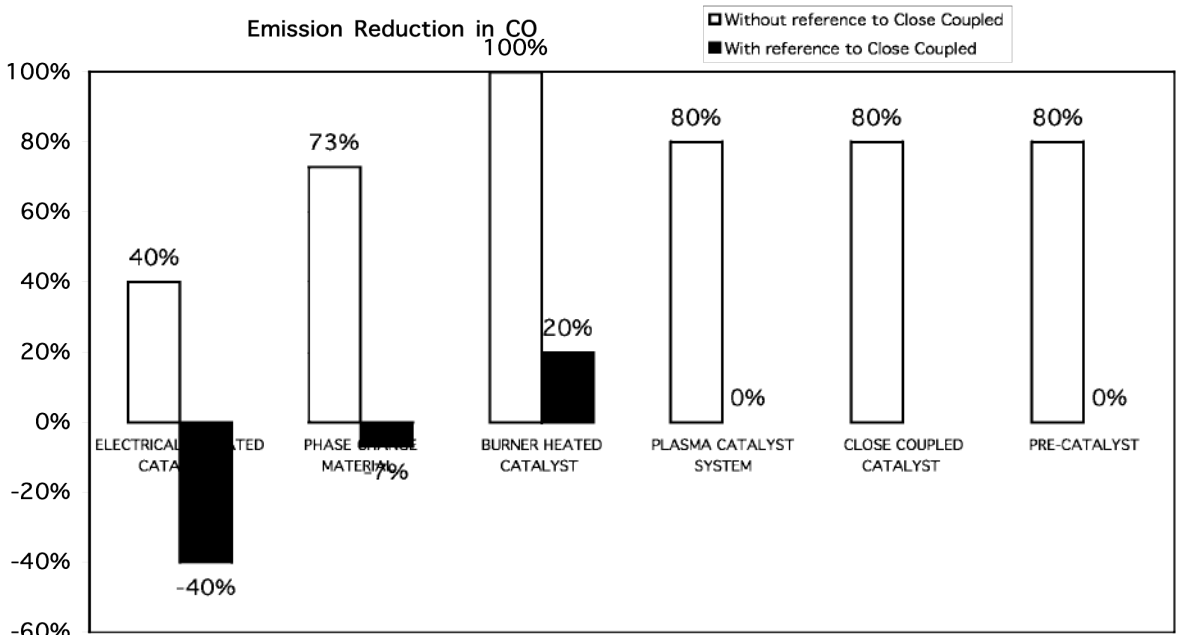

Figure 2: Emission Reduction in CO

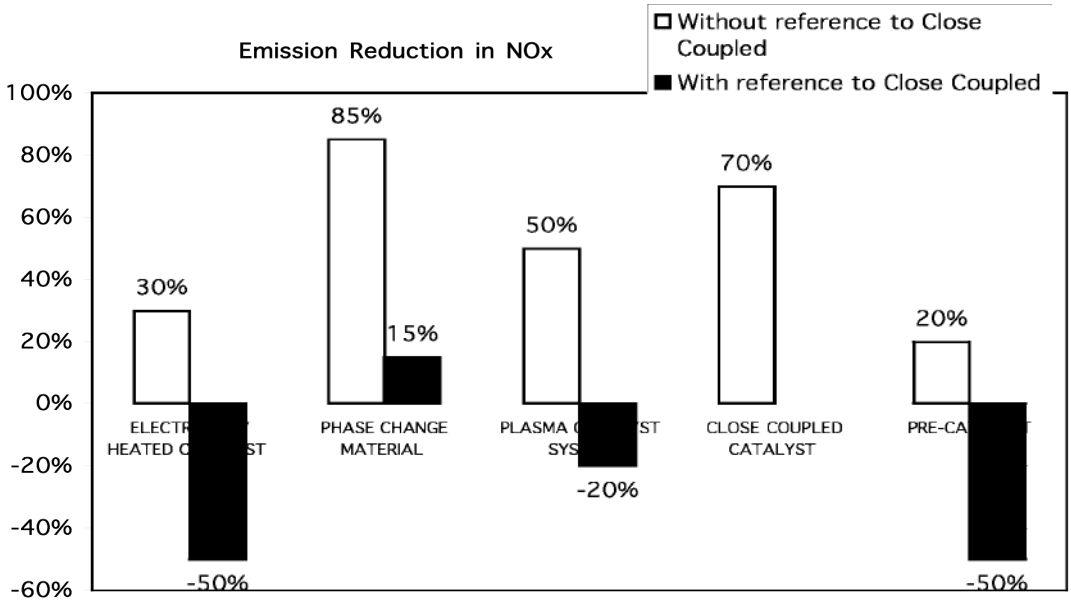

Figure 3: Emission Reduction in NO_x

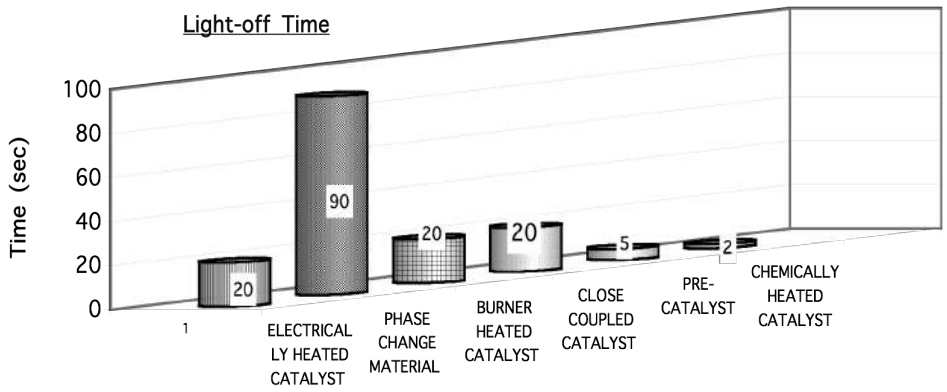

Figure 4: Light-off time

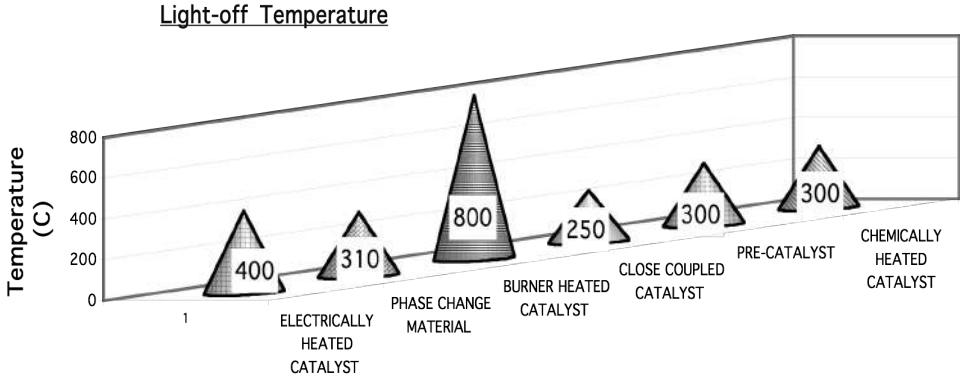

Figure 5: Light-off temperature

Conclusions

After studying carefully all the techniques discussed in this paper, it is fair to say that there are many different technologies to meet the requirements of ULEV. Reducing HC, CO and NO_x emitted by the exhaust gases can be achieved by either preheating the main converter, storing HC until light off temperature or adding a second pre-catalyst. Each one of the methods developed to improve cold-start emissions has some advantages and disadvantages. To sum up, one has to think which of the parameters discussed in the above technologies are the most important in a gasoline car behavior. The aim of this review paper is to help classify today's approaches on fast light off techniques in order to comply with emission legislation.

References

Association for Emission Control by Catalyst- AECC, Hydrocarbon Absorber Systems, http://www.aecc.be/en/next_technology.htm

DELPHI Automotive Systems, Close Coupled Catalytic Converters www.delphi.com/automotive/engine/exhaust

Herling, Darrell and Smith, Monty, (2000), Evaluation of Corona Reactors of Several Geometries for a Plasma Assisted Nitrogen Oxide Emission Reduction Device, SAE Tech. Paper 2000-01-2899.

Kirchner, T. and Eigenberger, G., (1997),On the dynamic behavior of automotive catalysts, Catalysis today, Vol. 38,pages 3-12, Elsevier Science Ltd.

Kirchner, T. and Eigenberg, G., (1996), Optimization of the cold- start behaviour of automotive catalysts using an electrically heated pre- catalyst, Chemical Engineering Science, Vol.51, No 10, pp2409-2418, Elsevier Science Ltd.

Koltsakis, C. Grigorios and Stamatelos, M. Anastasios, (1997), Catalytic Automotive Exhaust Aftertreatment, Prog. Energy Combust. Sci. Vol. 23, pp1-39, Elsevier Science Ltd.

Korin, E., Reshef, R., Tshernichovesky, D., and Sher, E. (1998), Improving Cold- Start Functioning of Catalytic Converters by Using Phase- Change Materials, SAE Tech. Paper 980671, 1998.

Laing, M. Paul, (1994), Development of an Alternator- Powered Electrically- Heated Catalyst System, SAE Tech. Paper 941042.

Litex- Corona Discharge Device, http://www.litexcorp.com/cdd/index.htm

Lynntech Inc, Chemically Heated Catalyst, www.lynntech.com/licensing/chc/index.shtml

Murphy, O. J., Kukreja, R.T., and Andrews, C.C., (1999), Electrically Initiated Chemically Heated Catalytic Converter to Reduce Cold- start Emissions from Automobiles, SAE Tech. Paper 199-01-1233.

Roychoudhury, S., Hixon, D., Pfefferle, W., Gibbs, E. R., Webster, J. W., Johnson R., and Wilson, G.(1994), Fast Light- off Non- Electrically and Electrically Heated Microlith Catalytic Converter, SAE Tech. Paper 940467, 1994.

Roychoudhury, S., Muench, G., Bianchi, F. J., Pfefferle, W. and Gonzales, F.(1997), Development and Performance of Microlith Light-off Preconverters for LEV/ ULEV, SAE Tech. Paper 971023, 1997.

Shimasaki, Y., Kato H., Abe, F., Hashimoto, S., Kaneko, T., (1997), Development of Extruded Electrically Heated Catalyst System for ULEV Standards, SAE Tech. Paper 971031.

Technology Brief, Keeping the Heat on Cold- start Emissions, www.nrel.gov

Truex, J. Timothy (1988), Development and Evaluation of Advanced Catalyst Technology for ULEV Emission Levels with Gasoline Fueled Vehicles, Final Report, February.

Volvo Car Corporation, www2.car.Volvo.se/vpc/press/releaser/990309e17.html

12th International Symposium "Transport and Air Pollution" / 12e Colloque international "Transports et pollution de l'air", Avignon, 16 -18 *June* / juin 2003
proceedings / actes, n°92, tome / Vol. 2, Inrets ed., Arcueil, France, 2003, p. 225-232

Comparison of the NO_2/NO_x Emissions of Heavy-Duty Euro-3 Diesel Engines with and without a CRT™ System

Patrik Soltic & Josef Rütter
EMPA, Überlandstrasse 129, 8600 Dübendorf, Switzerland -
Fax +41 (0)1 823 40 12 - email : patrik.soltic@empa.ch

Abstract
Traffic is the main source of anthropogenic nitrogen oxide (NO_x) emissions. Nitrogen oxide consists of nitric oxide (NO) and nitrogen dioxide (NO_2). NO_2 is an irritant, it destroys cells of plants and affects the visibility. NO_x plays, in combination with volatile hydrocarbons, a major role in the formation of tropospheric ozone. To estimate the partitioning of the NOx emissions for the actual heavy-duty diesel engines of the Euro-3 generation, on-line NO_x and NO_2 emission measurements are presented in this work. In total three engines were measured: Two engines had no exhaust gas aftertreatment systems and one engine was equipped with a CRT™ system.
The measurements show that all three engines produce similar NO_x and NO_2 concentrations after the turbine in similar operating conditions. The engines emit on average 6.3 volume-percent (9.4 mass-percent) of their NO_x as NO_2. The situation is completely different when using a CRT™ system: About 44 volume- percent (55 mass-percent) of the NO_x is emitted as NO_2 at tailpipe position. An inverse dependency of the NO_2 level on the exhaust gas temperature level can be observed: The lower the temperatures, the higher the NO_2 level. This behaviour indicates the exothermal NO to NO_2 conversion in the catalyst.
***Keys-words**: NO_x, NO_2, NO, CRT, ozone, VOC, heavy-duty diesel, partitioning, Euro-3, ESC.*

Introduction

Road traffic is the main source of anthropogenic nitrogen oxide emissions. The sum of nitric oxide (NO) and nitrogen dioxide (NO_2) is referred to as nitrogen oxide (NO_x) and is limited for heavy-duty engine homologation. NO_x, in conjunction with volatile organic compounds (VOC), plays a major role in the formation of ground-level ozone. The genesis of ground-level ozone during intense daylight in a “dirty” troposphere is driven by what is known as the photochemical NO_2/VOC cycle, where NO_2 acts as a catalyst and VOCs are the "fuel" for the reaction. For fairly high ozone concentrations, NO_2 is the limiting factor for ozone production. NO_2 is either emitted directly from combustion processes or converted in the environment by the oxidation of NO. However, NO_2 emissions are more harmful because they contribute directly to the ozone build-up while high NO emission rates can even lower the local ozone levels. For the understanding and modelling of the gas-phase chemistry of urban atmospheres it is therefore of particular importance to quantify the partitioning of the nitrogen oxide emissions of all sources.

The total amount as well as the partitioning of the NO_x emissions of three heavy-duty diesel engines, all with Euro-3 homologation, is analysed in this work. The measurements were performed in the raw exhaust gas. Two engines had no exhaust gas aftertreatment system and a rated power of approximately 330 kW respectively 250 kW. The third engine had a rated power of approximately 190 kW and was equipped with a CRT™ system fitted by the engine manufacturer. A CRT™ system consists of an oxidation catalyst followed by a filter capable of trapping soot and other particles, see Chatterjee et al (2001). The regeneration of the trap is enhanced at moderate temperatures by a high NO_2 level which the catalyst generates by the oxidation of NO. Therefore, it is interesting to analyse

the NO_2 levels before and after a modern CRT™ system and to compare the NO_2 levels of the three different Euro-3 engines of different manufacturers.

1 – Engines measured and measurement set-up

The technical data of the three engines, all of different manufacturers, is listed in Table 1. The engines 1 and 2 were Euro-3 engines without any exhaust gas aftertreatment system. Therefore, the engines were certified in the European Stationary Cycle (ESC) according to the EC directive (1999). The ESC is a 13-mode steady-state procedure. The engine 3 is a Euro-3 engine as well, but equipped with a CRT™ exhaust gas aftertreatment system. For engines with exhaust gas aftertreatment systems, the certification has to be performed in the European Transient Cycle (ETC). All engines were turbocharged and electronically controlled. The engine 1 was highly boosted using a turbocharger with variable turbine geometry. A peak brake mean effective pressure (bmep) of nearly 24 bar was measured. The other two engines were boosted moderately whereas engine 2 had no boost pressure control device and the boost pressure of engine 3 was controlled using a waste gate. All engines were equipped with an intercooler.

	Engine 1	**Engine 2**	**Engine 3**
Certification level	Euro-3	Euro-3	Euro-3
Configuration	6 cylinders in line	6 cylinders in V	6 cylinders in line
Displacement [litre]	10.3	12.0	7.3
Max. power	330 kW @ 1920 rpm	250 kW @ 1700 rpm	185 kW @ 2150 rpm
Max. torque [Nm]	1960	1730	1015
Max. bmep [bar]	23.9	18.1	17.5
Boosting device	Turbocharger	Turbocharger	Turbocharger
Boost pressure control	Variable turbine geometry	No	Waste gate
Intercooler	Yes	Yes	Yes
Injection system	Unit injection	Unit pump	In line pump
Engine control	Electronically	Electronically	Electronically
Exhaust system	w/o muffler	Muffler	CRT™ applied by the engine manufacturer

Table 1: Technical data of the engines.

The fuels used for the experiments were analysed and their main properties are listed in Table 2.

Fuel	**For engine 1**	**For engine 2**	**For engine 3**
Density (at 15°C) [kg/m^3]	838	832	834
Sulphur content [mg/kg]	52	346	8
Hydrogen [mass-%]	13.4	14.4	13.9
Carbon [mass-%]	86.3	85.9	86.1
Caloric value [MJ/kg]	43.44	42.74	43.03

Table 2: Diesel fuel properties.

The engines were mounted on a dynamic test bench and the exhaust gases were fed to a full flow CVS system. The raw exhaust gases were sampled with heated lines and analysed on-line. For the measurements of the engine equipped with the CRT™ system, an additional NO/NO_x analyser was placed between the engine and the CRT™ system to measure the raw exhaust gases. Table 3 gives a brief summary of the types and characteristics of the main devices used.

Brake	
Rated power [kW]	680
Rated Torque [Nm]	2500
Combustion Air	
Conditioning	Temperature + humidity controlled to 22 - 23 °C and 42 – 45 % rH
Fuel Processing	
Conditioning	Temperature controlled to 38 °C
CVS	
Type	Full flow dilution tunnel
Tunnel dimensions	Diameter 450 mm, length 4660 mm
Pump	Positive displacement (PDP)
Flow	25 - 100 Nm^3/min
Temperature control	50 ± 5 °C before PDP
Dilution Air	
Conditioning	Temperature controlled to 22 - 23 °C
Filtering	Coarse + charcoal + fine filters
Emission Measurement	
Main measurement system	Horiba MEXA 7400D (10 Hz sampling capability)
NO_x or NO analyser raw gas line 1	Horiba vacuum CLD (CLA-755A) in heated OVN (191 °C), wet measurement, repeatability within ± 0.5 % FS, carbon converter, NO_x coverter efficiency > 95 %
NO_x or NO analyser raw gas line 2	Horiba vacuum CLD (CLA-755A) in heated OVN (191 °C), wet measurement, repeatability within ± 0.5 % FS, carbon converter, NO_x coverter efficiency > 95 %
Simultaneous NO_x and NO analyser raw gas line pre-cat	Eco-Physics vacuum CLD (700 EL ht), heated sampling lines (190 °C), metal converter, linearity ± 1 % FS, NO_x coverter efficiency not specified

Table 3: Properties of the test facility.

The analysers measure the NO_x emissions such, that they first convert all NO_2 in NO and then measure the chemiluminiscent reaction of NO with ozone. If the converter is bypassed, only the NO emissions are measured. The concentration of the NO_2 emissions can therefore be calculated as the difference of the NO_x and the NO concentration. The raw gas sampling lines 1 and 2 sampled the same exhaust gases with the difference that one analyser was set to analyse NO_x and the other to analyse NO. The NO_2 emissions are soluble in water. The measurement set-up guarantees a proper measurement because the sample lines are heated to prevent the water from condensing. Figure 1 shows a sketch of the set-up.

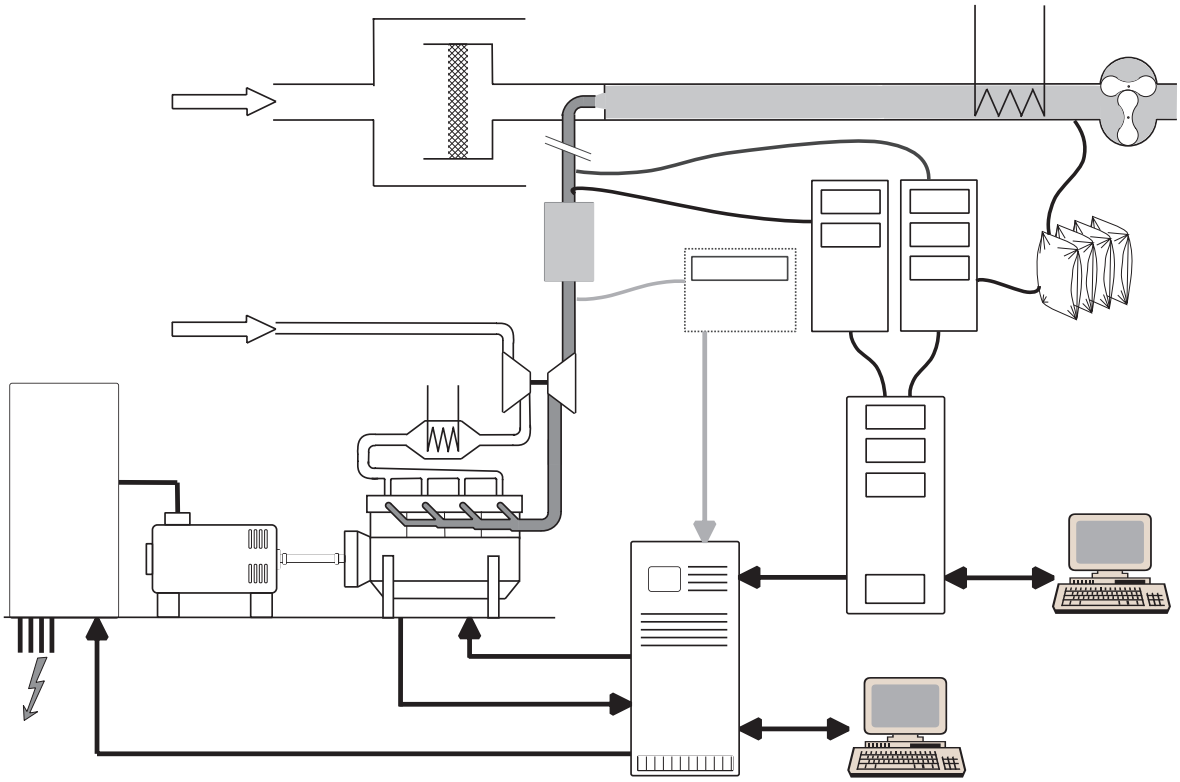

Figure 1: Measurement set-up.

2 – Performed measurements

The engines were measured, among many other cycles, in the ESC. The ESC consists of 13 successive engine operating points. The first operating point is engine idle (phase 1) where the engine is operated for four minutes. In each of the following twelve operating points, the engine is operated for two minutes. The ESC cycle is well suited to studying the dynamics of the NO_2/NO_x emissions in the phases where the operating points are quite rapidly changing as well as the stationary NO_2/NO_x behaviour in the phases when the emissions are stabilised. Figure 2 shows the operating points of the ESC.

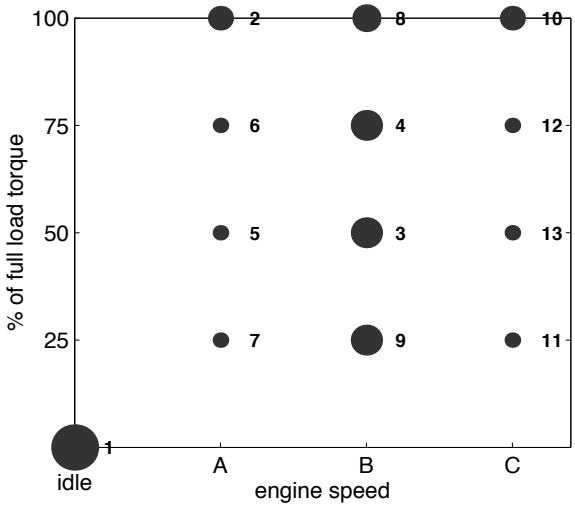

Figure 2: Operating points and order of the ESC (the diameter of the bullets represents the weighting for the particulate sampling of the several operating points for the ESC).

The speeds A, B and C are calculated for each engine individually. They depend on the power characteristic of the full load curve. To compare the behaviour of different engines, it is important to

compare similar operating points regarding the underlying physical processes. The thermo- and fluid dynamic conditions of two engines running at the same speed are different if the two engines have different strokes. Therefore, the mean piston speed and not the engine speed is a sensible measure. The mean piston speed (*mps* in m/s) is calculated from the engine angular speed (ω in rad/s) and the stroke (in m) as follows:

$$mps = 2 \cdot stroke \cdot \omega .$$

Two engines running at similar operating points have to run at the same mean piston speed and at the same brake mean effective pressure (bmep). The bmep for a four-stroke engine is calculated as follows:

$$bmep = T_e \frac{4\pi}{V_H}$$

where T_e is the engine brake torque. Figure 3 shows the resulting operating points for the three engines. It can clearly be seen that the highly boosted engine 1 is operated with higher specific engine load (i.e., more torque per displacement) than the lower boosted engines 2 and 3.

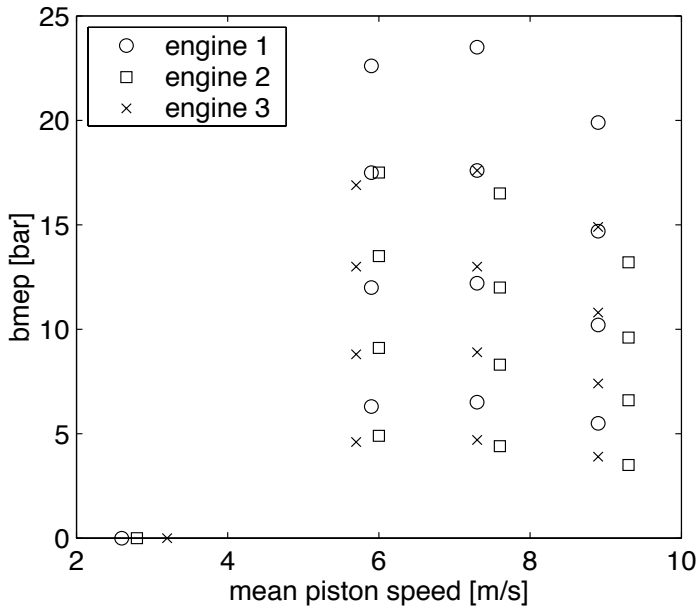

Figure 3: Mean piston speed (mps) and brake mean effective pressure (bmep) for the three engines in the different phases of the ESC.

3 – Results

The engines were warmed up prior to the start of the ESC at speed B and full load until all temperatures and emissions were stabilised. The concentrations of NO_x and NO_2 as well as the exhaust gas temperatures for the ESC measurements of the three engines are plotted in Figure 4. The 13 phases of the ESC are depicted as well (compare with Figure 2). It can clearly be seen, that the NO_x concentrations of engine 1 are the highest for each phase as one would expect because of the higher engine load. When similar operating points are compared (e.g. phase 6 for engine 1 and phase 2 for engine 2 and 3) the NO_x concentrations of all three engines are very alike. An interesting difference can be seen in idle engine operation (phase 1) where the NO_x emissions of engine 2 are clearly lower than for the other engines. Engine 2 is a V6 engine; the others have six cylinders in line. V6 configurations are more problematic regarding vibrations. Therefore, it is likely that engine 2 had different injection timing and thus different combustion behaviour to assure a smooth operation.

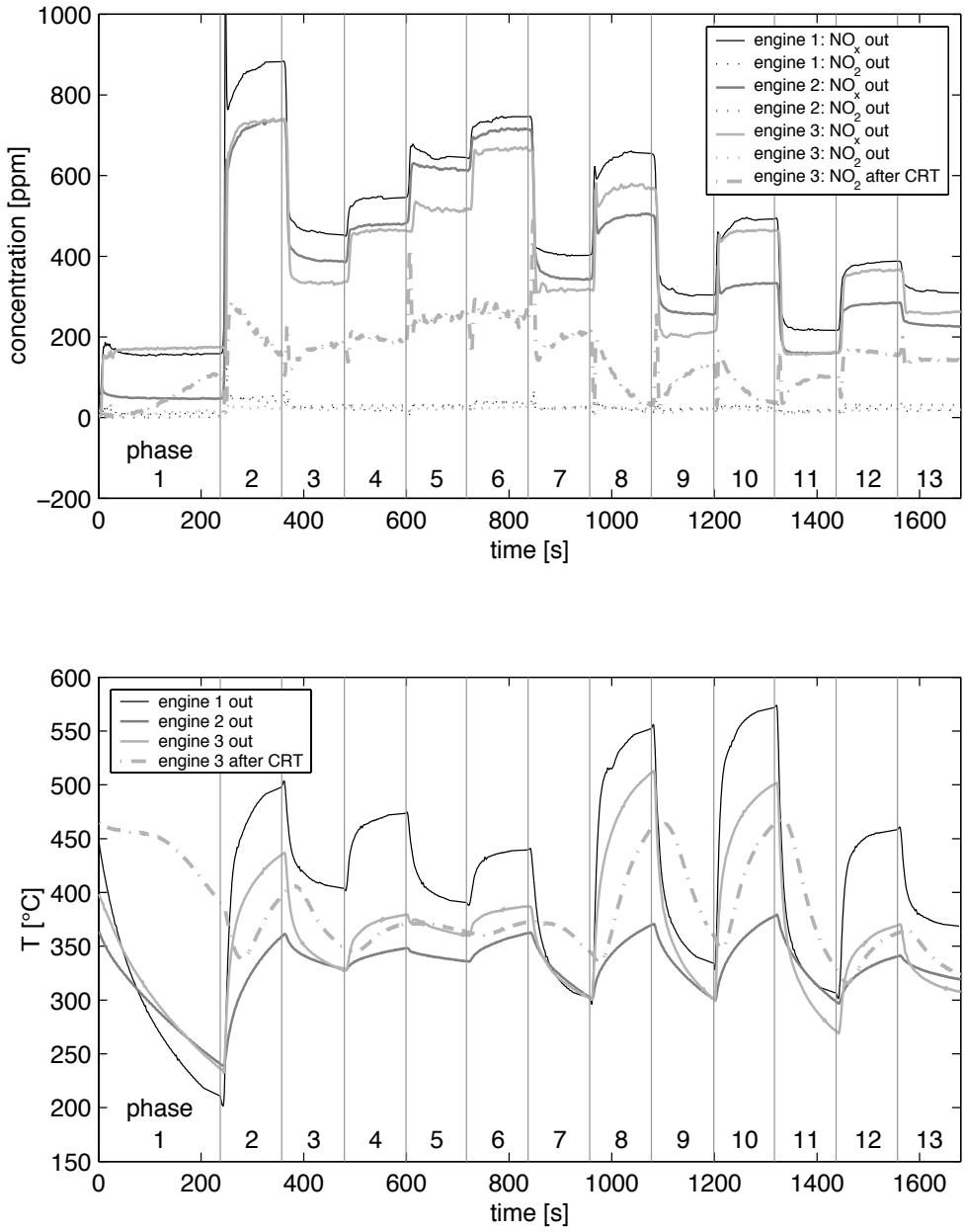

Figure 4: NO_x and NO_2 concentrations and temperatures after turbine and after CRT.

Looking at the exhaust gas temperatures after the turbine, it can be seen that a stationary level is almost never reached within a phase. This is because the whole energy to heat up or cool down the exhaust system (collectors, turbine and connections) has to be balanced via the exhaust gases. However, the NO_x emissions are stabilised faster because the dominant mechanisms depend on the in-cylinder thermodynamics and not on the temperature levels in the exhaust system. Engine 2 has the lowest temperature levels after the turbine. This is because a V6 configuration has a comparatively large exhaust manifold before the turbine that causes comparatively large heat losses.

The NO_2 emissions after the turbine are on a similar low level for all engines. The expected clear influence of the CRT™ system on the NO_2 emissions can be observed: The NO_2 level is much higher after the CRT™ system which indicates a large NO_2-slip in the soot oxidation process.

An inverse dependency of the NO_2 level on the exhaust gas temperature level can be observed: The lower the temperatures, the higher the NO_2 level. The NO_2 concentration fraction versus the exhaust gas temperature after the turbine respectively versus the average temperature between the turbine and after the CRT™ is plotted in Figure 5. Only a weak exothermal NO to NO_2 conversions can be

observed for the engine-out NO_x emissions (small negative slope in the reaction-rate versus temperature plot). The expected exothermal NO to NO_2 conversion in the catalyst of the CRT™ system is very efficient (large negative slope in the reaction-rate versus temperature plot).

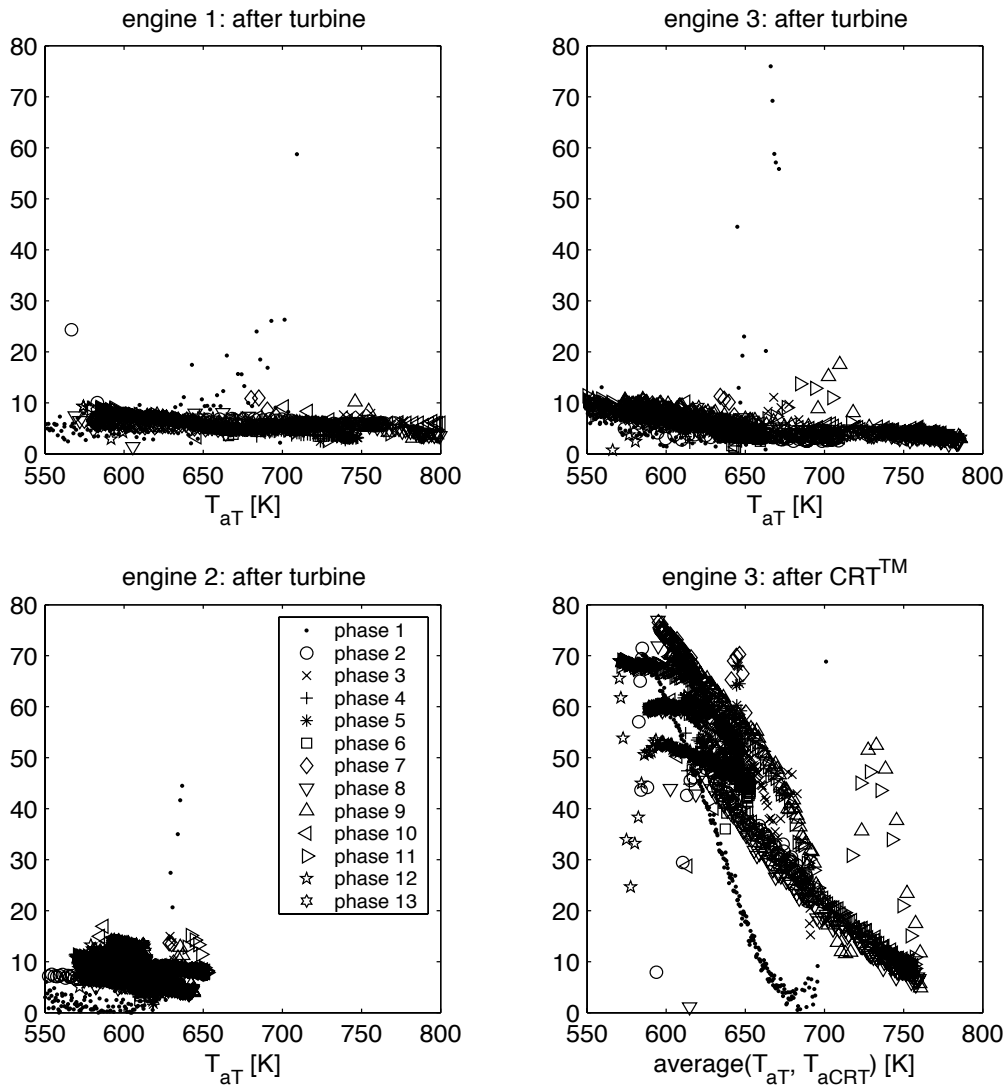

Figure 5: NO_2 concentration fractions versus the exhaust gas temperature after turbine (aT) and after CRT™ (aCRT).

The concentration fractions of NO_2 in the time-domain are plotted in Figure 6. The largest fraction can be observed at the end of phase 7 (speed A, 25 % load) where the NO_2 concentration fraction reaches 77 % (84 mass-%). These numbers are high compared to gasoline engines with three-way catalysts where maximum NO_2 mass fractions of 38 % can be observed, see Soltic and Weilenmann (2001).

	Engine 1 out	**Engine 2 out**	**Engine 3 out**	**Engine 3 after CRT**
Average NO_2 / NO_x concentration	5.9 %	7.1 %	6.1 %	44.1 %
Average NO_2 / NO_x mass	8.8 %	10.5 %	9.0 %	54.7 %

Table 4: Average NO_2 fractions for the whole ESC measurement.

The average NO_2/NO_x values are listed in Table 4. Please note that those numbers do not correspond to the official ESC procedure where only the last 30 seconds of each phase are evaluated but the average presented here is calculated over the whole measurement. The numbers correspond quite

well with numbers from the literature, e.g. from Gibbs (2000) and Grägg (2001).

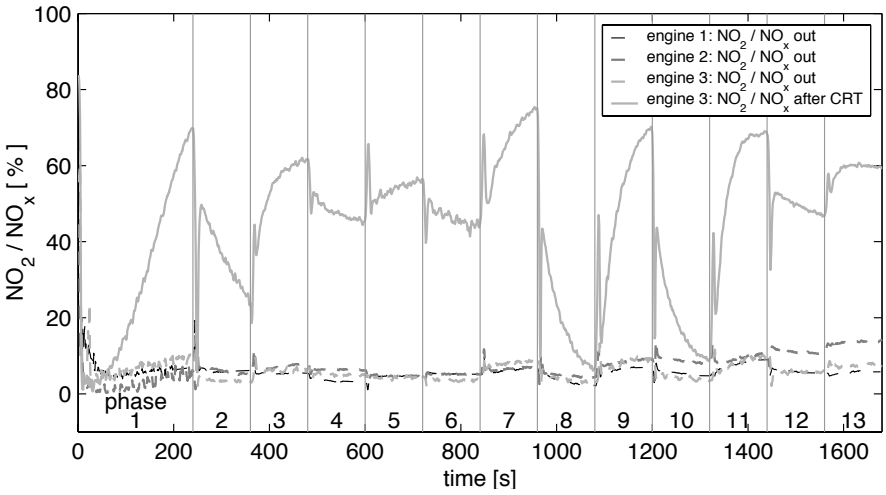

Figure 6: NO_2 concentration fractions for the ESC measurements.

Conclusion

The measurements of three electronically controlled heavy-duty diesel engines of different size, from different manufacturers, with different injection systems, driven with different diesel fuels but all of Euro-3 standard show similar low NO_2 fractions in the raw exhaust gas. The NO_2 fraction is most likely determined by the chemical kinetics during the combustion process and the composition is "frozen" thereafter. The well-known slip of NO_2 in CRT™ systems could be observed where up to 84 mass-percent of the NO_x emissions could be detected being emitted as NO_2. Such high fractions are emitted in conditions where the exhaust gases are comparatively cold. One solution to avoid such high NO_2 fractions could be a better thermal management of the exhaust gases before they reach the CRT™ systems. The measured NO_2 fraction of the Euro-3 engines is similar to the information found in literature for older heavy-duty diesel engines.

Acknowledgments

The authors wish to thank Rolf Ziegler for the excellent test-bench setups and Roland Graf for performing the experiments with great accuracy.

References

Chatterjee S., R. Conway & A. P. Walker (2001): Emission reduction in on-road heavy-duty diesel applications with the continuously regenerating technology (CrtSr) diesel particulate filter, SAE technical paper, 2001-28-0049.

Directive 1999/96/EC of the European Parliament and of the Council of 13 December 1999, Official journal L 044, 16/02/2000, p 1-155.

Soltic P. & M. Weilenmann (2001): Partitioning of NOx emissions for gasoline passenger cars and light duty trucks, Proc. Int. Symp. "Transport and air pollution", Graz, Austria, 19-21 June, 2001, p 49-56.

Gibbs R. (2000): Un-regulated emissions from CRT-equipped transit busses, 6th Diesel Engine Emission Reduction Workshop, San Diego, CA., available from the Energy, Science, & Technology Information Resource – U.S. Department of Energy (DOE) at www.osti.gov.

Grägg K. (2001): Efficiency of a catalytic muffler and CRT™ Systems for heavy duty vehicles, MTC report 511, MTC AB, Box 223, 136 23 Haninge, Sweden.

12th International Symposium "Transport and Air Pollution" / 12e Colloque international "Transports et pollution de l'air", Avignon, 16 -18 *June* / juin 2003
proceedings / actes, n°92, tome / Vol. 2, Inrets ed., Arcueil, France, 2003, p. 233-240

Cold start emission reduction via catalyst bypass

Anastasios Karkanis, Pantelis Botsaris & Panagiotis Sparis
Democritus Univ. of Thrace GR, Electrical & Computer Eng. Dep., Mechanical Eng. Lab.,
67100-GR Xanthi – Greece - Fax +30 25410 79518 - email : ankark@ee.duth.gr

Abstract
The present paper tests a new method for the reduction of pollutant emission during a cold start. The experimental results presented here indicate that there is significant reduction of the pollutant emissions during the cold start of an engine, with an adjustable three-way catalytic converter that reduces the catalyst active surface during start-up. There are strong indications that a quicker warm-up of the catalyst and a faster initiation of catalysis can be achieved by focusing the gas flow towards the center core of the monolith, resulting to a significant reduction of emitted CO and HC. The results of this paper show that at idle speed a reduction of approximately of 30% HC, CO can be achieved. By this method, the remaining ceramic body of the catalytic converter, at the start-up period, is used as a heat insulator.
Keywords: *three-way catalytic converter, emission control, cold-start.*

Résumé
Le papier actuel examine une nouvelle méthode pour la réduction d'émission de polluant pendant une démarrage à froid. Les résultats expérimentaux présentés ici indiquent qu'il y a réduction significative des émissions de polluant pendant la démarrage à froid d'un moteur, avec un convertisseur catalytique à trois voies réglable qui réduit la surface active de catalyseur pendant la mise en train. Il y a des indications fortes qu'un préchauffage plus rapide du catalyseur et un déclenchement plus rapide de catalyse peuvent être réalisé en focalisant l'écoulement de gaz vers le noyau central du monolith, donnant droit à une réduction significative de Co et de HC émis. Les résultats de cette exposition de papier qu'à la vitesse à vide une réduction d'approximativement de 30% HC, Co peut être réalisé. Par cette méthode, le corps en céramique restant du convertisseur catalytique, à la période de mise en train, est employé comme isolateur de la chaleur.
Mots-clefs : *convertisseur catalytique à trois voies - contrôle d'émission - froid-démarrez.*

Introduction

Although the problem of urban air pollution due to vehicle exhausts is still present, it appears that in the last decade it has found a temporary satisfactory answer with the development of the three-way catalysts and the necessary microprocessor controlled fuel injection, ignition and valve timing systems. As a result of this technological progress, the modern cars, as they leave the factory, are capable of a dependable, fuel economic operation with improved power output and largely reduced pollutant emissions. This pollution reduction during normal engine operation conditions amplified the effect of the exhaust gas emissions during cold start that became a considerable portion of the overall pollutant production. Various methods have been proposed that reduce cold start emissions with very good results, but with an increase of installation and operation cost, such as:

The Electrically Heated Catalyst (EHC) method, the Chemically Heated Catalyst (CHC) method, the Electrically Initiate Chemically Heated Catalyst (EICHC) method, the Exhaust Gas Ignition (EGI) method, the Precatalyst method, the Fuel/Air Ratio Variation method, the Ignition Delay method, the Phase-Change Materials method, the Heat Exchanger method and the Hydrocarbons Trapping method.

In this paper a new way of reducing the exhaust gas pollutants during cold start is being tested, that will adjust the area of the chemically active surface in the catalyst according to the volume of the exhaust gases. In this way, during the cold start period, when the engine operates at reduced exhaust gas temperatures and volumes, the catalyst cross section is suitably reduced and matched to the exhaust gas flow.

The advantages of this approach are: (a) The area used for catalysis is small and it can be heated faster than the whole catalyst, and, therefore, catalysis reaches its operating temperatures in a shorter time with considerably smaller delays. (b) The ceramic surrounding cover of the area where catalysis is taking place, and which is the part of the catalyst not reacting at the time, functions as a heat insulator.

Instrumentation and test procedures

The experimental measurements were carried out on a CIVIC coupe model CRX Honda D16Z5 engine. This is a 1590 cm^3 16-valve four-cylinder, multi point injection and variable timing engine with a 130 DIN PS output at 6800 rpm and 14,6 Nm at 5700 rpm. The exhaust pollutants of the engine upstream of the catalyst varied from 0.8% to 1% for the CO and 120ppm to 150ppm for the HC at constant idle speed.

During tests, the catalyst inlet and outlet temperature measurements, the engine water and oil temperature were measured and recorded via the ADVANTECH PCI-1710HG Data Acquisition cart, installed at a Pentium II PC at 266Mhz, with on-board Cold Junction Compensation circuit for direct K-type thermocouple measurement. The thermocouples used have a flexible stainless steel shielding and a 0-1000ºC temperature range with and accuracy of ±0,25ºC.

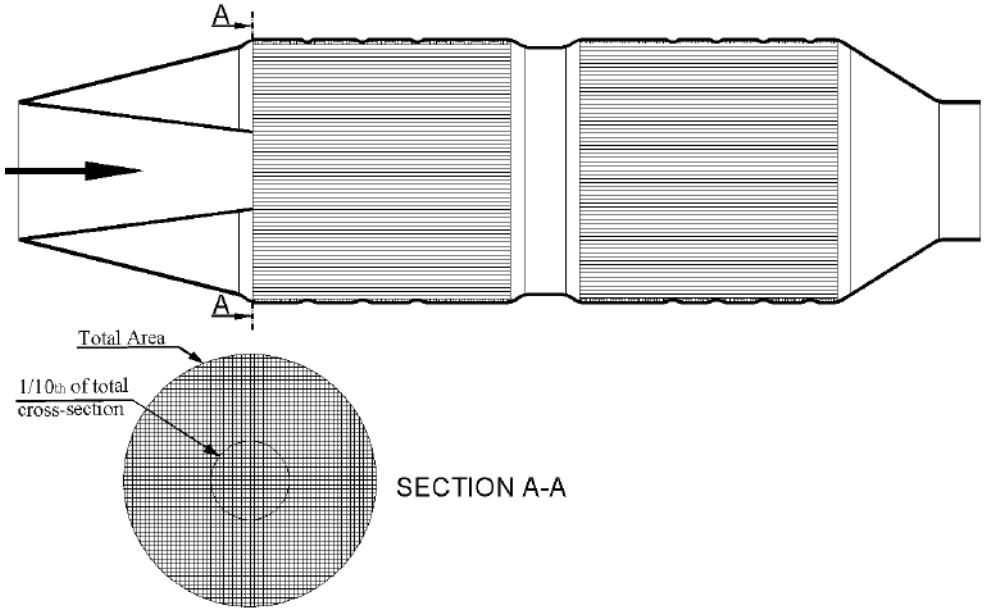

Figure 1: The two piece structure of the catalyst and the cross-section of a partially utilized catalyst is illustrated. In this case only 1/10th of the total cross-section is in the flow of the exhaust gases during start-up

Figure 1: La structure de deux pièces du catalyseur et du catalyseur et la section transversale d'un catalyseur partiellement employé est illustrée. Dans ce cas-ci seulement le 1/10th de toute la section transversale est dans l'écoulement des gaz d'échappement pendant la mise en train.

Also the exhaust gases composition and λ upstream of the catalyst. were measured and recorded via a HORIBA MEXA-574GE analyzer with the following ranges:CO: 0-10% Volume, CO_2: 0-20% Volume,HC: 0-10000 ppm,O_2: 0-25% Volume

There is also a λ computation hardware option, corresponds to the catalyst outlet, using the formula: $\lambda = 2.088 \times A/F\{(100 + 0.4475CO_2 - 0.6075CO - 10HC)/(CO_2 + CO + 10HC)\} / 14.8$

The operating principle of this unit for the CO_2, CO, HC measurements is the Infrared Non Dispersive Spectrometry. The time response for the CO_2, CO, HC measurements is <=10 s. For the O_2 measurement a galvanic type cell is used with a time response of <=25 s. This unit is adequate for the steady state operation measurements required. The unit has a ±2% accuracy and a ±2% repeatability.

For the speed measurements in rpm an ignition pulse detector was used. This particular measuring system and software completed a scanning cycle per channel every 0.1second approximately. It was not considered necessary to measure the back-pressure as shown in this series of experiments.

It should be noted that due to the two brick structure of the catalyst (figure 1), that the vehicle exhaust manufacturer uses, it was impossible to use the full length of its catalytic surface but only its first part (only the front brick was constricted). Therefore, better results could be expected as far as reducing the exhaust pollutants if catalysts with full-length monoliths were used. These catalyst are the one used by the research team at the present time.

Experimental results

During the tests, the engine was starting up cold in room temperature and was working with idle speed, following the cycle curve determined by the ECU program of the manufacturer as indicated in terms of rpm variation in Figure 2. No attempt has been made to alter this schedule at this stage of the development.

The exhaust gas catalysis starts as soon as the upstream temperature reaches approximately the 250 ºC.

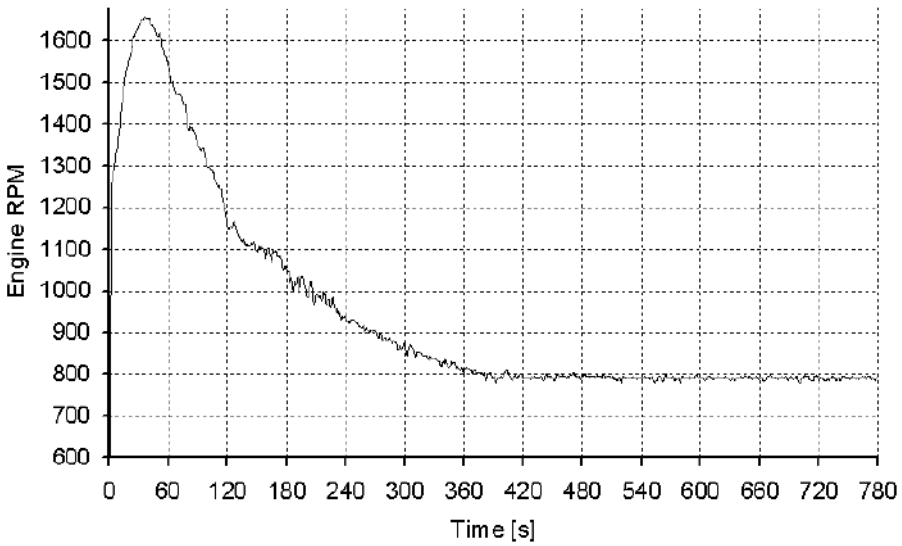

Figure 2 : The rpm variation during cold start.
Figure 2 : Variation de T/MN pendant la démarrage à froid.

When the downstream temperature is about 250 ºC, we can assume that we have catalysis on the whole catalyst surface. So light-off occurs. This behavior is typical for all catalytic engines, but it is possible that it might be altered at a later stage of the system development.

Six sets of experiments were carried out with a minimum number of three repetitions for each set with negligible variations of the data measured. The environmental temperature for all sets of experiments varied from 17 ºC to 25 ºC and the atmospheric pressure from 1002mbar to 1015mbar. Different environmental conditions had little effect on the outcome of the experiments.

The first set of experiments, illustrated in Figure 3, was carried out using the normal catalyst

geometry provided by the car manufacturer without any intervention to the exhaust gas flow. The data measured indicate that the catalyst light off is happening in approximately 220s. The operation of the engine and the inlet and outlet exhaust gas temperatures are stabilized around 265ºC and 305ºC respectively after approximately 6 minutes.

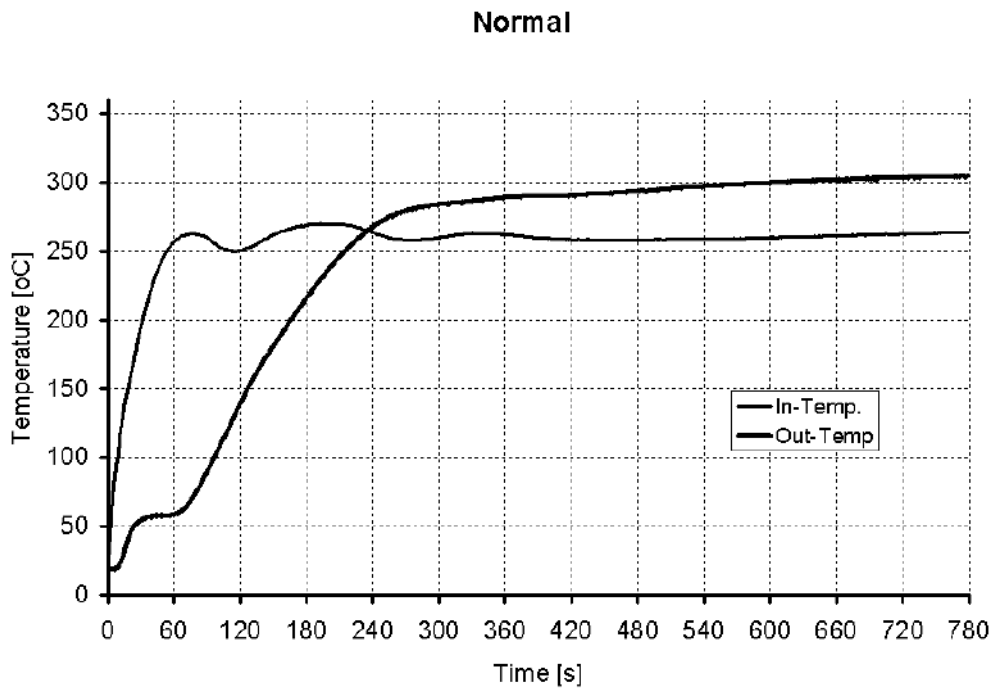

Figure 3: The temperatures before and after the catalyst without any intervention to the exhaust gas flow.

Figure 3 : Températures avant et après catalyseur sans toute interposition à l'écoulement de gaz d'échappement.

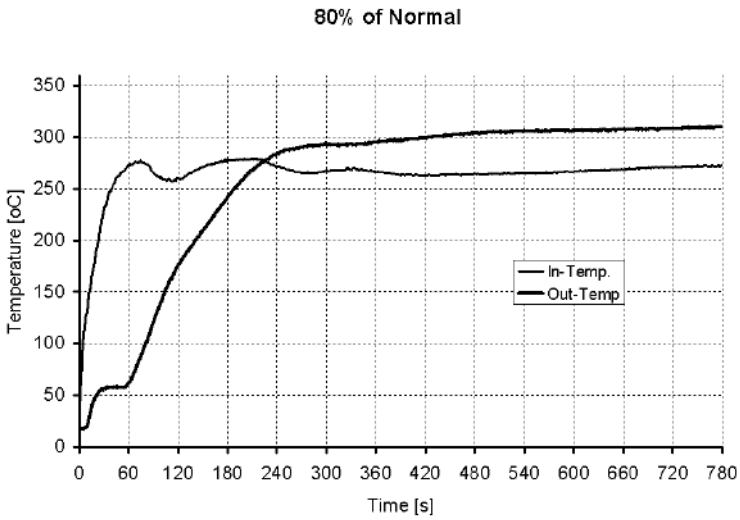

Figure 4: The catalyst temperatures when using the 80% of the Total Catalyst Surface.

Figure 4 : Températures de catalyseur en utilisant 80% de toute la surface de catalyseur.

The reduction of the catalyst cross section was effected by the use of suitable cones that concentrated the gas flow onto the catalyst central core forcing the exhaust gas to pass through the 80%, 40%, 20%, 10% and 5% of the Total Catalyst Surface (TCS). Naturally, when the system is fully realized, an appropriate servomechanism will carry out the flow adjustments.

In the figures 4, through 8 the corresponding inlet, outlet temperature variation are illustrated for the cases of 80%, 40%, 20%, 10%, 5% respectively.

During these sets of experiments, where the total amount of exhaust gas was forced to pass through the corresponding ratios of TCS, it was ascertained that the catalyst's light off was happening at

approximately 190s, 150s, 110s, 90s and 80s respectively.

As shown in figures 4 through 8 the inlet and outlet temperatures were stabilized respectively at:

for 80% of TCS,	for 40% of TCS,	for 20% of TCS,	for 10% of TCS,	for 5% of TCS
270ºC and 310ºC	270ºC and 320ºC	270ºC and 335ºC	280ºC and 355ºC	285ºC and 330ºC

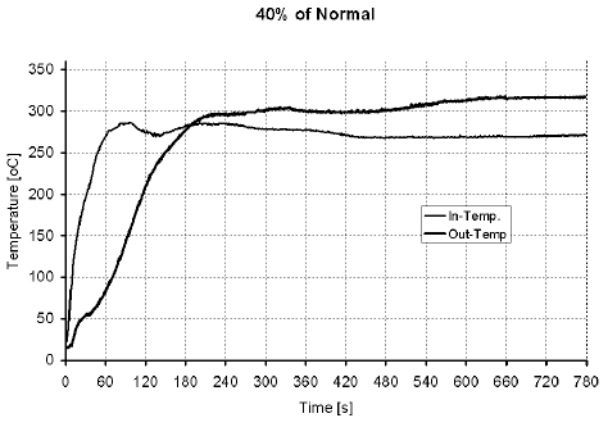

Figure 5: The catalyst temperatures when using 40% of the Total Catalyst Surface.

Figure 5 : Températures de catalyseur en utilisant 40% de toute la surface de catalys.Eur.

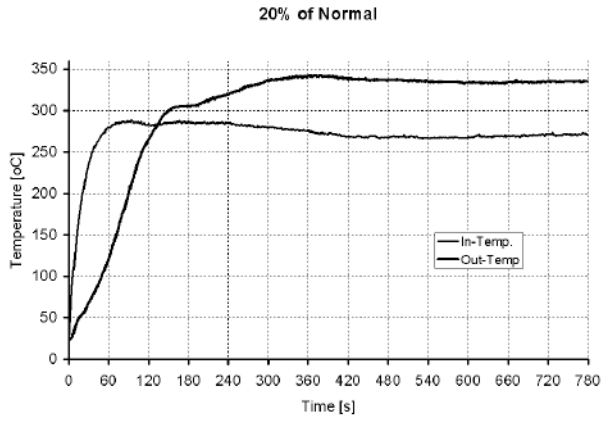

Figure 6 The catalyst temperatures when using the 20% of the Total Catalyst Surface.

Figure 6 : Températures de catalyseur en utilisant 20% de toute la surface de catalyseur.

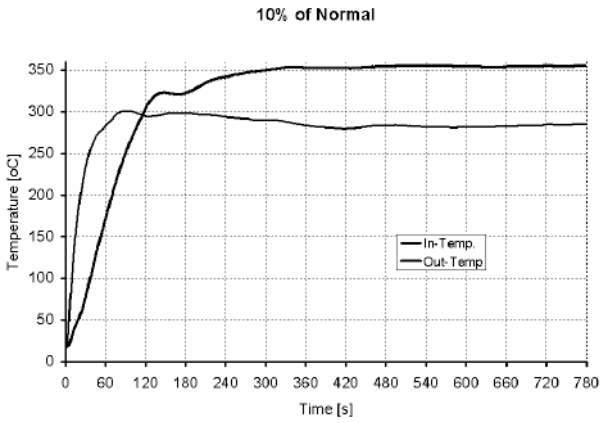

Figure 7: The catalyst temperatures when using the 10% of the Total Catalyst Surface.

Figure 7 : Températures de catalyseur en utilisant 10% de toute la surface de catalys.Eur.

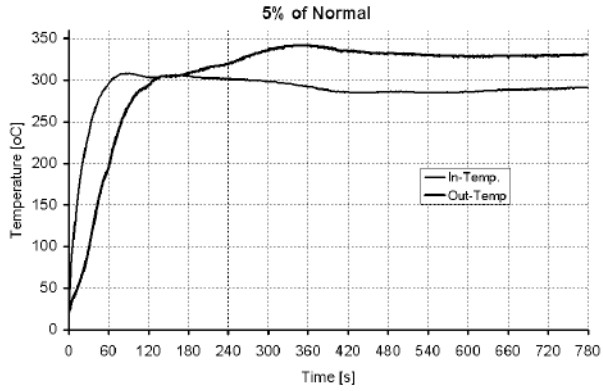

Figure 8: The catalyst temperatures when using the 5% of the Total Catalyst Surface.

Figure 8 : Températures de catalyseur en utilisant 5% de toute la surface de catalyseur.

At this series of experiments the upstream temperature shows that the exhaust gases could pass through the smaller section of the catalyst with no problem, as it was done without the constriction, until the 20% of TCS. At 10% and 5% of the TCS there is a gradient increase of the upstream temperature. This increase is a sign of increased back-pressure at those sections, since the gas flow was the same in all cases.

From the above data it is clear that as the rate of contraction increases, the exhaust gas temperature at the exit tends also to increase, a fact that indicates an improvement of catalytic efficiency. However, with the excessive constriction of the flow to just 5% of normal the exit temperature reverses trend and this is a clear sign of catalysis efficiency deterioration.

By comparing those sets of curves, it is clear that when using a part of the catalyst's surface during cold start, the light-off catalysis occurs considerably sooner.

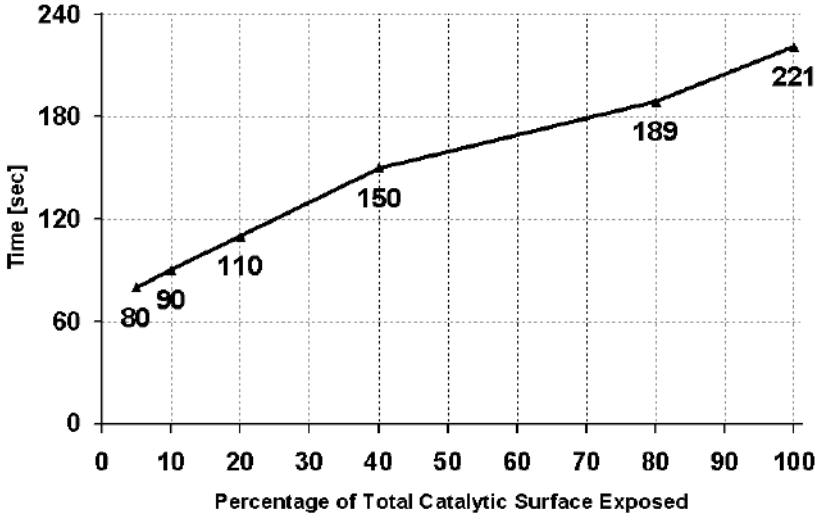

Figure 9: The light-off delay is plotted versus the percentage of the active catalytic surface.
Figure 9 : L'allumage retardé en fonction du pourcentage de la surface catalytique active.

In the case of 20% of TCS, the maximum overall reduction is of the order of 50% (110 vs 221 seconds). In the case of even greater constrictions the light off time reduced, but the gas velocity through the catalyst become so great that a large mass of gas is "breaking through" unconverted by catalysis.

In figures 10, 11 the HC, CO content of the exhaust gases is illustrated respectively for all the tests. During the initial 180s there is a confusing mixing of the corresponding curves for each case. This is the result of random effects, as ignition delays, catalyst contamination, etc. that temporary increased the fuel/air ratio during start-up. Nevertheless, after this period the beneficial effect of flow constriction is evident.

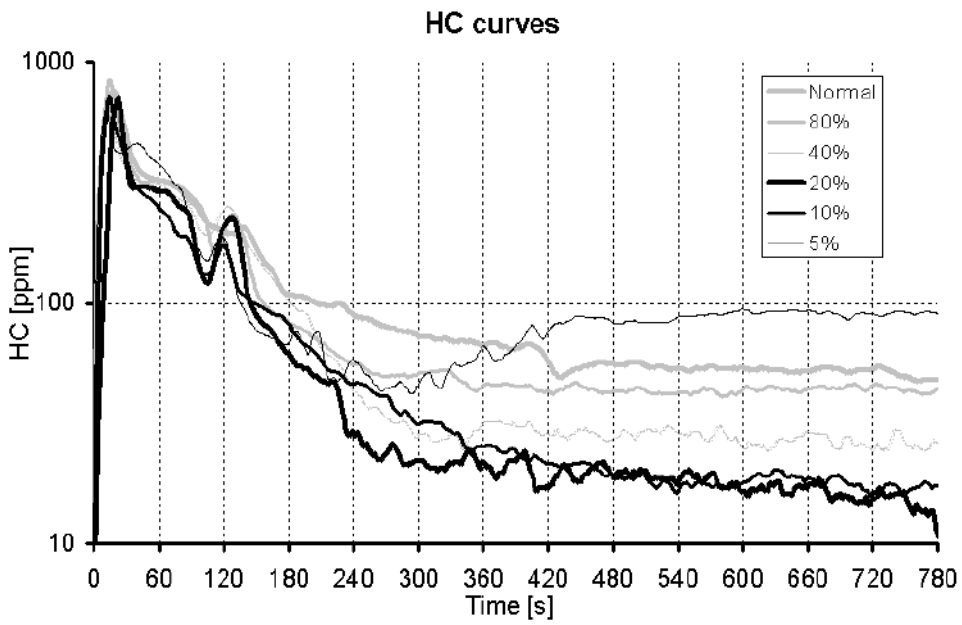

Figure 10 : The HC content of the exhaust gases.
Figure 10 : Teneur en HC des gaz d'échappement

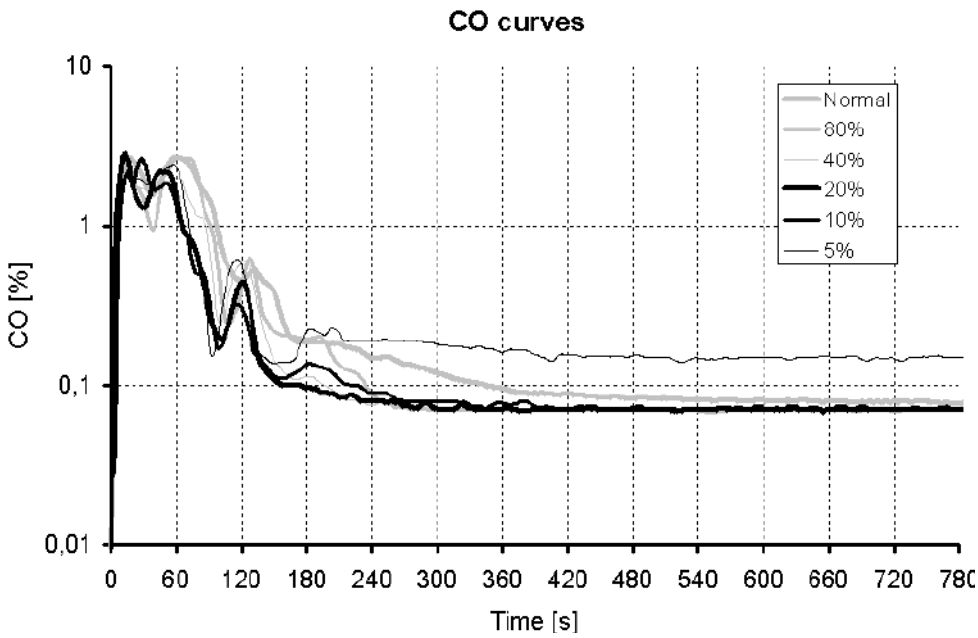

Figure 11: The CO content of the exhaust gases
Figure 11: Teneur en CO des gaz d'échappement

Comparing those sets of curves, it is clear that when using a part of the catalyst's surface during cold start, the amount of the exhaust pollutants HC, CO is reduced, except in case of the 5% of TCS where a considerable increase is noted, especially for the HC. It is clear that in case of the 5% of TCS the catalytic surface is excessively reduced, so there is a detrimental effect on the catalysis efficiency due to "break through".

It should also be noticed that in the case of CO (fig. 11) after 360s all curves except 5%, tend to approximately 0.07%. On the other hand, in the case of HC (fig. 10) the effect of constriction is permanent.

Conclusion

A new idea for reducing the emitted pollutants in exhaust gas during an engine's cold start is presented in this paper. The experimental results have shown that, during the cold start of an engine, if the central core of the catalysts' surface is used, then the process of the catalysis starts sooner and there is a significant reduction of emitted CO and HC. The results of this paper show that at idle speed a reduction of approximately 30% of HC, CO can be achieved after 6 minutes from the ignition of the engine by constricting the flow to the 10-20% of the total catalyst surface.

The back-pressure effect seams to occur for constrictions more than 20%. This phenomenon is under research in other set of experiments that made with a vehicle driven on Europe ECE-15 cycle.

Further more, it is important to note that the use of the proposed method for the reduction of the time required to reach the light-off point can be used in combination with any other method to that effect (EHC, CHC, EICHC, EGI, etc.).

References

Bissett and Oh (1999) "Electrically heated converters for automotive emission control: determination of the best size regime for the heated element", Chemical Engineering Science 54 p 3957-3966

Crane at all (1997) "Reduced Cold-Start Emissions Using Rapid Exhaust Port Oxidation (REPO) in a Spark-Ignition Engine", SAE Paper 970264.

Drake et all (1996) "Effect of Fuel/Air Variation on Catalyst Performance and Hydrocarbon Emissions During Cold-Star and Warm-Up, Society of Automotive Engineers, Inc, SAE paper No 962075.

Golben et all (1997) "Hydride-based cold-start heater for automotive catalyst", Journal of Alloys and Compounds 253-254, p 686-688.

Ichikawa et all (1999) "Development of Low Light-off Three Way Catalyst", SAE Paper 99010307.

Kirchner and Eigenberger (1996) "Optimization of the cold-start behaviour of automotive catalysts using an electrically heated pre-ctalyst", Chemical Engineering Science, Vol. 51, No 10, p 2409-2418.

Korin et all (1998) "Improving Cold-Start Functioning of Catalytic Converters by Using Phase-Change Materials", Society of Automotive Engineers, Inc, SAE paper No 980671.

Lafyatis et all (1998) "Ambient temperature light-off for automobile emission control", Applied Catalysis B: Environmental 18, p 123-135.

Laing (1994) "Development of an Alternator-Powered Electrically-Heated Catalyst System", Society of Automotive Engineers, Inc, SAE paper No 941042.

Langen et all (1994) "Heated Catalytic Converter Competing Technologies to Meet LEV Emission Standards", SAE Paper 940470.

Murphy et all (1999) "Electrically Initiated Chemically Heated Catalytic Converter to Reduce Cold-Start Emissions from Automobiles", Society of Automotive Engineers, Inc, SAE paper No 1999-01-1233.

Nishizawa et all (1997) "Technologies for Reducing Cold-Star Emissions of V6 ULEVs", SAE Paper 971022.

Roychoudhury et all (1994) "Fast Lightoff Non-Electrically and Electrically Heated Microlith Catalytic Converter", Society of Automotive Engineers, Inc, SAE paper No 940467.

Roychoudhury et all (1997) "Development and Performance of Microlith™ Light-Off Preconverters for LEV/ULEV", Society of Automotive Engineers, Inc, SAE paper No 971023.

Shimasaki et all (1997) "Development of Extruded Electrically Heated Catalyst System for ULEV Standards", Society of Automotive Engineers, Inc, SAE paper No 971031.

Umehara et all (1997a) "Advanced Ceramic Substrate: Catalytic Performance Improvement by High Geometric Surface Area and Low Heat Capacity", SAE Paper 97102.

Umehara et all (1997b) "HC reduction system for cold start and warm-up phases – Improvement of catalyst warm-up by retarded ingnition", Technical Notes / JSAE Review 18, p 67-68

Yaegashi et all (1994) "New Technology for Reducing the Power Consumption of Electrically Heated Catalysts", Society of Automotive Engineers, Inc, SAE paper No 940464.

12th International Symposium "Transport and Air Pollution" / 12e Colloque international "Transports et pollution de l'air", Avignon, 16 -18 *June* / juin 2003
proceedings / actes, n°92, tome / Vol. 2, Inrets ed., Arcueil, France, 2003, p. -

On Board Diagnostics System of Oxygen Sensor Malfunction, Meeting OBD II Requirements

Eugene Golgotiu & Radu Drosescu
*Internal Combustion Engine & Automotive Department, Technical University "Gh. Asachi", 60 av. D. Mangeron, 6600, Iasi, Romania - Tel/Fax: +40.232.232337, email: egolgoti@mec.tuiasi.ro

Abstract
The OBD II regulation requires for a diagnostic system of an oxygen sensor, to monitor the output voltage, response rate, and any other parameter of the sensor that can give us information about his state. For a heated oxygen sensors (Lambda probe), the heater circuit must be checked when the current or voltage drop within the circuit deteriorates below the manufacturer's specifications for a proper operation. The algorithm studied in this paper detects an oxygen sensor's fault, measuring directly or indirectly the internal resistance of the sensor and comparing with a predetermined value. The paper presets a method able to evaluate this huge value of the internal resistance using an external voltage applied to the sensor and a high input impedance operational amplifier connected like an impedance converter between sensor and acquisition circuitry. This method able us to test the lambda sensor immediately after a cold start and in the same time it gives the possibility to measure, indirectly, the sensor temperature.
Key words: *OBD, lambda probe, lambda probe temperature, and oxygen sensor.*

Introduction

For most emission control system and components, the OBD II regulation requires malfunctions to be identified before any problem becomes serious enough to cause emission exceed the standards by more than 50 percent (i.e., when emissions exceed 1.5 times the standards). Since the oxygen sensor is a critical component of a vehicle's fuel and emission controls, the proper monitoring and diagnosis must be assured for most of operating conditions in order to maintain low emissions. Oxygen sensor's faults are generally one of the most difficult faults to diagnose and repair because of the substantial number of possible causes of these faults. The readiness operation estate of the lambda probe must be checked not only during normal operation, but also during the warming-up phase.

Ordinary gasoline engines work at best efficiencies when the air/fuel ratio approximates the stoichiometric ratio, i.e. 14.65 – 14.7 by weight. The employment of the stoichiometric air/fuel ratio is advantageous also to the proper function of so-called, three-way catalyst, which can promote not only the oxidation of carbon monoxide CO and hydrocarbons HC but also the reduction of oxides of nitrogen NO_x in the exhaust gas of the engine. At this ratio, the noxious components in the exhaust gases of automotive engines may, for example, be converted to harmless compound such as CO_2, nitrogen, and water, by exposing the exhaust gases to after-burning by conducting the exhaust gases through a catalyst at temperatures above 300°C.

The deviation of the air/fuel mixture from the stoichiometric ratio is commonly indicated by the term excess air factor λ, which is the ratio of the amount of air in the combustible mixture to that in the stoichiometric mixture of the same components. Accordingly, the value of λ is larger than 1.0 for a lean mixture and smaller than 1.0 for a rich mixture.

1. Oxygen sensor used in automotive field

There are primarily two types of oxygen sensors available that differ in price and performances. First sensor type, the exhaust gas oxygen (EGO) is a discrete sensor, with switching point around the stoichiometric value, (see Fig. 1). It gives a high voltage signal ($0.85 \approx 1$ V) when $\lambda < 1$ and a low voltage signal ($0.1 \approx 0{,}2$ V) when $\lambda > 1$. Since the EGO signal behaves like a relay we can only sense a lean or a rich air fuel mixture. Almost every modern SI engine equipped automotive uses an EGO sensor because it gives acceptable performance at a low cost.

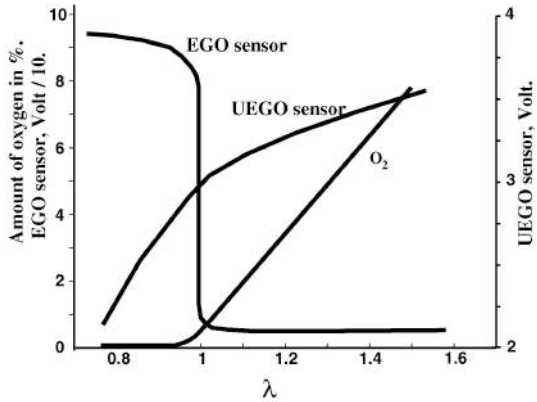

Figure 1: Characteristics for EGO and UEGO sensors related to the oxygen contents

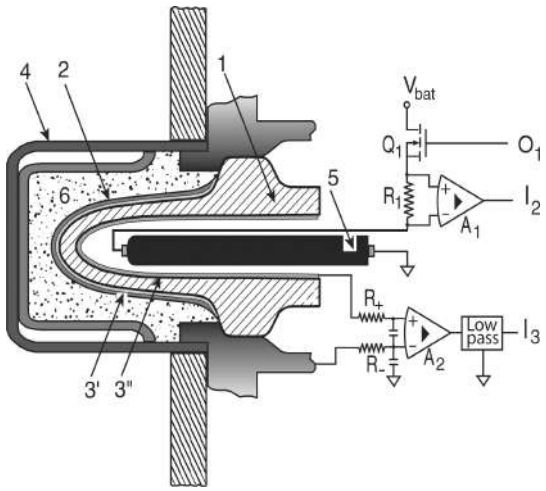

Figure 2: HEGO basic cell; 1- ion-conducting solid electrolyte; 2- porous protective coating, 3',3" – porous platinum electrode layers, 4- external protective tube with slots, 5- heater, 6- exhaust gases

There are two basic types of EGO sensors. One type is the potentiometric sensor, also known as the lambda sensor, which is well known and the details of which are described, for example in the referenced literature. Another type of EGO sensor is the limit-current type sensor patented by Bosch, Dietz et al. (1997) .

The other sensor type is the universal exhaust gas oxygen (UEGO) sensor. We note that it has a continuous behavior, and it is possible to measure an absolute lambda value over the whole engine operating range ($0.8 < \lambda < 1.3$).

Both EGO and UEGO sensors need an operating temperature above 350°C. Most of today sensors are preheated (HEGO, HUEGO), but it's still one of the reasons to use open loop control during starts.

2. EGO, HEGO model

Most of the EGO sensors use a solid electrolyte that responds to the oxygen concentration of a gas with respect to a reference oxygen concentration, for example free air. In one such structure, a voltage is generated which depends on whether the sensor senses oxygen or not. The structure of a such kind of sensor, (see Fig. 2), includes a solid electrolyte 1, which has a gas permeable (porous) measuring electrode applied to one face, 3', usually the face exposed to the gas to be tested, 6; the other face of the solid electrolyte has a permeable reference electrode, 3", which is exposed to the reference gas of known oxygen concentration (free air). The solid electrolyte having ion conductive proprieties is sandwiched between the two electrodes.

When a gas mixture such as an engine exhaust gas, 6, is present on one side of the sensor and a

reference gas such as air is present on the other side, the electromotive force, U_λ, across the sensor depends on the ratio of the oxygen partial pressure of electromotive force depends not only on the the reference gas to that of the gas mixture. The mixture concentration, λ, but also on the sensor temperature, T_λ. Because the temperature of the exhaust gas of the engine corresponds to the temperature of the sensor element, and the response time of the oxygen sensor is not better than 40-50 ms (at 650 °C), we have used a K thermocouple to measure T_λ.

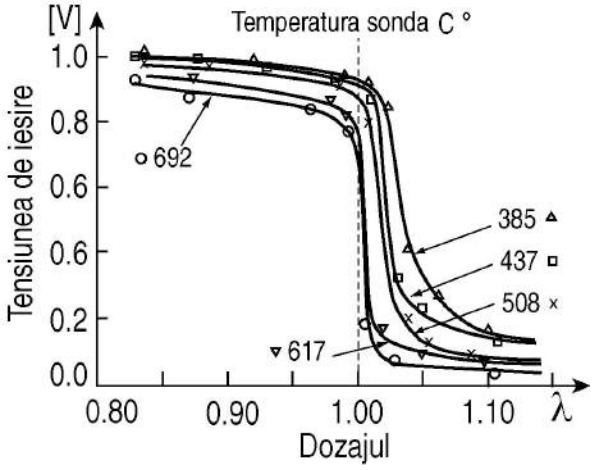

Figure 3: Experimental measurements points and theoretical curves for the output voltage of the oxygen sensor

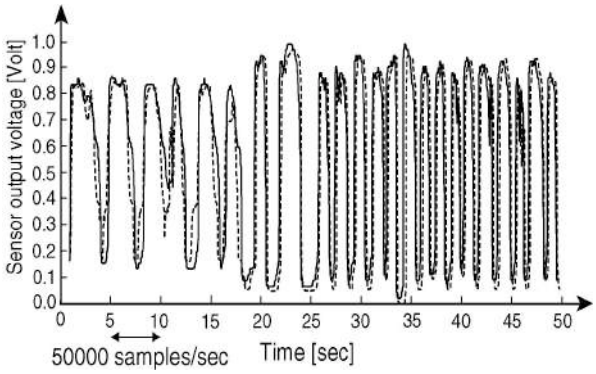

Figure 4: Theoretical curves (dashed line) and corresponding measured curves (continuous line)

The steady state measurements of voltage curves for a Bosch sensor are shown in Fig. 3. A National Instruments data acquisition board PCI-6052E has been used to control the heater and acquire data from the sensors. The interfaces and signal conditioning electronics are implemented by the author in order to offer good evaluations of used variables and to achieve the various test algorithms

Mathematical models for an oxygen sensor are well known, Fleming (1977), Fleming (1978) or Voltz et al. (1973). However, the mathematical relation of the sensor output voltage was estimated by curve fitting to the voltage data measured for different λ values. For reference λ values, a Bosch UEGO probe, LSM 11 was used in parallel with the HEGO sensor.

Estimated values (dotted line), and measured points (continuous curves) for the output voltage of the O_2 sensor are shown in Fig. 4. Because of the curve fitting procedure which was used, theoretical curves match with a good approximation the corresponding experimental curves.

For the auto-diagnosis algorithms, a simplified equivalent circuit of a zirconia solid electrolyte oxygen sensor is shown in Fig. 5. With a good approximation, the oxygen sensor may be represented as an equivalent circuit including an internal electromotive force potential U_λ which is dependent on the temperature of the exhaust gas, connected in series with a temperature dependent resistor, R_λ. The output voltage of the oxygen sensor, U_s shown in Fig. 3, must not be confused with the electromotive force U_λ. If R_{ex} denotes the input impedance of the control circuit which processes the output voltage of the O_2 sensor, and U_b is an external bias voltage, then:

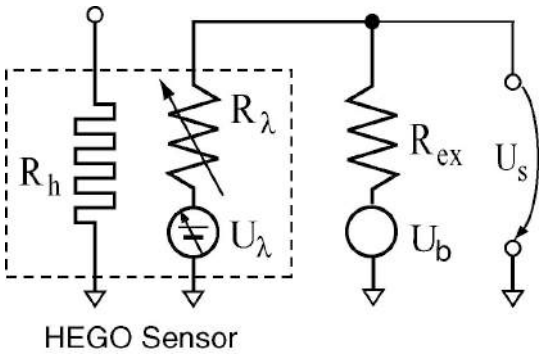

Figure 5: Simplified equivalent circuit of the HEGO sensor

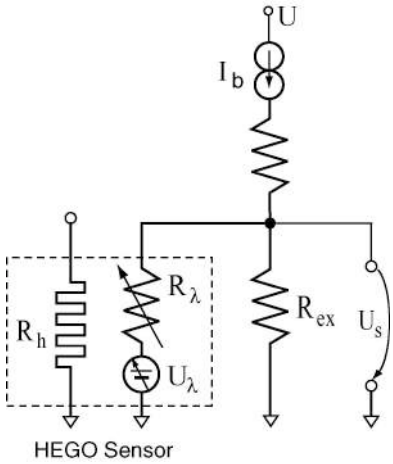

Figure 6: Biasing oxygen sensor with a constant current

$$U_s = \frac{U_\lambda \cdot R_{ex} + U_b \cdot R_\lambda}{R_\lambda + R_{ex}} \quad (1)$$

If U_b=0, then:

$$U_s = \frac{U_\lambda \cdot R_{ex}}{R_\lambda + R_{ex}} \quad (2)$$

Only when R_{ex} is very high (open circuit or $R_{ex} > 10^9\ \Omega$) we have: $U_\lambda = U_s$. An O_2 sensor can be bias not only with a voltage source, but also with a current source as is shown in Fig. 6. Using the superposition principle, the sensor output voltage, U_s results from the equation:

$$U_s = \frac{R_{ex}}{R_\lambda + R_{ex}} \cdot \left(U_\lambda + I_b \cdot R_\lambda\right) \quad (3)$$

$$U_s = U_\lambda + I_b \cdot R_\lambda \quad (4)$$

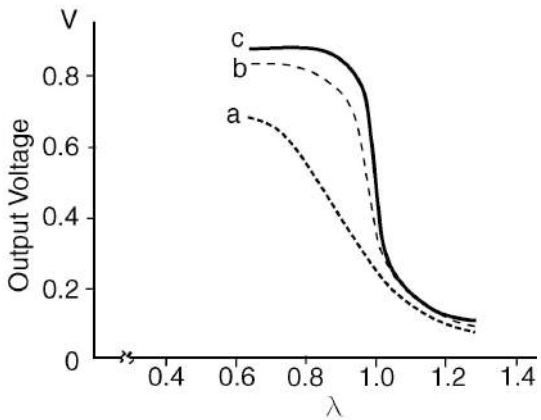

Figure 7: Characteristic curves of an output voltage relative to A/F of the O_2 sensor in a normally state, b and wear state, a or c.

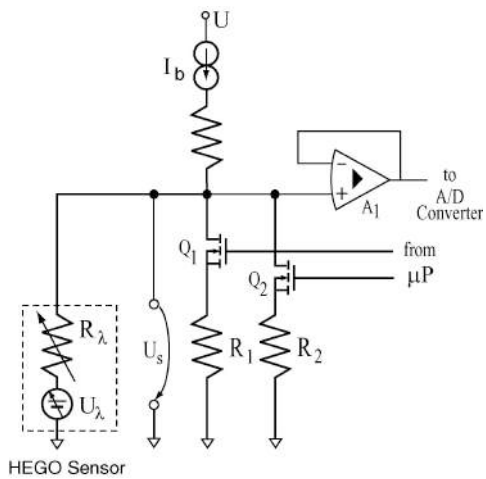

Figure 8: Internal resistance measurement circuit

It is obvious that when the O_2 sensor is interfaced with high impedance amplifier ($R_{ex} > 10^9\ \Omega$), the voltage developed across its internal impedance represents a DC voltage, which is (4). Without a properly biasing of an oxygen sensor it is very difficult to make good measurements of the sensor internal impedance versus temperature, or to use the sensor output voltage for a control process.

The internal resistance can vary from less than 100 Ω at 800°C, to 10-15 MΩ at 200°C depending on the temperature of the sensor element. A cold sensor has a very high internal resistance, which drastically decreases once the sensor reaches an operating temperature about 300 °C, the heating

time dependent on engine operating conditions and also on engine temperature (ex. 20-30 sec). *If the exhaust gas electrode does not promote chemical reactions, for example due to a high internal resistance, the gas composition detected at the electrode will not bear a reliable relationship to engine air-fuel ratio*. During this warm-up period, the engine operates in an open loop where data from the sensor is not used to regulate the fuel mixture. The heater brings the sensor to its operating temperature faster than it would if heated by the engine exhaust gases alone.

3. Testing methods of EGO, HEGO sensor

The hostile environment of the hot, corrosive and fast flowing exhaust gases causes wear on the portion of the O_2 sensor exposed to such gases. As a result, the electromotive force of the sensor will decrease accordingly. When U_λ decreases, the output voltage, U_s, of the O_2 sensor is reduced as result from relation (2) or (3). The output voltage of the sensor is shown by the characteristic curve **a** (see Fig. 7) and it can be seen that the air-fuel ratio, A/F, deviates to the smaller side toward rich mixture ($\lambda<1$).

When the current flows out of the O_2 sensor, the output voltage U_s decreases as the internal resistance R_λ increases as shown by the characteristic curve **a** (see Fig. 7) and the A/F deviates to rich side. Conversely, when the current I_b flows into the O_2 sensor, Fig. 6, the output voltage U_s increase as the internal resistance R_λ increases (4) as shown by a characteristic curve **c** (see Fig.7) and the A/F deviates to the leaner side ($\lambda>1$).

The restoration of the internal impedance of the sensor to the original internal impedance of the sensor when new, such as by injecting a bias current or as by using heating means to increase the temperature of the sensor until the desired internal impedance is reached, may have the beneficial results of restoring the original response time. Thus, the internal impedance of such a sensor is found to be a good indication of the sensor deterioration state Fig. 8 shows a partial circuit diagram used to measure the impedance of an O_2 sensor. In fact, it represents the basic circuit (see Fig. 8) provided with two switches, Q_1 and Q_2 to modify the external impedance of the O_2 sensor. On the first step, transistor Q_1 is saturated and Q_2 turn off so that the external impedance is given by R_1.

Accordingly with relation (3), the voltage measured from the A/D converter, U_1 is given by the equation (5).

$$U_1 = \frac{R_1}{R_\lambda + R_1} \cdot \left(U_\lambda + I_b \cdot R_\lambda\right) \quad (5)$$

On the next step, the transistor Q_2 is saturated so that the sensor gives a decreases impedance formed by $R_1 \parallel R_2$. The sensor output measured with the A/D converter, U_2 results from the relation (6).

$$U_2 = \frac{R_1 \parallel R_2}{R_\lambda + R_1 \parallel R_2} \cdot \left(U_\lambda + I_b \cdot R_\lambda\right) \quad (6)$$

The sensor resistance results from relations (5), respectively (6), and it is proportional with the difference of the two voltages (7).

$$R_\lambda = \Delta U \cdot \frac{R_2}{U_1 - \left(1 + \frac{R_2}{R_1}\right) \cdot \Delta U} \quad (7)$$

$$\Delta U = U_1 - U_2$$

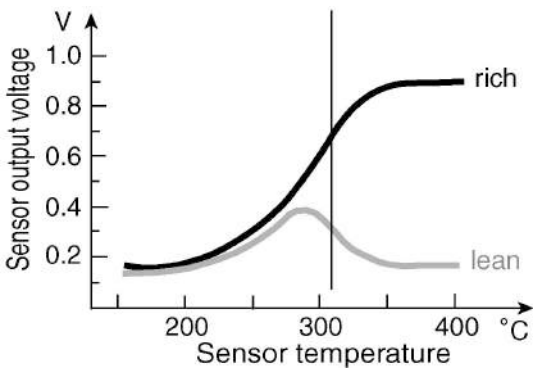

Figure 9: Electromotive force of the O_2 sensor for rich and lean mixtures as a temperature function

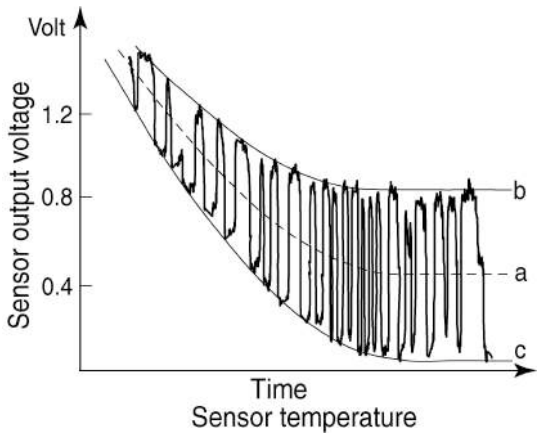

Figure 10: Sensor output voltage amplitude depending on temperature

This absolute sensor impedance is useful in monitoring changes in the sensor resistance with the aging of the sensor, for possible recalibration or early detection of approaching failure.

The above circuit is also useful in order to extend the operating range of the exhaust gas sensor to low temperatures. When a bias current, I_b is injected into the O_2 sensor, the voltage developed across its internal resistance represents a DC voltage, which is given by relation (4). Since U_λ takes on the high and low voltage levels in response to rich and lean mixtures conditions (see Fig. 9), and the internal resistance decreases with the temperature and hence with the time, the output voltage of the O_2 sensor adopts a curve **b** which is an envelope of the maximum peak values representing rich mixtures and a curve **c** which is an envelope of the minimum peak values representing lean mixtures, (see Fig. 10). When the resistance of the sensor is greater than a predetermined value, a bias current is injected in order to force the output voltage of the sensor to vary and to adopt the curve **a** (see Fig. 10).

Conclusions

Determining the internal resistance of an O_2 sensor may be a precise method used to recognize its non-operational (not readiness) or its wearing state. The indirect measurement of the internal resistance was achieved by feeding to the sensor a bias current of a suitable and well defined magnitude, thereby producing a voltage drop across the sensor which will normally be substantially larger than the threshold voltage and hence can be appropriately interpreted. Because it does not affect the primary control function of the lambda probe, this method can be implemented like an auto-diagnose method for an OBD II system.

References

H. Dietz et al. (1997), "Electrochemical Sensors for the Analysis of Gases", Bosch Technical Report, Stuttgart.

W. Fleming, (1977) "Device Model of the Zirconia Oxygen Sensor, "SAE Paper 770400, Automotive Engineering Congress, Detroit.

W. Fleming, (1978) "Physical Principles Governing Nonideal Behavior of the Zirconia Oxygen Sensor," J. Electrochemical Society, Vol. 124, No.1, 1978

S. Voltz, C., Morgan, et al. (1973) "Kinetic Study of Carbon Monoxide and Propylene Oxidation of Platinum Catalysts", Ind. Engr. Chem. Prod. Res. Devlop, Vol. 12, No.4, pp. 294-301.

12th International Symposium "Transport and Air Pollution" / 12e Colloque international "Transports et pollution de l'air", Avignon, 16 -18 *June* / juin 2003
proceedings / actes, n°92, tome / Vol. 2, Inrets ed., Arcueil, France, 2003, p. 247-252

Conversion Capability Estimation Method of an Automotive Catalytic Converter

Radu Drosescu & Eugene Golgotiu
*Internal Combustion Engine & Automotive Department, Technical University "Gh. Asachi", 60 av. D. Mangeron, 6600, Iasi, Romania - Tel/Fax: +40.232.232337, email: egolgoti@mec.tuiasi.ro

Abstract
This paper presents a method able to estimate the mass of the oxygen gas flowing through the catalyst. The oxygen storage capacity of the catalyzer is a measure of its exhaust gas oxidation capability, and thereby an accurate determination of the catalyzer conversion efficiency. In practice, the oxygen storage capacity is the main parameter for a correct appreciation of the catalyst deterioration degree and aging status. If the catalyst is not able to retain the oxygen from exhaust gas flow, the conversion of pollutant substances cannot be made, and the efficiency of the catalyst converter is compromised.
The oxygen storage capacity of the catalyst can be appreciated by computing the times integrals of the product between the gas mass flow and the control lambda value, respectively the time integrals of the product between the gas mass flow and the control lambda value. The measure of the deterioration of the catalyst is given by the difference between the two integrals or the ratio of the integrals can be used .
Key Words: *TWC, catalytic converter, oxygen storage, lambda sensor, catalyst deterioration.*

Introduction

A conversion catalyst in good state has a big oxygen storage capacity. The oxygen comes from the exhaust gases, if the air / fuel ratio is lean. This oxygen, stored in his volume, is release when the air - fuel mixture is richer and a plus of oxygen it is needed to complete the oxidation of the exhaust gas pollutant, especially CO and HC.

The modern self-diagnosis on board device (OBD) is able to determine the state of the catalytic converter using the ratio or the difference between the DC output voltage of two lambda sensors placed one up-stream from the catalytic converter and one down-stream. The first lambda sensor (the control sensor) is part of the automatic loop-control that corrects the fuel quantity delivered to the engine, depending on the oxygen content in the exhaust gases. The second is the test sensor of the converter (see Fig. 1). His roll is to establish the amount of oxygen in the exhaust gases after the converter. This is the principle of the tree way catalyst converter (TWC) test circuit arrangement.

The oxygen mass stored in the catalyst volume it is considered as the most accurate parameter that characterized the conversion capacity of the catalyst and his deterioration degree, Clemmens (1990).

When the TWC is in a good shape, the second sensor, the test one, registers constantly $\lambda = 1$.

If the TWC deteriorates during the normal use, or because of an accident, his oxygen storage capacity decrees and the test sensor registers a bigger oxygen quantity in the exhaust gases after the TWC, $\lambda > 1$ (lean mixture), and $\lambda < 1$ when the engine run with a rich mixture. The indication of the sensor are far from the constant "1" value, which characterize a good catalyst.

1. Usual methods to estimate the deterioration degree of the TWC

The control system of the air / fuel ratio which processes the information received from the control lambda sensor, is usually, a PID regulator (regulator in two stapes, all or nothing). Do to the system inertia and do to the operation mode of the PID, the exhaust gas composition oscillates between maxim and minim values, an average been established. This oscillations detectable in the outgoing voltage of the control sensor, defines the specific frequency of the loop control, or the time limit of the loop.

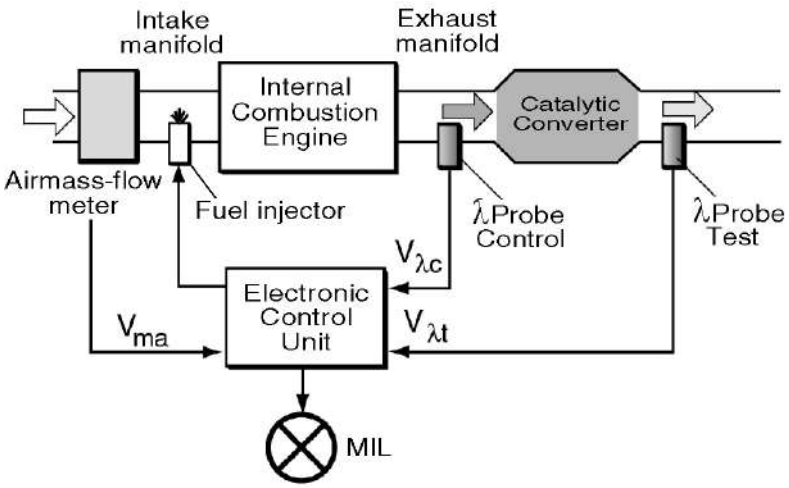

Figure 1: The block-diagram of an internal combustion engine with catalytic converter and two lambda-sensors one as control ad command probe and the second one as test probe.

The signal of the second lambda sensor, placed after the TWC is different from the signal of the first sensor. The amplitude of the test sensor voltage is different from the first one and considerable smaller. For the ideal case, this voltage amplitude is ZERO.

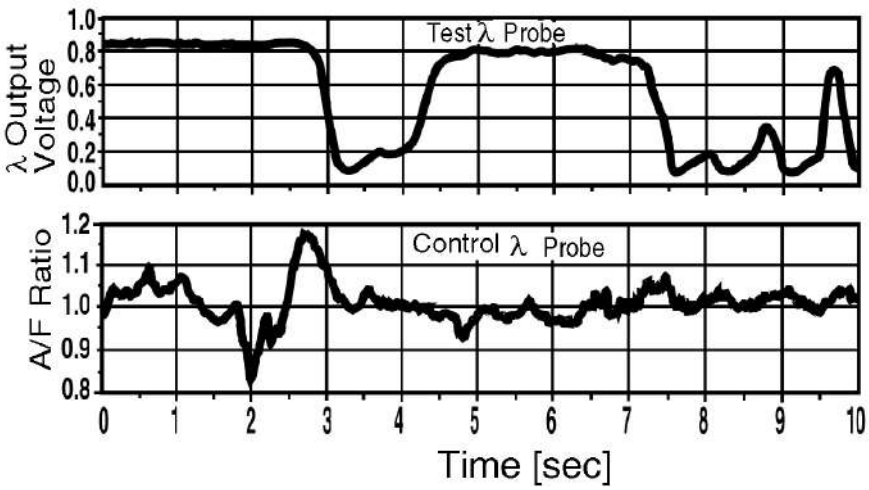

Figure 2: The amplitude of the output of the test probe voltage and λ value detected by the control probe when the engine regime is not stable.

In reality (see Fig. 2), the average value of the test-sensor voltage amplitude indicates the residual oxygen content of the exhaust gases after TWC, smaller the signal amplitude, better the exhaust gas conversion in the catalytic converter. Practically, the amplitude of the signal is growing proportionally with the decrees of the efficiency of the TWC, (see Fig. 3).

The test-sensor signal amplitude is deeply dependent to the moment when the converter it is saturated with oxygen, Drosescu (1999). In Figure 3, it can be seen that, earlier the "t_2" appearance moment, bigger the amplitude of the test-sensor signal. The amplitude of the test signal is in a very close relation with the oxygen storage capacity of the catalyst and this is for, this signal it is intensively used in practice to test the state of the TWC. For example:

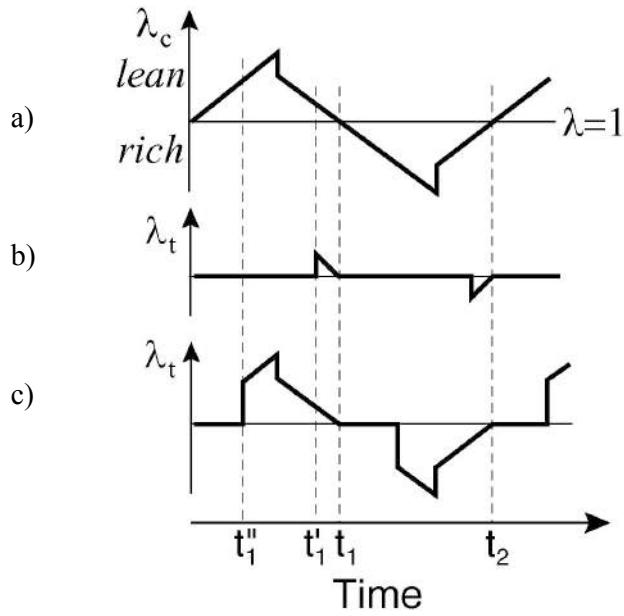

Figure 3: *(a) In time variation of the control lambda value "λ_c".*
(b) The lambda value given by the test probe for a converter a little bit aged.
(c) The lambda value given by the test probe for an aged converter.

a) The OBD self-diagnosis system, determines the oxygen storage capacity of the converter using the difference or the ratio between the amplitude of the two signals, one from the control sensor and one from the test-sensor.

This method has his limitation do to the loop-control system that, if it is not very precise, can' t maintains a precise air / fuel ratio for the engine, close enough to the stoechiometric value. The consequence it is that the test-sensor indicates a smaller oxygen storage capacity that it is in reality. Is the case at idling, in load transition mode and overrun mode.

b) The Federal Test Procedure (FTP) imposes two ways to test the efficiency of the catalyst. The first procedure use the test-sensor in the automatic loop-control of the air / fuel ratio, only for the test period, Yasui (2000). The second procedure measures the proper frequency of the loop-control to the changes of the "λ" value, compared with the value of a cartogram, depending on engine speed or engine load. The frequency of the loop-control, which is the reversed period, it is in a reversed proportionality with the oxygen storage capacity of the catalyst. The tests prove a strong connection between this frequency and the efficiency of the catalytic converter;

c) Other indicator of the converter wear is the difference between the time-answer of the two oxygen sensors, to the changes of the air / fuel ratio, Hepburn (1994) and Clemmens (1990). This indicator it is known as "purification factor" of the catalyst and it is defined based on the deviation of thus specific two temporal differences, for two specific engine function points, from a reference value.

2. Estimation of the oxygen flow trough the converter catalyst

This method use to estimate the conversion efficiency of the converter compares the DC voltage value output from the two sensors, detecting in the same time the sense of the transition detected on both sensors, from lean to rich mixture or from rich to lean. To accomplish this goal, if the two sensors detect the same sense for the transition, the following steeps it must be fallowed:

- Determine the value of the exhaust gases flow trough the converter;

- Compute the time-integer between the gas flow and the control-sensor voltage value;

- Compute the time-integer between the gas flow and the test-sensor voltage value;

- Compute the ratio or the difference between the two integers, as a measure of the converter

efficiency.

The block diagram of the installation include (see Fig. 4), an electronic block for the conditioning of the signals which come from the two sensors and the signal which comes from the hot wire flow-meter adapted to the engine air manifold. The original structure of the engine command-block connectors it is maintain, the voltage signals from the sensors it is collected directly from the transducer trough a splitter. Other signals as the advanced to the spark ignition moment, or the air / fuel ratio, can be followed with a UCE scanner-tester.

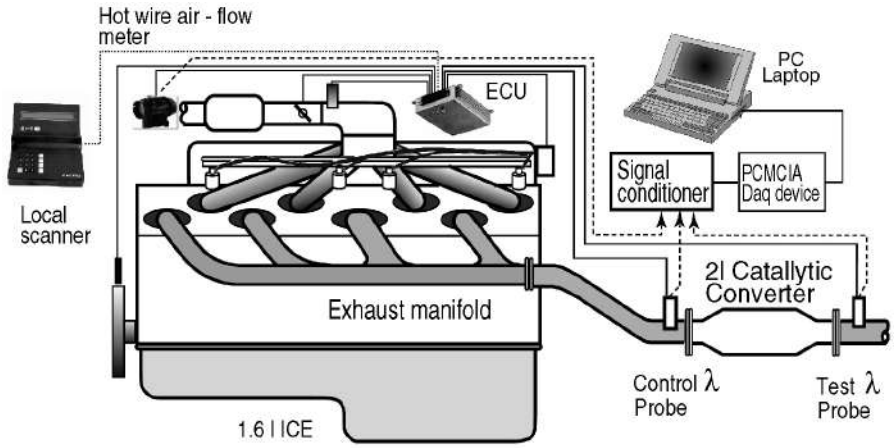

Figure 4: The block- diagram of the engine monitoring system

The test program of the catalytic converter is done with the help of an acquisition data device, type PCMCIA connected to the UCE and to a laptop.

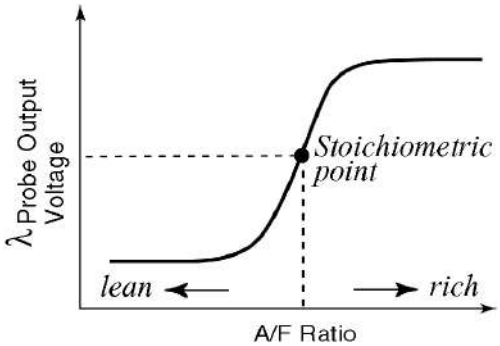

Figure 5: Hego lambda probe output characteristic

The both lambda-sensors are HEGO (pre-heated), type Bosch LSU4, the original ones for the studied engine. The output signal of this type of sensor has a "step" shape, (see Fig.5).

If the catalytic converter volume is "Vc" and it is considered as an open system submit to the low of mass conservation, the oxygen flow which come into the converter "$\dot{q}_{o2}$", it is directly proportional with the air mass flow "$\dot{q}_{air}$" and considering "k" a proportional factor (percent of the oxygen in the air), the mass flow of the oxygen in the exhaust gases after the engine and before the catalyst is:

$$\dot{q}_{o2} = k \cdot \dot{q}_{air} \cdot (\lambda c - 1) \qquad (1)$$

λc – lambda value give by the control sensor before the catalyst.

A similar relation is available for the oxygen flow after the catalytic converter "$\dot{q}'_{o2}$":

$$\dot{q}'_{o2} = k \cdot \dot{q}_{air} \cdot (\lambda t - 1) \qquad (2)$$

λt – lambda value given by the test sensor after the catalyst.

Coming back, (see Fig.3) the wave shape marked with **"a",** show the value of the oxygen excess

variation to the catalyst entrance. This value oscillates and it has an symmetric amplitude around the λ=1 value. At the moment t_1 becomes the transition from a lean mixture, $\lambda c > 1$, to a rich mixture, $\lambda c < 1$, and at the moment t_1 the transition is in reverse order. The signal has a triangle shape to simplify the representation and for a better understanding of the phenomena. The PID regulation system of the air / fuel ratio works exclusive with the integer component "I" and the sensor signal it is filtrated from the induced components do to the main control signal of the air / fuel ratio control system generated by the UCE.

The area between the lambda sensor signal and the lambda value "one", correspond with a time

$$\int(\lambda c - 1)\cdot d\tau \qquad (3) \qquad\qquad \int(\dot{q}_{O_2})\cdot d\tau \qquad (4) \qquad\qquad \int_{t_2}^{t_1}(\lambda t - 1)\cdot d\tau \qquad (5)$$

integer (3). If the income gas flow trough the catalyst is supposed to be uniform (on stable engine work regime), the area is proportional with the integer (4). As result, the graph area between the points "t_1" and "t'_1" is equivalent with the oxygen quantity, which transit the catalyst converter in this temporal integer window. This oxygen quantity is supposed to be enough to oxidize the entire pollutant quantity existent in the exhaust gas flow in the same time window.

If the output value of the test sensor shows that to the catalyst exit, that means the catalyst is in good condition. He is able to store enough oxygen for a complete oxidation of CO and HC quantities emitted from the engine.

Figure 3b. show the output signal of the test sensor for a catalyst witch become less effective. In this case, the catalyst it is no more capable to store all the oxygen available in the lean ratio period. The lost oxygen quantity can be compute trough the time integer (5).

Figure 3c. show the case of an inefficient catalyst converter, used or deteriorated, with a very low oxygen storage capacity. The output signal of the control sensor and test sensor are almost identically. The oxygen quantity stored in the catalyst can be compute with the equation (6).

This difference (6) is a direct measure of the storage capacity of the catalyst and in the same time the measure of the catalyst efficiency.

$$\Delta m_{O_2} = \int_{t_1'}^{t_1}(\dot{q}_{O_2})\cdot d\tau - \int_{t_1'}^{t_1}(\dot{q}'_{O_2})\cdot d\tau \qquad (6)$$

The Figure 6 presents the experimental data obtained with a 2-liter catalyst converter after 50.000 Km. The Figure 6.a represents the lambda value variation in time, around "one", if the engine it is commanded to accelerate successively at idling.

To evaluate the value of equation (6) it has been used, as integer method, the trapez method, with integer step "k". In this case, the numerical formula for equation (6) become (7), where "T" is the

$$\Delta m_{O_2}(k) = \Delta m_{O_2}(k-1) + [\dot{m}_{O_2}(k) + \dot{m}_{O_2}(k-1)]\cdot\frac{1}{T} \qquad (7)$$

time interval between the calculated value at "k-1" moment and respectively "k", and it is corresponding with the sample rate of the sensor signal. The Figure 6.b. show the shape of the integer signal past trough to PID. This signal represents the oxygen storage capacity of the catalyst in grams/seconds.

Thus integer relation it has been transposed in a discrete form, to be accessible to the micro-controller of the central unit.

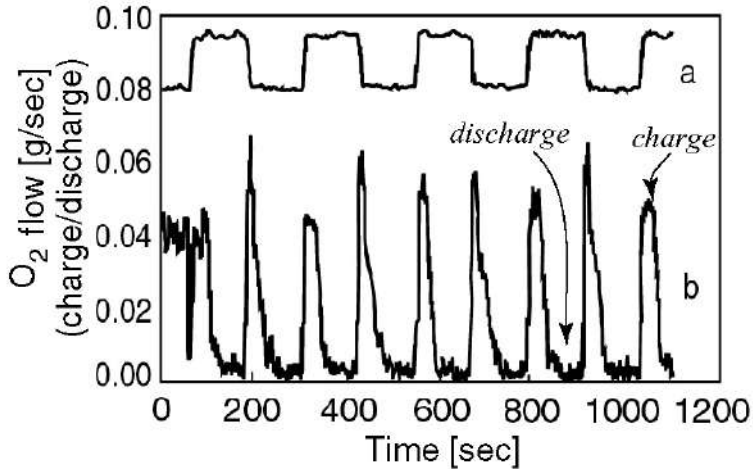

Figure 6: *The oxygen storage capabilities of a two liter converter catalyst.*

Conclusion

The method presented in this paper has the advantage to allow a precise evaluation of the catalytic converter efficiency.

It is also possible to estimate the gas flow trough the catalyst, and as consequence is possible a direct determination of the oxygen storage capacity of the catalyst, that gives the efficiency of this one.

Because the Δm_{o2} variable is not dependent from the shape of the lambda sensor signal, or from the airflow, Δm_{o2} it can be used to evaluate the state of the catalyst almost for the entire engine load.

As disadvantage, this method can't be used if the engine is functioning in overrun mode. In this case the fuel injection system cut off the fuel and as result the air quantity detected by the lambda sensor is out of the normal range ($\lambda >>1$).

Other disadvantage that can be considered is the necessity of a bigger calculation power for he UCE, which collects and evaluates the mathematical relation presented.

References

Clemmens W., et al. ,(1990), "Detection of catalyst Performance Loss Using On-Board Diagnostics", SAE Technical Paper 900062.

Drosescu R. (1999), "Cercetari privind achizitia, prelucrarea si modelarea parametrilor motarelor cu ardere interna la standul de incercari" Doctoral disertation, U.T.Iasi.

Hepburn S., J., Et al, (1994), "A Review of the Dual EGO Sensorr Method for OBD- II Catalyst Efficiency" SAE Technical Paper 942057.

Yasui Y,. Akasazaki S., et al.(2000), "SecondaryO2 Feedback Using Prediction and Identification Type Sliding Mode Control", SAE Technical Paper 2000-01- 0936.

Clemmens E., et al.(1990), "Detection of Catalyst Performance Loss Using On-Board Diagnostics", U.S. Environmental Protection Agency, SAE Congres Detroit.

12th International Symposium "Transport and Air Pollution" / 12e Colloque international "Transports et pollution de l'air", Avignon, 16 -18 *June* / juin 2003
proceedings / actes, n°92, tome / Vol. 2, Inrets ed., Arcueil, France, 2003, p. 253-255

Ag-Ti-V Impregnated Alumina for Controlling Carbon Monoxide and Hydrocarbons from Auto-exhaust

S.K.Rajput, S.Sarkar & D.K.Ghosh
Environmental Engineering Laboratory, Indian Institute of Technology, Kanpur-208016, India
Email: dkg@iitk.ac.in

Abstract
A laboratory scale set-up has been used in the present work for studying the performance of catalysts bed of alumina pellets impregnated with silver (Ag), titanium (Ti) and vanadium (V) to investigate its feasibility as a novel catalyst, which may replace expensive noble metal catalysts for controlling carbon monoxide (CO) and hydrocarbon (HC) emissions from automobiles. The effects of temperature, flow rate and time of catalyst bed usage on conversion have been studied. Ag-Ti-V impregnated alumina was found to be effective catalyst system for oxidation of both CO and HC.
Keywords*: Air pollution, Automobile exhaust, Catalysts, Impregnated alumina*

Introduction

Automobile exhaust emissions in India significantly contribute in making the air we breathe increasingly polluted and unsafe. In fact, the air quality monitoring done by Central Pollution Control Board in India indicates that concentration of fine particulate matter (PM_{10}), carbon monoxide, hydrocarbons, benzene are generally above the prescribed standard. Major initiative for vehicular emission control and fuel quality improvement was taken in India when emission standards for vehicles were notified in 1991 under the Environment (Protection) Act 1986. Now significant improvement in vehicular norms and fuel quality has been achieved through total phasing out of lead additives in petrol and supply of low sulphur (0.05%) diesel in major cities in India. However, suitable catalyst system shall be used to meet the standards.

Noble metals (Pt group metals), base metals and rare earth elements may be used as catalysts for automobile emission control. Noble metal group catalysts are good for automotive emission control, but they are expensive. Transition group elements may be used as oxidation catalysts since they do have more than one oxidation states. Oxides of Cu, Ni, Fe, V, Mo, Ti, Ag etc. can be used as catalyst for oxidation of CO and HC. Pathak (1998) studied catalyst system comprising of a bed of alumina pellets impregnated with nickel and molybdenum for oxidation of CO; and he found that alumina pellets impregnated with 4.4% Mo (pre-treated with 5.6%Ni) was effective catalyst. Jha (2000) used the Cu/Ni and Mo/V impregnated alumina as model auto-exhaust catalyst for CO-NO redox reactions. In the present work mixture of silver, titanium and vanadium impregnated alumina have been used to investigate its feasibility for controlling carbon monoxide and hydrocarbon emissions. The choice of Ag, Ti and V as catalysts has been made because of their affinity for CO and HC molecules.

Methodology of the study

A laboratory scale set-up (Rajput, 2001) has been used for studying the performances of the catalyst bed (alumina impregnated with Ag, Ti and V) to oxidise carbon monoxide (CO) and hydrocarbon (HC) with air at various operating conditions. The main emphasis has been to find the effective composition of the catalysts for the catalytic conversion of CO and HC. Carbon monoxide was

generated in the laboratory by the dehydration of formic acid with sulphuric acid. The flow of air from the compressor was controlled by regulating valve, and it was mixed with CO gas to get the desired CO concentration. Hydrocarbon was generated in the laboratory by bubbling the mixture of gasoline and groundnut oil in 1/5 ratio. Air was used as a carrier for the HC to get the desired concentration of HC. The concentration of CO and HC was measured by Auto Exhaust Gas Analyser (Model SAGEM-5040, SAGEM SOURIAU System, France), which is based on the principle of nondispersive infrared (NDIR) absorption of radiation by polyatomic gases in the IR region of the spectrum (2-15 micron), which does not disperse spectrally.

The size of alumina pellets were chosen judiciously in order to avoid the channelling due to large size and excessive head loss because of small size. Three different catalysts have been used in this study. They are Ag/Al_2O_3, Ti/Al_2O_3 and V/Al_2O_3. They were prepared by impregnating the pellets with solutions of $AgNO_3$, titanium butoxide and ammonium vanadate, respectively. A packed bed reactor was used for studying the conversion of CO and HC to CO_2 and H_2O. Different catalyst compositions of V, Ti and Ag impregnated alumina were tested. The emphasis has been given on finding effective composition of the catalysts for the catalytic conversion of CO and HC; and to study the performance of the catalysts at different temperatures and flow rates as well as with time of catalyst bed usage. The temperature range of 300 to 510^0C and flow rates 3 to 0.66 lpm were maintained. Concentration of CO in feed gas was maintained between 2 and 4 percent, and that of HC was in the range of 600 to 900 ppm. The system is also being studied with feed gas containing CO, HC and NO_x, which will be reported in future paper.

Results and discussions

Various combinations of catalysts (Ag, Ti and V impregnated alumina) were tested for different catalyst sequence as shown in Fig 1 (a) and (b): V-Ag-Ti, V-Ti-Ag, Ti-V-Ag, Ti-Ag-V, Ag-Ti-V and Ag-V-Ti. The catalyst sequence (Vi-Ti-Ag) comes out to be most effective in the conversion of both CO and HC. So this sequence of catalysts was used throughout the experiment for finding the most efficient catalyst composition under various operating conditions. The minimum conversion of CO and HC was observed in case of Ti-V-Ag and Ag-Ti-V catalyst sequence. The experimental data for the conversion of CO and HC at different temperatures for different catalyst sequence have been shown in the Fig 1 (a) and Fig 1 (b). The present study revealed that when the percentage of silver is increased, keeping the percentage of titanium and vanadium constant, the percentage increase in conversion of HC was more than the increase in percentage conversion of CO. When we increase the percentage of Ti, keeping percentage of Ag and V fixed, the gradual increase was found in both CO and HC concentration.

Conclusion

The present study shows the potential of a low-cost catalytic system for the oxidation of CO and HC. The main findings can be summarized as follows:

- Activated alumina impregnated with 1.1% Ag, 7% Ti and 7% V was found to be the most effective catalyst composition for oxidation of CO and HC
- When the gas stream comprising CO and HC with air was passed through the catalyst bed, conversion of gasses increases with increase in temperature of gas stream, and decreases with increase in flow rate
- This conversion was good enough at temperature higher than 400^0C

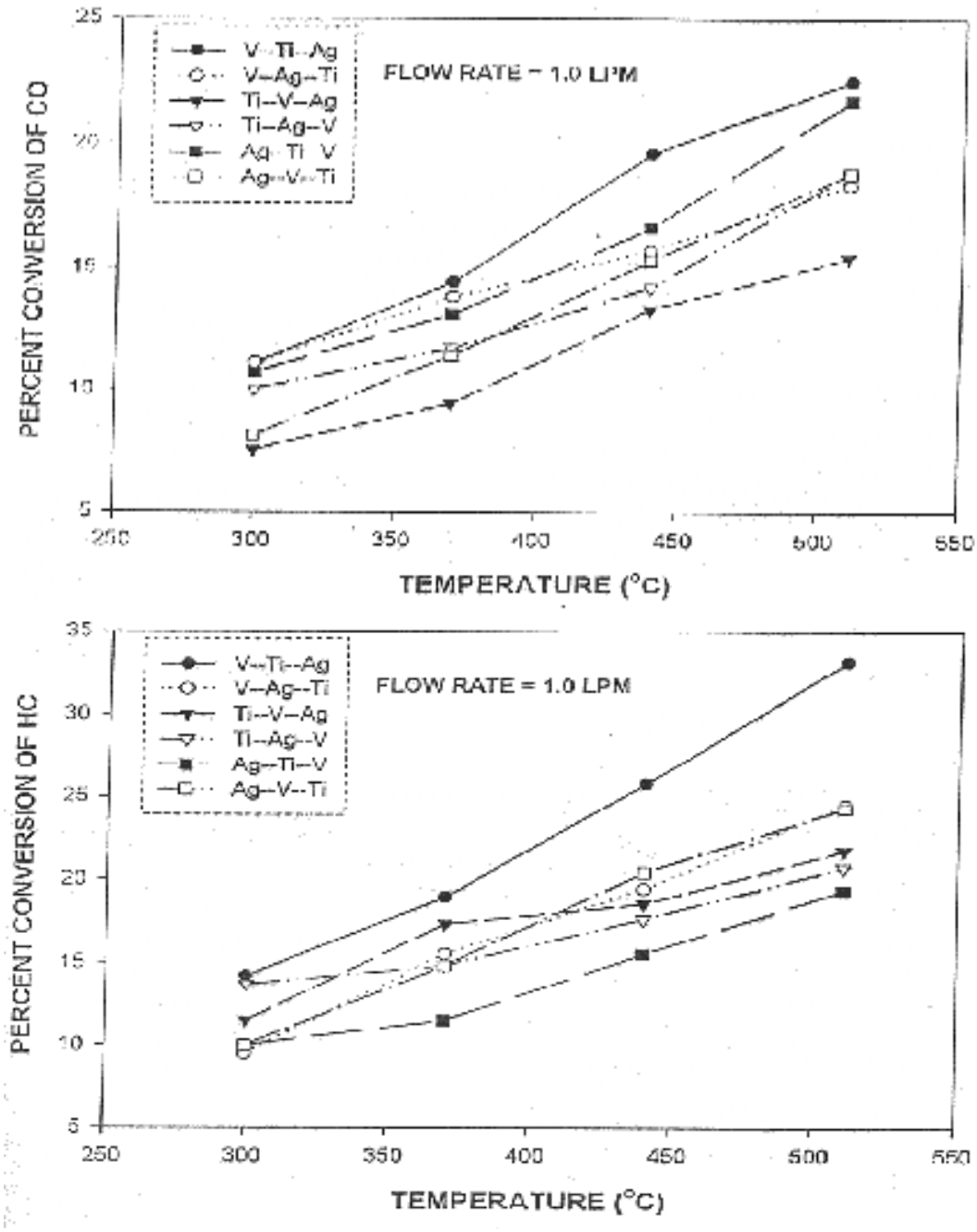

Figure 1: Conversion dependance on catalyst sequence for (a) CO, and (b) HC. Catalyst composition : V 5%,Ti 5% and Ag 0.7%.

References

Jha R. (2000) " Copper/Nickel and Molybdenum/Vanadium impregnated alumina as a model auto-exhaust catalyst for CO-NO redox reactions", M.Tech Thesis, IIT Kanpur

Pathak V. K. (1998) "Nickel and Molbdenum impregnated activated alumina for the catalytic conversion of CO to CO_2 in relevance to auto-exhaust", M.Tech Thesis, IIT Kanpur

Rajput S. K. (2001) "Ag-Ti-V impregnated alumina as a model auto-exhaust catalyst for catalytic conversion of CO and HC", M.Tech Thesis, IIT Kanpur

12th International Symposium "Transport and Air Pollution" / 12e Colloque international "Transports et pollution de l'air", Avignon, 16 -18 *June* / juin 2003
proceedings / actes, n°92, tome / Vol. 2, Inrets ed., Arcueil, France, 2003, p. 257-261

Nickel and Molybdenum Impregnated Catalytic System for Controlling Carbon Monoxide from Auto-exhaust

V. K. Pathak, S. Sarkar & D. K. Ghosh
Environmental Engineering Laboratory, Civil Engineering Department, Indian Institute of Technology, Kanpur-208016, India

Abstract
A laboratory scale set-up has been used in the present work for studying the performance of catalyst bed (allumina pellets impregnated with nickel and molybdenum) to oxidize carbon monoxide to carbon dioxide with air at various operating conditions. The emphasis has been given in this study to find the effective catalytic composition for catalytic conversion. Nickel has been chosen to trap carbon monoxide as it can readily form carbonyl compound, which in turn can be thermally decomposed. The experimental data revealed that for a given temperature, conversion of carbon monoxide decreases with increase in space velocity; and for a given space velocity, conversion of carbon monoxide increases with increase in temperature. The conversion of carbon monoxide did not decrease significantly with time of catalyst bed usage. This catalytic system being less expensive compared to noble group metal catalysts appears to be an economically viable one.
Keys- words: *Automobile exhaust, Carbon monoxide, Catalytic conversion, Impregnated catalytic system.*

Introduction

Automobile exhaust is a significant and growing source of air pollutants such as carbon monoxide, oxides of nitrogen and hydrocarbons. The need for controlling carbon monoxide from auto-exhaust will be necessary till automobiles are powered by non-polluting energy source. The various methods for the control of carbon monoxide emission include control of fuel, composition, modification of engine operating conditions, use of devices such as direct flame afterburners, adsorption canisters and catalytic converters. Catalytic converter is the most effective and feasible for controlling emission of carbon monoxide from automobiles exhaust. Such catalytic converter, already in use, consists of a porous ceramic element that is impregnated with a thin layer of platinum, palladium, rhodium or other noble metals of platinum group for oxidising carbon monoxide to carbon dioxide. Noble metals are however, very expensive. Further research is needed to identify other inexpensive catalyst for replacing noble metals usage in catalytic converter. A laboratory scale set-up has been used in the present work for studying the performance of catalyst bed (alumina pellets impregnated with nickel and molybdenum) to oxidise carbon monoxide to carbon dioxide with air at various operating conditions. The emphasis has been given in this study of finding the effective catalytic composition for catalytic conversion of carbon monoxide to carbon dioxide in relevance of auto-exhaust. Furthermore, the objective of present work is to identify a relatively inexpensive catalyst (as compared to the noble metal group catalysts) for converting carbon monoxide to carbon dioxide. Nickel has been chosen to trap carbon monoxide as it can readily form carbonyl compound, which in turn can be thermally decomposed. Earlier studies (Babu *et al*., 1992) at I.I.T Kanpur showed that molybdenum was a good oxidising agent for carbon monoxide. Hence molybdenum has been chosen as an oxidation catalyst.

1-Background Information

Transportation sources, primarily gasoline powered internal combustion engines, are the major anthropogenic source of carbon monoxide. The constituents of automobile exhaust are carbon monoxide, oxides of nitrogen, hydrocarbons, particulate matter and trace quantities of sulphur dioxide, formaldehyde and lead. Carbon monoxide and hydrocarbons result from the incomplete combustion of the fuel whereas oxides of nitrogen are formed from the nitrogen present in the fuel and the reactions between atmospheric oxygen and nitrogen inducted into the engine.

Impact of Air-Fuel Ratio

The ratio of the mass of air required per unit mass of fuel for combustion is defined as air-fuel ratio. As the air-fuel ratio is increased from around 11, the unburned hydrocarbons and carbon monoxide concentrations decrease. The concentration of oxide of nitrogen increases to a maximum at stoichiometric air-fuel ratio, i.e. 14.5 which give a minimum of unburned hydrocarbons and carbon monoxide. A further increase in air-fuel ratio results in a decrease of oxide of nitrogen, but an increase in hydrocarbons.

Catalytic Reactors

The use of catalysts to clean vehicle exhaust gasses started in USA in 1974 with the oxidising catalyst, which was able to oxidise hydrocarbons and carbon monoxide. However, this catalyst could not handle the oxides of nitrogen emissions and in 1979, the three-way catalyst was commercialised. This system is capable of simultaneously oxidising carbon monoxide and hydrocarbons and reducing the oxide of nitrogen.

The main oxidation reactions that occur in the catalyst are:

$C_XH_Y + (X+\frac{1}{4}Y)O_2 \rightarrow X\,CO_2 + \frac{1}{2}Y\,H_2O$ and $CO + \frac{1}{2}\,O_2 \rightarrow CO_2$

The main reduction reactions are:

$NO + CO \rightarrow \frac{1}{2}\,N_2 + CO_2$, $NO + H_2 \rightarrow \frac{1}{2}\,N_2 + H_2O$ and

$(2 + \frac{1}{2}Y)\,NO + C_XH_Y \rightarrow (1+\frac{1}{4}Y)\,N_2 + X\,CO_2 + \frac{1}{2}Y\,H_2O$

Undesired reduction reactions are:

$2\,NO + 5\,CO + 3H_2O \rightarrow 2\,NH_3 + 5CO_2$, $2\,NO + 5\,H_2 \rightarrow 2\,NH_3 + 2\,H_2O$

$2\,NO + CO \rightarrow N_2O + CO_2$ and $2\,NO + H_2 \rightarrow N_2O + H_2O$

The desired products are N_2, CO_2 and H_2O. These reaction products are thermodynamically favoured at typical exhaust temperature. The overall conversion is determined not only by the activity of the catalysts to promote the first five reactions mentioned above, but also by the availability of the oxidising and the reducing agents.

When an air pollution control catalyst is employed, the reaction is heterogeneous and goes through five basic phases:

1. Organic constituents must diffuse from the bulk of the untreated gas over the surface of the catalyst.
2. Organic materials must be adsorbed on the catalysts.
3. Adsorbed substances must then react on the catalyst surface.
4. Newly formed materials must be desorbed after reaction.
5. Desorbed products must once more diffuse into the body of the gas.

The catalyst offers new pathways for the reactions above, and lowers the activation energies so that the reactions can occur at normal exhaust temperatures (400-600^{0}C).

Catalyst Supports

The role and purpose of support for the catalyst component in auto-exhausts catalysts have been the subjects of some rather unique technology. As in all heterogeneous technology, the support or carrier is used to stabilise the catalyst component, increase the surface area of the catalyst and increase the degree of the dispersion of the catalytic component. Supports for the automobile exhaust catalysts are of two general types: alumina pellets and ceramic monoliths coated with a thin wash-coat. Both support types have perceived advantages and disadvantages, which have influenced their selection. Factors considered include converter size and cost, catalyst performance and durability on a particular vehicle, availability of support material from suppliers and ease of replacements.

Pelleted catalyst supports used in automobile catalytic converters are spherical particles (2.5 to 5mm in diameter) composed on thermally stable transitional alumina phase often stabilised by incorporation of metal and metal oxides (Gauguin *et al.,* 1975). Monoliths supports are thin walled ceramic honey combs composed mostly of cordierite (Bagley *et al*., 1973). A thin wash-coat of alumina applied to the surface of cordierite serves to increase the area of the surface to which the metals are applied. Characteristics of the monoliths that make them attractive catalyst supports are the low thermal expansion of ceramic, their small sizes, fast heat-up, low backpressure, and low vibration attrition and design flexibility.

Selection of catalyst for catalytic converter

Oxidation catalysts exist in more than one valance states. They accept and donate electrons easily and hence they can stay either in reduced or oxidised state depending on availability of elements. The ease of change of the valance state of metal cation in the oxide determines its effectiveness as an oxidation catalyst (Satterfield *et al*., 1982). The high cost of noble metals encourages manufacturers to find means to search for alternative to noble metals. The transition group elements may be used as oxidation catalysts since they do have more than one oxidation states. Oxides of Cu, Ni, Fe, V, Mo, Ti, and Ag etc can be used as catalysts for oxidation of carbon monoxide and hydrocarbon in auto-exhaust. Sometimes two or more metal oxides in combination are used as catalysts.

2-Experimental Section

In the present work carbon monoxide was generated in the laboratory by the dehydration of formic acid with sulphuric acid. A regulating valve controlled airflow from the compressor, and it was mixed with carbon monoxide gas to get the desired carbon monoxide concentration. A three-way valve was utilised to divert the flow of gas stream to facilitate the monitoring of inlet carbon monoxide concentration and to allow the mixed gas stream to pass through the catalyst bed reactor. Outlet and inlet carbon monoxide concentrations were measured with the help of Auto Exhaust Analyser (Model NPM CH-1, Netal Chromatograph). The temperature of the feed gas to the catalyst bed reactor was raised with the help of cylindrical oven and the temperature was controlled by regulating current through the heating coil with the help of voltage regulator. Temperature was recorded with the help of cromel-alumel thermocouple. The reactor used in the present study was cylindrical tube 23 cm long and inside diameter 23 mm.

Alumina pellets (mean size 1.55 mm) were washed with distilled water and dried before impregnation. These pellets were first impregnated in Nickel Nitrate solution for six hours and dried at room temperature. These dried pellets were impregnated in Ammonium Molybdate solution for six hours, dried at room temperature and then heated in an oven at 500^0C for three hours, to convert molybdenum and nickel in oxide form. Activated alumina used was acquired from Indian Petrochemicals Ltd. Distilled water and analytical grade chemicals were used in the preparation of reagents.

In the present work a packed bed reactor was used for studying the conversion of CO to CO_2. Diameter and length of the bed were 23 mm and 120 mm respectively. Temperature of feed gas ranged between 300 and 500^0C. The space velocities were kept between 0.188 and 1.197 sec^{-1}.

Different catalyst compositions of Ni and Mo impregnated alumina were tested for getting maximum conversion of CO to CO_2. Then the catalyst was tested for catalytic conversion of CO to CO_2 under different operating conditions, namely, temperature, space velocity and inlet CO concentration.

3-Results and Discussions

In this study, attempts were made to develop a low cost catalyst (alumina pellets impregnated with Mo and Ni) for catalytic conversion of CO to CO_2 in presence of air. The emphasis was given on finding effective operating conditions for conversion of CO to CO_2. Table 1 shows the important experimental data for the catalytic conversion of carbon monoxide under different operating conditions:

Catalyst Composition	Temperature (^{0}C)	Flow Rate Q (lpm)	Space Velocity (sec^{-1})	Conversion (%)
6%Ni, 4%Mo	300	1.00	0.311	20.00
		0.66	0.197	30.76
	440	1.00	0.361	38.23
		0.66	0.227	50.00
	500	1.00	0.376	48.48
		0.66	0.233	64.28
4%Ni, 6%Mo	300	1.50	0.463	21.62
		0.66	0.202	25.00
	440	1.50	0.548	35.71
		0.66	0.240	36.36
	500	1.50	0.578	42.85
		0.66	0.250	47.05
5.5%Ni, 4.5%Mo	300	1.40	0.404	40.00
		0.66	0.188	43.75
	440	1.40	0.472	56.00
		0.66	0.218	60.10
	500	1.40	0.468	76.56
		0.66	0.213	84.37
5.6%Ni, 4.4%Mo	300	1.00	0.296	33.33
		0.66	0.189	41.93
	440	1.00	0.328	62.50
		0.66	0.203	76.56
	500	1.00	0.329	80.00
		0.66	0.210	86.66

Table 1: Conversion of Carbon Monoxide (Average Inlet Conc. of CO = 3%)

It is evident from the above table that the activated alumina impregnated with 4.40% Mo (pre-treated with 5.60% Ni) was found to be most effective catalyst combination for oxidation of CO to CO_2. Electron Paramagnetic Resonance (EPR) as a probe was used to understand the chemistry involved in the observed conversion of CO to CO_2. EPR spectra of different catalyst combinations indicate that Mo was acting as primary oxidising agent while Ni acted as a secondary catalyst and activated CO molecules for oxidation to CO_2.

It may be mentioned that the oxidation of CO to CO_2 mediated by Mo^{vi} concomitant to its reduction to Mo^{v}, which in turn gets re-oxidised by aerial oxygen to regenerate Mo^{vi} to participate in the subsequent catalytic cycles. The expected equations are

[1] $2Mo^{vi}O_3 + CO \rightarrow Mo^{v}_2O_5 + CO_2$

[2] $Mo^{v}_2O_5 + {}^1/_2O_2 \rightarrow 2Mo^{vi}O_3$

Attempts have been made to understand the role of Ni to activate CO for its subsequent oxidation by Mo^{vi}. As it is well known that Ni compounds readily trap CO to form nickel carbonyl, which can be readily identified by infrared spectroscopy where the bonded carbonyl stretching frequency appeared around 2000 cm^{-1} (Cotton and Wilkinson, 1979). The study of Ni with CO is well known and Ni does form nickel carbonyl very readily. We believe that the free CO binds to Ni, which is thermally unstable whereby the carbonyl that is activated in turn reacts with Mo^{vi} to respond to the subsequent redox reaction (equation [1] and [2]). It was observed that when the catalyst is made first by impregnating Ni salt followed by molybdate then, it has higher activity in contrast when the catalyst is made in the reverse order. The possible explanation for this is that in the first case CO molecules diffuse Mo layer to reach the Ni site where it is activated followed by oxidation by Mo^{vi} leading to higher conversion. In contrast when the outer layer contains Ni the activated CO immediately gets released outside and it diffuse the Mo layer to give small percentage of conversion.

Conclusion

The experimental data revealed that for a given temperature conversion of CO decreases with increase in space velocity; and for a given space velocity conversion of CO increases with increase in temperature. It has been observed that at lower space velocities (0.20 to 0.30 sec^{-1}), as temperature is increased to 500 degree centigrade there is an appreciable increase in conversion of CO to CO_2. The temperature of auto-exhaust gasses also lie in the range 663 to 773K (Kathleen (1984)) indicating feasibility and worthiness of this catalyst to be used in an automobile exhaust catalytic converter. The conversion of CO was not reduced significantly with time of catalyst bed usage. Re-oxidation of Mo^{v} to Mo^{vi} was found to be the rate-limiting step. This catalytic system being less expensive compared to noble group metal catalysts appears to be an economically viable one.

The present study shows the potential of Ni-Mo catalytic system as a possible low-cost catalytic system in controlling carbon monoxide levels. However, the aspects of catalyst poisoning by lead, sulphur, and phosphorus compounds have to be studied before designing a three-way catalyst system for automobile exhaust emissions control.

References

Babu, N., "Catalytic Conversion of CO to CO_2 with Air Using a Cheap Catalyst in Relevance to Auto-exhaust", M. Tech. Thesis, I.I.T Kanpur (1992)

Begley, R. D.; Doman, R. C.; Duke, D. A. and McNally, R. N., “Paper No.730274”, presented to Society of Automotive Engineers (1973)

Cotton, F.A. and Wilkinson, G., "Advance Inorganic Chemistry", 3rd ed., Wiley Eastern Limited (1979)

Gauguin, R; Graulier, M. and Papee, D., “Catalysis for control of Automotive pollutants”, Adv. Chem. Ser. 143, Am. Chem. Soc., Washington D.C. (1975)

Kathleen, C.T., "Automobile Catalytic Converters", Applied Catalysis, Vol. 5, Springer-Verlag (1984)

Satterfield, C. N., Heterogeneous Catalysis in Practice, McGraw Hill Book Company, Inc., USA (1982)